UNIVERSITY OF CALIFORNIA,
IRVINE

Elucidating the Structures of Amyloid Oligomers with Chemical Model Systems

DISSERTATION

submitted in partial satisfaction of the requirements
for the degree of

DOCTOR OF PHILOSOPHY

in Chemistry

by

Johnny D. Pham

Dissertation Committee:
Professor James S. Nowick, Chair
Professor Zhibin Guan
Professor Kenneth J. Shea

2014

© 2014 Johnny D. Pham

Table of Contents

List of Figures

List of Schemes

List of Tables

Acknowledgements

There are many people I wish to recognize that helped me in my pursuit of a doctorate degree, and in my development as a scientist. I am very grateful for these people that have offered me professional and personal guidance and support during my time at UC Irvine.

I would like to first thank my advisor, Prof. James Nowick, for allowing me to join his research group and for being such a great mentor. During my first year as a graduate student in the Medicinal Chemistry and Pharmacology (MCP) program, I had some difficulties with being placed in a research lab during the initial selection process. Fortunately, James let me join his group. Under his tutelage, I learned a great deal in thinking about science, in properly communicating ideas clearly and succinctly, and in becoming a detail-oriented problem-solver and researcher. His dedication and curiosity in chemistry and attention to detail inspires me to question everything and be meticulous as well. I will be forever grateful of his mentorship.

I would like to thank Dr. Celia Goulding and her research group for providing me with assistance in learning X-ray crystallography. Members of her group, Dr. Nicholas Chim, Angie Iniguez, Heidi Contreras, Dr. Rodrigo Torres, Parker Johnson and Robert Morse were especially helpful in guiding me through the steps of growing and collecting crystals, collecting diffraction data, and in solving structures.

Professors in the chemistry department are incredible resources in providing career and professional advice. I would like to thank Kenneth Shea and Zhibin Guan for being on my dissertation committee and for providing helpful advice, Prof. Andrej Luptak for being a helpful advisor during my first year in the MCP program and in my Ph. D. career, and Profs. Elizabeth

Jarvo, Jennifer Prescher, Aaron Esser-Kahn, Stephen Hanesian, and Christopher Vanderwal for additional guidance.

Research group members are also valuable resources for my development as a scientist. I would like to thank former group member Dr. Pin-Nan Cheng for being such a great mentor and friend during graduate school. Dr. Cheng offered much assistance when he was a senior graduate student in the lab and I was just a junior graduate student getting acclimated to the group. Prior and current group members that I would also like to thank are: Dr. Omid Khakshoor, Dr. Mandy Zheng, Dr. Suchitra Datta, Kim V. Le, Ryan Spencer, Kevin Chen, Yilin Wang, Adam Kreutzer, Matthew Klun, Nick Truex, Andrew Lam, Hao Li, Andrew Lam, and Chun-Ching Huang.

I would like to thank friends that I have met in the department that have been very helpful in graduate school. I would like to thank: Dr. Michael Shaghafi, Dr. Ivelina Yonova, Dr. Greg Williams, Dr. Jessica Arter, Dr. Dave Schaffer, Dave McCutcheon, David Patterson, Dave Jackson, and Jonathan Lam.

Lastly, I would like to thank my family and cousins for their incredible love and support, and I would like to thank my friends that have also supported me during graduate school.

Curriculum Vitae
Johnny D. Pham

Education

University of California, Irvine, Department of Chemistry, Ph. D., 2008-2014
San Francisco State University, Department of Chemistry, M. S. Program, 2006-2008
University of California, Berkeley, Department of Chemistry, B. A., 1997-2002

Research and Work Experience

Graduate Student Researcher, University of California, Irvine, 2008-present
Advisor: Prof. James S. Nowick
Invented a new class of macrocyclic β-sheet peptides to study amyloid oligomer formation. Solved X-ray crystallographic structures of macrocyclic β-sheet peptides. Synthesized and studied inhibitors of amyloid-β (Aβ) aggregation. Mentored undergraduate and graduate students. Maintained and repaired HPLC, high-vacuum system, solvent dispenser system, peptide synthesizer, and lyophilizer equipment.

Medicinal Chemistry and Pharmacology Gateway Program, Irvine, 2008-2009
Involved in the inaugural interdisciplinary program that included coursework in pharmaceutical sciences and research rotations through a pharmacology laboratory and total synthesis laboratory prior to joining the chemistry department for completion of PhD degree.

Graduate Student Researcher, San Francisco State University, 2006-2008
Advisor: Prof. Marc O. Anderson
Synthesized and characterized analogs of nordihydroguaiaretic acid (NDGA) for use as inhibitors of several tyrosine kinase receptors implicated in breast cancer. Supervised an undergraduate student.

Senior Research Associate, Nano-Tex, Inc., Emeryville, CA, 2002-2005
Designed new chemical formulations in applying new functionality to textiles. Assisted in the regulatory compliance and commercialization of such new products.

Undergraduate Researcher, University of California, Berkeley, 2001-2002
Advisor: Prof. Peidong Yang
Synthesized nanowires using chemical vapor deposition (CVD). Analyzed, researched and studied nanowire and nanoribbon formation for advancements in nanotechnology.

Manufacturing Intern, Bayer Corporation, Berkeley, CA, 2000-2001
Ran alert modules, created alert-limit charts using statistical methods and designed a database to simplify data entry in the quality assurance department using Microsoft Access. Investigated factor VIII coagulation lab data and procedures for statistical analysis.

Publications

8) **Pham, J. D**.; Spencer, R. K.; Chen, K. H.; Nowick, J. S. "A Fibril-like Assembly of Oligomers of a Peptide Derived from β-Amyloid," manuscript submitted to *J. Am. Chem. Soc.*

7) **Pham, J. D**.; Demeler, B.; Nowick, J. S. "Polymorphism of Oligomers of a Peptide from β-Amyloid," *J. Am. Chem. Soc.* **2014**, *136*, 5432–5442. Highlighted in *JACS Spotlights* **2014**, *136*, 5525–5526.

6) **Pham, J. D**.; Chim, N.; Goulding, C. W.; Nowick, J. S. "Structures of Oligomers of a Peptide from β-Amyloid," *J. Am. Chem. Soc.* **2013**, *135*, 12460–12467.

5) Cheng, P.-N.; **Pham, J. D.**; Nowick, J. S. "The Supramolecular Chemistry of β–Sheets," *J. Am. Chem. Soc.* **2013**, *135*, 5477–5492.

4) Li, F.; **Pham, J. D.**; Anderson, M. O.; Youngren, J. F. "Nordihydroguaiaretic Acid Inhibits Transforming Growth Factor Beta Type 1 Receptor Activity and Downstream Signaling" *Eur. J. Pharm*. **2009**, *616*, 31–37.

3) Yan, H.; Johnson, J.; Law, M.; He, R.; Knutsen, K.; McKinney, J. R.; **Pham, J.**; Saykally, R.; Yang, P. " ZnO Nanoribbon Microcavity Lasers " *Adv. Mater.* **2003**, *22*, 1907–1911.

2) Yang, P.; Yan, H.; **Pham, J.**; He, R. "Morphogenesis of One-Dimensional ZnO Nano- and Microcrystals" *Adv. Mater.* **2003**, *15*, 402–405.

1) Yang, P.; Yan, H.; Mao, S.; Russo, R.; Johnson, J.; Saykally, R.; Morris, N.; **Pham, J.**; He, R.; Choi, H. "Controlled growth of ZnO Nanowires and their optical properties," *Adv. Funct. Mater.* **2002**, *12*, 323–331.

Recognition

- UCI Regents' Dissertation Fellowship, 2013
- AAPPTec Travel Award for the 23rd American Peptide Symposium, 2013
- UCI Faculty Endowed Fellowship, 2012 and 2013
- American Chemical Society Travel Award for Spring National Convention at San Diego, 2012
- SFSU Alumni Association, Academic Recognition, 2007
- SFSU Summer Research Fellowship, 2007

Oral and Poster Presentations

Pham, J. D.; Chim, N.; Goulding, C. W.; Nowick, J. S. "Structures of Oligomers of a β-Amyloid Peptide," American Peptide Society, Hilton Waikoloa Village, Hawaii, June 22-27, 2013, Poster (Semi-Finalist).

Pham, J. D.; Chim, N.; Goulding, C. W.; Nowick, J. S. "Structures of Oligomers of a β-Amyloid Peptide," Emerging Scientists Symposium on Neurological Disorders, University of California, Irvine, February 21, 2013, Presentation.

Pham, J. D.; Nowick, J. S. "Oligomer Structures of a β-Amyloid Peptide," Vertex Symposium, University of California, Irvine, December 6, 2012, Presentation.

Pham, J. D.; Nowick, J. S. "New Macrocyclic β-Sheets featuring a Nonapeptide Strand," ACS Spring Meeting and Expo, San Diego Convention Center in San Diego, CA, March 27, 2012, Presentation.

Pham, J. D.; Nowick, J. S. "New Macrocyclic β-Sheets Featuring a Nonapeptide Strand that Forms a Well-Defined Tetramer," Gordon Research Seminar on Peptides, Chemistry and Biology, Ventura Beach Marriott in Ventura Beach, CA, February 18–19, 2012, Poster.

Pham, J. D.; Nowick, J. S. "A New Class of Macrocyclic β-Sheets that form Well-Defined Oligomers," Vertex Symposium, University of California, Irvine, October 28, 2011, Presentation.

Pham, J. D.; Nowick, J. S. "Artificial Macrocyclic β-Sheets for Inhibiting β-Amyloid Aggregation and the Use of Disulfide Staples to Construct β-Sandwich Structure," Post-Doctoral and Graduate Student Colloquium, University of California, Irvine, April 23, 2010, Presentation.

Teaching Experience

Teaching assistant, Department of Chemistry, University of California, Irvine, 2009-2013
Taught general chemistry lectures and laboratory courses, organic chemistry lectures and laboratory courses, and upper division organic chemistry and chemical biology laboratory courses.

Instructor, Bridges to Baccalaureate Minority Science Program, Department of Biology, Summer 2011
Developed and taught introductory organic chemistry curriculum for underrepresented minority students interested in biomedical sciences making the transition to college-level organic classes.

Teaching assistant, Department of Chemistry, San Francisco State University, 2006-2007
Taught general chemistry and organic chemistry laboratory courses.

Services

- Student-Hosted Seminar Committee, 2012–2013
  Organized and arranged a lecture series from invited professors from around the country.
- Graduate Student Outreach, 2011–2012
  Conducted chemistry demonstrations at nearby elementary and middle schools to help children foster an interest in science at an early age.

ABSTRACT OF THE DISSERTATION

Elucidating the Structures of Amyloid Oligomers Using Chemical Model Systems

By

Johnny D. Pham

Doctor of Philosophy in Chemistry

University of California, Irvine, 2014

Professor James S. Nowick, Chair

While amyloid plaques and fibrils are a visible hallmark of Alzheimer's disease, smaller assemblies of Aβ, termed *oligomers*, are now widely thought to be the Aβ species that cause neurodegeneration. Since the structures of the oligomers are not known and not well understood, determination of the structure of amyloid oligomers is one of the most important problems in structural biology. The Nowick group uses chemical model systems to study β-sheet structures and interactions, and these systems can also be used to stabilize oligomers for structural studies. This dissertation describes chemical model systems to elucidate different amyloid oligomer assemblies using an amyloidogenic sequence from Aβ and to gain a structure-based understanding of how natural Aβ may form toxic oligomers.

Chapter 1 describes the use of chemical model systems in the research group in helping us understand the types of supramolecular interactions in protein quaternary structure and in amyloids. The model systems are macrocyclic β-sheet peptides that contain artificial turn and template units that mimic β-sheet structure and interactions. Studies of the macrocyclic β-sheet peptides by X-ray crystallography illustrate the importance of edge-to-edge hydrogen bonding

interactions and the face-to-face hydrophobic interactions between proteins and amyloid peptides. The macrocycles were used in inhibition studies against amyloid aggregation assays.

Chapter 2 describes the X-ray crystallographic structures of oligomers of a new chemical model system of a macrocyclic β-sheet peptide that incorporates an amyloidogenic sequence $A\beta_{15\text{-}23}$ from the Aβ peptide. In the solid state structure, the macrocycle folds well as an artificial β-sheet and forms a cruciform tetramer that are made up of antiparallel, hydrogen-bonded dimers. The cruciform tetramers assemble into triangular dodecamers, and the triangular dodecamers further assemble into a lattice. The lattice features a hexagonal cavity, which can be thought of as a porelike assembly, and may disrupt cell membranes by serving as a channel for water or metal cations. The cruciform tetramers also organize into a linear assembly through the lattice. The self-association of the β-sheet macrocycle seen in the crystal structure provides clues into the self-assembly mechanism of amyloid oligomers. Chapter 2 culminates with the use of the crystal structure to model similar oligomer structures using the linear sequence of Aβ (Ac-QKLVFFAED-NHMe, Ac-$A\beta_{15–23}$-NHMe); the modeling suggests that natural Aβ can form similar structures.

Chapter 3 complements the work conducted in Chapter 2 and describes a series of macrocyclic β-sheet peptides that differs in the solution structure vs. the solid-state structure. In the study, the macrocyclic β-sheets dimerize in a shifted, antiparallel fashion as observed by ^{1}H-NMR spectroscopy. Additional studies by ^{1}H-NMR and DOSY spectroscopy suggest that the shifted, β-sheet dimers self-associate into a tetramer through face-to-face interaction. Supramolecular interactions of the peptide were explored with different mutations. The results show the structural importance of incorporating Aβ residues and the polymorphism observed in the solution-state structure in comparison to the solid-state structure.

Chapter 4 is an extension of the work from Chapter 2 that describes the discovery of a new motif of a macrocyclic β-sheet peptide that forms a fibril-like assembly of oligomers. The results bridge the gap between amyloid oligomers and amyloid fibrils, showing how amyloid oligomers can form fibrillar assemblies in the solid state. In the new macrocycle, the template strand is substituted with an $A\beta_{15–23}$ hybrid strand. The macrocycle forms a tetramer in aqueous solution, and in X-ray crystallographic studies, the solid-state structure of the macrocycle suggests an alternate mode of assembly for Aβ peptides.

CHAPTER 1

Chemical Models of β-Sheets

Preamble

Chapter 1 is part of a *Perspective* in the *Journal of the American Chemical Society* that I co-wrote with another graduate student in our research group, Dr. Pin-Nan Cheng during 2012.[1] This chapter addresses the common themes in the supramolecular interactions of β-sheets through chemical model systems developed in Prof. James Nowick's laboratory. The chemical model systems offer our research group the ability to study important types of supramolecular interactions in β-sheets relevant to proteins and amyloid structures. The chemical model systems are smaller, simpler and easy to manipulate in comparison to larger globular proteins.

Working on this chapter and the perspective paper helped with my early development as a Ph.D. scientist by allowing me to gain experience in the proper preparation of a scientific article. I was able to work alongside James in learning the art of scientific writing and the meticulous process that goes into preparing high quality images. I also had the chance to utilize computer software such as Illustrator and PyMOL necessary for communicating our research work.

By reviewing our research group's work, I gained a deeper understanding of β-sheet structures and interactions. I applied some of this knowledge that led to the development of the projects described in the subsequent chapters.

Reproduced in part with permission from Cheng, P.-N.; Pham, J. D.; Nowick, J. S. *J. Am. Chem. Soc.* **2013**, *135*, 5477–5492. Copyright 2013 American Chemical Society.

Introduction

Chemical model systems provide a powerful platform with which to study and control the rich supramolecular chemistry of β-sheets. Our laboratory has developed macrocyclic β-sheet peptides containing artificial turn and template units as chemical models of β-sheet structure and interactions. The macrocyclic β-sheets contain a natural peptide β-strand, turns based on δ-linked ornithine ($^{\delta}$Orn),[2] and templates based on the unnatural amino acid *Hao*,[4] which mimics the hydrogen-bonding edge of a tripeptide β-strand while blocking the other edge. Macrocycles **1.1**–**1.3** are the three most important classes of macrocyclic β-sheets that we have thus far published (Figure 1.1).[5,6,7,8,9,10,11]

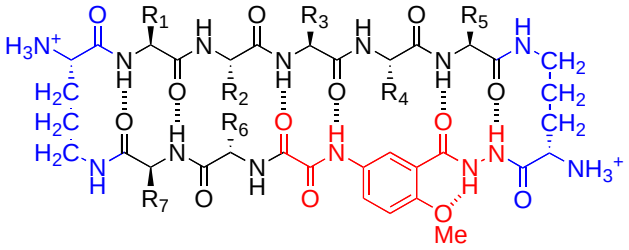

macrocyclic β-sheet **1.1**

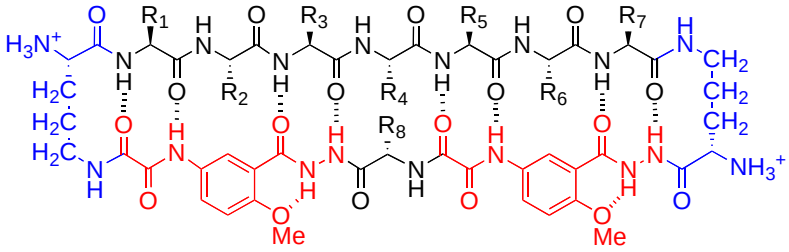

macrocyclic β-sheet **1.2**

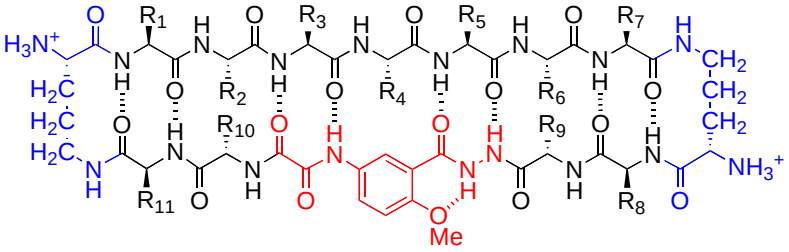

macrocyclic β-sheet **1.3**

Figure 1.1. Macrocyclic β-sheets **1.1-1.3**. The tripeptide mimic Hao is shown in red and the δ-linked ornithine turn units are shown in blue. Intramolecular hydrogen-bonds are shown with dashed lines.

Macrocyclic β-sheet **1.1** is a 42-membered ring containing a pentapeptide (upper strand, R_1–R_5), two $^{\delta}$Orn turn units (shown in blue), one Hao template (shown in red), and two additional amino acids (R_6 and R_7).[6,9,10,12] Macrocyclic β-sheet **1.2** is a 54-membered ring containing a heptapeptide (upper strand, R_1–R_7), two $^{\delta}$Orn turn units, two Hao templates, and one additional amino acid (R_8).[5,7,8] Macrocyclic β-sheet **1.3** is a 54-membered ring containing a heptapeptide (upper strand, R_1–R_7), two $^{\delta}$Orn turn units, one Hao template, and four additional amino acid (R_8–R_{11}).[11]

Macrocyclic β-sheets **1.1–1.3** exhibit a rich supramolecular chemistry. The penta- and heptapeptide strands of these macrocycles provide one exposed edge that can participate in edge-to-edge hydrogen-bonding interactions. The Hao-containing strands help preorganize the other edge by intramolecular hydrogen bonding, while blocking further hydrogen-bonding interactions. The side chains of the alternate amino acids of the penta- and heptapeptide strands, above and below the hydrogen-bonded backbones, make up the "top" and "bottom" faces of the β-sheet.

Table 1 illustrates some of the macrocyclic β-sheets that we have studied that demonstrate edifying supramolecular chemistry in the solid state or in solution. Many of these macrocycles contain penta- and heptapeptides derived from amyloidogenic or other β-sheet peptides and proteins. The pentapeptides of **1.1a**, **1.1b**, and **1.1e** are based on residues 17–21 and 30–34 of Aβ, while those of **1.1c** and **1.1d** are based on residues 306–310 of tau. The heptapeptides of **1.2a** and **1.2b** are based on protein G variant NuG2.[13,14] The heptapeptides of **1.3a** and **1.3b** are based on residues 30–36 and 16–22 of Aβ, while that of **1.3c** is based on residues 63–69 of human β_2-microglobulin (hβ_2M) and that of **1.3d** is based on human α-synuclein (hαSyn).

Table 1.1: Amino acids in macrocycles **1.1-1.3**[a]

Macrocycle	R_1	R_2	R_3	R_4	R_5	R_6	R_7	R_8	R_9	R_{10}	R_{11}
1.1a (based on $A\beta_{17-21}$)	Leu	Val	Phe	Phe	Ala	Leu	Lys				
1.1b (based on $A\beta_{30-34}$)	Ala	Ile	Ile	Phe	Leu	Tyr	Lys				
1.1c (based on $Tau_{306-310}$)	Val	Gln	Ile	Val	Phe^{Br}	Lys	Leu				
1.1d (based on $Tau_{306-310}$)	Val	Gln	Ile	Val	Tyr	Lys	Leu				
1.1e (based on $A\beta_{30-34}$)	Ala	Ile	Ile	Gly	Leu	Tyr	Lys				
1.2a (based on NuG2)	Thr	Ser	Phe	Thr	Tyr	Thr	Ser	Lys			
1.2b (based on NuG2)	Thr	Tyr	Phe	Thr	Tyr	Phe^{Br}	Ser	Lys			
1.3a (based on $A\beta_{30-36}$)	Ala	Ile	Ile	Gly	Leu	Met	Val	Lys	Phe	Phe^{Br}	Lys
1.3b (based on $A\beta_{16-22}$)	Lys	Leu	Val	Phe	Phe	Ala	Glu	Lys	Leu	Ile	Glu
1.3c (based on $h\beta_2M_{63-69}$)	Tyr	Leu	Leu	Tyr	Tyr	Thr	Glu	Lys	Val	Val	Lys
1.3d (based on $h\alpha Syn_{75-81}$)	Thr	Ala	Val	Ala	Asn	Lys	Thr	Val	Phe	Tyr	Lys

[a] Standard three-letter abbreviations are used; Phe^{Br} represents *p*-bromophenylalanine, which was incorporated to faciliate X-ray crystallographic analysis.

Folding of Macrocyclic β-Sheets. The X-ray crystallographic structures of macrocycles **1.1a**–**1.1c**, **1.2b**, and **1.3a** reveal well-folded β-sheet structures in the solid state.[8,9,11] The main chains of 42-membered ring macrocycles **1.1a**–**1.1c** have six intramolecular hydrogen bonds between the upper and lower strands and adopt similar conformations (Figure 1.2).[9] The main chains of 54-membered ring macrocycles **1.2b** and **1.3a** have eight intramolecular hydrogen bonds between the upper and lower strands (Figure 1.3).[8,11]

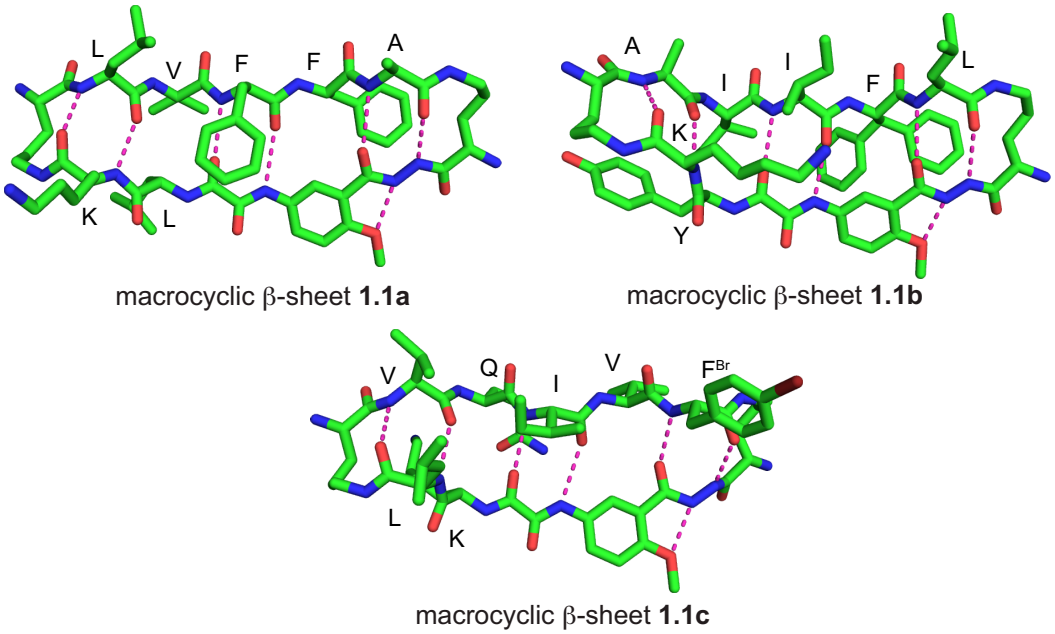

Figure 1.2: Crystal structures of macrocyclic β-sheets **1.1a–1.1c** (PDB: 3Q9H, 3Q9J, and 3Q9G). Intramolecular hydrogen bonds are shown with dashed lines. The phenylalanine residue of **1.1b** exhibits partial occupancy; the two rotameric orientations of the side chain are shown.

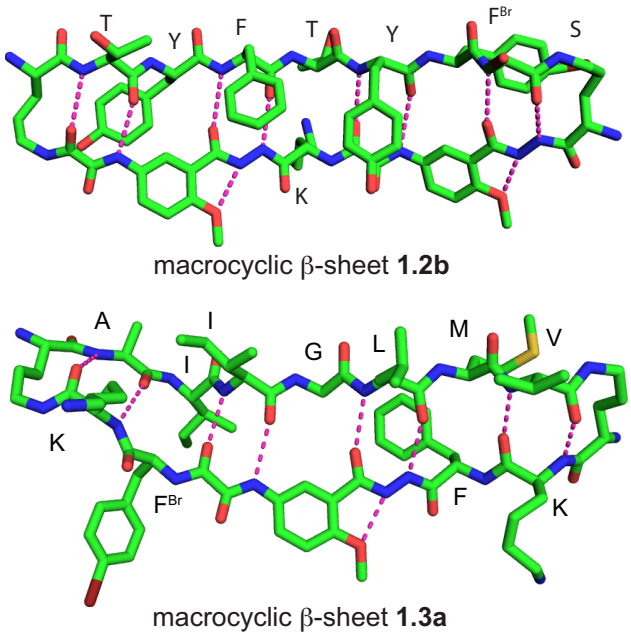

Figure 1.3. Crystal structures of macrocyclic β-sheets **1.2b** and **1.3a** (PDB: 3NI3 and 3T4G). Intramolecular hydrogen bonds are shown with dashed lines.

The X-ray crystallographic structures of macrocycles **1.1b**, **1.1c**, and **1.3a** exhibit a pronounced twist. This twist can stabilize the folded structure of macrocycle **1.1** through hydrophobic or van der Waals interactions between residues R_4 and R_6 and the two ᵈOrn turn units (Figure 1.4). These interactions can be observed in the X-ray crystallographic structures of macrocycles **1.1b** and **1.1c**. ^{1}H NMR spectroscopic studies of macrocycles **1.1** suggests that bulky and branched residues at the R_4 and R_6 positions also enhance the formation of folded β-sheet structures in aqueous solution.[6] This twist can also stabilize the folded structure of macrocycle **1.3** through hydrophobic or van der Waals interactions between residues R_6 and R_{10} and the two ᵈOrn turn units. The interaction between R_6 and the adjacent ᵈOrn turn unit is observed in the X-ray crystallographic structure of macrocycle **1.3a**, while that between R_{10} is supplanted by other crystal packing interactions. These interactions can, in turn, stabilize the twist of the macrocycles.

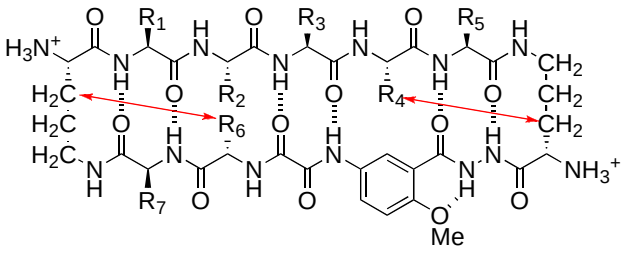

Figure 1.4. Stabilizing interactions between residues R_4 and R_6 and the two ᵈOrn turn units in macrocycle **1.1** facilitated by the natural right-handed twist of the β-sheet (represented with red arrows).

Dimerization of Macrocyclic β-Sheets through Edge-to-Edge Hydrogen Bonding.

Macrocycles **1.1a**–**1.1c**, **1.2b**, and **1.3a** do not occur as isolated monomers in the solid state, but rather dimerize through edge-to-edge hydrogen bonding. All of the macrocycles form dimers in which the two monomers interact to form an antiparallel β-sheet; macrocycle **1.1a** forms both

parallel and antiparallel β-sheet dimers in the same lattice. Figures 1.5 to 1.7 illustrate the structures of the six observed dimers with line drawings; Figures 1.8 and 1.9 show the crystal structures.

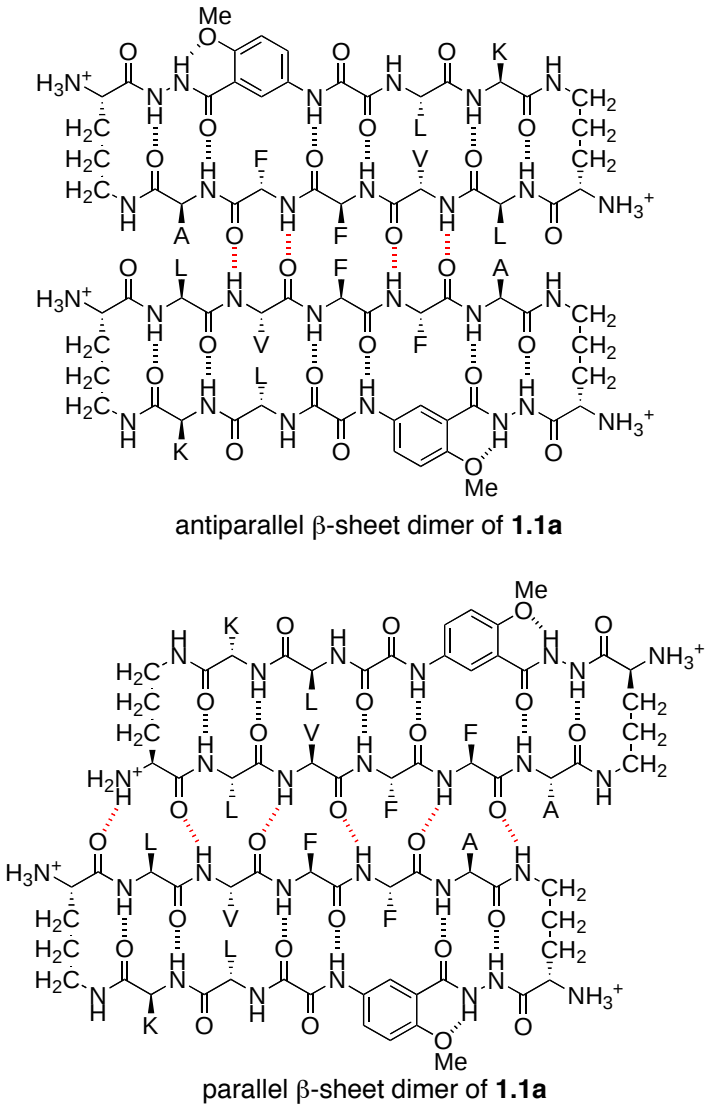

Figure 1.5. Dimers of macrocyclic β-sheets **1.1a** observed by X-ray crystallography. Intermolecular hydrogen bonds are shown with red dashed lines.

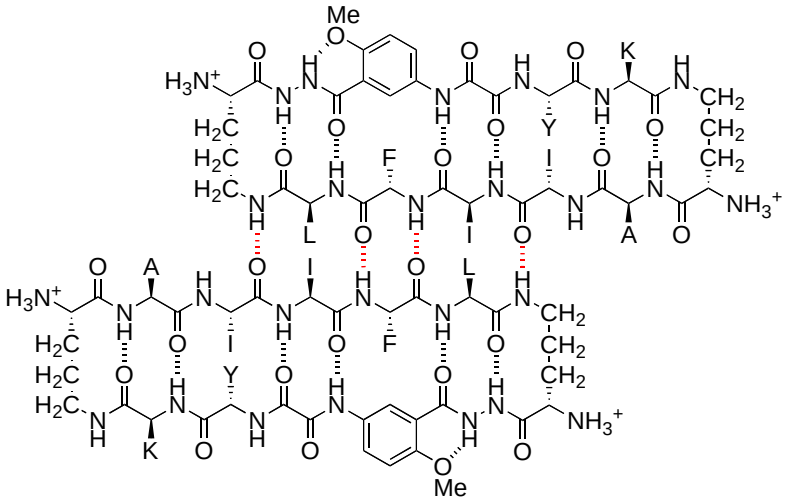

antiparallel β-sheet dimer of **1b**

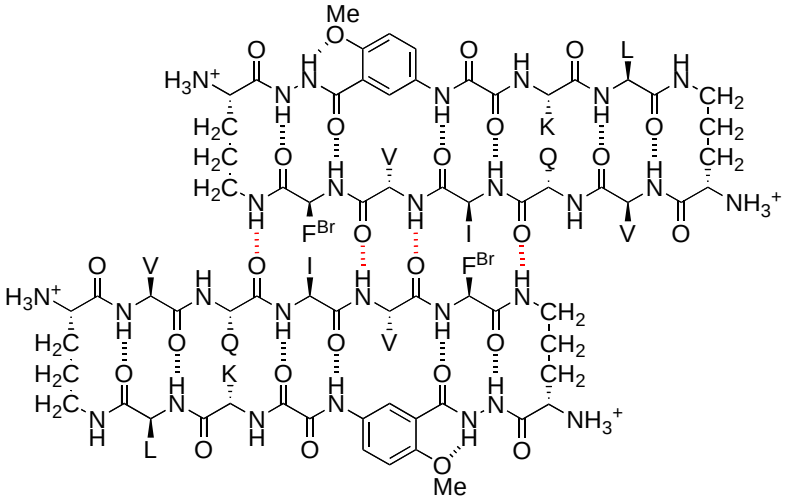

antiparallel β-sheet dimer of **1c**

Figure 1.6. Dimers of macrocyclic β-sheets **1.1b-1.1c** observed by X-ray crystallography. Intermolecular hydrogen bonds are shown with red dashed lines.

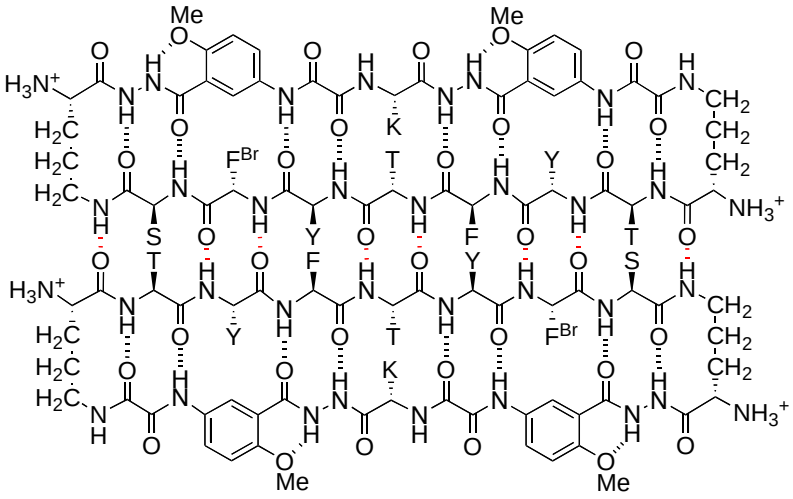

antiparallel β-sheet dimer of **2b**

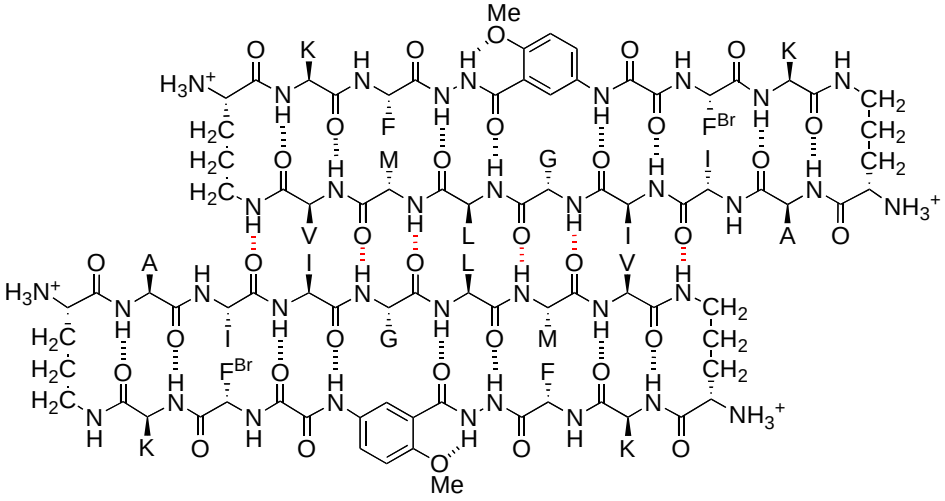

antiparallel β-sheet dimer of **3a**

Figure 1.7. Dimers of macrocyclic β-sheets **1.2b** and **1.3a** observed by X-ray crystallography. Intermolecular hydrogen bonds are shown with red dashed lines.

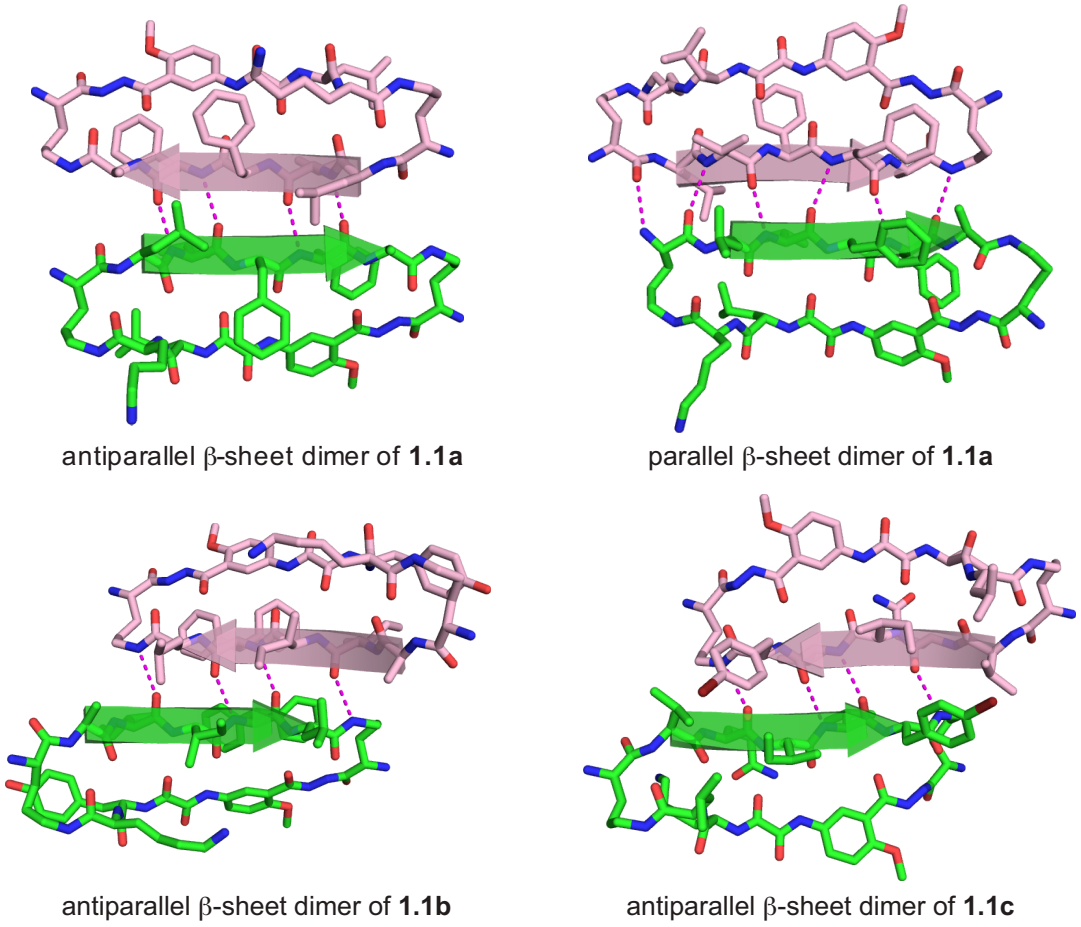

Figure 1.8. Crystal structures of dimers of macrocyclic β-sheets **1.1a–1.1c** (PDB: 3Q9H, 3Q9J, and 3Q9G). Intermolecular hydrogen bonds are shown with dashed lines.

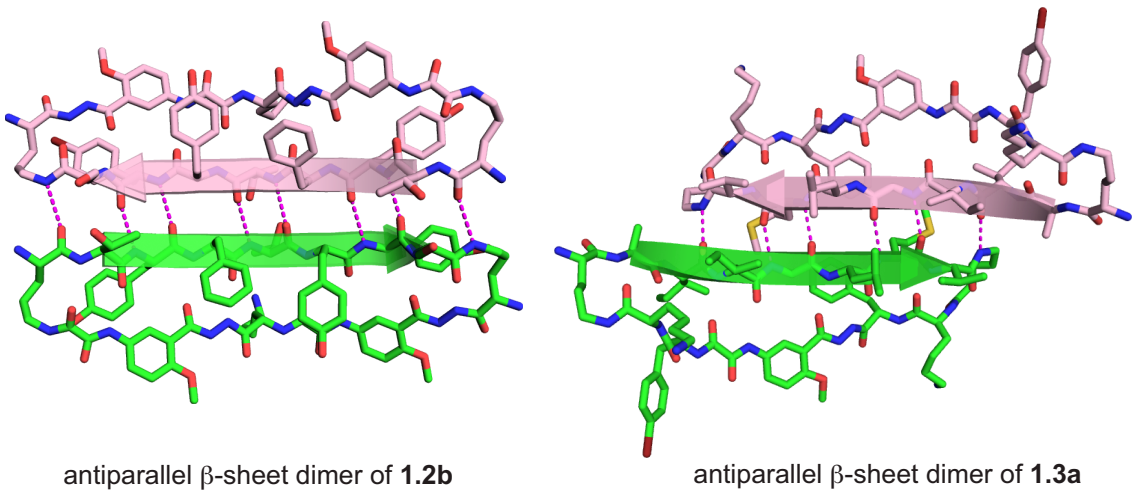

Figure 1.9. Crystal structures of dimers of macrocyclic β-sheets **1.2b** and **1.3a** (PDB: 3NI3 and 3T4G). Intermolecular hydrogen bonds are shown with dashed lines.

Of the five antiparallel β-sheet dimers observed, two (**1.1a** and **1.2b**) are in register, with all residues aligned, while three (**1.1b**, **1.1c**, and **1.3a**) are out of register, shifted by two residues. The parallel β-sheet dimer of macrocycle **1.1a** is shifted out of register by one residue, because the topology of the macrocycles prevents the formation of the type of parallel in-register β-sheets that occur in most amyloid fibrils.

All three of the out-of-register antiparallel β-sheet dimers shift by two residues in the same direction—toward the *C*-terminus. Shifting by two residues, rather than by one or three, is necessary to hydrogen bond; shifts of homodimers of antiparallel β-sheets by an even number of residues is possible; shifts of homodimers of antiparallel β-sheets by an odd number of residues is not. While shifting toward the *C*-terminus costs hydrogen bonds, it can provide better hydrophobic or van der Waals interactions. Shifting by two residues brings together the bulky isoleucine and leucine residues in the non-hydrogen-bonded rings of the **1.1b** dimer interface and the bulky isoleucine, leucine, and valine residues in the non-hydrogen-bonded rings of the **1.3a** dimer interface. The resulting hydrophobic patch helps stabilize the further assembly of each dimer into a tetramer, as described in the following section.

The twist of the antiparallel β-sheets brings together residues in *adjacent* non-hydrogen-bonded rings and helps create additional favorable hydrophobic or van der Waals interactions. The β-sheet dimerization interface of macrocycle **1.3a** illustrates these stabilizing interactions (Figure 1.10). In addition to the three sets of primary intersheet interactions between the side chains of the valine and isoleucine, leucine and leucine, and isoleucine and valine, there are four sets of secondary intersheet interactions, between the valine and alanine, leucine and isoleucine, isoleucine and leucine, and alanine and valine. These interactions, in turn, stabilize the twist of the β-sheets.

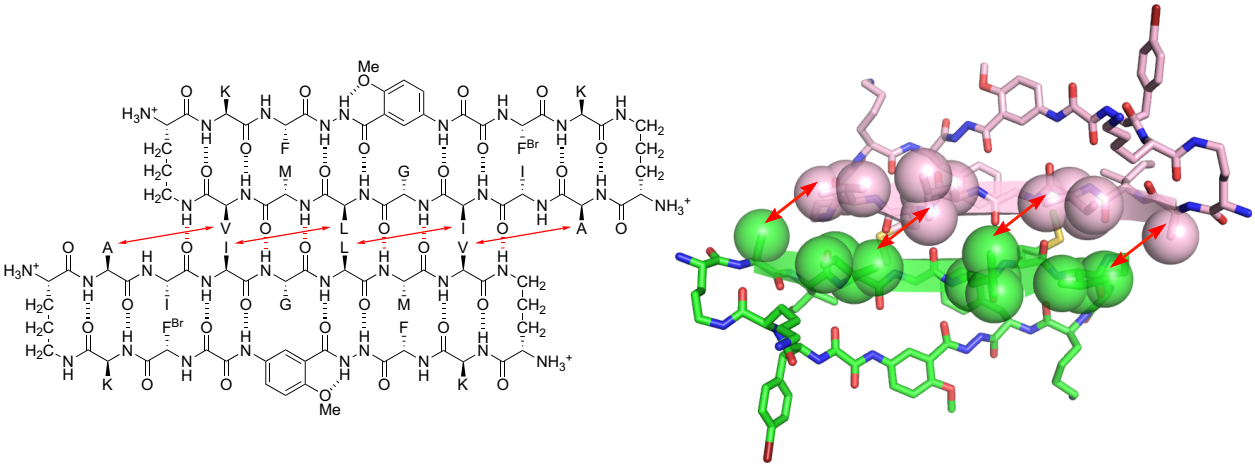

Figure 1.10. Dimer of macrocyclic β-sheet **1.3a** showing stabilizing secondary interactions facilitated by the natural right-handed twist of the β-sheet (represented with red arrows).

Face-to-Face Interactions of Macrocyclic β-Sheets. The dimers of macrocycles **1.1a**–**1.1c**, **1.2b**, and **1.3a** pack in the solid state through face-to-face interactions to form tetramers and related higher-order assemblies. Macrocycle **1.1c** packs in the lattice as tetramers comprising dimers of dimers that interact through hydrophobic face-to-face interactions (Figure 1.11). The dimer subunits of the tetramers pack in a symmetrical face-to-face fashion, rather than an unsymmetrical face-to-back fashion. These inner faces present the hydrophobic valine (R_1), isoleucine (R_3), and *p*-bromophenylalanine (R_5) residues of the pentapeptide in the upper strand, as well as the hydrophobic leucine (R_7) residue in the lower strand. These residues pack together to make up the hydrophobic core of the tetramer. The layers of the sheets are rotated at nearly right angles with respect to each other, allowing the twisted β-sheets to clasp together and create a tightly packed hydrophobic core. The tetramers are relatively isolated, having little contact with each other, except stacking interactions between the Hao templates.

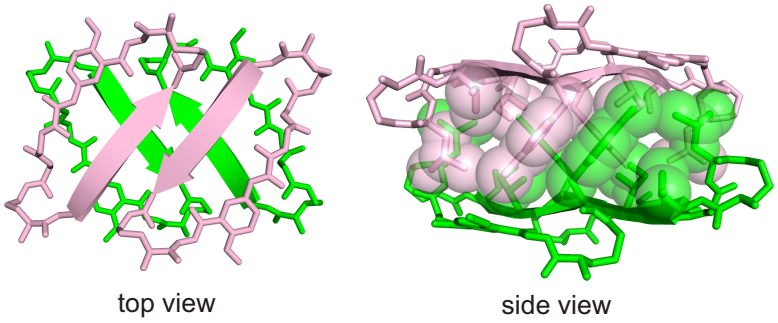

Figure 1.11. Crystal structure of the tetramer of macrocyclic β-sheet **1c** (PDB: 3Q9G). The top view shows the relative orientations of the macrocycles. The side view shows the hydrophobic core. Selected side chains are omitted for clarity.

Macrocycle **1.1b** also packs in the lattice as tetramers comprising dimers of dimers that interact through hydrophobic face-to-face interactions (Figure 1.12). The hydrophobic alanine (R_1), isoleucine (R_3), and leucine (R_5) residues of the pentapeptide in the upper strand pack together to make up the hydrophobic core of the tetramer. The tetramers stack loosely on each other through interactions among the phenylalanine groups on the outer faces of the tetramers. Zinc ions, which crystallized with **1.1b**, coordinate to the ᵈOrn turn units and both span and bridge the tetramer units.

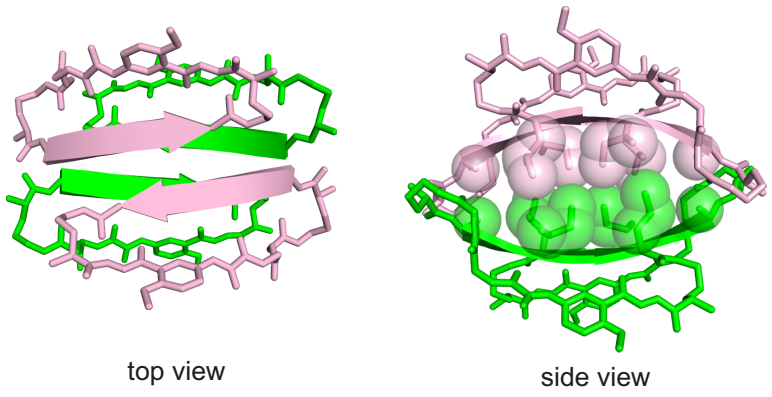

Figure 1.12. Crystal structure of the tetramer of macrocyclic β-sheet **1.1b** (PDB: 3Q9J). The top view shows the relative orientations of the macrocycles. The side view shows the hydrophobic core. Zinc ions and selected side chains are omitted for clarity.

Macrocycle **1.1a** forms stacks of four dimers in the lattice that make up a four-layered β-sandwich structure, with the parallel β-sheet dimers as the top and bottom layers of the stack and the antiparallel β-sheet dimers as the middle two layers of the stack. These stacks may be thought of as encompassing two types of tetramers: a face-to-face tetramer composed of two antiparallel β-sheet dimers (tetramer 1), and an unsymmetrical tetramer composed of an antiparallel β-sheet dimer and a parallel β-sheet dimer (tetramer 2). Figure 1.13 illustrates these tetramers. Residues R_1–R_5 of the macrocycle are all hydrophobic, making both faces of the pentapeptide hydrophobic and allowing both types of tetramers to have hydrophobic cores.

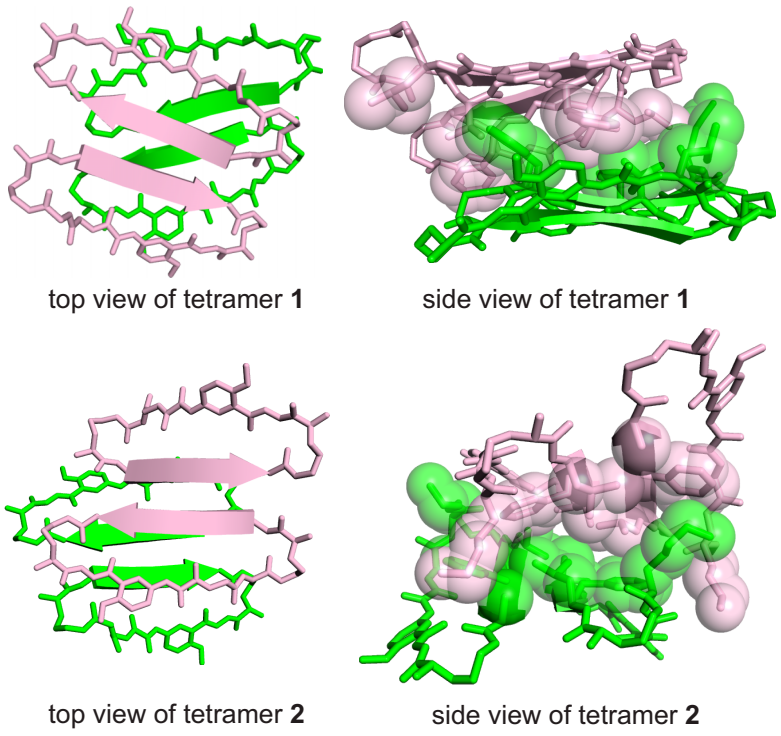

Figure 1.13. Crystal structure of the tetramers of macrocyclic β-sheet **1.1a** (PDB: 3Q9H). The top views show the relative orientations of the macrocycles. The side views show the hydrophobic cores. Selected side chains are omitted for clarity.

Macrocycle **1.3a** also forms stacks of β-sheet dimers that may be thought of as comprising two types of tetramer: a face-to-face tetramer (tetramer 1) and a back-to-back

tetramer (tetramer 2). Figure 1.14 illustrates these tetramers. The isoleucine (R_3), leucine (R_5), and valine (R_7) residues of the heptapeptide in the upper strand create the hydrophobic core of the face-to-face tetramer. The methionine (R_6) residue of the heptapeptide in the upper strand and the phenylalanine (R_9) in the lower strand create the hydrophobic core of the back-to-back tetramer. The layers of the sheets of the back-to-back tetramer (tetramer 2) are rotated at nearly right angles with respect to each other and clasp together, like those of the tetramer of macrocycle **1.1c**. The layers of the face-to-face tetramer (tetramer 1), on the other hand, are aligned and twist in a laminated fashion.

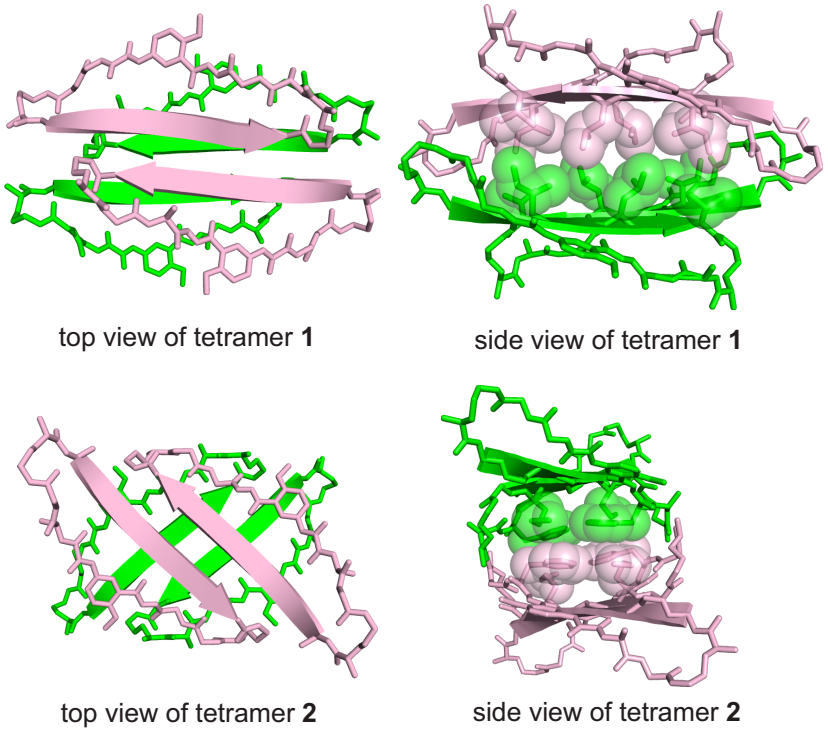

Figure 1.14. Crystal structures of the tetramers of macrocyclic β-sheet **1.3a** (PDB: 3T4G). The top views show the relative orientations of the macrocycles. The side views show the hydrophobic cores. Selected side chains are omitted for clarity.

Macrocycle **1.2b** crystallizes as hexamers comprising trimers of dimers, rather than tetramers comprising dimers of dimers. The hexamer may be thought of as a β-sandwich in

which one of the layers has been tilted upward by 60° and another dimer has been added to create a triangular assembly. In solution, homologue **1.2a** forms tetramers comprising dimers of dimers, in which the phenylalanine (R_3) and tyrosine (R_5) residues of the heptapeptide in the upper strand pack together to create a hydrophobic core. This tetramer resembles the tetramers formed by macrocycles **1.1a–1.1c** and **1.3a**.

The tetramers formed by these macrocyclic β-sheets may shed light on the structures of the oligomers that are central to the toxicity of amyloids in Alzheimer's and other neurodegenerative diseases. In the tetramers, hydrophobic or van der Waals interactions act in conjunction with hydrogen bonding to create recognizable assemblies with common structural themes: folded monomers with β-sheet structures that assemble to hydrogen-bonded dimers that pack face-to-face or back-to-back to form layered structures. All of these features reflect the self-complementarity of these peptides and hence their ability to form oligomers. When the layers of the sheets are substantially rotated with respect to each other, the twist of the β-sheets creates a special additional complementarity in which two corners of the upper sheet clasp two corners of the lower sheet. This clasping together of the rotated twisted β-sheets may help create oligomers with well-packed cores, enhanced stability, and unique biological properties.

Macrocyclic β-Sheets that Inhibit Amyloid Aggregation. Macrocyclic β-sheets containing amyloid-derived peptide sequences can control the aggregation of amyloidogenic peptides and proteins through the same types of supramolecular interactions that occur among β-sheets. The macrocycles are designed to bind to β-sheet intermediates involved in the aggregation process and block further aggregation. Macrocyclic β-sheet **1.1d** inhibits the aggregation of an amyloidogenic hexapeptide from the protein tau, which aggregates to form neurofibrillary

tangles in Alzheimer's disease and certain frontotemporal dementias.[10] Both edge-to-edge hydrogen bonding and face-to-face hydrophobic interactions are essential to the binding process, and the macrocycle appears to interact with the offset layered β-sheets of the amyloidogenic hexapeptide through hydrogen-bonding interactions with an exposed hydrogen-bonding edge and hydrophobic interactions with a hydrophobic ledge. The inhibition appears to involve two molecules binding cooperatively to the two layers of the aggregating β-sheets.

Macrocyclic β-sheet **1.3b** inhibits Aβ aggregation and reduces the toxicity of amyloid aggregates.[11] Macrocyclic β-sheet **1.3c** inhibits the aggregation of human β_2-microglobulin (hβ_2M), which is associated with dialysis-related amyloidosis.[11] Macrocyclic β-sheet **1.3d** inhibits the aggregation of human α-synuclein (hαSyn), which is associated with Parkinson's disease.[10] Heterodivalent compounds comprising macrocyclic β-sheets **1.1a** and **1.1e** connected by a polyethyene-glycol-based linker inhibit Aβ aggregation more strongly than the monovalent components **1.1a** and **1.1e** or homodivalent molecules containing two copies of **1.1a** or **1.1e** connected by a polyethylene-glycol-based linker.[12]

Conclusion and Outlook

Our chemical model systems have given us deeper insights into the rich supramolecular chemistry of β-sheets and have helped us better understand the types of supramolecular interactions in protein quaternary structure and in amyloids. A unifying theme that has emerged in both the model systems and natural proteins and amyloids is the confluence of edge-to-edge hydrogen-bonding interactions and face-to-face hydrophobic interactions among β-sheets that result in layered sandwich-like structures. The characteristic right-handed twist of β-sheets can help stabilize edge-to-edge interactions among β-sheets through favorable secondary interactions

between hydrophobic side chains in adjacent non-hydrogen-bonded rings. Complementarity among the faces of the β-sheets is particularly important, through features such as aligned and offset hydrophobic contacts, interdigitation, and knob-hole interactions. The orientation of layered β-sheets helps maximize the complementarity of the layered structures. Twisted β-sheets can clasp together in rotated layered structures to create compact oligomers with well-packed cores. Offset layered β-sheets with hydrogen-bonding edges over hydrophobic ledges have special potential for further interactions and may be especially important in β-sheet aggregation. By understanding and applying these principles, it may be possible to gain unique insights with which to further control β-sheet interactions in Alzheimer's and other diseases and to ultimately develop therapies.

References

1 Cheng, P.-N.; Pham, J. D.; Nowick, J. S.; *J. Am. Chem. Soc.* **2013**, *135*, 5477–5492.

2 Nowick, J. S.; Lam, K. S.; Khasanova, T. V.; Kemnitzer, W. E.; Maitra, S.; Mee, H. T.; Liu, R. *J. Am. Chem. Soc.* **2002**, *124*, 4972–4973.

3 Nowick, J. S.; Brower, J. O. *J. Am. Chem. Soc.* **2003**, *125*, 876–877.

4 Nowick, J. S.; Chung, D. M.; Maitra, K.; Maitra, S.; Stigers, K. D.; Sun, Y. *J. Am. Chem. Soc.* **2000**, *122*, 7654–7661.

5 Khakshoor, O.; Demeler, B.; Nowick, J. S. *J. Am. Chem. Soc.* **2007**, *129*, 5558–5569.

6 Woods, R. J.; Brower, J. O.; Castellanos, E.; Hashemzadeh, M.; Khakshoor, O.; Russu, W.A.; Nowick, J. S. *J. Am. Chem. Soc.* **2007**, *129*, 2548–2558.

7 Khakshoor, O.; Nowick, J. S. *Org. Lett.* **2009**, *11*, 3000–3003.

8 Khakshoor, O.; Lin, A. J.; Korman, T. P.; Sawaya, M. R.; Tsai, S.-C.; Eisenberg, D.; Nowick, J. S. *J. Am. Chem. Soc.* **2010**, *132*, 11622–11628.

9 Liu, C.; Sawaya, M. R.; Cheng, P.-N.; Zheng, J.; Nowick, J. S.; Eisenberg, D. *J. Am. Chem. Soc.* **2011**, *133*, 6736–6744.

10 Zheng, J.; Liu, C.; Sawaya, M. R.; Vadla, B.; Khan, S.; Woods, R. J.; Eisenberg, D.; Goux, W. J.; Nowick, J. S. *J. Am. Chem. Soc.* **2011**, *133*, 3144–3157.

11 Cheng, P.-N.; Liu, L.; Zhao, M.; Eisenberg, D. Nowick, J. S. *Nat. Chem.* **2012**, *4*, 927–933.

12 Cheng, P.-N.; Spencer, R.; Woods, R. J.; Glabe, C. G.; Nowick, J. S. *J. Am. Chem. Soc.* **2012**, *133*, 14179–14184.

13 Nauli, S.; Kuhlman, B.; Baker, D. *Nat. Struct. Biol.* **2001**, *8*, 602−605.

14 Nauli, S.; Kuhlman, B.; Le Trong, I.; Stenkamp, R. E.; Teller, D.; Baker, D. *Protein Sci.* **2002**, *11*, 2924−2931.

CHAPTER 2

Structures of Oligomers of a Peptide from β-Amyloid

Preamble

Chapter 2 describes the X-ray crystallographic structures of oligomers and oligomer assemblies formed by a new chemical model system that I developed containing the $A\beta_{15-23}$ nonapeptide sequence. A discussion that I had with Dr. Pin-Nan Cheng about the pentapeptide and heptapeptide strands in the macrocycles described in Chapter 1 inspired me to develop a new macrocycle that would display a larger number of amino acids on the upper strand to increase the edge-to-edge hydrogen-bonding interaction. The increased size of the strand could facilitate the study of fibril-forming amyloid peptides that contain long β-strands, comprising nine or more amino acids. Thus, I invented a 66-membered macrocyclic β-sheet peptide that incorporates nine amino acids from the central hydrophobic region (QKLVFFAED) from the Aβ peptide.

In studying the new macrocycle, I utilized X-ray crystallography as a tool to study the structure and the oligomer assemblies the macrocycle forms in the solid state. For this project, I envisioned gaining the knowledge and skills necessary to solve the structure independently. To learn the new skill, I looked to Prof. Celia Goulding and her research group for expertise in growing well diffracting crystals and to learn a suite of software programs for solving the X-ray crystallographic structure of the new macrocyclic β-sheet peptide.

In addition to X-ray crystallography, I utilized the modeling software program Maestro to investigate if the oligomer assemblies formed by the new macrocycle can also be formed by the linear nonapeptide sequence (QKLVFFAED). In the study, I was able to learn how to construct different structures in the software program and to generate energy-minimized structures. This

chapter reports the crystallographic and molecular modeling studies which provides insights into the role of oligomers in amyloid diseases.

This chapter is adapted from that paper that I published in the *Journal of the American Chemical Society*.[1]

Reproduced in part with permission from Pham, J. D.; Chim, N.; Goulding, C. W.; Nowick, J. S. *J. Am. Chem. Soc.* **2013**, *135*, 12460–12467. Copyright 2013 American Chemical Society.

Introduction

The structures of the toxic amyloid oligomers associated with neurodegenerative diseases remain largely elusive. The plaques formed by amyloid-β peptide (Aβ) are a visible hallmark of Alzheimer's disease, and their component fibrils have been found to consist of long networks of layered β-sheets comprising thousands of molecules of the 40- and 42-amino acid polypeptide.[2,3,4] Smaller oligomers, consisting of as few as two molecules or as many as tens of molecules, are now widely thought to be the Aβ species that cause neurodegeneration.[5,6,7,8,9,10,11,12,13] The mechanism or mechanisms by which these oligomers cause neurodegeneration are still not certain, with possibilities including binding to cell-surface receptors, generation of pores of channels in cell membranes, or otherwise perturbing membrane structure.[12]

The structures of the oligomers formed by Aβ and other amyloidogenic peptides and proteins are difficult to study because amyloid oligomers are heterogeneous and unstable. Small oligomers of Aβ, including dimers, trimers, tetramers, hexamers, and dodecamers, have been observed, as well as larger oligomer assemblies with spherical and annular morphologies.[14,15,16,17,18,19,20] Most efforts to study the oligomers have relied upon techniques that provide relatively little structural information, such as gel electrophoresis, size-exclusion chromatography, ion mobility-mass spectrometry, transmission electron microscopy, atomic force microscopy, and use of oligomer-specific antibodies. Determining the structure of the oligomers of full-length Aβ at atomic resolution simply is not possible. Chemical model systems that are simpler than full-length Aβ can interact in controlled fashions to form well-defined oligomers and oligomer assemblies. These model systems can afford structures at atomic resolution that provide insights into the structures and modes of assembly of amyloid oligomers.

Thus far, there are no chemical model systems that provide deep insights into the structures of Aβ oligomers at atomic resolution. Model systems containing sequences derived from amyloidogenic peptides and proteins have provided glimpses of hydrogen bonding and hydrophobic interactions and geometrical aspects in amyloid oligomer formation.[21,22,23,24,25,26,27,28] Pioneering work by Eisenberg and coworkers revealed the structure of a small toxic oligomer of amyloidogenic peptides derived from the protein αB crystallin to be a barrel-shaped hexamer consisting of six β-strands hydrogen bonded to form a cylindrical β-sheet.[27]

In the current study I set out to observe oligomers and oligomer assemblies formed by the important central region of Aβ by incorporating residues 15–23 into a macrocycle containing a molecular template that controls intermolecular association and blocks the formation of fibrils. To reduce this idea to practice, I combined the nonapeptide QKLVFFAED ($A\beta_{15-23}$) with the unnatural amino acid *Hao*,[29] two δ-linked ornithine turn units,[30] and three additional amino acids in a 66-membered ring to create macrocyclic peptide **2.1**. I incorporated a *p*-bromophenylalanine (F^{Br}) residue to facilitate phase determination of the X-ray crystallographic structure through single anomalous dispersion (SAD) phasing. I initially prepared two different macrocycles; one macrocycle with F^{Br} substituting for F_{19} and tyrosine substituting for F_{Br} on the template strand, and the second macrocycle with F^{Br} substituting for F_{20} on the recognition strand and tyrosine substituting for F^{Br} on the template strand. Only small crystals and amorphous aggregates were observed in attempts to crystallize the respective macrocycles, which led to collection of poor diffraction data. Ultimately macrocycle **2.1** where afforded crystals suitable for X-ray crystallography.

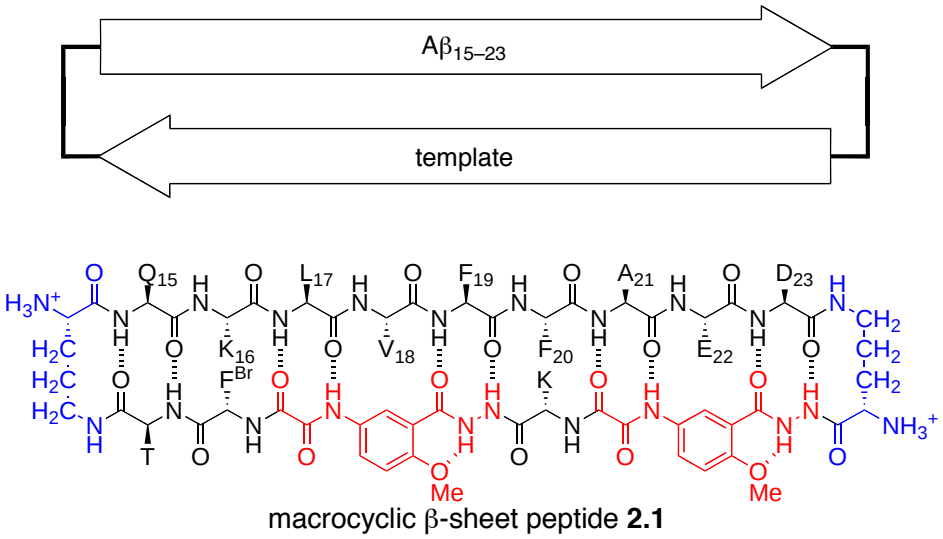

macrocyclic β-sheet peptide **2.1**

Results

1. Synthesis of Macrocyclic β-Sheet Peptide 2.1. Macrocyclic peptide **2.1** was synthesized by Fmoc-based solid-phase synthesis of the turn, template, and $A\beta_{15–23}$ units on chlorotrityl resin, followed by cleavage of the protected peptide from the resin, solution-phase cyclization, deprotection, and purification by RP-HPLC (Scheme 1). Macrocyclic peptide **2.1** was synthesized as illustrated in Figure Scheme 1 in a fashion similar to procedures previously reported for the synthesis of other macrocyclic β-sheet peptides.[31,32] Boc-Orn(Fmoc)-OH was used to introduce the δ-linked ornithine turn units. Fmoc-Hao-OH[30] was used to introduce the unnatural amino acid Hao.[33] Standard Fmoc-protected amino acids were used to introduce the other residues. Details of the synthesis along with HPLC and mass spectrometry data are described in the experimental section of the chapter.

Scheme 2.1. Synthesis of Macrocyclic β-sheet peptide **2.1**

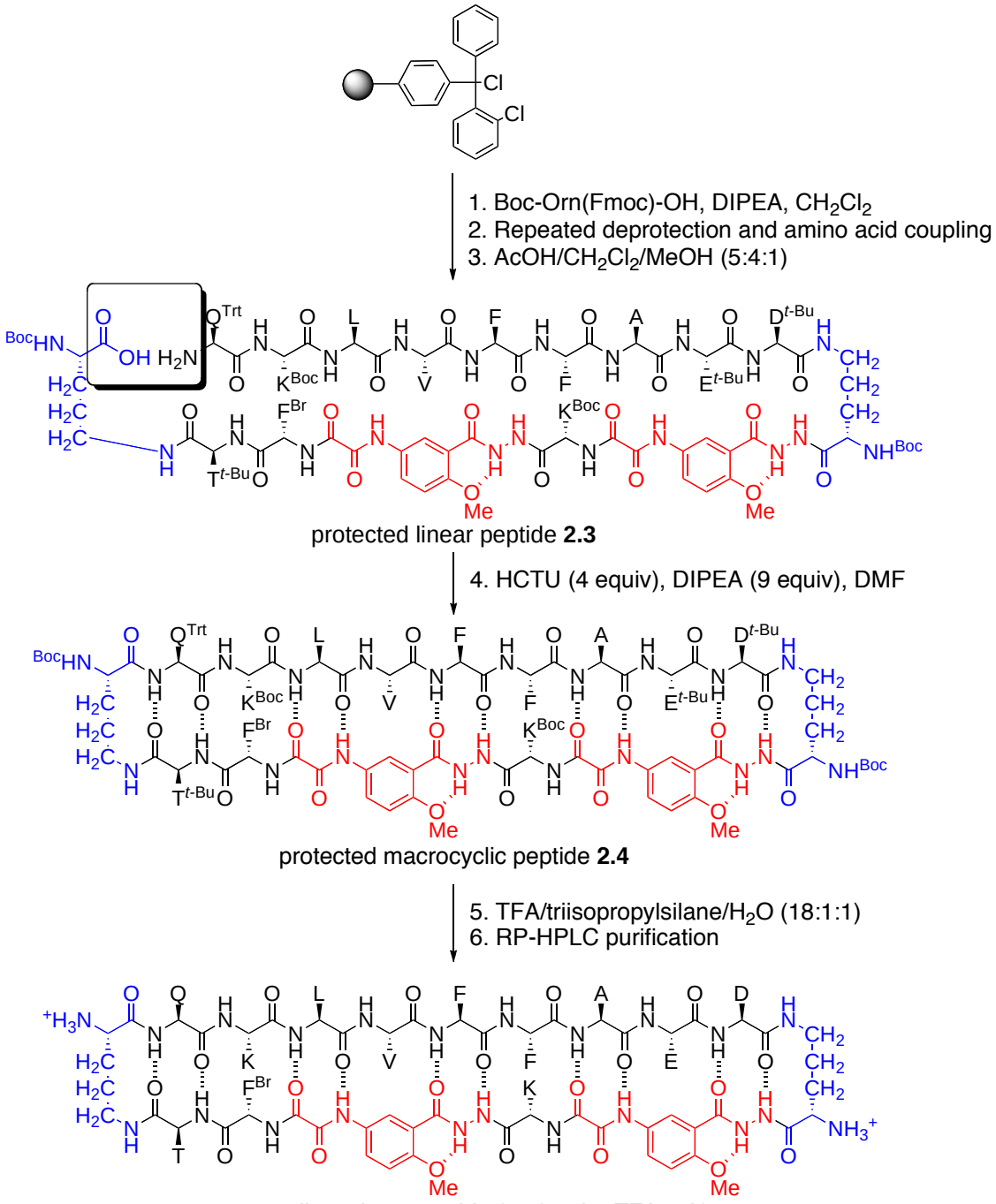

macrocyclic β-sheet peptide **2.1** (as the TFA salt)
28 mg (12% yield based on initial loading)

molecular weight calculated for $C_{101}H_{140}BrN_{25}O_{28} \bullet 4CF_3CO_2H$ (TFA salt of **2.1**): 2688.34
exact mass calculated for $C_{101}H_{140}BrN_{25}O_{28}$ (free base of **2.1**): 2229.95

2. Crystallization of Macrocyclic β-Sheet 2.1. A solution of 7 mg/mL macrocyclic β-sheet peptide **2.1** in water was used for crystallization trials. Three sparse-matrix screens from Hampton Research (Crystal Screen, PEG/Ion, and Index) and two from Qiagen (PACT Suite and JCSG Suite) were used to find initial crystallization conditions. Each screen consisted of a 96-well plate with 100 μL solutions of different salts, reagents, and pH values. The screens were prepared using the TTP LabTech Mosquito nanodispenser instrument with a 1:1 ratio (600 nL total) of dissolved peptide and well solution. The initial condition 0.1 M sodium citrate tribasic dihydrate pH 5.6 and 35% *tert*-butanol produced small, 0.1 mm rectangular crystals. Adding 1% poly(ethylene glycol) (PEG) 3350 from the Hampton Research Additive Screen was found to improve the quality of the crystals. After additional optimization of conditions, a well-diffracting crystal was grown using the hanging-drop vapor-diffusion method at room temperature with 0.5 M sodium citrate tribasic dihydrate, pH 7.2, 35% *tert*-butanol, 1% PEG 3350. The rectangular crystals were collected without soaking in cryoprotectant and flash frozen in liquid nitrogen prior to data collection.

3. X-ray Diffraction Data Collection, Processing, and Structure and Refinement. A SAD dataset was collected at 100 K at the Advanced Light Source (Berkeley, CA) with Beamline 8.2.1 using the bromine absorption edge wavelength (0.92 Å). The dataset was indexed, integrated and scaled using the HKL2000 Suite.[34] Macrocycle β-sheet peptide **2.1** was found to crystallize in space group P622 with unit cell dimensions 45.1 x 45.1 x 29.2 Å and one molecule of macrocyclic β-sheet **2.1** in the asymmetric unit. Conversion of scalepack to mtz file format was performed with CCP4i suite.[35] A single bromine site was located using Phaser and an initial

model was built using Autosol in PHENIX.[36] Additional model building and refinement was carried out with COOT[37] and Refmac5.[38]

Solvent and ions were incorporated in the refinement to account for electron density beyond macrocycle β-sheet peptide **2.1**. One molecule of *tert*-butanol and two molecules of water were identified per asymmetric unit. One sodium ion at 50% occupancy was also identified. Incorporating a sodium ion into a region of positive electron density observed in the F_o-F_c difference map lowered R values by 1.5% (Figure 2.1). Although water could also be a reasonable choice instead of Na^+, a sodium ion was chosen because water and the carbonyl group of 4-bromophenylalanine are located appropriately as ligands after symmetry operations, creating a tetracoordinate environment of roughly square-planar geometry. A final TLS model was used for refinement with Refmac5.

The structure was solved and refined in space group P622 at 1.77 Å resolution to give a model with R_{work} = 22.4% and R_{free} = 27.1% (Figure 2.1 & Table 2.1). Each asymmetric unit was found to contain a single molecule of macrocyclic peptide **2.1**. One molecule of *tert*-butanol (*t*-BuOH), two molecules of water, and one sodium ion at 50% occupancy on a twofold axis were included in each asymmetric unit. The crystal structure was deposited to the Protein Data Bank (PDB) with PDB code 4IVH.

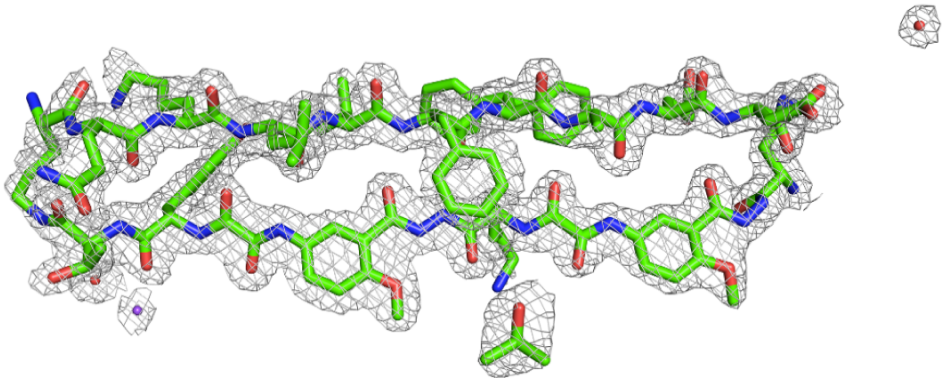

Figure 2.1. X-ray crystallographic structure and electron density map of the asymmetric unit of macrocyclic β-sheet peptide **2.1**. A $2F_o$-F_c difference map contoured at 1σ is shown in grey mesh. Macrocyclic β-sheet peptide **2.1** and *tert*-butanol are shown as sticks. Two molecules of water are shown as red spheres. One sodium ion at 50% occupancy on a twofold axis is shown as a purple sphere.

PyMOL was used to generate images from the crystallographic data.[39] A β-strand of nine glycine residues (G_9) was used to generate a cartoon of the molecular template Hao-K-Hao-F^{Br}-T. Specifically, the pdb coordinates from each unnatural amino acid Hao were used to generate tri-glycine segments, and the pdb coordinates of the threonine, *p*-bromophenylalanine, and lysine residues were also used to generate three glycine residues of the G_9 β-strand.

Table 2.1. X-ray Crystallographic Data Collection and Refinement Statistics for Macrocyclic β-Sheet Peptide **2.1**.

Crystal parameters	
Space group	P622
a, b, c (Å)	45.1, 45.1, 29.2
α, β, γ (°)	90, 90, 120
Molecules per asymmetric unit	1
Data collection	
Synchrotron beam line	ALS Beam line 8.2.1
Wavelength (Å)	0.92
Resolution (Å)	50–1.77 (1.83–1.77)
Total reflections	38242
Unique reflections	1909
Completeness (%)[a]	98.8 (96.7)
Multiplicity[a]	20.0 (17.8)
R_{merge} (%)[a,b]	12.3 (45.6)
I/σ(I)[a]	16.8 (8.87)
Refinement	
Resolution (Å)	1.77
R_{work} (%)[c]	22.4
R_{free} (%)[d]	27.1
RMS bond lengths (Å)	0.029
RMS bond angles (°)	2.81
Ligand	*tert*-butanol (1), sodium (1)
Water	2
Ramachandran favored (%)	100
Ramachandran outliers (%)	0
Wilson B-factor (Å^2)	32.8
Average B-factor (Å^2)	42.1

[a]Statistics for the highest resolution shell are shown in parentheses

[b]$R_{merge} = \sum|I - \langle I \rangle|/\sum I$

[c]$R_{work} = \sum|F_{obs} - F_{calc}|/\sum F_{obs}$

[d]R_{free} was computed identically as R_{work} except where all reflections belong to a test set of 8% randomly selected data.

4. X-ray Crystallographic Studies of Macrocyclic β-Sheet Peptide 2.1. The X-ray crystallographic structure of macrocyclic peptide **2.1** shows a folded monomer that forms hydrogen-bonded dimers, which further assemble to form the crystal lattice. The $A\beta_{15–23}$ nonapeptide adopts a β-strand conformation and forms ten intramolecular hydrogen bonds with the template to make a cyclic β-sheet (Figure 2.2A). The side chains of the nonapeptide project above and below the plane of the β-sheet, with the side chains of Q_{15}, L_{17}, F_{19}, A_{21}, and D_{23} projecting on the upper face and the side chains of K_{16}, V_{18}, F_{20}, and E_{22} projecting on the lower face. The side chain of F_{20} exhibits partial occupancy of two rotamers with χ_1= 176° and 310° (Figure 2.2D).

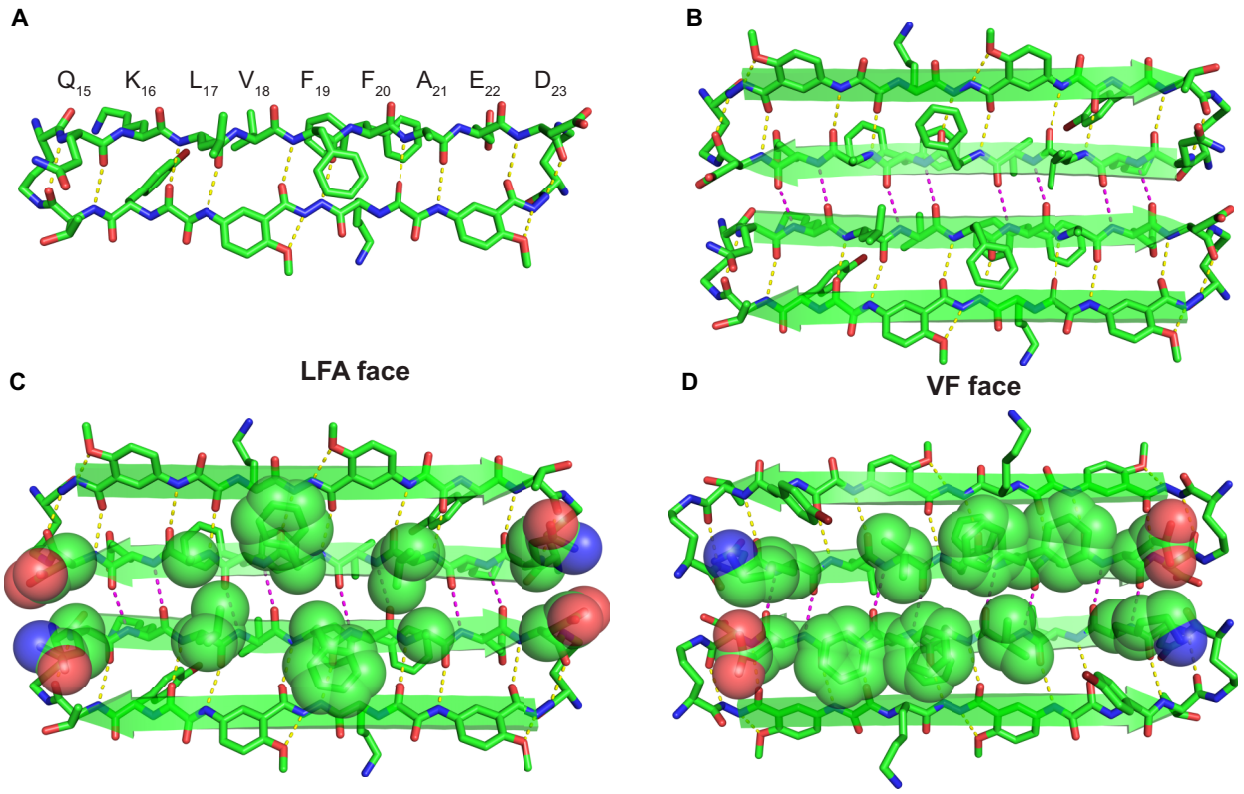

Figure 2.2. X-ray crystallographic structure of macrocyclic β-sheet peptide **2.1**. (A) Monomeric subunit. (B) Hydrogen-bonded dimer. (C) Hydrogen-bonded dimer illustrating relationship of Q_{15}, L_{17}, F_{19}, A_{21}, and D_{23} (LFA face view). (D) Hydrogen-bonded dimer illustrating relationship of K_{16}, V_{18}, F_{20}, and E_{22} (VF face view). The side chain of F_{20} exhibits partial occupancy of two rotamers; both rotamers are shown.

Macrocyclic β-sheet peptide **2.1** forms a hydrogen-bonded dimer in which the two $A\beta_{15–23}$ nonapeptide strands align and form eight hydrogen bonds to make a four-stranded antiparallel β-sheet (Figure 2.2B).[40,41,42,43,44] The hydrophobic side chains of L_{17}, F_{19}, and A_{21} make a hydrophobic patch that is flanked by the polar side chains of Q_{15} and D_{23} on the upper face of the β-sheet (Figure 2.2C); the hydrophobic side chains of V_{18} and F_{20} make a hydrophobic patch that is flanked by the polar side chains of K_{16} and E_{22} on the lower face of the β-sheet (Figure 2.2D). Based on the residues projected on each face, I use the term the *LFA face* and the *VF face* to

represent the upper and lower faces in order to distinguish between the two faces and for subsequent discussion of the assembly of the dimers,

The hydrogen-bonded dimers pack in a hexagonal fashion to form the crystal lattice (Figure 2.3A). The lattice has triangular and hexagonal cavities, which are readily apparent in a space-filling model (Figure 2.3B). The LFA faces line the triangular cavities, while the VF faces pack to create a hydrophobic network that separates the triangular cavities. The polar residues (Q_{15}, K_{16}, E_{22}, and D_{23}) and δ-linked ornithine turn units meet at the hexagonal cavities. The triangular cavities are about 1 nm across, while the hexagonal cavities are about 1.5 nm in diameter. The *t*-BuOH resides in the hydrophobic triangular cavities, while the sodium ion and water reside in the hydrophilic hexagonal cavities (Figure 2.3C).

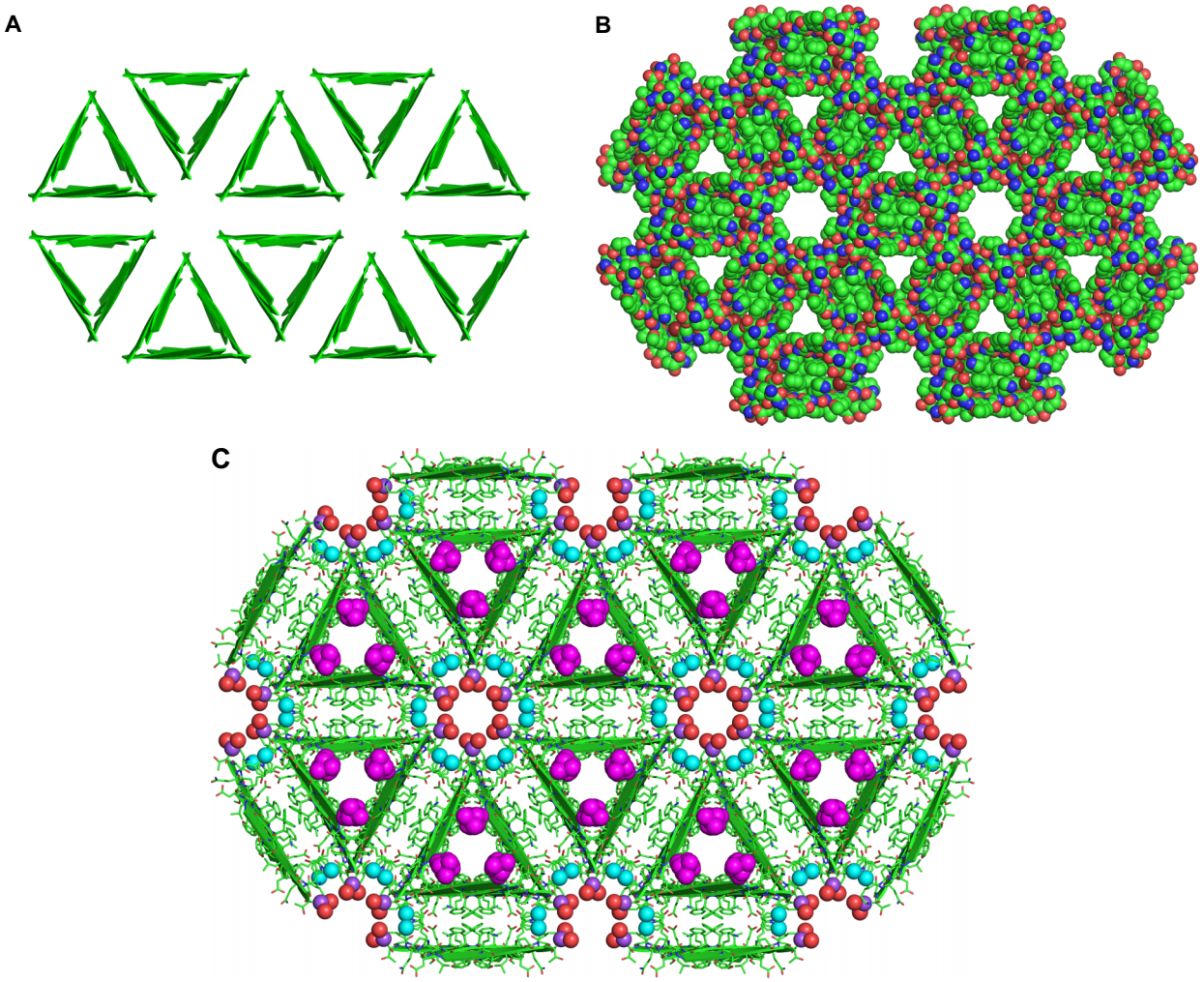

Figure 2.3. Crystal packing of macrocyclic β-sheet peptide **2.1**. (A) The crystal lattice (cartoon, top view). (B) The crystal lattice (space filling model, top view). (C) The crystal lattice showing solvent and ions (top view): *t*-BuOH (magenta, in the triangular cavities), Na^+ (purple, in the hexagonal cavities), H_2O ligands for Na^+ (red, in the hexagonal cavities), additional H_2O (cyan, in the hexagonal cavities).

The lattice may be thought of as comprising two types of oligomers: *cruciform tetramers* and *triangular dodecamers*. The hydrogen-bonded dimers pack through the VF faces to create tetramers (Figure 2.4). In the tetramers the β-sheets of the dimers are nearly orthogonal, oriented at an 83° angle. These cruciform tetramers are about 3 nm wide and 2 nm thick. The V_{18} and F_{20} side chains pack through hydrophobic and aromatic interactions, and aromatic stacking

interactions occur between the side chains of the bromophenyalanine residues. These interactions help stabilize the tetramer.

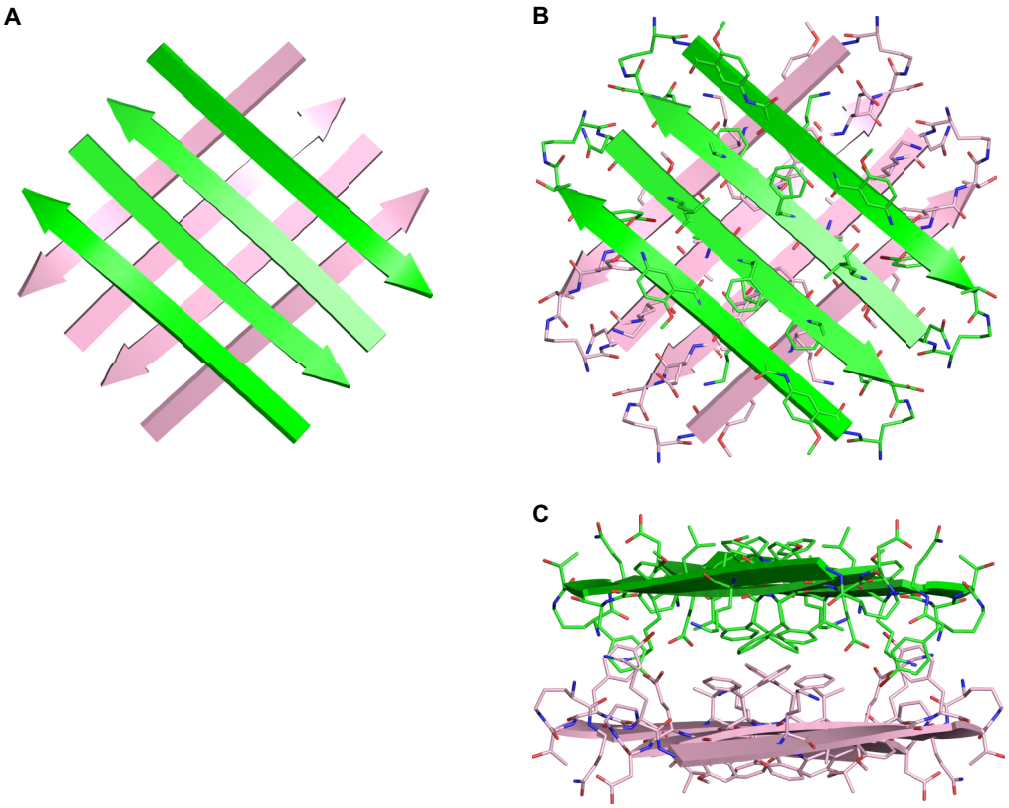

Figure 2.4. Cruciform tetramer of macrocyclic β-sheet peptide **2.1.** (A) Cruciform tetramer within the crystal lattice (top view). (B) Cruciform tetramer within the crystal lattice (top view) with detail of the crystal structure . (C) Cruciform tetramer within the crystal lattice (side view) with detail of the crystal structure.

Three cruciform tetramers pack in a triangular arrangement to form a triangular dodecamer (Figure 2.5). The dodecamer is about 4–5 nm across and 3 nm thick. The L_{17}, F_{19}, and A_{21} side chains line the interior of the triangular dodecamer creating a hydrophobic cavity. The three interior walls of the dodecamer (shown in green in Figure 2.5) and three exterior walls of the dodecamer (shown in pink in Figure 2.4) each consist of the hydrogen-bonded dimers of

macrocyclic β-sheet peptide **2.1**. The F^{Br} residues abut at the juncture between the interior walls, forming a weak pair of hydrogen bonds (Figure 2.6).

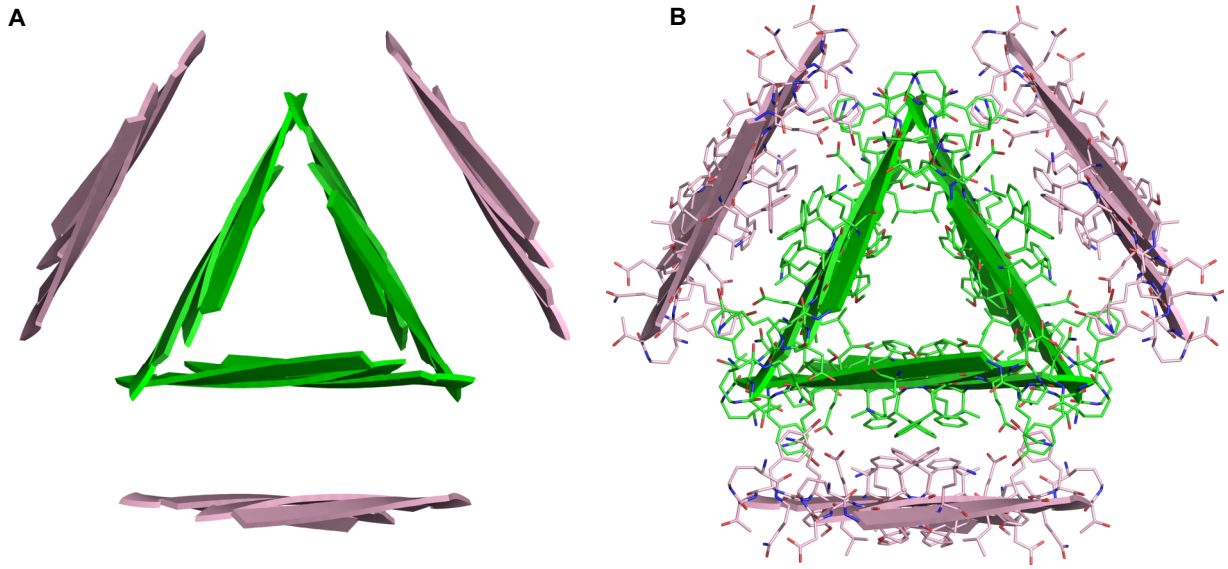

Figure 2.5. Triangular dodecamers of macrocyclic β-sheet peptide **2.1.** (A) Triangular dodecamer within the crystal lattice comprising three tetrameric subunits (top view). (B) Three tetrameric subunits of the infinite linear assembly are shown (side view) with detail of the crystal structure.

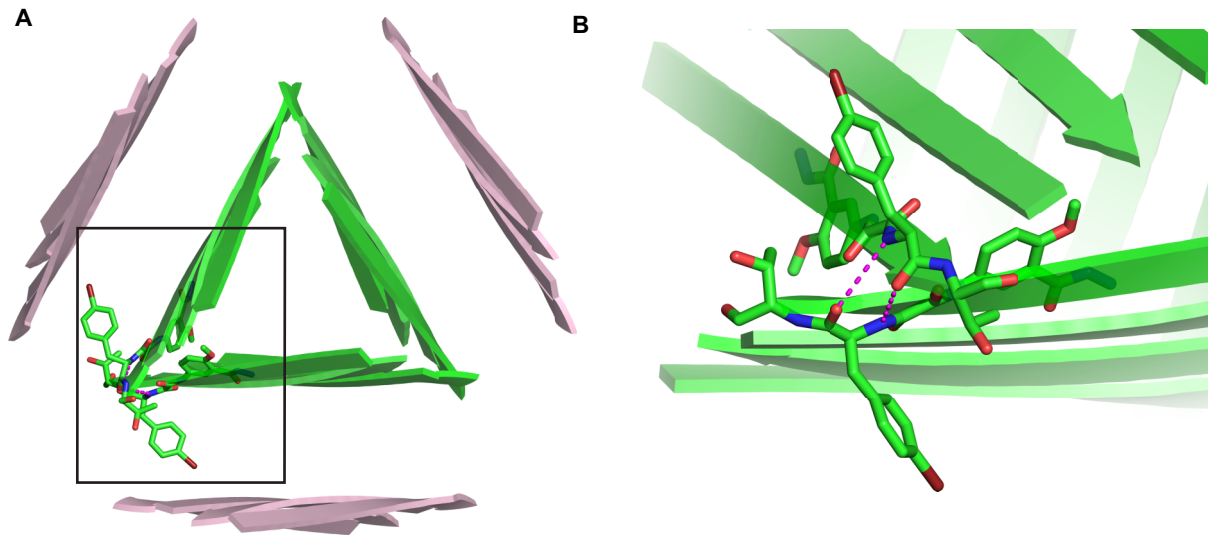

Figure 2.6. Contacts between the cruciform tetramer units of the triangular dodecamer in the X-ray crystallographic structure of macrocyclic β-sheet peptide **2.1**. (A) Triangular dodecamer formed by three tetramer subunits. (B) Detail of the contact between two cruciform tetramer units of the triangular dodecamer showing hydrogen bonding between the F^{Br} residues.

The cruciform tetramers fit together to form infinite linear assemblies that run through the lattice (Figure 2.7A). The β-sheet interfaces between the tetramer units are shifted out of alignment by six residues toward the *N*-termini. The Hao units of the template strands abut at the interface between tetramer units, creating an overlap equivalent in length to three residues, but without any hydrogen bonds (Figure 2.7B). The triangular cavities are formed from the convergence of three such infinite linear assemblies and may be thought of as infinite stacks of triangular dodecamers that run through the lattice.

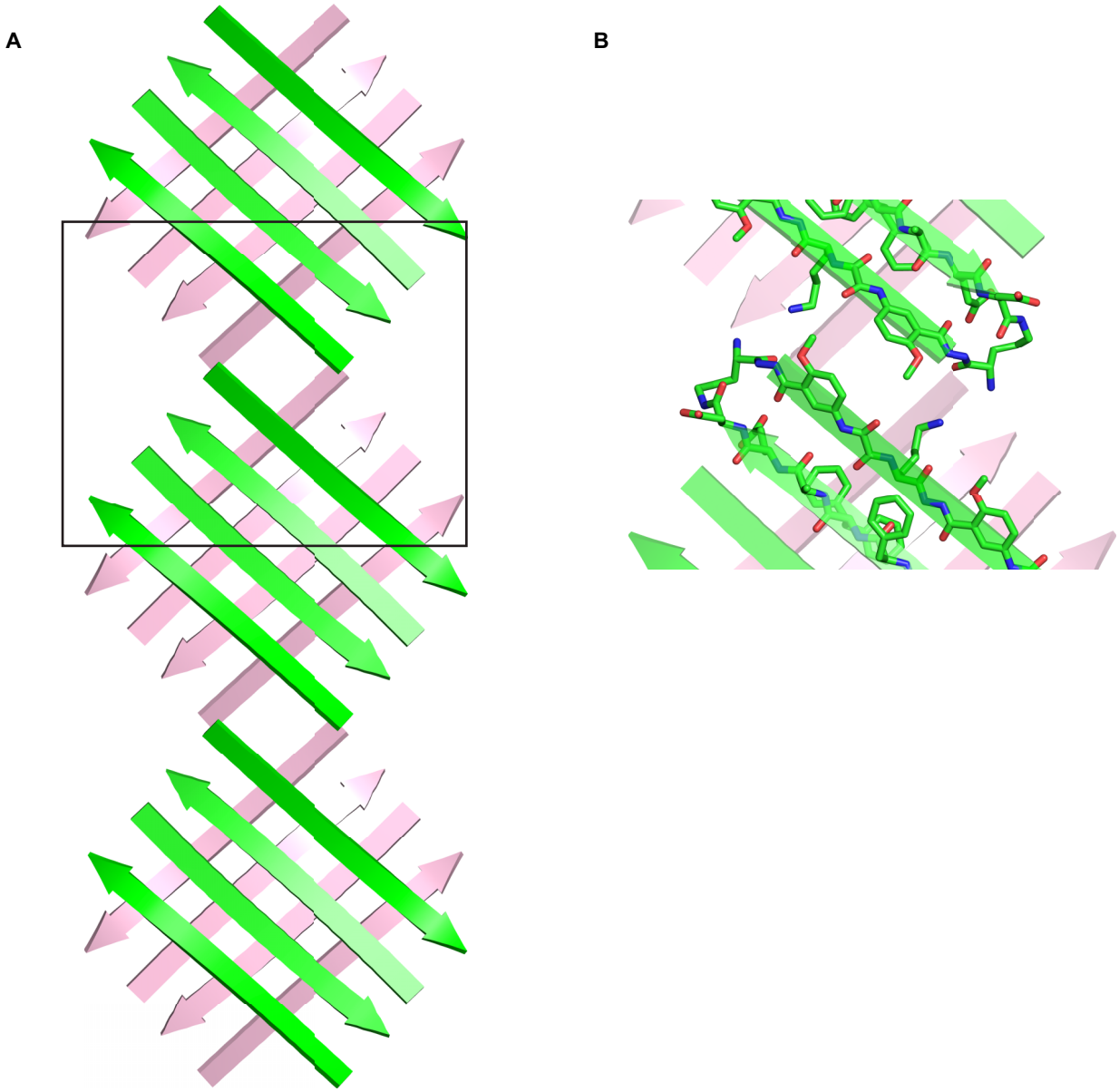

Figure 2.7. Interface between the cruciform tetramer units within the lattice in the X-ray crystallographic structure of macrocyclic β-sheet peptide **2.1**. (A) Linear assembly of cruciform tetramers within the crystal lattice. Three tetrameric subunits of the infinite linear assembly are shown. (B) Detail of the interface between the cruciform tetramer units showing contacts between *Hao* amino acids.

Discussion

To envision how the X-ray crystallographic structure of macrocyclic β-sheet peptide **2.1** reflects the structures of amyloid oligomers of natural peptides and proteins, we used the structure to model assemblies of $A\beta_{15–23}$ homologous to the cruciform tetramer, the triangular dodecamer, and the linear assembly of tetramers. We modeled each of these assemblies by replacing the QKLVFFAED nonapeptide strand and the template strand of macrocyclic β-sheet peptide **2.1** with linear peptide **2.2** (Ac-QKLVFFAED-NHMe, Ac-$A\beta_{15–23}$-NHMe) and generating a minimum energy structure using molecular mechanics with the Merck Molecular Force Field (MMFF) and GB/SA water solvation (Figure 2.8). Figure 2.9 illustrates the resulting structures of the eight-stranded cruciform oligomer, twenty-four-stranded triangular oligomer, and linear assembly of cruciform oligomers modeled with linear peptide **2.2**.

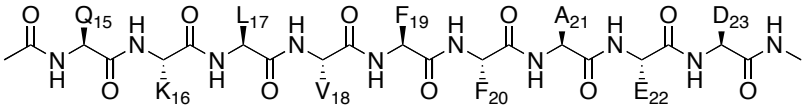

linear peptide **2.2**

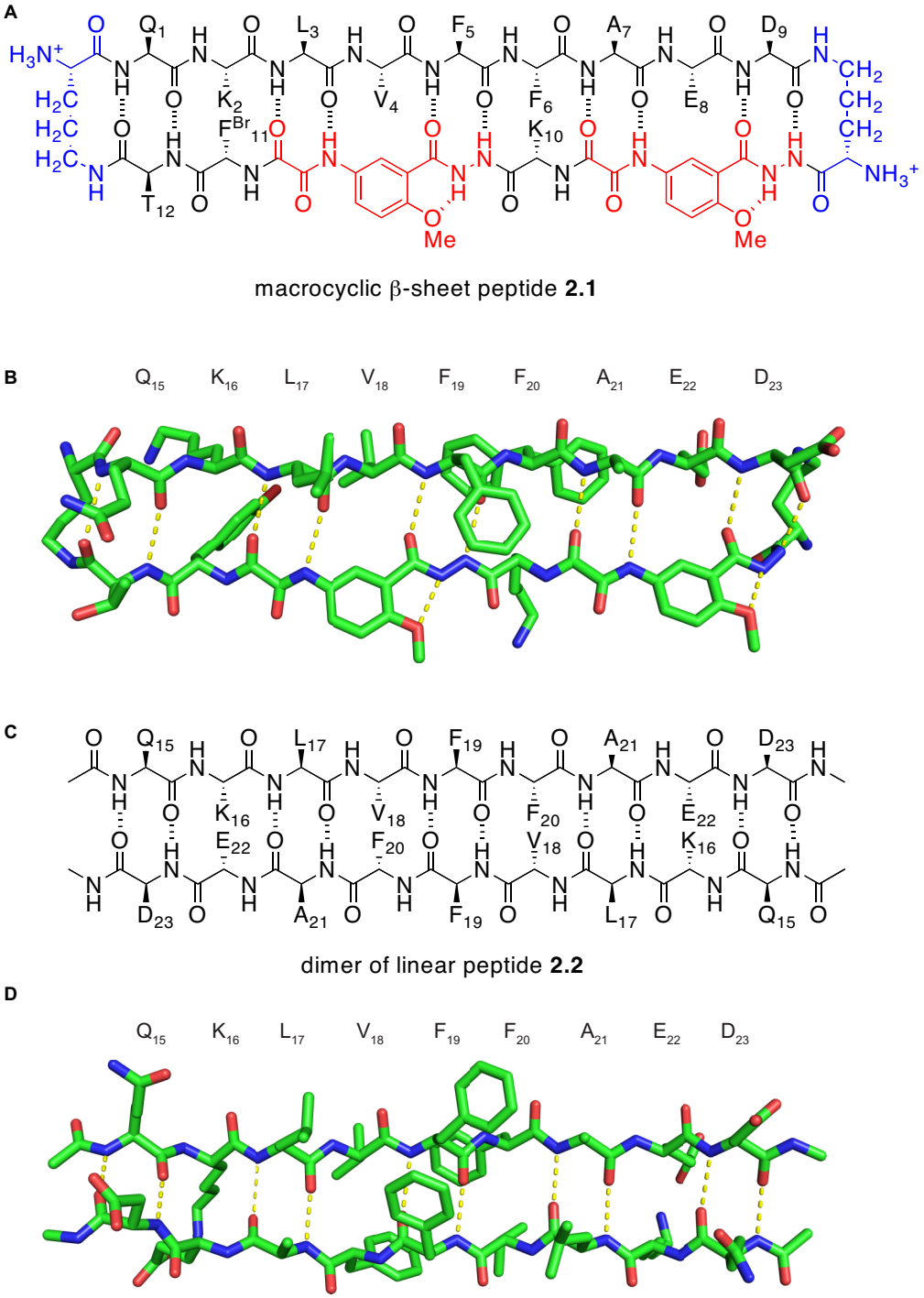

Figure 2.8. X-ray crystallographic structure of macrocyclic β-sheet peptide **2.1** and crystallographically-based molecular models of a dimer of $A\beta_{15–23}$. (A) Macrocyclic β-sheet peptide **2.1**. (B) X-ray crystallographic structure of macrocyclic β-sheet peptide **2.1**. (C) Dimer of linear peptide **2.2** (Ac-QKLVFFAED-NHMe, Ac-$A\beta_{15–23}$-NHMe). (D) Crystallographically-based molecular model of an antiparallel β-sheet dimer of linear peptide **2.2**.

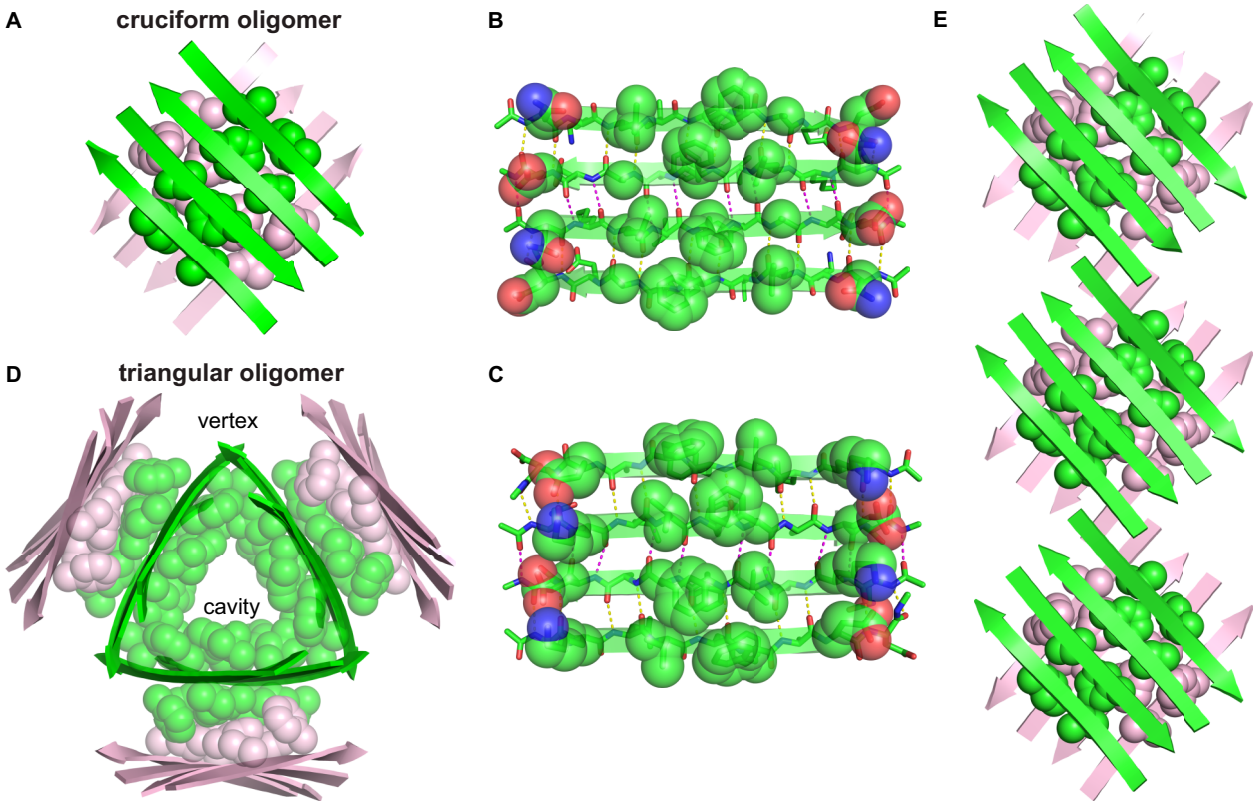

Figure 2.9. Crystallographically-based molecular models of oligomers of $A\beta_{15–23}$. (A) Eight-stranded cruciform oligomer of linear peptide **2.2** (Ac-QKLVFFAED-NHMe, Ac-$A\beta_{15–23}$-NHMe). Model is based upon tetramer of macrocyclic β-sheet peptide **2.1** (Figure 2.4). Side chains of V_{18} and F_{20} in the hydrophobic core are shown. (B) Antiparallel β-sheet comprising four strands of linear peptide **2.2** (LFA face view). Model is one layer of the eight-stranded cruciform oligomer. (C) Antiparallel β-sheet comprising four strands of linear peptide **2.2** (VF face view). Model is one layer of the eight-stranded cruciform oligomer. (D) Twenty-four-stranded triangular oligomer of linear peptide **2.2**. Model is based upon dodecamer of macrocyclic β-sheet peptide **2.1** (Figure 2.5). Side chains of L_{17}, F_{19}, and A_{21} lining the triangular cavity and V_{18} and F_{20} forming the hydrophobic cores between the interior and exterior walls are shown. Side chains of Q_{15}, K_{16}, E_{22}, and D_{23} (not shown) converge at the vertices. (E) Linear assembly of cruciform oligomers of linear peptide **2.2**. Model is based upon assembly of tetramers of macrocyclic β-sheet peptide **2.1** (Figure 2.7). Side chains of V_{18} and F_{20} in the hydrophobic cores are shown.

The cruciform oligomer modeled from linear peptide **2.2** consists of two four-stranded antiparallel β-sheets packed through hydrophobic interactions (Figure 2.9A). In each four-stranded antiparallel β-sheet, the hydrophobic side chains of L_{17}, F_{19}, and A_{21} make a hydrophobic patch that is flanked by the polar side chains of Q_{15} and D_{23} on the LFA face

(Figure 2.9B), and the hydrophobic side chains of V_{18} and F_{20} make a hydrophobic patch that is flanked by the polar side chains of K_{16} and E_{22} on the VF face (Figure 2.9C). The two four-stranded antiparallel β-sheets pack through the VF faces and are nearly orthogonal. The methylene groups of the K_{16} and E_{22} side chains may further pack with the V_{18} and F_{20} side chains to stabilize the hydrophobic core of the cruciform oligomer.

The width of each four-stranded β-sheet is roughly comparable to the length of the seven-amino acid β-strand region from K_{16} to E_{22}—each is about 2 nm. The formation of a cruciform structure between these two β-sheets may reflect a general mode of β-sheet interaction in amyloid oligomers, in which β-sheets of about four peptide strands in width and seven amino acids in length assemble in a crisscross fashion through hydrophobic interactions.[24,25] Hydrophobic interactions through either the VF or the LFA faces should be possible (Figure 2.10). Both antiparallel and parallel β-sheets should be able to interact in this fashion (Figure 2.10). The β-strands comprising the β-sheets may be of the same or different sequences. For example, $A\beta_{16–22}$ (KLVFFAE) should be able to interact both with itself and with hydrophobic sequences from the *C*-terminal region of Aβ, such as $A\beta_{30–36}$ (AIIGLMV).[20,21] Thus, an eight-stranded cruciform oligomer could form from as few as four molecules of $A\beta_{1–40}$ or $A\beta_{1–42}$, with loops connecting the $A\beta_{15–23}$ and *C*-terminal β-strands (Figure 2.11).

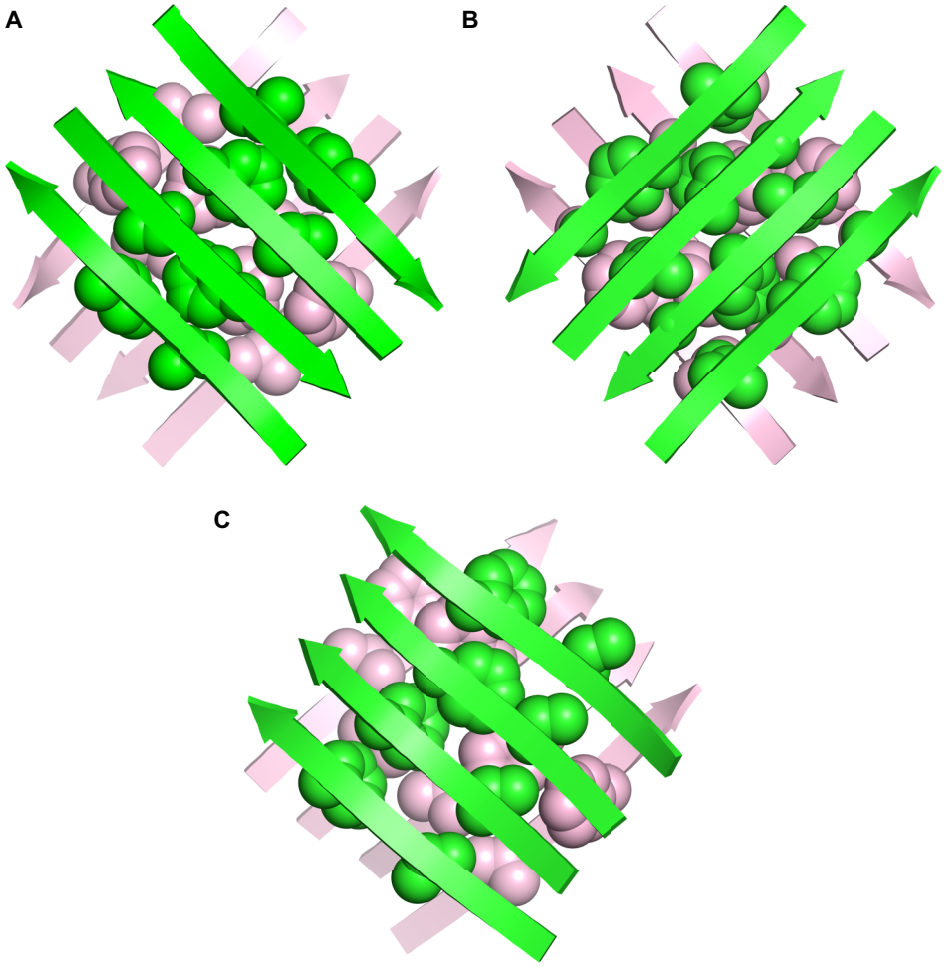

Figure 2.10. Crystallographically-based molecular models of cruciform oligomers of $A\beta_{15–23}$. (A) Eight-stranded cruciform oligomer of peptide **2.2** (Ac-QKLVFFAED-NHMe, Ac-$A\beta_{15–23}$-NHMe) with hydrophobic core formed by VF faces (Figure 2.9A). Model is based upon tetramer of macrocyclic β-sheet peptide **2.1** (Figure 2.4A). Side chains of V_{18} and F_{20} in the hydrophobic core are shown. (B) Eight-stranded cruciform oligomer of peptide **2.2** with hydrophobic core formed by LFA faces. Model is based upon tetramer of macrocyclic β-sheet peptide **2.1** (Figure 2.4A). Side chains of L_{17}, $F_{19,}$ and A_{21} in the hydrophobic core are shown. (C) Eight-stranded cruciform oligomer of peptide **2.2** composed of *parallel* β-sheets. Model is based upon tetramer of macrocyclic β-sheet peptide **2.1** (Figure 2.4A). Side chains of V_{18} and F_{20} in the hydrophobic core are shown.

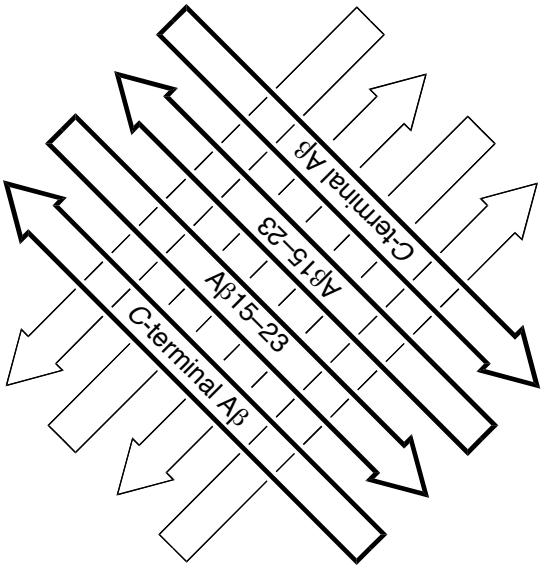

Figure 2.11. Cartoon of an eight-stranded cruciform oligomer comprising the $A\beta_{15–23}$ and *C*-terminal β-strands.

The triangular oligomer modeled from linear peptide **2.2** consists of three cruciform oligomers in a triangular arrangement (Figure 2.9D). The hydrophobic L_{17}, F_{19}, and A_{21} side chains line the triangular cavity, and the hydrophobic V_{18} and F_{20} side chains pack to form the hydrophobic cores between the interior and exterior walls. The E_{22} residues abut at the juncture between the interior walls forming a pair of hydrogen bonds. The polar side chains of Q_{15}, K_{16}, E_{22}, and D_{23} converge at the vertices of the triangles.

In a triangular oligomer formed from $A\beta_{1–40}$ or $A\beta_{1–42}$ the polypeptide chains would extend beyond the vertices (Figure 2.9D) and create additional stabilizing hydrophobic and polar contacts. The side chains of H_{13} and H_{14} would converge at the vertices, along with those of E_{22} and D_{23}. These side chains would create rich ligating environments for metal ions, which could further stabilize the oligomer, much akin to the sodium ions in the lattice (Figure 2.3C). Lipids could further stabilize the oligomer by binding inside the triangular cavity, in a fashion similar to

the *t*-BuOH in the lattice (Figure 2.3C). A triangular oligomer formed from $A\beta_{1–40}$ or $A\beta_{1–42}$ need not consist only of the *N*-terminal hydrophobic region of Aβ and could also incorporate hydrophobic sequences from the *C*-terminal region. Thus, a triangular oligomer could form from as few as twelve molecules of $A\beta_{1–40}$ or $A\beta_{1–42}$, with loops connecting the β-strands.

The linear assembly of oligomers modeled from linear peptide **2.2** consists of three cruciform oligomers in a linear arrangement (Figure 2.9E). The nonapeptide strands of the cruciform oligomers are shifted out of alignment by six residues at the juncture between the tetramer units. Because the assemblies lack the Hao units, the *N*-termini of the β-strands at the juncture are able to hydrogen bond, and each β-strand creates a three-residue hydrogen-bonded β-sheet between the cruciform oligomer units. Assemblies of cruciform oligomers can also occur through overlap of the *C*-termini of the β-strands (e.g., Figure 2.12).

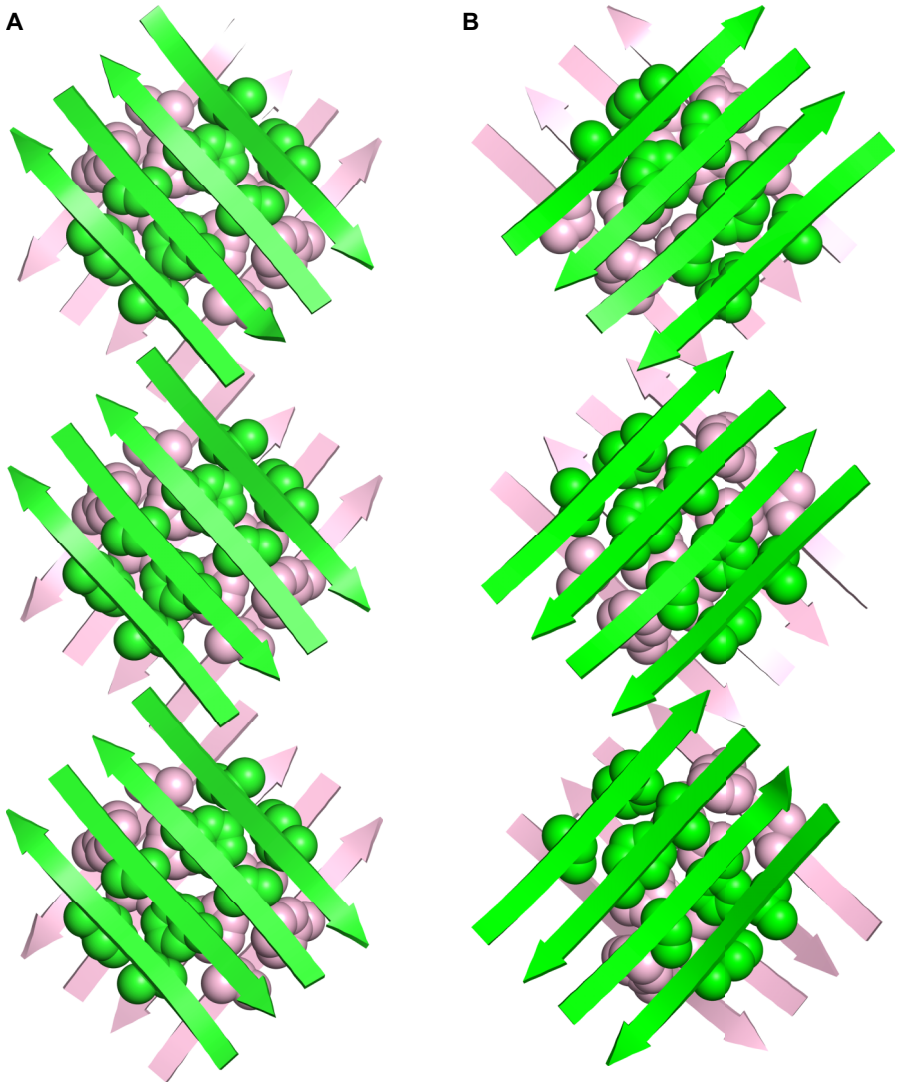

Figure 2.12. Crystallographically-based molecular models of linear assemblies of cruciform oligomers of $A\beta_{15–23}$. (A) Linear assembly of cruciform oligomers of peptide **2.2** (Ac-QKLVFFAED-NHMe, Ac-$A\beta_{15–23}$-NHMe) formed by overlap of the *N*-termini of the β-strands (Figure 2.9E). Model is based upon assembly of tetramers of macrocyclic β-sheet peptide **2.1** (Figure 2.7). Side chains of V_{18} and F_{20} in the hydrophobic cores are shown. (B) Linear assembly of cruciform oligomers of peptide **2.2** formed by overlap of the *C*-termini of the β-strands. Model is based upon assembly of tetramers of macrocyclic β-sheet peptide **2.1** (Figure 2.7). Side chains of V_{18} and F_{20} in the hydrophobic cores are shown.

The crystal lattice of macrocyclic β-sheet peptide **2.1** (Figure 2.3) suggests the potential for incorporation of cruciform and triangular oligomers of Aβ into lipid bilayer membranes. The triangular cavities in the lattice are surrounded by the hydrophobic L_{17}, F_{19}, and A_{21} side chains.

The lipophilic *t*-BuOH in these cavities suggests the potential for the oligomers to assemble in lipid bilayer membranes and be stabilized by interactions of the hydrophobic LFA faces with lipids. The hexagonal cavities in the lattice (Figures 2.3) suggest the potential for the creation of hydrophilic pores in lipid bilayer membranes that could disrupt membrane integrity toward water or ions. The hexagonal cavities in the lattice are surrounded by the polar Q_{15}, K_{16}, E_{22}, and D_{23} side chains. The presence of sodium ions and water in these cavities suggests that six cruciform oligomers or three triangular oligomers could form a hexagonal pore in a membrane that could serve as a conduit for water or metal cations (Figure 2.13). If oligomers from $A\beta_{1–40}$ or $A\beta_{1–42}$ were to form such pores, the side chains of H_{13} and H_{14} would line the pores, along with those of E_{22} and D_{23}, further facilitating the binding and transport of metal cations. The hexagonal arrangement of oligomers in the crystal lattice appear to be consistent in size and morphology with the hexagonal and annular porelike structures observed for Aβ and other amyloidogenic peptides and proteins. [45,46,47,48] The X-ray crystallographic structure of macrocyclic β-sheet **2.1** may thus provide a glimpse into the molecular basis of Aβ oligomer toxicity. [49,50,51,52]

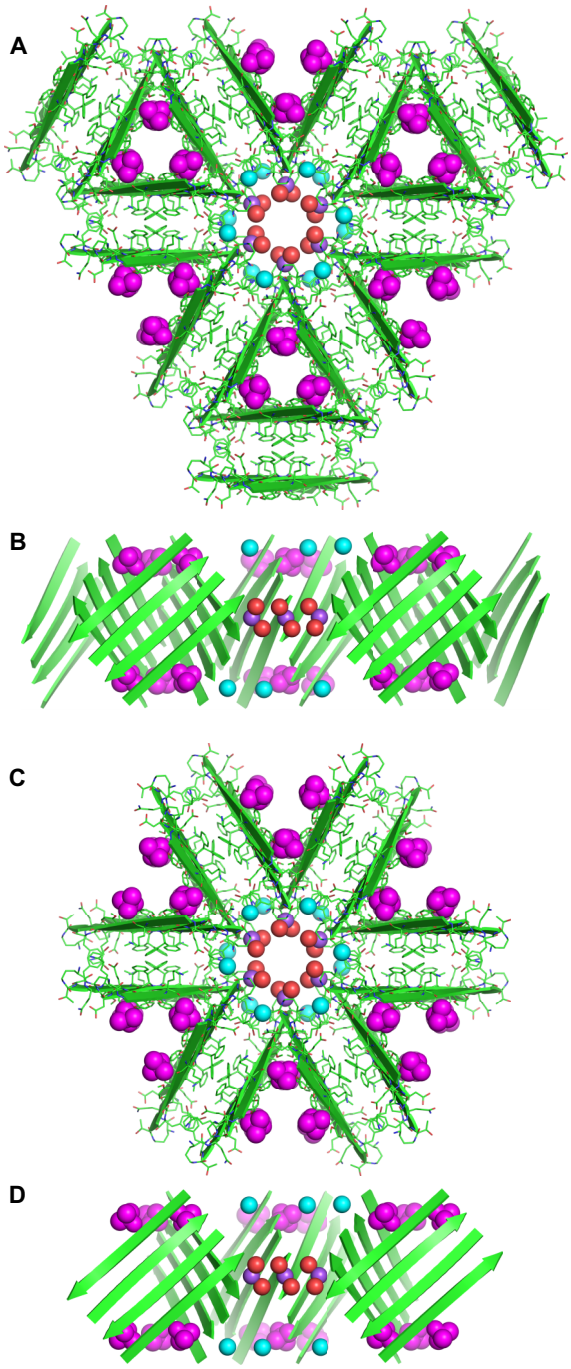

Figure 2.13. Hexagonal pores within the crystal lattice of macrocyclic β-sheet peptide **2.1**. (A) Hexagonal pore formed by three triangular dodecamers (top view): *t*-BuOH (magenta, in the triangular cavities), Na^+ (purple, in the hexagonal cavities), H_2O ligands for Na^+ (red, in the hexagonal cavities), additional H_2O (cyan, in the hexagonal cavities). (B) Hexagonal pore formed by three triangular dodecamers (cutaway side view). (C) Hexagonal pore formed by six cruciform tetramers (top view). (D) Hexagonal pore formed by six cruciform tetramers (cutaway side view).

The cruciform and triangular oligomers observed for macrocyclic β-sheet peptide **2.1** and modeled for linear peptide **2.2** reflect common themes observed in amyloidogenic peptides. $A\beta_{1-40}$, $A\beta_{1-42}$, islet amyloid polypeptide, and small peptides derived from human prions, tau, and insulin form fibrils composed of layered β-sheets.[1,2,3,53,54,55] In the fibrils, the β-sheets form long networks of β-strands and the component β-strands are nearly orthogonal to the fibril axis. The cruciform oligomer described here is similar to the fibrils in that it consists of a layered pair of β-sheets with a central hydrophobic core. It differs in that the β-sheets are nearly orthogonal and are composed of only four β-strands apiece. Under suitable conditions, $A\beta_{1-40}$ can form three-fold symmetrical assemblies consisting of layered pairs of β-sheets in a triangular arrangement around the fibril axis.[3] The triangular oligomer described here is similar to the triangular fibril assemblies in that the three-fold symmetrical structure consists of layered pairs of β-sheets. It differs in that the β-sheets are at nearly a 45° angle to the threefold axis.

The triangular core of the triangular oligomer of macrocyclic β-sheet peptide **2.1** is a *homologated cylindrin*, similar to the previously reported barrel-shaped hexamer structure of amyloid oligomers derived from αB crystallin but expanded from six β-strands to twelve (Figure 2.14).[26] The core of the triangular oligomer consists of three four-stranded β-sheet subunits that are hydrogen bonded to make a cylindrical twelve-stranded β-sheet.[27] The β-strands of three β-sheet subunits are fully aligned, but are then shifted out of alignment by six residues, toward the *C*-terminus, at the juncture between the three subunits. In the previously reported cylindrin structures, the junctures between the three aligned two-stranded β-sheet subunits shift out of alignment by two residues, toward the *N*-terminus, giving a net shift of one residue per β-strand and a right-handed propeller structure. In the triangular core of the triangular oligomer of macrocyclic β-sheet peptide **2.1**, there is a net shift of one and a half residues per β-strand and a

right-handed propeller structure. As a result of the larger net shift, the β-strands of this cylindrin are at a larger angle with respect to the cylinder axis than those of αB crystallin. This difference may reflect the blocking of hydrogen bonding by the Hao units.

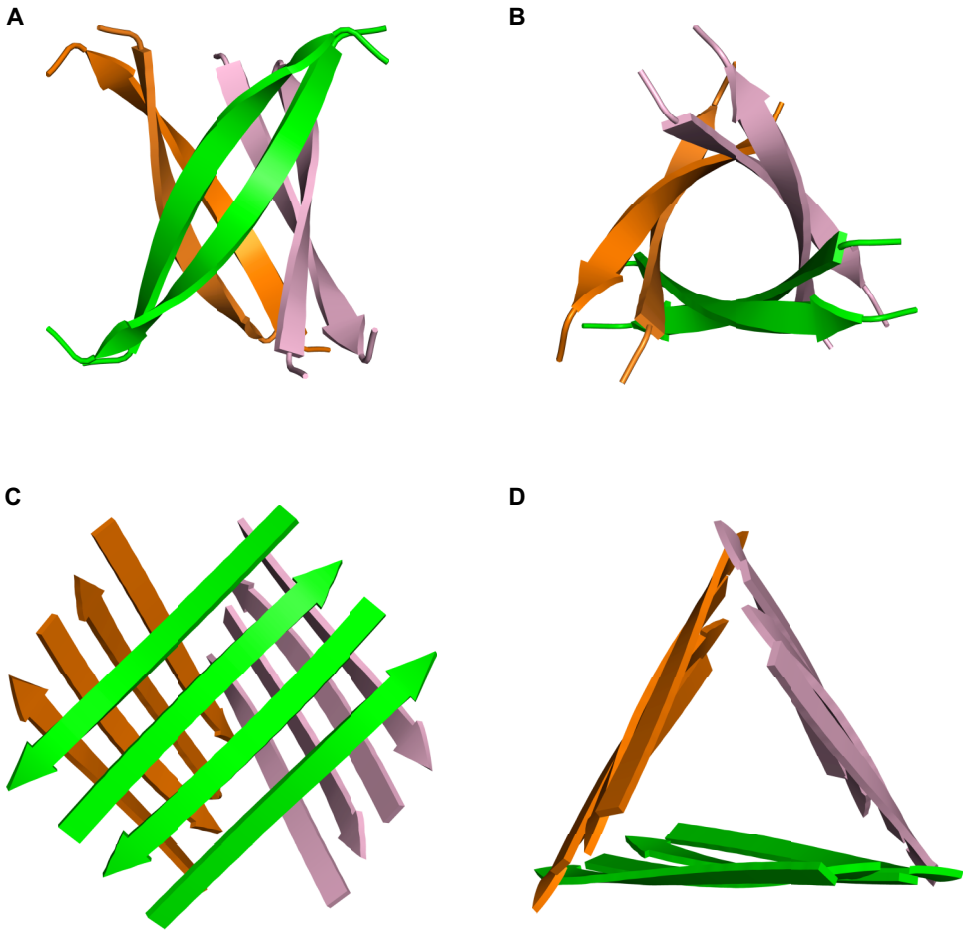

Figure 2.14. X-ray crystallographic structures of the amyloid oligomer derived from αB crystallin and the triangular core of the triangular oligomer of macrocyclic β-sheet peptide **2.1**. (A) Cylindrin oligomer of the undecapeptide KVKVLGDVIEV from αB crystallin (PDB ID 3SGO, side view). (B) Cylindrin oligomer of the undecapeptide KVKVLGDVIEV from αB crystallin (PDB ID 3SGO, top view). (C) Homologated cylindrin structure of the triangular core of the triangular oligomer of macrocyclic β-sheet peptide **2.1** (side view). (D) Homologated cylindrin structure of the triangular core of the triangular oligomer of macrocyclic β-sheet peptide **2.1** (top view).

Conclusion

The X-ray crystallographic structure of Aβ-derived peptide **2.1** provides a unique window into the supramolecular assembly of β-amyloid peptides and perhaps amyloidogenic peptides in general. Assembly of peptide strands into small β-sheets that further assemble in a crisscross fashion creates cruciform oligomers. The cruciform oligomers can assemble in a hierarchical fashion to create larger oligomers and oligomer assemblies. Three cruciform oligomers can assemble in a propeller-like fashion to form triangular oligomers. The cruciform oligomers can also assemble in a linear fashion to form linear assemblies. Three triangular oligomers or six cruciform oligomers can assemble to form hexagonal pores lined with hydrophilic ionophoric groups. The hydrophobic surfaces of the cruciform oligomers and oligomer assemblies may provide a means by which these structures can insert into lipid bilayer membranes, facilitate the transport of water or metal cations, and disrupt cellular homeostasis.

References

1 Pham, J. D.; Chim, N.; Goulding, C. W.; Nowick, J. S. N. *J. Am. Chem. Soc.* **2013**, *135*, 12460–12467.

2 Lührs, T; Ritter, C.; Adrian, M.; Riek-Loher, D.; Bohrmann, B.; Döbeli, H.; Schubert, D.; Riek, R. *Proc. Natl. Acad. Sci. U.S.A.* **2005**, *102*, 17342–17347.

3 Petkova, A. T.; Yau, W.-M.; Tycko, R. *Biochemistry* **2006**, *45*, 498–512.

4 Paravastu, A. K.; Leapman, R. D.; Yau, W.-M.; Tycko, R. *Proc. Natl. Acad. Sci. U.S.A.* **2008**, *105*, 18349–18354.

5 Kayed, R.; Head, E.; Thompson, J. L.; McIntire, T. M.; Milton, S. C.; Cotman, C. W.; Glabe, C. G. *Science* **2003**, *300*, 486–489.

6 Haass, C.; Selkoe, D. J.; *Nat. Rev. Mol. Cell Bio.* **2007**, *8*, 101–112.

7 Walsh, D. M.; Selkoe, D. J.; *J. Neurochem.* **2007**, *101*, 1172–1184.

8 Selkoe, D. J. *Behav. Brain Res.* **2008**, *192*, 106–113.

9 Glabe, C. G. *J. Biol. Chem.* **2008**, *283*, 29639–29643.

10 Kayed, R.; Canto, I.; Breydo, L.; Rasool, S.; Lukacsovich, T.; Wu, J.; Albay III, R.; Pensalfini, P.; Yeung, S.; Head, E.; Marsh, J. L.; Glabe, C. *Mol. Neurodegener.* **2010**, *5*, 1–10.

11 Fändrich, M. *J. Mol. Biol.* **2012**, *421*, 427–440.

12 Benilova, I.; Karran, E.; De Stooper, B. *Nat. Neurosci.* **2012**, *15*, 349–357.

13 Nussbaum, J. M.; Schilling, S.; Cynis, H.; Silva, A.; Swanson, E.; Wangsanut, T.; Tayler, K.; Wiltgen, B.; Hatami, A.; Rönicke, R.; Reymann, K.; Hutter-Paier, B.; Alexandru, A.; Jagla, W.; Graubner, S.; Glabe, C. G.; Demuth, H.-U.; Bloom, G. S. *Nature* **2012**, *485*, 651–655.

14 Chen, Y.-R.; Glabe, C. G. *J. Biol. Chem.* **2006**, *281*, 24414–24422.

15 Lesné, S.; Koh, M. T.; Kotilinek, L.; Kayed, R.; Glabe, C. G.; Yang, A.; Gallagher, M.; Ashe, K. H. *Nature* **2006**, *440*, 352–357.

16 Shankar, G. M.; Li, S.; Mehta, T. H.; Garcia-Munoz, A.; Shepardson, N. E.; Smith, I.; Brett, F. M.; Farrell, M. A.; Rowan, M. J.; Lemer, C. A.; Regan, C. M.; Walsh, D. M.; Sabatini, B. L.; Selkoe, D. J. *Nat. Med.* **2008**, *14*, 837–842.

17 Bernstein, S. L.; Dupuis, N. F.; Lazo, N. D.; Wyttenbach, T.; Condron, M. M.; Bitan, G.; Teplow, D. B.; Shea, J.-E.; Ruotolo, B. T.; Robinson, C. V.; Bowers, M. T. *Nat. Chem.* **2009**, *1*, 326–331.

18 Ono, K.; Condron, M. M.; Teplow, D. B. *Proc. Natl. Acad. Sci. U.S.A.* **2009**, *106*, 14745–14750.

19 Zhang, R.; Hu, X.; Khant, H.; Ludtke, S. J.; Chiu, W.; Schmid, M. F.; Frieden, C.; Lee, J.-M. *Proc. Natl. Acad. Sci. U.S.A.* **2009**, *106*, 4653–4658.

20 Miller, Y.; Ma, B.; Tsai, C.-J.; Nussinov, R. *Proc. Natl. Acad. Sci. U.S.A.* **2010**, *107*, 14128–14133.

21 Hoyer, W.; Grönwall, C.; Jonsson, A.; Ståhl, S.; Härd, T. *Proc. Natl. Acad. Sci. U.S.A.* **2008**, *105*, 5099–5104.

22 Sandberg, A.; Luheshi, L. M.; Söllvander, S.; de Barros, T. P.; Macao, B.; Knowles, T. P. J.; Biverstål, H.; Lendel, C.; Ekholm-Petterson, F.; Dubnovitsky, A.; Lannfelt, L.; Dobson, C. M.; Härd, T. *Proc. Natl. Acad. Sci. U.S.A.* **2010**, *107*, 15595–15600.

23 Yu, L.; Edalji, R.; Harlan, J. E.; Holzman, T. F.; Lopez, A. P.; Labkovsky, B.; Hillen, H.; Barghorn, S.; Ebert, U.; Richardson, P. L.; Miesbauer, L.; Solomon, L.; Bartley, D.; Walter, K.; Johnson, R. W.; Hajduk, P. J.; Olejniczak, E. T. *Biochemistry* **2009**, *48*, 1870–1877.

24 Miller, Y.; Ma, B.; Nussinov, R. *Chem. Rev.* **2010**, *110*, 4820–4838.

25 Liu, C.; Sawaya, M. R.; Cheng, P.-N.; Zheng, J.; Nowick, J. S.; Eisenberg, D. *J. Am. Chem. Soc.* **2011**, *133*, 6736–6744.

26 Liu, C.; Zhao, M.; Jiang, L.; Cheng, P.-N.; Park, J.; Sawaya, M. R.; Pensalfini, A.; Gou, D.; Berk, A. J.; Glabe, C. G.; Nowick, J. S.; Eisenberg, D. *Proc. Natl. Acad. Sci. U.S.A.* **2012**, *109*, 20913–20918.

27 Laganowsky, A.; Liu, C.; Sawaya, M. R.; Whitelegge, J. P.; Park, J.; Zhao, M.; Pensalfini, A.; Soriaga, A. B.; Landau, M.; Keng, P. K.; Cascio, D.; Glabe, C. G.; Eisenberg, D. *Science* **2012**, *335*, 1228–1231.

28 Apostol, M. I.; Perry, K.; Surewicz, W. K. *J. Am. Chem. Soc.* **2013**, *135*, 10202–10205.

29 Nowick, J. S.; Chung, D. M.; Maitra, K.; Maitra, S.; Stigers, K. D.; Sun, Y. J. *J. Am. Chem. Soc.* **2000**, *122*, 7654–7661.

30 Nowick, J. S.; Brower, J. O. *J. Am. Chem. Soc.* **2003**, *125*, 876–877.

31 Cheng, P.-N.; Nowick, J. S. *J. Org. Chem.* **2011**, *76*, 3166–3173.

32 Cheng, P-N.; Liu, C.; Zhao, M.; Eisenberg, D.; Nowick, J. S. *Nat. Chem.* **2012**, *4*, 927–933.

33 Nowick, J. S.; Chung, D. M.; Maitra, K.; Maitra, S.; Stigers, K. D.; Sun, Y. J. *J. Am. Chem. Soc.* **2000**, *122*, 7654–7661.

34 Otwinowski, Z.; Minor, W. *Methods Enzymol.* **1997**, *276*, 307–326.

35 Winn, M. D.; Ballard, C. C.; Cowtan, K. D.; Dodson, E. J.; Emsley, P.; Evans, P. R.; Keegan, R. M.; Krissinel, E. B.; Leslie, A. G. W.; McCoy, A.; McNicholas, S. J.; Murshudov, G. N.; Pannu, N. S.; Potterton, E. A.; Powell, H. R.; Read, R. J.; Vagin, A.; Wilson, K. S. *Acta Crystallogr. D Biol. Crystallogr.* **2011**, *67*, 235–242.

36 Adams, P. D.; Grosse-Kunstleve, R. W.; Hung, L.-W.; Ioerger, T. R.; McCoy, A. J.; Moriarty, N. W.; Read, R. J.; Sacchettini, J. C.; Sauter, N. K.; Terwilliger, T. C. *Acta*

Crystallogr. D Biol. Crystallogr. **2002**, *58*, 1948–1954.

37 Emsley, P.; Cowtan, K. *Acta Crystallogr. D Biol. Crystallogr.* **2004**, *60*, 2126–2132.

38 Murshudov, G. N.; Vagin, A. A.; Dodson, E. J. *Acta Crystallogr. D Biol. Crystallogr.* **1997**, *53*, 240–255.

39 The PyMOL Molecular Graphics System, Schrödinger, LLC, available at www.pymol.org.

40 Tjernberg, L. O.; Callaway, D. J. E.; Tjernberg, A.; Hahne, S.; Lilliehöök, C.; Terenius, L.; Thyberg, J.; Nordstedt, C. *J. Biol. Chem.* **1999**, *274*, 12619–12625.

41 Balbach, J. J.; Ishii, Y.; Antzutkin, O. N.; Leapman, R. D.; Rizzo, N. W.; Dyda, F.; Reed, J.; Tycko, R. *Biochemistry* **2000**, *39*, 13748–13759.

42 Mehta, A. K.; Lu, K.; Childers, W. S.; Liang, Y.; Dublin, S. N.; Dong, J.; Snyder, J. P.; Pingali, S. V.; Thiyagarajan, P.; Lynn, D. G. *J. Am. Chem. Soc.* **2008**, *130*, 9829–9835.

43 Liang, Y.; Pingali, S. V.; Jogalekar, A. S.; Snyder, J. P.; Thiyagarajan, P.; Lynn, D. G. *Biochemistry* **2008**, *47*, 10018–10026.

44 Qiang, W.; Yau, W-M.; Luo, Y.; Mattson, M. P.; Tycko, R. *Proc. Natl. Acad. Sci. U.S.A.* **2012**, *109*, 4443–4448.

45 Lin, H.; Bhatia, R.; Lal, R. *FASEB J.* **2001**, *15*, 2433–2444.

46 Lashuel, H. A.; Hartley, D.; Petre, B. M.; Walz, T.; Lansbury Jr., P. T. *Nature* **2002**, *418*, 291.

47 Quist, A.; Doudevski, I.; Lin, H.; Azimova, R.; Ng, D.; Frangione, B.; Kagan, B.; Ghiso, J.; Lal, R. *Proc. Natl. Acad. Sci. U.S.A.* **2005**, *102*, 10427–10432.

48 Kayed, R.; Pensalfini, A.; Margol, L.; Sokolov, Y.; Sarsoza, F.; Head, E.; Hall, J.; Glabe, C. G. *J. Bio. Chem.* **2009**, *284*, 4230–4237.

49 Lashuel, H. A.; Lansbury Jr., P. T.; *Quart. Rev. Biophys.* **2006**, *39*,167–201.

50 Butterfield, S. M.; Lashuel, H. A. *Angew. Chem. Int. Ed.* **2010**, *49*, 5628–5654.

51 Kayed, R. Sokolov, Y.; Edmonds, B.; McIntire, T. M.; Milton, S. C.; Hall, J. E.; Glabe, C. G. *J. Biol. Chem.* **2004**, *279*, 46363–46366.

52 Lasagna-Reeves, C. A.; Glabe, C. G.; Kayed, R. *J. Biol. Chem.* **2011**, *286*, 22122–22130.

53 Luca, S.; Yau, W.-M.; Leapman, R.; Tycko, R. *Biochemistry* **2007**, *46*, 13505–13522.

54 Nelson, R.; Sawaya, M. R.; Balbirnie, M.; Madsen, A. Ø.; Riekel, C.; Grothe, R.; Eisenberg, D. *Nature* **2005**, *435*, 773–778.

55 Sawaya, M. R.; Sambashivan, S.; Nelson, R.; Ivanova, M. I.; Sievers, S. A.; Apostol, M. I.; Thompson, M. J.; Balbirnie, M.; Wiltzius, J. J. W.; McFarlane, H. T.; Madsen, A. Ø.; Riekel, C.; Eisenberg, D. *Nature* **2007**, *447*, 453–457.

Experimental Section For Chapter 2

Materials and Methods:

*Synthesis of macrocyclic β-sheet peptide **2.1**.*

Macrocyclic peptide **2.1** was synthesized as illustrated in Scheme 2.1 in a fashion similar to procedures previously reported for the synthesis of other macrocyclic β-sheet peptides.[1,2] Boc-Orn(Fmoc)-OH was used to introduce the δ-linked ornithine turn units. Fmoc-Hao-OH[1] was used to introduce the unnatural amino acid Hao.[3] Standard Fmoc-protected amino acids were used to introduce the other residues. Details of the synthesis are described below:

Loading of resin: A 10 mL Bio-Rad Poly-Prep chromatography column was charged with 2-chlorotrityl choride resin (357 mg, 1.2 mmol/g loading, 0.428 mmol) and ca. 6 mL of CH_2Cl_2. After 30 min, the solvent was drained, a premixed solution of Boc-Orn(Fmoc)-OH (68 mg, 0.15 mmol, 0.35 mol equiv) and *N*,*N*-diisopropylethylamine (DIPEA, 0.05 mL, 0.3 mmol, 0.7 mol equiv) in 10 mL of CH_2Cl_2 was added, and the mixture was shaken for 12 hours. The solution was drained and the resin was washed with CH_2Cl_2 (2 x 5 mL). Unreacted sites were capped by shaking the resin with a mixture of CH_2Cl_2/MeOH/DIPEA (17:2:1 v/v, 2 x 7 mL, 5 min. each time). The resin was washed with CH_2Cl_2 and dried under a stream of nitrogen. The resin loading

---

1 Cheng, P.-N.; Nowick, J. S. *J. Org. Chem.* **2011**, *76*, 3166–3173.

2 Cheng, P-N.; Liu, C.; Zhao, M.; Eisenberg, D.; Nowick, J. S. *Nat. Chem.* **2012**, *4*, 927–933.

3 Nowick, J. S.; Chung, D. M.; Maitra, K.; Maitra, S.; Stigers, K. D.; Sun, Y. J. *J. Am. Chem. Soc.* **2000**, *122*, 7654–7661.

was analyzed spectrophotometrically[4] and was determined to be 0.24 mmol/g (56% loading efficiency of Boc-Orn(Fmoc)-OH).

Peptide coupling and cleavage: The PS-2-chlorotrityl-Orn(Fmoc)-Boc resin from the previous step was washed with DMF (1 x 5 mL) and submitted to cycles of standard Fmoc-based solid phase peptide synthesis on an automated PS3^{TM} Peptide Synthesizer (Protein Technologies, Inc.) using Fmoc-protected amino acid building blocks (4 equiv, with HCTU as coupling agent and 2,4,6-collidine as base). Hao was introduced using Fmoc-Hao-OH (3 equiv, with HCTU as coupling agent and 2,4,6-collidine as base) with double coupling and 1 hour coupling times to ensure complete coupling. The final step involved Fmoc deprotection of the terminal amino acid.

The linear peptide was then cleaved from resin by agitating the resin with a solution of AcOH/CH_2Cl_2/MeOH (5:4:1 v/v, ca. 7 mL) for 1.5 hr. The cleavage solution was concentrated under vacuum to a yellow oil. The oil was dissolved with 5 mL of CH_2Cl_2 and ca. 100 mL of hexanes, and concentrated under vacuum to dryness. The dissolution and rotary evaporation was repeated two more times to afford 208 mg of protected linear peptide **2.3** as a white solid (81% yield of crude product based on resin loading). The unpurified material was used in the next step without further purification.

Cyclization: A 250 mL one-neck round-bottom flask equipped with a magnetic stirring bar and a pressure-equalizing addition funnel fitted with a nitrogen-inlet adapter was charged with HCTU (105 mg, 0.25 mmol, 3.7 equiv) and DIPEA (0.10 mL, 0.61 mmol, 9.0 mol equiv) in 75 mL DMF. A solution of the protected linear peptide **2.3** (208 mg) in 75 mL DMF was added in drops over 1 h. The solution was stirred for 2 days. The DMF was then removed under

[4] Beck, F. *Methods Mol. Biol.* **2002**, *208*, 29–41.

vacuum to give a yellow waxy solid. The solid was stirred vigorously with 100 mL CH_2Cl_2 and 100 mL H_2O for 10 min. The organic layer was separated and concentrated under vacuum to afford protected macrocyclic peptide **2.4** as a yellowish brown solid. The unpurified material was used in the next step without further purification.

Global deprotection and purification: Protected macrocyclic peptide **2.4** was stirred with 10 mL of trifluoroacetic acid/triisopropylsilane/water (18:1:1 v/v) for 1.5 hours. The solution was concentrated under vacuum. The residue was dissolved in ca. 5 mL of water/acetonitrile (1:1), filtered through a 0.45 micron filter, and purified by RP-HPLC on a C_{18} column (elution with acetonitrile and water containing 0.1% TFA, linear gradient from 35-55% acetonitrile over 50 min). The pure fractions were lyophilized to yield 28 mg of macrocyclic β-sheet **2.1** (12% yield based on resin loading): ESI-MS *m/z* for $C_{101}H_{142}BrN_{25}O_{28}$ $[M + 2H]^{2+}$ calcd 1115.98, found 1116.01.

*Crystallization of macrocyclic β-sheet **2.1***.

A solution of 7 mg/mL macrocyclic β-sheet peptide **2.1** in water was used for crystallization trials. Three sparse-matrix screens from Hampton Research (Crystal Screen, PEG/Ion, and Index) and two from Qiagen (PACT Suite and JCSG Suite) were used to find initial crystallization conditions. Each screen consisted of a 96-well plate with 100 μL solutions of different salts, reagents, and pH values. The screens were prepared using the TTP LabTech Mosquito nanodispenser instrument with a 1:1 ratio (600 nL total) of dissolved peptide and well solution. The initial condition 0.1 M sodium citrate tribasic dihydrate pH 5.6 and 35% *tert*-butanol produced small, 0.1 mm rectangular crystals. Adding 1% poly(ethylene glycol) (PEG) 3350 from the Hampton Research Additive Screen was found to improve the quality of the

crystals. After additional optimization of conditions, a well-diffracting crystal was grown using the hanging-drop vapor-diffusion method at room temperature with 0.5 M sodium citrate tribasic dihydrate, pH 7.2, 35% *tert*-butanol, 1% PEG 3350. The rectangular crystals were collected without soaking in cryoprotectant and flash frozen in liquid nitrogen prior to data collection.

X-ray diffraction data collection, processing, and structure and refinement.

A single anomalous dispersion (SAD) dataset was collected at 100 K at the Advanced Light Source (Berkeley, CA) with Beamline 8.2.1 using the bromine absorption edge wavelength (0.92 Å). The dataset was indexed, integrated and scaled using the HKL2000 Suite.[5] Macrocycle β-sheet peptide **2.1** was found to crystallize in space group P622 with unit cell dimensions 45.1 x 45.1 x 29.2 Å and one molecule of macrocyclic β-sheet **2.1** in the asymmetric unit. Conversion of scalepack to mtz file format was performed with CCP4i suite.[6] A single bromine site was located using Phaser and an initial model was built using Autosol in PHENIX.[7] Additional model

---

[5] Otwinowski, Z.; Minor, W. *Methods Enzymol.* **1997**, *276*, 307–326.

[6] Winn, M. D.; Ballard, C. C.; Cowtan, K. D.; Dodson, E. J.; Emsley, P.; Evans, P. R.; Keegan, R. M.; Krissinel, E. B.; Leslie, A. G. W.; McCoy, A.; McNicholas, S. J.; Murshudov, G. N.; Pannu, N. S.; Potterton, E. A.; Powell, H. R.; Read, R. J.; Vagin, A.; Wilson, K. S. *Acta Crystallogr. D Biol. Crystallogr.* **2011**, *67*, 235–242.

[7] Adams, P. D.; Grosse-Kunstleve, R. W.; Hung, L.-W.; Ioerger, T. R.; McCoy, A. J.; Moriarty, N. W.; Read, R. J.; Sacchettini, J. C.; Sauter, N. K.; Terwilliger, T. C. *Acta Crystallogr. D Biol. Crystallogr.* **2002**, *58*, 1948–1954.

building and refinement was carried out with COOT[8] and Refmac5.[9]

Solvent and ions were incorporated in the refinement to account for electron density beyond macrocycle β-sheet peptide **2.1**. One molecule of *tert*-butanol and two molecules of water were identified per asymmetric unit. One sodium ion at 50% occupancy was also identified. Incorporating a sodium ion into a region of positive electron density observed in the F_o-F_c difference map lowered R values by 1.5% (Figure 2.1). Although water could also be a reasonable choice instead of Na^+, a sodium ion was chosen because water and the carbonyl group of 4-bromophenylalanine are located appropriately as ligands after symmetry operations, creating a tetracoordinate environment of roughly square-planar geometry. A final TLS model was used for refinement with Refmac5. The crystal structure was deposited to the Protein Data Bank (PDB) with PDB code 4IVH.

PyMOL was used to generate images from the crystallographic data.[10] A β-strand of nine glycine residues (G_9) was used to generate a cartoon of the molecular template Hao-K-Hao-F^{Br}-T. Specifically, the pdb coordinates from each unnatural amino acid Hao were used to generate tri-glycine segments, and the pdb coordinates of the threonine, *p*-bromophenylalanine, and lysine residues were also used to generate three glycine residues of the G_9 β-strand.

---

[8] Emsley, P.; Cowtan, K. *Acta Crystallogr. D Biol. Crystallogr.* **2004**, *60*, 2126–2132.

[9] Murshudov, G. N.; Vagin, A. A.; Dodson, E. J. *Acta Crystallogr. D Biol. Crystallogr.* **1997**, *53*, 240–255.

[10] The PyMOL Molecular Graphics System, Schrödinger, LLC, available at www.pymol.org.

*Modeling of oligomers of linear peptide **2.2**.*

Modeling of an antiparallel β-sheet dimer of linear peptide **2.2** (Figure 2.8): An antiparallel β-sheet dimer of linear peptide **2.2** was modeled from the X-ray crystallographic structure of macrocyclic β-sheet **1**. In PyMOL, one copy of linear peptide **2.2** (Ac-QKLVFFAED-NHMe) was created from the $A\beta_{15–23}$ strand of macrocyclic β-sheet **2.1**. The rotamer of F_{20} with $\chi_1 = 310°$ was selected to avoid inter-chain steric clashes. A second copy of linear peptide **2.2** was then overlaid on the Hao-K-Hao-F^{Br}-T strand of macrocyclic β-sheet **2.1**. Macrocyclic β-sheet **2.1** was then deleted. The dimer was imported into MacroModel.[11] Hydrogen atoms were added. Hydrogen-bonding constraints were applied between the main chains (1.8 Å NH—O distance) and the structure was minimized with the MMFFs force field with GB/SA water solvation. The hydrogen-bonding constraints were removed, and minimization was repeated with the MMFFs force field with GB/SA water solvation to generate a local minimum energy structure.

Modeling of an eight-stranded cruciform oligomer of linear peptide **2.2**, a twenty-four-stranded triangular oligomer of linear peptide **2.2**, and a linear assembly of cruciform oligomers of linear peptide **2.2** (Figure 2.9): Oligomers of linear peptide **2.2** were modeled from the X-ray crystallographic structure of macrocyclic β-sheet **2.1**. In PyMOL, one copy of linear peptide **2.2** (Ac-QKLVFFAED-NHMe) was created from the $A\beta_{15–23}$ strand of macrocyclic β-sheet **2.1**. The rotamer of F_{20} with $\chi_1 = 310°$ was selected to avoid inter-chain steric clashes. A second copy of linear peptide **2.2** was then overlaid on the Hao-K-Hao-F^{Br}-T strand of macrocyclic β-sheet **2.1**. Macrocyclic β-sheet **2.1** was then deleted. Oligomers then were generated by symmetry

[11] Suite 2012: MacroModel, version 9.9, Schrödinger, LLC, New York, NY, 2012.

operations. Each oligomer was imported into MacroModel. Hydrogen atoms were added. Hydrogen-bonding constraints were applied between appropriate main chains (1.8 Å NH—O distance) and the structure was minimized with the MMFFs force field with GB/SA water solvation. The hydrogen-bonding constraints were removed, and minimization was repeated with the MMFFs force field with GB/SA water solvation to generate a local minimum energy structure.

Modeling of alternative eight-stranded cruciform oligomers of peptide **2.2** (Figs. 2.10B&C): Alternative oligomers of linear peptide **2.2** were modeled from the eight-stranded cruciform oligomer of linear peptide **2.2** shown in Figure 2.9A and Figure 2.10A. In PyMOL, the strands of linear peptide **2.2** were translated to create contact between the LFA faces or rotated to create parallel β-sheets. Each oligomer was imported into MacroModel. Hydrogen-bonding constraints were applied between appropriate main chains (1.8 Å NH—O distance) and the structure was minimized with the MMFFs force field with GB/SA water solvation. The hydrogen-bonding constraints were removed, and minimization was repeated with the MMFFs force field with GB/SA water solvation to generate a local minimum energy structure.

Modeling of an alternative linear assembly of cruciform oligomers of linear peptide **2.2** (Figure 2.12B): An alternative linear assembly of cruciform oligomers of linear peptide **2.2** was modeled from the linear assembly of cruciform oligomers of linear peptide **2.2** shown in Figure 2.19E and Figure 2.12A. In PyMOL, the eight-stranded cruciform oligomers in the linear assembly of cruciform oligomers of linear peptide **2.2** were rotated and translated to create assemblies of cruciform oligomers through overlap of the *C*-termini of the β-strands. The oligomer was imported into MacroModel. Hydrogen-bonding constraints were applied between appropriate main chains (1.8 Å NH—O distance) and the structure was minimized with the

MMFFs force field with GB/SA water solvation. The hydrogen-bonding constraints were removed, and minimization was repeated with the MMFFs force field with GB/SA water solvation to generate a local minimum energy structure.

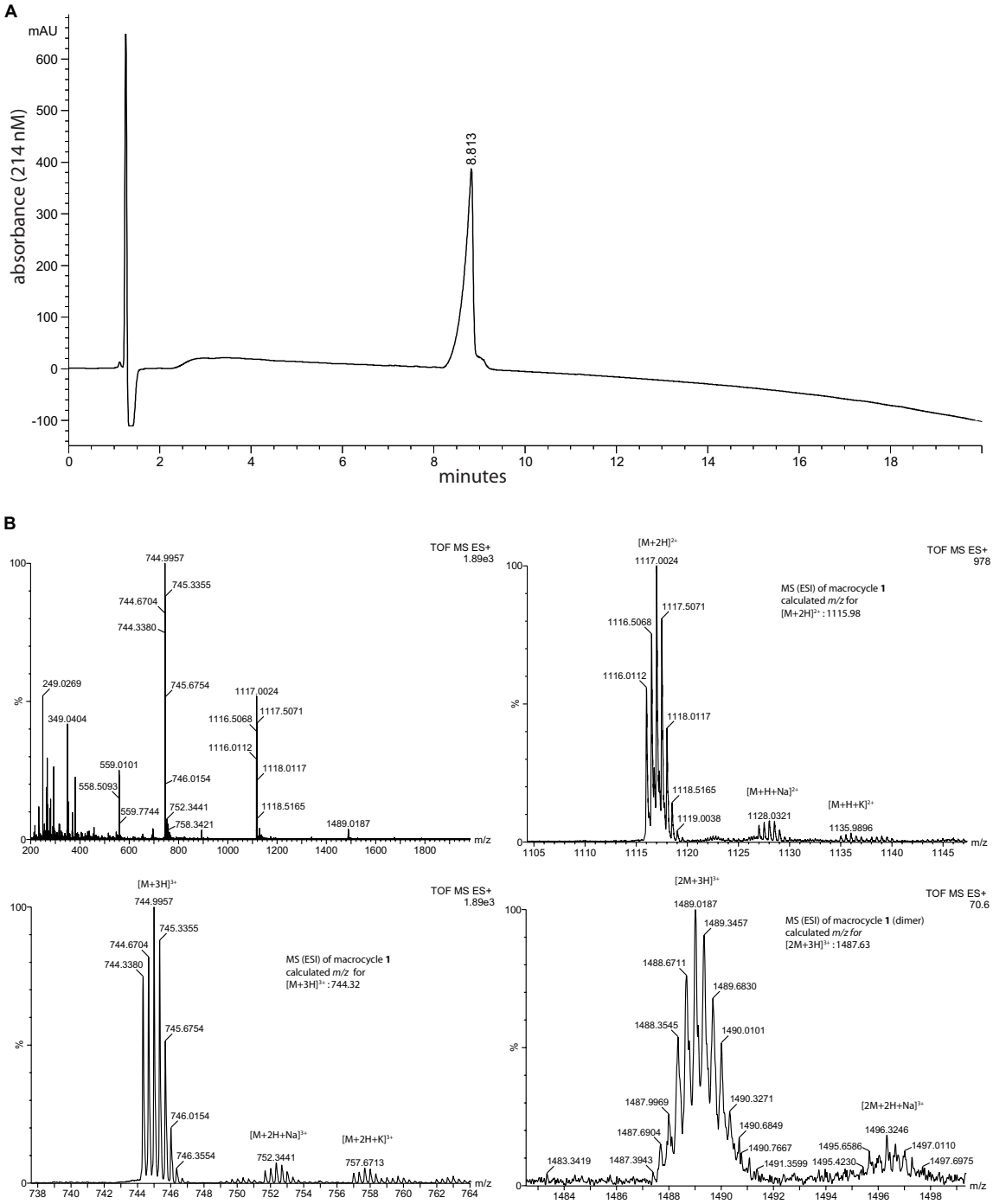

Analytical RP-HPLC trace and electrospray ionization mass spectrum of macrocyclic β-sheet peptide **2.1**. (A) Analytical RP-HPLC trace of macrocyclic β-sheet peptide **2.1**. RP-HPLC was performed with a gradient of 5-100% CH_3CN in H_2O with 0.1% TFA and a flow of 1.0 mL/min over 20 min on an Agilent Zorbax SB-C18 column (50 mm x 4.6 mm). (B) Electrospray ionization mass spectrum (ESI-MS) of macrocyclic β-sheet peptide **2.1** with expansions.

CHAPTER 3

Polymorphism of Oligomers of a Peptide from β-Amyloid

Preamble

Chapter 3 describes solution-phase studies of oligomers of the macrocyclic β-sheet peptide **3.1** (previously described as **2.1** in Chapter 2) and for homologues of the peptide. While the X-ray crystallographic structure of peptide **3.1** is described in Chapter 2, the NMR studies were conducted first for peptide **3.1**. The difference of the structures formed by **3.1** and its homologues in solution state and in solid state is significant and will be discussed in the chapter.

Studies of homologues of **3.1** confirm that the peptide tetramerizes on the LFA face in solution in comparison to the VF face in solid state. While initial findings suggest that peptide **3.1** assembles as a dimer of dimers, further investigations into the types of sheet β-sheet interactions displayed by peptide **3.1** as it assembles warranted further experiments. Thus, I perturbed the hydrogen bonding edge and probed the faces of the peptide by hydroxylating key residues of peptide **3.1**. The results of these experiments confirm that **3.1** tetramerizes as a dimer of hydrogen bonded dimers through the LFA face.

The work conducted in the studies provided me with substantial experience with NMR spectroscopy, which is a necessary tool for organic chemists. In characterizing my structures with utmost detail, I gained an appreciation for the meticulous nature involved with the characterization of large molecules, and for properly organizing the data for this chapter. This chapter reports how the oligomers that form in solution differ from those that form in the solid state, and is an important contribution in supramolecular chemistry beyond the amyloid studies as well.

This chapter is adapted from the paper that I published in the *Journal of the American Chemical Society*.[1]

Reproduced in part with permission from Pham, J. D.; Demeler, B.; Nowick, J. S. *J. Am. Chem. Soc.* **2014**, *136*, 5432–5442. Copyright 2014 American Chemical Society.

Introduction

Soluble amyloid oligomers are now thought to be the main toxic species that cause neurodegeneration in Alzheimer's and other amyloid diseases.[2,3,4,5,6,7,8,9,10,11] Small assemblies made up of dimers, trimers, and tetramers of the β-amyloid peptide (Aβ), as well as larger assemblies such as dodecamers, have been shown to disrupt synaptic activity and cause neuronal cell death. [12,13,14,15,16,17,18] Atomic-level details of the structures of amyloid oligomers are desperately needed in order to understand how the oligomers form and the molecular basis by which they cause neurodegeneration.

The oligomers are polymorphic and dynamic, forming as different species and equilibrating slowly with the monomer and with β-amyloid fibrils, which are generally more stable.[9,10,19,20,21] While the structures of amyloid oligomers are still largely unknown, a number of approaches have been taken to gain insights into their structures. β-Sheet structure and interactions — a common feature of amyloid fibril formation — are generally thought to be important in the structures and interactions of amyloid oligomers.[21,22,23,24,25,26] Incorporation of amyloidogenic peptides into larger proteins can control amyloid supramolecular assembly and allow observation of oligomeric assemblies at atomic resolution.[27] Peptide fragments can also serve as chemical models of oligomers; X-ray crystallographic studies of these peptide fragments have provided insights into the structures of amyloid oligomers.[28,29] Chemical crosslinks within amyloidogenic monomers that stabilize folded β-sheet conformations can promote oligomer formation and help prevent fibril formation.[30,31,32] These crosslinked systems are more amenable to study and can provide simpler and more stable chemical models of the unstable oligomers formed by amyloidogenic peptides and proteins. Computational models of oligomers have been

constructed from atomic-level structures of amyloid fibrils, which are understood far better at atomic resolution than the oligomers.[33,34,35]

Our laboratory is gaining insights into the structures and interactions of amyloid oligomers by combining fragments of amyloidogenic peptides and proteins with molecular templates to create macrocycles that promote β-sheet structure and interactions while blocking amyloid fibril formation.[36,37] We recently reported the X-ray crystallographic structures of oligomers of a peptide from β-amyloid.[38] We incorporated the nonapeptide sequence QKLVFFAED ($A\beta_{15\text{-}23}$) into macrocyclic β-sheet peptide **3.1**, with δ-linked ornithine turn units and a template strand that features an unnatural amino acid, Hao.[39,40] In the solid state, the macrocycle folds to form a β-sheet. The β-sheet forms a hydrogen-bonded dimer, which assembles face-to-face to make a cruciform tetramer, which is a key subunit of the lattice. The cruciform tetramers assemble into triangular dodecamers, and the triangular dodecamers further assemble into the lattice.

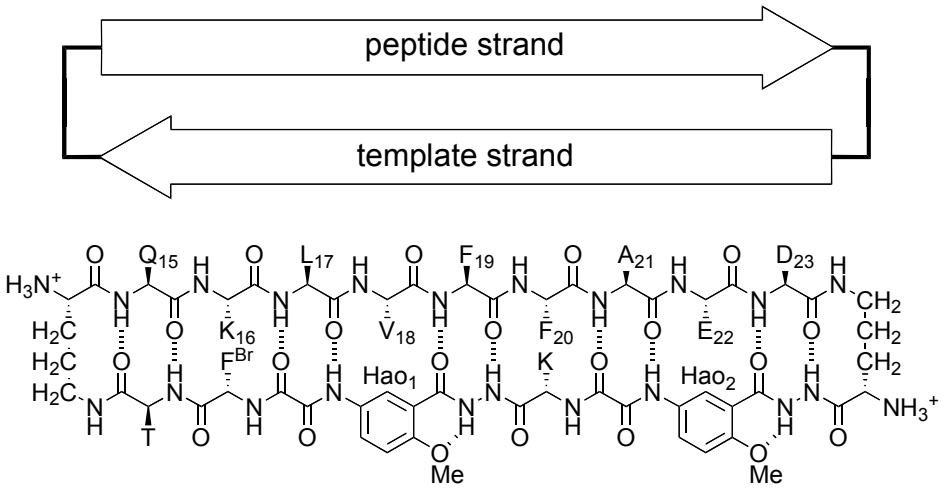

macrocyclic β-sheet peptide **3.1**

The hydrogen-bonded dimers are antiparallel, and the β-strands are fully aligned, with residues 17–23 of one of the macrocycles aligned with residues 23–17 of the other. The resulting four-stranded β-sheet forms a plane, with the side chains projecting from the upper and lower faces of the plane. Residues K_{16}, V_{18}, F_{20}, and E_{22} of each macrocycle project from one face of the plane (the *VF face*), and residues Q_{15}, L_{17}, F_{19}, A_{21}, D_{23} of each macrocycle project from the other face of the plane (the *LFA face*). The VF face has the hydrophobic residues V_{18} and F_{20} flanked by the polar residues K_{16} and E_{22}. The LFA face has the hydrophobic residues L_{17}, F_{19}, and A_{21} flanked by the polar residues Q_{15} and D_{23}. The hydrogen-bonded dimers assemble in a crisscross fashion through hydrophobic interactions between the VF faces to give the cruciform tetramers. Figure 3.1 illustrates the faces of the macrocycle and the structure of the cruciform tetramer.

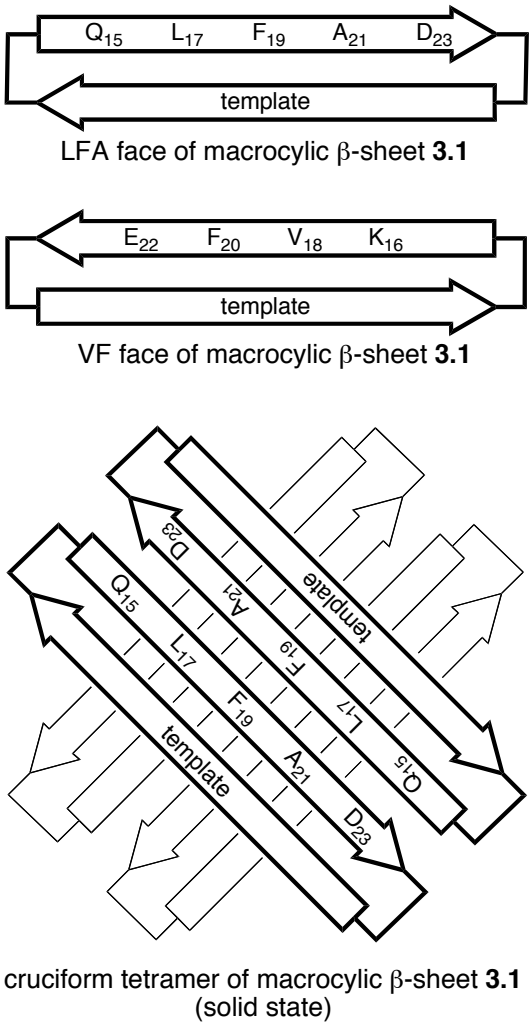

Figure 3.1. Cartoon illustrating the LFA and VF faces of macrocyclic β-sheet **3.1** and the cruciform tetramer formed in the solid state. The VF faces form the inner hydrophobic core of the cruciform tetramer, and the LFA faces form the outer surface.

In the current study, we set out to determine how macrocyclic β-sheet peptides containing the $A\beta_{15\text{-}23}$ nonapeptide assemble in solution. We began by using ^{1}H NMR spectroscopy to study how macrocyclic β-sheet peptide **3.2a** folds and oligomerizes in aqueous solution. We had envisioned macrocyclic β-sheet **3.1** as a homologue of macrocyclic β-sheet **3.2a**. The two molecules differ only in that **3.1** contains a *p*-bromophenylalanine (F^{Br}) in the template strand, for single anomalous dispersion (SAD) phasing in X-ray crystallographic structure

determination, while **3.2a** contains a tyrosine.[38] As our studies of macrocyclic β-sheet **3.2a** unfolded, we prepared additional homologues (**3.2b**, **3.2c**, **3.3**, and **3.4**) to interrogate the assembly process. The following describes these studies and elucidates how the tetramer that forms in solution differs from that which forms in the solid state.

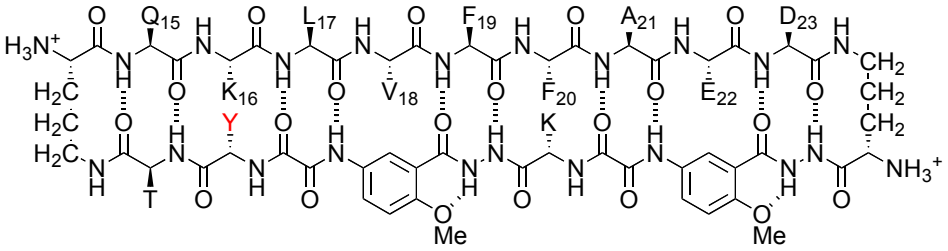

macrocyclic β-sheet peptide **3.2a**

Results

1. Tetramerization of Macrocyclic β-Sheet Peptides 3.1 and 3.2a. We investigated the folding and assembly of the macrocyclic β-sheets in D_2O and in H_2O-D_2O solution by NMR spectroscopy. At millimolar concentrations, the ^{1}H NMR spectrum of macrocyclic β-sheet **3.2a** is disperse, with methyl resonances from L_{17} and A_{21} unusually upfield (-0.35 and 0.49 ppm), aromatic resonances from F_{19} unusually upfield (6.28 and 6.52 ppm), and many of the amino acid α-protons unusually downfield (≥ 5.0 ppm). One of the resonances from one of the Hao amino acids (the H_4 resonance of Hao_1) appears unusually downfield at 9.17 ppm. The upfield shifting of the aromatic and aliphatic resonances is characteristic of the formation of an oligomer with a well-packed hydrophobic core comprising aromatic residues (Hao, Phe, etc.) and aliphatic residues (Leu, Ala, etc.). Minor additional resonances, associated with a monomer lacking a

hydrophobic core are also present, most notably at 0.69–0.79 ppm (L_{17} and V_{18}). Figure 3.2 illustrates the ^{1}H NMR spectrum of macrocyclic β-sheet **3.2a** at 2.0 mM in D_2O solution.

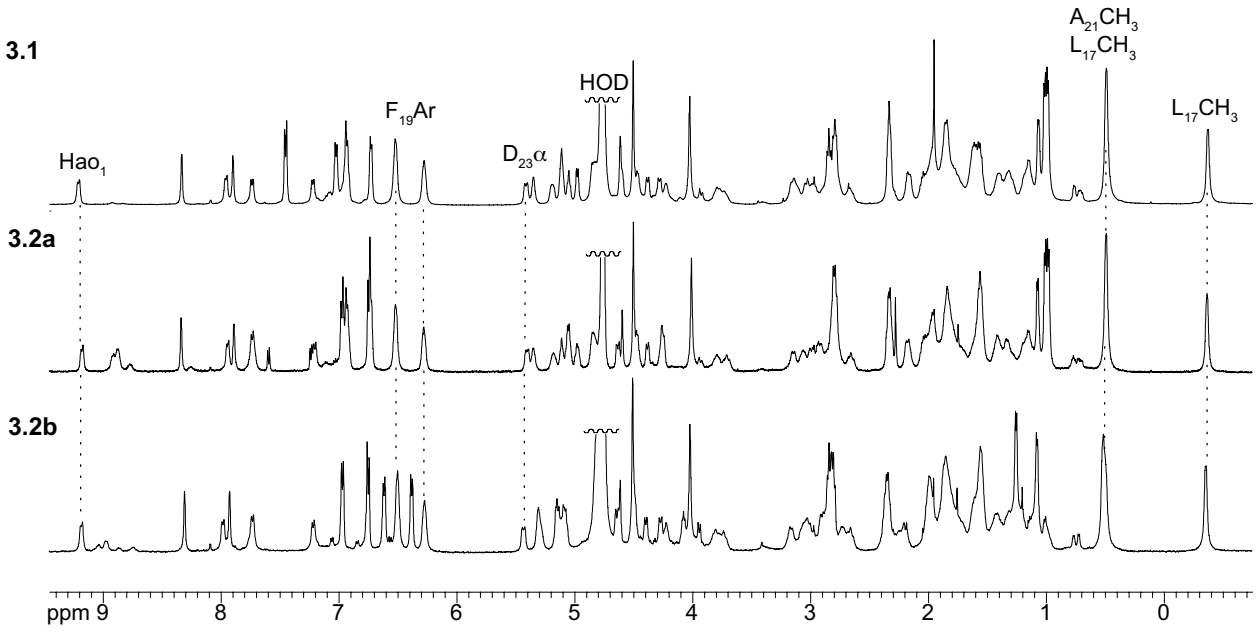

Figure 3.2. ^{1}H NMR spectra of macrocyclic β-sheet peptides **3.1**, **3.2a**, and **3.2b** at 2.0 mM in D_2O at 500 MHz and 298 K. Noteworthy resonances that reflect important shared features of the folding and assembly of these peptides are labeled and highlighted with dashed lines.

The ^{1}H NMR spectrum of macrocyclic β-sheet **3.1** is virtually identical to that of macrocyclic β-sheet **3.2a**, indicating that both peptides fold and oligomerize in a similar fashion in solution. The ^{1}H NMR spectrum of macrocyclic β-sheet **3.1** also exhibits additional minor resonances from L_{17} and V_{18} associated with a monomer lacking a hydrophobic core. These resonances are similar in intensity to those of macrocyclic β-sheet **3.2a**, indicating that the oligomers formed by both macrocycles are similar in association constant (K_{assoc}) as well as in structure.

^{1}H NMR NOESY studies establish the formation of hydrogen-bonded dimers that are antiparallel, with the β-strands of residues 17–23 shifted out of alignment by two residues toward the C-termini (Figure 3.4). Notably, the NOESY spectrum in D_2O exhibits strong NOEs between

the α-protons of L_{17} and D_{23} and between the α-protons of F_{19} and A_{21} (Figure 3.5). These NOEs reflect dimer formation. Additional strong NOEs associated with β-sheet folding of the macrocycles occur between the α-protons of K_{16} and Y and between the α-protons of F_{20} and K (Figure 3.5).

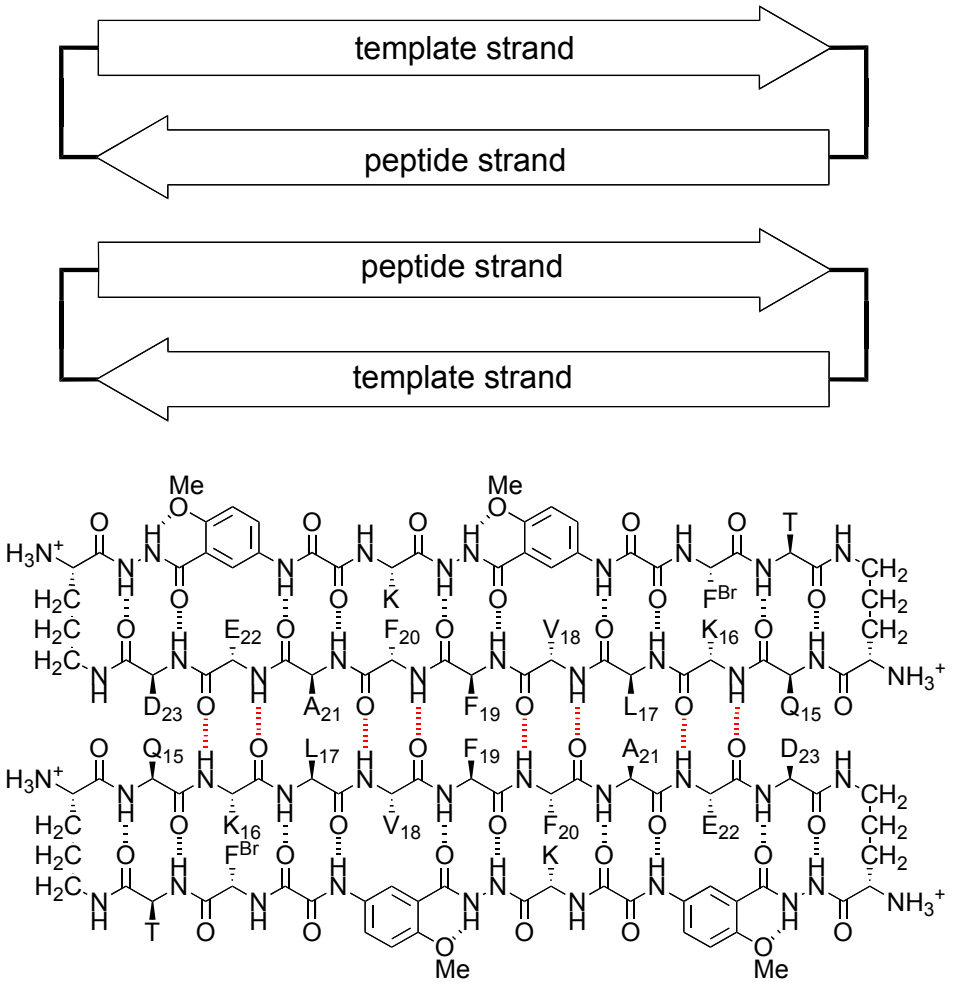

Figure 3.3. Cartoons and chemical structure illustrating the hydrogen-bonded dimer formed by macrocyclic β-sheet peptide **3.1** in the solid state. The hydrogen-bonded dimer is antiparallel where residues 17–23 of one of the macrocycles align with residues 23–17 of the other.

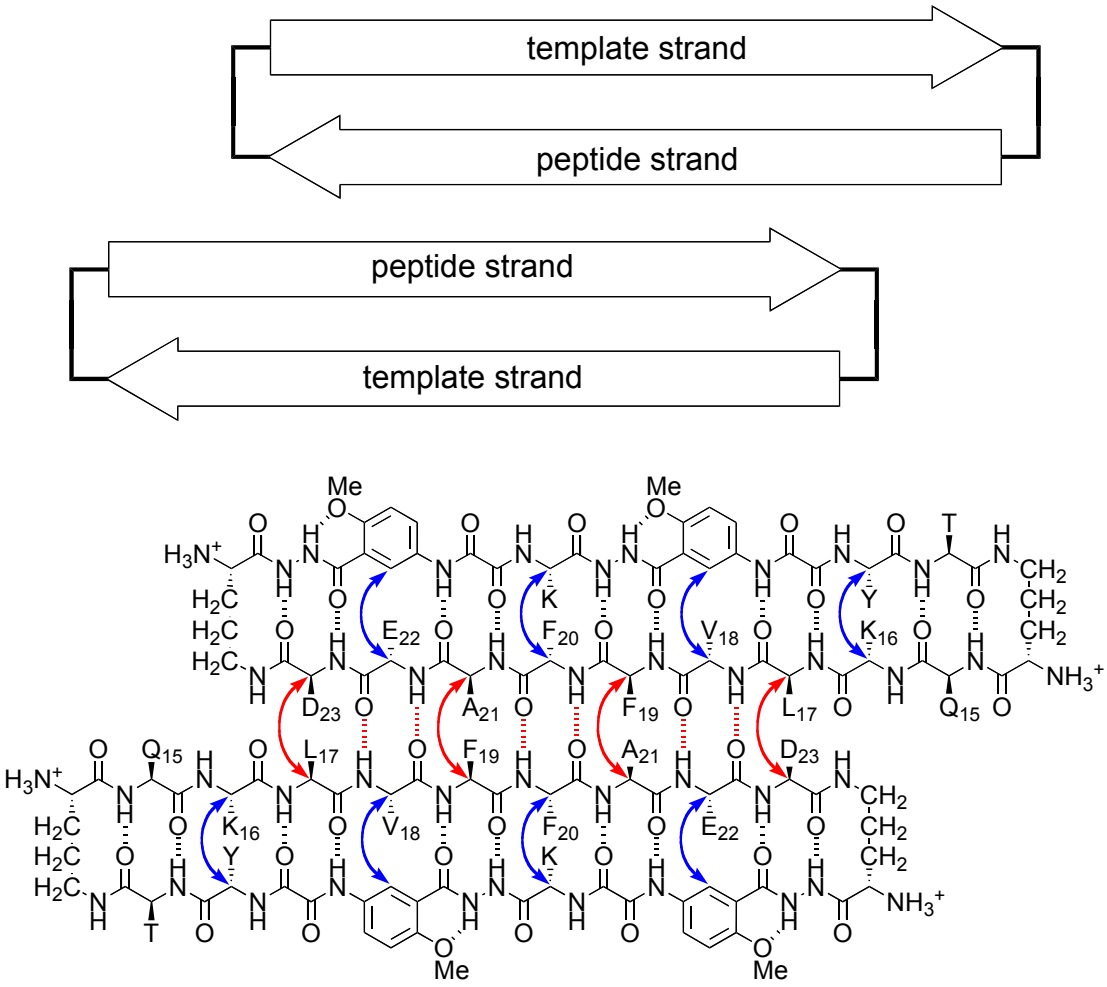

Figure 3.4. Cartoons and chemical structure illustrating the hydrogen-bonded dimer formed by macrocyclic β-sheet peptide **3.1, 3.2a,** and **3.2b** in the solution. The hydrogen-bonded dimer is antiparallel where the β-strands are shifted out of alignment by two residues toward the C-termini. Key NOEs associated with solution-state dimerization and folding of **3.2a** are shown with red and blue arrows.

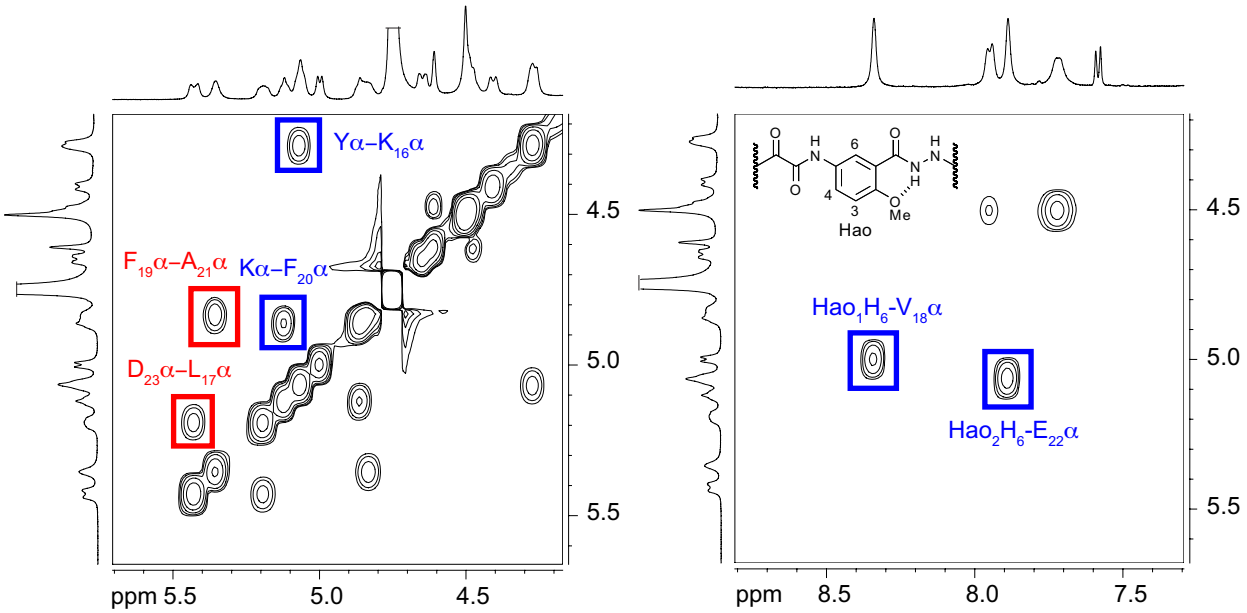

Figure 3.5. Selected expansions of the NOESY spectrum of macrocyclic β-sheet peptide **3.2a** at 8.0 mM in D_2O at 500 MHz and 300.5 K. Key intermolecular interstrand NOEs associated with dimerization are highlighted in red; key intramolecular interstrand NOEs associated with folding are highlighted in blue.

Other NOEs characteristic of folding are described in detail in Figure 3.6, as are additional NOEs associated with folding and dimerization that are seen in the NOESY spectrum in H_2O–D_2O (90:10) (Figure 3.7). Macrocyclic β-sheet **3.1** exhibits similar patterns of NOEs, indicating that it folds and dimerizes in a similar fashion to macrocycle **3.2a** (Figures 3.8 & 3.9). The shifted structure of the dimers formed by the macrocycles in solution stands in sharp contrast to the aligned structure of macrocycle **3.1** in the solid state (Figure 3.3).

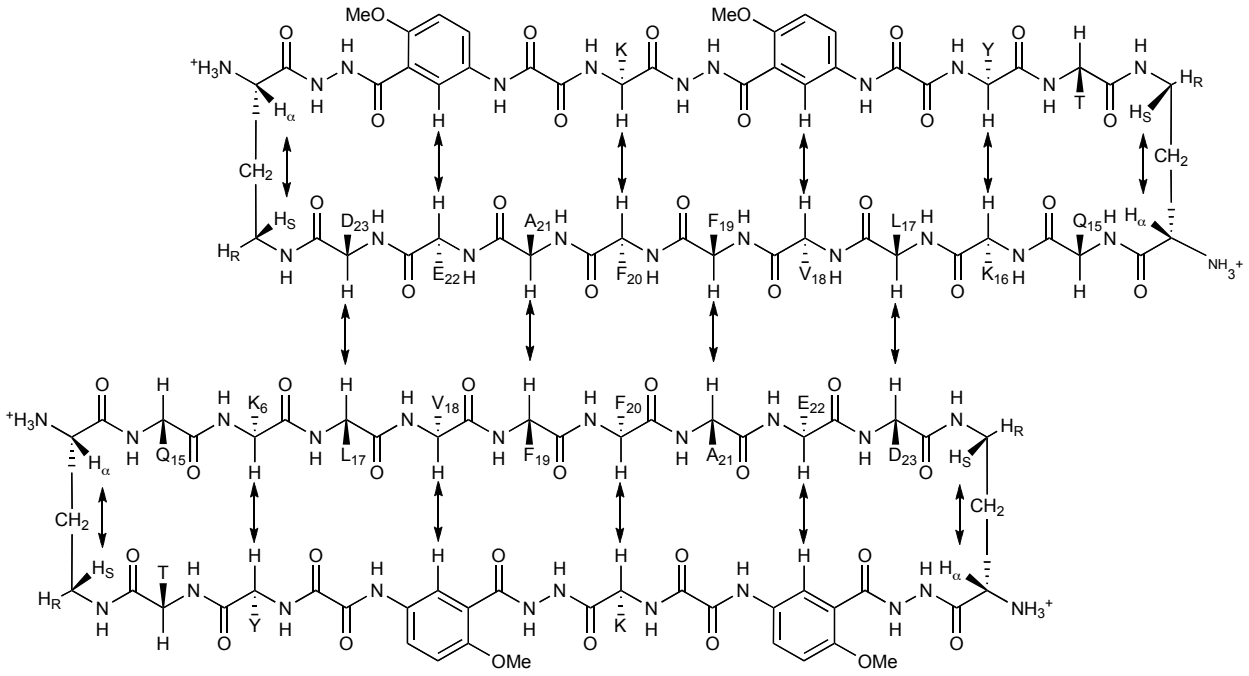

Figure 3.6. Key NOEs associated with folding and dimerization of macrocyclic β-sheet peptide **3.2a**. Interstrand main chain-main chain NOEs were observed for **3.2a** in the NOESY 800 MHz spectrum with WATERGATE (8.0 mM in H2O-D2O (9:1) and 298 K).

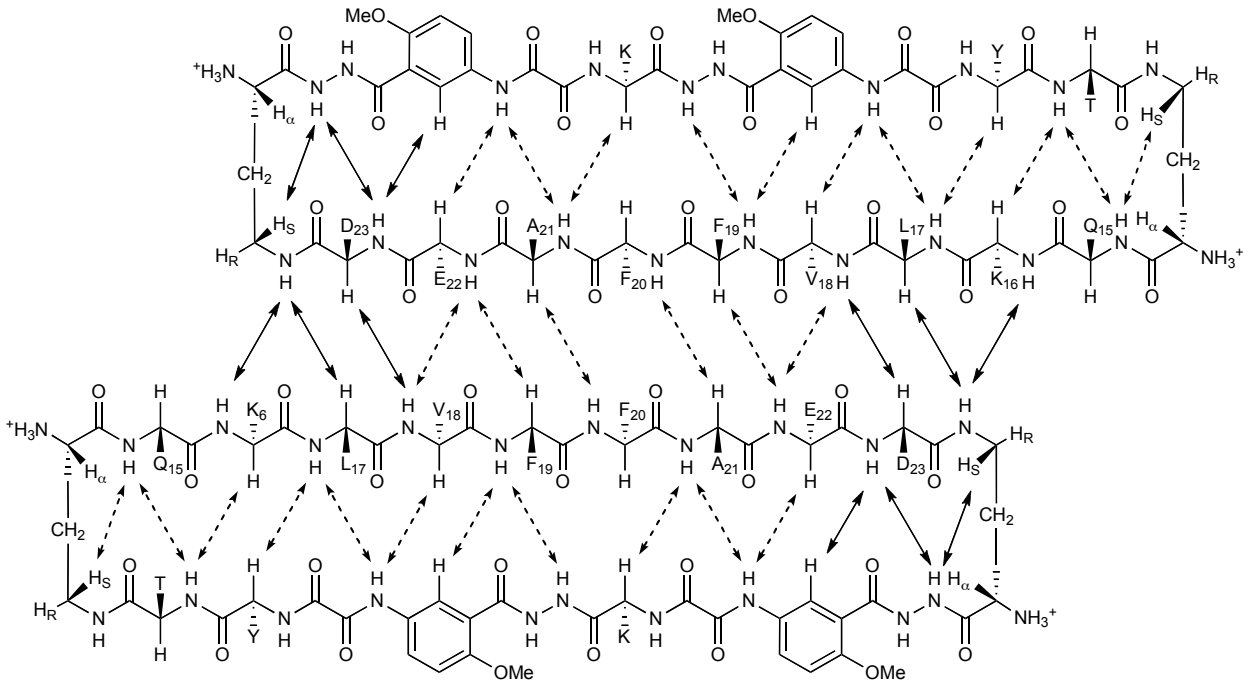

Figure 3.7. Key NOEs associated with folding and dimerization of macrocyclic β-sheet peptide **3.2a**. Interstrand main chain-main chain NOEs were observed for **3.2a** in the NOESY 800 MHz spectrum with WATERGATE (8.0 mM in H2O-D2O (9:1) and 298 K). Dashed lines represent weak or ambiguous NOEs.

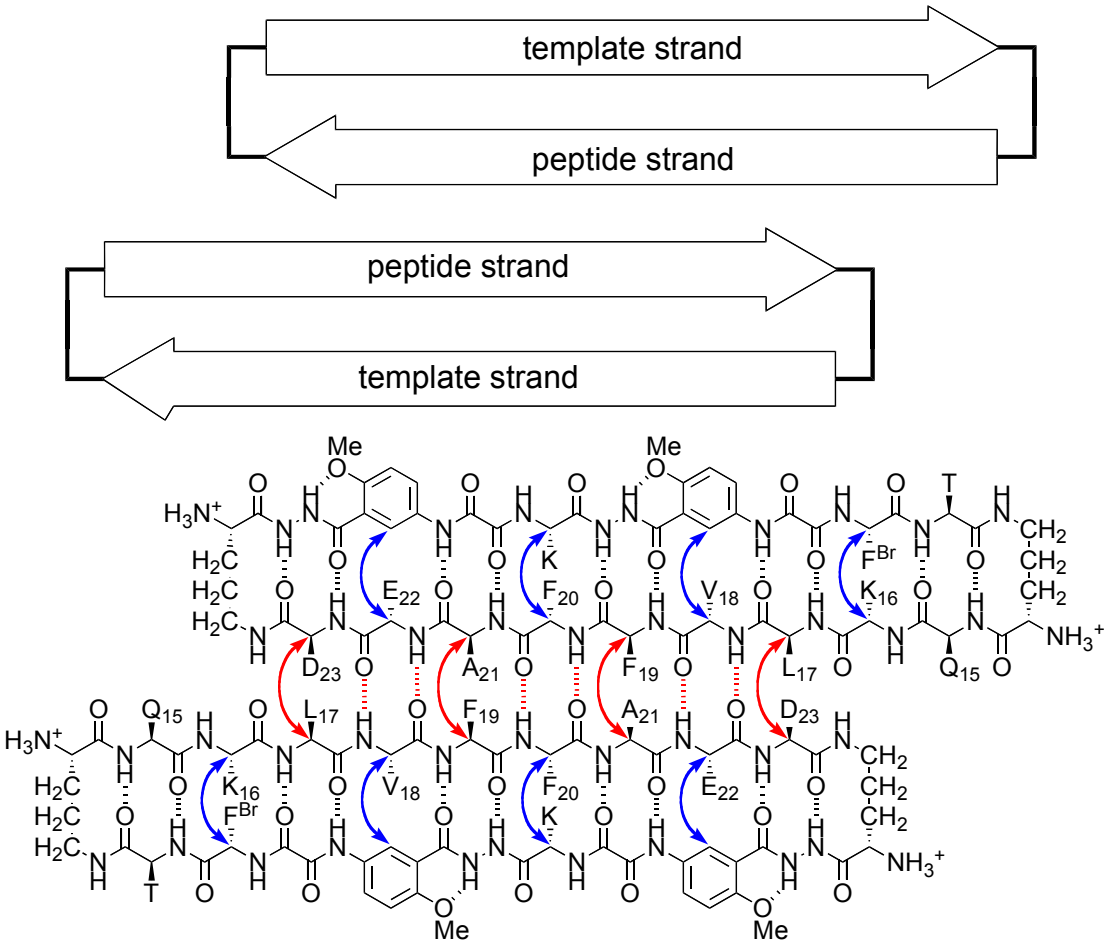

Figure 3.8. Cartoon and chemical structure illustrating the hydrogen-bonded dimer formed by macrocyclic sheet β-peptide **3.1** in solution. Key NOEs associated with solution-state dimerization and folding of **3.1** are shown with red and blue arrows.

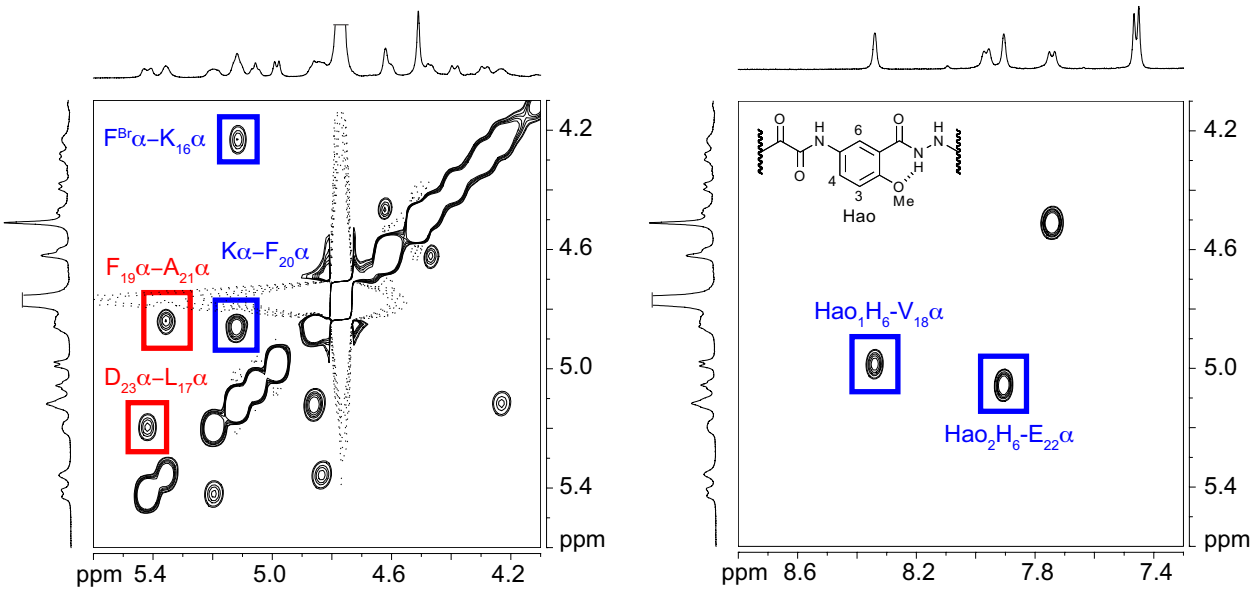

Figure 3.9. Selected expansions of the NOESY spectrum of macrocyclic β-sheet peptide **3.1** at 2.0 mM in D_2O at 500 MHz and 298 K. Key intermolecular interstrand NOEs associated with dimerization are highlighted in red; key intramolecular interstrand NOEs associated with folding are highlighted in blue.

At low concentrations (e.g., ≤ 0.1 mM), the monomer predominates in the ^{1}H NMR spectrum of macrocyclic β-sheet **3.2a**. The methyl resonances from L_{17} and V_{18} of the monomer are prominent at 0.69–0.79 ppm, and the methyl resonances from L_{17} and A_{21} of the oligomer at -0.35 and 0.49 ppm are small. As the concentration of **3.2a** is increased, the relative intensities of the resonances from the oligomer increase and the relative intensities of the resonances from the monomer decrease (Figure 3.10). At 0.2 mM, the resonances of the monomer and oligomer are roughly equal in intensity. At 0.2 mM, if the oligomer is a tetramer, then the molar concentration of the tetramer is roughly one-fourth the molar concentration of the monomer (i.e., [**3.2a**$_4$] ≈ 0.025 mM and [**3.2a**] ≈ 0.1 mM). These concentrations correspond to an equilibrium constant K_{assoc} for monomer-to-tetramer association of roughly 2.5 x 10^{11} M^{-3}. At high concentrations (e.g., 8.0 mM), the resonances of the monomer are barely visible. The strong concentration

dependence of the monomer-oligomer equilibrium is not consistent with a simple monomer-dimer equilibrium, but rather reflects cooperative association in which the dimers are a subunit of a higher-order oligomer — in this case a tetramer consisting of a dimer of dimers.

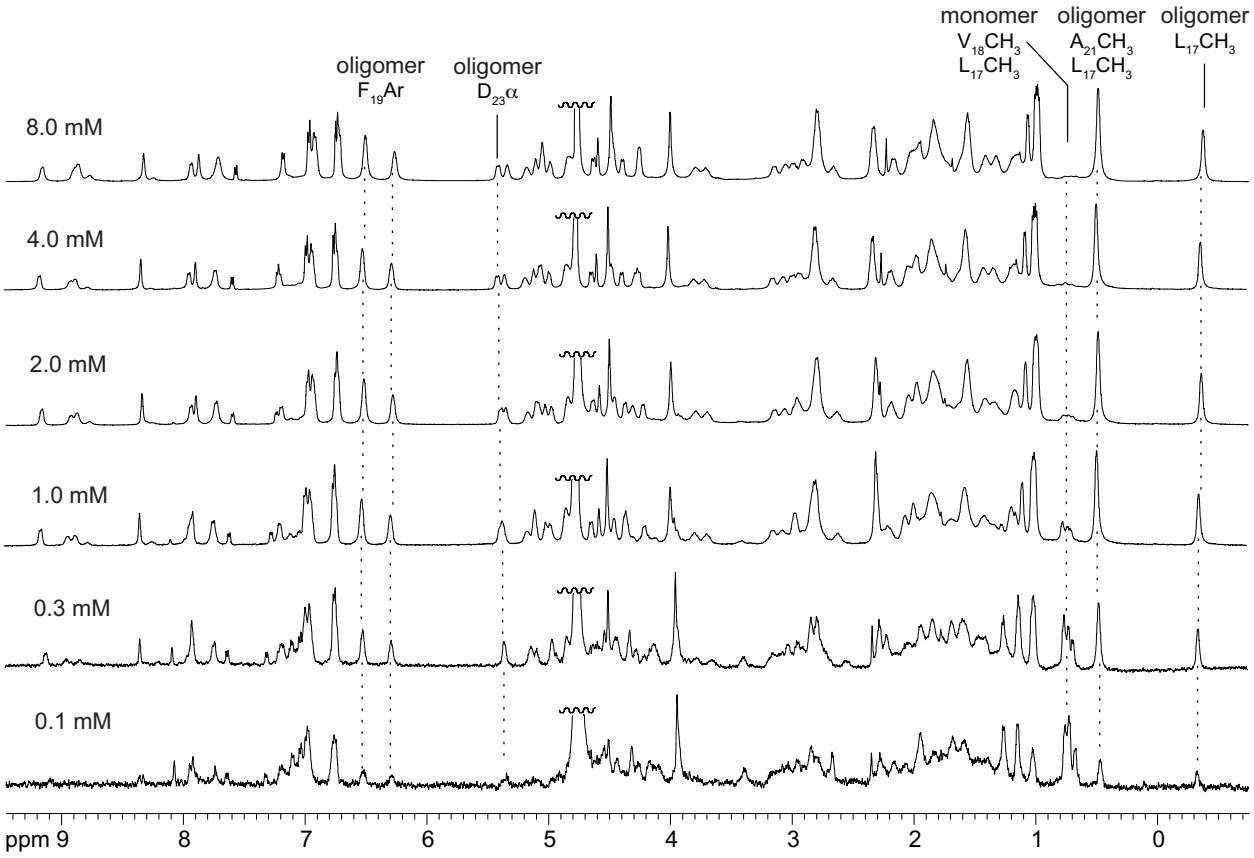

Figure 3.10 ^{1}H NMR spectra of macrocyclic β-sheet peptide **3.2a** at various concentrations in D_2O at 500 MHz and 298 K. Noteworthy characteristic resonances of the monomer and the oligomer are labeled and highlighted with dashed lines.

An EXSY experiment of macrocyclic β-sheet peptide **3.2a** shows that the oligomer is in equilibrium with the monomer. The EXSY experiment was carried out using a ROESY pulse sequence at 2.0 mM in D_2O at 350 K with a mixing time of 200 ms for **3.2a**. Exchange crosspeaks have the same phase as the diagonal while ROESY crosspeaks have the opposite phase to the diagonal. Crosspeaks from chemical exchange between the methyl resonances of the

monomer and the oligomer for L_{17} are seen in the EXSY spectrum (Figure 3.11). Crosspeaks from chemical exchange between the methyl resonances of the monomer and the oligomer for V_{18} and A_{18} are also seen in the EXSY spectrum (Figure 3.11). Additional EXSY crosspeaks involving the aromatic resonances from F_{19} and various α-proton resonances are also seen. (experimental data for Chapter 3).

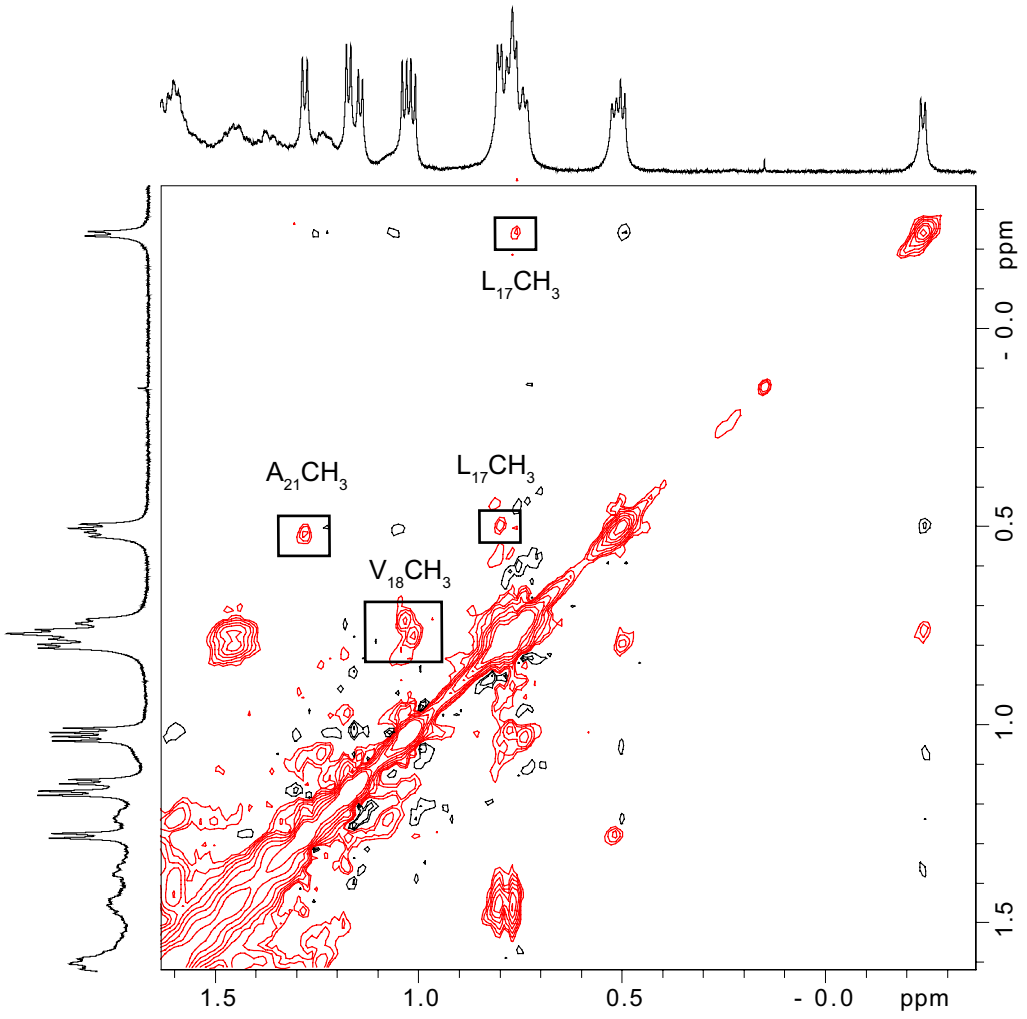

Figure 3.11. Selected expansion of the ROESY spectrum of macrocyclic β-sheet peptide **3.2a** at 2.0 mM in D_2O at 600 MHz and 350 K. EXSY crosspeaks in the ROESY spectrum have the same phase as the diagonal and are shown in red; ROESY crosspeaks have the opposite phase and are shown in black). Key EXSY crosspeaks associated with exchange between monomer and tetramer are highlighted.

The NOESY spectrum of macrocyclic β-sheet **3.2a** shows additional crosspeaks that are

consistent with a tetramer in which two hydrogen-bonded dimers form a sandwich-like assembly. Notably, the NOESY spectrum in D_2O exhibits NOEs between Hao_2 and threonine and between Hao_2 and Hao_1 that only make sense as interlayer NOEs between the hydrogen-bonded dimers. Specifically, the methoxy group of Hao_2 gives NOEs with the methyl group of threonine, and the H_3 and H_4 protons of Hao_2 give NOEs with the H_3 and H_4 protons of Hao_1. Figure 3.12 illustrates these interlayer NOE crosspeaks in the NOESY spectrum; Figure 3.13 illustrates the sandwich-like assembly consistent with these NOEs. Additional interlayer NOEs consistent with the sandwich-like assembly shown in Figure 3.14 are summarized in Table 3.1. Figure 3.14 and Table 3.1 provide additional data.

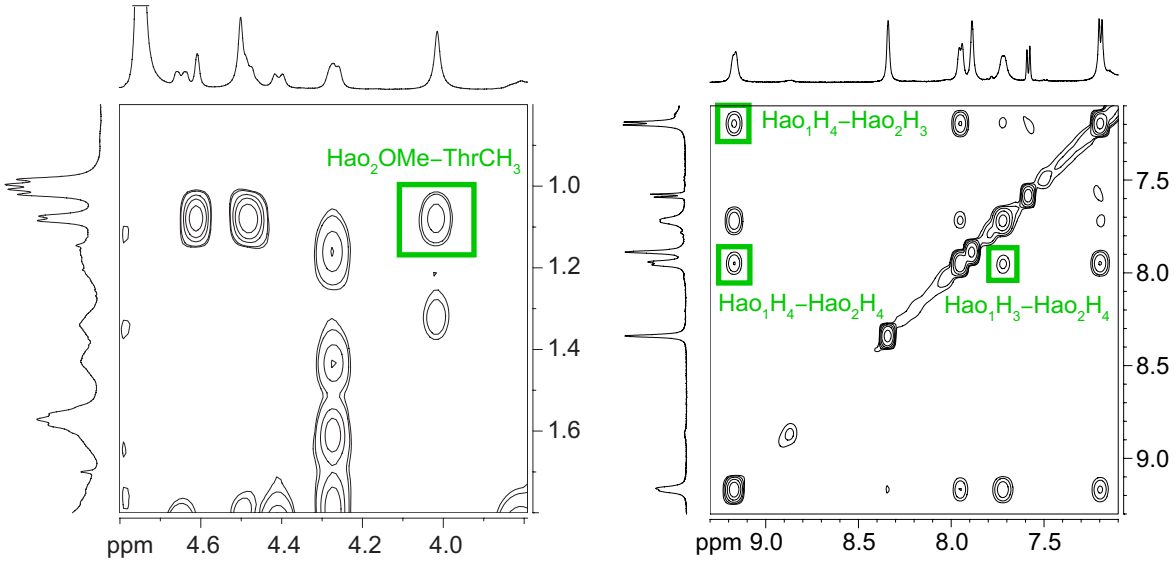

Figure 3.12. Selected expansions of the NOESY spectrum of macrocyclic β-sheet peptide **3.2a** at 8.0 mM in D_2O at 500 MHz and 300.5 K. Key interlayer NOEs associated with tetramerization are highlighted in green.

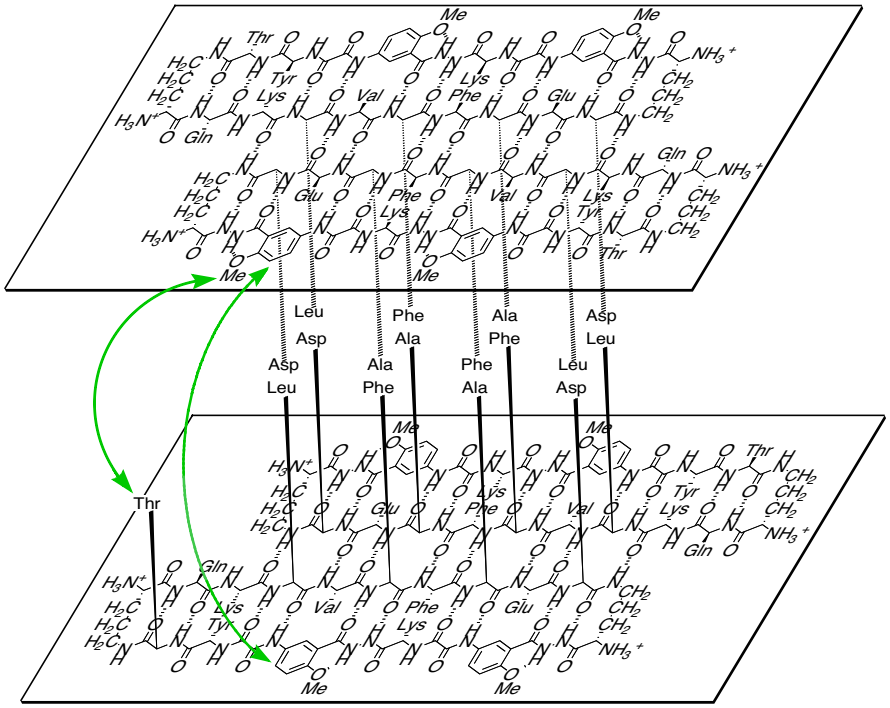

Figure 3.13. Illustration of the tetramer formed as a sandwich-like assembly of two hydrogen-bonded dimers of macrocyclic β-sheet peptide **3.2a** in aqueous solution. The green arrow shows key NOEs between the layered β-sheets. Four sets of these interactions can occur in the tetramer. (For clarity, only one set is shown.) Macrocyclic β-sheet peptide **3.1** forms a similar sandwich-like tetramer in solution.

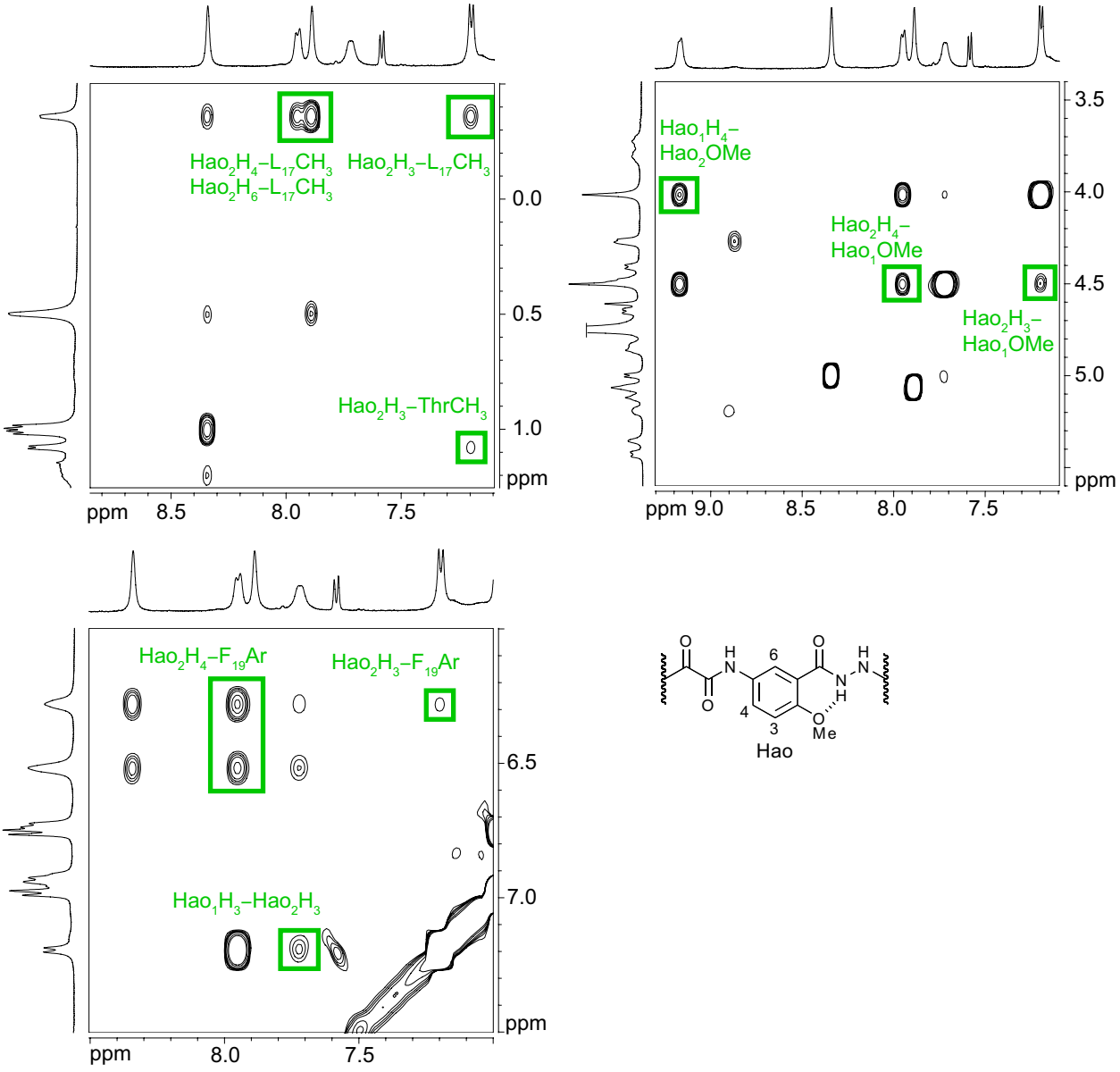

Figure 3.14. Selected expansions of the NOESY spectrum of macrocyclic β-sheet peptide **3.2a** at 8.0 mM in D_2O at 500 MHz and 300.5 K. Key interlayer NOEs associated with tetramerization are highlighted in green.

Table 3.1. Key NOEs associated with interlayer contacts in tetramer formation of 3.2a.[a]

	Hao_2H_3	Hao_2H_4	Hao_2H_6	Hao_2OMe
$F_{19}Ar$	weak	strong	-	-
$L_{17}\delta$	medium	medium	strong	-
$T\gamma$	weak	-	-	medium
Hao_1H_3	weak	medium	-	-
Hao_1H_4	strong	strong	-	strong
Hao_1OMe	weak	strong	-	-

[a]Interlayer contacts are observed in Figure 3.12 and Figure 3.14.

The four threonines of the tetramer point toward the interior of the sandwich-like assembly, as do all of the residues on the LFA faces of the β-sheets (Q_{15}, L_{17}, F_{19}, A_{21}, and D_{23}). The magnetic anisotropy from the packed aromatic groups of the resulting hydrophobic core shift the methyl resonances of L_{17} and A_{21} upfield. The magnetic anisotropy also shifts the aromatic ring protons of F_{19} upfield. Thus, the structure of this solution-state tetramer, in which the LFA faces make up the hydrophobic core, differs markedly from the structure of the solid-state tetramer, in which the VF faces make up the hydrophobic core. In the solid-state structure, the LFA faces are on the exterior of the tetramer and the VF faces are on the interior; in the solution-state structure, the VF faces are on the exterior and the LFA faces are on the interior.

2. Disruption of Tetramer Formation. To probe the assembly of the tetramer, we studied macrocyclic β-sheet peptide **3.3**. Macrocyclic β-sheet **3.3** is a homologue of **3.2a** with a lysine in place of the threonine in the template strand. At 1.0 mM essentially no tetramer is observed in the ^{1}H NMR spectrum of **3.3** (Figure 3.15). As the concentration is increased to 2.0 and 4.0 mM, resonances for the tetramer appear; at 8.0 mM the tetramer predominates. The tetramerization is far weaker than that of macrocyclic β-sheet **3.2a**, in which the tetramer is observed at 0.1 mM and predominates at 0.3 mM.

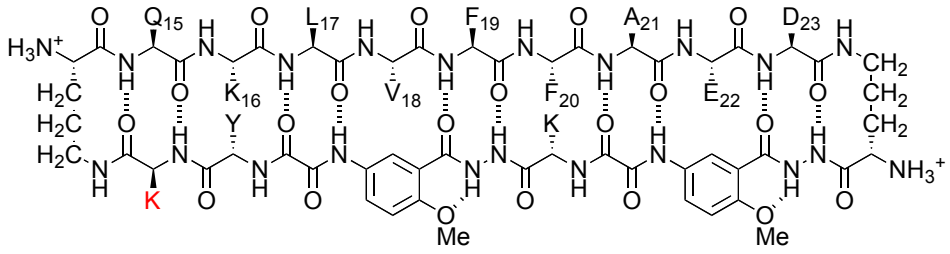

macrocyclic β-sheet peptide **3.3**

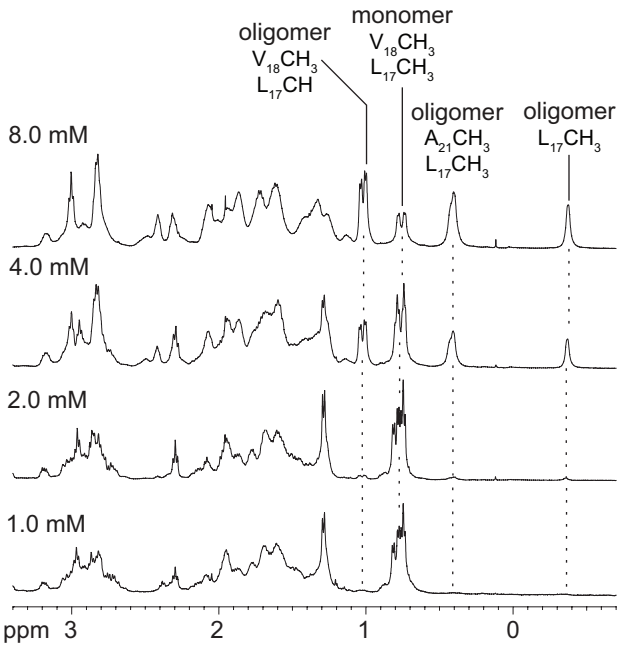

Figure 3.15. Expansions of the ^{1}H NMR spectra of macrocyclic β-sheet peptide **3.3** at various concentrations in D_2O at 500 MHz and 298 K. Noteworthy characteristic resonances of the monomer and the oligomer are labeled and highlighted with dashed lines.

Addition of salt (NaCl) augments tetramer formation, suggesting that intermolecular ionic repulsion is partially responsible for the diminished tetramerization of macrocyclic β-sheet **3.3**. Without NaCl, macrocyclic β-sheet **3.3** is 46% tetramerized at 4.0 mM; with 25 mM NaCl, it is 70% tetramerized; with 150 mM NaCl, it is 80% tetramerized (Figure 3.16 and Table 3.2). The loss of hydrophobic interactions between the methyl group of threonine and the methoxy group

of Hao_2 may also contribute to the diminished stability of the tetramer of macrocyclic β-sheet **3.3**.

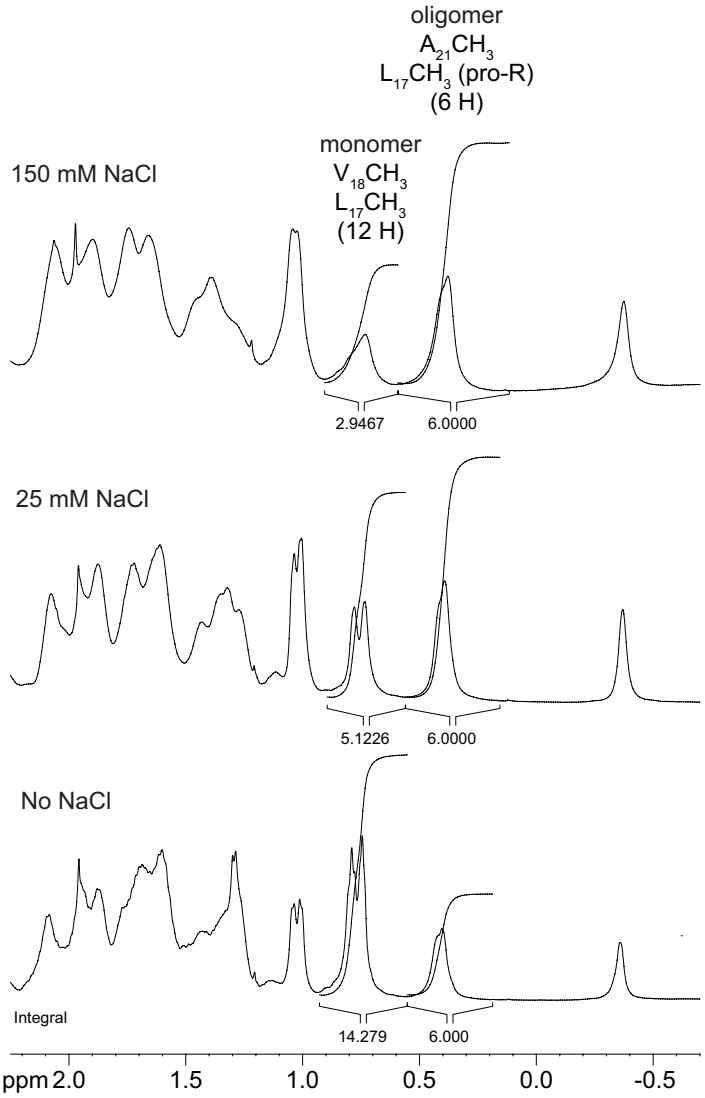

Figure 3.16. Expansions of the ^{1}H NMR spectra of macrocyclic β-sheet peptide **3.3** at 4.0 mM in D_2O at 500 MHz and 298 K with 0 mM, 25 mM NaCl, and 150 mM NaCl.

Table 3.2. Percentage of monomer and tetramer of 3.3 at 4.0 mM with 0, 25, and 150 mM NaCl (based on the relative integrals for selected ^{1}H NMR resonances).

[NaCl] (mM)	$L_{17}CH_3$, $V_{18}CH_3$ (as monomer)	$L_{17}CH_3$ (*pro*-R), $A_{21}CH_3$ (as oligomer)	% Monomer	% Tetramer
0	1.19/H	1.00/H	54.3	45.7
25	0.43/H	1.00/H	29.9	70.1
150	0.25/H	1.00/H	19.7	80.3

In comparison to macrocyclic β-sheet **3.2a**, addition of salt also augments tetramer formation of macrocyclic β-sheet **3.2a**: Without NaCl, macrocylic β-sheet **3.2a** is 56% tetramerized at 0.3 mM; with 25 mM NaCl, it is 82% tetramerized (Figure 3.17 and Table 3.3).

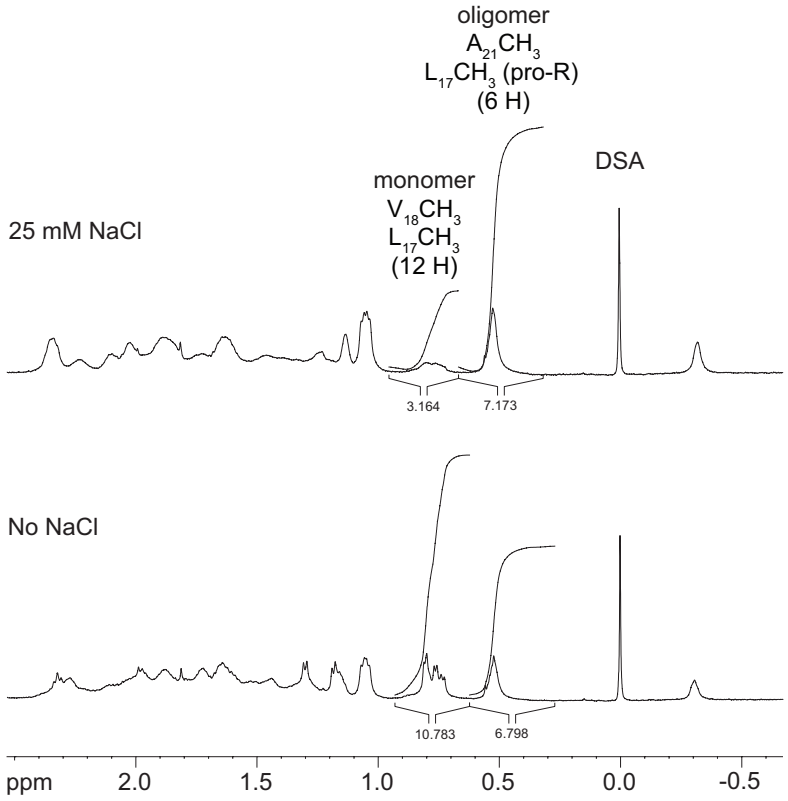

Figure 3.17. Expansions of the ^{1}H NMR spectra of macrocyclic β-sheet peptide **3.2a** at 0.3 mM in D_2O at 500 MHz and 298 K with 0 mM and 25 mM NaCl. (DSA = 4,4-dimethyl-4-silapentane-1-ammonium trifluoroacetate.)

Table 3.3. Percentage of monomer and tetramer of 3.2a at 0.3 mM with 0 and 25 mM NaCl (based on the relative integrals for selected ^{1}H NMR resonances).

[NaCl] (mM)	$L_{17}CH_3$, $V_{18}CH_3$ (as monomer)	$L_{17}CH_3$ (*pro*-R), $A_{21}CH_3$ (as oligomer)	% Monomer	% Tetramer
0	0.90/H	1.13/H	44.2	55.8
25	0.26/H	1.20/H	18.1	81.9

Diffusion-ordered spectroscopy (DOSY) NMR studies support the formation of a tetrameric species.[41,42] Measurement of the DOSY spectrum of macrocyclic β-sheet peptide **3.2a** in D_2O at 2.0 mM and 8.0 mM and 298 K gave a diffusion coefficient of 10.0 x 10^{-7} cm^2/s and 10.1 x 10^{-7} cm^2/s, respectively, for the oligomer.[43] As is expected, the diffusion coefficient of the tetramer of **3.2a** is slightly lower than that of a lighter tetramer of a smaller peptide that we had studied previously. Dr. Omid Khakshoor reported a diffusion coefficient value of 12.0 x 10^{-7} cm^2/s for a 6.4 kDa tetramer while **3.2a** has a diffusion coefficient value of 10.0 x 10^{-7} cm^2/s for a 8.9 kDa tetramer.

The diffusion coefficient does not vary from 2.0 mM to 8.0 mM, suggesting the presence of a single oligomerization state. The low concentration of monomer precluded measurement of its diffusion coefficient for comparison. Measurement of the DOSY spectrum of macrocyclic β-sheet peptide **3.3** in D_2O at 2.0 mM and 298 K gave a diffusion coefficient of 16.4 x 10^{-7} cm^2/s for the corresponding monomer. Consistent with tetramer formation, the diffusion coefficient of the oligomer of macrocyclic β-sheet peptide **3.2a** is 0.61 times that of the monomer of macrocyclic β-sheet peptide **3.3**.[42,43,44,45]

3. Facial Control of Tetramerization in Macrocyclic β-Sheet Peptides 3.2b and 3.2c.

To further study the assembly of the tetramer, we mutated residues on the LFA and VF faces to examine how the hydrophobic residues on each face control tetramer formation. We created two double mutants of **3.2a**, in which either the hydrophobic residues V_{18} and F_{20} or the hydrophobic residues F_{19} and A_{21} were rendered more hydrophilic by hydroxylation. In double mutant **3.2b**, V_{18} was replaced with threonine and F_{20} was replaced with tyrosine ($V_{18}T$,$F_{20}Y$). In

double mutant **3.2c**, F_{19} was replaced with tyrosine and A_{21} was replaced with serine ($F_{19}Y$,$A_{21}S$).

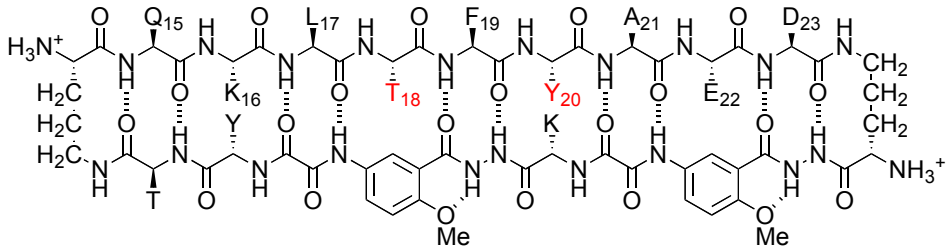

macrocyclic β-sheet peptide **3.2b**

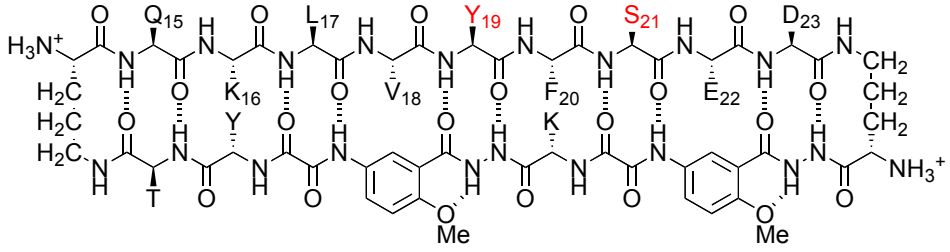

macrocyclic β-sheet peptide **3.2c**

The ^{1}H NMR spectrum of the $V_{18}T$,$F_{20}Y$ double mutant **3.2b** is strikingly similar to that of macrocyclic β-sheet **3.2a** (Figure 3.2), indicating that **3.2a** and **3.2b** fold and oligomerize in a similar fashion in aqueous solution. The methyl resonances from L_{17} and A_{21} appear unusually upfield, the aromatic resonances from F_{19} also appear unusually upfield, and many of the amino acid α-protons appear unusually downfield. The ^{1}H NMR spectra of both compounds reflect similar monomer-oligomer equilibria. At 0.1 mM, the monomer predominates and only small resonances from the tetramer are present; at 1.0 mM, the resonances from the tetramer predominate and only small resonances from the monomer are present. Thus, $V_{18}T$,$F_{20}Y$ double mutation does not substantially alter the equilibrium constant for tetramer formation.

The ^{1}H NMR spectrum of the $F_{19}Y$,$A_{21}S$ double mutant **3.2c** differs markedly from those

of **3.2a** and **3.2b (**Figure 3.18). The methyl resonances from L_{17} do not appear unusually upfield and the amino acid α-protons do not appear unusually downfield. These observations indicate that $F_{19}Y,A_{21}S$ double mutation disrupts the formation of the tetramer. The ^{1}H NMR spectrum of macrocyclic β-sheet **2c** shows some minor broadened resonances at 2.0 mM, which diminish at lower concentrations, suggesting that some weaker non-specific self-association may persist when tetramer formation is disrupted.

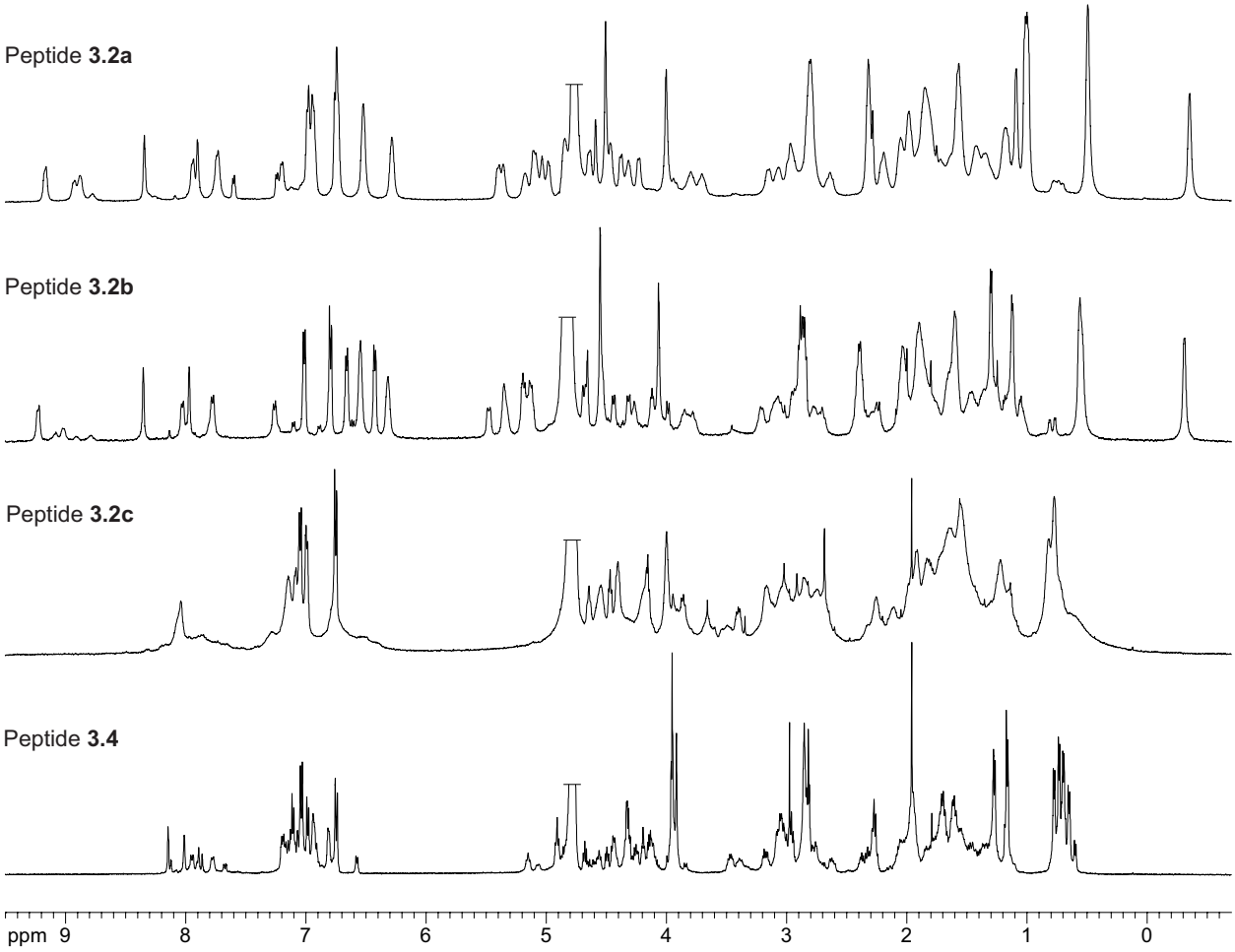

Figure 3.18. ^{1}H NMR spectra of macrocyclic β-sheet peptides at 2.0 mM at 298 K in D_2O at 500 MHz: **3.2a** (tetramer predominates), **3.2b** (tetramer predominates), **3.2c** (monomer predominates), and **3.4** (monomer predominates). The spectrum of **3.4** shows multiple sets of resonances, which are associated with amide-bond rotamers.

The dramatic differences between macrocyclic β-sheets **3.2b** and **3.2c** further

demonstrate the importance of hydrophobic interactions of the LFA face of the macrocycle in tetramer formation. When the LFA face is hydroxylated, tetramer formation is disrupted, but when the VF face is hydroxylated, tetramer formation is not affected.

4. Hydrogen-Bonding Edge Control of Tetramerization in Macrocyclic β-Sheet Peptide 3.4. To probe the role of hydrogen bonding in tetramer formation, we blocked the hydrogen-bonding edge of the macrocycle by *N*-methylation. Macrocyclic β-sheet **3.4** is a homologue of macrocyclic β-sheet **3.2a** with *N*-methylphenylalanine in place of phenylalanine at position 20. The $F_{20}F^{N\text{-Me}}$ mutation is designed to block formation of the hydrogen-bonded dimer and thus the assembly of a tetramer comprising a dimer of hydrogen-bonded dimers. The ^{1}H NMR spectrum of macrocyclic β-sheet **3.4** also differs markedly from those of **3.2a** and **3.2b** (Figure 3.17). The methyl resonances from L_{17} and A_{21} do not appear unusually upfield and the amino acid α-protons do not appear unusually downfield. The disruption of tetramer formation by *N*-methylation demonstrates that hydrogen bonding is also essential for tetramer formation.

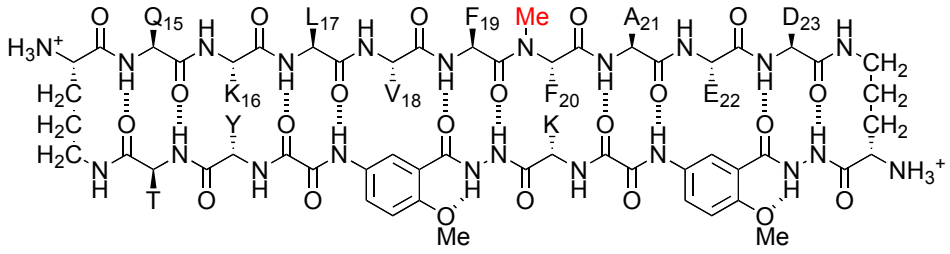

macrocyclic β-sheet peptide **3.4**

5. Diffusion Studies of Macrocyclic β-Sheet Peptides 3.1–3.4. DOSY NMR studies of macrocyclic β-sheets **3.1–3.4** suggest that **3.1**, **3.2a**, and **3.2b** are tetrameric at millimolar concentrations, while **3.2c**, **3.3**, and **3.4** are monomeric.[41,42,43] As mentioned above, the

oligomeric **3.2a** exhibits a diffusion coefficient of 10.0 x 10^{-7} cm^2/s in D_2O at 298 K, while monomeric **3.3** exhibits a diffusion coefficient of 16.4 x 10^{-7} cm^2/s. The ratio of these diffusion coefficients — about 0.6 — is consistent with tetramer formation.[42,43,44,45] Macrocyclic β-sheets **3.1** and **3.2b** exhibit diffusion coefficients similar to that of **3.2a**, while macrocyclic β-sheets **3.2c** and **3.4** exhibit diffusion coefficients similar to that of **3.3** (Table 3.4).

Table 3.4. Diffusion Coefficients (D) of Peptides 3.1–3.4 in D_2O at 298 K

peptide	$MW_{monomer}$[a] (Da)	$MW_{tetramer}$[a] (Da)	D (10^{-7} cm^2/s)	oligomer state
3.1	2232	8929	10.1[b]	tetramer
3.2a	2169	8677	10.0[b]	tetramer
			10.1[c]	
3.2b	2187	8749	10.3[b]	tetramer
			10.1[c]	
3.2c	2201	NA	16.5[b]	monomer
3.3	2196	8785	16.4[b]	monomer
3.4	2183	NA	17.6[b]	monomer

[a] Molecular weight calculated for the neutral (uncharged) macrocycle. [b]Diffusion coefficient measured at 2.0 mM. [c]Diffusion coefficient measured at 8.0 mM.

6. Analytical Ultracentrifugation Studies of Macrocyclic β-Sheet Peptide 3.2b. To corroborate the DOSY studies, analytical ultracentrifugation (AUC) sedimentation velocity studies (SV) on macrocyclic β-sheet **3.2b** were performed.[46,47,48] AUC is useful tool that was used previously in our group to obtain equilibrium data for an oligomer species.[43] AUC experiments characterize the solution-state behavior of macromolecules and can identify dynamic processes such as mass-action driven reversible associations by observing the sedimentation and diffusion behavior of all species in a mixture, and report their partial concentrations, molecular weights, and anisotropies. Analysis of multiple loading concentrations can reveal shifts in the sedimentation profile, corresponding to increasing amounts of higher oligomeric forms in response to mass action. Reversible reactions can be fitted directly to

solutions of the Lamm equation to obtain the equilibrium coefficients of the reactions, and to obtain mass and anisotropy of the reacting species.[48] These studies were conducted by Dr. Borries Demeler at the Center for Analytical Ultracentrifugation of Macromolecular Assemblies (CAUMA) located in the Department of Biochemistry at the University of Texas Health Science Center, San Antonio, TX.

The AUC studies are best performed in non-zero ionic strength to avoid nonideality resulting from charge interactions between the large cationic molecules. Thus, AUC sedimentation velocity studies were performed in the presence of salt, using 0.10, 0.30, and 0.66 mM solutions of macrocycle **3.2b** in H_2O containing 25 mM NaCl at 293 K.

A comparison of sedimentation profiles measured at 344 nm from multiple loading concentrations (98.7 μM, 304.0 μM, and 657.6 μM) indicated a mass-action driven shift in the sedimentation profile, suggesting the presence of a reversible reaction (Figure 3.19). Genetic algorithm – Monte Carlo fitting of the individual concentrations suggested the presence of monomer and tetramer species at different ratios, depending on concentration. From these ratios, we estimated K_{assoc} = 1.93 x 10^{14}, 5.66 x 10^{15}, and 8.89 x 10^{14} M^{-3} for the respective experiments. Detailed hydrodynamic fitting results for these fits are shown in Table 3.5. Based on these results, we fitted the lowest concentration — which displayed the largest signal for the monomer — to a reversible self-associating model for a monomer-tetramer equilibrium using a 200-iteration genetic algorithm-Monte Carlo analysis.[47,48] This treatment resulted in a very good fit to the monomer-tetramer model — with random residuals (Figure 3.20 and Table 3.6).

Collectively, the sedimentation velocity data fit well to a reversible monomer-tetramer equilibrium with slow exchange on the time scale of the experiment (hours). The tetramer predominated at all three concentrations, with the greatest fraction of monomer present at 0.10

mM. Analysis of the data from the 0.10 mM experiment gave a good fit to a monomer-tetramer equilibrium with a 2.14 kDa monomer and at 8.55 kDa tetramer and a K_{assoc} of 1.93 x 10^{14} M^{-3}. A K_{assoc} of 1.93 x 10^{14} M^{-3} corresponds to a 1:1 molar ratio of monomer and tetramer at 0.086 mM total concentration of **3.2b** and a 4:1 molar ratio of monomer and tetramer at 0.022 mM total concentration of **3.2b**. The stronger self-association of **3.2b** under these conditions, as compared to the NMR studies shown in Figure 3.10, may be explained by the NaCl and lower temperature used for the AUC studies.

In comparison to the studies with **3.2b**, macrocyclic β-sheet **3.2a** was found to form high molecular weight aggregates when subjected to AUC studies under similar conditions. The formation of high molecular weight aggregates may reflect enhanced self-association and aggregation promoted by salt (NaCl).

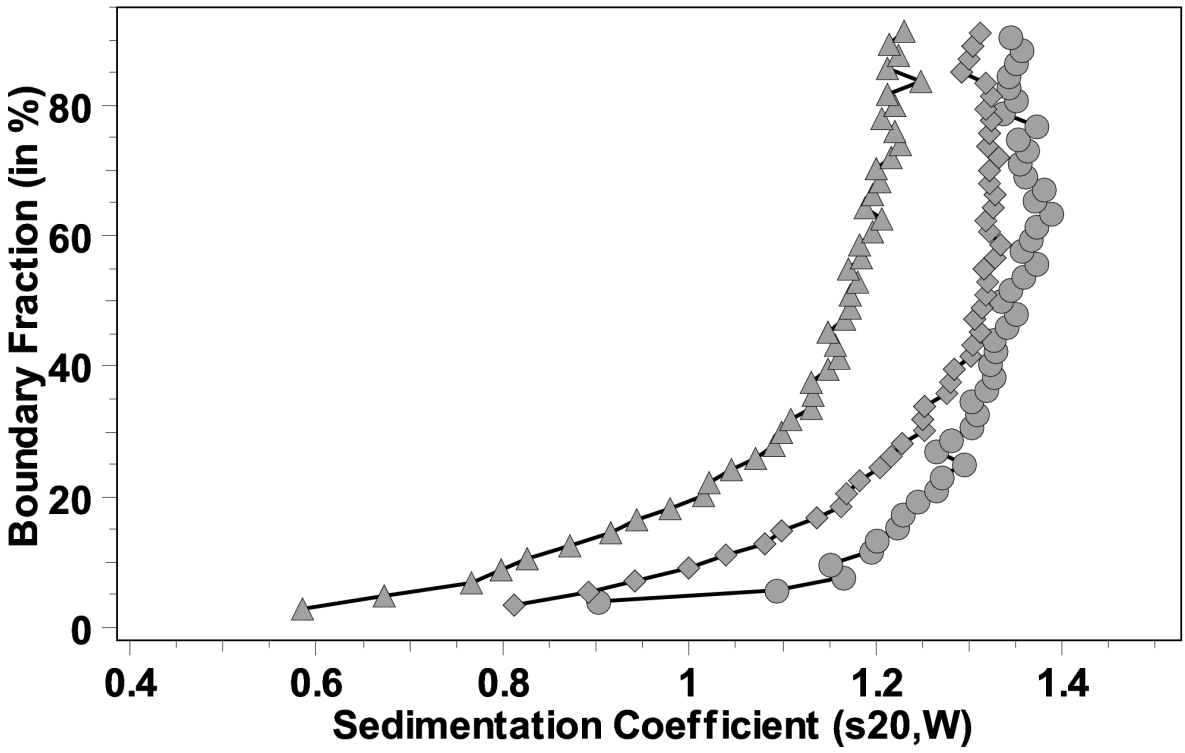

Figure 3.19. Sedimentation coefficient distributions of macrocyclic β-sheet peptide **3.2b** for loading concentrations at 98.7 μM (triangles), 304.0 μM (squares) and 657.6 μM (circles) obtained from sedimentation velocity experiments performed at 344 nm. The increase in sedimentation coefficient as a function of increase in loading concentration suggests the presence of a mass-action driven self-association reaction.

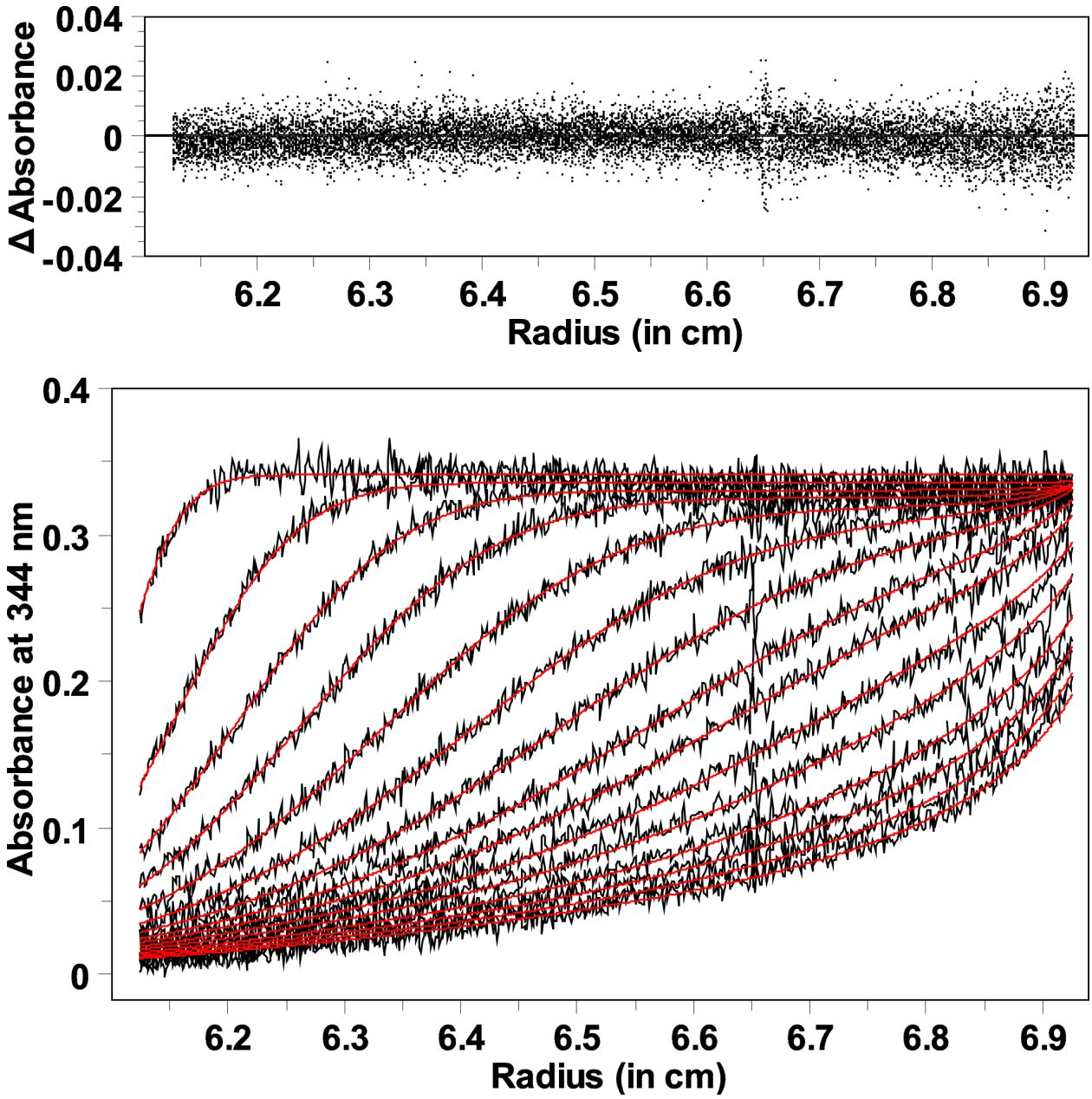

Figure 3.20. Sedimentation velocity data (black lines, lower plot) for macrocyclic β-sheet peptide **3.2b** (98.7 μM) when fitted with a reversible model for a monomer-tetramer equilibrium[47,48] using genetic algorithm-Monte Carlo analysis (red lines). Residuals are random, and shown in the upper portion of this plot. For clarity, only every fifth scan in this experiment is shown.

Table 3.5. Hydrodynamic measurements for macrocyclic β-sheet peptide **3.2b**.[a]

	Monomer (98.7 µM)	**Tetramer (98.7 µM)**	**Monomer (304.0 µM)**	**Tetramer (304.0 µM)**	**Monomer (657.6 µM)**	**Tetramer (657.6 µM)**
Partial concentration (% of total OD)	31.06%	68.94%	12.02%	87.98%	2.73%	97.27%
Molecular weight (Da)	2752.8	8946.4	3316.4	8947.7	2548.6	8507.2
Sedimentation Coefficient (x 10^{13} s)	0.60	1.30	0.59	1.27	0.65	1.25
Diffusion Coefficient (x 10^{7} cm^2/s)	18.75	12.50	15.22	14.33	21.94	15.60
Anisotropy (f/f_0)	1.24	1.26	1.44	1.24	1.09	1.21
K_{assoc} (M^{-3})	1.93 x 10^{14}		5.66 x 10^{15}		8.89 x 10^{14}	

[a]Hydrodynamic measurements for macrocyclic β-sheet **3.2b** from a genetic algorithm-Monte Carlo fit to a non-interacting model with 50 iterations, fitting each loading concentration individually.Only two species were detected in each sample, corresponding in molecular weight to the monomer and tetramer of **3.2b**. The shift in partial concentration is consistent with a reversible self-association model for a monomer-tetramer equilibrium. K_{assoc} is estimated based on the relative amounts of monomer and tetramer determined in the genetic algorithm-Monte Carlo analysis, but due to the low amount of monomer in the two higher concentrations, the K_{assoc} from the lowest concentration is considered to be the most reliable.

Table 3.6. Hydrodynamic measurements for macrocyclic β-sheet peptide **3.2b** at 98.7 mM from a genetic algorithm-Monte Carlo fit to a reversible monomer-tetramer model.[a]

	Monomer	**Tetramer**
Molecular weight (Da)	2137.0 (2116.5, 2157.6)	8548.0 (8466.0, 8630.4)
Sedimentation Coefficient (x 10^{13} s)	0.514 (0.511, 0.518)	1.223 (1.220, 1.225)
Diffusion Coefficient (x 10^{7} cm^2/s)	21.27 (21.17, 21.36)	12.64 (12.54, 12.74)
Anisotropy (f/f_0)	1.18 (1.17, 1.19)	1.25 (1.24, 1.26)
K_{assoc} (M^{-3})	1.93 (1.80, 2.05) x 10^{14}	

[a]Hydrodynamic measurements for macrocyclic β-sheet **3.2b** from a genetic algorithm-Monte Carlo fit to a reversible self-association model for a monomer-tetramer with 200 iterations.[47] The K_{assoc} observed in this fit matched well the K_{assoc} observed with the non-interacting fit. Values in parenthesis reflect the 95% confidence intervals for each parameter.

7. Folding of Macrocyclic β-Sheet Peptides 3.1–3.4. The magnetic anisotropy of the diastereotopic δ-protons of the δ-linked ornithine turn units in the ^{1}H NMR spectra reflect that the tetramers of **3.1a**, **3.2a**, and **3.2b** form well-folded β-sheets, while the monomers of **3.2c**, **3.3**, and **3.4** are only partially-folded. In a well-folded macrocyclic β-sheet, the difference in the chemical shifts (Δδ) of the diastereotopic *pro-S* and *pro-R* δ-protons of the δ-linked ornithine turn units ($^{\delta}$Orn) is about 0.6 ppm in aqueous solution.[39,43,49] Values substantially lower than 0.6 ppm reflect the formation of partially folded macrocyclic β-sheet structures. At 2.0 mM and 298 K in D_2O, the tetramers of **3.1**, **3.2a**, and **3.2b** exhibit large magnetic anisotropies, while the monomers of **3.2c**, **3.3**, and **3.4** exhibit smaller magnetic anisotropies (Table 3.7). Thus, oligomerization promotes folding.

Table 3.7. Magnetic Anisotropies of the δ-Protons of the δ-Linked Ornithine Turn Units of Peptides **3.1–3.4** in D_2O at 298 K

peptide	$^{\delta}$Orn$_1$ Δδ (ppm)	$^{\delta}$Orn$_2$ Δδ (ppm)	folding
3.1[a]	0.64	0.70	folded tetramer
3.2a[a]	0.64	0.72	folded tetramer
3.2b[a]	0.64	0.70	folded tetramer
3.2c[a]	0.23[d]	0.45[d]	partially folded monomer
3.3[b]	0.54[d]	0.24[d]	partially folded monomer
3.3[c]	0.58[d]	0.66[d]	folded tetramer
3.4[a]	0.30[d]	0.32[d]	partially folded monomer

[a] oligomer at 2.0 mM. [b] monomer at 2.0 mM. [c] oligomer at 8.0 mM.
[d] assignment of $^{\delta}$Orn$_1$ and $^{\delta}$Orn$_2$ is arbitrary.

To further investigate the folding and oligomerization of macrocylic β-sheet **3.2a**, we compared the ^{1}H NMR chemical shifts of the α-protons of the **3.2a** tetramer to those of acyclic control peptide **3.5**.[50] Peptide **3.5** contains the A$\beta_{15\text{-}23}$ nonapeptide and two δ-linked ornithine

units but lacks the lower template strand. The α-proton resonances of $A\beta_{15\text{-}23}$ in the **3.2a** tetramer appear 0.04–1.04 ppm downfield of those of acyclic control, with an average downfield shifting of 0.66 ppm (Figures 3.21 and 3.22). The large downfield shifting of the α-protons suggests the formation of a well-folded β-sheet structure.

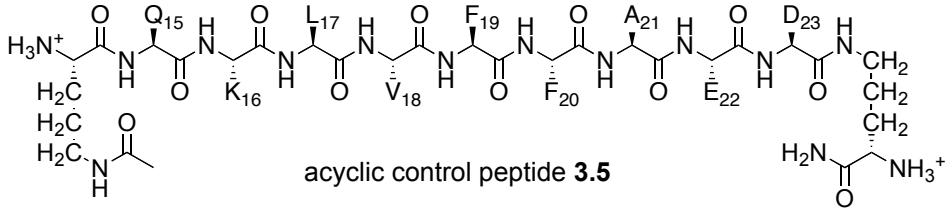

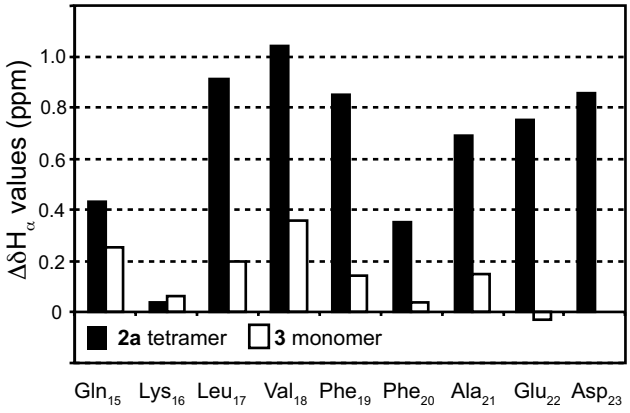

Figure 3.21. Downfield shifting of the ^{1}H NMR α-proton resonances of the **3.2a** tetramer and the **3.3** monomer, relative to acyclic control **5**. The ^{1}H NMR spectrum of **3.2a** was recorded at 8.0 mM in D_2O at 500 MHz and 300.5 K. The ^{1}H NMR spectra of **3.3** and **3.5** were recorded at 2.0 and 1.2 mM respectively in D_2O at 500 MHz and 298 K.

Table 3.7. ^{1}H NMR chemical shifts of the α-protons of the **3.2a** tetramer, the **3.3** monomer, and linear peptide **3.5**.

Residue	Peptide **3.2a** δ (ppm)	Peptide **3.3** δ (ppm)	Peptide **3.5** δ (ppm)	Δδ (ppm) **3.2a – 3.5**	Δδ (ppm) **3.3 – 3.5**
Q_{15}	4.67	4.49	4.24	0.43	0.25
K_{16}	4.29	4.31	4.25	0.04	0.06
L_{17}	5.22	4.51	4.31	0.91	0.20
V_{18}	5.03	4.35	3.99	1.04	0.36
F_{19}	5.38	4.67	4.55[a]	0.85[a]	0.14[a]
F_{20}	4.88	4.57	4.51[a]	0.35[a]	0.04[a]
A_{21}	4.86	4.32	4.17	0.69	0.15
E_{22}	5.10	4.32	4.35	0.75	-0.03
D_{23}	5.45	4.59	4.59	0.86	0.00

[a] assignment of F_{19} and F_{20} of peptide **3.5** arbitrary. The average d for F_{19} and F_{20} of peptide **3.5** was used in calculating Δδ.

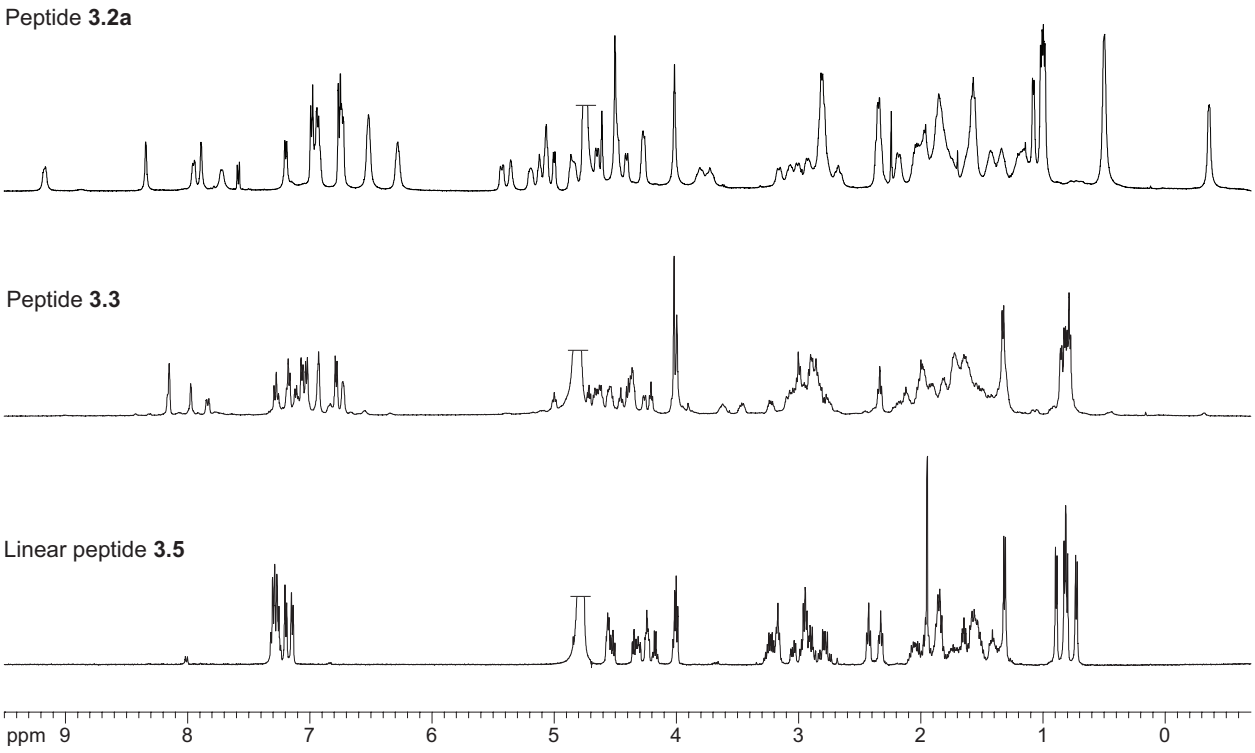

Figure 3.22. ^{1}H NMR spectra of macrocyclic β-sheet peptide **3.2a** at 8.0 mM at 300.5 K in D_2O at 500 MHz (tetramer predominates), macrocyclic β-sheet peptide **3.3** at 2.0 mM at 298 K in D_2O at 500 MHz (monomer predominates), and linear peptide **3.5** at 1.2 mM at 298 K in D_2O at 500 MHz (monomer).

In contrast, the α-proton resonances of the monomer of **3.2a** are not nearly as far downfield shifted. Although it is not feasible to identify all of the α-proton resonances of the monomer of **3.2a** because the tetramer predominates even at submillimolar concentrations, it is possible to do so in the close homologue **3.3**, which is largely monomeric at low millimolar concentrations. The α-proton resonances of $A\beta_{15\text{-}23}$ in the **3.3** monomer show far less downfield shifting, with an average of only 0.13 ppm (Figures 3.21 and 3.22). The smaller downfield shifting of the α-protons of the monomers of **3.2a** and **3.3** reflects the formation of β-sheet structures that are only partially folded.

Discussion

The tetramers formed by macrocyclic β-sheets containing the $A\beta_{15–23}$ nonapeptide are remarkable. Although the individual peptide monomer units are only partially folded, the tetramers that form exhibit secondary, tertiary, and quaternary structure reminiscent of proteins. The unusually well-defined structures of the tetramers are reflected in the strong NOEs observed and in the large magnetic anisotropies of the L_{17}, F_{19}, and A_{21} side chains and many of the α-protons in the ^{1}H NMR spectra.

To gain further insight into the structure of the tetramers formed by the macrocyclic β-sheets in aqueous solution, we used the X-ray crystallographic structure of the tetramer of macrocyclic β-sheet **3.1** to create a model of the solution-state tetramer of macrocyclic β-sheet **3.2a**. We generated the initial coordinates for the model in PyMOL by (1) changing the *p*-bromophenylalanine of **3.1** to tyrosine, (2) shifting the crystallographic dimers out of alignment by two residues toward the C-termini, (3) moving the dimers to pack through the LFA faces instead of the VF faces, (4) selecting appropriate rotamers of F_{20}, and (5) orienting the dimers to

approximately match the observed interlayer NOEs between the methoxy group of Hao_2 and the methyl group of threonine. We then generated a minimum-energy structure (local minimum) of the tetramer in MacroModel with the Maestro user interface using the MMFFs force field with GB/SA water solvation, minimizing first with distance constraints to match the observed NOEs between α-protons (Figure 3.4–3.5) and between the layers of the β-sheets (Figures 3.12–3.14) and then without constraints.

Figure 3.23 illustrates the resulting model of the tetramer. The tetramer consists of a dimer of hydrogen-bonded dimers and is essentially symmetrical, consisting of four roughly symmetrical monomers arranged in roughly D_2 symmetry. Residues L_{17}, F_{19}, and A_{21} of the dimers pack tightly to form a hydrophobic core within the tetramer (Figures 3.23B and 3.23C). The methyl group of A_{21} sits over the phenyl group of F_{19} in the opposing layer of the sandwich-like structure, consistent with the observed upfield shifting of the methyl resonance of A_{21} in the ^{1}H NMR spectrum. The *pro-S* methyl group of L_{17} sits over the aromatic ring of Hao_2 in the opposing layer, consistent with the pronounced upfield shifting of one of the methyl resonances of L_{17} in the ^{1}H NMR spectrum. The methyl group of the threonine is close to the methoxy group of Hao_2, and Hao_1 is close to Hao_2, consistent with the observed NOEs between these groups (Figures 3.23D, 3.12 and 3.14).

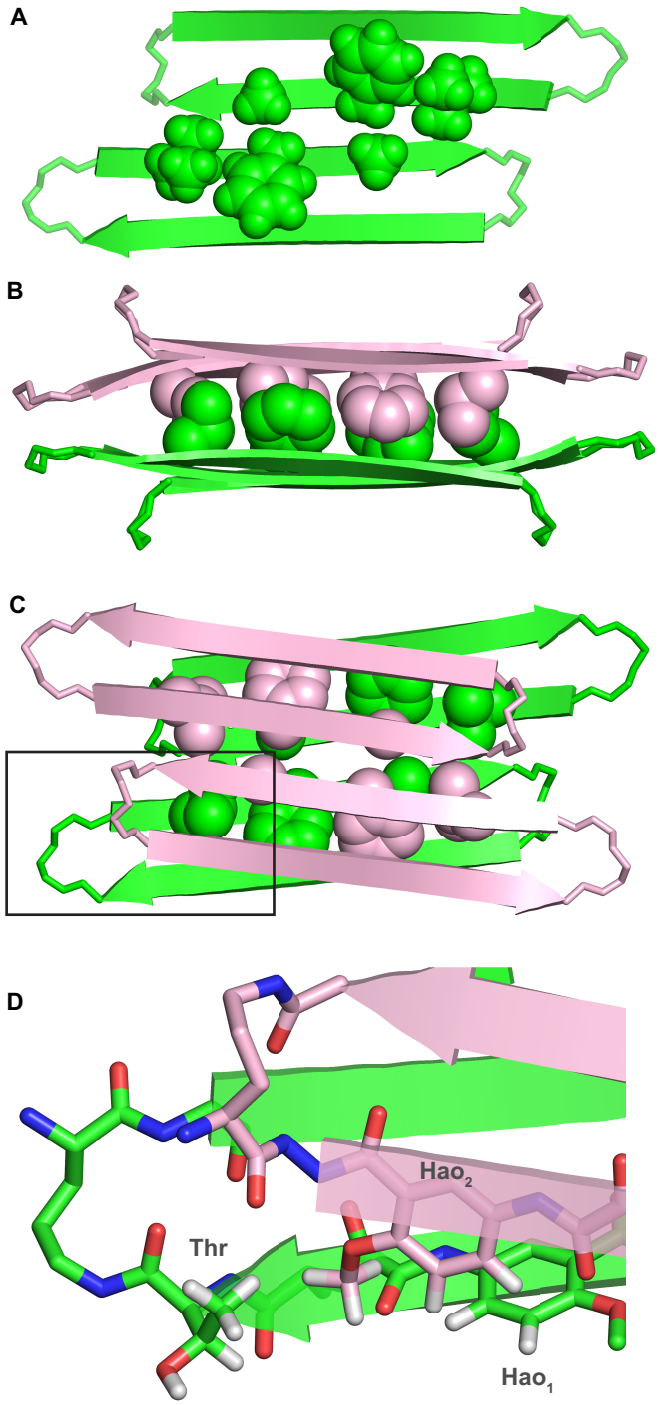

Figure 3.23. Model of macrocyclic β-sheet peptide **3.2a** as a tetramer, based on the NOE cross peaks of **3.2a** and the X-ray crystallographic structure of **1**. (A) Hydrogen-bonded dimers within the tetramer. The hydrogen-bonded dimers are antiparallel and shifted out of alignment by two residues toward the C-termini. Residues L_{17}, F_{19}, and A_{21} of the hydrophobic core are shown (the LFA face). (B) Side view of **3.2a** as a tetramer. (C) Top view of **3.2a** as a tetramer. The LFA faces that form the hydrophobic core of the tetramer are shown. (D) Detail of the contacts between threonine, Hao_1, and Hao_2, which give rise to the interlayer NOE crosspeaks that are shown in Figure 3.12 and 3.14.

The solution-state tetramers formed by macrocyclic β-sheets **3.1**, **3.2a**, and **3.2b** differ from the solid-state tetramer observed for macrocyclic β-sheet **3.1** in three notable ways: Although both tetramers comprise antiparallel β-sheet dimers, the solution-state dimers are out of register, shifted out of alignment by two residues towards the C-termini, while the solid-state dimers are in register, with all residues aligned (Figure 3.24). The solution-state dimers are sandwiched through the LFA faces, while the solid-state dimers are sandwiched through the VF faces (Figure 3.25). The two solution-state dimers that form the tetramer are nearly parallel to each other, while the two solid-state dimers are nearly orthogonal; the former are oriented at roughly 15°, while the latter are oriented at roughly 83° (Figure 3.25).

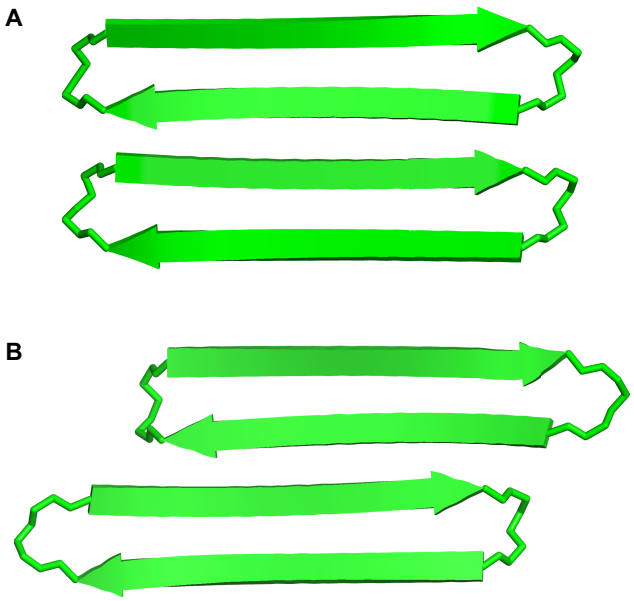

Figure 3.24. Model of macrocyclic β-sheet peptide **3.2a** and the X-ray crystallographic structure of **3.1** as dimers. (A) X-ray crystallographic structure of hydrogen-bonded dimers of **3.1** that are antiparallel and fully aligned. (B) Solution-state structure of hydrogen-bonded dimers of **3.2a** that are antiparallel and shifted out of alignment by two residues toward the C-termini.

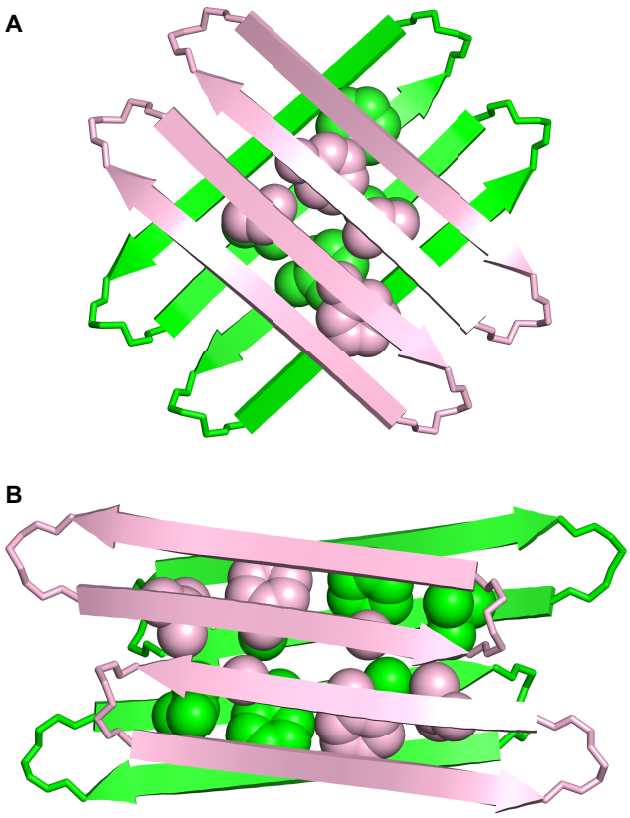

Figure 3.25. Model of macrocyclic β-sheet peptide **3.2a** and the X-ray crystallographic structure of **3.1** as tetramers. (A) Top view of the X-ray crystallographic structure of **3.1** as a tetramer. Residues V_{18} and F_{20} of the hydrophobic core are shown (the VF face). One rotamer of residue F_{20} for each monomer is shown. (B) Top view of solution-state structure of **3.2a** as a tetramer. Residues L_{17}, F_{19}, and A_{21} of the hydrophobic core are shown (the LFA face).

The differences between the solution-state tetramer and the solid-state tetramer may reflect the need to maximize hydrophobic contacts in aqueous solution. In aqueous solution, hydrophobic contacts within the tetramer are important. The LFA face of the dimer presents six hydrophobic residues from $A\beta_{15-23}$, while the VF face presents only four (Figure 3.25). Hydrophobic contact is maximized in the aqueous tetramer through contact between these six residues. The bulky hydrophobic side chains of L_{17} and F_{19} pack well with the small hydrophobic side chain of A_{21} in the opposing dimer of the tetramer. In the solid state, the tetramer is part of a lattice in which there are additional intermolecular contacts. The tetramers are in contact with

other tetramers, as well as with water and organic co-crystallants, and these contacts likely help stabilize the tetramer. Differences in pH and protonation state may also be important in the differences between the solution-state and solid-state tetramers. In assessing the extent of the hydrophobic contacts, buried surface areas were calculated as the difference between the solvent-accessible surface areas of the individual monomer components and that of the tetramer using the areaimol program in the CCP4 suite.[51] The buried surface area of the solution-state tetramer is 3401 $Å^2$, while that of the solid-state tetramer is 2785 $Å^2$. The greater buried surface area of the solutions-state tetramer reflects well the greater hydrophobic contacts in comparison to the solid-state tetramer.

The differing morphology of the solution-state and solid-state tetramers is significant, because it may provide a glimpse into some of the structural bases for polymorphism among Aβ oligomers in Alzheimer's disease. Polymorphism has previously been observed at atomic resolution in Aβ fibrils, but not in oligomers.[52,53,54] Only polymorphism studies of Aβ oligomers and mixed oligomers derived from Aβ and tau peptides has been observed in computational studies.[55] Because little is known about the structures of amyloid oligomers, little is known about the structural bases of oligomer polymorphism. Much of what is currently known about amyloid oligomer polymorphism focuses on differences in reactivity toward oligomer-specific antibodies or differences in size and shape that can be observed by electron microscopy, atomic-force microscopy, gel electrophoresis, or mass spectrometry. These techniques do not provide detail at atomic resolution. The contrasting structures of the solution-state and solid-state tetramers described here demonstrate subtle differences among oligomers that can be observed at atomic resolution. Differing facial pairings of the β-sheets give rise to unique stable structures. Differing alignment of the β-strands within the β-sheets also gives rise to unique structures. While not seen

in the two types of tetramers here, both parallel and antiparallel β-sheet structures may also be possible.

Conclusion

Macrocyclic β-sheet peptides containing the $A\beta_{15-23}$ nonapeptide exhibit rich supramolecular chemistry, forming tetramers with well-defined structures in aqueous solution and in the solid state.[56] The solution-state and solid-state tetramers exhibit noteworthy polymorphism, differing in the alignment of the monomers within the hydrogen-bonded dimers, the faces of the hydrogen-bonded dimers involved in tetramer formation, and the rotational orientation of the hydrogen-bonded dimers within the tetramers (Figure 3.26). Both hydrogen bonding and hydrophobic interactions are important in tetramer formation. Residues L_{17}, F_{19}, and A_{21} are critical in the formation of the hydrophobic core of the tetramers in solution, and the size complementarity of the small A_{21} residue and large L_{17} and F_{19} residues may play a special role in their stability.

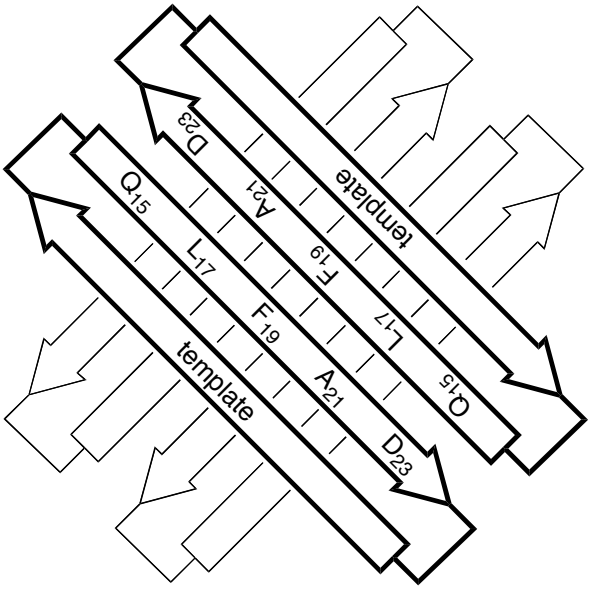

solid-state tetramer

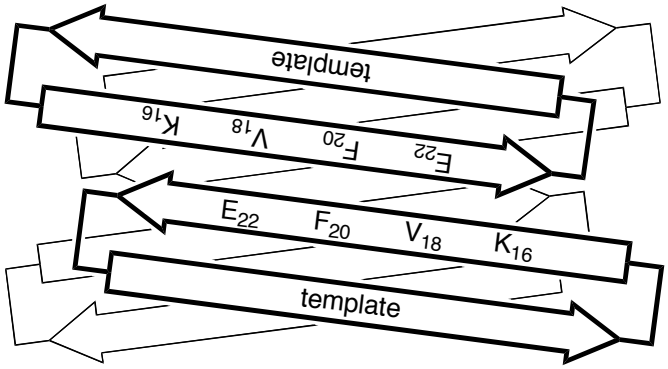

solution-state tetramer

Figure 3.26. Cartoon illustrating the structure of the solid-state tetramer of macrocyclic β-sheet **3.1** (top), and the solution-state tetramer of macrocyclic β-sheets **3.1** and **3.2a** (bottom). The VF faces form the inner hydrophobic core of the solid-state tetramer of **3.1**, and the LFA faces form the outer surface. The LFA faces form the inner hydrophobic core of the solution-state tetramer of **3.1** and **3.2a**, and the VF faces form the outer surface.

The supramolecular assembly of amyloidogenic peptides to form soluble oligomers is almost impossible to study at atomic resolution with natural full-length amyloidogenic peptides, because the oligomers that form are heterogeneous in size and morphology and because the oligomers are dynamic and can ultimately form insoluble amyloid. Chemical model systems that

limit uncontrolled supramolecular assembly and contain important segments of the amyloidogenic peptides can help identify modes in which the peptides interact. We anticipate that chemical model systems based on macrocyclic peptides will prove widely useful in elucidating the supramolecular assembly and oligomer formation of other amyloidogenic peptides with future studies from our group.

References

1 Pham, J. D.; Demeler, B.; Nowick, J. S. *J. Am. Chem. Soc.* **2014**, *136*, 5432–5442.

2 Kayed, R.; Head, E.; Thompson, J. L.; McIntire, T. M.; Milton, S. C.; Cotman, C. W.; Glabe, C. G. *Science* **2003**, *300*, 486–489.

3 Lacor, P. N.; Buniel, M. C.; Chang, L.; Fernandez, S. J.; Gong, Y.; Viola, K. L.; Lambert, M. P.; Velasco, P. T.; Bigio, E. H.; Finch, C. E.; Krafft, G. A.; Klein, W. L. *J. Neurosci.* **2004**, *24*, 10191–11200.

4 Haass, C.; Selkoe, D. J. *Nat. Rev. Mol. Cell Bio.* **2007**, *8*, 101–112.

5 Walsh, D. M.; Selkoe, D. J. *J. Neurochem.* **2007**, *101*, 1172–1184.

6 Glabe, C. G. *J. Biol. Chem.* **2008**, *283*, 29639–29643.

7 Kayed, R.; Canto, I.; Breydo, L.; Rasool, S.; Lukacsovich, T.; Wu, J.; Albay III, R.; Pensalfini, P.; Yeung, S.; Head, E.; Marsh, J. L.; Glabe, C. *Mol. Neurodegener.* **2010**, *5*, 1–10.

8 Umeda, T.; Tomiyama, T.; Sakama, N.; Tanaka, S.; Lambert, M. P.; Klein, W. L.; Mori, H. *J. Neurosci. Res.* **2011**, *89*, 1031–1042.

9 Fändrich, M. *J. Mol. Biol.* **2012**, *421*, 427–440.

10 Benilova, I.; Karran, E.; De Stooper, B. *Nat. Neurosci.* **2012**, *15*, 349–357.

11 Nussbaum, J. M.; Schilling, S.; Cynis, H.; Silva, A.; Swanson, E.; Wangsanut, T.; Tayler, K.; Wiltgen, B.; Hatami, A.; Rönicke, R.; Reymann, K.; Hutter-Paier, B.; Alexandru, A.; Jagla, W.; Graubner, S.; Glabe, C. G.; Demuth, H.-U.; Bloom, G. S. *Nature* **2012**, *485*, 651–655.

12 Chromy, B. A.; Nowak, R. J.; Lambert, M. P.; Viola, K. L.; Chang, L.; Velasco, P. T.; Jones, B. W.; Fernandez, S. J.; Lacor, P. N.; Horowitz, P.; Finch, C. E.; Krafft, G. A.; Klein, W. L. *Biochemistry* **2003**, *42*, 12749–12760.

13 Cleary, J. P.; Walsh, D. M.; Hofmeister, J. J.; Shankar, G. M.; Kuskowski, M. A.; Selkoe, D. J.; Ashe, K. H. *Nat. Neurosci.* **2005**, *8*, 79–84.

14 Lesné, S.; Koh, M. T.; Kotilinek, L.; Kayed, R.; Glabe, C. G.; Yang, A.; Gallagher, M.; Ashe, K. H. *Nature* **2006**, *440*, 352–357.

15 Shankar, G. M.; Li, S.; Mehta, T. H.; Garcia-Munoz, A.; Shepardson, N. E.; Smith, I.; Brett, F. M.; Farrell, M. A.; Rowan, M. J.; Lemer, C. A.; Regan, C. M.; Walsh, D. M.; Sabatini, B. L.; Selkoe, D. J. *Nat. Med.* **2008**, *14*, 837–842.

16 Ono, K.; Condron, M. M.; Teplow, D. B. *Proc. Natl. Acad. Sci. U.S.A.* **2009**, *106*, 14745–14750.

17 Selkoe, D. J. *Behav. Brain Res.* **2008**, *192*, 106–113.

18 Larson, M. E.; Lesné, S. E. *J. Neurochem.* **2012**, *192* (Suppl. 1), 125–139.

19 Vivekanandan, S.; Brender, J. R.; Lee, S. Y.; Ramamoorthy, A. *Biochem. Biophys. Res. Commun.* **2011**, *411*, 312–316.

20 Bernstein, S. L.; Dupuis, N. F.; Lazo, N. D.; Wyttenbach, T.; Condron, M. M.; Bitan, G.; Teplow, D. B.; Shea, J.-E.; Ruotolo, B. T.; Robinson, C. V.; Bowers, M. T. *Nat. Chem.* **2009**, *1*, 326–331.

21 Miller, Y.; Ma, B.; Nussinov, R. *Chem. Rev.* **2010**, *110*, 4820-4838.

22 Lührs, T; Ritter, C.; Adrian, M.; Riek-Loher, D.; Bohrmann, B.; Döbeli, H.; Schubert, D.; Riek, R. *Proc. Natl. Acad. Sci. U.S.A.* **2005**, *102*, 17342–17347.

23 Petkova, A. T.; Yau, W.-M.; Tycko, R. *Biochemistry* **2006**, *45*, 498–512.

24 Cerf, E.; Sarroukh, R.; Tamamizu-Kato, S.; Breydo, L.; Derclaye, S.; Dufrênes, Y. V.; Narayanaswami, V.; Goormaghtigh, E.; Ruysschaert, J.-M.; Raussens, V. *Biochem. J.* **2009**, *421*, 415–423.

25 Chimon, S.; Shaibat, M. A.; Jones, C. R.; Calero, D. C.; Aizezi, B.; Ishii, Y. *Nat. Struc. Mol. Bio.* **2010**, *14*, 1157–1164.

26 Strodel, B; Lee, J. W.; Whittleston, C. S.; Wales, D. J. *J. Am. Chem. Soc.* **2010**, *132*, 13300–13312.

27 Streltsov, V. A.; Varghese, J. N.; Masters, C. L.; Nuttall, S. D. *J. Neurosci.* **2011**, *31*, 1419–1426.

28 Laganowsky, A.; Liu, C.; Sawaya, M. R.; Whitelegge, J. P.; Park, J.; Zhao, M.; Pensalfini, A.; Soriaga, A. B.; Landau, M.; Keng, P. K.; Cascio, D.; Glabe, C. G.; Eisenberg, D. *Science* **2012**, *335*, 1228–1231.

29 Apostol, M. I.; Perry, K.; Surewicz, W. K. *J. Am. Chem. Soc.* **2013**, *135*, 10202–10205.

30 Hoyer, W.; Grönwall, C.; Jonsson, A.; Ståhl, S.; Härd, T. *Proc. Natl. Acad. Sci. U.S.A.* **2008**, *105*, 5099–5104.

31 Sandberg, A.; Luheshi, L. M.; Söllvander, S.; de Barros, T. P.; Macao, B.; Knowles, T. P. J.; Biverstål, H.; Lendel, C.; Ekholm-Petterson, F.; Dubnovitsky, A.; Lannfelt, L.; Dobson, C. M.; Härd, T. *Proc. Natl. Acad. Sci. U.S.A.* **2010**, *107*, 15595–15600.

32 Yu, L.; Edalji, R.; Harlan, J. E.; Holzman, T. F.; Lopez, A. P.; Labkovsky, B.; Hillen, H.; Barghorn, S.; Ebert, U.; Richardson, P. L.; Miesbauer, L.; Solomon, L.; Bartley, D.; Walter, K.; Johnson, R. W.; Hajduk, P. J.; Olejniczak, E. T. *Biochemistry* **2009**, *48*, 1870–1877.

33 Horn, A. H. C.; Sticht, H. *J. Phys. Chem. B* **2010**, *114*, 2219–2226.

34 Xu, J.; Zhang, J. Z. H.; Xiang, Y. *J. Phys. Chem. A* **2013**, *117*, 6373–6379.

35 Miller, Y.; Ma, B.; Tsai, C.-J.; Nussinov, R. *Proc. Natl. Acad. Sci. U.S.A.* **2010**, *107*, 14128–14133.

36 We began these studies through a fruitful collaboration with the laboratory of Professor David Eisenberg: (a) Zheng, J.; Liu, C.; Sawaya, M. R.; Vadla, B.; Khan, S.; Woods, R. J.; Eisenberg, D.; Goux, W. J.; Nowick, J. S. *J. Am. Chem. Soc.* **2011**, *133*, 3144–3157. (b) Liu, C.; Sawaya, M. R.; Cheng, P.-N.; Zheng, J.; Nowick, J. S.; Eisenberg, D. *J. Am. Chem. Soc.* **2011**, *133*, 6736–6744. (c) Cheng, P.-N.; Liu, C.; Zhao, M.; Eisenberg, D.; Nowick, J. S. *Nat. Chem.* **2012**, *4*, 927–933. (d) Liu, C.; Zhao, M.; Jiang, L.; Cheng, P.-N.; Park, J.; Sawaya,. M. R.; Pensalfini, A.; Gou, D.; Berk, A. J.; Glabe, C. G.; Nowick, J. S.; Eisenberg, D. *Proc. Natl. Acad. Sci. U. S. A.* **2012**, *109*, 20913–20918.

37 (a) Zheng, J.; Baghkhanian, A. M.; Nowick, J. S. *J. Am. Chem. Soc.* **2013**, *135*, 6846–6852. (b) Buchanan, L. E.; Dunkelberger, E. B.; Tran, H. Q.; Cheng, P.-N.; Chiu, C.-C.; Cao, P.; Raleigh, D. P.; de Pablo, J. J.; Nowick, J. S.; Zanni, M. T. *Proc. Natl. Acad. Sci. U. S. A.* **2013**, *110*, 19285–19290.

38 Pham, J. D.; Chim, N.; Goulding, C. W.; Nowick, J. S. *J. Am. Chem. Soc.* **2013**, *135*, 12460–12467.

39 Nowick, J. S.; Brower, J. O. *J. Am. Chem. Soc.* **2003**, *125*, 876–877.

40 Nowick, J. S.; Chung, D. M.; Maitra, K.; Maitra, S.; Stigers, K. D.; Sun, Y. J. *J. Am. Chem. Soc.* **2000**, *122*, 7654–7661.

41 (a) Berger, S.; Braun, S. *200 and More NMR Experiments: A Practical Course*; Wiley-VCH:

Weinheim, 2004; pp 515–517. (b) Findeisen, M; Berger, S. *50 and More Essential NMR Experiments*; Wiley-VCH: Weinheim, 2012; pp 163–166.

42 (a) Altieri, A. S.; Hinton, D. P.; Byrd, R. A. *J. Am. Chem. Soc.* **1995**, *117*, 7566–7567. (b) Johnson, C. S. *Progr. NMR Spectrosc.* **1999**, *34*, 203–256. (c) Yao, S.; Howlett, G. J.; Norton, R. S. *J. Biomol. NMR* **2000**, *16*, 109–119. (d) Cohen, Y.; Avram, L.; Frish, L. *Angew. Chem. Int. Ed.* **2005**, *44*, 520–554. (e) Cohen, Y.; Avram, L.; Evan-Salem, T.; Slovak, S.; Shemesh, N.; Frish, L. In *Analytical Methods in Supramolecular Chemistry*, 2nd ed.; Schalley, C. A., Ed; Wiley-VCH: Weinheim, 2012; 197–285.

43 Khakshoor, O.; Demeler, B.; Nowick, J. S. *J. Am. Chem. Soc.* **2007**, *129*, 5558–5569.

44 Teller, D. C.; Swanson, E.; DeHaen, C. *Methods Enzymol.* **1979**, *61*, 103–124.

45 Polson, A. *J. Phys. Colloid Chem.* **1950**, *54*, 649–652.

46 Demeler, B. *Current Protocols in Protein Science*; Wiley: Hoboken, NJ, **2010**; unit 7.13, Chapter 7.

47 Demeler, B.; Brookes, E.; Wang, R.; Schirf, V.; Kim, C. A. *Macromol. Biosci.* **2010**, *7*, 775–782.

48 (a) Cao, W.; Demeler, B. *Biophys. J.* **2005**, *89*, 1589–1602. (b) Cao, W.; Demeler, B. *Biophys. J.* **2008**, *95*, 54-65.

49 Woods, J. R.; Brower, J. O.; Castellanos, E.; Hashemzadeh, M.; Khakshoor, O.; Russu, W. A.; Nowick, J. S. *J. Am. Chem. Soc.* **2007**, *129*, 2548–2558.

50 Wishart, D. S.; Sykes, B. D. *Methods Enzymol.* **1994**, *239*, 363–392.

51 Winn, M. D.; Ballard, C. C.; Cowtan, K. D.; Dodson, E. J.; Emsley, P.; Evans, P. R.; Keegan, R. M.; Krissinel, E. B.; Leslie, A. G. W.; McCoy, A.; McNicholas, S. J.; Murshudov, G. N.;

Pannu, N. S.; Potterton, E. A.; Powell, H. R.; Read, R. J.; Vagin, A.; Wilson, K. S. *Acta Crystallogr. D Biol. Crystallogr.* **2011**, *67*, 235–242.

52 Petkova, A. T.; Leapman, R. D.; Guo, Z.; Yau, W.-M.; Mattson, M. P.; Tycko, R. *Science* **2005**, 307, 262–265

53 Paravastu, A. K.; Leapman, R. D.; Yau, W.-M.; Tycko, R. *Proc. Natl. Acad. Sci. U.S.A.* **2008**, *105*, 18349–18354.

54 Qiang, W.; Yau, W.-M.; Luo, Y.; Mattson, M. P.; Tycko, R. *Proc. Natl. Acad. Sci. U.S.A.* **2012**, *109*, 4443–4448.

55 (a) Miller, Y.; Ma, B.; Nussinov, R. *Biophys. J.* **2009**, *97*, 1168–1177. (b) Raz, Y.; Miller, Y. *PLoS One* **2013**, *8*, e73303.

56 Cheng, P.-N.; Pham, J. D.; Nowick, J. S. *J. Am. Chem. Soc.* **2013**, *135*, 5477–5492.

Experimental Section For Chapter 3

Materials and Methods:

Peptides **3.1–3.5** were prepared and studied as the trifluoroacetate (TFA) salts.

*Synthesis of macrocyclic β-sheet peptides **3.1–3.4**.*

Macrocyclic peptide **3.1** was synthesized as described previously, by automated solid-phase peptide synthesis of the corresponding linear peptide on chlorotrityl resin, followed by solution-phase cyclization, deprotection, and purification.[1] Macrocyclic peptides **3.2a-3.2c, 3.3,** and **3.4** were synthesized in a similar fashion, using procedures previously reported for the synthesis of **3.1** and of other macrocyclic β-sheet peptides.[1,2,3] Boc-Orn(Fmoc)-OH was used to introduce the δ-linked ornithine turn units. Fmoc-Hao-OH[2] was used to introduce the unnatural amino acid Hao.[4] Standard Fmoc-protected amino acids were used to introduce the other residues: Fmoc-Ala-OH, Fmoc-Asp(OtBu)-OH, Fmoc-Gln(Trt)-OH, Fmoc-Glu(OtBu)-OH, Fmoc-Leu-OH, Fmoc-Lys(Boc)-OH, Fmoc-Phe-OH, Fmoc-N(Me)-Phe-OH, Fmoc-Ser(OtBu)-OH, Fmoc-Thr(OtBu)-OH, Fmoc-Tyr(OtBu)-OH, Fmoc-Val-OH. In the synthesis of macrocyclic peptide **3.4**, Fmoc-N(Me)-Phe-OH was introduced using normal coupling times and

---

1 Pham, J. D.; Chim, N.; Goulding, C. W.; Nowick, J. S. *J. Am. Chem. Soc.* **2013**, *135,* 12460−12467.

2 Cheng, P.-N.; Nowick, J. S. *J. Org. Chem.* **2011**, *76*, 3166–3173.

3 Cheng, P.-N.; Liu, C.; Zhao, M.; Eisenberg, D.; Nowick, J. S. *Nat. Chem.* **2012**, *4*, 927–933.

4 Nowick, J. S.; Chung, D. M.; Maitra, K.; Maitra, S.; Stigers, K. D.; Sun, Y. J. *J. Am. Chem. Soc.* **2000**, *122*, 7654–7661.

conditions (20 min coupling with HCTU) and the subsequent amino acid, Fmoc-Phe-OH, was introduced by double coupling with HOAT (4 equiv.), HATU (4 equiv.), and 1 hour coupling times using automated solid phase peptide synthesis.

*Synthesis of linear peptide **3.5**.*

A 10 mL Bio-Rad Poly-Prep chromatography column was charged with Rink amide resin (300 mg, 0.73 mmol/g loading, 0.22 mmol) and ca. 6 mL of CH_2Cl_2. After 30 min, the solvent was drained and the resin was washed with ca. 3 mL of DMF. The resin was then submitted to cycles of standard Fmoc-based solid phase peptide synthesis on a PS3 automated peptide synthesizer (Protein Technologies, Inc.) using Fmoc-protected amino acid building blocks (4 equiv, with HCTU as coupling agent and 2,4,6-collidine as base). The final step of the synthesis of the protected peptide involved acetylating the amino-terminus by treating the resin with 2 mL of acetic anhydride on the PS3 synthesizer using 2,4,6-collidine as base. The resin was stirred with 10 mL of trifluoroacetic acid/triisopropylsilane/water (38:1:1 v/v) for 4 hours under nitrogen. The solution was concentrated under vacuum. The residue was dissolved in ca. 5 mL of water/acetonitrile (1:1), and centrifuged for 5 min at 14,000 rpm. The liquid portion was decanted from the supernatant, then filtered through a 0.45 micron filter, and purified by RP-HPLC on a C18 column (elution with acetonitrile and water containing 0.1% TFA, linear gradient from 20-35% acetonitrile over 38 min). The pure fractions were lyophilized to yield 3.1 mg of acyclic control peptide **3.5** (1% yield based on resin loading): ESI-MS m/z for $C_{64}H_{102}N_{16}O_{17}$ $[M + 2H]^{2+}$ calcd 683.37, found 683.34.

*NMR sample preparation, data collection, and data processing of peptides **3.1–3.5**.*

^{1}H NMR experiments of macrocyclic β-sheet peptides **3.1–3.5** were performed in D_2O at 500 MHz and 600 MHz at varying temperatures. Solutions of the peptides were prepared gravimetrically by dissolving an appropriate weight of each peptide in an appropriate volume of solvent. In calculating molecular weights, all amino groups were assumed to be protonated as the TFA salts. The HOD peak was used as a reference after the HOD peak was calibrated based on temperature.[5] All macrocyclic β-sheet peptides were allowed to stand for 6 hours to 36 hours to allow full hydrogen-deuterium exchange of the amide and ammonium hydrogens. 2D TOCSY, 2D COSY, 2D ROESY and 2D NOESY spectra were collected with 2048 data points in the f_2 domain and 512 data points in the f_1 domain. 2D TOCSY, 2D COSY and 2D ROESY data were processed to a 1024 x 1024 real matrix with a Qsine weighting function and with forward linear prediction in the f_1 domain. 2D NOESY data were processed to a 1024 x 1024 real matrix with a Qsinc weighting function, a forward linear prediction in the f_1 domain, and with the parameter GB set at 0.05 in the f_2 and f_1 domain. The data were processed with the Bruker XwinNMR software.

In order to observe amide resonances for further resonance assignments, ^{1}H NMR studies of macrocyclic β-sheet peptide **3.2a** were also performed in a H_2O/D_2O mixture (9:1) at 800 MHz and 298 K using WATERGATE. 2D TOCSY and 2D NOESY data for **3.2a** in the H_2O/D_2O mixture (9:1) were collected with 4096 data points in the f_2 domain and 512 data points in the f_1 domain. The collected data were processed with zero filling to a final matrix of 4096 x

---

5 Gottlieb, H. E.; Kotllyar, V.; Nudelman, A. *J. Org. Chem.* **1997**, *62,* 7512–7515.

1024 real points with a Qsine weighting function and with a forward linear prediction in the f_1 domain. The data were processed with the Bruker XwinNMR software.

*Modeling of the solution-state tetramer of macrocyclic β-sheet peptide **3.2a**.*

We used the X-ray crystallographic structure of the tetramer of macrocyclic β-sheet **1** to create a model of the solution-state tetramer of macrocyclic β-sheet **3.2a**. We generated the initial coordinates for the model in PyMOL by (1) changing the *p*-bromophenylalanine of **1** to tyrosine, (2) shifting the crystallographic dimers out of alignment by two residues toward the C-termini, and (3) moving the dimers so that they packed through the LFA faces, instead of the VF faces. The rotamer of F_{20} with χ_1=180° was then selected to avoid inter-chain steric clashes, and the shifted dimer layers were oriented to approximately match the observed interlayer NOEs between the methoxy group of Hao_2 and the methyl group of threonine.

The resulting initial structure was then imported into Maestro and a minimum-energy structure was generated by applying distance constraints to match observed NOEs as follows: Using MacroModel with the Maestro user interface, NOE constraints to match the observed intra- and intermolecular NOEs illustrated in Figures 3.4, 3.5, 3.12, and 3.13 were applied. Distance constraints of 2.2 to 2.8 Å were applied for the following intramolecular NOEs: $K_{16}\alpha$–$Y\alpha$, $F_{20}\alpha$–$K\alpha$, $V_{18}\alpha$–Hao_1H_6, and $E_{22}\alpha$–Hao_2H_6 (16 constraints total within the tetramer). Distance constraints of 2.2 to 3.6 Å were applied for the following intermolecular intralayer NOEs: $L_{17}\alpha$–$D_{23}\alpha$ and $F_{19}\alpha$–$A_{21}\alpha$ (8 constraints total within the tetramer). Distance constraints of 2.2 to 5.0 Å were applied for the following intermolecular interlayer NOEs: Hao_2OMe–$ThrCH_3$, Hao_1H_4–Hao_2H_4, Hao_1H_4–Hao_2H_3, and Hao_1H_3–Hao_2-H_4 (16 constraints total between the layers of the tetramer). The structure was minimized with these constraints using the MMFFs

force field with GB/SA water solvation. The NOE constraints were removed, and minimization was repeated using the MMFFs force field with GB/SA water solvation to generate a minimum-energy structure (local minimum).

This minimum-energy was then imported into PyMOL, and PyMOL was used to generate the images in Figures 3.23, 3.24B, and 3.25B.[6] A β-strand of nine glycine residues (G9) was used to generate a cartoon of the template strand Hao-K-Hao-Y-T. Specifically, the pdb coordinates from each unnatural amino acid Hao were used to generate tri-glycine segments, and the pdb coordinates of the threonine, tyrosine, and lysine residues were also used to generate three glycine residues of the G9 β-strand.

*Diffusion-ordered spectroscopy (DOSY) experiments of macrocyclic β-sheet peptides **3.1–3.4**.*

The diffusion coefficients of macrocyclic β-sheet peptides **3.1**-**3.4** were determined by DOSY experiments on a Bruker Avance 600 MHz spectrometer in D_2O at 298 K. The experiments comprised a series of 16 pulsed field gradient spin-echo experiments in which the gradient strength was incremented to allow ca. 5–95% signal attenuation with a linear ramp. A 75-ms diffusion delay was used. Diffusion gradient lengths of 1.75 – 3.0 ms were selected to achieve appropriate attenuation of each macrocyclic β-sheet peptide. Data were processed to give a pseudo-2D spectrum. The residual HOD peak in D_2O was set as a reference (19.0×10^{-10} m^2/s at 298 K).[7]

---

[6] The PyMOL Molecular Graphics System, Schrödinger, LLC, available at www.pymol.org.

[7] Longsworth, L. G. *J. Phys. Chem.* **1960**, *64*, 1914–1917.

*Analytical ultracentrifugation studies of macrocyclic β-sheet peptide **3.2b**.*

Analytical ultracentrifugation (AUC) sedimentation velocity (SV) studies were performed on macrocyclic β-sheet **3.2b** to further elucidate its self-association behavior. Solutions of **3.2b** were prepared gravimetrically as 0.10, 0.30, and 0.60 mM and determined spectrophotometrically to be 98.7, 304.0, and 657.6 μM based on a molar extinction coefficient of 2897 $M^{-1}cm^{-1}$ at 344 nm and a molar extinction coefficient of 22,260 $M^{-1}cm^{-1}$ at 280 nm,[8,9] Sedimentation experiments were performed with a Beckman Optima XL-I at the Center for Analytical Ultracentrifugation of Macromolecular Assemblies at the University of Texas Health Science Center at San Antonio. All measurements were made in intensity mode, measuring at 344 nm in 25 mM aqueous NaCl. The experimental data were collected at 20°C, and at 60,000 rpm, using 1.2 cm titanium 2-channel centerpieces for the 98.7 μM and 304.0 μM samples, and a 3 mm titanium 2-channel centerpiece for the 657.6 μM sample. Hydrodynamic corrections for buffer density, viscosity and partial specific volume (0.7179 ml/g for **3.2b**)[10] were made according

---

[8] The extinction coefficient of **3.2b** was calculated to be 22,260 $M^{-1}cm^{-1}$ from the extinction coefficient of Hao (9850 $M^{-1}cm^{-1}$) and Tyr (1280 $M^{-1}cm^{-1}$) at 280 nm.

[9] Khakshoor, O.; Demeler, B.; Nowick, J. S. *J. Am. Chem. Soc.* **2007**, *129*, 5558–5569.

[10] The partial specific volume of the Hao subunit was determined to be 0.65 cm^3/g as described previously.[9] The molar mass of the Hao subunit is 235.12 g.

to methods outlined in Laue et al.[11] and as implemented in UltraScan.[12]

The experimental data from SV experiments were analyzed with UltraScan v. 9.9 [10,13] and modeled with solutions of the Lamm equation.[14,15] Optimization was performed by 2-dimensional spectrum analysis (2DSA)[16] with simultaneous removal of time- and radially-invariant noise contributions.[17] 2DSA solutions are subjected to parsimonious regularization by

---

[11] Laue, T. M.; Shah, B. D.; Ridgeway, T. M.; Pelletier, S. L. Computer-aided interpretation of analytical sedimentation data for proteins. In *Analytical Ultracentrifugation in Biochemistry and Polymer Science*; Harding, S. E., Rowe, A. J., Horton, J. C., Eds.; Cambridge, Royal Society of Chemistry: Cambridge, United Kingdom, 1992; 90–125.

[12] Demeler, B. UltraScan: A Comprehensive Data Analysis Software Package for Analytical Ultracentrifugation Experiments. In *Modern Analytical Ultracentrifugation: Techniques and Methods;* Scott, D. J., Harding, S. E., Rowe, A. J., Eds.; Royal Society of Chemistry: Cambridge, United Kingdom, 2005; 210–229

[13] Demeler B. UltraScan-II version 9.9, release 1528 - A comprehensive data analysis software package for analytical ultracentrifugation experiments, 2011, University of Texas Health Science Center at San Antonio, Dept. of Biochemistry. http://www.ultrascan.uthscsa.edu

[14] Cao, W.; Demeler, B. *Biophys. J.* **2005**, *89*, 1589–1602.

[15] Cao, W.; Demeler, B. *Biophys. J.* **2008**, *95,* 54–65.

[16] Brookes, E.; Cao, W; Demeler, B. *Eur. Biophys. J.* **2010**, *39,* 405–414.

[17] Schuck, P; Demeler, B. *Biophysical J.* **1999**, *76,* 2288–2296.

genetic algorithm analysis,[18] and are further refined using Monte Carlo analysis to determine confidence limits for the determined parameters.[19] The calculations are computationally intensive and are carried out on high-performance computing platforms.[20] All calculations were performed on the Lonestar and Ranger clusters at the Texas Advanced Computing Center at the University of Texas at Austin, and on the Jacinto cluster at the Bioinformatics Core Facility at the University of Texas Health Science Center at San Antonio.

A comparison of sedimentation profiles measured at 344 nm from multiple loading concentrations (98.7 μM, 304.0 μM, and 657.6 μM) indicated a mass-action driven shift in the sedimentation profile, suggesting the presence of a reversible reaction (Figure 3.19). Genetic algorithm – Monte Carlo fitting of the individual concentrations suggested the presence of monomer and tetramer species at different ratios, depending on concentration. From these ratios, we estimated K_{assoc} = 1.93 x 10^{14}, 5.66 x 10^{15}, and 8.89 x 10^{14} M^{-3} for the respective experiments.[21] Detailed hydrodynamic fitting results for these fits are shown in Table 3.6. Based on these results, we fitted the lowest concentration — which displayed the largest signal for the monomer — to a reversible self-associating model for a monomer-tetramer equilibrium using a

---

[18] Brookes, E.; Demeler, B. Parsimonious Regularization using Genetic Algorithms Applied to the Analysis of Analytical Ultracentrifugation Experiments. In GECCO Proceedings, ACM 978-1-59593-697-4/07/0007, **2007**.

[19] Demeler, B.; Brookes, E. *Colloid Polym. Sci.* **2008**, *286,*129–137.

[20] Brookes, E.; Demeler, B. *Colloid Polym. Sci.* **2008**, *286,* 138–148.

[21] A K_{assoc} of 1.93 x 10^{14} M^{-3} corresponds to a 1:1 molar ratio of monomer and tetramer at 0.086 mM total concentration of **3.2b** and a 4:1 molar ratio of monomer and tetramer at 0.022 mM total concentration of **3.2b**.

200-iteration genetic algorithm-Monte Carlo analysis.[13,22] This treatment resulted in a very good fit to the monomer-tetramer model — with random residuals (Figure 3.19) — and gave K_{assoc} = 1.93 x 10^{14} M^{-3}.

[22] Demeler, B.; Brookes, E.; Wang, R.; Schirf, V.; Kim, C. A. *Macromol. Biosci.* **2010**, *10,* 775–782.

1D ^{1}H NMR spectrum of macrocyclic β-sheet **3.1**
2 mM in D_2O, 500 MHz, 298 K
tetramer predominates, monomer denoted with asterisk (*)

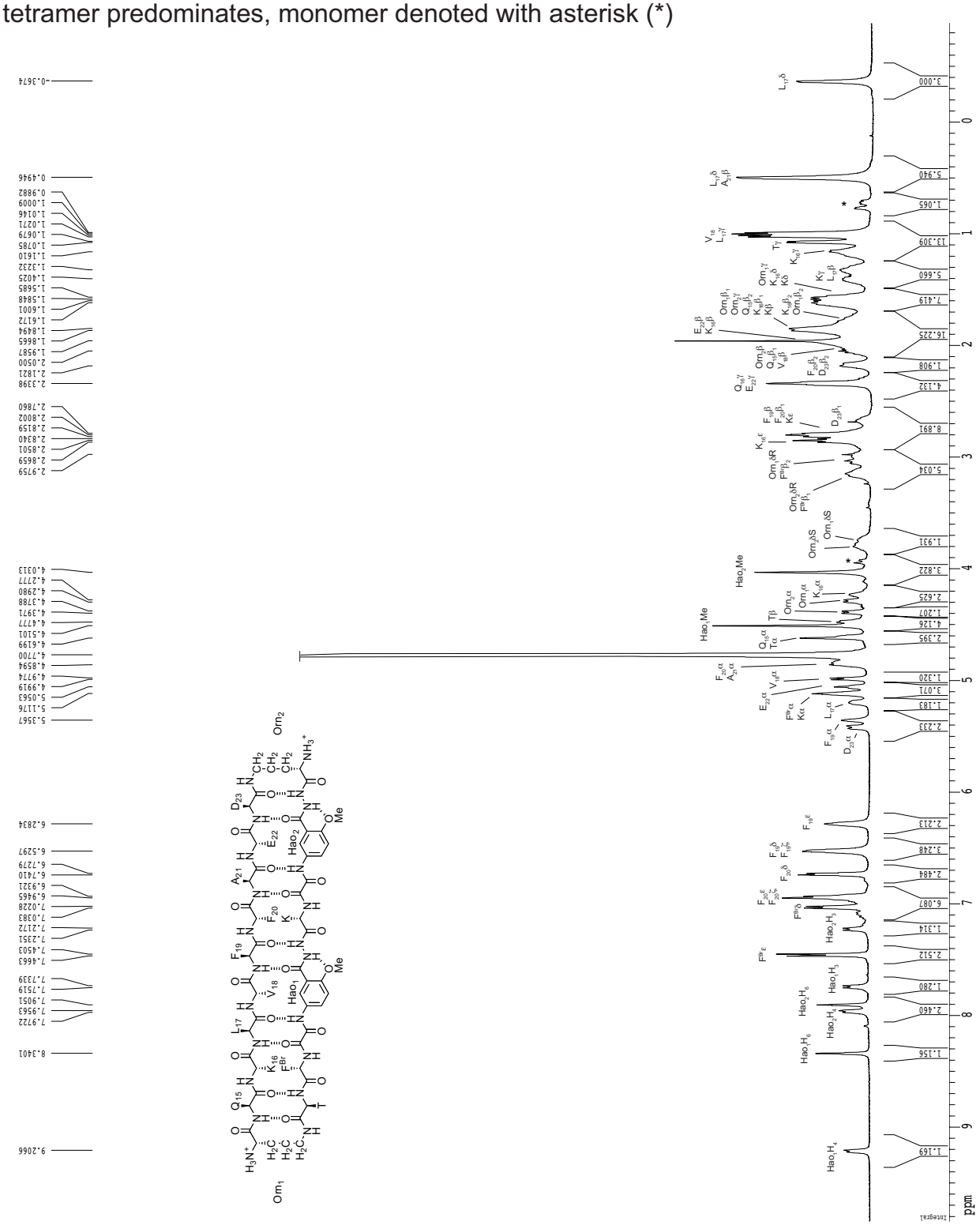

2D TOCSY spectrum of macrocyclic β-sheet **3.1** as tetramer
2 mM in D_2O, 500 MHz, 298 K, 150-ms spin-locking mixing time
tetramer predominates, monomer denoted by asterisk (*)

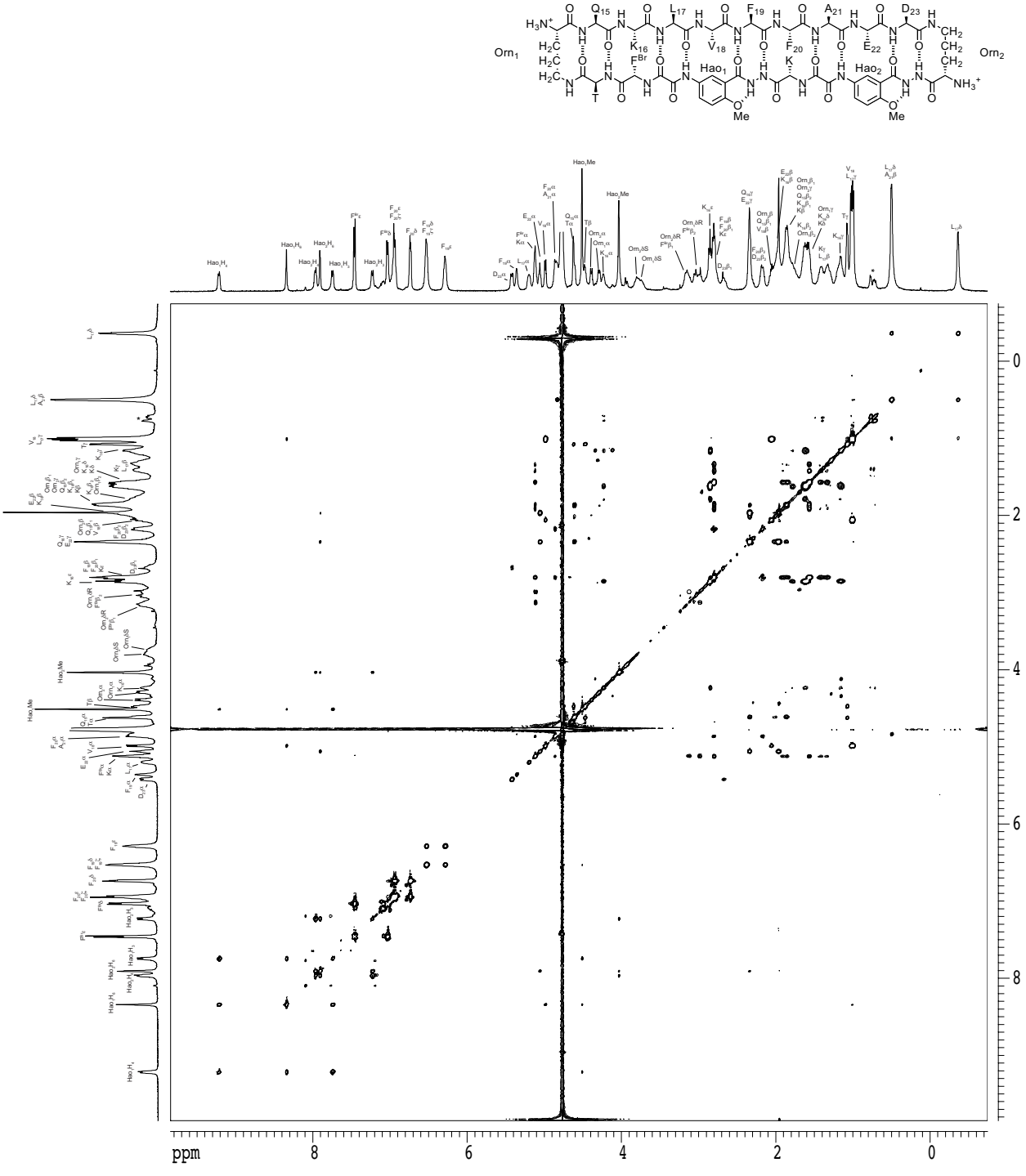

2D TOCSY spectrum of macrocyclic β-sheet **3.1** as tetramer
2 mM in D_2O, 500 MHz, 298 K, 150-ms spin-locking mixing time
tetramer predominates, monomer denoted by asterisk (*)

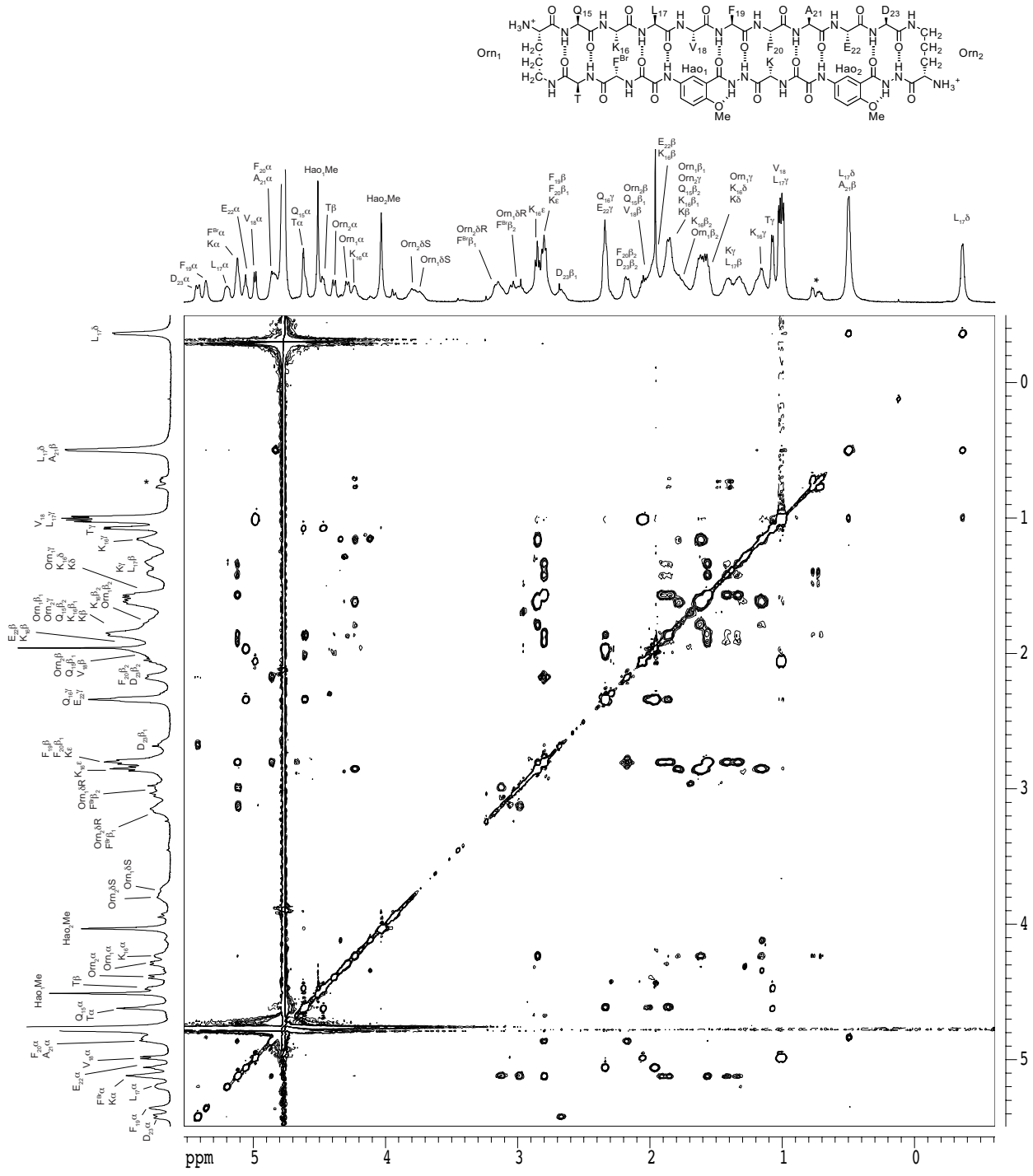

2D TOCSY spectrum of macrocyclic β-sheet **3.1** as tetramer
2 mM in D_2O, 500 MHz, 298 K, 150-ms spin-locking mixing time
tetramer predominates

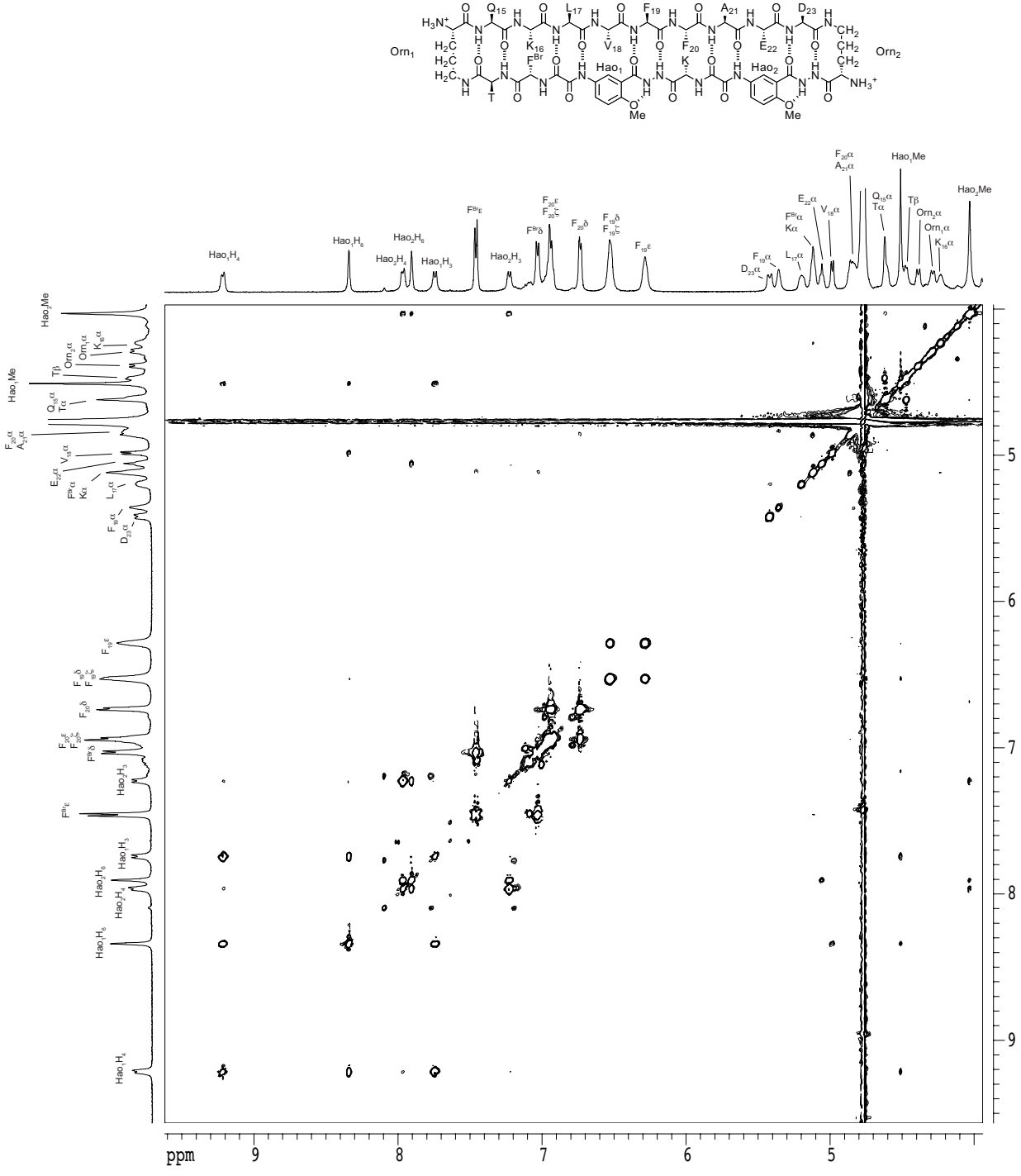

2D NOESY spectrum of macrocyclic β-sheet **3.1** as tetramer
2 mM in D_2O, 500 MHz, 298 K, 200-ms spin-locking mixing time
tetramer predominates, monomer denoted by asterisk (*)

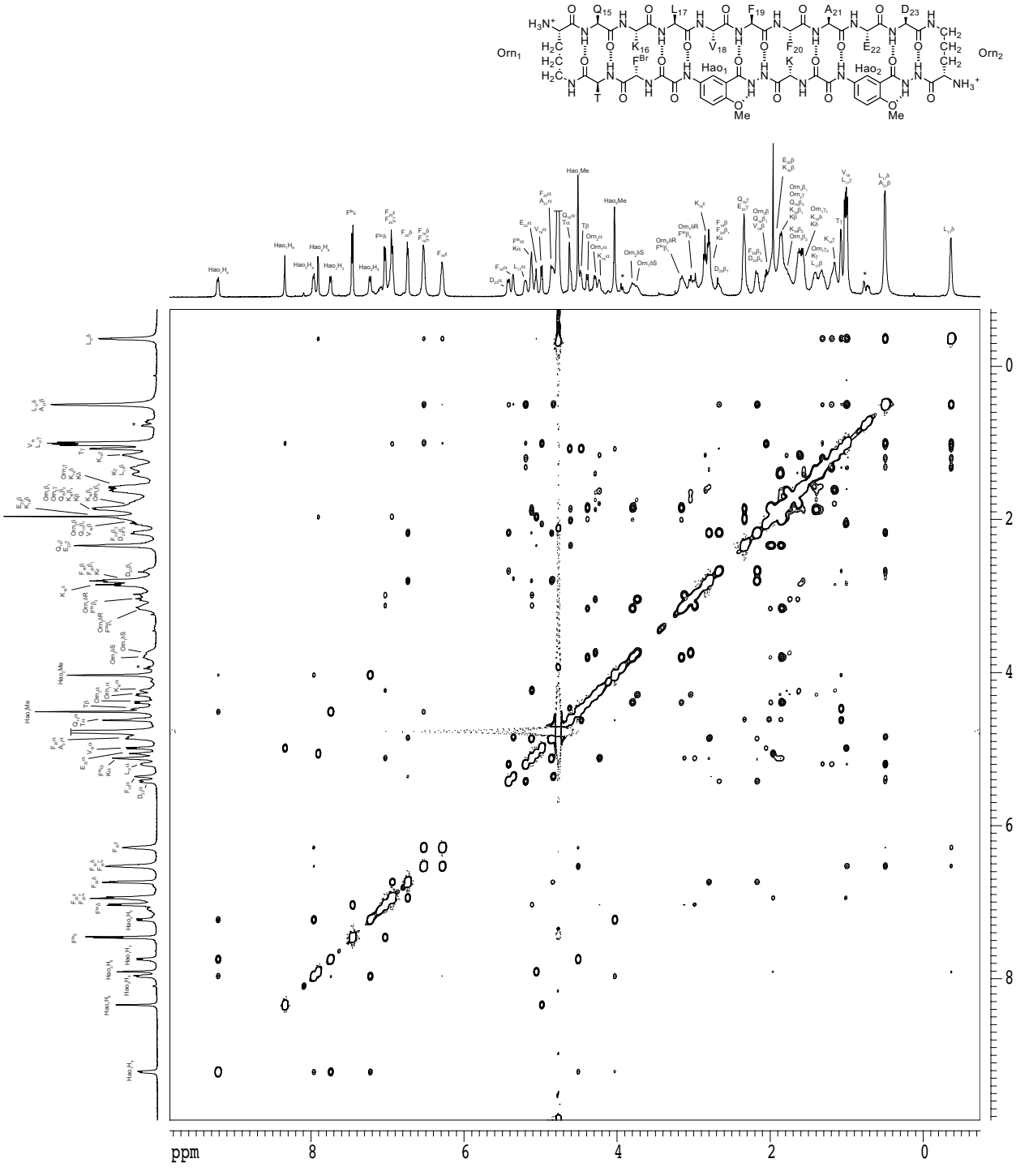

2D NOESY spectrum of macrocyclic β-sheet **3.1** as tetramer
2 mM in D_2O, 500 MHz, 298 K, 200-ms spin-locking mixing time
tetramer predominates, monomer denoted by asterisk (*)
#select NMR crosspeaks are labeled

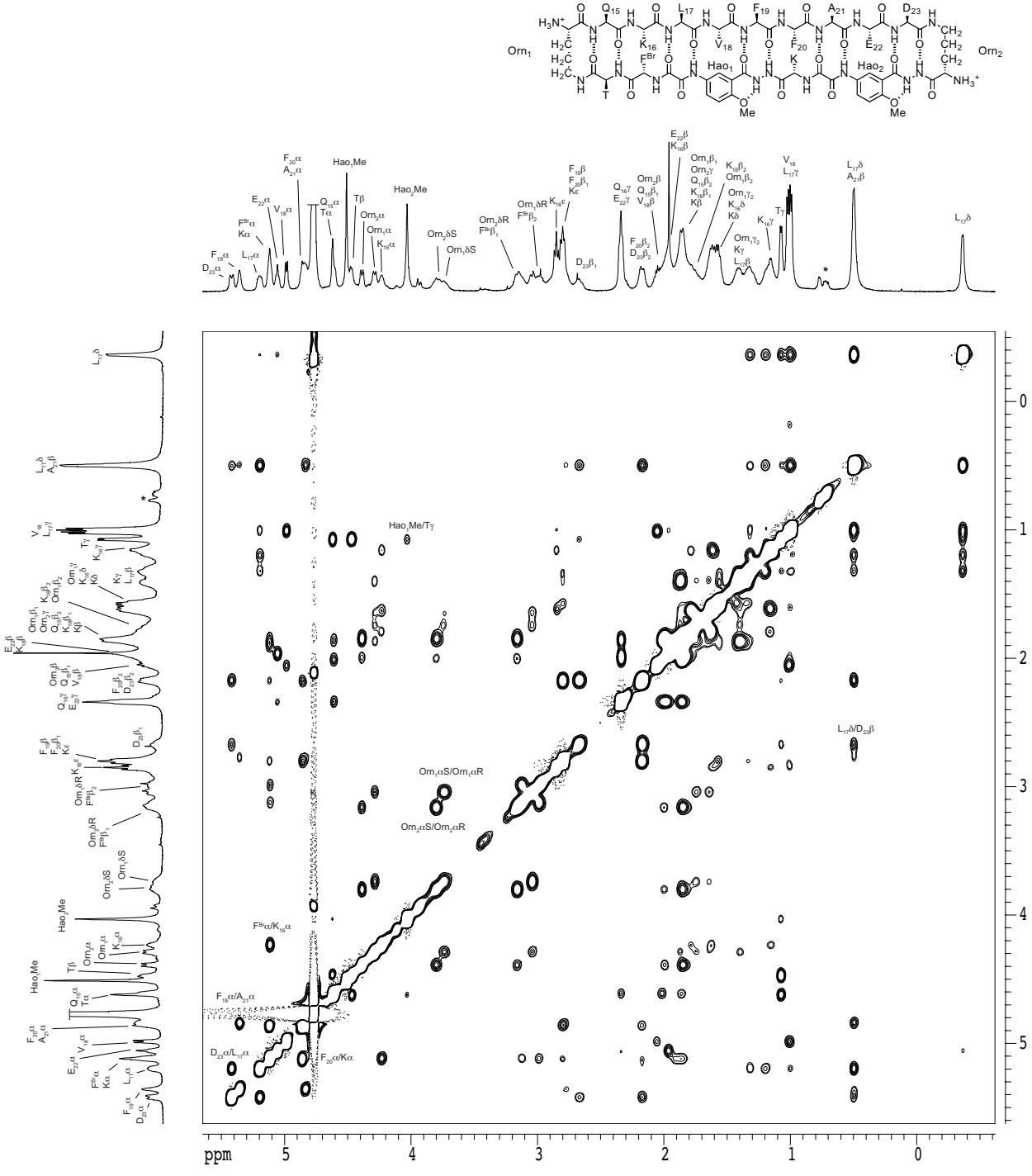

2D NOESY spectrum of macrocyclic β-sheet **3.1**
2 mM in D_2O, 500 MHz, 298 K, 200-ms spin-locking mixing time
tetramer predominates, monomer denoted by asterisk (*)
[#]select NMR crosspeaks are labeled

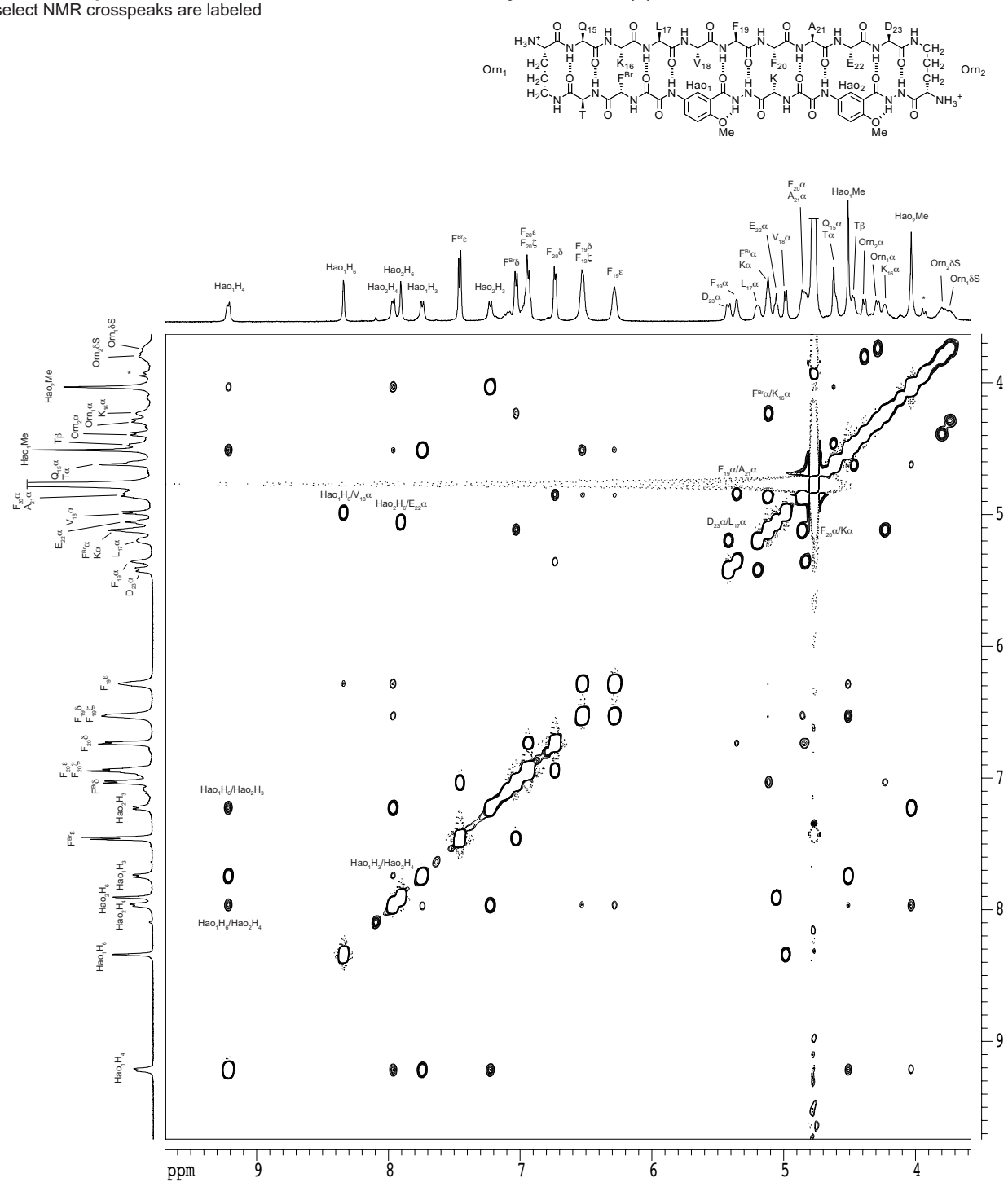

2D DOSY spectrum of macrocyclic β-sheet **3.1**
2 mM in D_2O, 600 MHz, 298 K
tetramer predominates

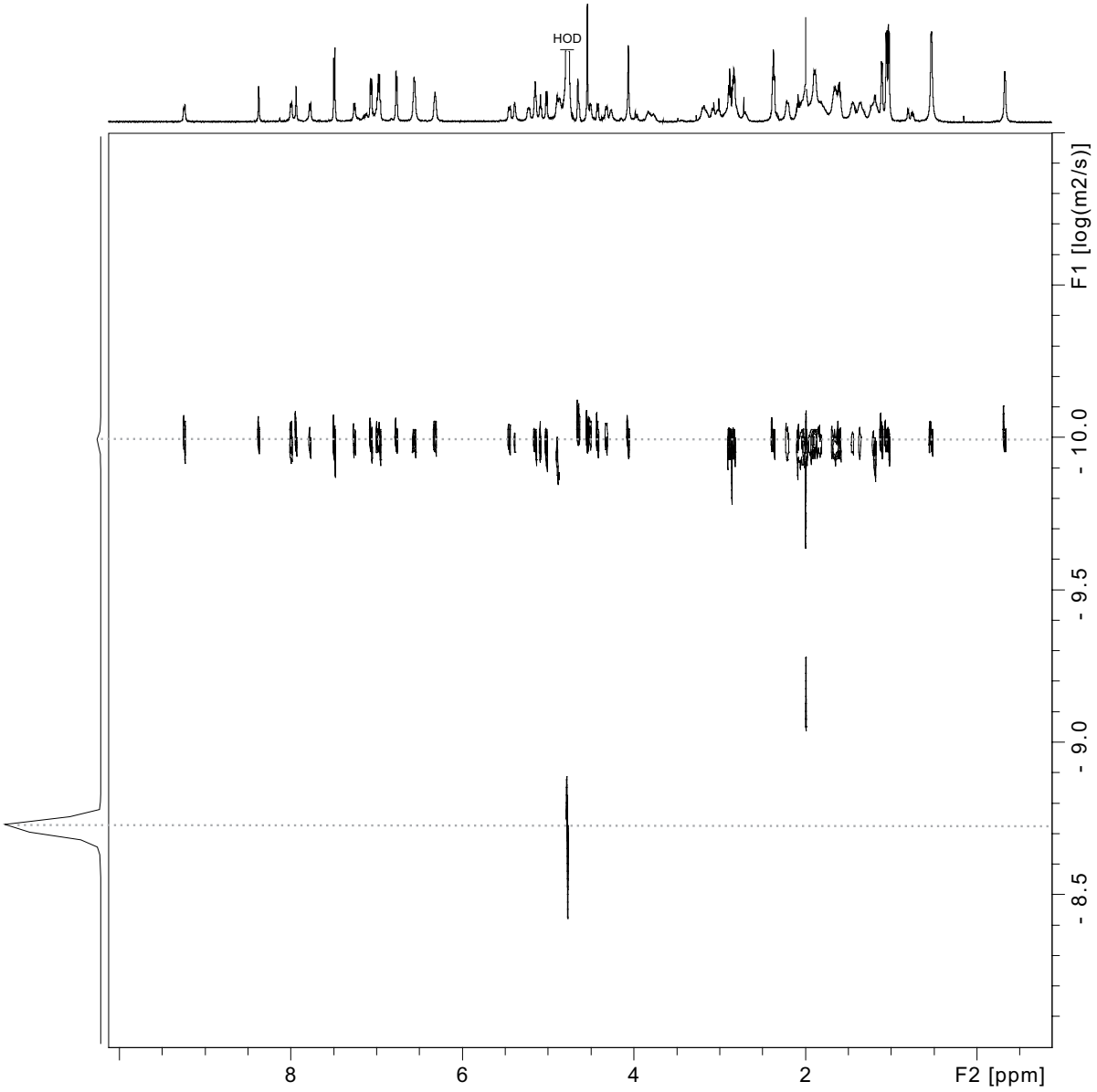

Calculation for 3.1 at 2.0 mM

DC_{HOD} = 19.0 x 10^{-10} m^2/s [a]
log DC_{HOD} = -8.721

For 3.1 tetramer, log DC (m^2/s) = -9.99(7), DC = $10^{-9.997}$ m^2/s = 10.1 x 10^{-11} m^2/s = 10.1 x 10^{-7} cm^2/s

[a] Longsworth, L. G. J. Phys. Chem. 1960, 64, 1914–1917.

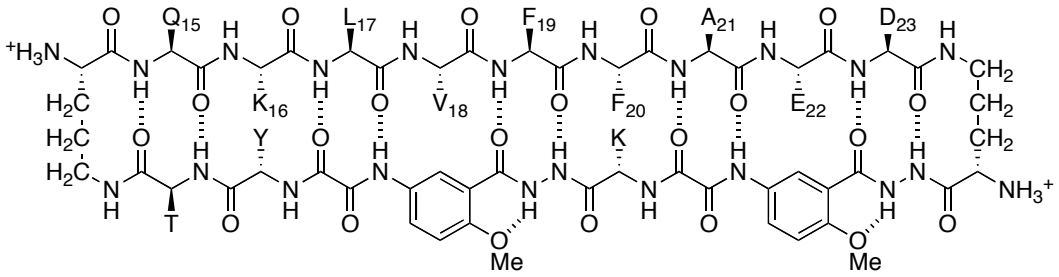

macrocyclic β-sheet peptide **3.2a** (as the TFA salt)

molecular weight calculated for $C_{101}H_{141}N_{25}O_{29} \cdot 4CF_3CO_2H$ (TFA salt of **3.2a**): 2625.44
molecular weight calculated for $C_{101}H_{141}N_{25}O_{29}$ (free base of **3.2a**): 2169.35
exact mass calculated for $C_{101}H_{141}N_{25}O_{29}$ (free base of **3.2a**): 2168.03

Analytical RP-HPLC of macrocyclic β-peptide **3.2a**

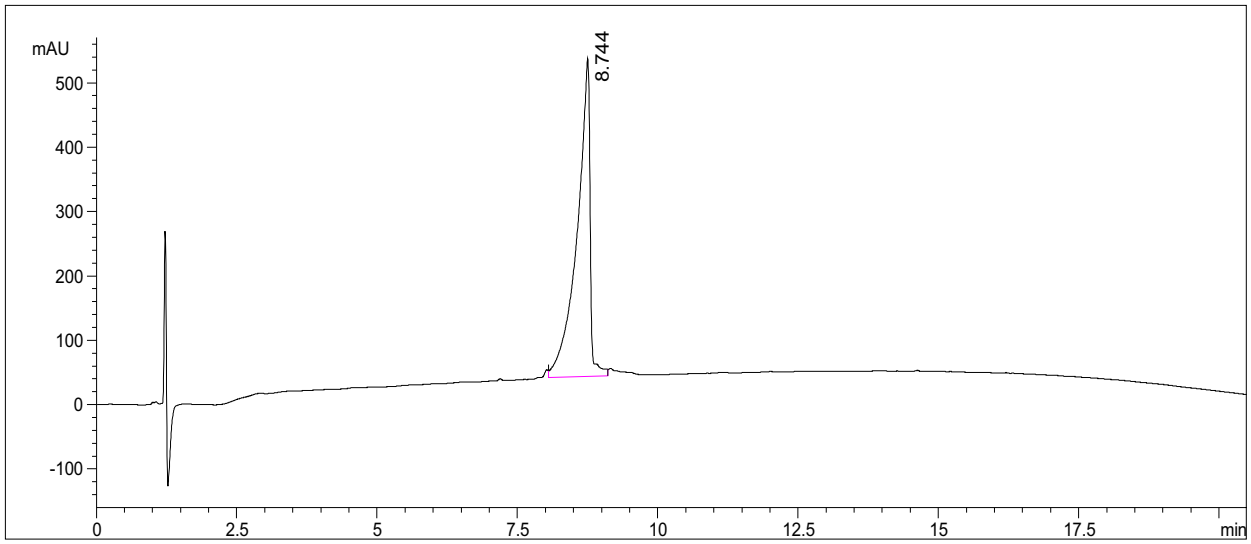

Signal 1: VWD1 A, Wavelength=214 nm

Peak #	RetTime [min]	Type	Width [min]	Area mAU *s	Height [mAU]	Area %
1	8.744	VV	0.2105	7939.88721	494.81061	100.0000
Totals :				7939.88721	494.81061	

Macrocyclic β-sheet peptide **3.2a**

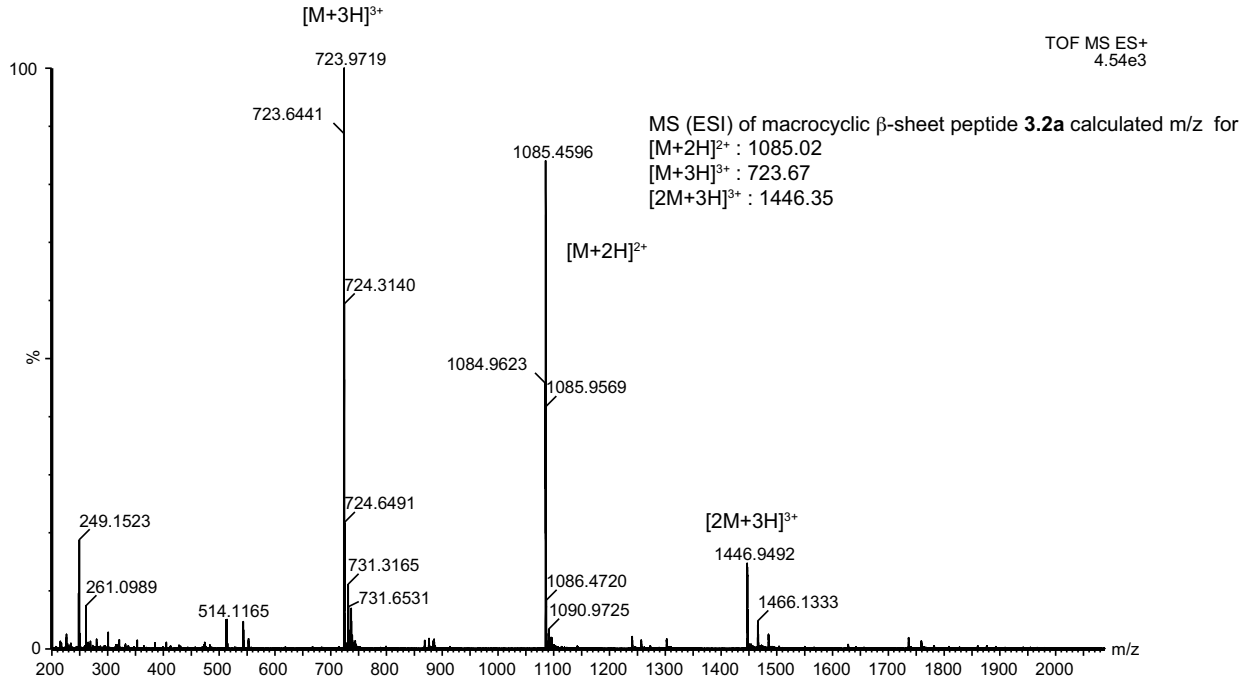

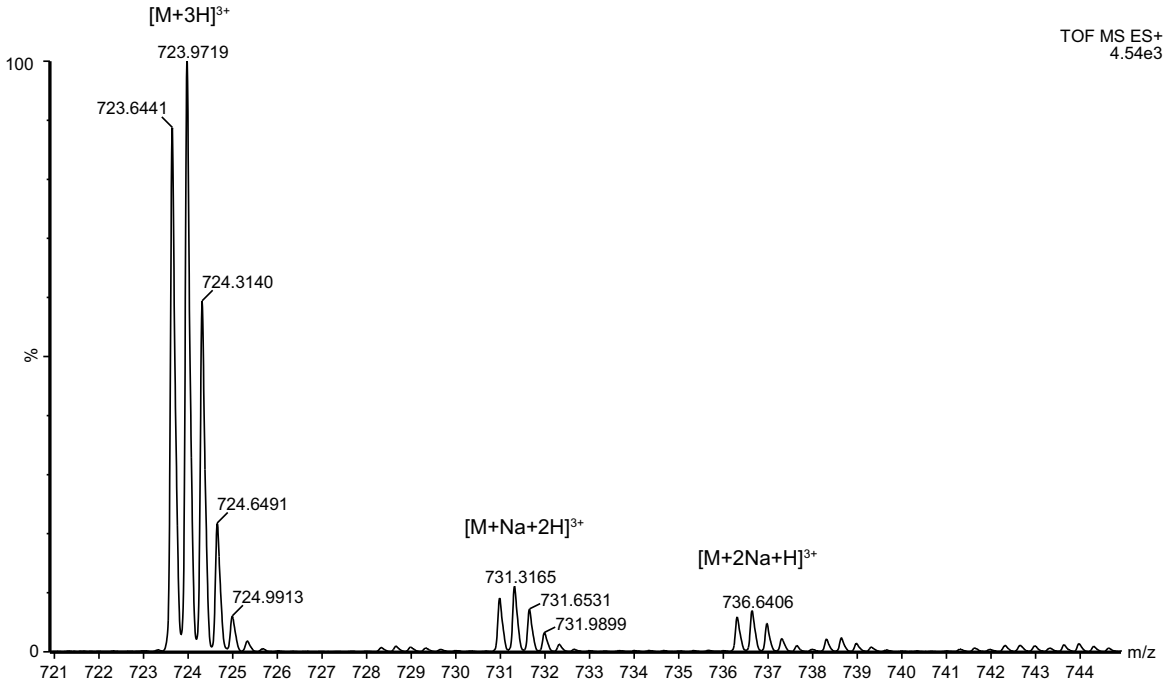

Macrocyclic β-sheet peptide **3.2a**

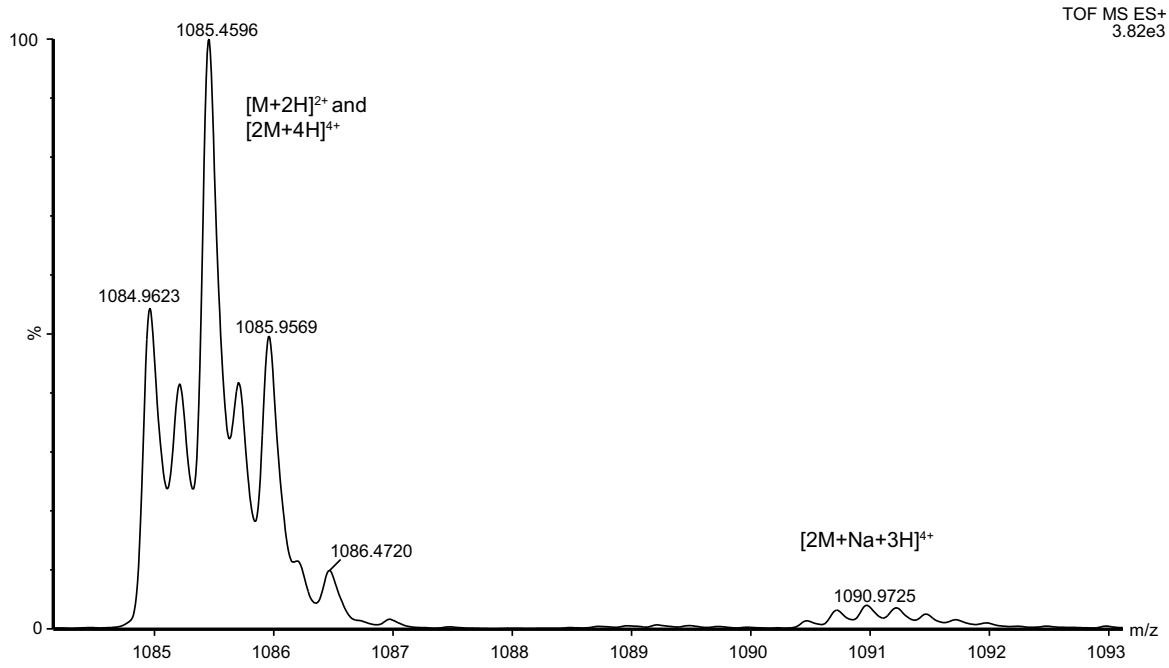

1D ^{1}H NMR spectrum of macrocyclic β-sheet **3.2a**
8 mM in D_2O, 500 MHz, 300.5 K
tetramer predominates

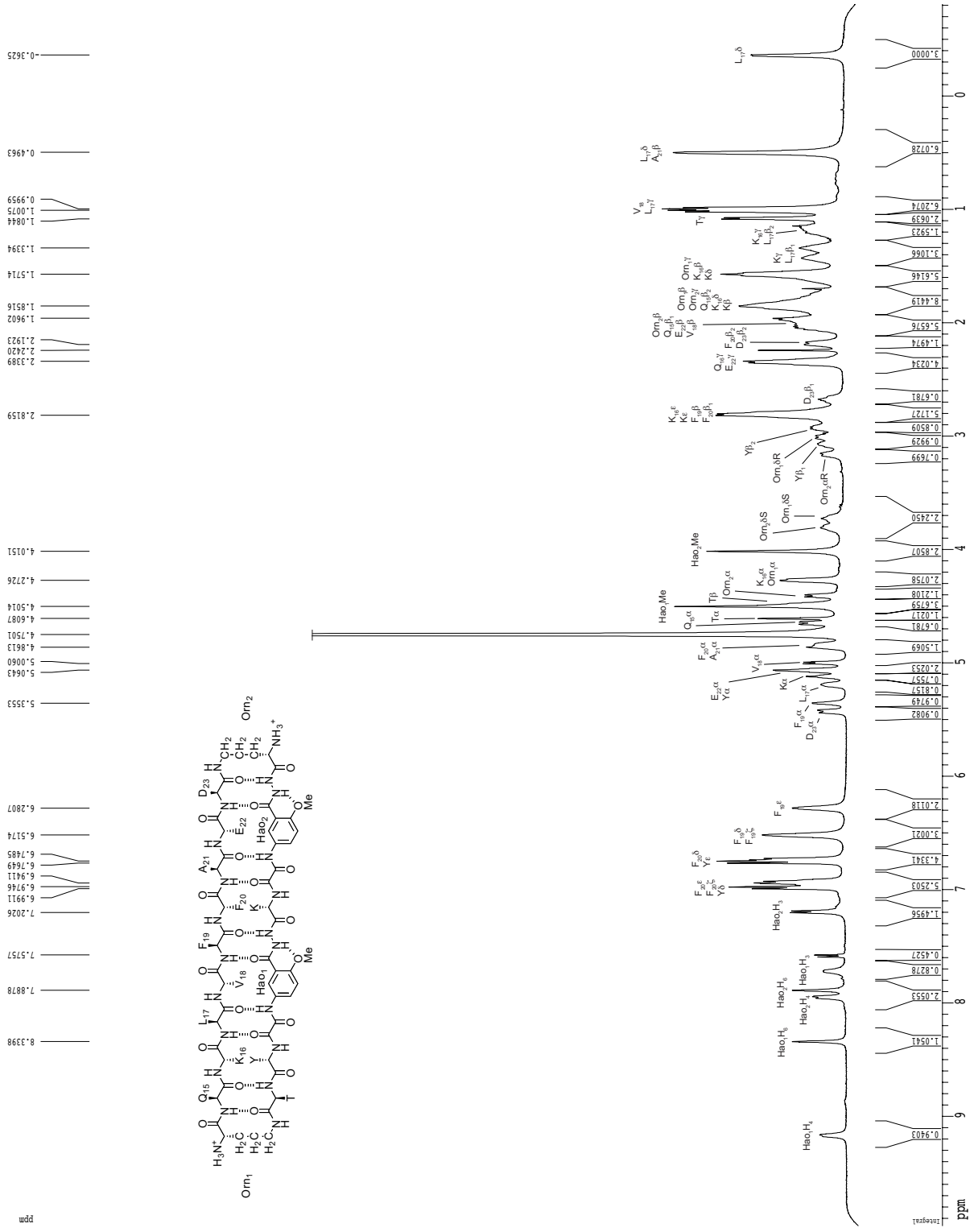

2D TOCSY spectrum of macrocyclic β-sheet **3.2a**
2 mM in D_2O, 500 MHz, 300.5 K, 150-ms spin-locking mixing time
tetramer predominates, monomer denoted with an asterisk (*)

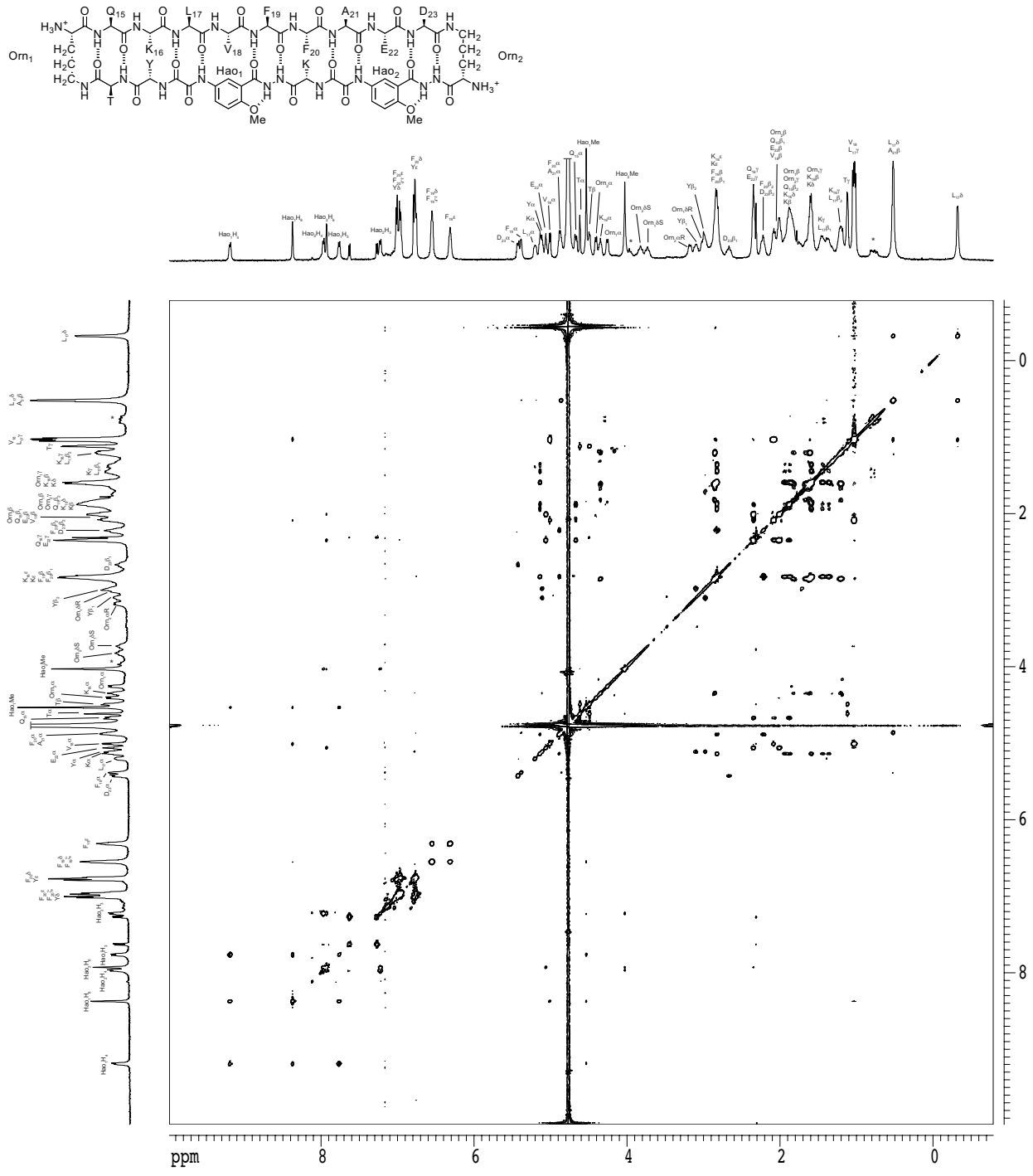

2D TOCSY spectrum of macrocyclic β-sheet **3.2a**
2 mM in D_2O, 500 MHz, 300.5 K, 150-ms spin-locking mixing time
tetramer predominates, monomer denoted with an asterisk (*)

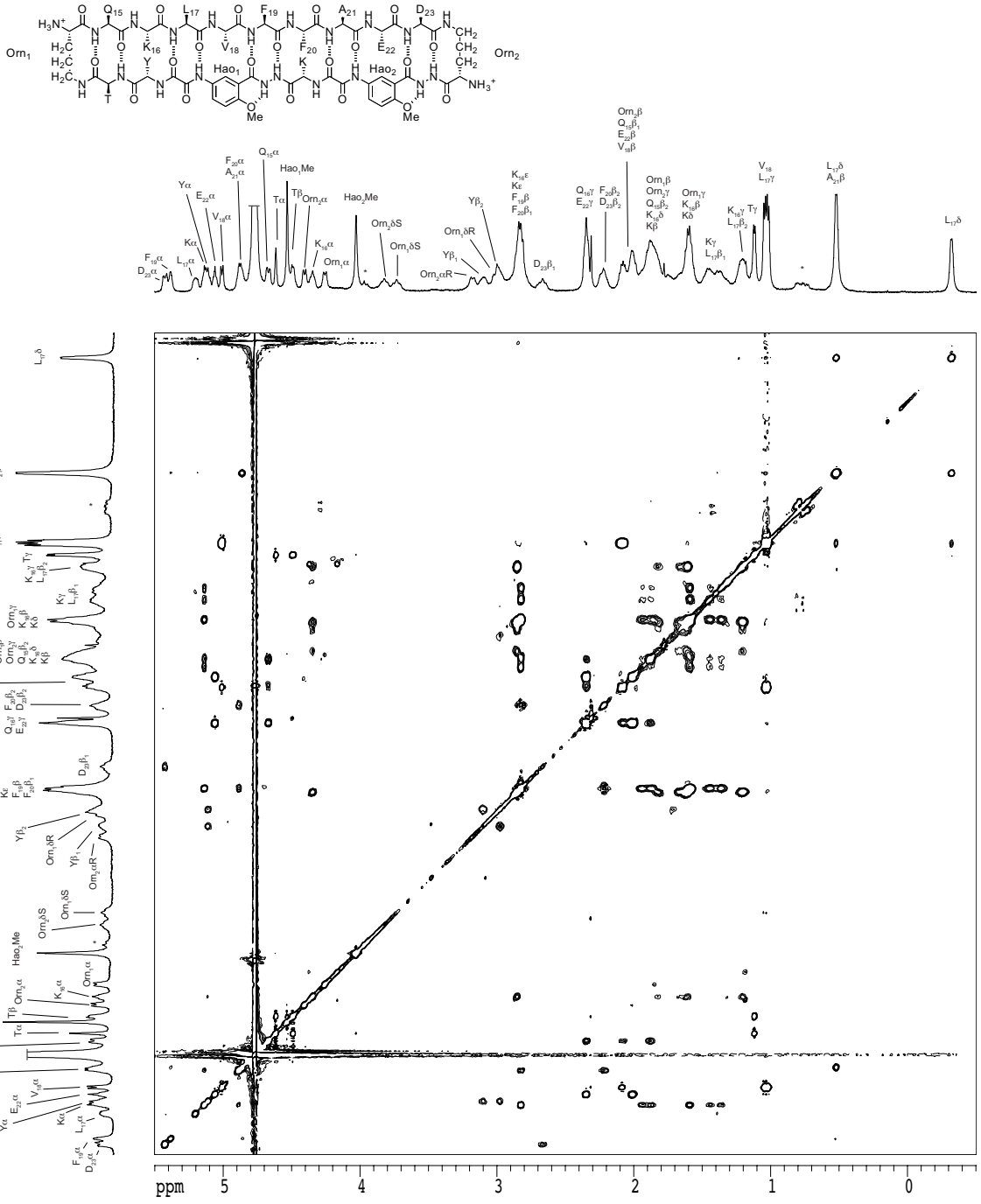

2D TOCSY spectrum of macrocyclic β-sheet **3.2a**
2 mM in D_2O, 500 MHz, 300.5 K, 150-ms spin-locking mixing time
tetramer predominates, monomer denoted with an asterisk (*)

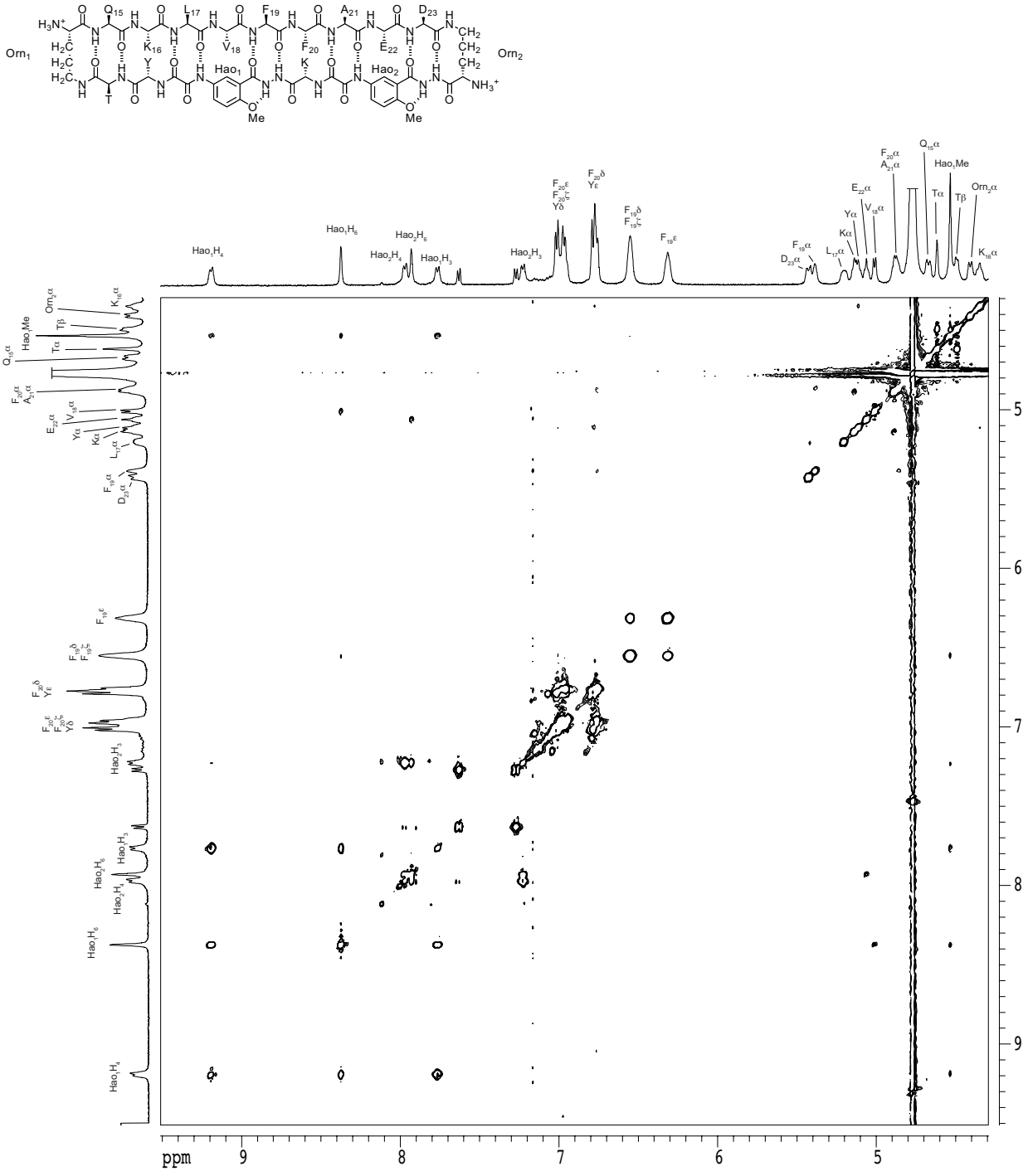

2D NOESY spectrum of macrocyclic β-sheet **3.2a**
8 mM in D_2O, 500 MHz, 300.5 K, 150-ms spin-locking mixing time
tetramer predominates

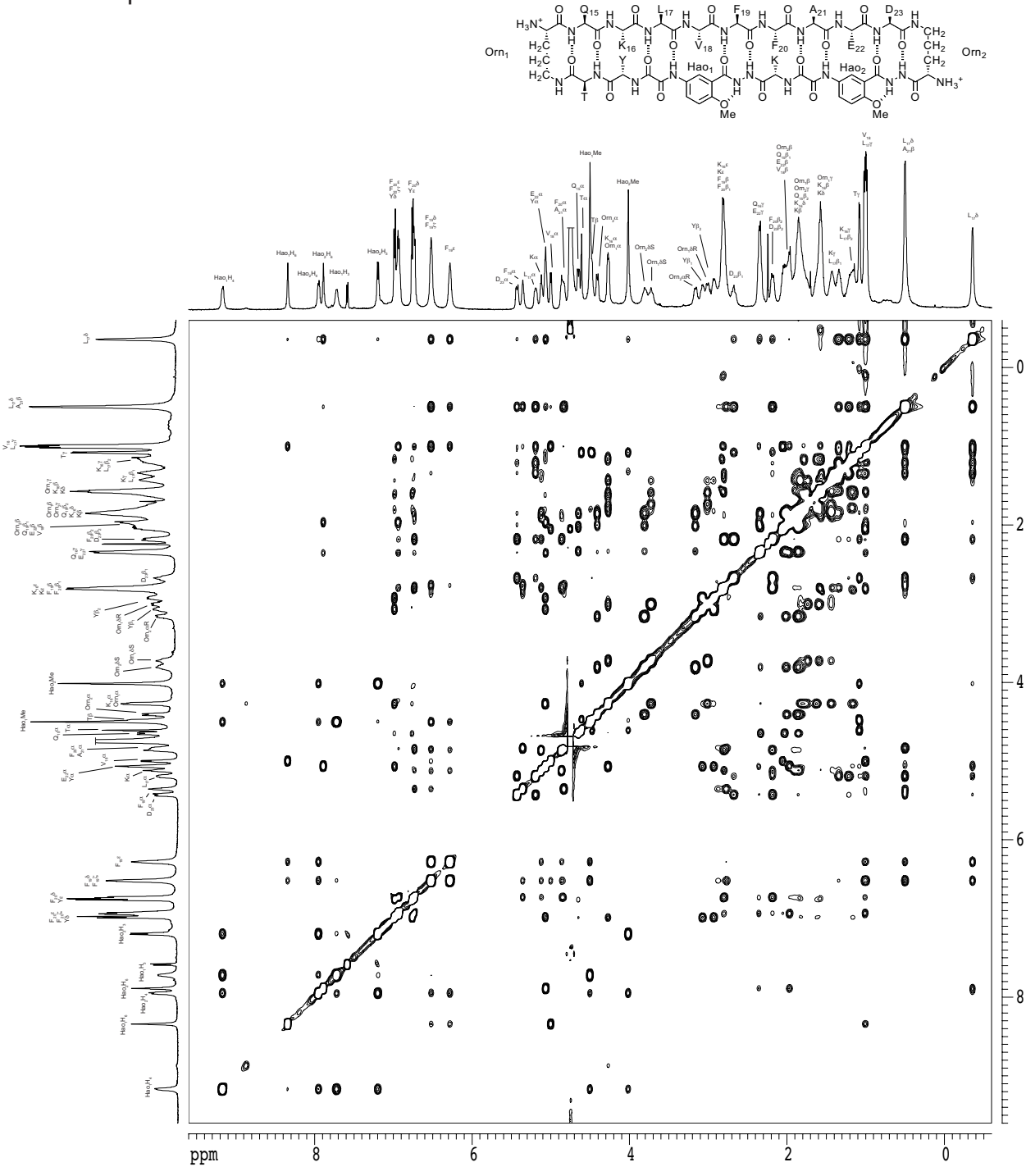

2D NOESY spectrum of macrocyclic β-sheet **3.2a**
8 mM in D_2O, 500 MHz, 300.5 K, 150-ms spin-locking mixing time
tetramer predominates
#select NMR crosspeaks are labeled

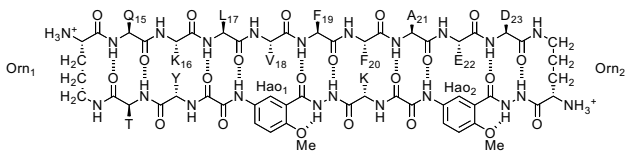

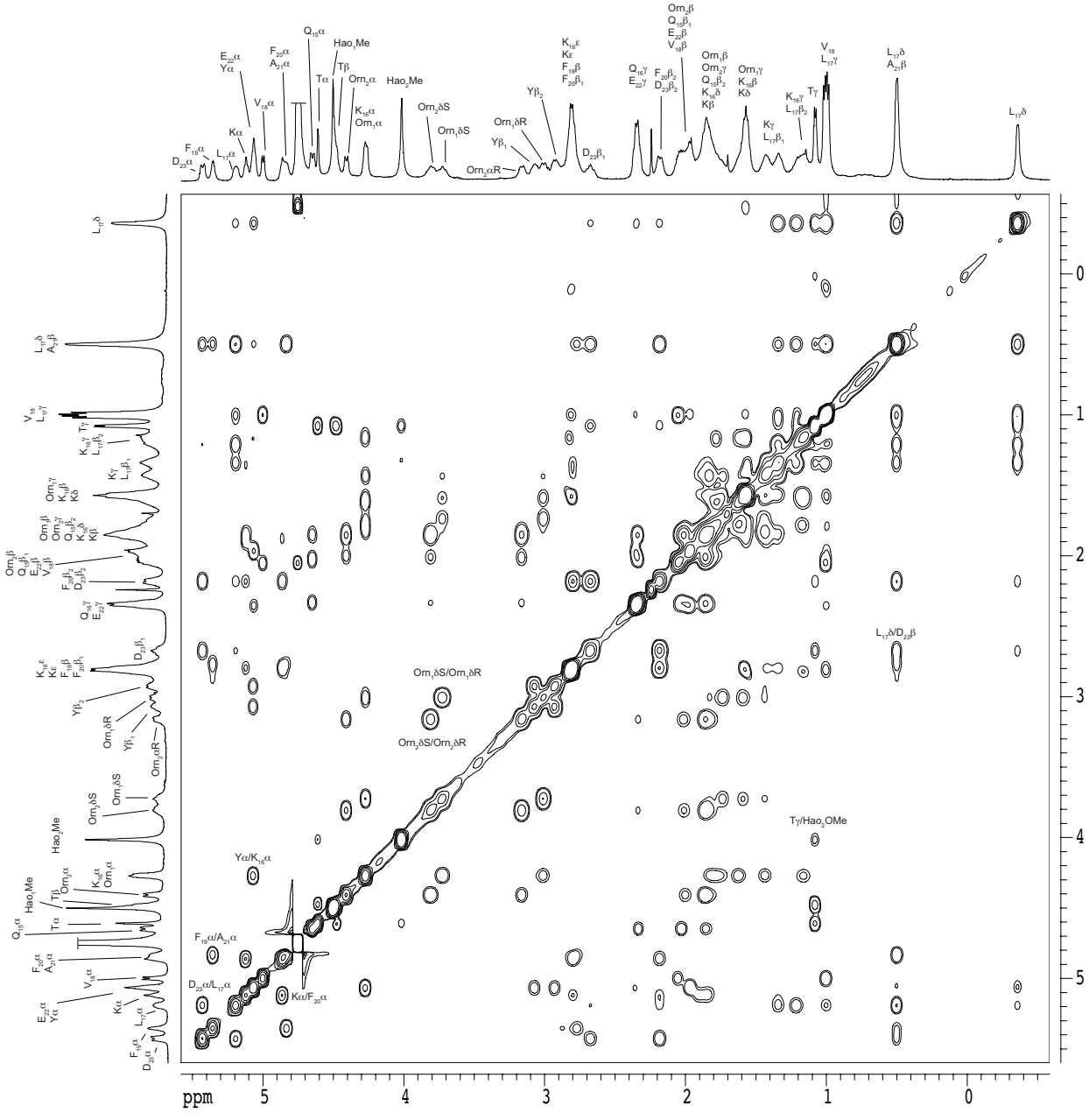

2D NOESY spectrum of macrocyclic β-sheet **3.2a**
8 mM in D_2O, 500 MHz, 300.5 K, 150-ms spin-locking mixing time
tetramer predominates

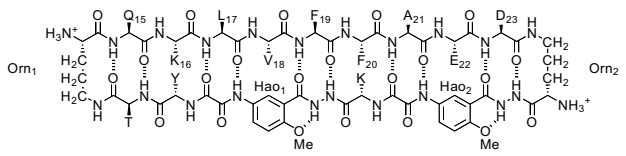

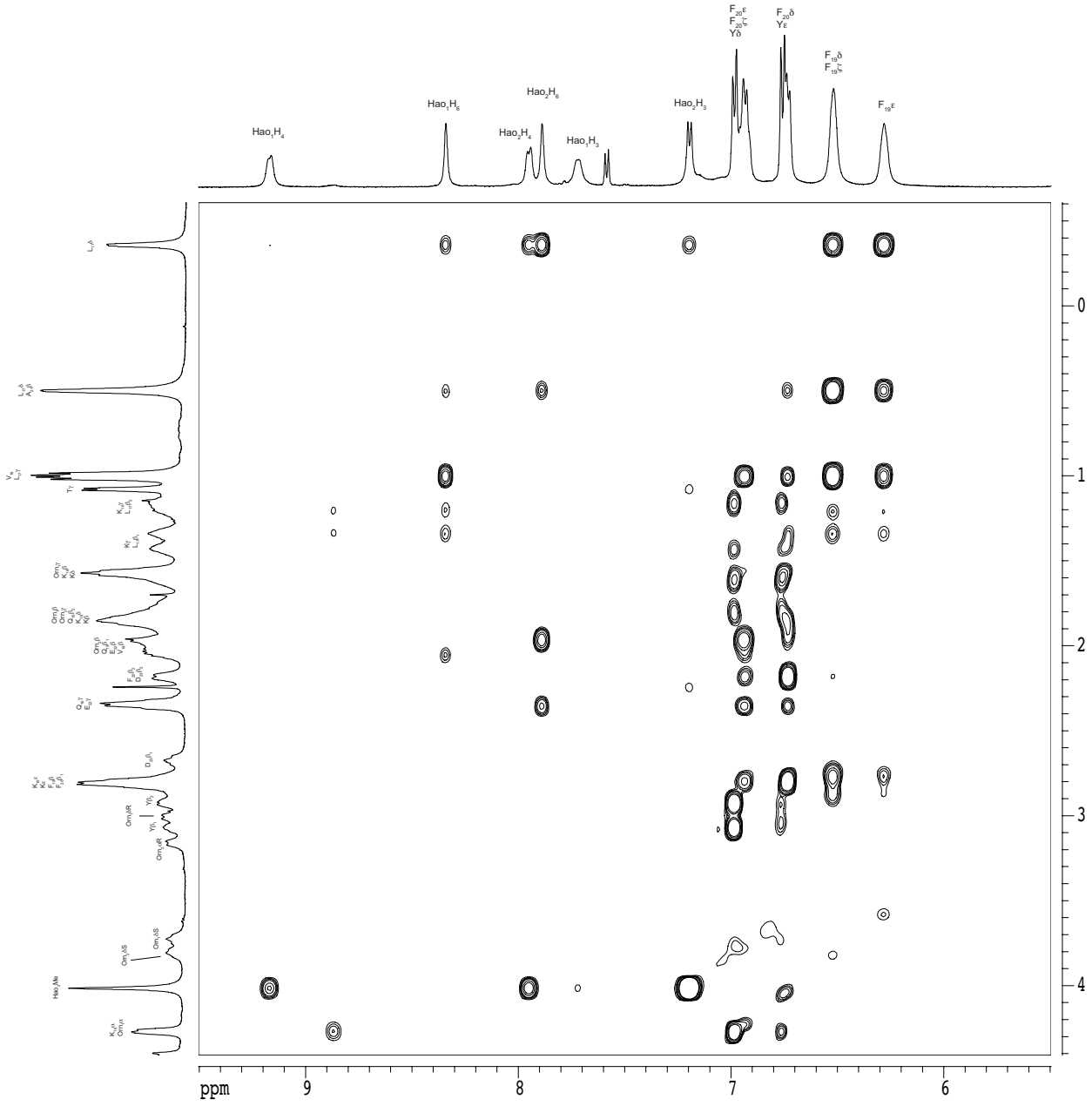

2D NOESY spectrum of macrocyclic β-sheet **3.2a**
8 mM in D_2O, 500 MHz, 300.5 K, 150-ms spin-locking mixing time
tetramer predominates
#select NMR crosspeaks are labeled

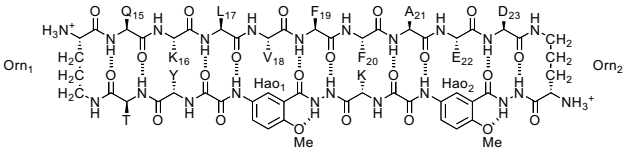

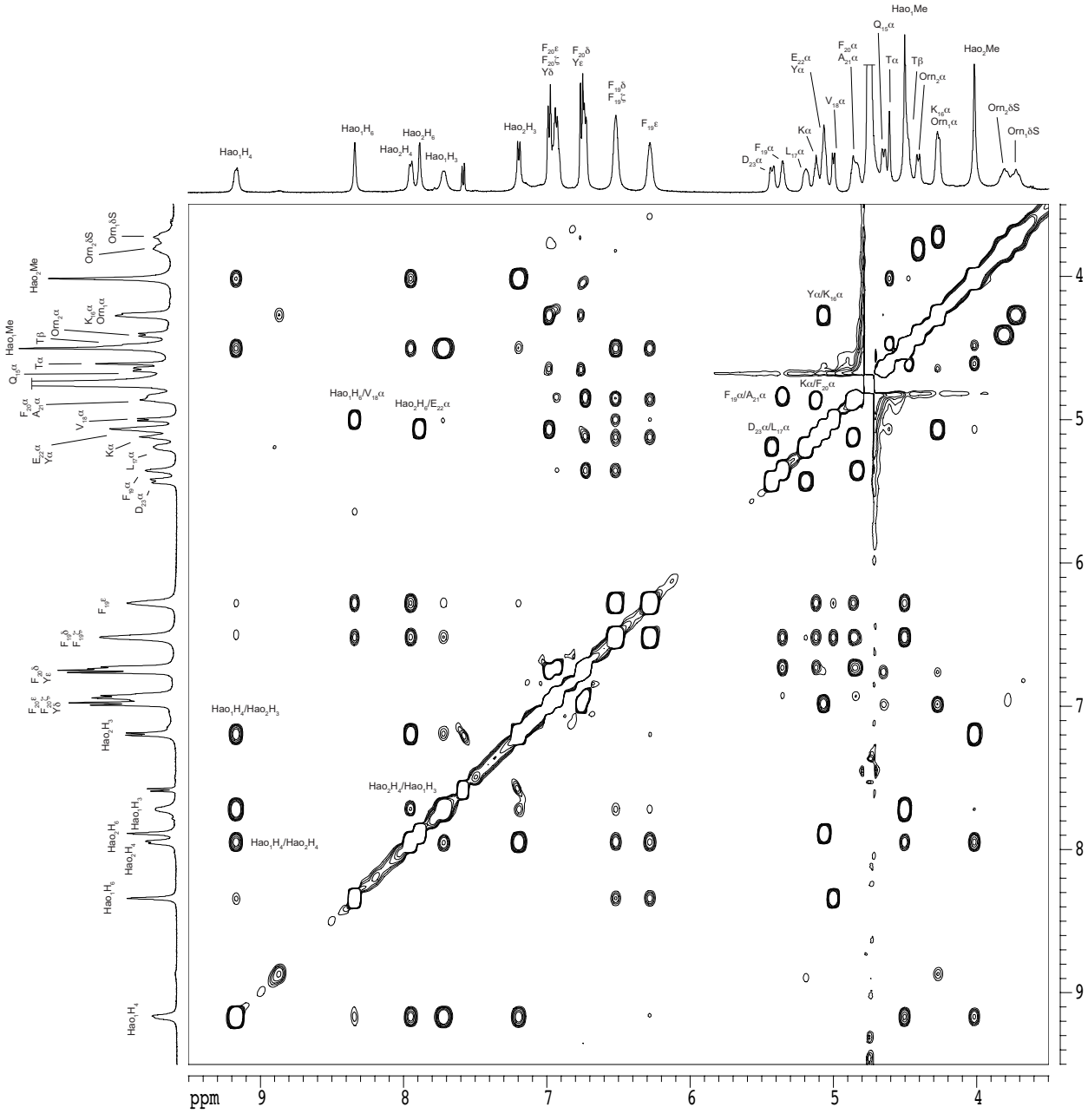

1D ^{1}H NMR spectrum of macrocyclic β-sheet **3.2a**
with WATERGATE
8 mM in 9:1 H_2O/D_2O, 800 MHz, 298 K
tetramer predominates

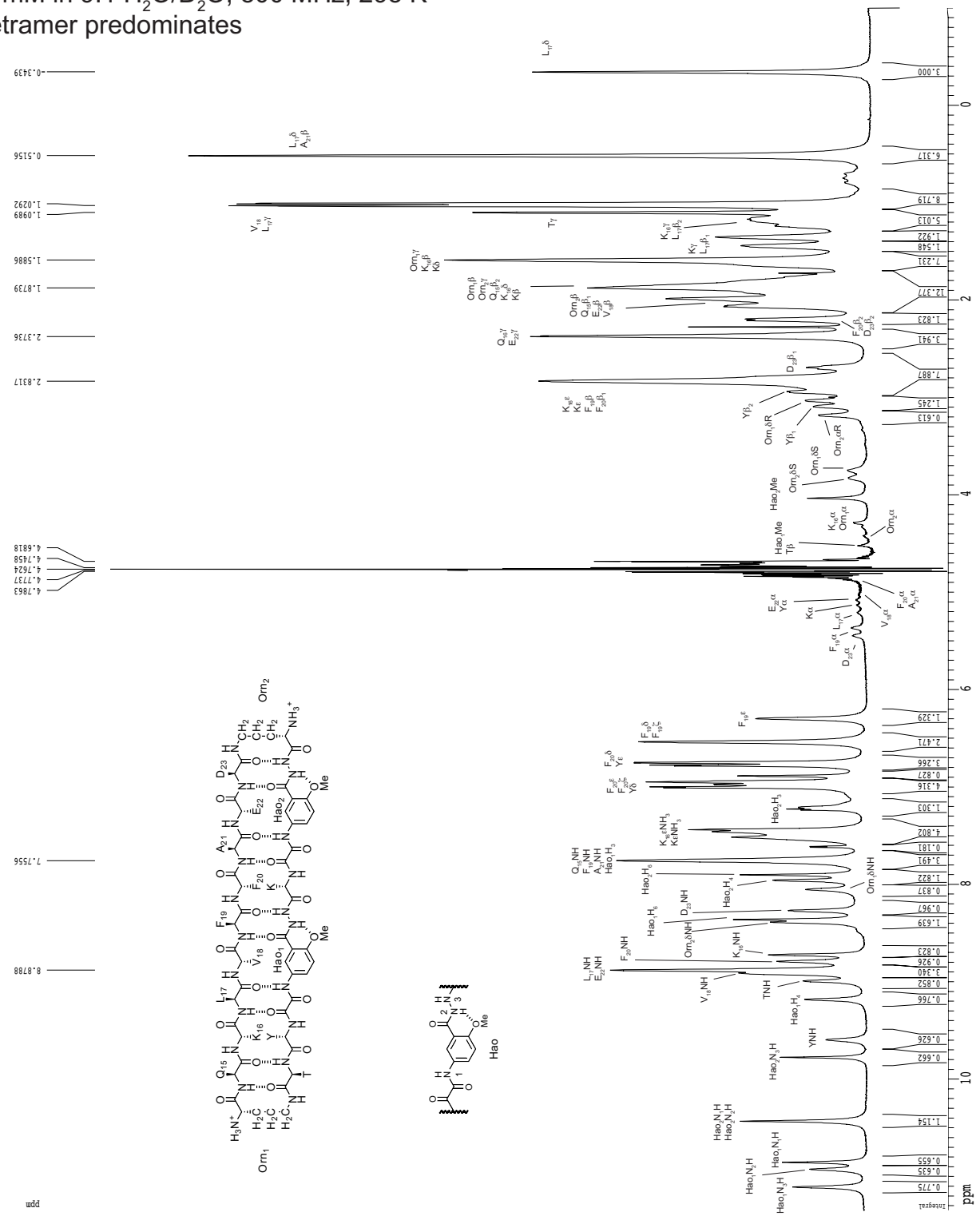

2D TOCSY spectrum of macrocyclic β-sheet **3.2a** with WATERGATE
8 mM in 9:1 H_2O/D_2O, 800 MHz, 298 K
75-ms spin-locking mixing time
tetramer predominates

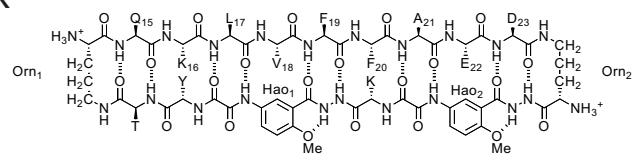

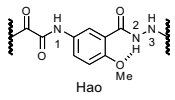

2D TOCSY spectrum of macrocyclic β-sheet **3.2a** with WATERGATE
8 mM in 9:1 H_2O/D_2O, 800 MHz, 298 K
75-ms spin-locking mixing time
tetramer predominates

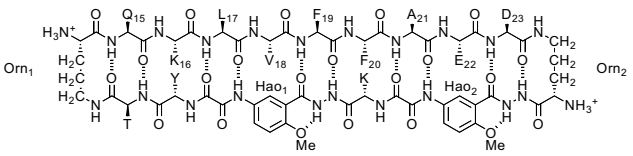

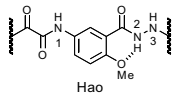

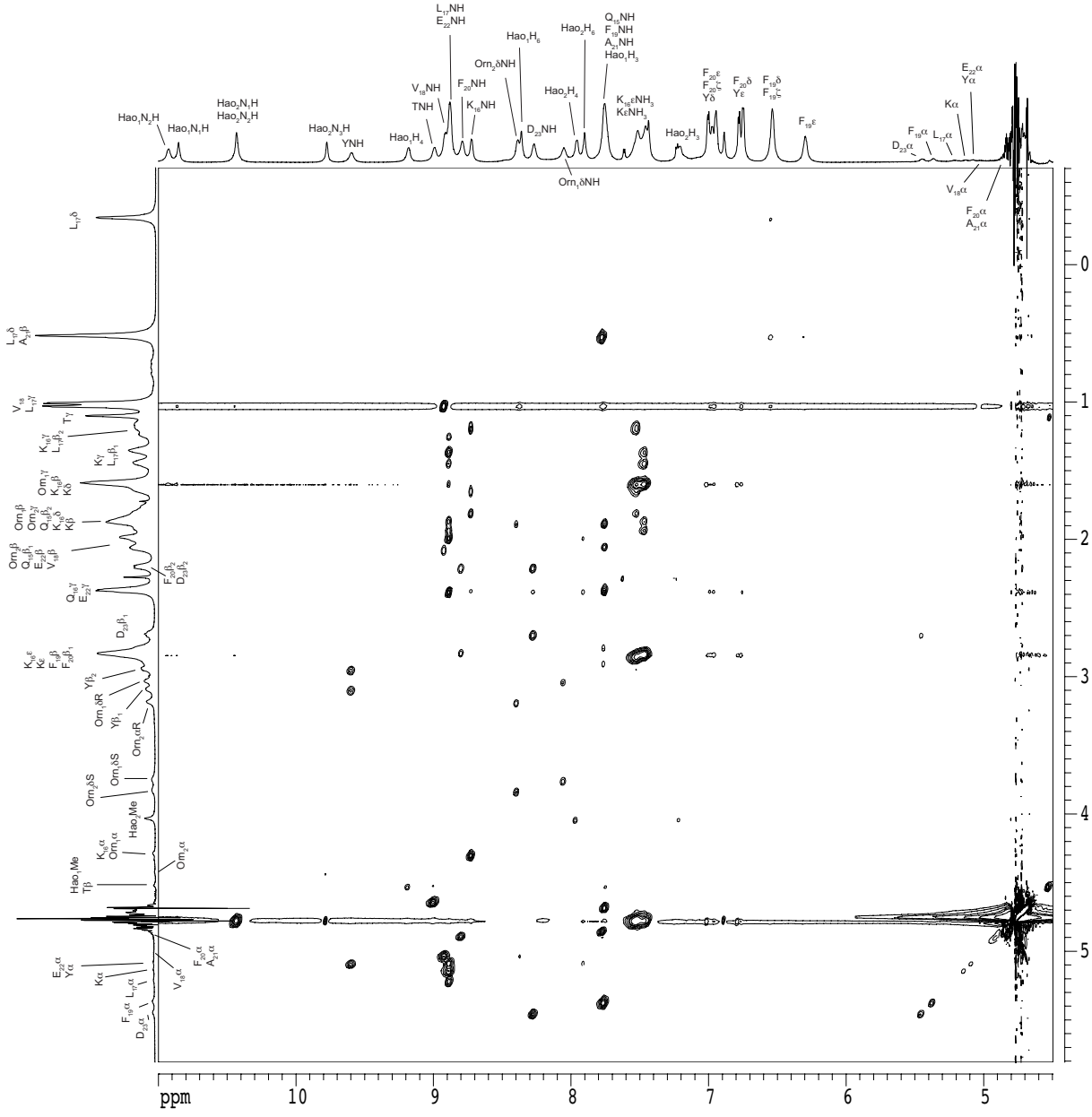

2D TOCSY spectrum of macrocyclic β-sheet **3.2a** with WATERGATE
8 mM in 9:1 H_2O/D_2O, 800 MHz, 298 K
75-ms spin-locking mixing time
tetramer predominates

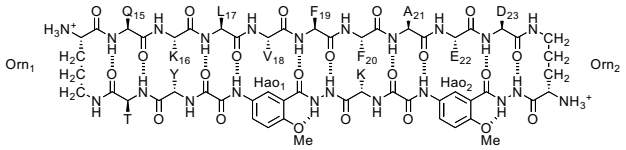

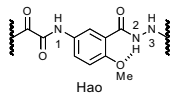

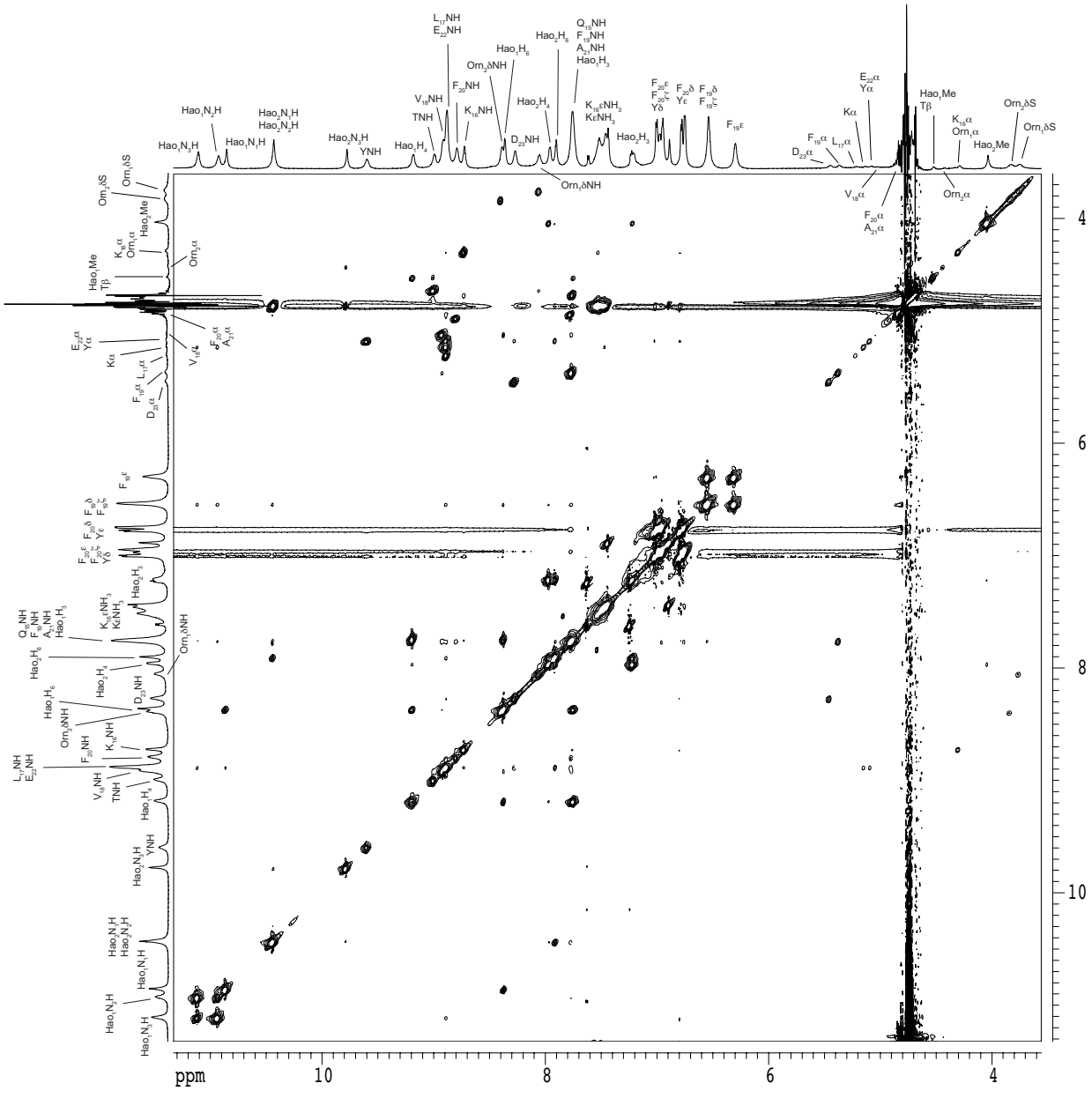

2D NOESY spectrum of macrocyclic β-sheet **3.2a** with WATERGATE
8 mM in 9:1 H_2O/D_2O, 800 MHz, 298 K
225-ms spin-locking mixing time
tetramer predominates

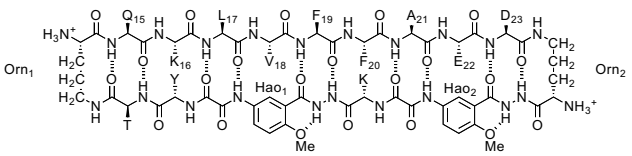

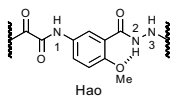

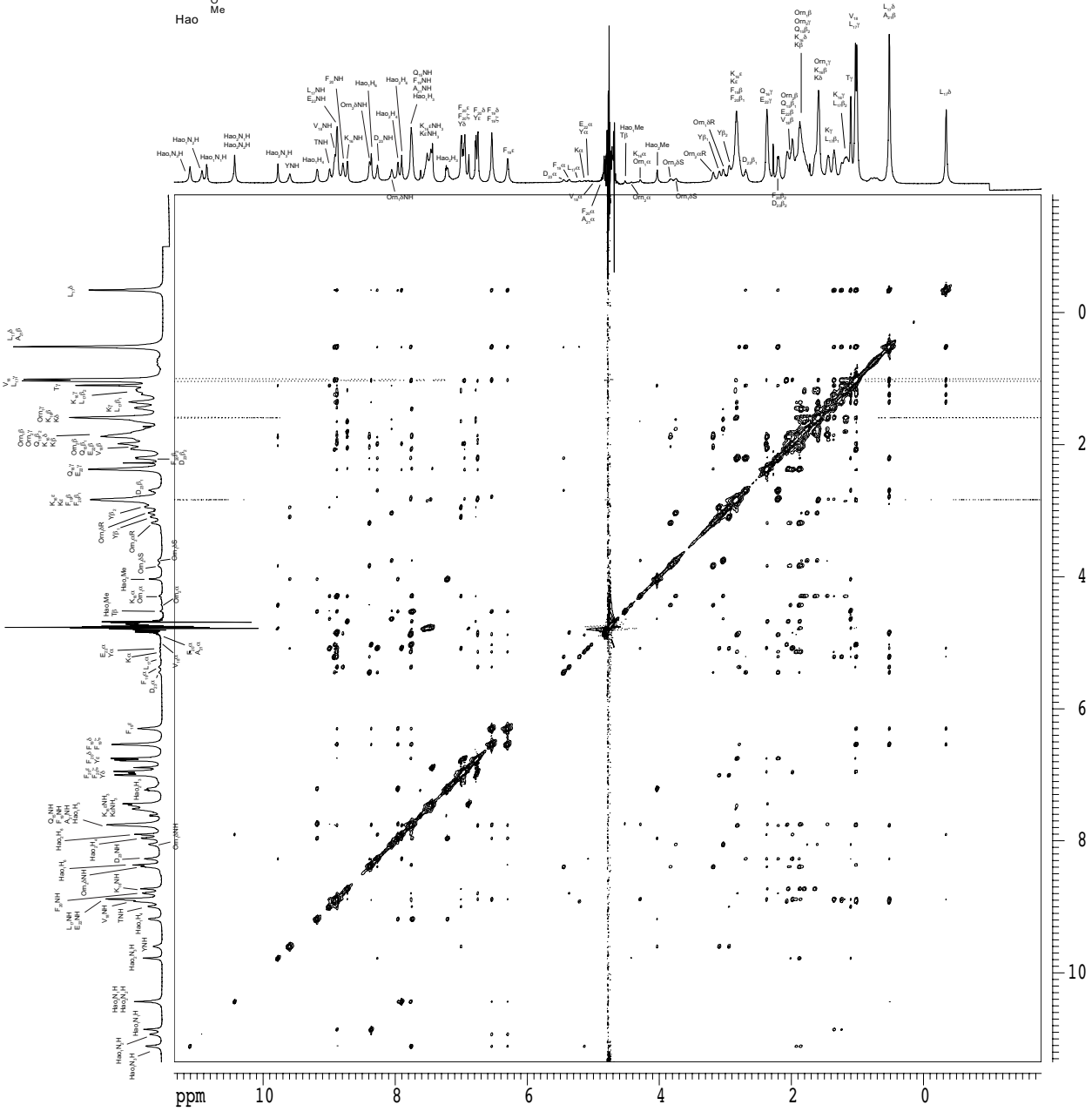

2D NOESY spectrum of macrocyclic β-sheet **3.2a** with WATERGATE
8 mM in 9:1 H_2O/D_2O, 800 MHz, 298 K
225-ms spin-locking mixing time
tetramer predominates

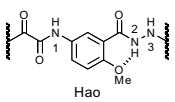

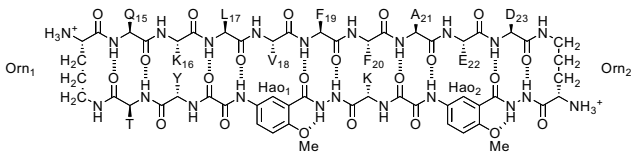

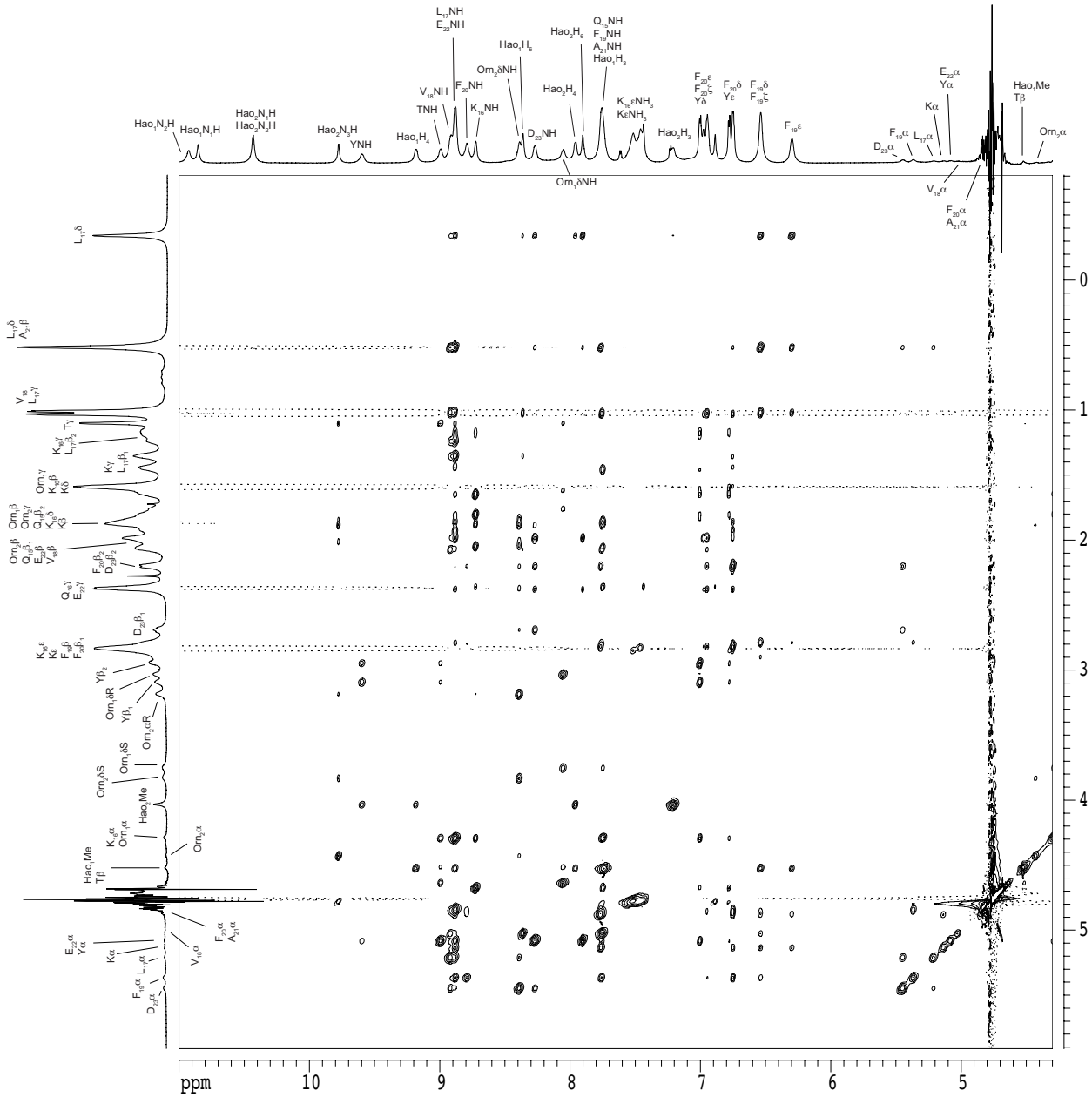

2D NOESY spectrum of macrocyclic β-sheet **3.2a** with WATERGATE
8 mM in 9:1 H_2O/D_2O, 800 MHz, 298 K
225-ms spin-locking mixing time
tetramer predominates
#select NMR crosspeaks are labeled

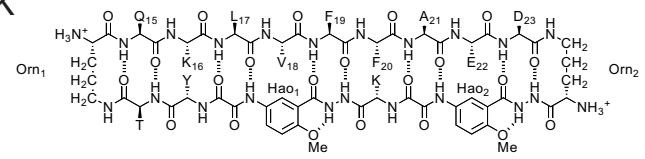

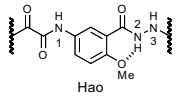

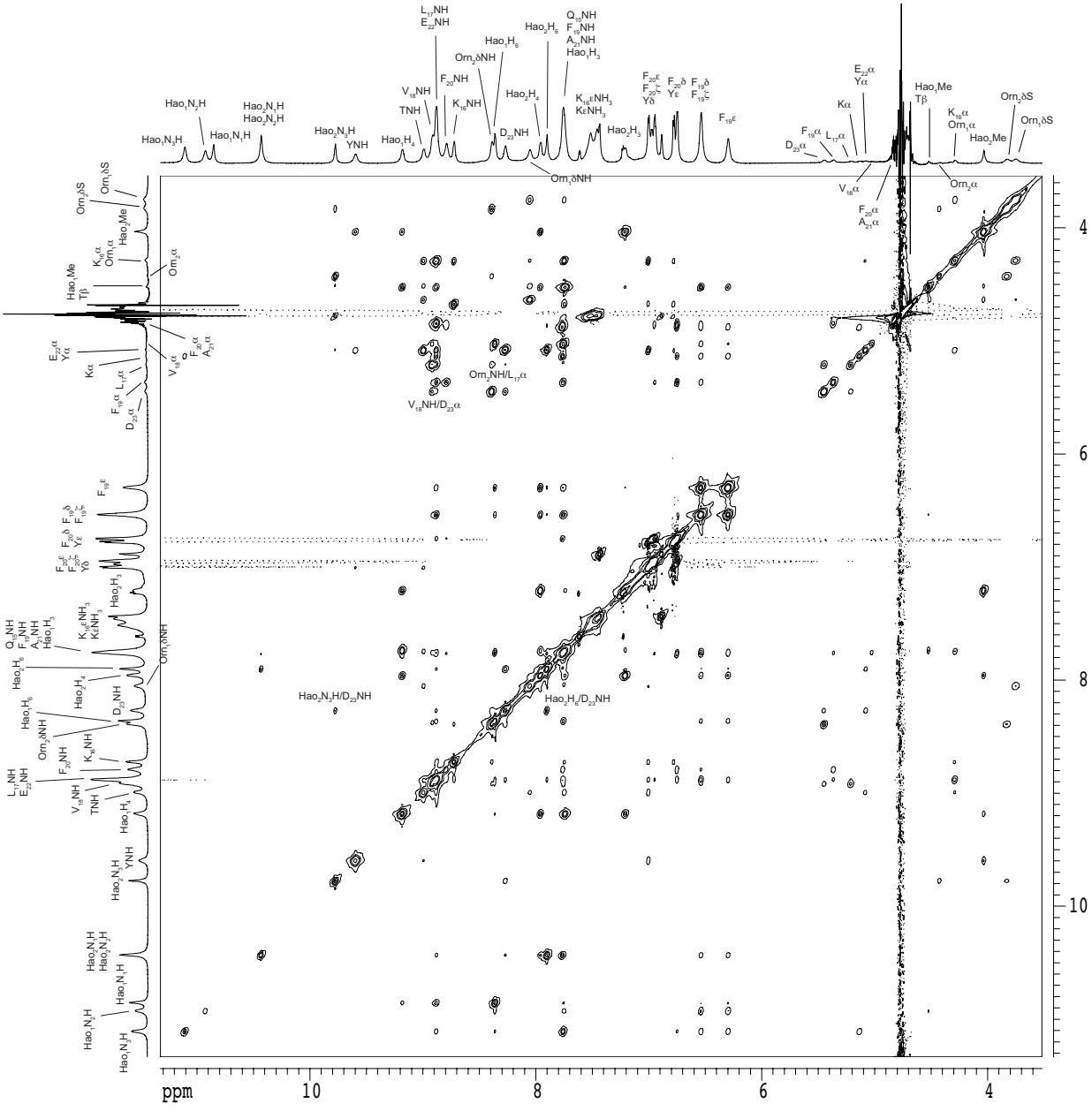

^{1}H NMR 2D EXSY (ROESY spectra showing exchange crosspeaks)
Peptide **3.2a**, 2 mM in D_2O, 600 MHz, 350 K
200 ms spin-locking time
Exchange crosspeaks shown in red; ROE crosspeaks shown in black

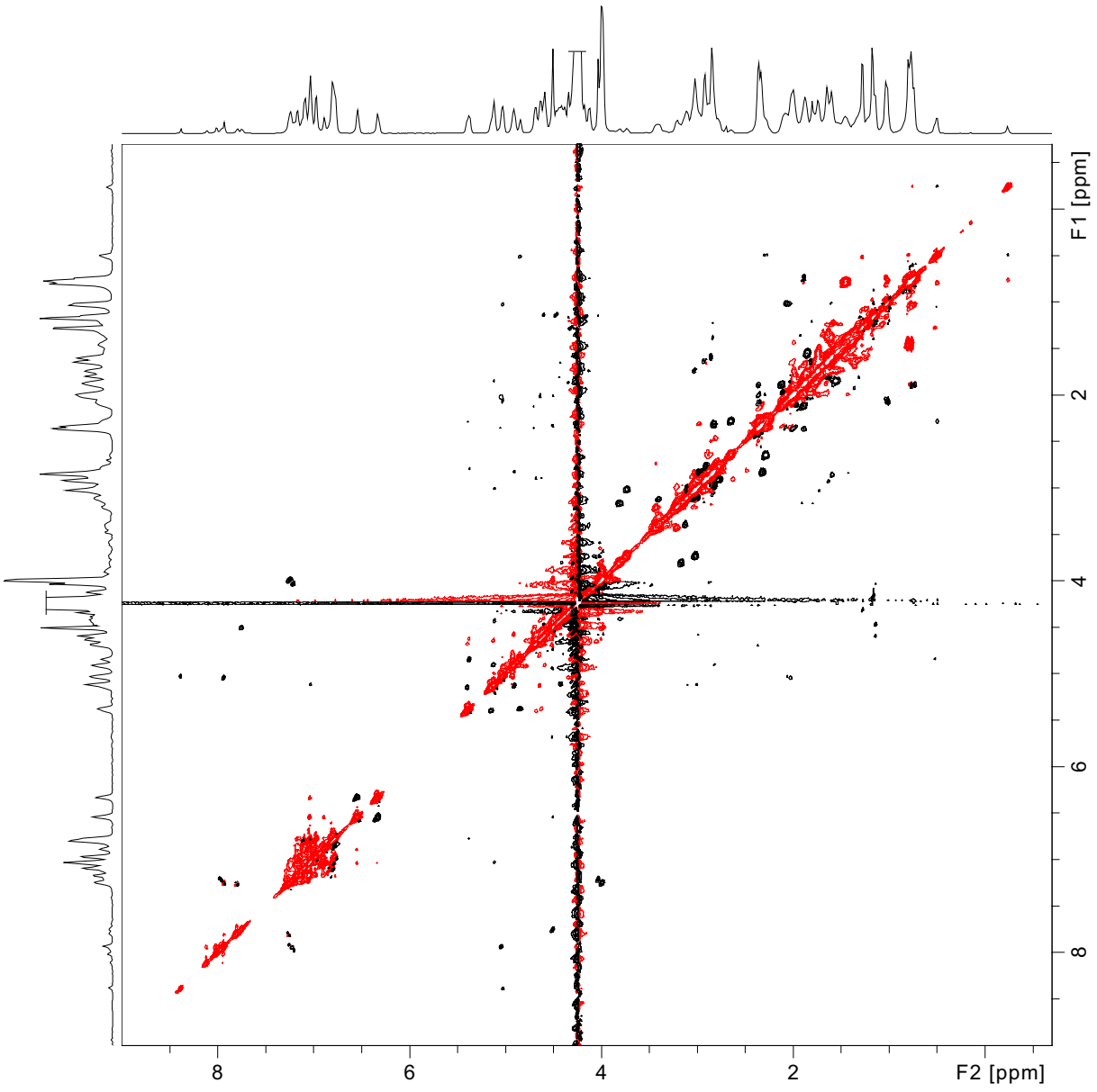

^{1}H NMR 2D EXSY (ROESY spectra showing exchange crosspeaks)
Peptide **3.2a**, 2 mM in D_2O, 600 MHz, 350 K
200 ms spin-locking time
Exchange crosspeaks shown in red; ROE crosspeaks shown in black

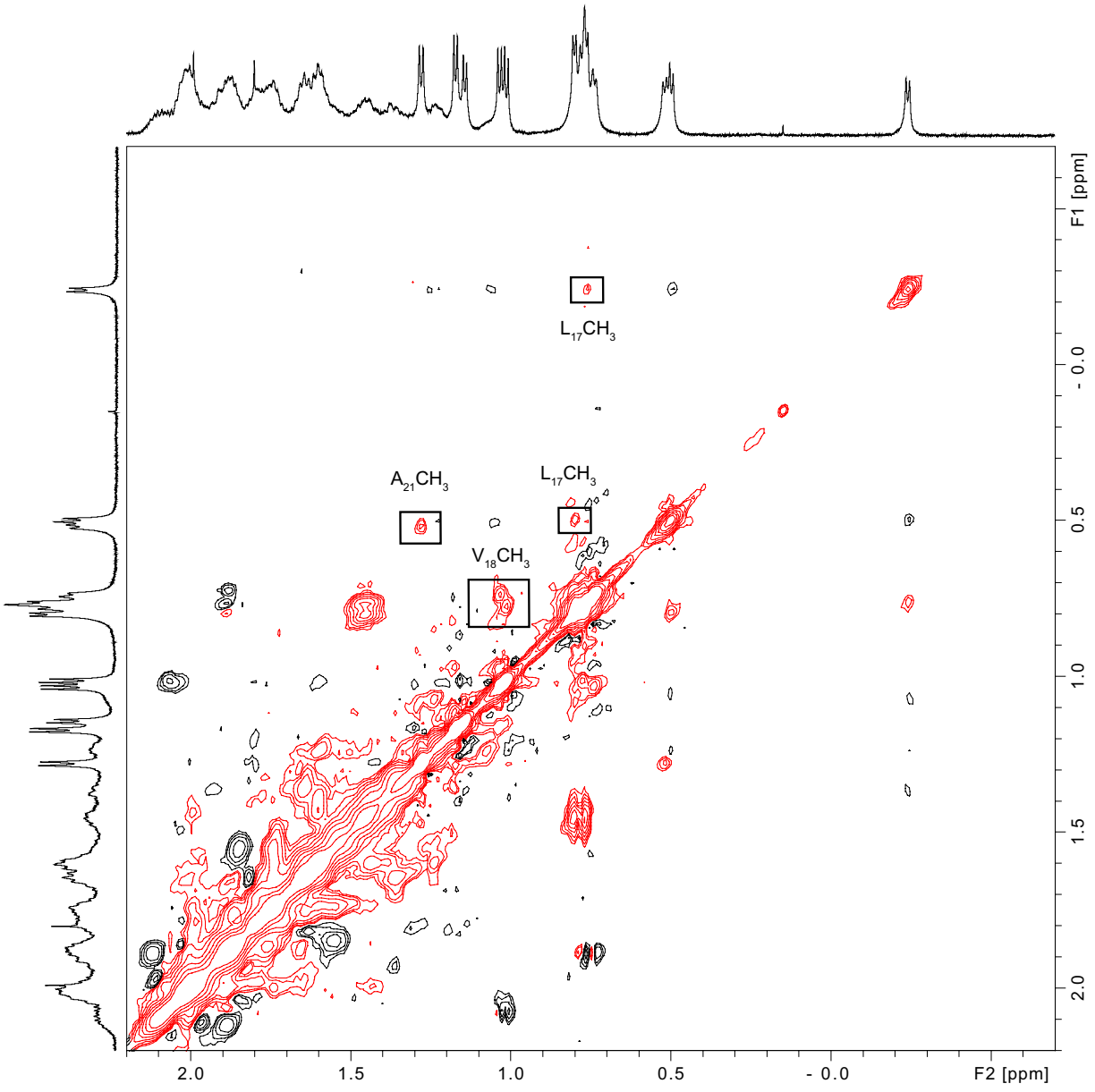

^{1}H NMR 2D EXSY (ROESY spectra showing exchange crosspeaks)
Peptide **3.2a**, 2 mM in D_2O, 600 MHz, 350 K
200 ms spin-locking time
Exchange crosspeaks shown in red; ROE crosspeaks shown in black

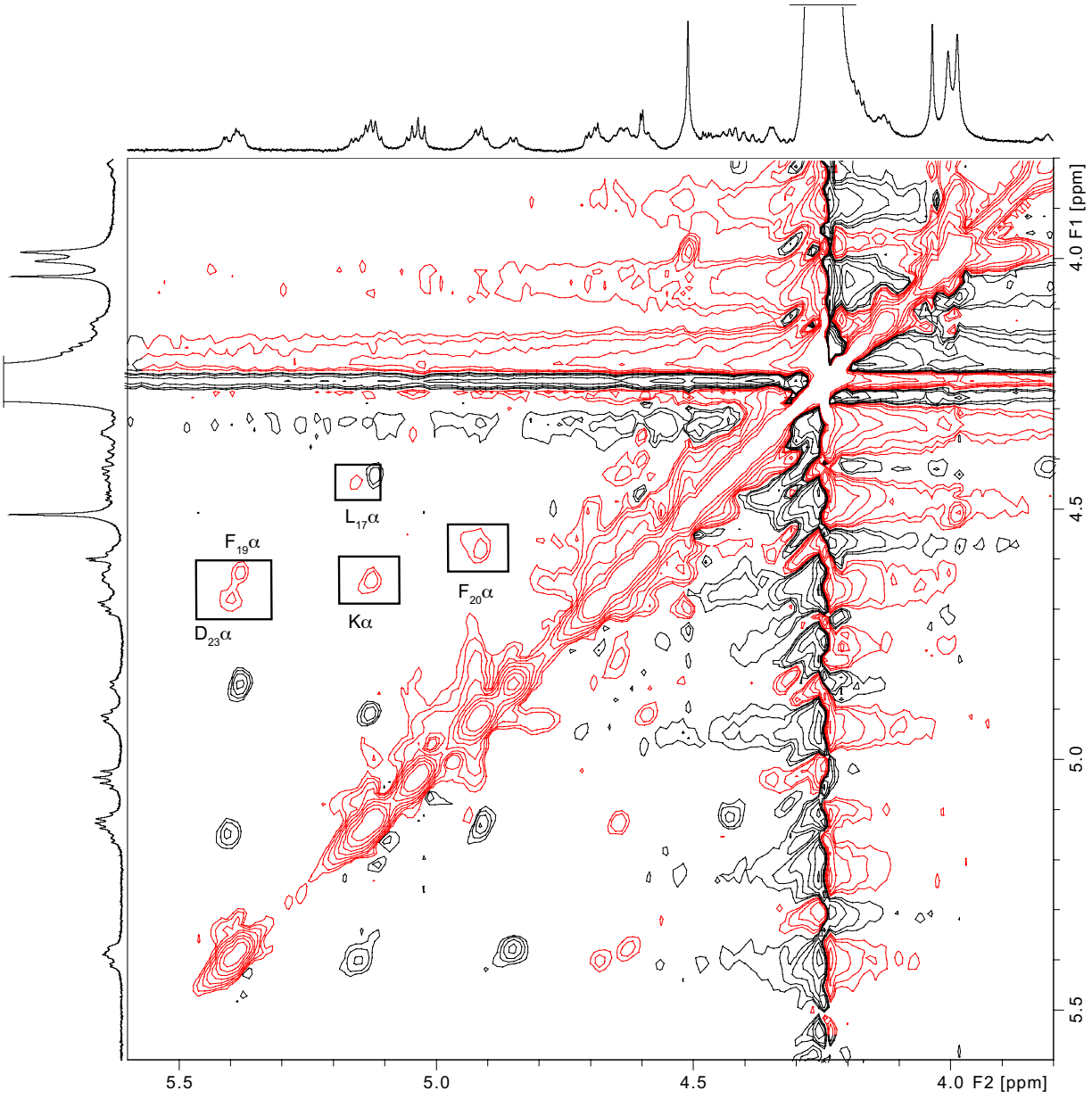

^{1}H NMR 2D EXSY (ROESY spectra showing exchange crosspeaks)
Peptide **3.2a**, 2 mM in D_2O, 600 MHz, 350 K
200 ms spin-locking time
Exchange crosspeaks shown in red; ROE crosspeaks shown in black

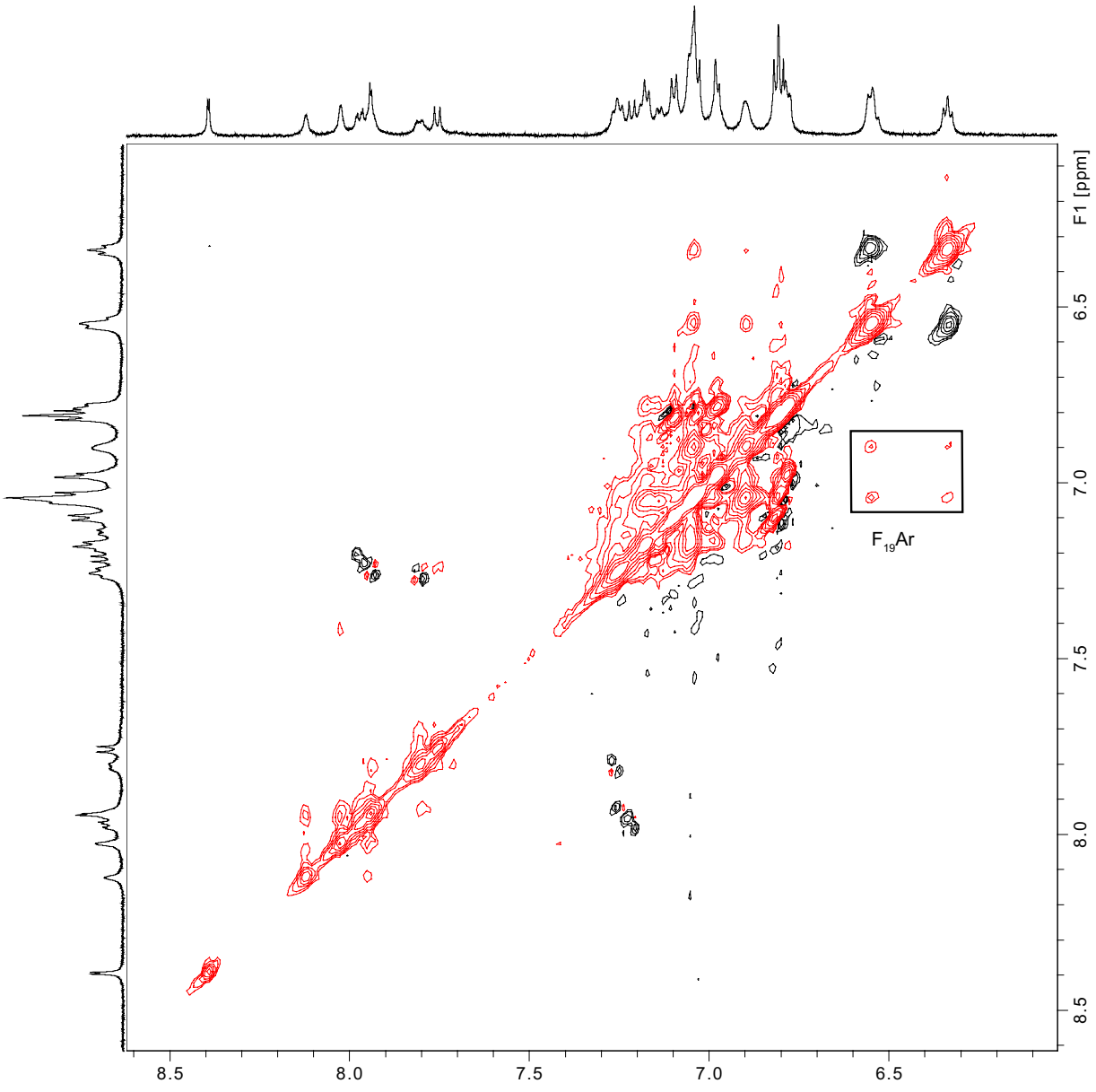

2D DOSY spectrum of macrocyclic β-sheet **3.2a**
2 mM in D_2O, 600 MHz, 298 K
tetramer predominates

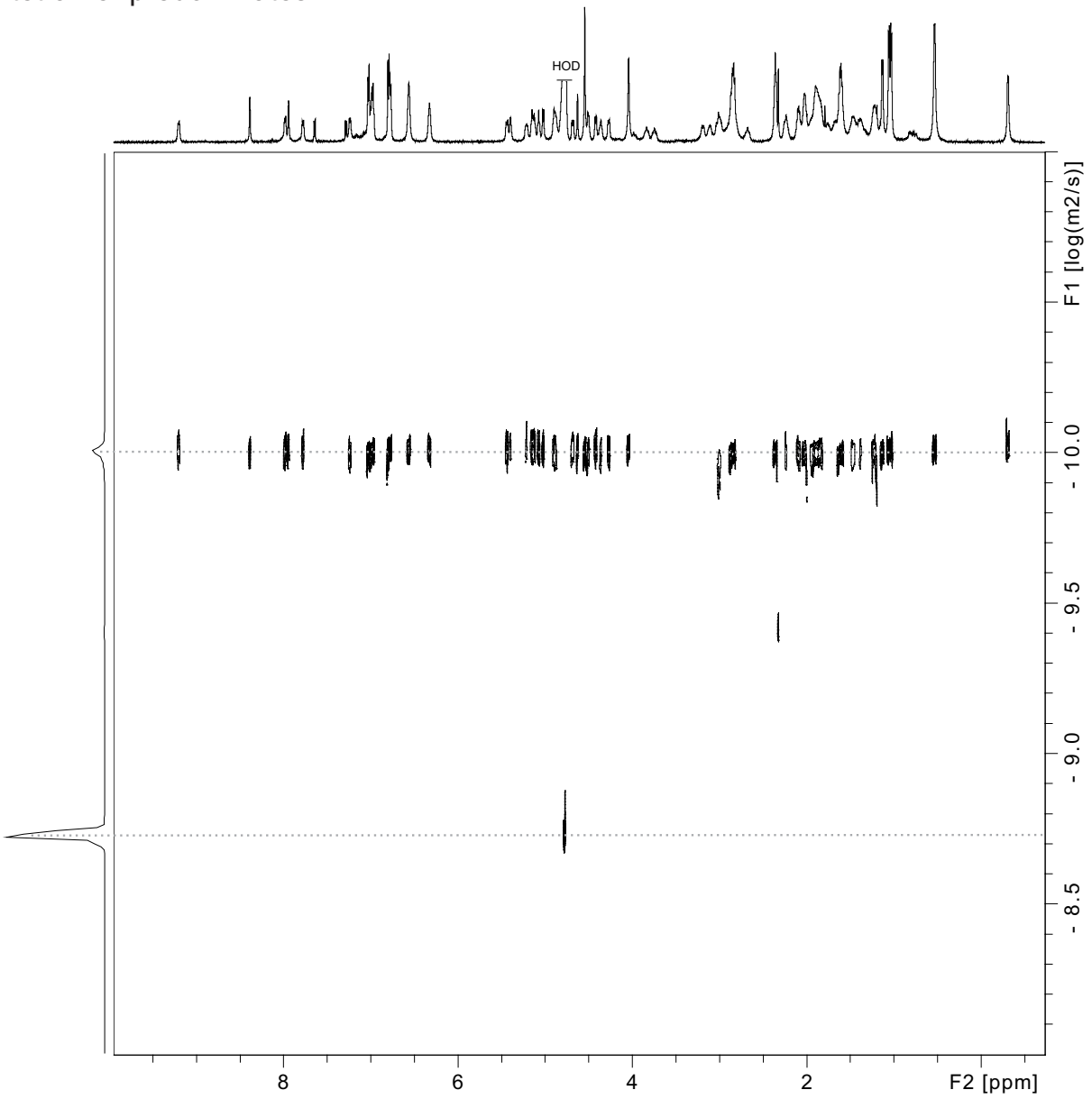

Calculation for 3.2a at 2.0 mM

$DC_{HOD} = 19.0 \times 10^{-10}$ m^2/s [a]
log $DC_{HOD} = -8.721$

For 3.2a tetramer, log DC (m^2/s) = -10.00(1), DC = $10^{-10.001}$ m^2/s = 10.0×10^{-11} m^2/s = 10.0×10^{-7} cm^2/s

[a] Longsworth, L. G. J. Phys. Chem. 1960, 64, 1914–1917.

2D DOSY spectrum of macrocyclic β-sheet **3.2a**
8 mM in D_2O, 600 MHz, 298 K
tetramer predominates

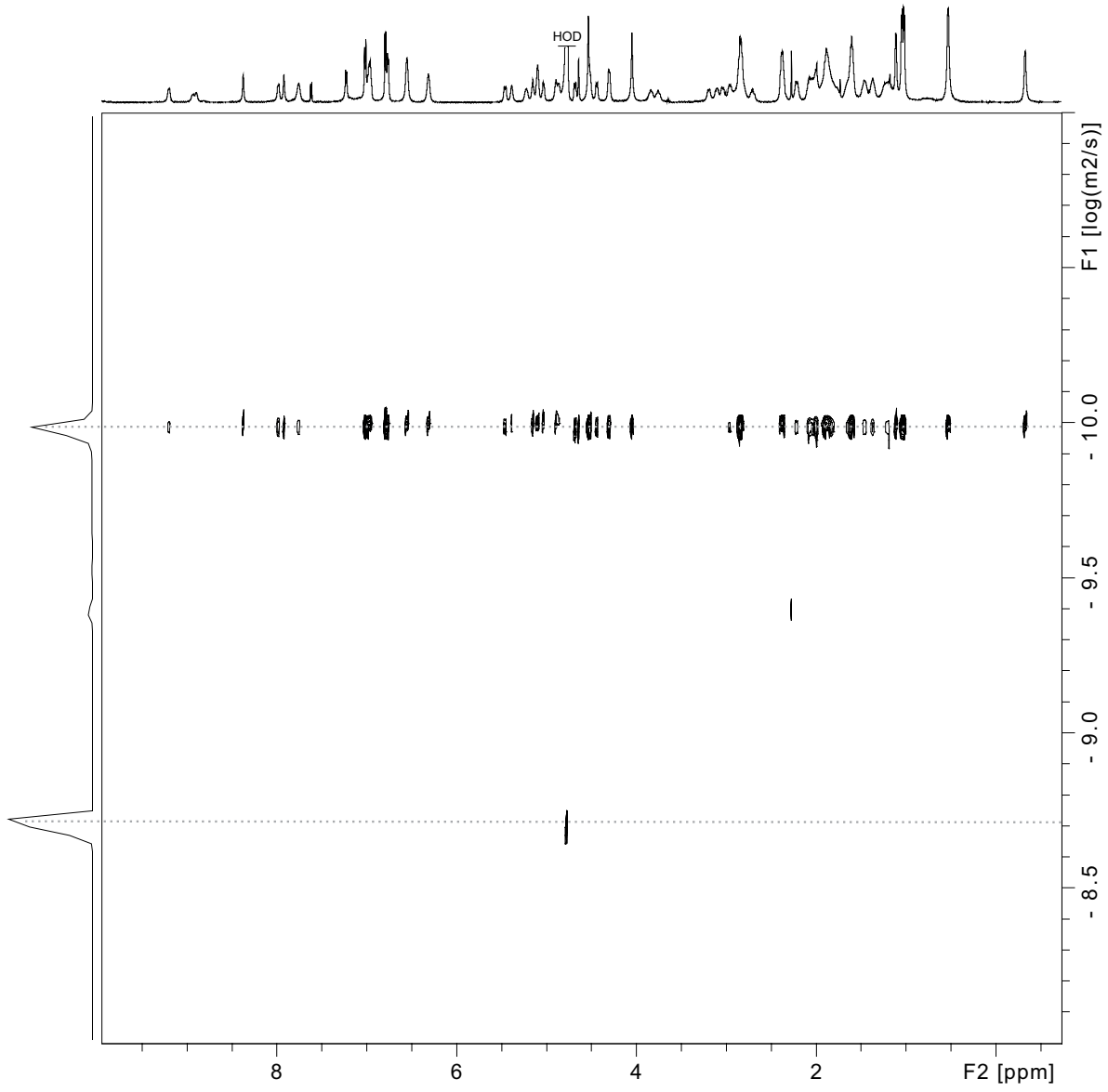

Calculation for 3.2a at 8.0 mM

$DC_{HOD} = 19.0 \times 10^{-10}$ m^2/s [a]
$\log DC_{HOD} = -8.721$

For 3.2a tetramer, log DC (m^2/s) = -9.99(4), DC = $10^{-9.994}$ m^2/s = 10.1×10^{-11} m^2/s = 10.1×10^{-7} cm^2/s

[a] Longsworth, L. G. J. Phys. Chem. 1960, 64, 1914–1917.

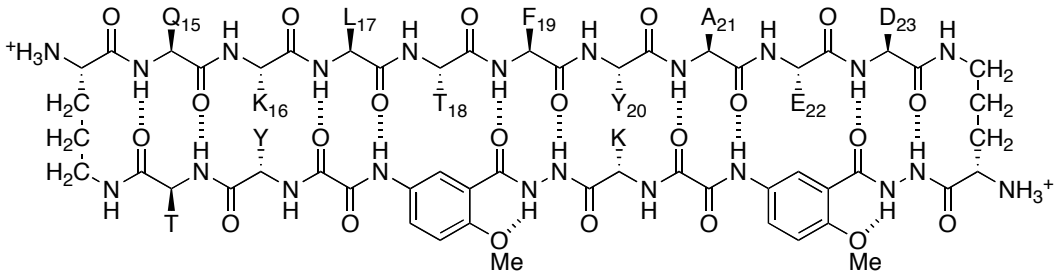

macrocyclic β-sheet peptide **3.2b** (as the TFA salt)

molecular weight calculated for $C_{100}H_{139}N_{25}O_{31} \cdot 4CF_3CO_2H$ (TFA salt of **3.2b**): 2643.42
molecular weight calculated for $C_{100}H_{139}N_{25}O_{31}$ (free base of **3.2b**): 2187.32
exact mass calculated for $C_{100}H_{139}N_{25}O_{31}$ (free base of **3.2b**): 2186.01

Analytical RP-HPLC of macrocyclic β-peptide **3.2b**

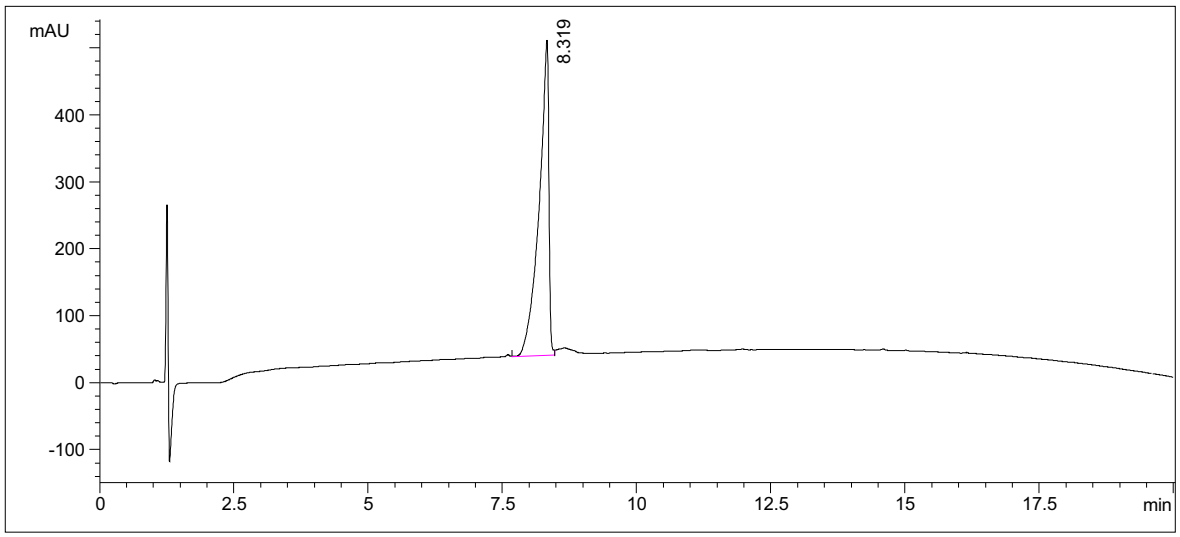


```
Signal 1: VWD1 A, Wavelength=214 nm

Peak RetTime Type  Width     Area      Height     Area
  #   [min]        [min]  mAU   *s    [mAU   ]      %
----|-------|----|-------|----------|----------|--------|
   1   8.319 VV    0.1667 5902.40332  470.60681 100.0000

Totals :                  5902.40332  470.60681
```

Macrocyclic β-sheet peptide **3.2b**

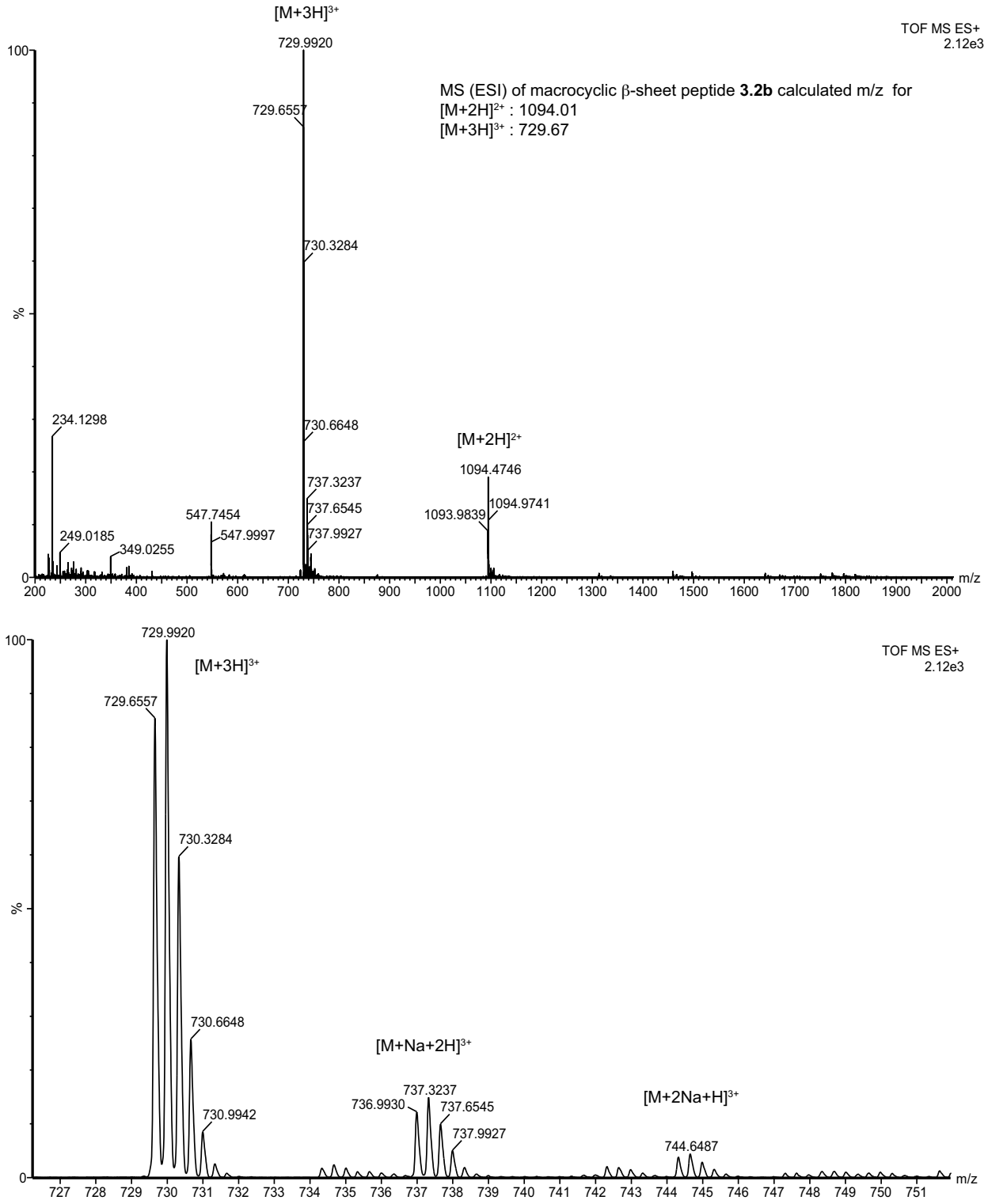

Macrocyclic β-sheet peptide **3.2b**

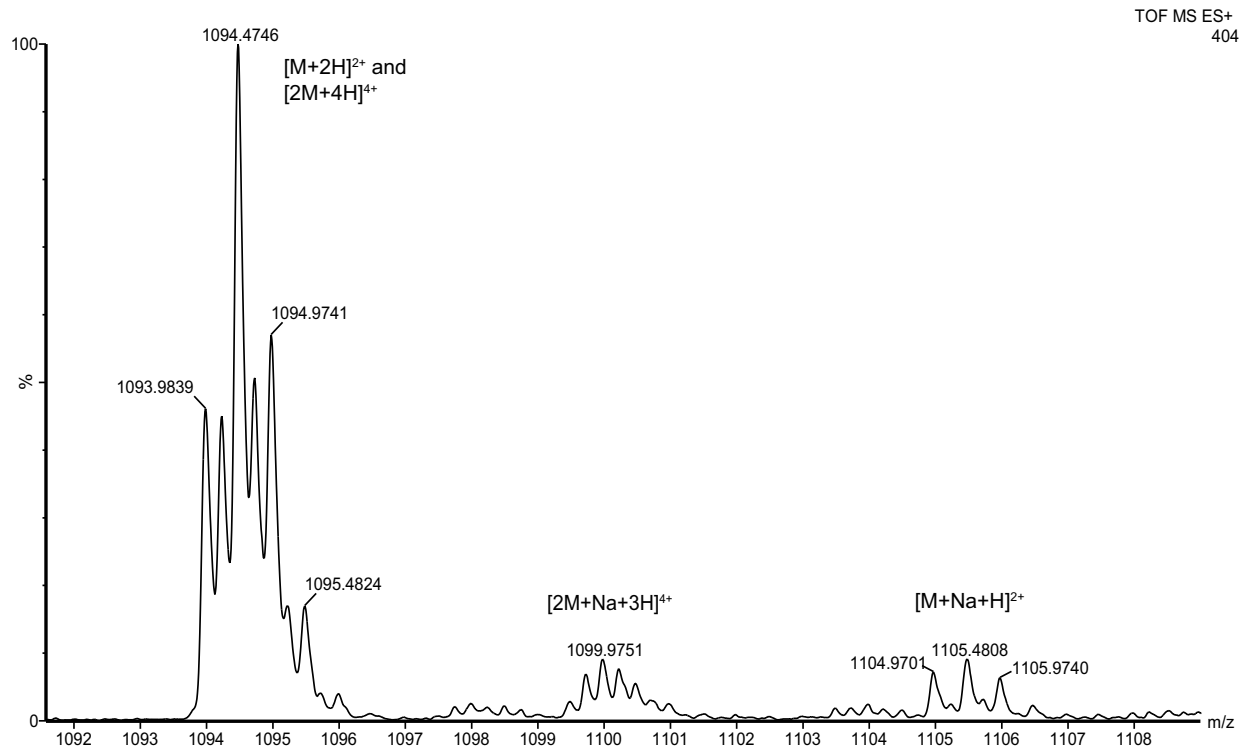

1D ^{1}H NMR spectrum of macrocyclic β-sheet **3.2b**
2 mM in D_2O, 500 MHz, 285 K
tetramer predominates

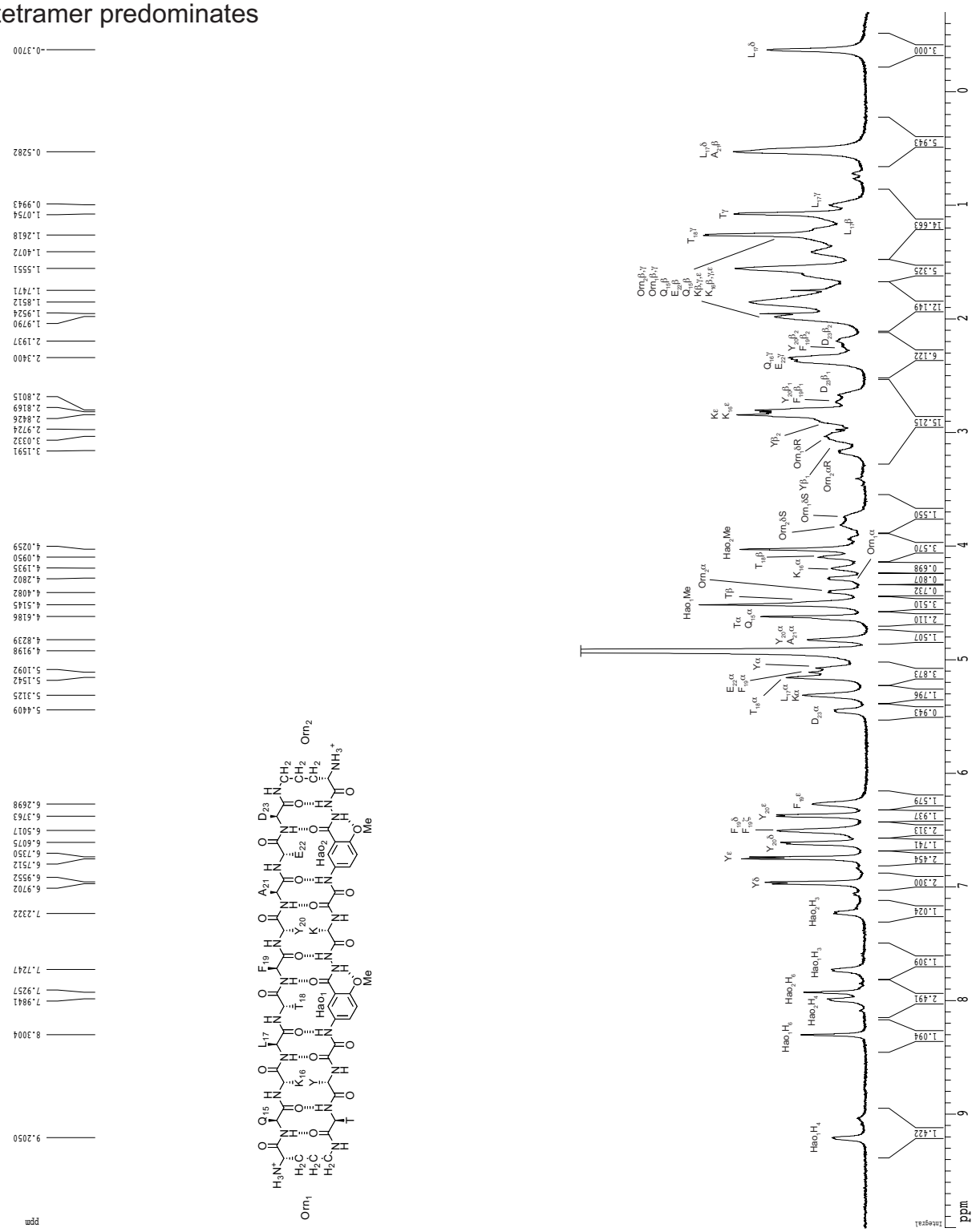

2D TOCSY spectrum of macrocyclic β-sheet **3.2b** as tetramer
2 mM in D_2O, 500 MHz, 285 K
150-ms spin-locking mixing time
tetramer predominates

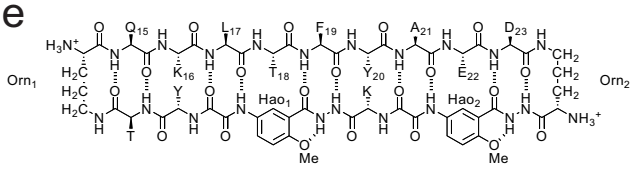

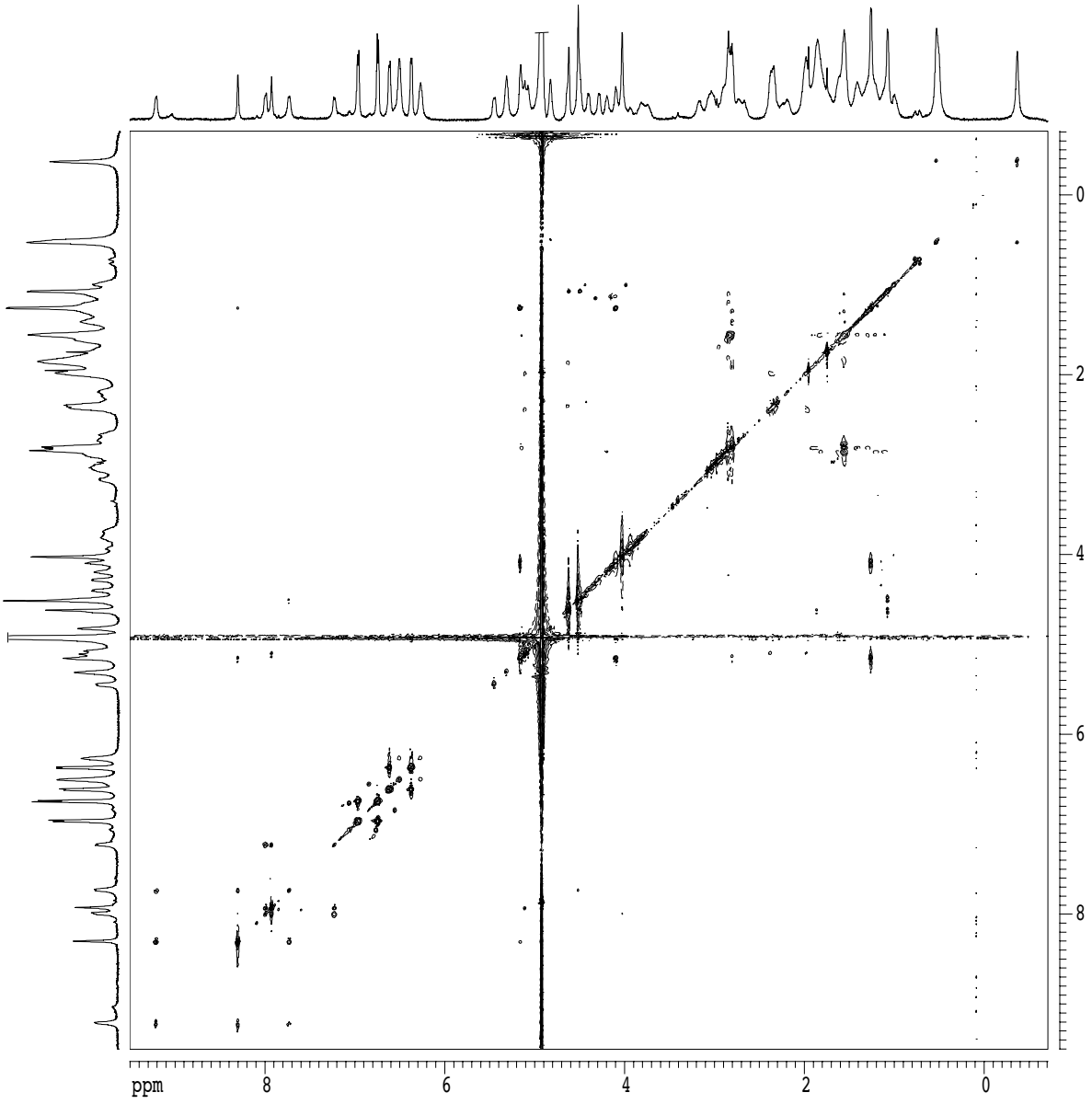

2D COSY spectrum of macrocyclic β-sheet **3.2b** as tetramer
2 mM in D_2O, 500 MHz, 285 K
tetramer predominates

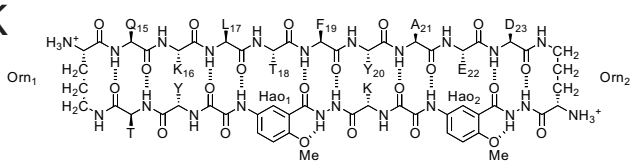

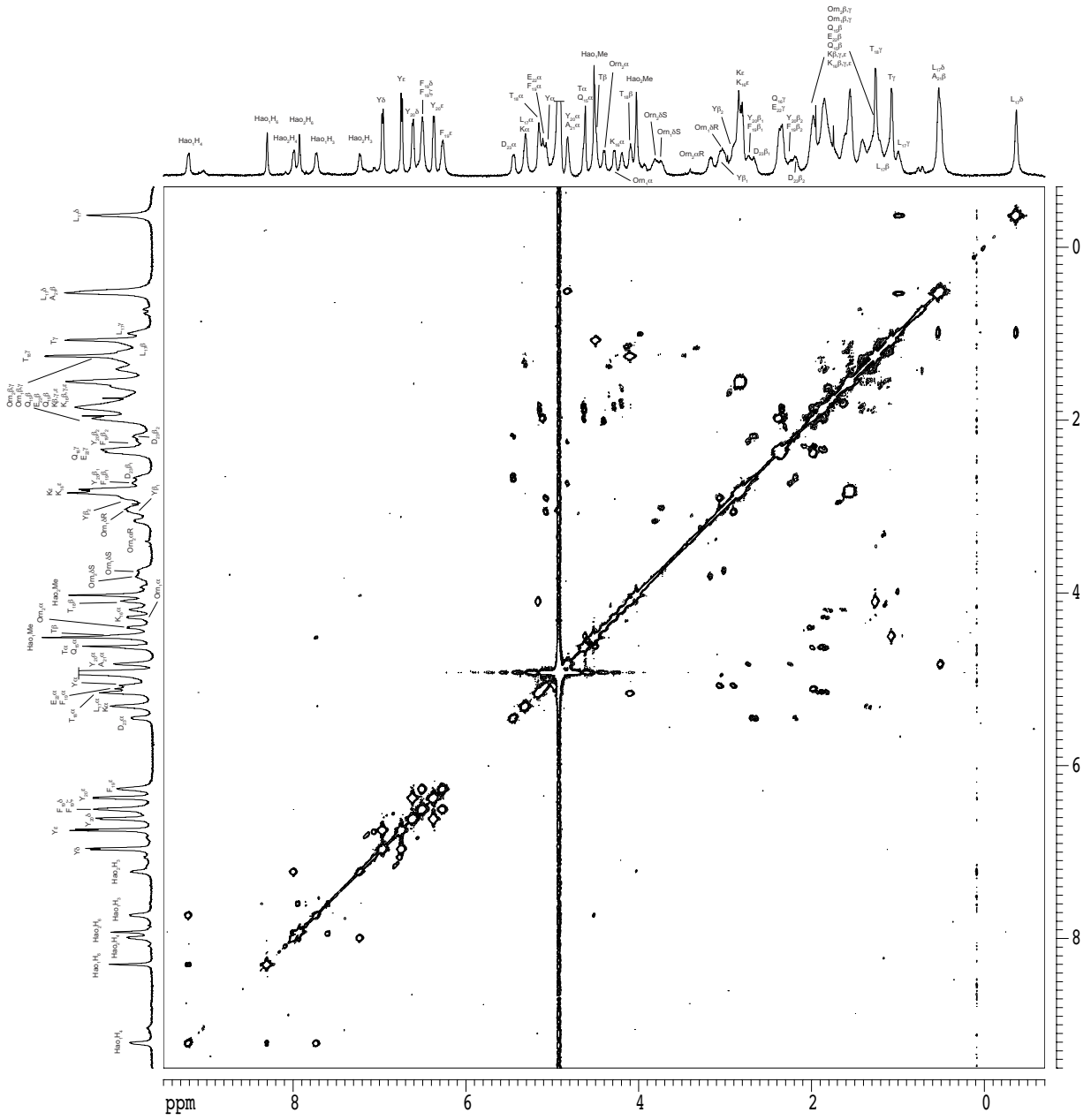

2D NOESY spectrum of macrocyclic β-sheet **3.2b** as tetramer
2 mM in D_2O, 500 MHz, 285 K
150-ms spin-locking mixing time
tetramer predominates

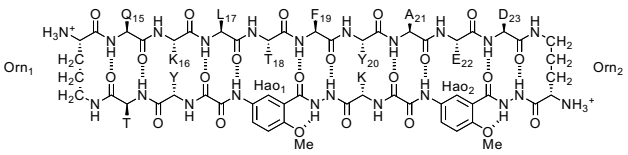

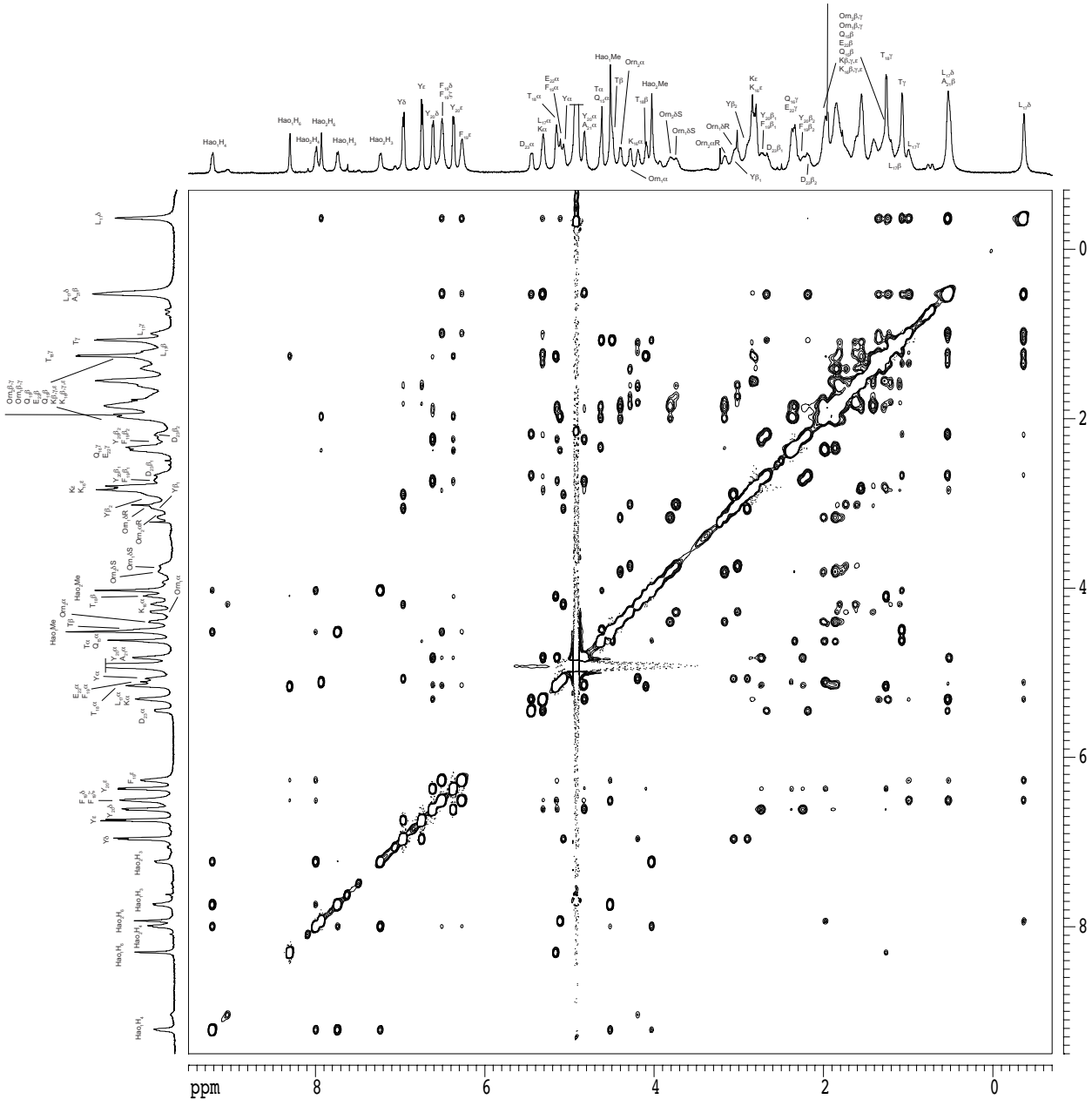

2D NOESY spectrum of macrocyclic β-sheet **3.2b** as tetramer
2 mM in D_2O, 500 MHz, 285 K
150-ms spin-locking mixing time
tetramer predominates
#select NMR crosspeaks are labeled

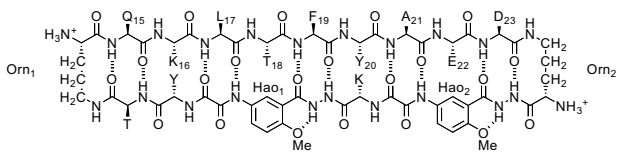

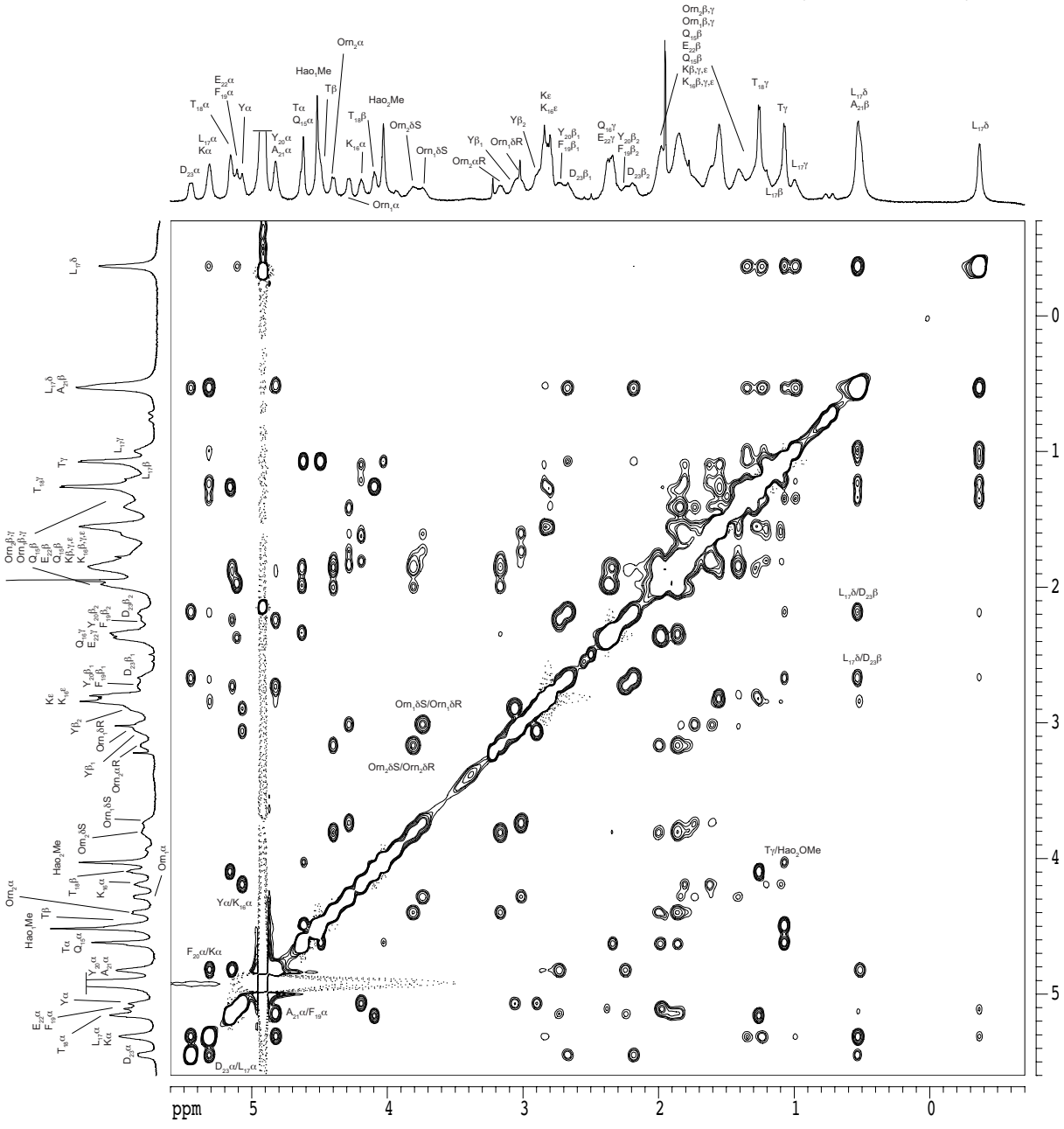

2D NOESY spectrum of macrocyclic β-sheet **3.2b** as tetramer
2 mM in D_2O, 500 MHz, 285 K
150-ms spin-locking mixing time
tetramer predominates
#select NMR crosspeaks are labeled

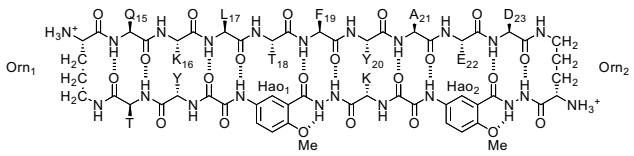

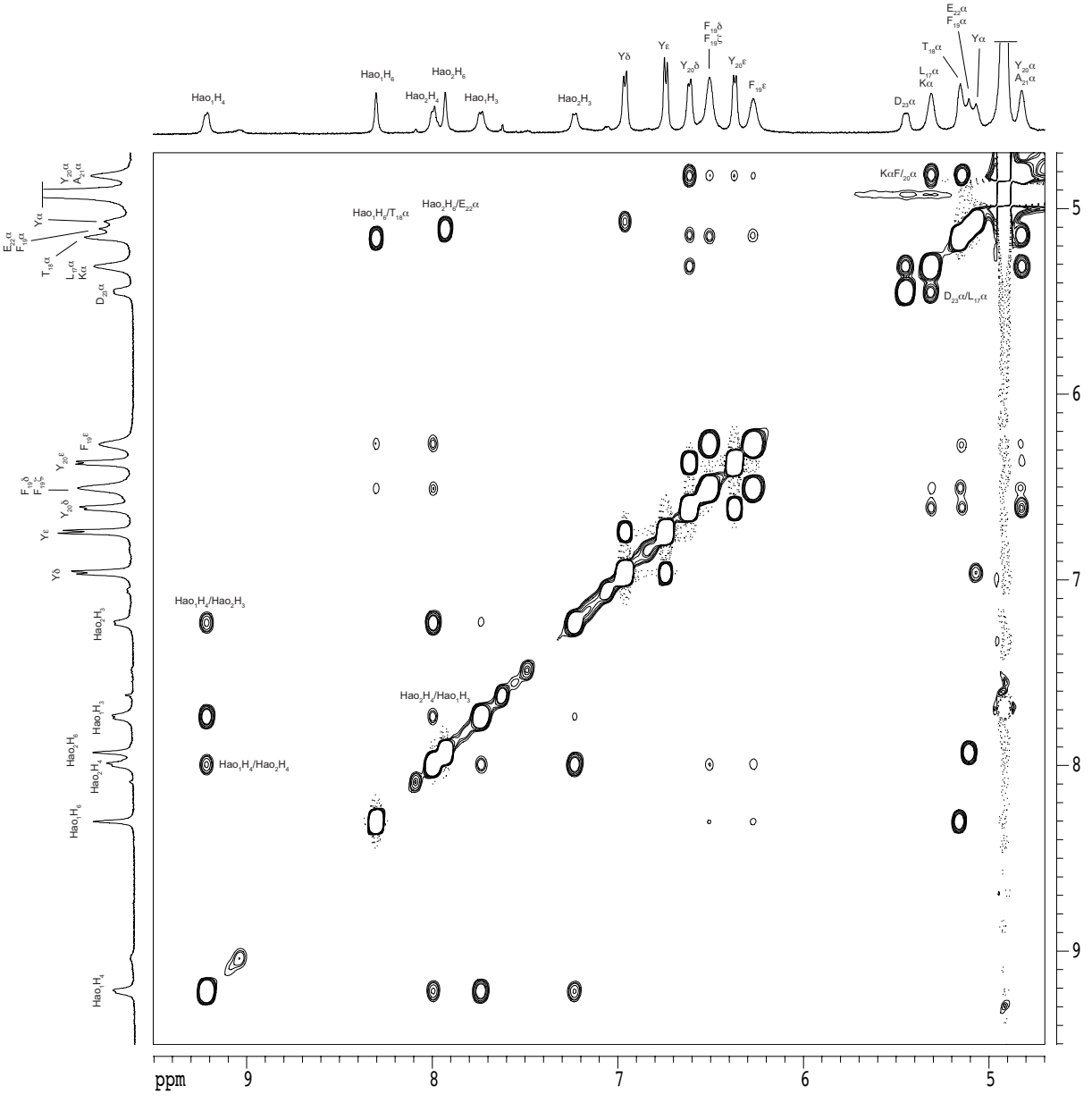

2D DOSY spectrum of macrocyclic β-sheet **3.2b**
2 mM in D_2O, 600 MHz, 298 K
tetramer predominates

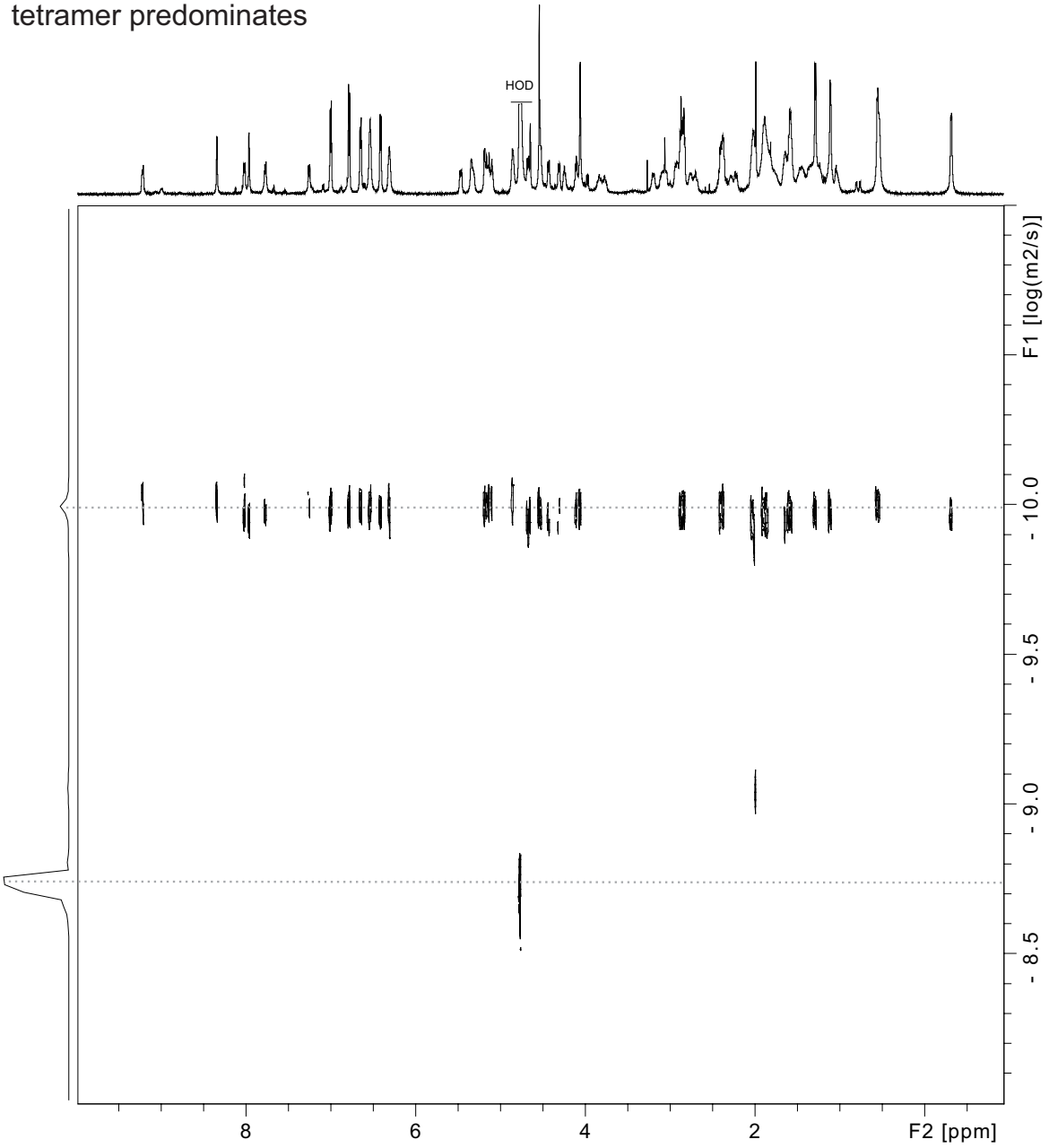

Calculation for 3.2b at 2.0 mM

DC_{HOD} = 19.0 x 10^{-10} m^2/s [a]
log DC_{HOD} = -8.721

For 3.2b tetramer, log DC (m^2/s) = -9.98(6), DC = $10^{-9.986}$ m^2/s = 10.3 x 10^{-11} m^2/s = 10.3 x 10^{-7} cm^2/s

[a] Longsworth, L. G. J. Phys. Chem. 1960, 64, 1914–1917.

2D DOSY spectrum of macrocyclic β-sheet **3.2b**
8 mM in D_2O, 600 MHz, 298 K
tetramer predominates

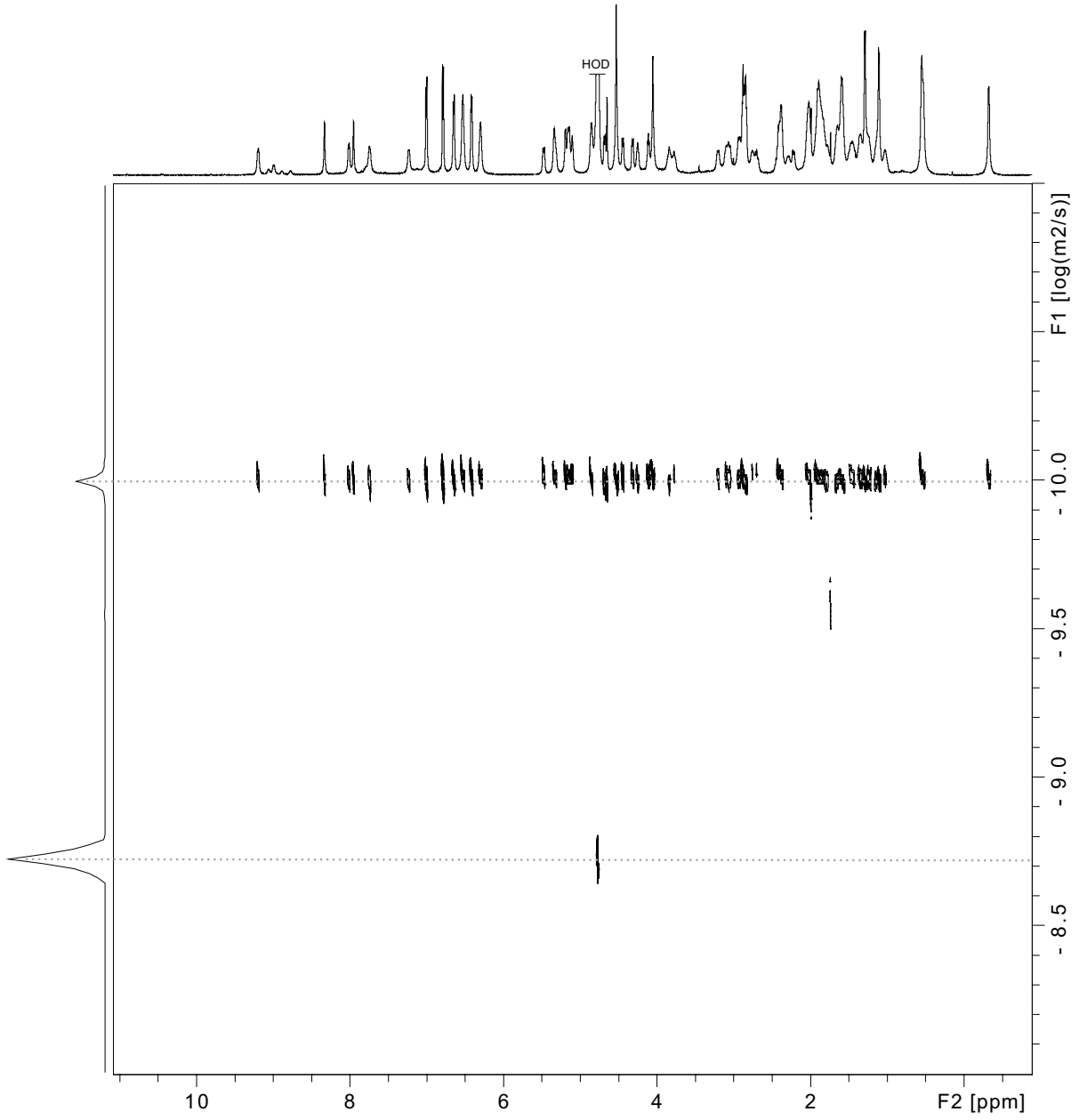

Calculation for 3.2b at 8.0 mM

DC_{HOD} = 19.0 x 10^{-10} m^2/s [a]
log DC_{HOD} = -8.721

For 3.2b tetramer, log DC (m^2/s) = -9.99(4), DC = $10^{-9.994}$ m^2/s = 10.1 x 10^{-11} m^2/s = 10.1 x 10^{-7} cm^2/s

[a] Longsworth, L. G. J. Phys. Chem. 1960, 64, 1914–1917.

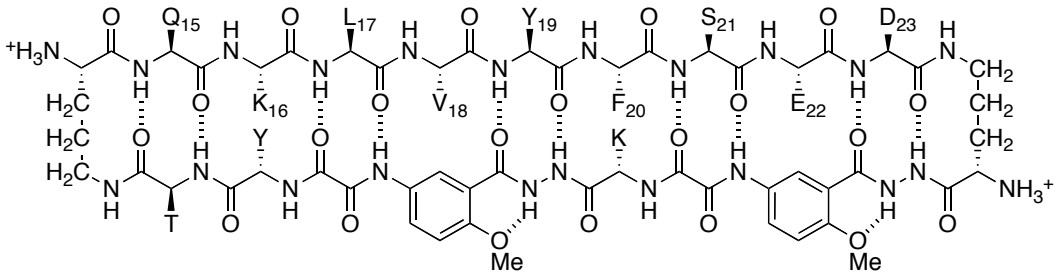

macrocyclic β-sheet peptide **3.2c** (as the TFA salt)

molecular weight calculated for $C_{101}H_{141}N_{25}O_{31} \cdot 4CF_3CO_2H$ (TFA salt of **3.2c**): 2657.44
molecular weight calculated for $C_{101}H_{141}N_{25}O_{31}$ (free base of **3.2c**): 2201.35
exact mass calculated for $C_{101}H_{141}N_{25}O_{31}$ (free base of **3.2c**): 2200.02

Analytical RP-HPLC of macrocyclic β-sheet peptide **3.2c**

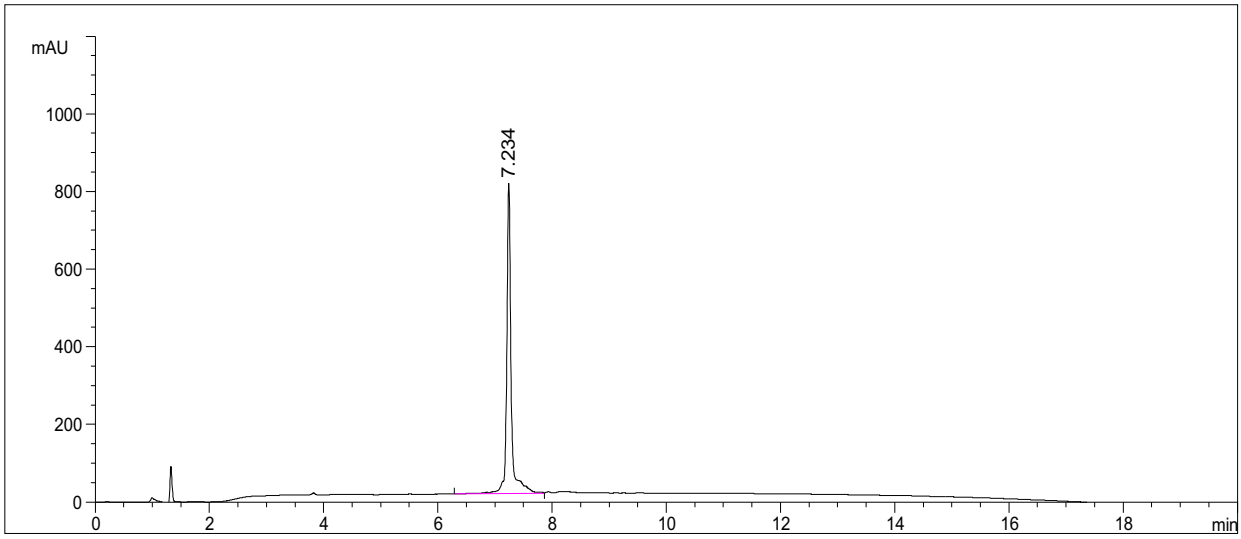


```
Signal 1: VWD1 A, Wavelength=214 nm

Peak RetTime Type  Width     Area      Height     Area
  #   [min]        [min]  mAU   *s   [mAU   ]      %
----|-------|----|-------|----------|----------|--------|
   1   7.234 BV    0.0780 4340.98779  798.37006 100.0000

Totals :                  4340.98779  798.37006
```

Macrocyclic β-sheet peptide **3.2c**

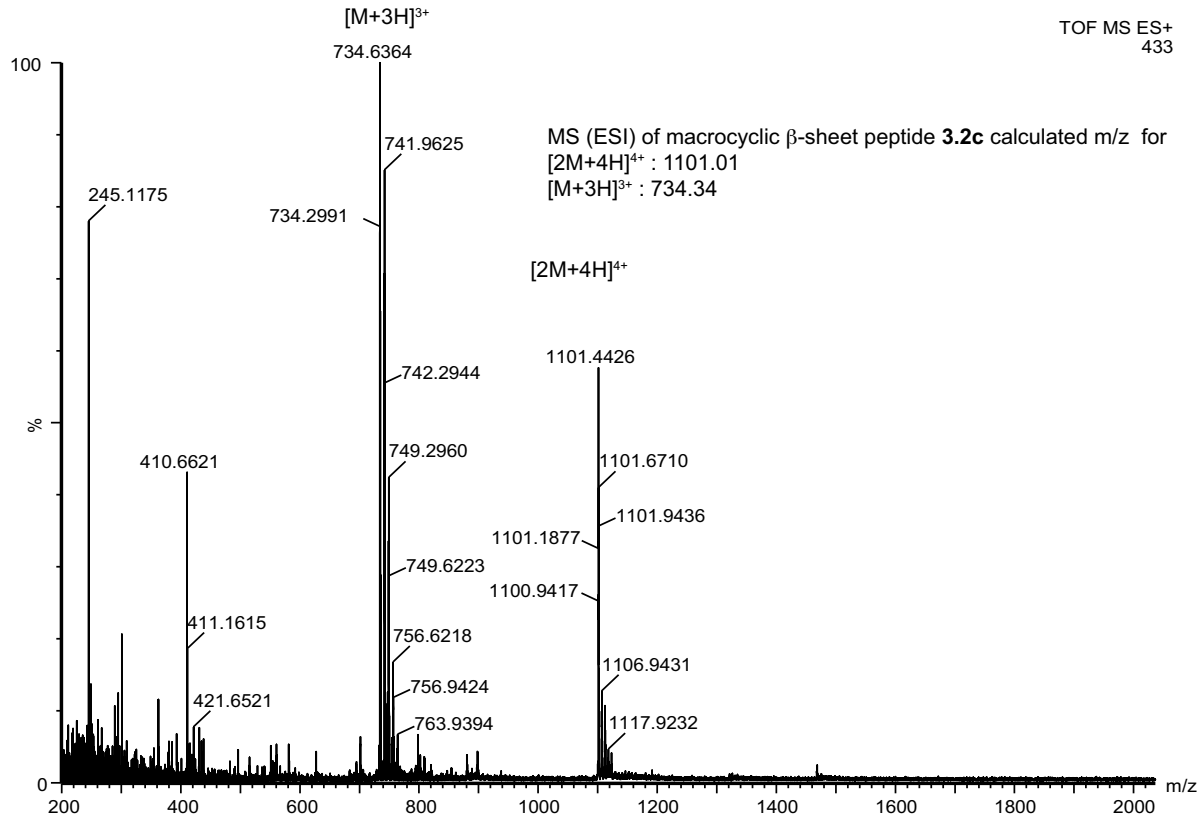

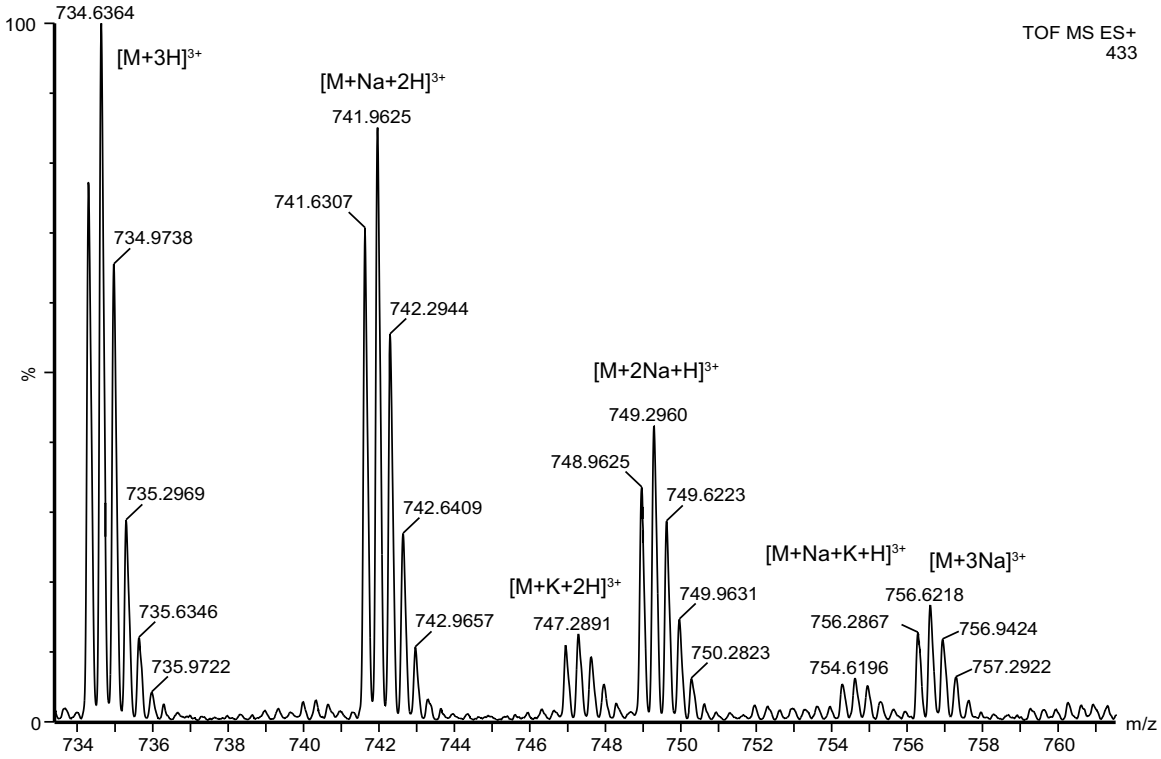

Macrocyclic β-sheet peptide **3.2c**

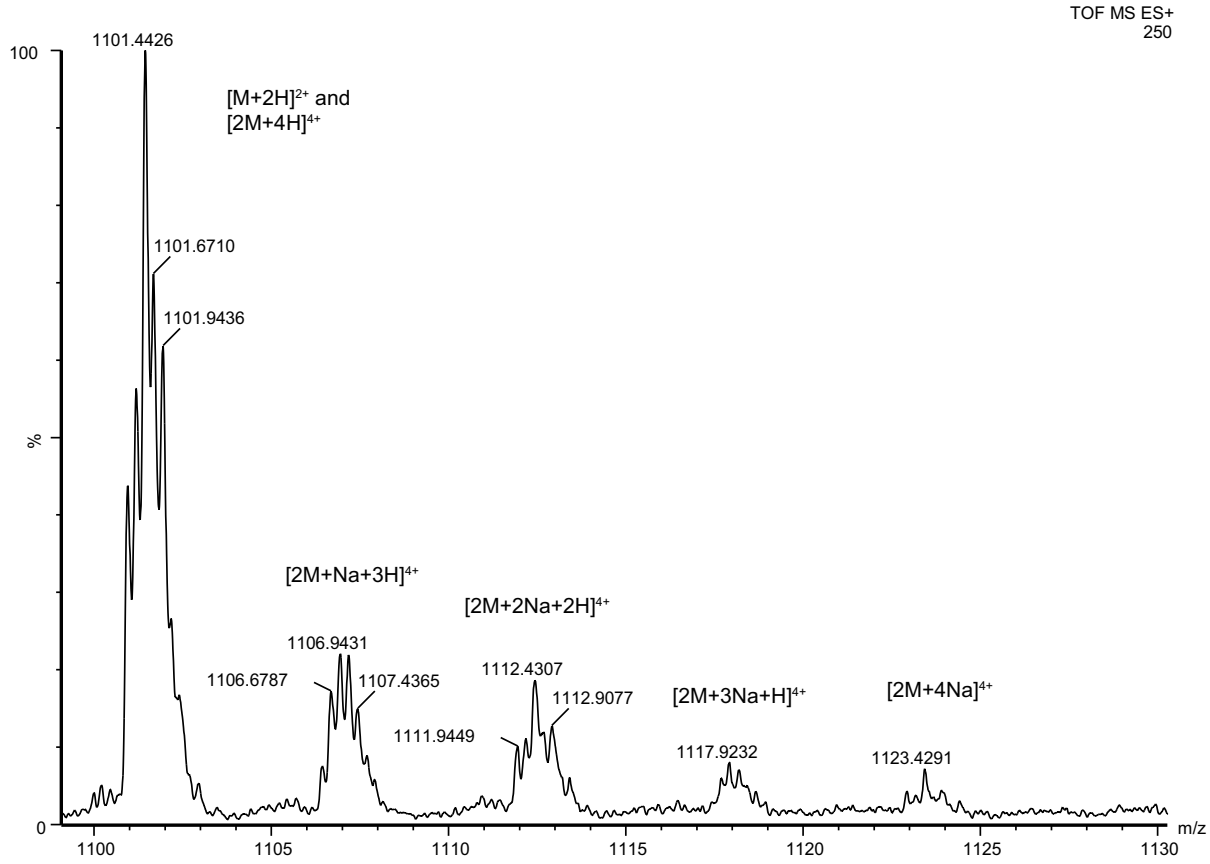

1D ^{1}H NMR spectrum of macrocyclic β-sheet **3.2c**
2 mM in D_2O, 500 MHz, 298 K

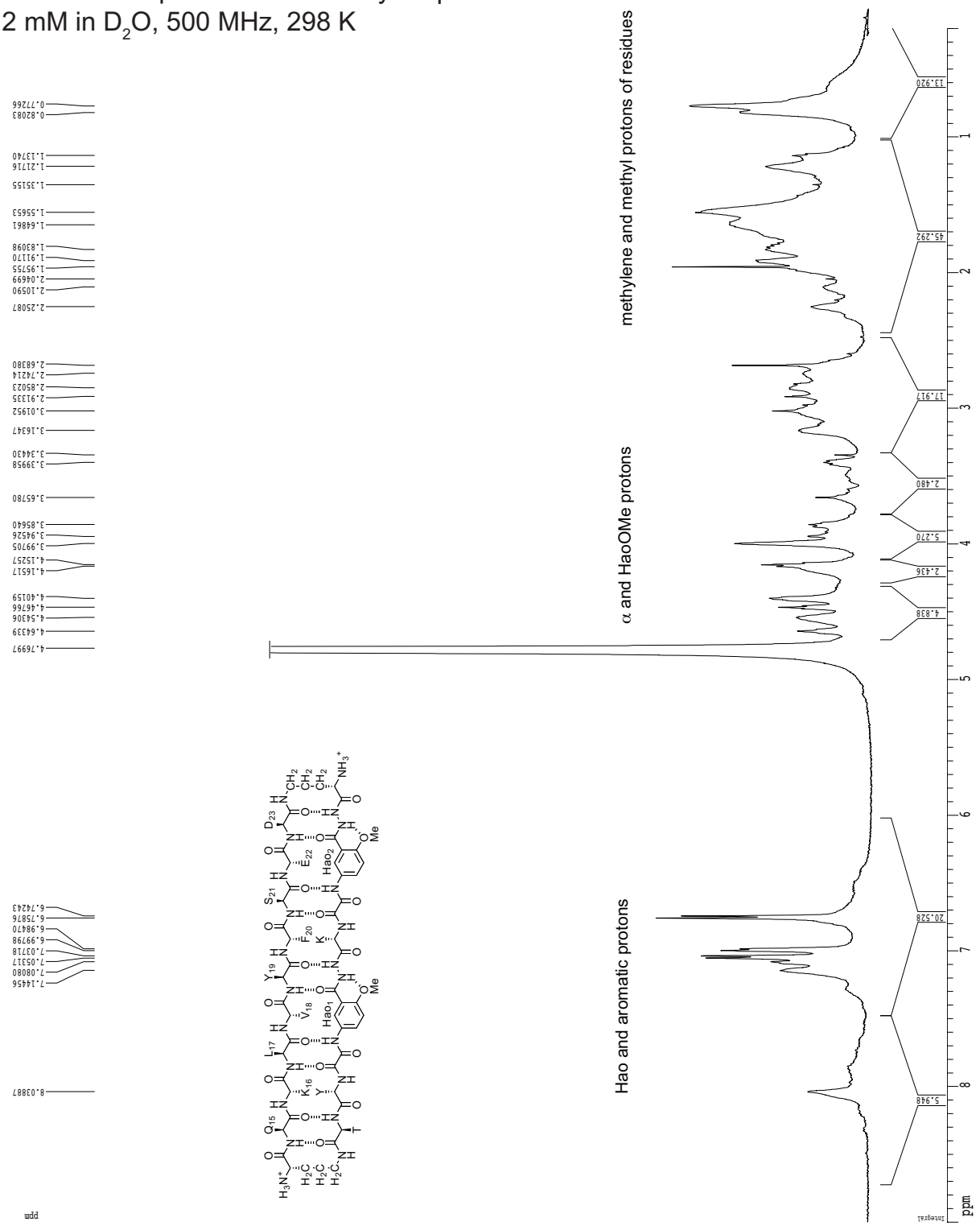

2D TOCSY spectrum of macrocyclic β-sheet **3.2c**
2 mM in D_2O, 500 MHz, 298 K
150-ms spin-locking mixing time

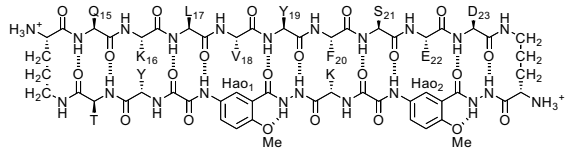

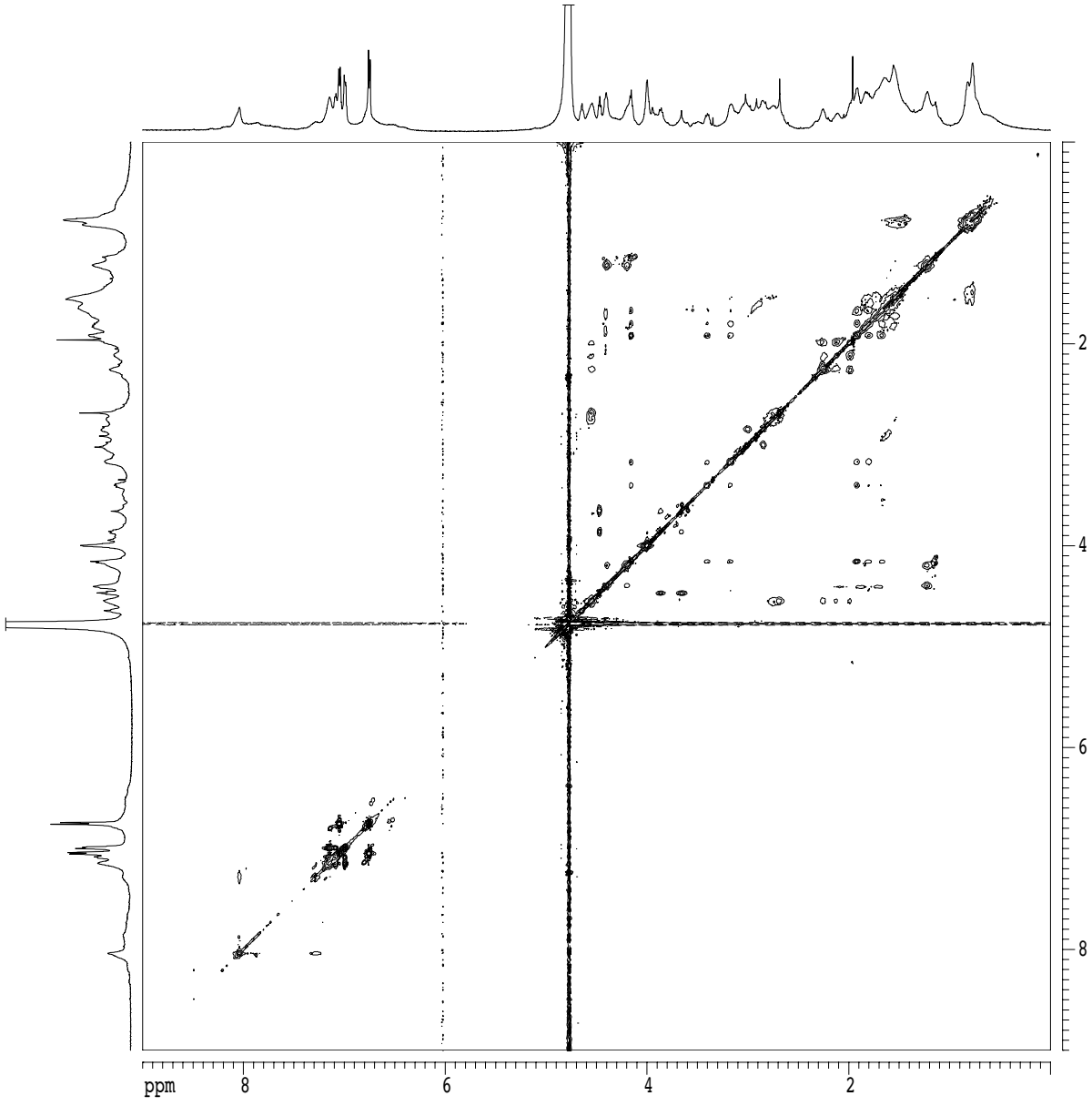

2D TOCSY spectrum of macrocyclic β-sheet **3.2c**
2 mM in D_2O, 500 MHz, 298 K
150-ms spin-locking mixing time

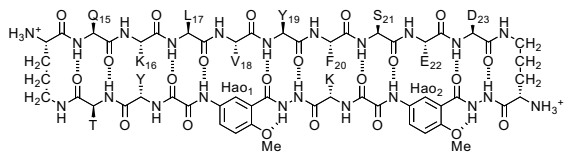

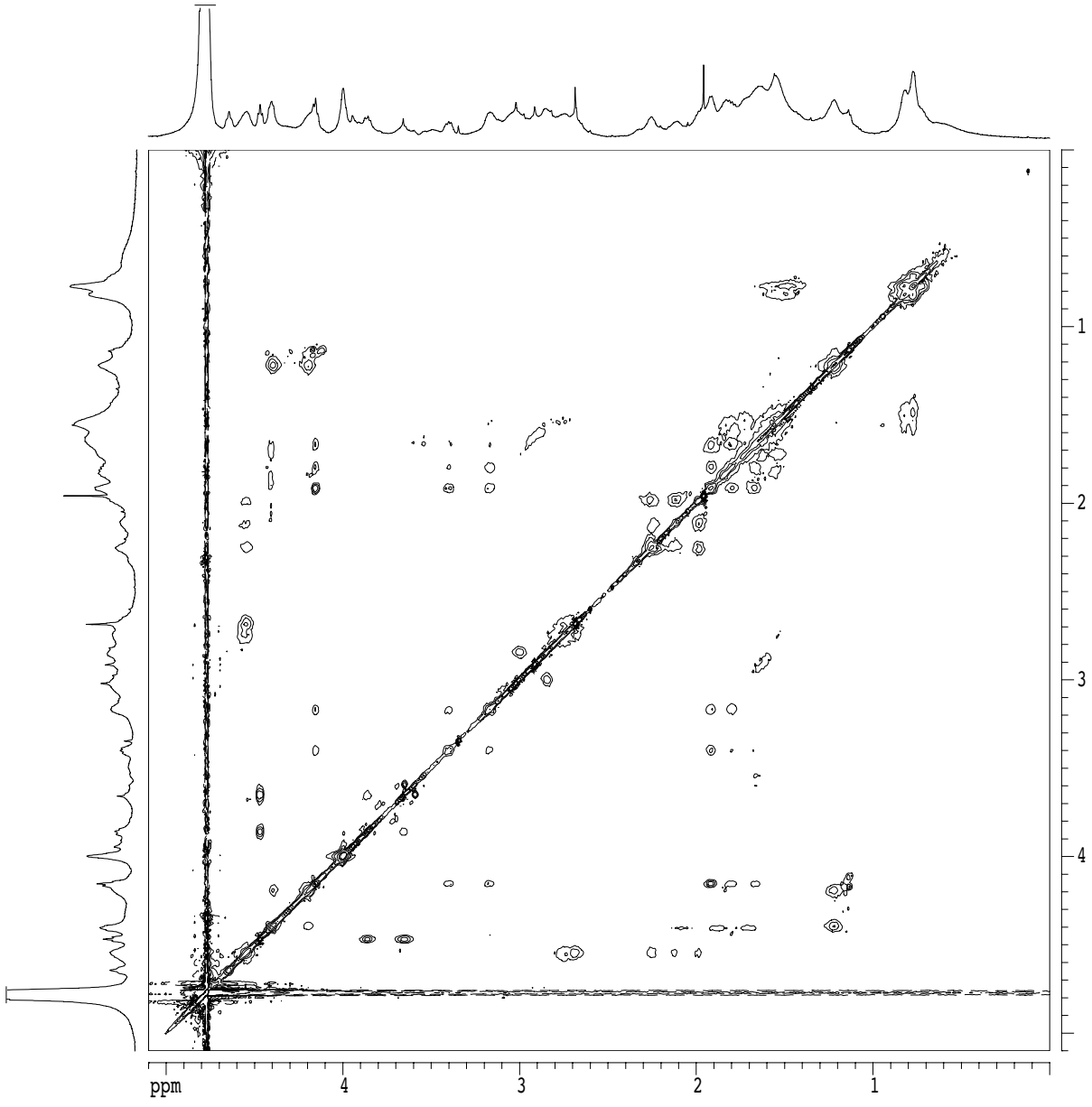

2D TOCSY spectrum of macrocyclic β-sheet **3.2c**
2 mM in D_2O, 500 MHz, 298 K
150-ms spin-locking mixing time

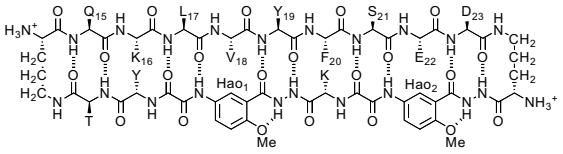

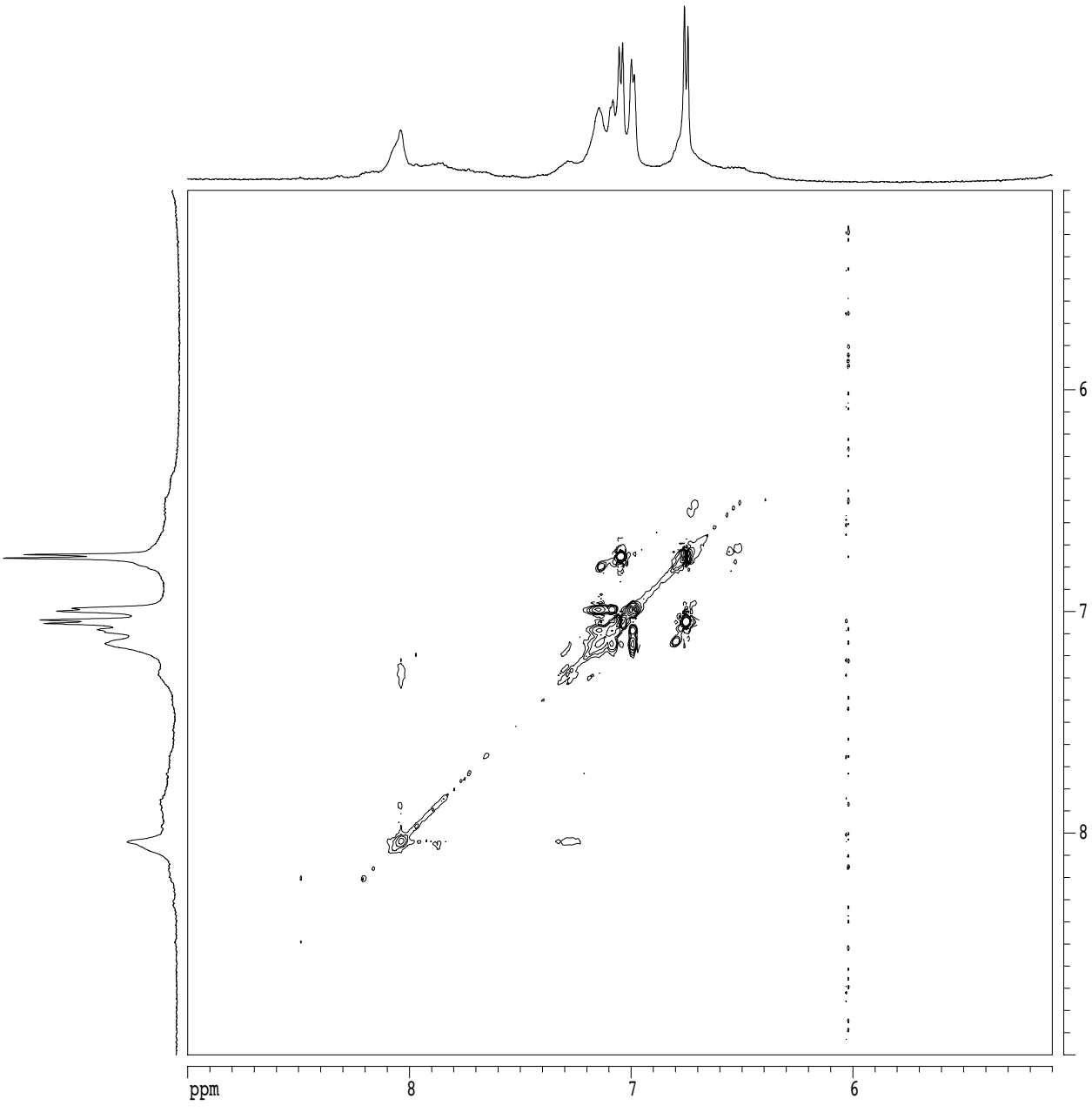

2D NOESY spectrum of macrocyclic β-sheet **3.2c**
2 mM in D_2O, 500 MHz, 298 K
250 ms spin-locking time

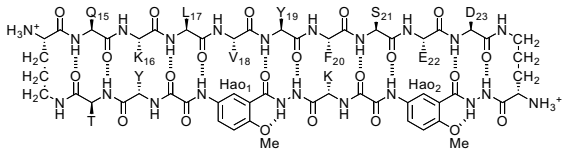

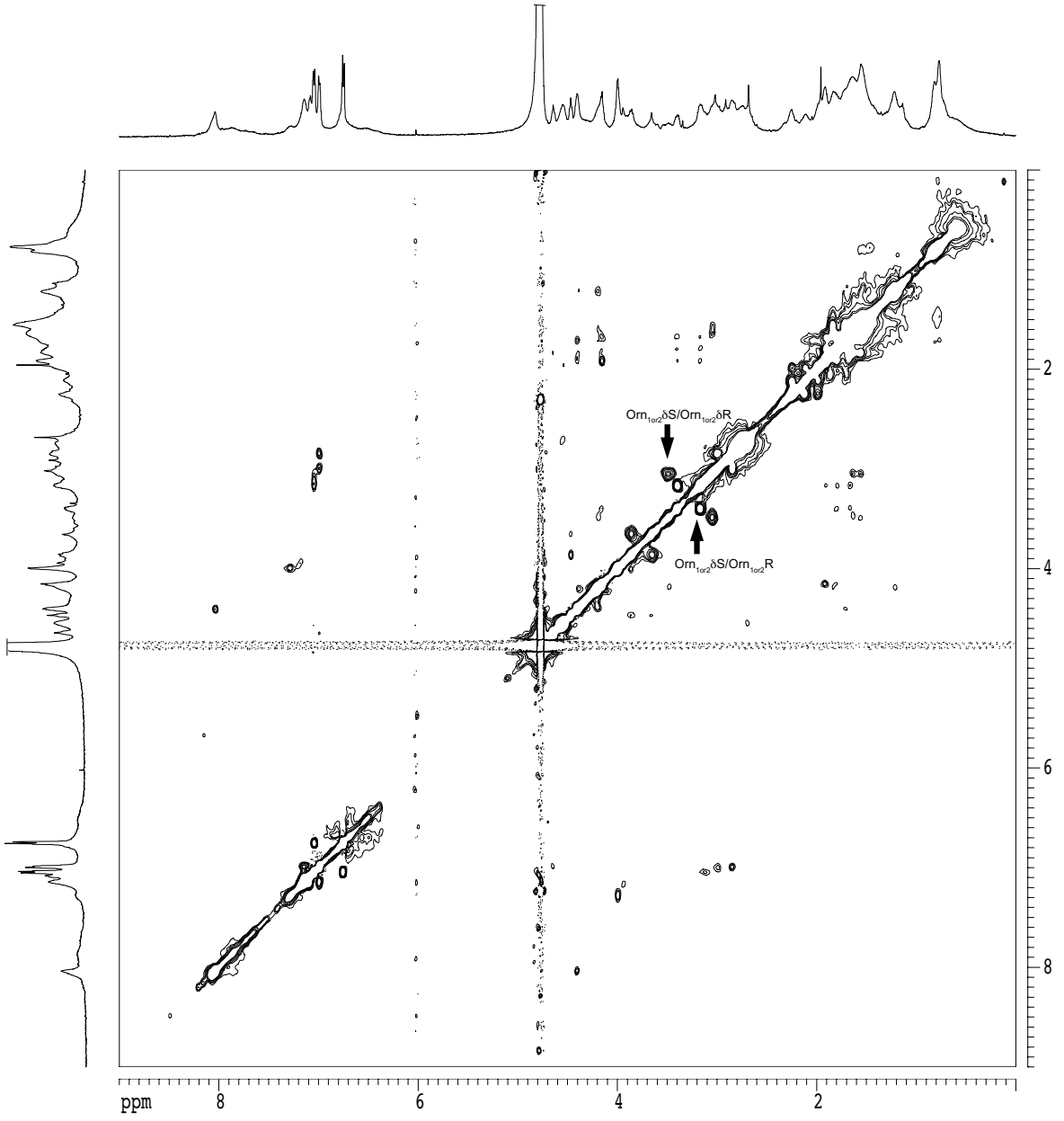

2D DOSY spectrum of macrocyclic β-sheet **3.2c**
2 mM in D_2O, 600 MHz, 298 K
monomer predominates

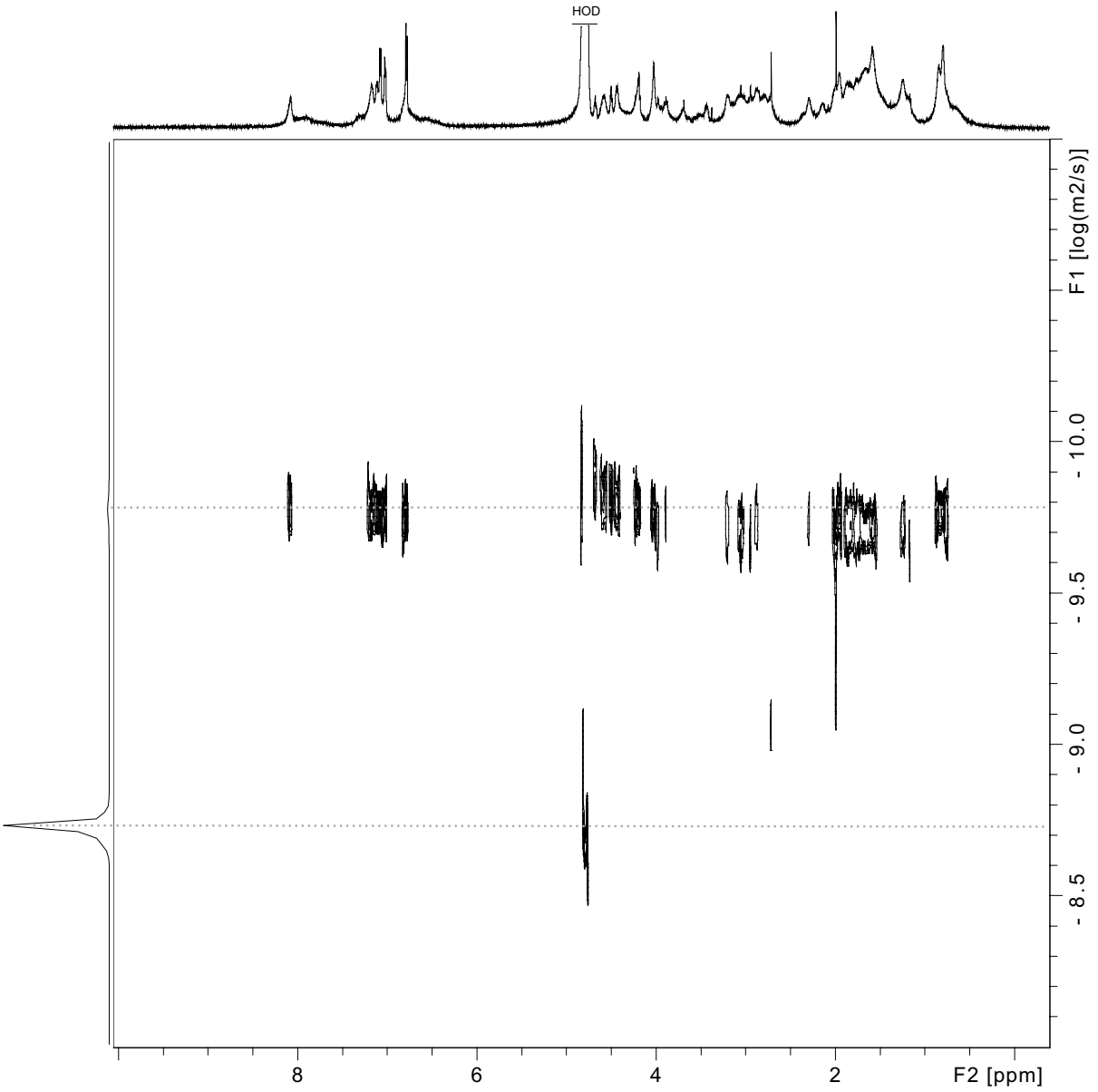

Calculation for 3.2c at 2.0 mM

DC_{HOD} = 19.0 x 10^{-10} m^2/s [a]
log DC_{HOD} = -8.721

For 3.2c tetramer, log DC (m^2/s) = -9.78(3), DC = $10^{-9.783}$ m^2/s = 16.5 x 10^{-11} m^2/s = 16.5 x 10^{-7} cm^2/s

[a] Longsworth, L. G. J. Phys. Chem. 1960, 64, 1914–1917.

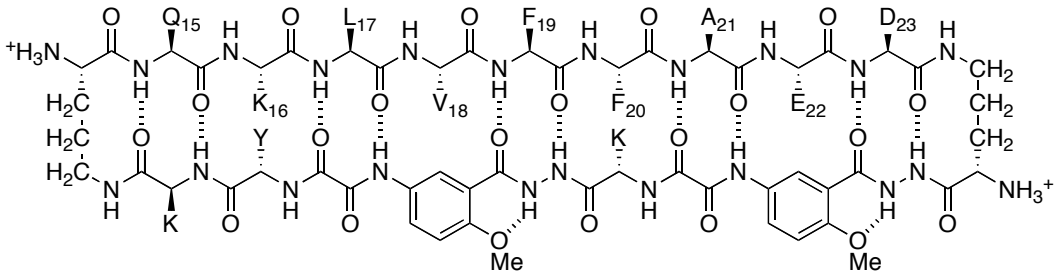

macrocyclic β-sheet peptide **3.3** (as the TFA salt)

molecular weight calculated for $C_{103}H_{146}N_{26}O_{28} \cdot 5CF_3CO_2H$ (TFA salt of **3.3**): 2766.54
molecular weight calculated for $C_{103}H_{146}N_{26}O_{28}$ (free base of **3.3**): 2196.42
exact mass calculated for $C_{103}H_{146}N_{26}O_{28}$ (free base of **3.3**): 2195.08

Analytical RP-HPLC of macrocyclic β-sheet peptide **3.3**

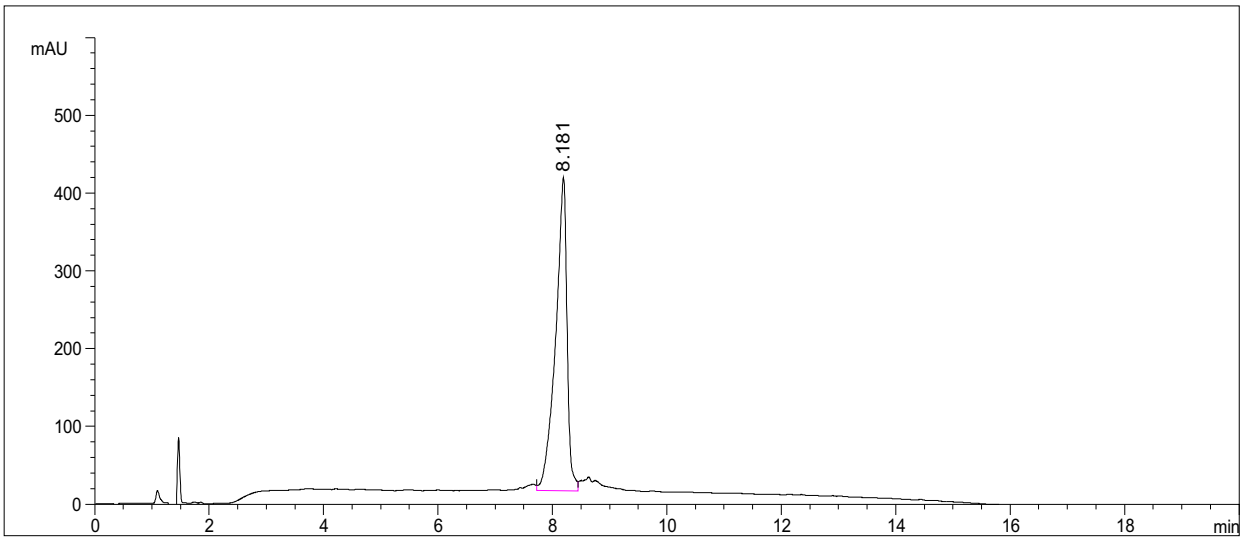

Signal 1: VWD1 A, Wavelength=214 nm

Peak #	RetTime [min]	Type	Width [min]	Area mAU *s	Height [mAU]	Area %
1	8.181	VV	0.1970	5600.01514	403.11060	100.0000
Totals :				5600.01514	403.11060	

Macrocyclic β-sheet peptide **3.3**

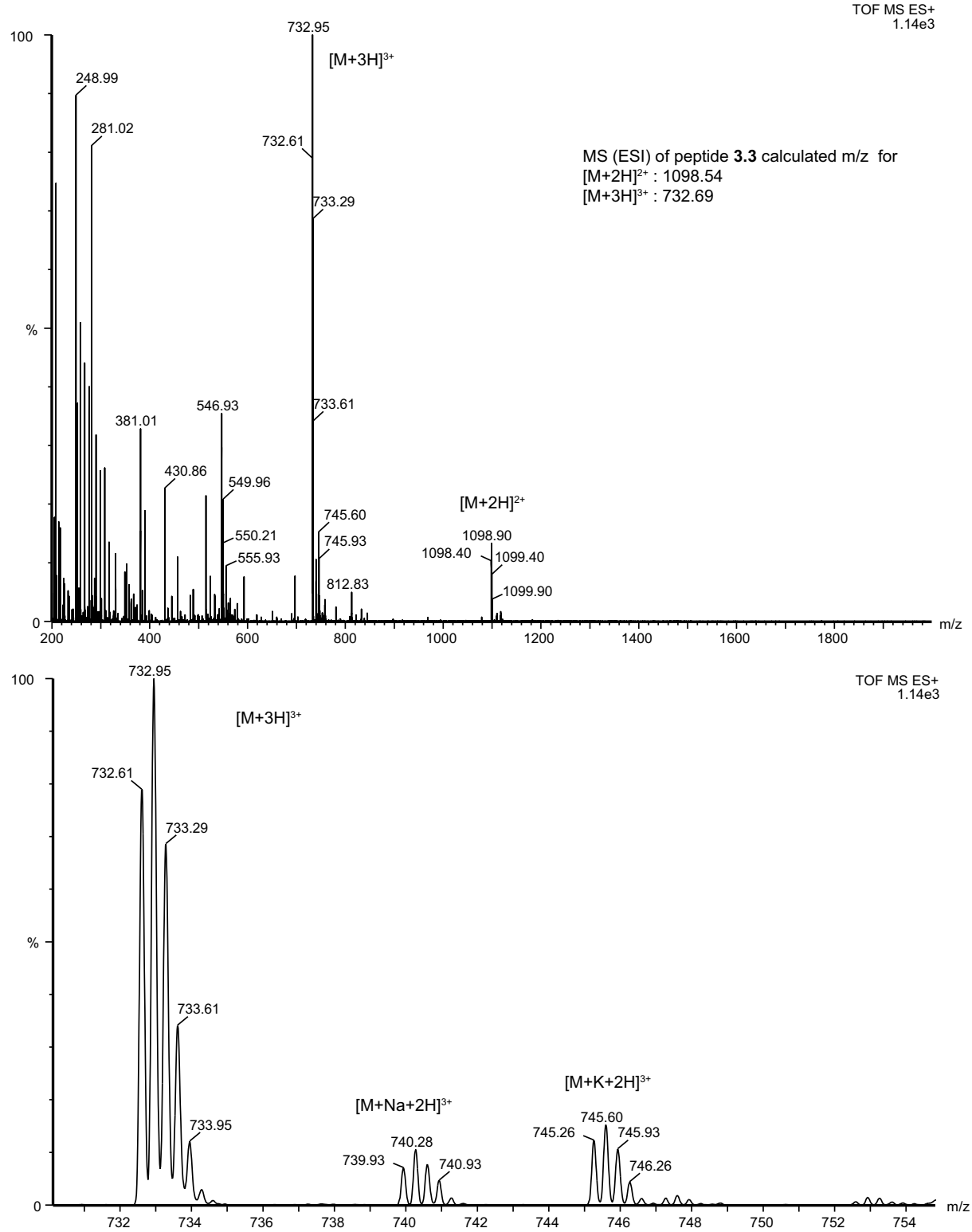

Macrocyclic β-sheet peptide **3.3**

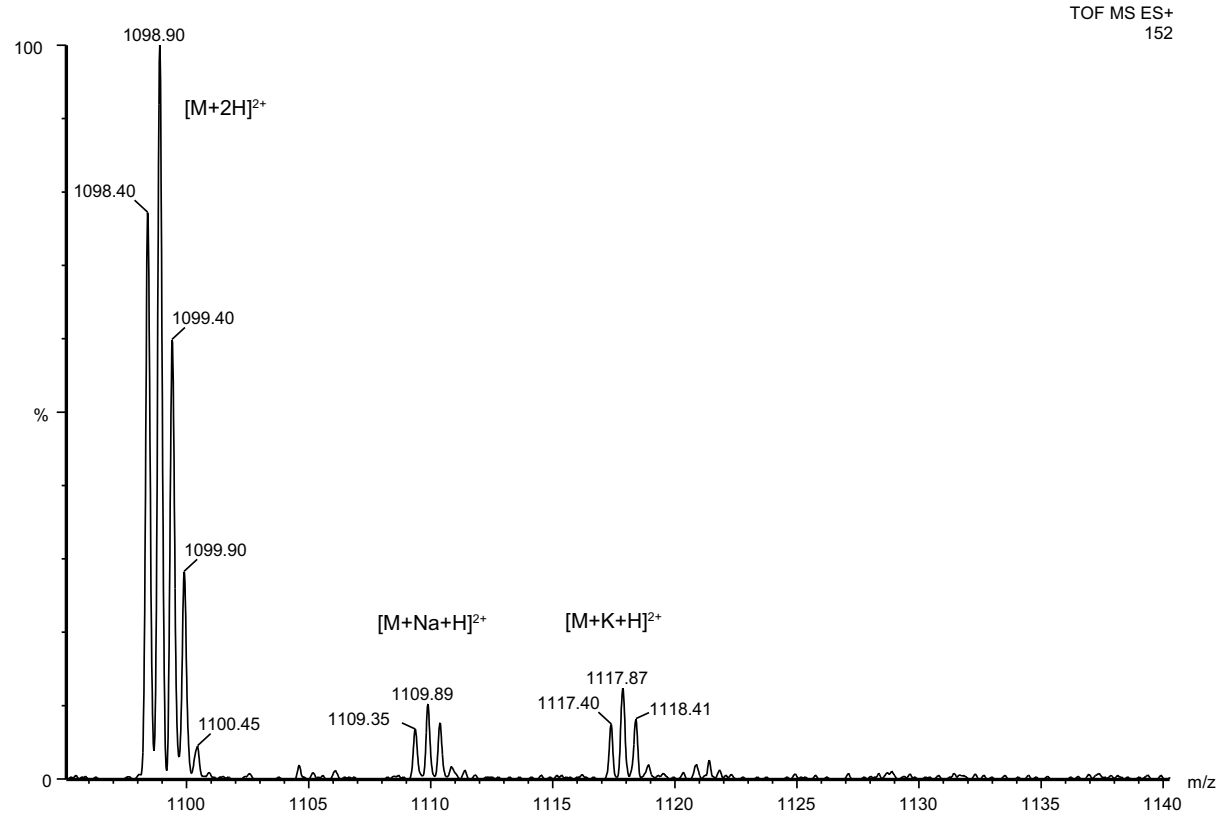

1D ^{1}H NMR spectrum of macrocyclic β-sheet **3.3**
2 mM in D_2O, 500 MHz, 298 K
monomer predominates, small resonances are from tetramers

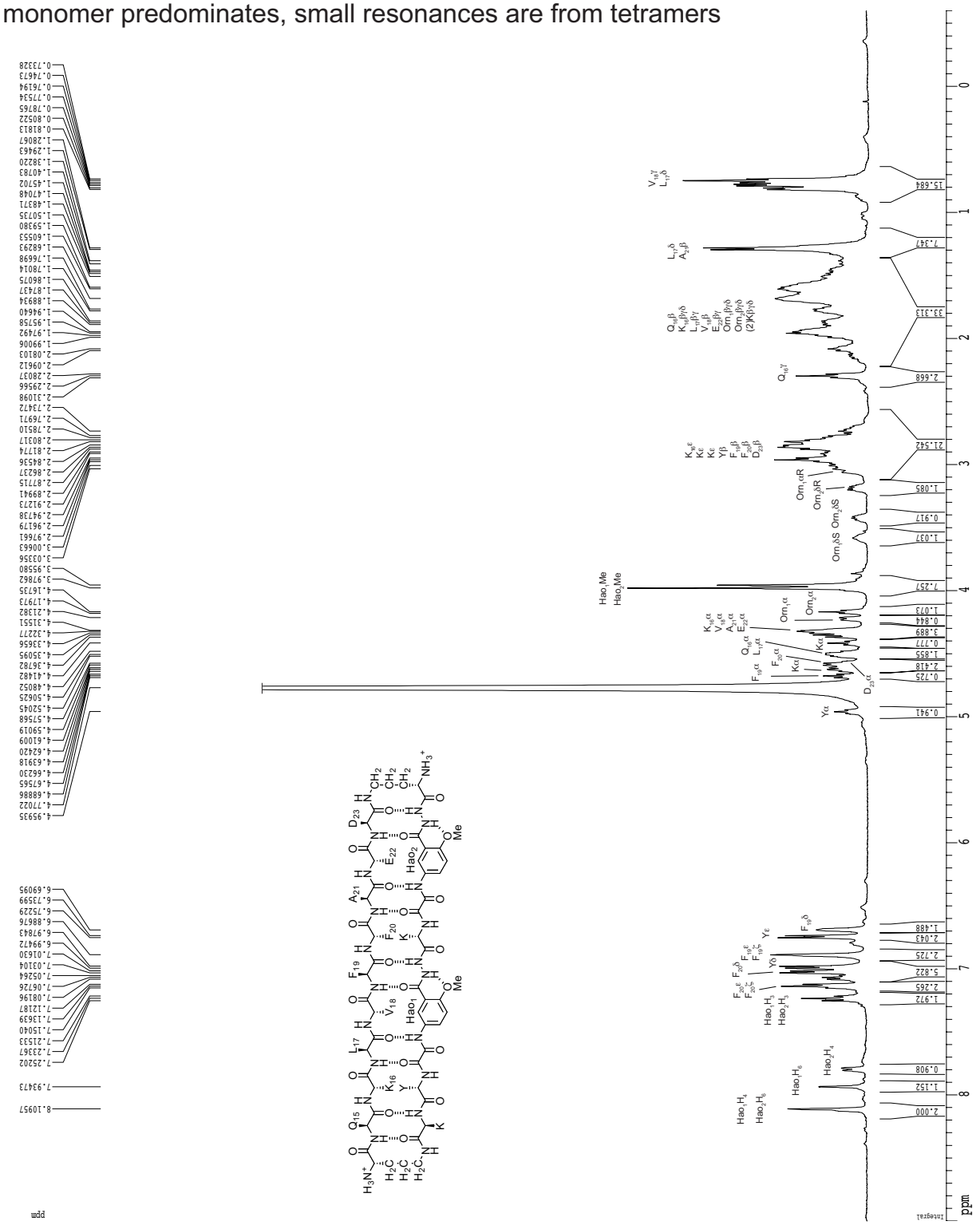

2D TOCSY spectrum of macrocyclic β-sheet **3.3**, 2 mM in D_2O, 500 MHz, 298 K
150-ms spin-locking mixing time
monomer predominates, small resonances from tetramer

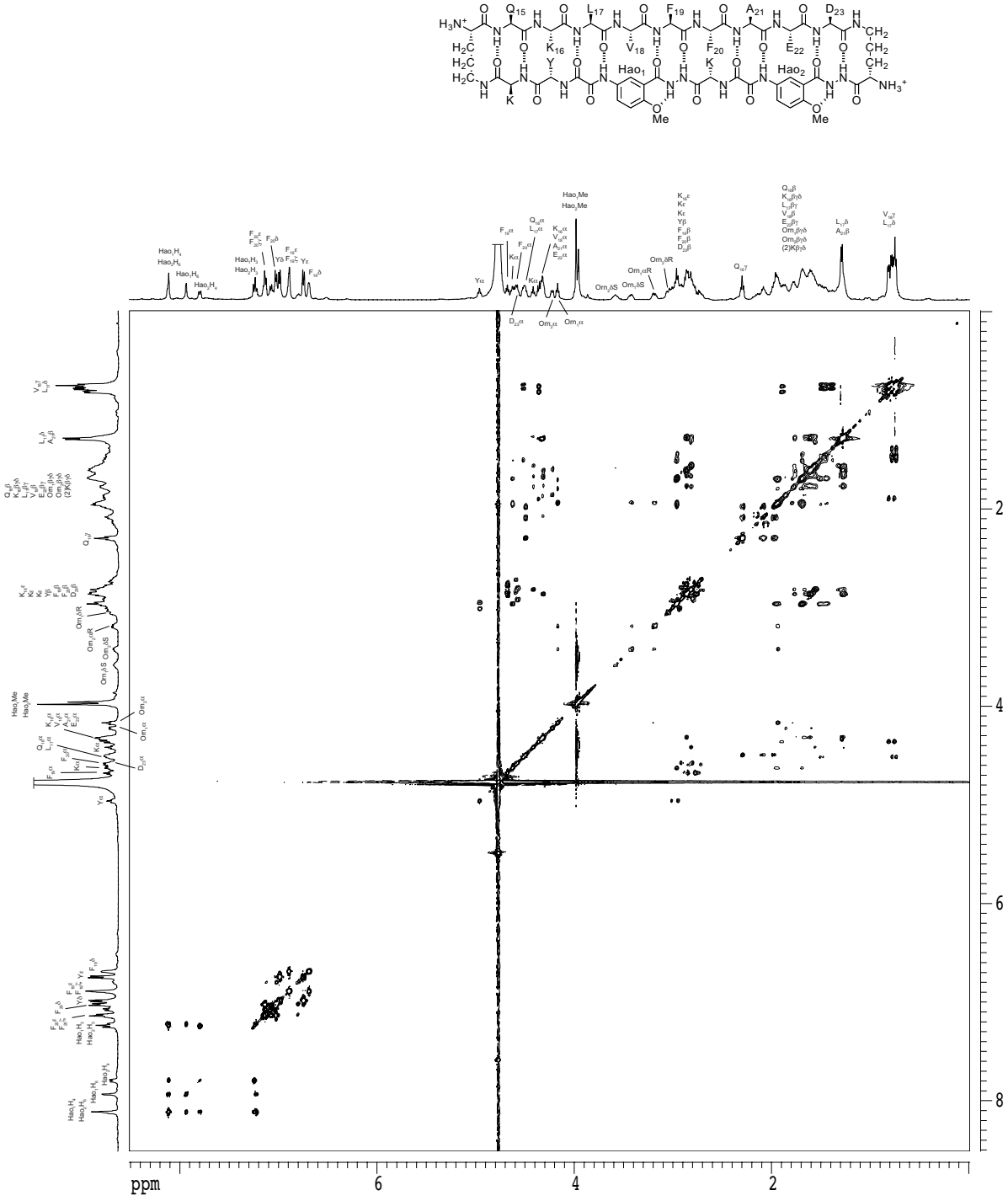

2D TOCSY spectrum of macrocyclic β-sheet **3.3**, 2 mM in D_2O, 500 MHz, 298 K
150-ms spin-locking mixing time
monomer predominates, small resonances from tetramer

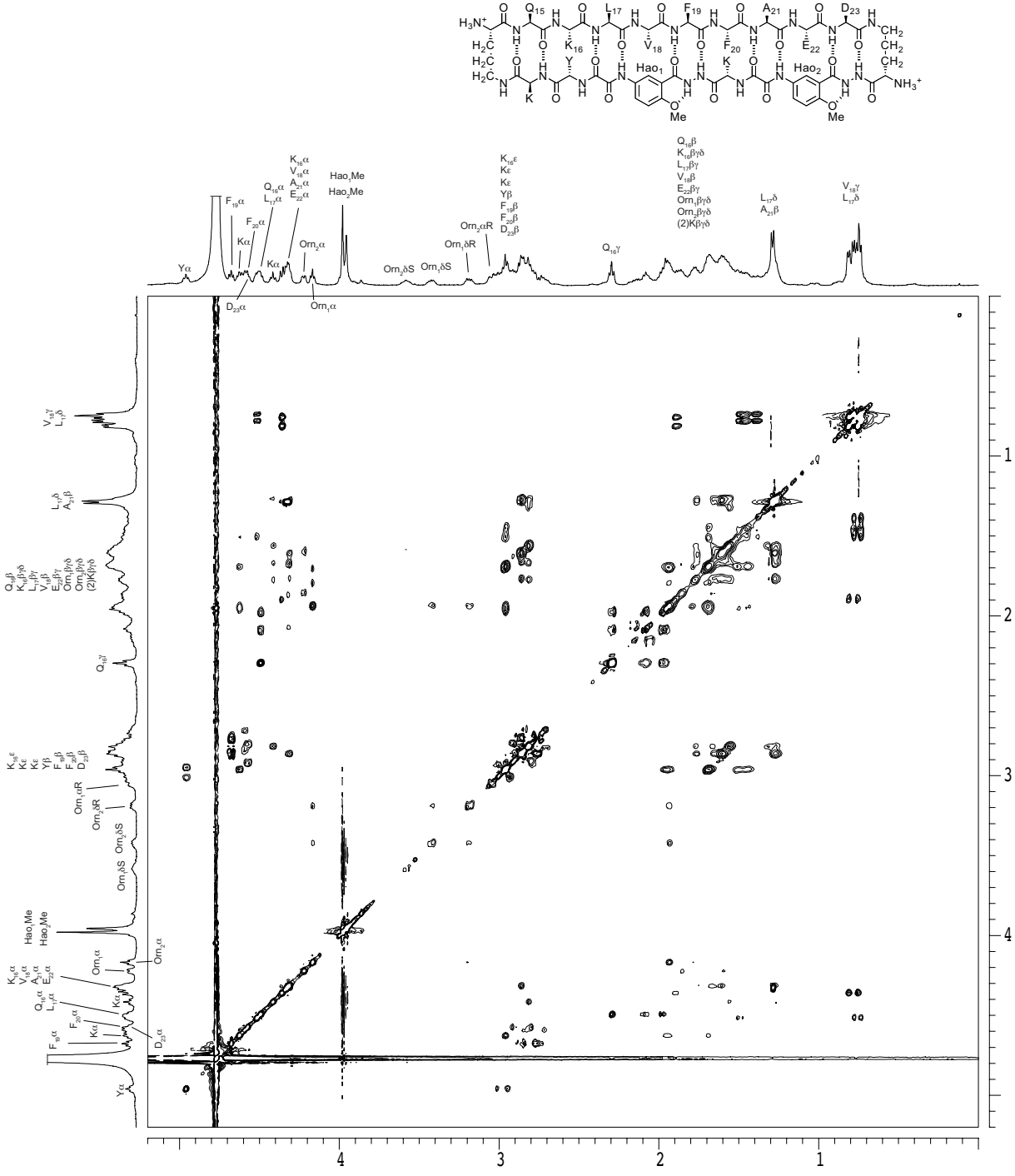

2D TOCSY spectrum of macrocyclic β-sheet **3.3**, 2 mM in D_2O, 500 MHz, 298 K
150-ms spin-locking mixing time
monomer predominates, small resonances from tetramer

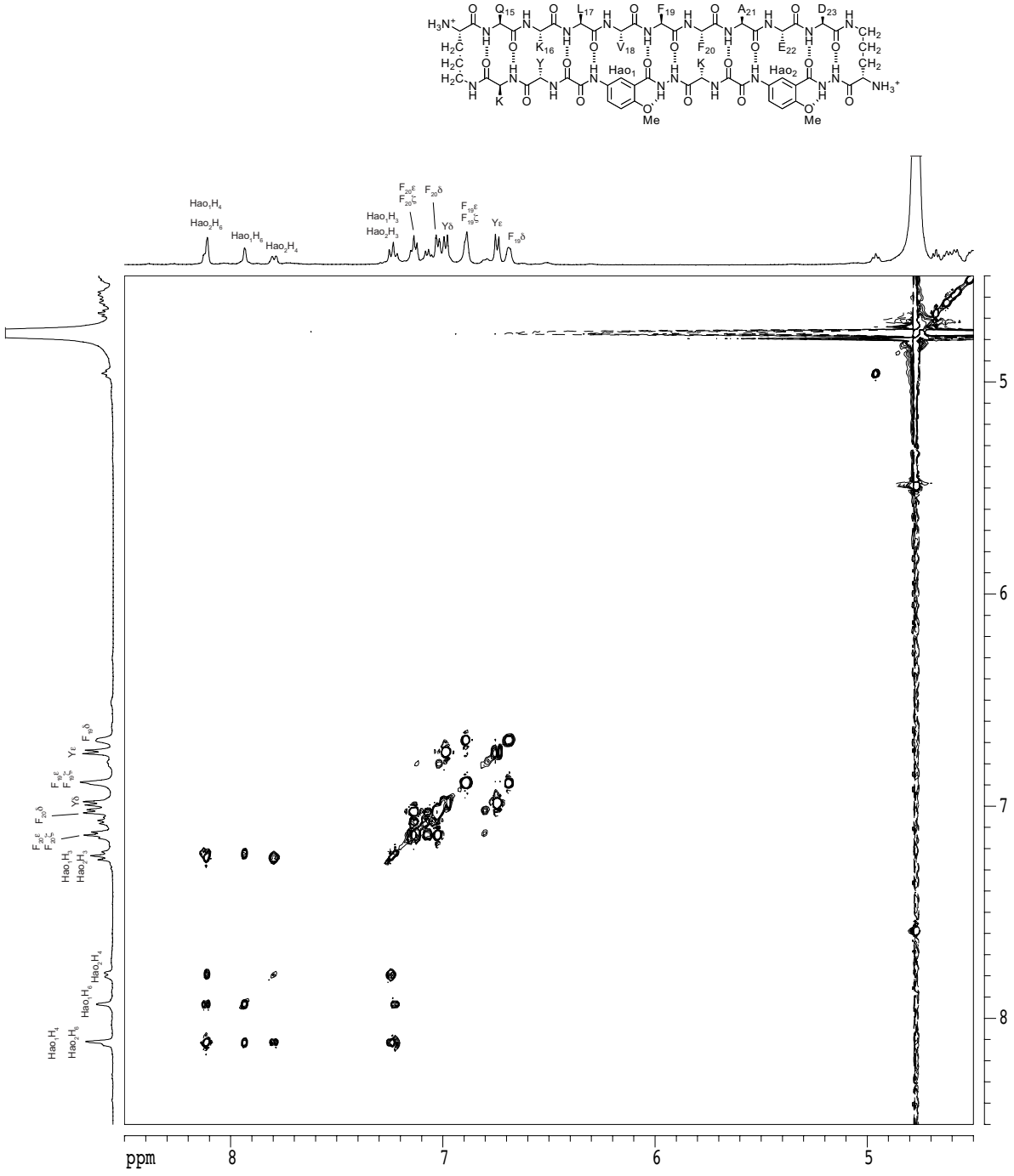

2D NOESY spectrum of macrocyclic β-sheet **3.3**
2 mM in D_2O, 500 MHz, 298 K
200-ms spin-locking mixing time
monomer predominates, small resonances are from tetramers

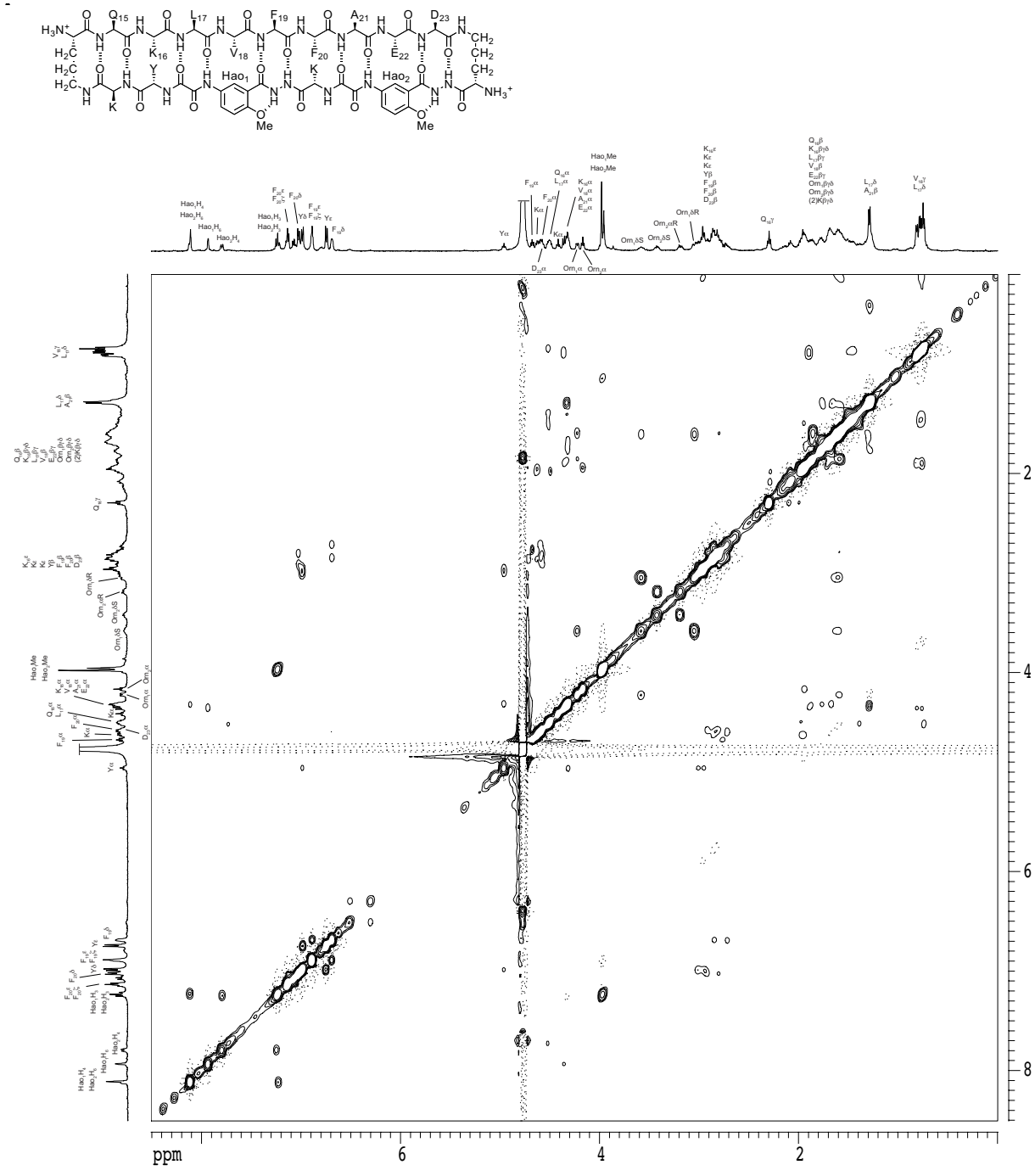

2D NOESY spectrum of macrocyclic β-sheet **3.3**, 2 mM in D_2O, 500 MHz, 298 K
200-ms spin-locking mixing time
monomer predominates, small resonances are from tetramers

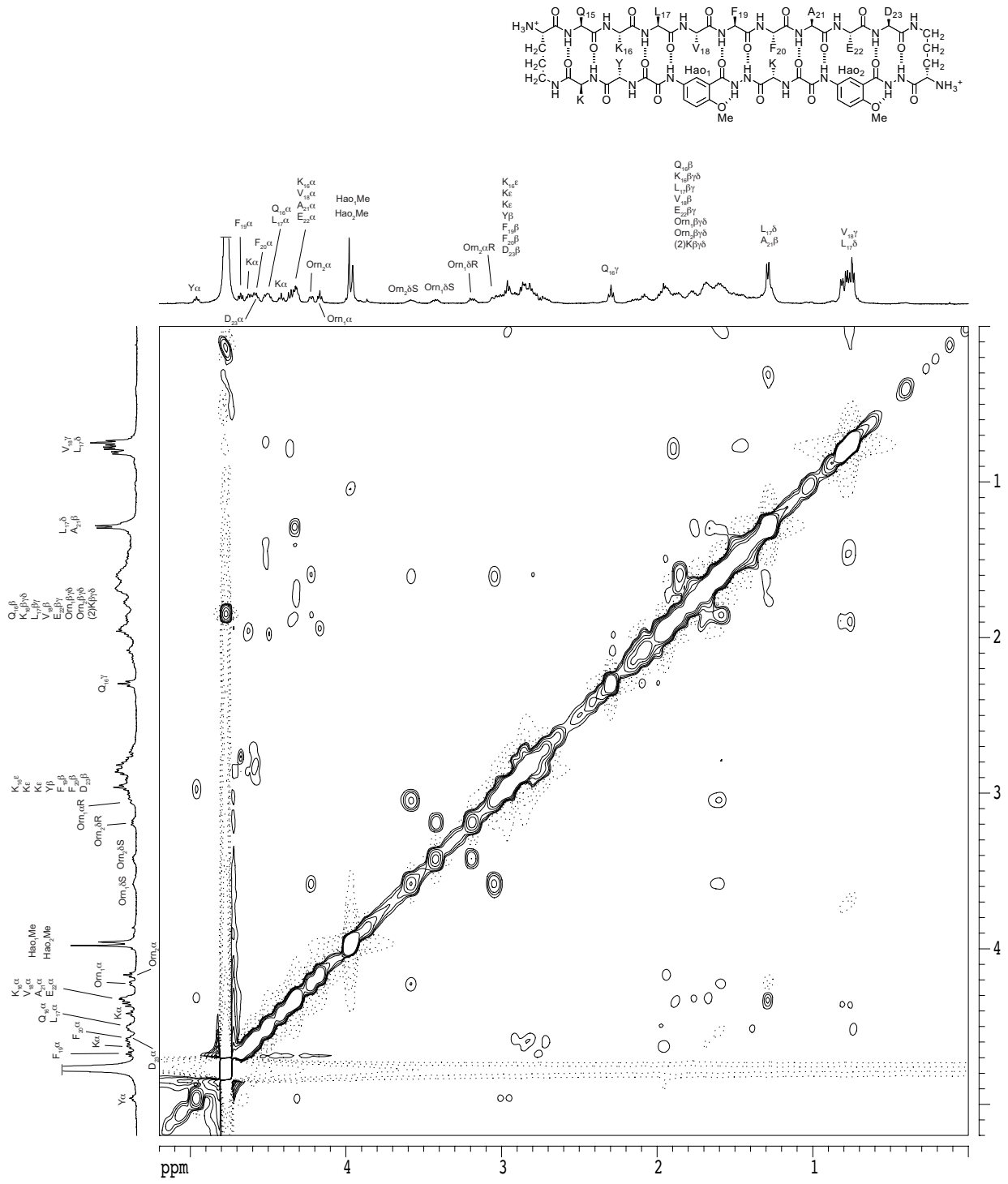

2D NOESY spectrum of macrocyclic β-sheet **3.3**, 2 mM in D_2O, 500 MHz, 298 K
200 ms spin-locking time
monomer predominates, small resonances are from tetramer

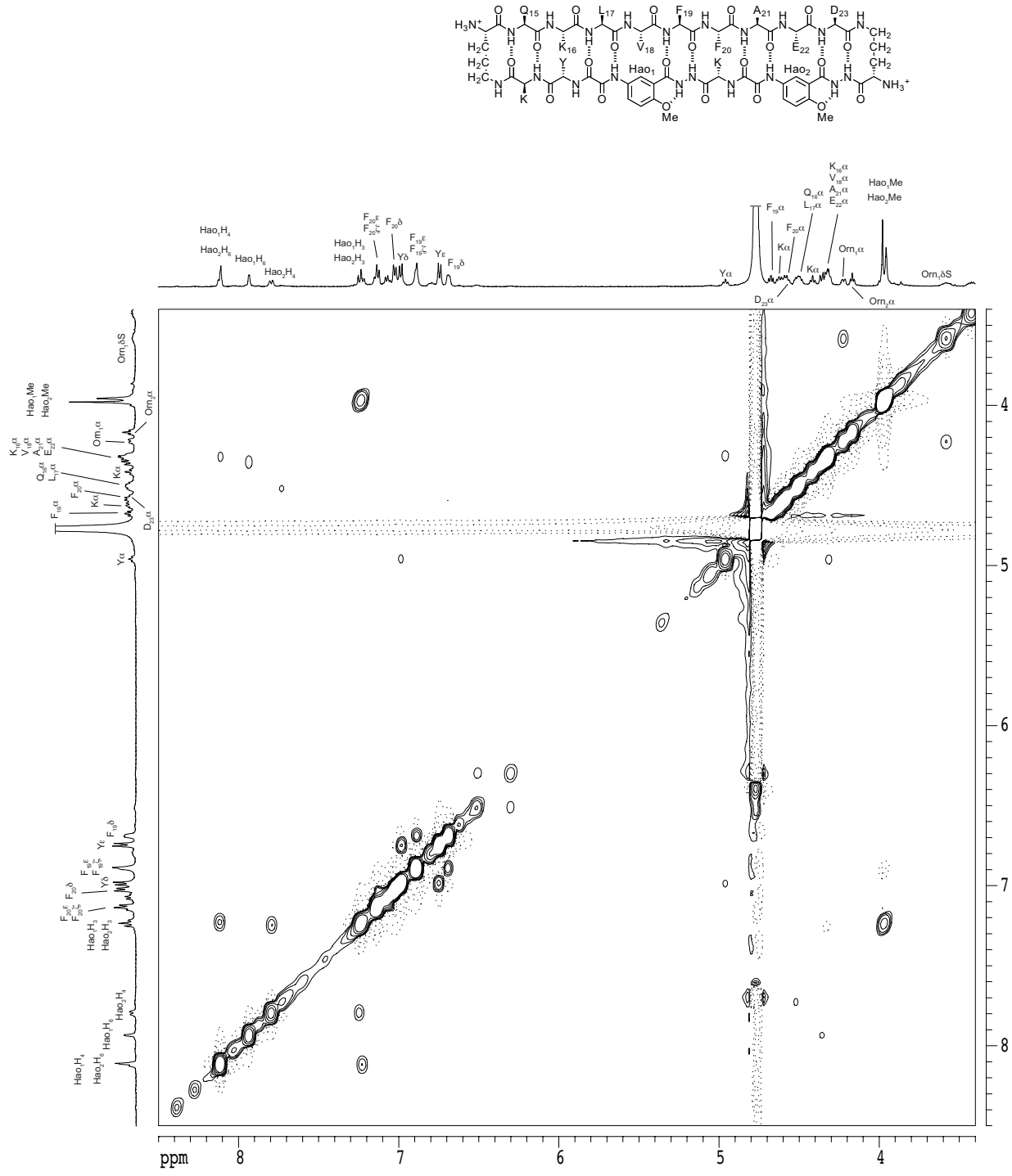

1D ^{1}H NMR spectrum of macrocyclic β-sheet **3.3**, 8 mM in D_2O, 500 MHz, 298 K
40/60 ratio of monomer to tetramer
resonances from tetramer are labeled

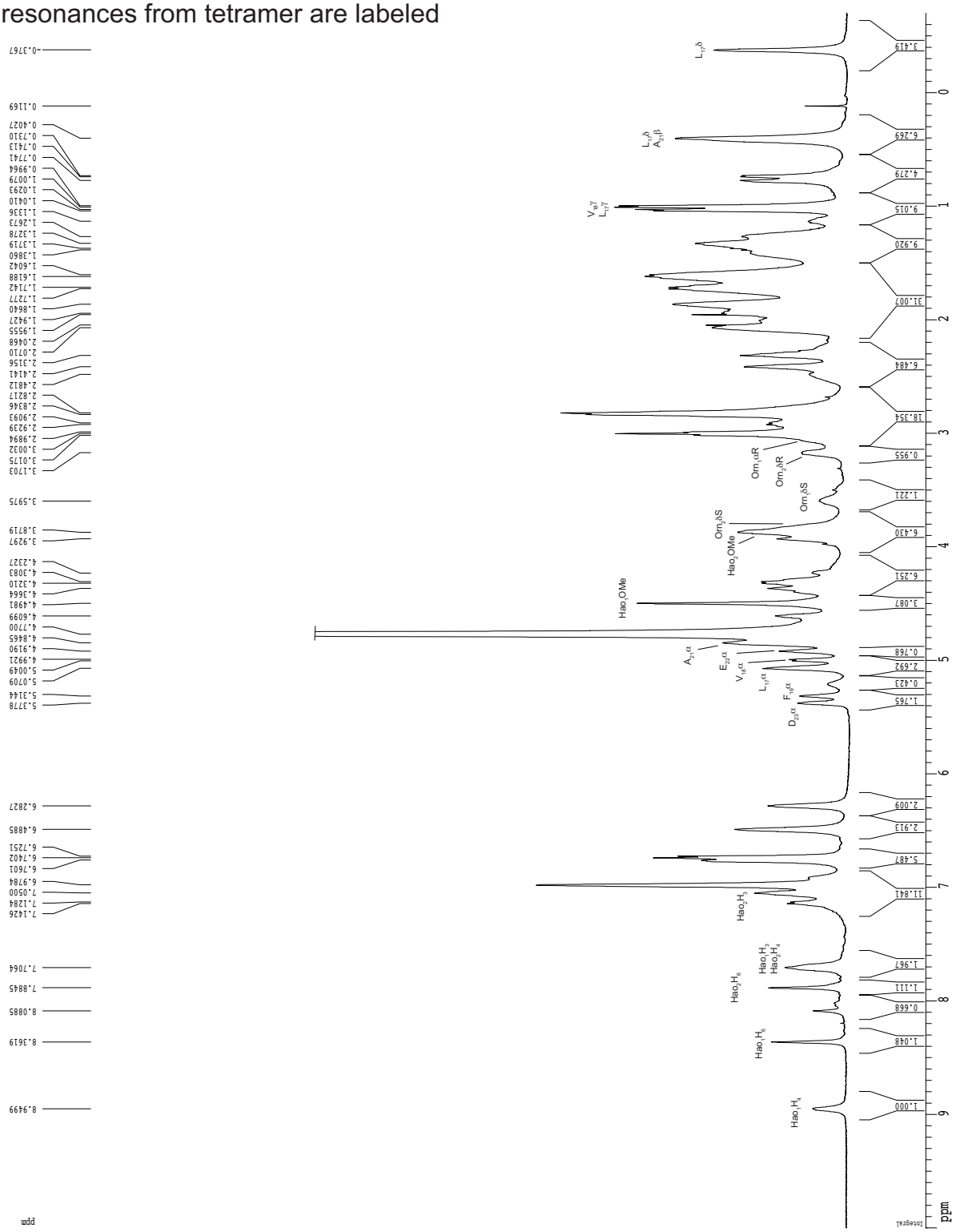

2D TOCSY spectrum of macrocyclic β-sheet **3.3**, 8 mM in D_2O, 500 MHz, 298 K
150-ms spin-locking mixing time
40/60 ratio of monomer to tetramer
resonances from tetramer are labeled

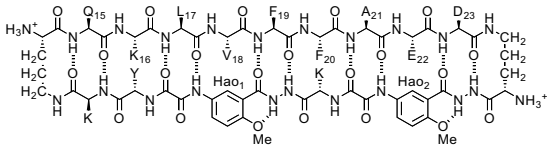

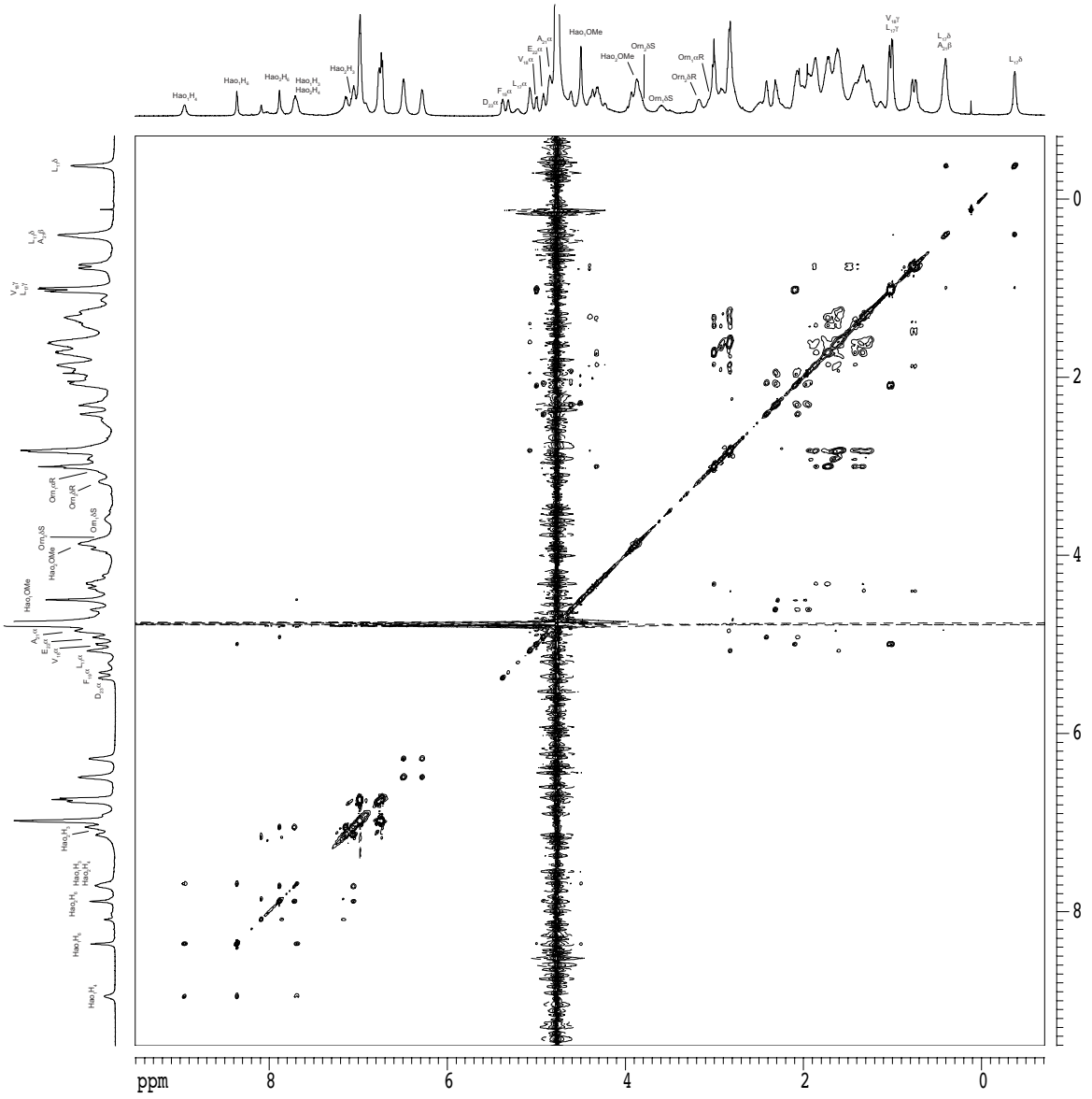

2D NOESY spectrum of macrocyclic β-sheet **3.3**, 8 mM in D_2O, 500 MHz, 298 K
200-ms spin-locking mixing time
40/60 ratio of monomer to tetramer
resonances from tetramer are labeled

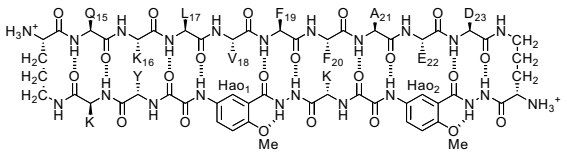

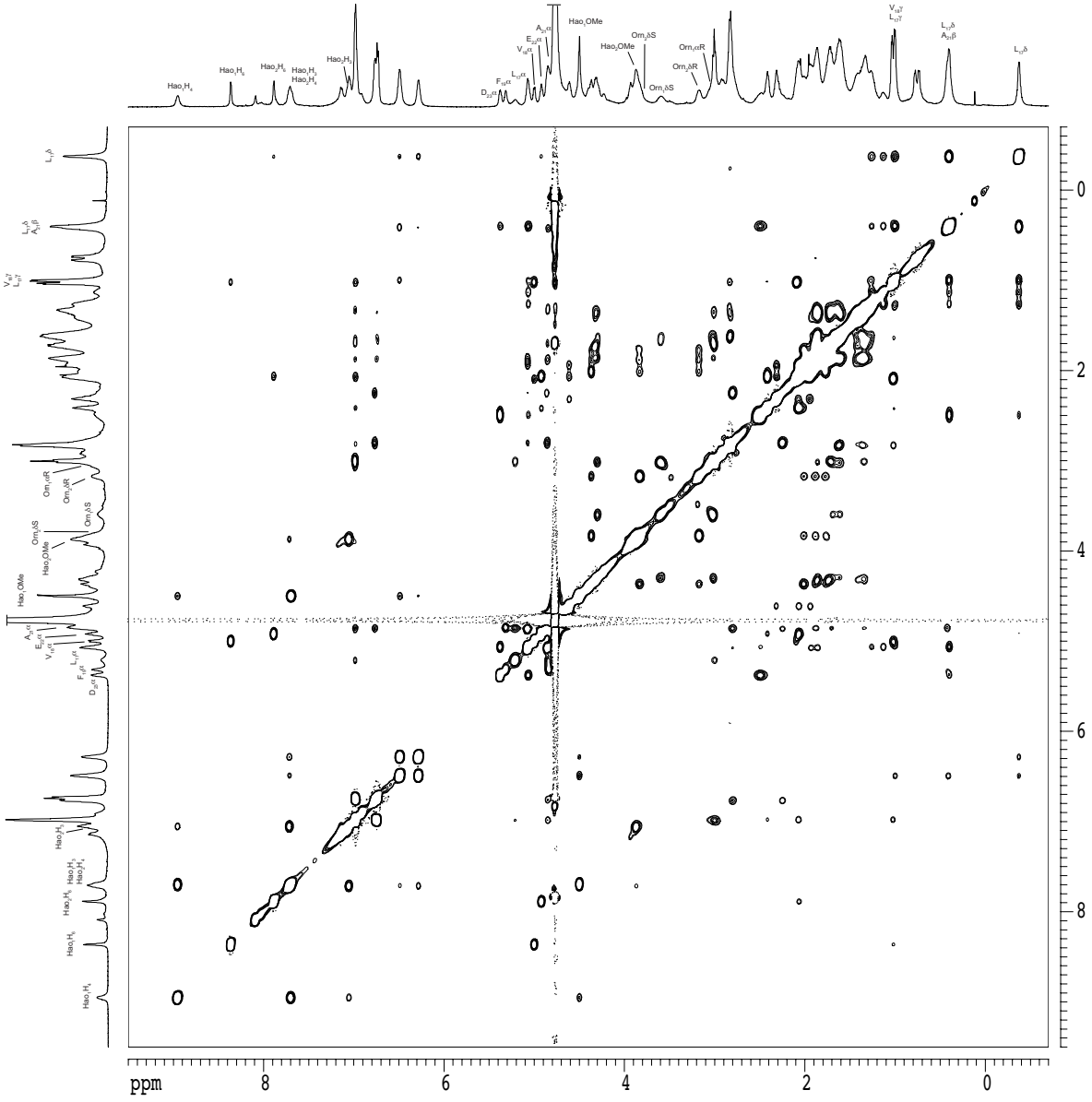

^{1}H NMR 2D EXSY (ROESY spectra showing exchange crosspeaks)
Peptide **3.3**, 4 mM in D_2O, 600 MHz, 340 K
200 ms spin-locking time
Exchange crosspeaks shown in red; ROE crosspeaks shown in black

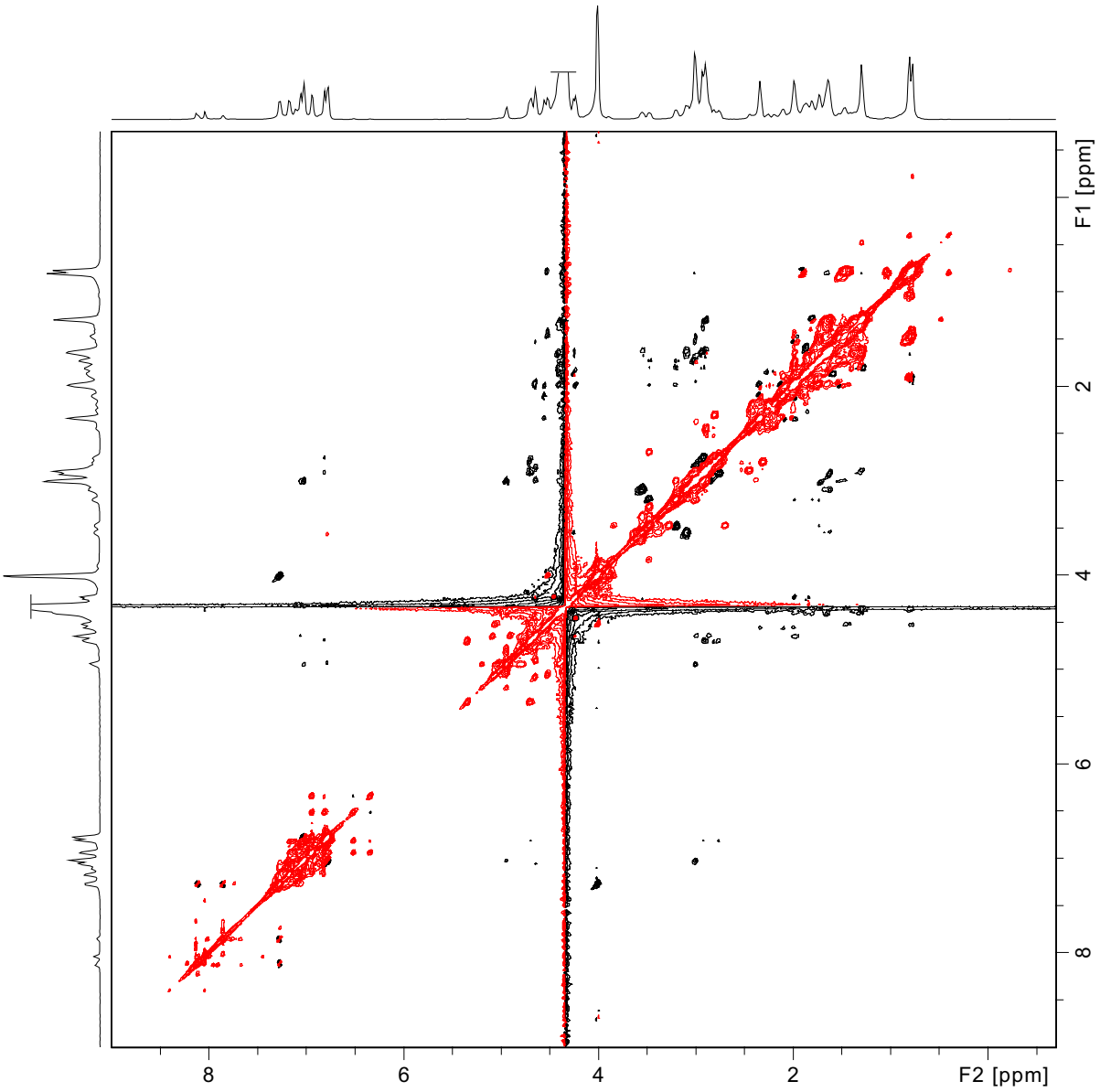

^{1}H NMR 2D EXSY (ROESY spectra showing exchange crosspeaks)
Peptide **3.3**, 4 mM in D_2O, 600 MHz, 340 K
200 ms spin-locking time
Exchange crosspeaks shown in red; ROE crosspeaks shown in black

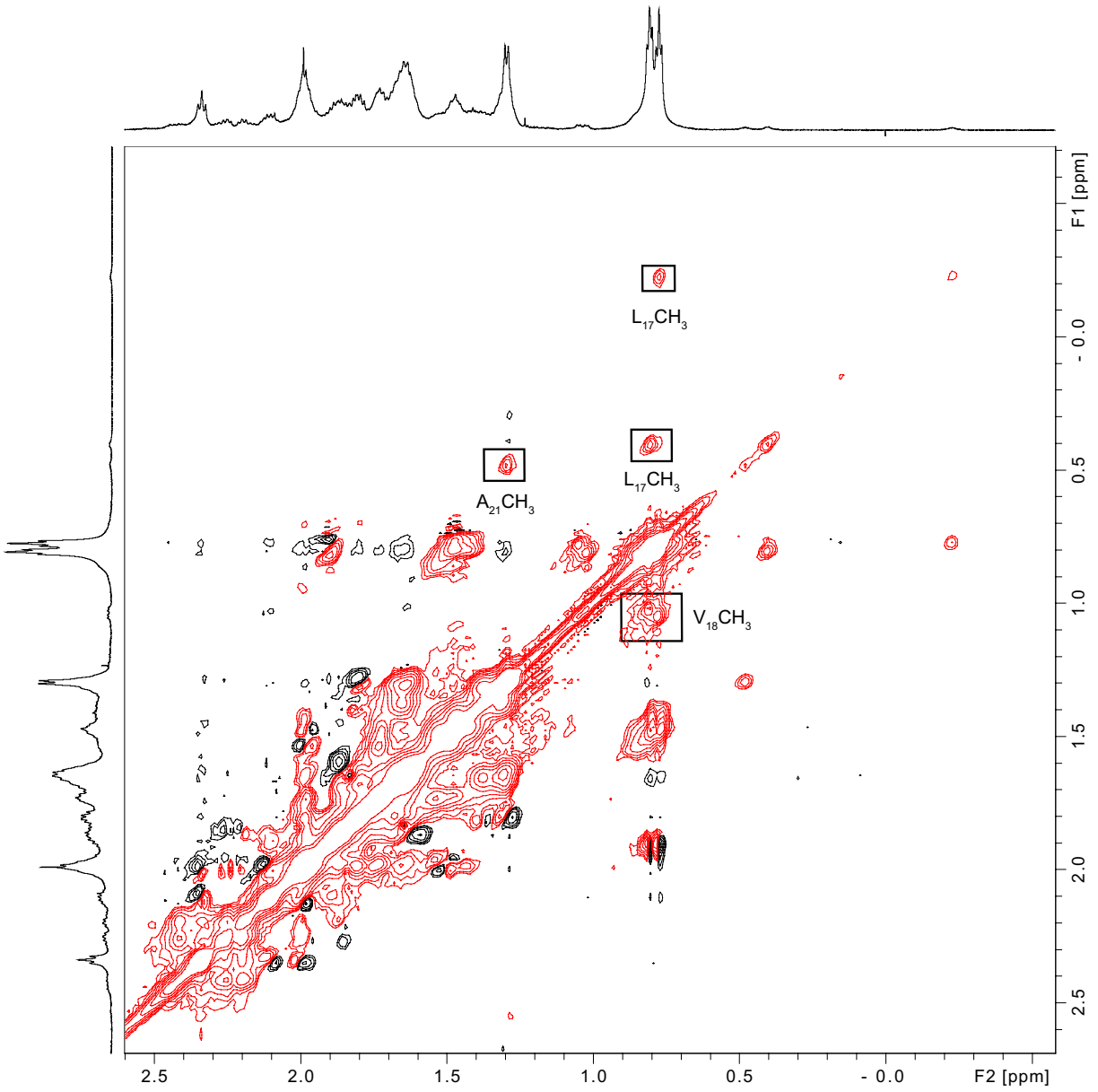

^{1}H NMR 2D EXSY (ROESY spectra showing exchange crosspeaks)
Peptide **3.3**, 4 mM in D_2O, 600 MHz, 340 K
200 ms spin-locking time
Exchange crosspeaks shown in red; ROE crosspeaks shown in black

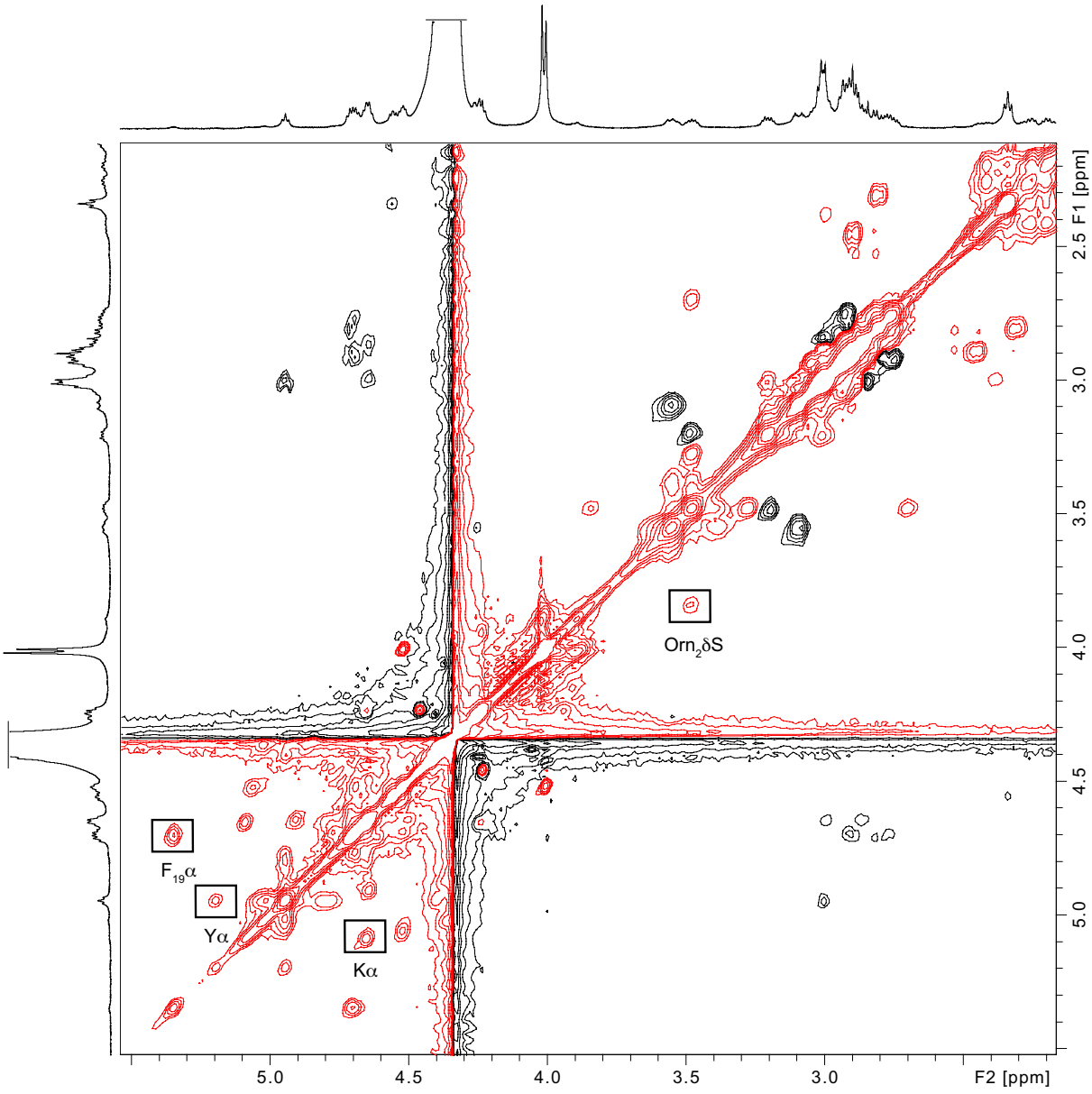

^{1}H NMR 2D EXSY (ROESY spectra showing exchange crosspeaks)
Peptide **3.3**, 4 mM in D_2O, 600 MHz, 340 K
200 ms spin-locking time
Exchange crosspeaks shown in red; ROE crosspeaks shown in black

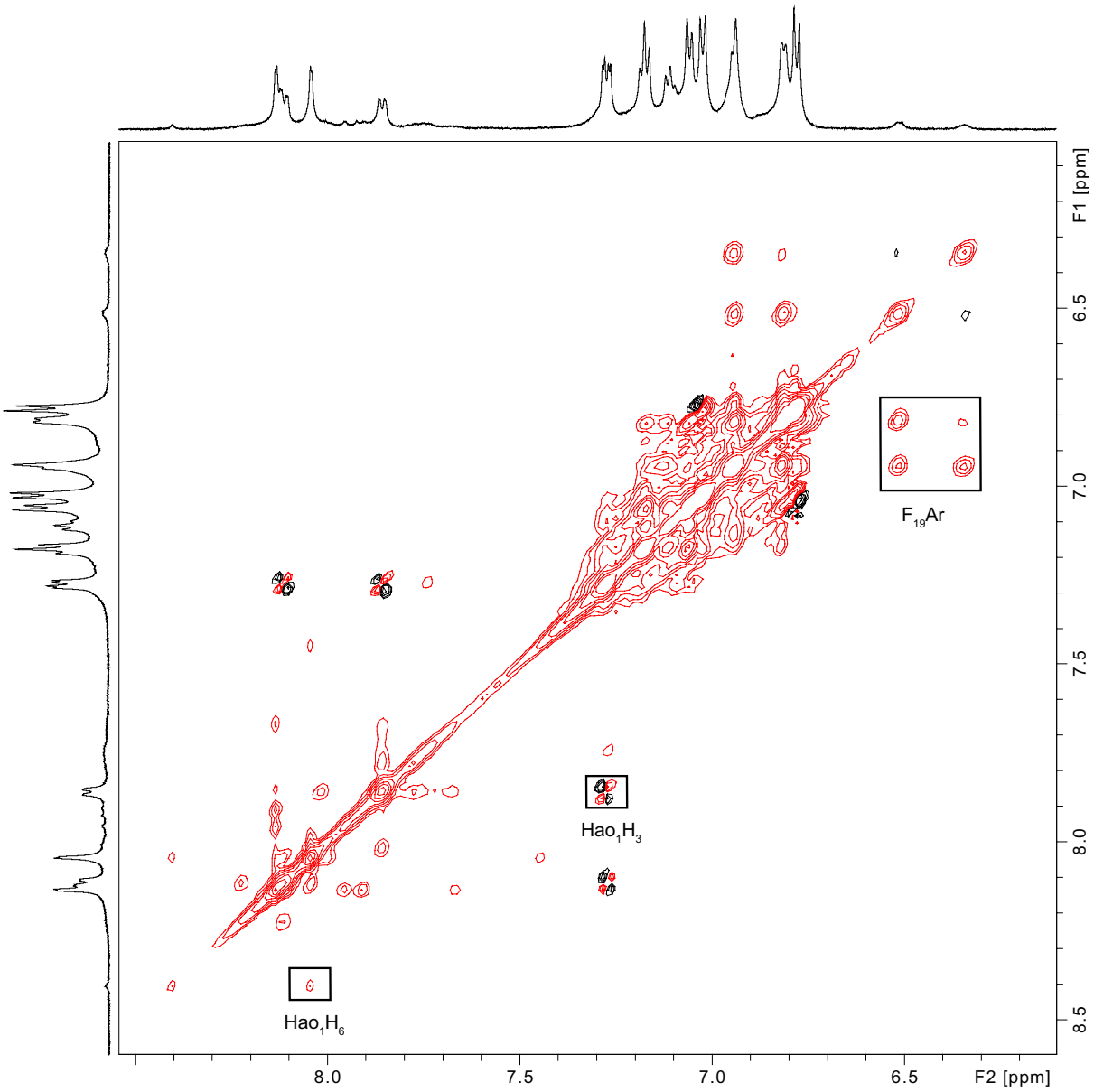

2D DOSY spectrum of macrocyclic β-sheet **3.3**
2 mM in D_2O, 600 MHz, 298 K
monomer predominates,
small resonances from tetramer

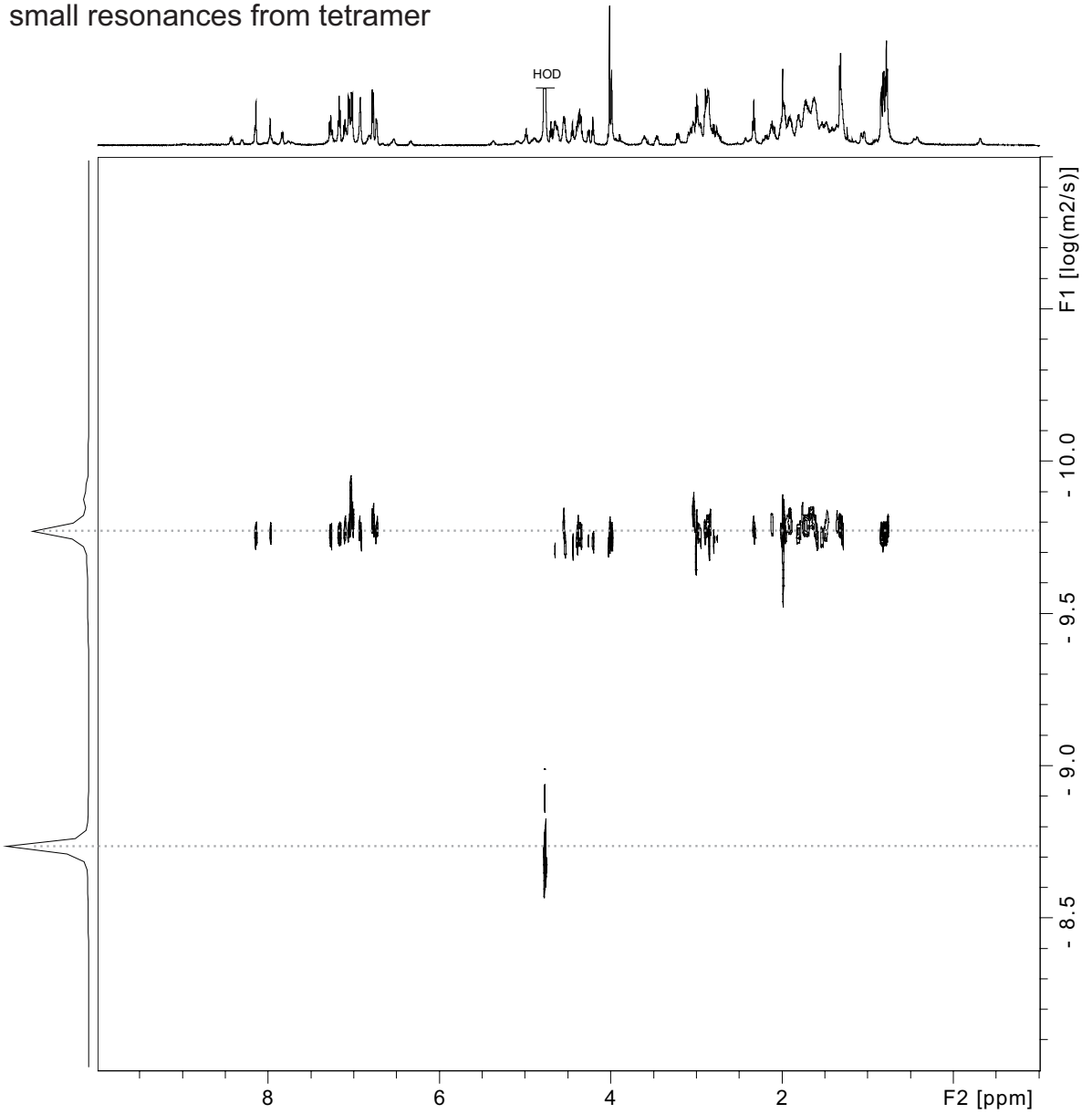

Calculation for 3.3 at 2.0 mM

DC_{HOD} = 19.0 x 10^{-10} m^2/s [a]
log DC_{HOD} = -8.721

For 3.3 tetramer, log DC (m^2/s) = -9.78(5), DC = $10^{-9.785}$ m^2/s = 16.4 x 10^{-11} m^2/s = 16.4 x 10^{-7} cm^2/s

[a] Longsworth, L. G. J. Phys. Chem. 1960, 64, 1914–1917.

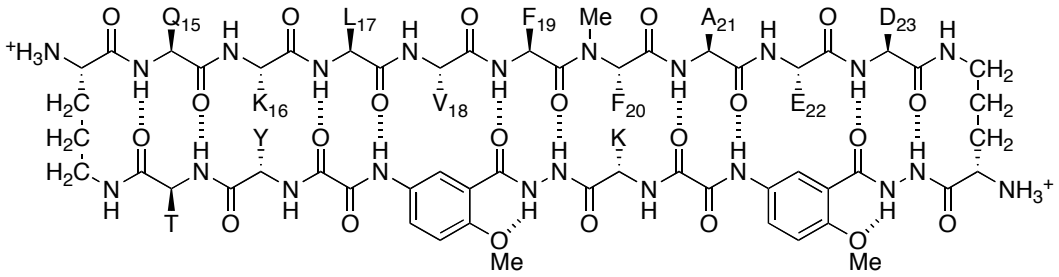

macrocyclic β-sheet peptide **3.4** (as the TFA salt)

molecular weight calculated for $C_{102}H_{143}N_{25}O_{29} \cdot 4CF_3CO_2H$ (TFA salt of **3.4**): 2639.47
molecular weight calculated for $C_{102}H_{143}N_{25}O_{29}$ (free base of **3.4**): 2183.38
exact mass calculated for $C_{102}H_{143}N_{25}O_{29}$ (free base of **3.4**): 2182.04

Analytical RP-HPLC of macrocyclic β-peptide **3.4**

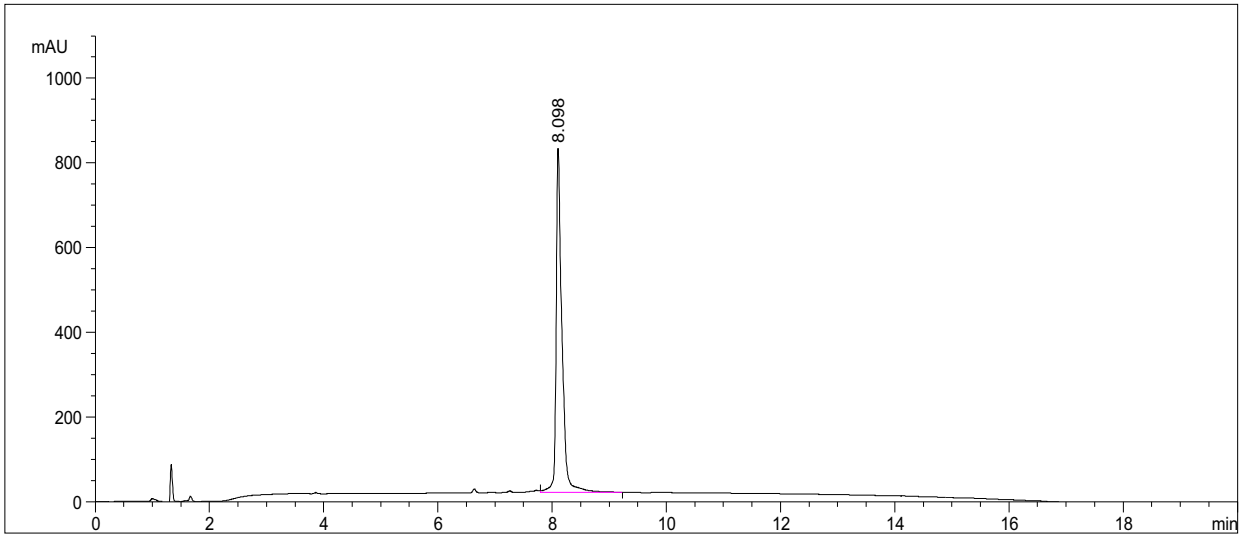

Signal 1: VWD1 A, Wavelength=214 nm

Peak #	RetTime [min]	Type	Width [min]	Area mAU *s	Height [mAU]	Area %
1	8.098	VV	0.1003	5771.48926	812.59326	100.0000
Totals :				5771.48926	812.59326	

Macrocyclic β-sheet peptide **3.4**

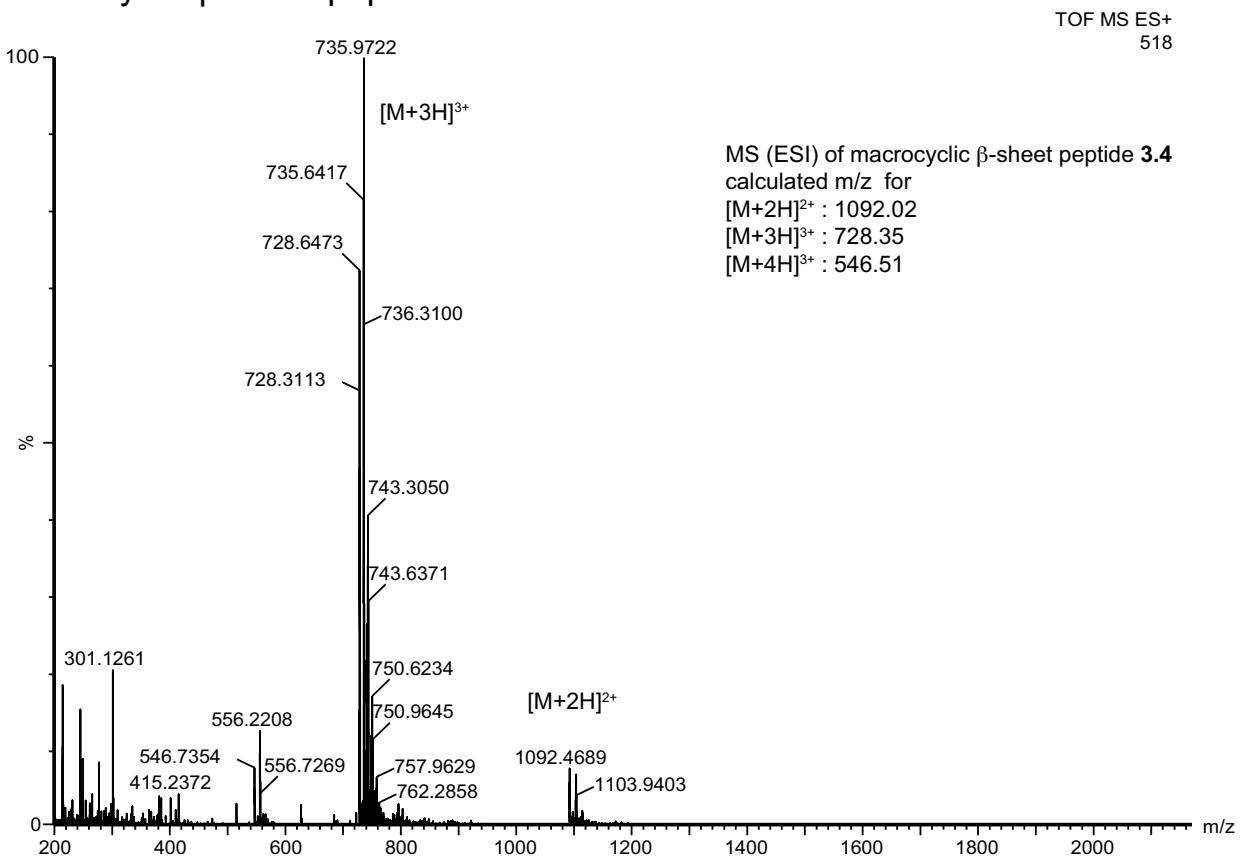

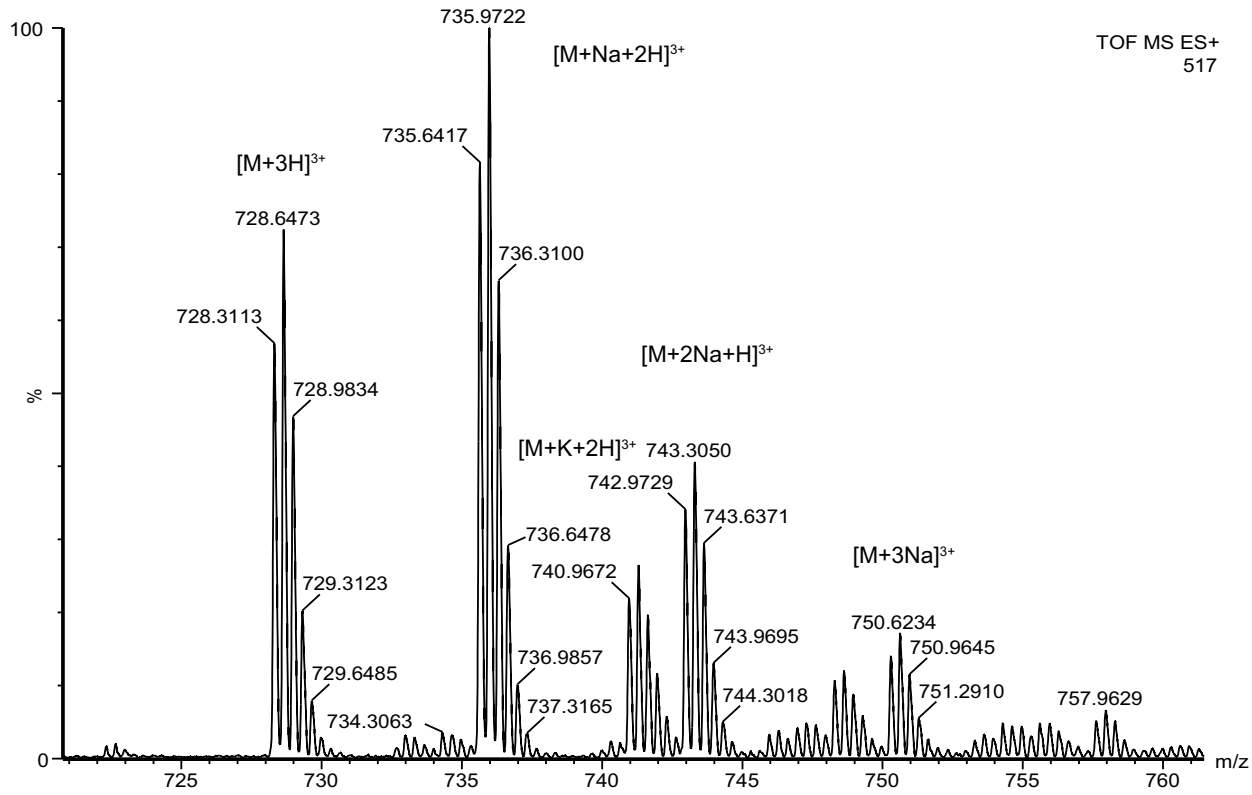

Macrocyclic β-sheet peptide **3.4**

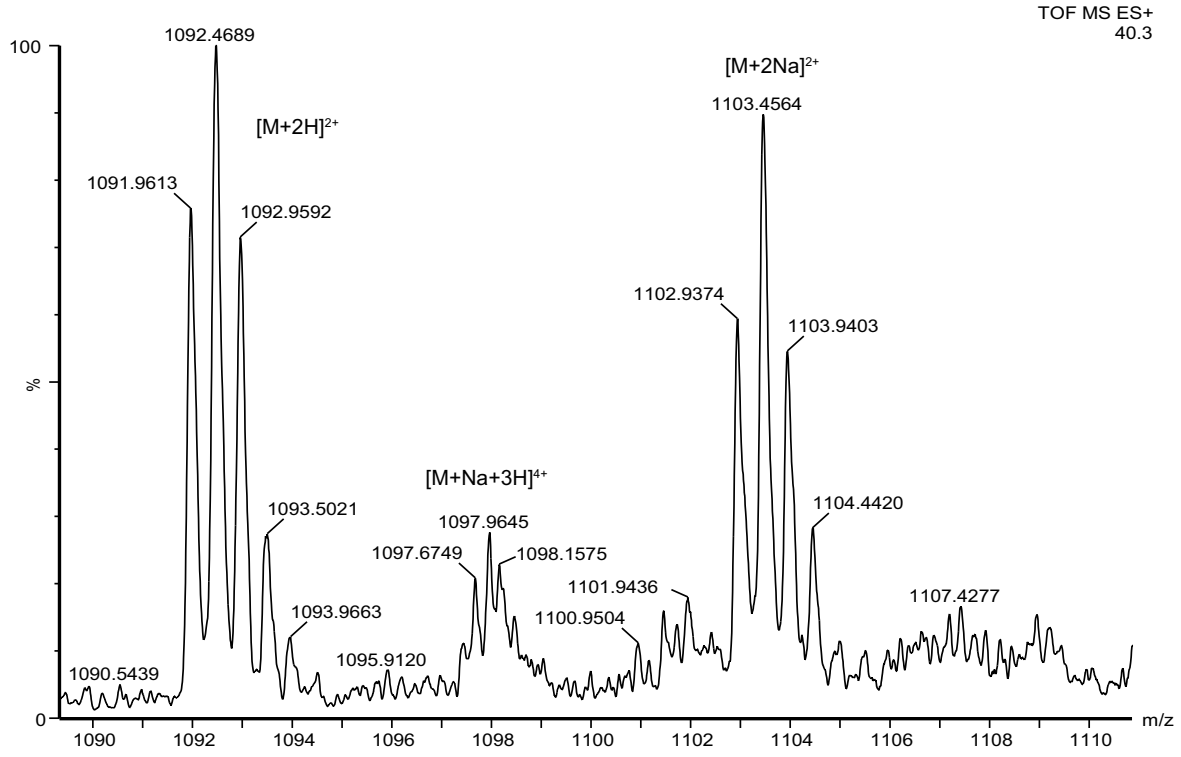

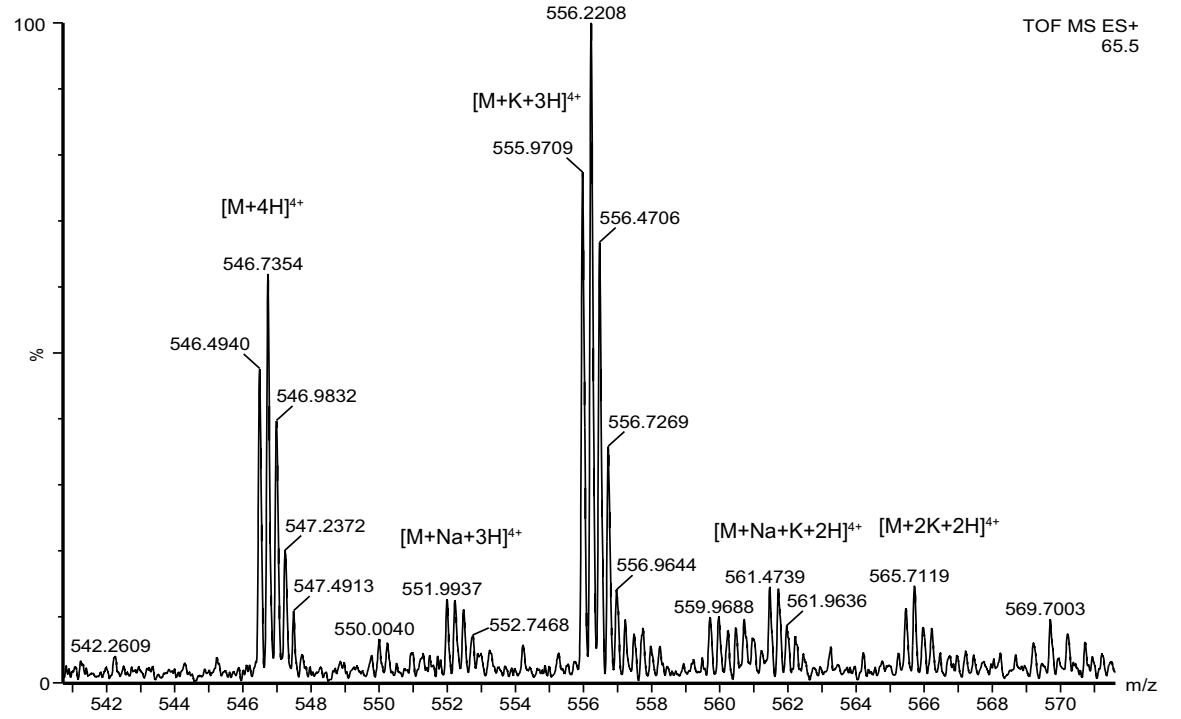

1D ^{1}H NMR spectrum of macrocyclic β-sheet peptide **3.4**
2 mM in D_2O, 500 MHz, 298 K

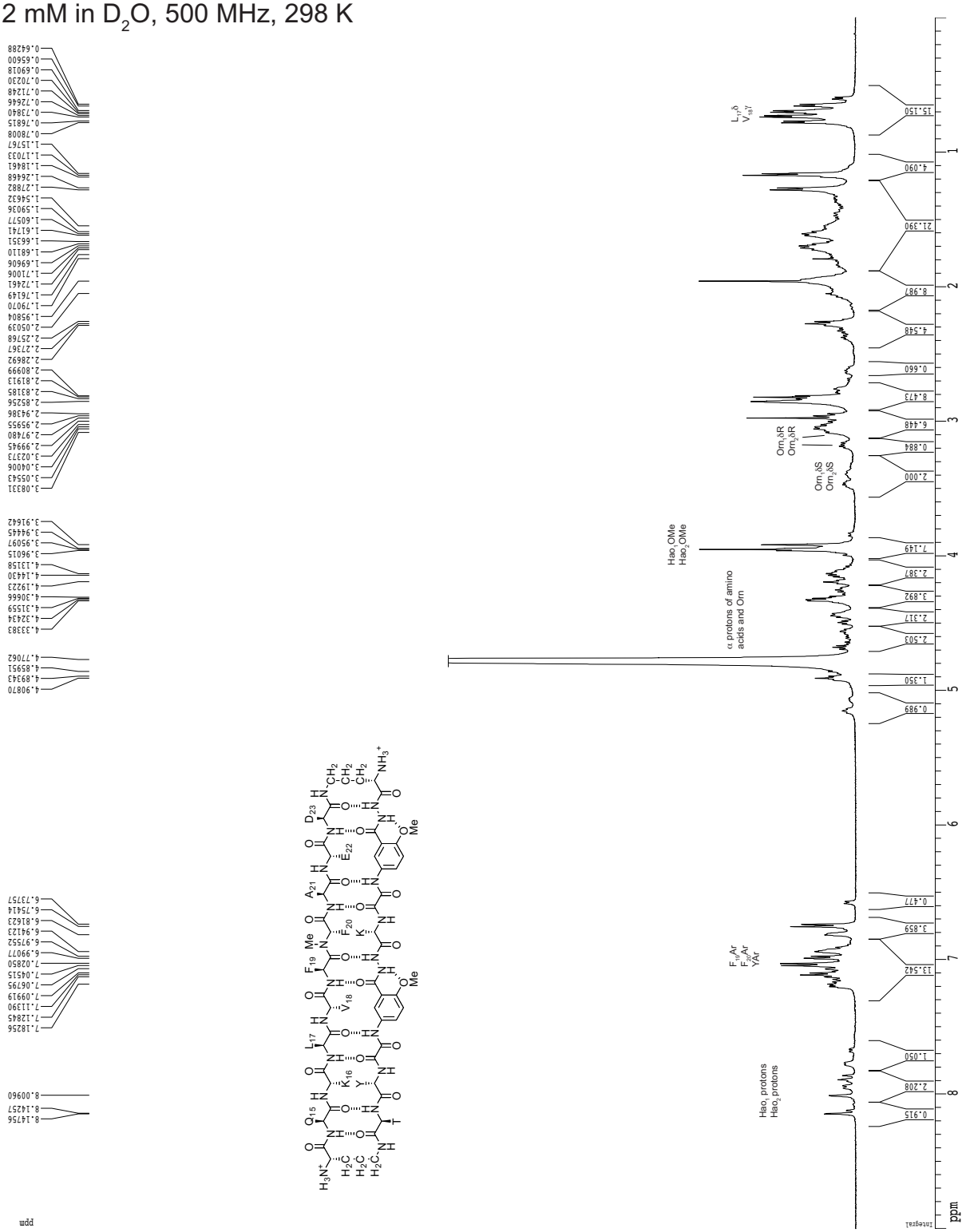

2D TOCSY spectrum of macrocyclic β-sheet peptide **3.4** as monomer
2 mM in D_2O, 500 MHz, 298 K
150 ms spin-locking time

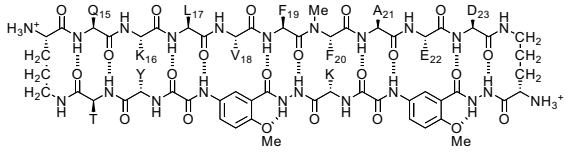

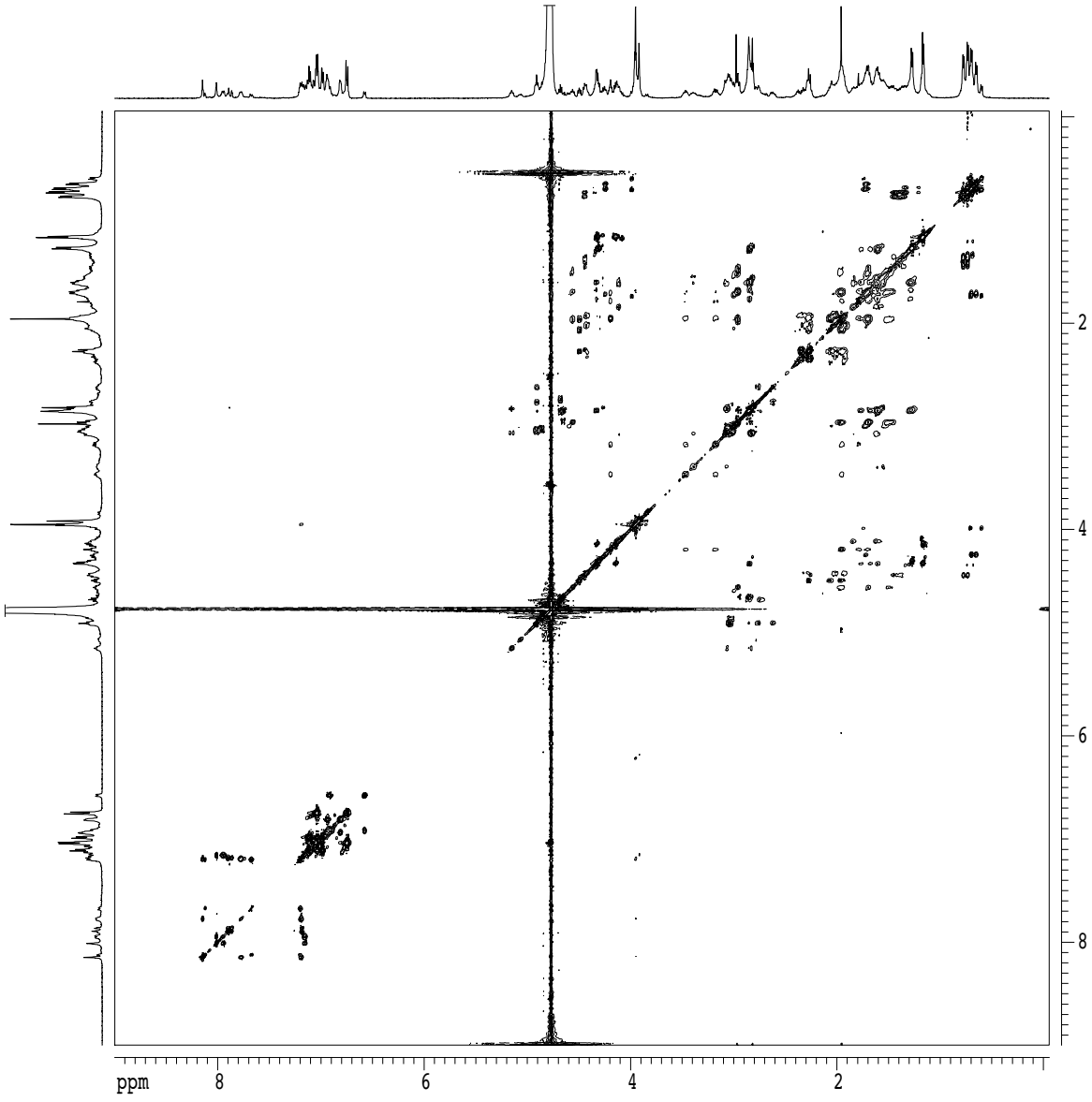

2D ROESY spectrum of macrocyclic β-sheet peptide **3.4**
2 mM in D_2O, 500 MHz, 298 K
200 ms spin-locking time

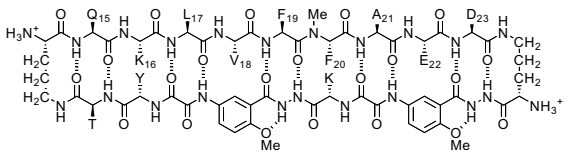

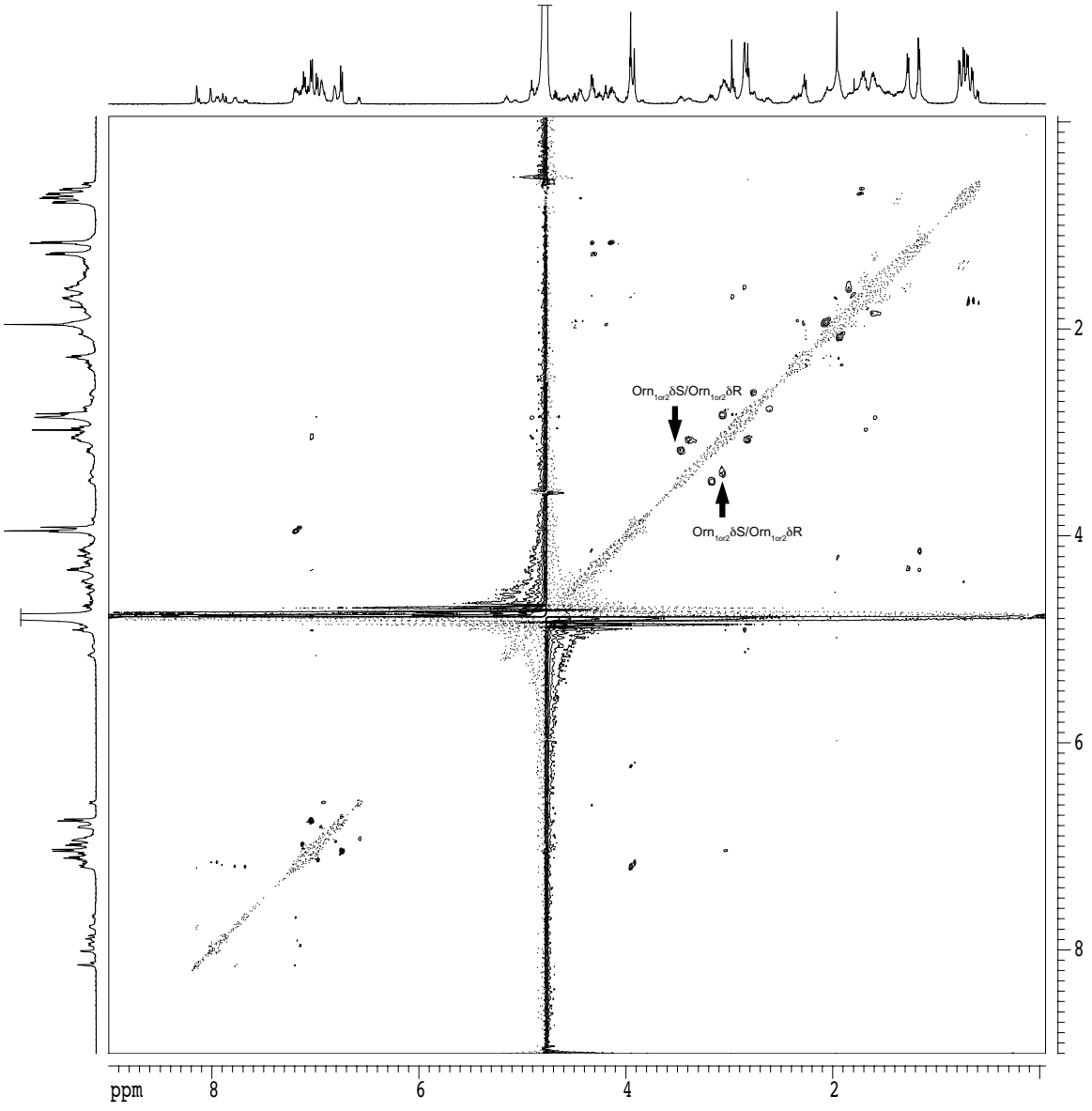

2D DOSY spectrum of macrocyclic β-sheet **3.4**
2 mM in D_2O, 600 MHz, 298 K
monomer predominates

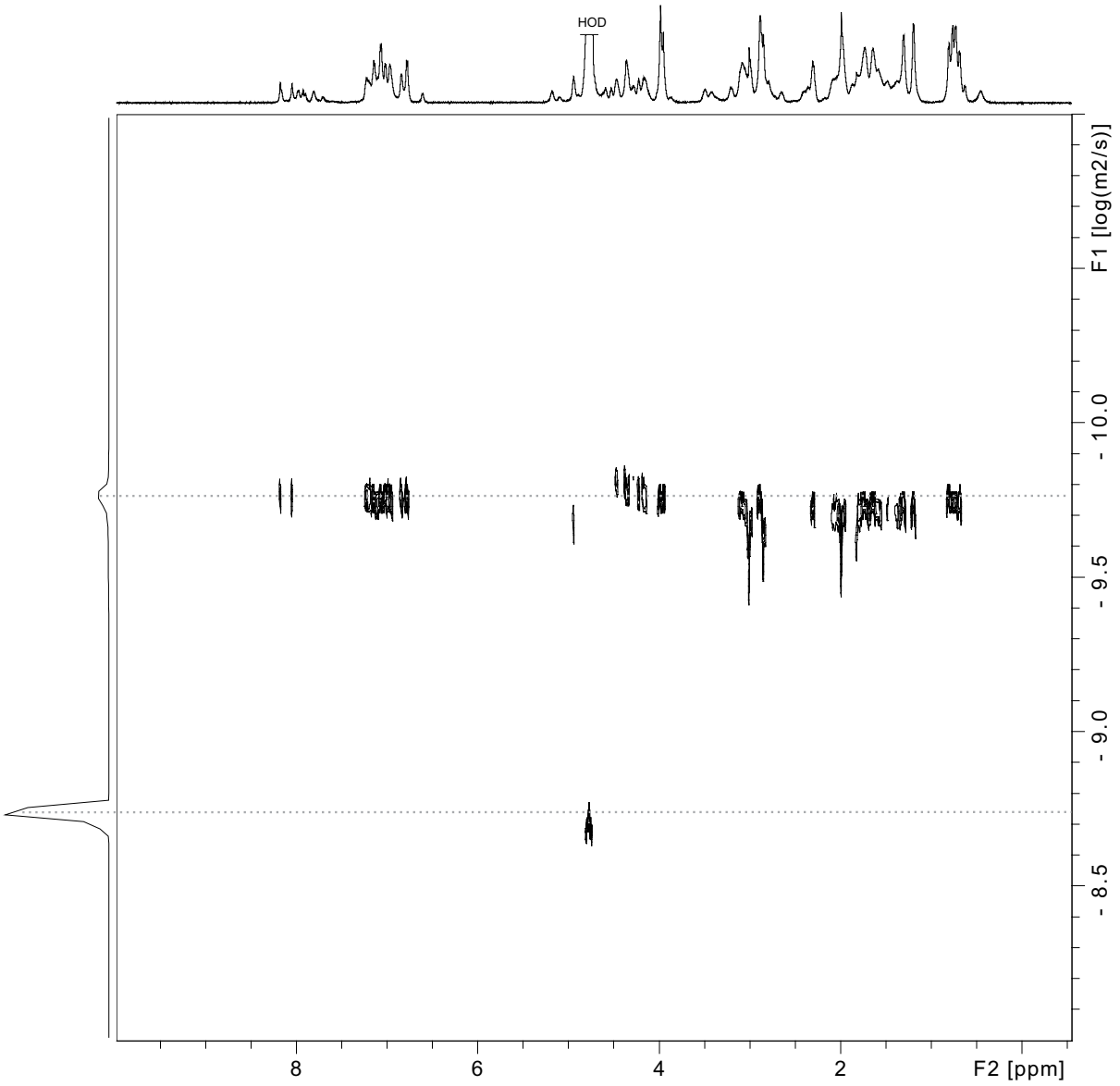

Calculation for 3.4 at 2.0 mM

DC_{HOD} = 19.0 x 10^{-10} m^2/s [a]
log DC_{HOD} = -8.721

For 3.4 tetramer, log DC (m^2/s) = -9.75(4), DC = $10^{-9.754}$ m^2/s = 17.6 x 10^{-11} m^2/s = 17.6 x 10^{-7} cm^2/s

[a] Longsworth, L. G. J. Phys. Chem. 1960, 64, 1914–1917.

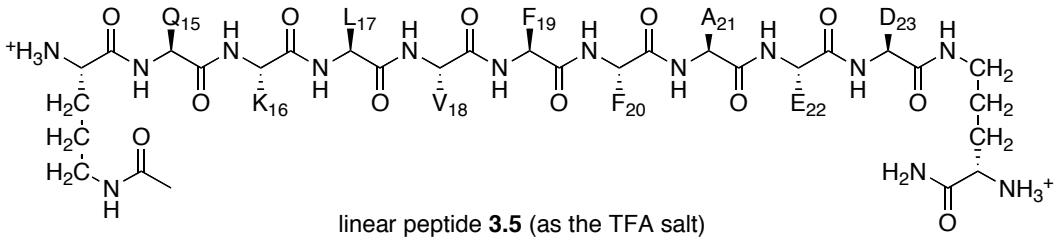

linear peptide **3.5** (as the TFA salt)

molecular weight calculated for $C_{64}H_{100}N_{16}O_{17} \cdot 3CF_3CO_2H$ (TFA salt of **3.5**): 1707.65
molecular weight calculated for $C_{64}H_{100}N_{16}O_{17}$ (free base of **3.5**): 1365.58
exact mass calculated for $C_{64}H_{100}N_{16}O_{17}$ (free base of **3.5**): 1364.75

Analytical RP-HPLC of linear peptide **3.5**

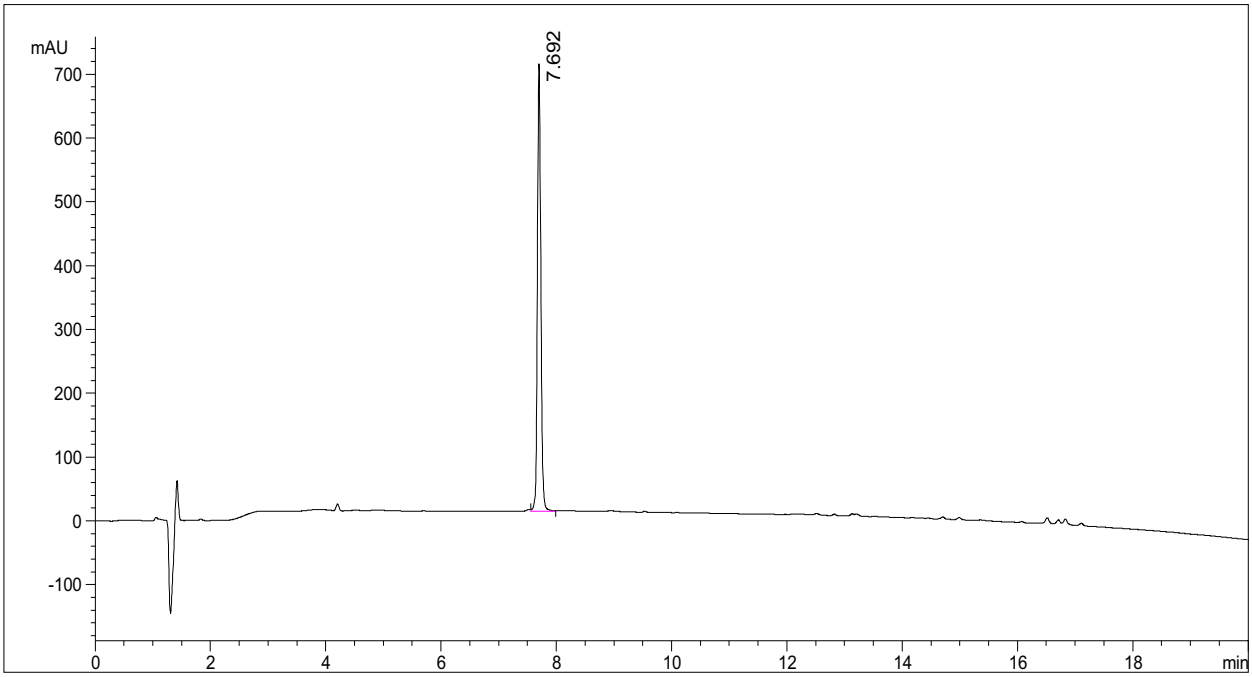

Signal 1: VWD1 A, Wavelength=214 nm

Peak #	RetTime [min]	Type	Width [min]	Area mAU *s	Height [mAU]	Area %
1	7.692	VV	0.0657	2891.74707	698.99927	100.0000
Totals :				2891.74707	698.99927	

Linear peptide **3.5**

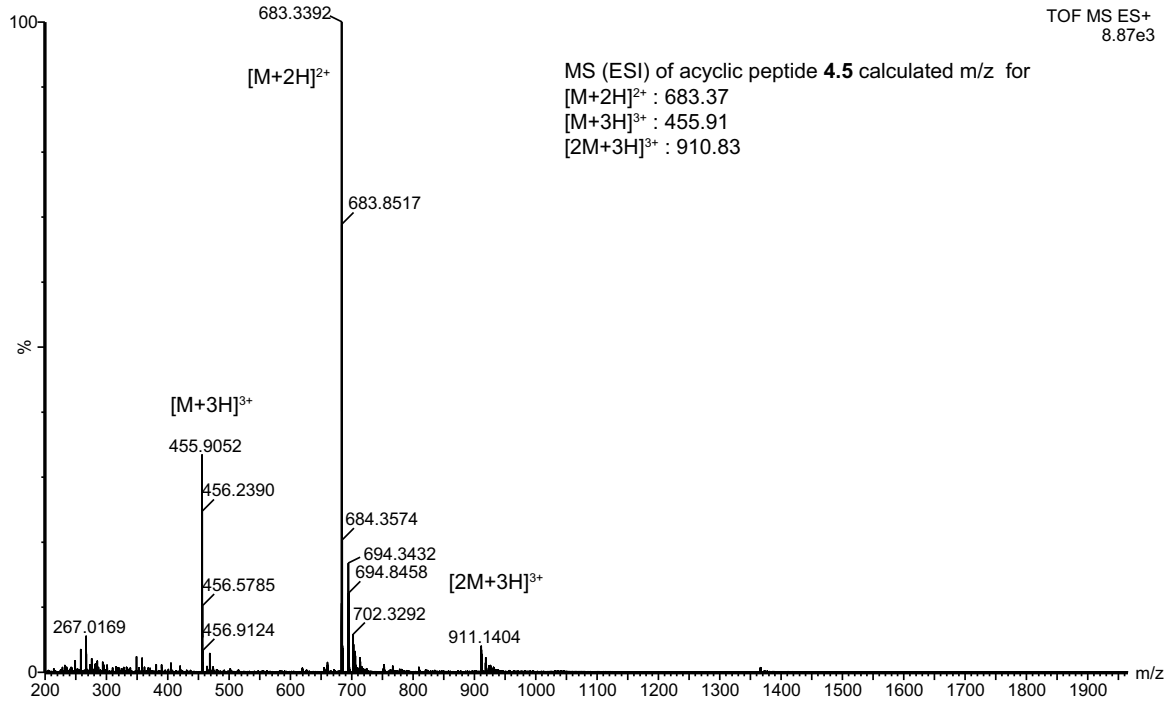

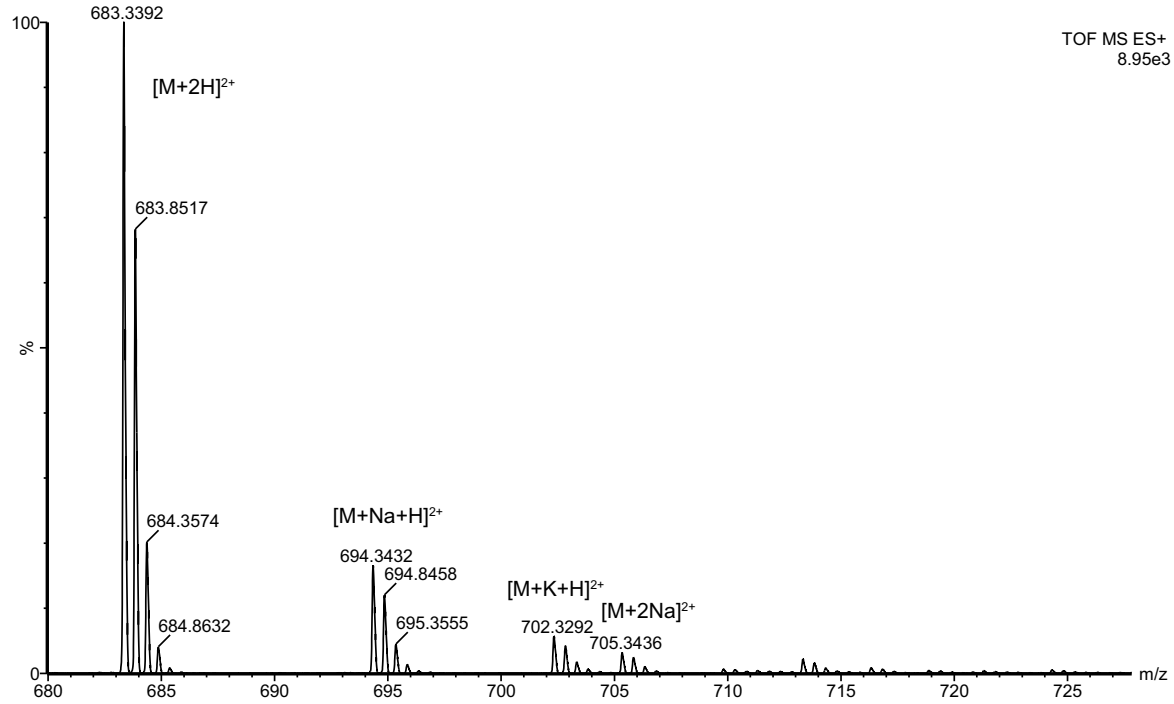

Linear peptide **3.5**

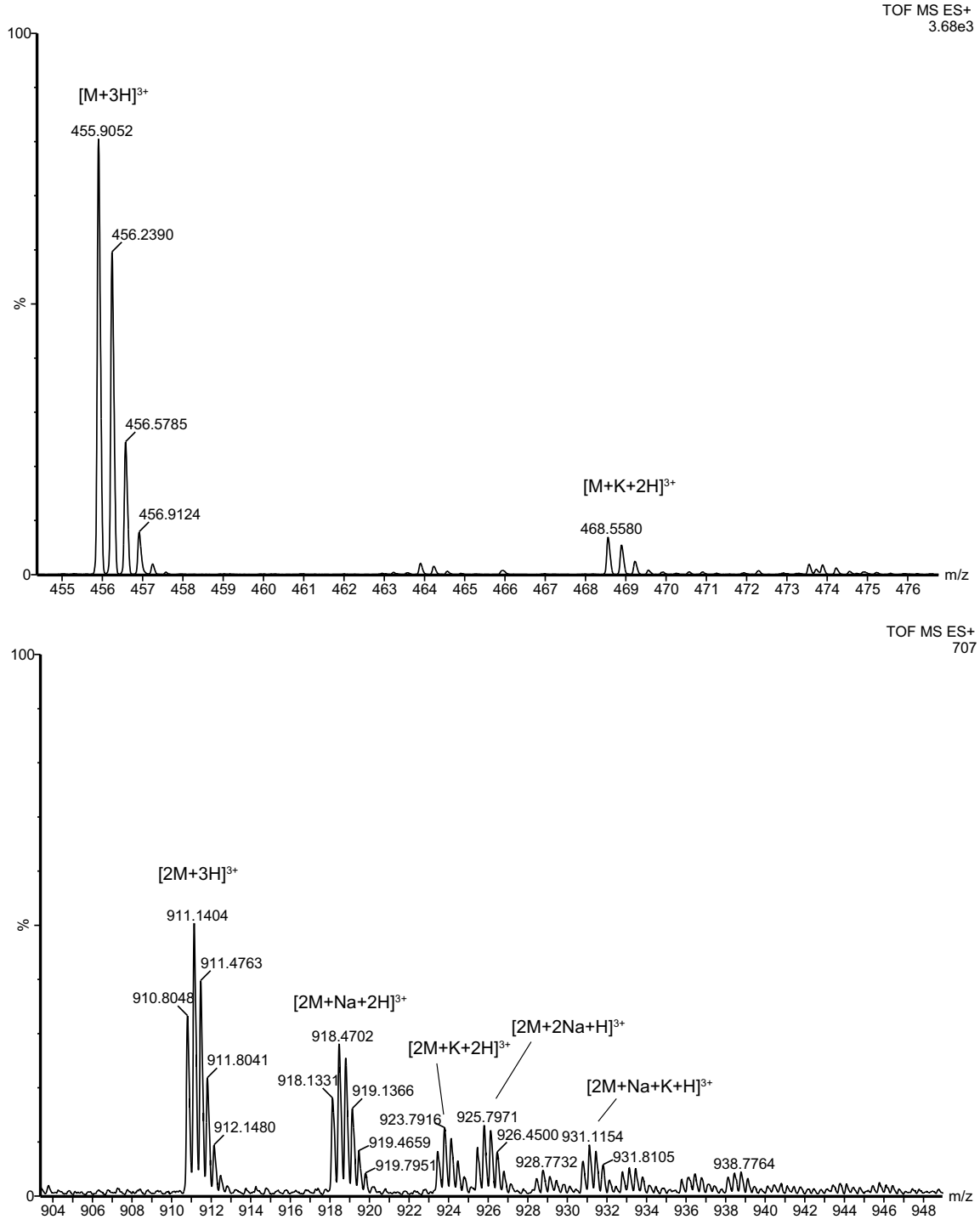

1D ^{1}H NMR spectrum of linear peptide **3.5** as control
1.2 mM in D_2O, 500 MHz, 298 K

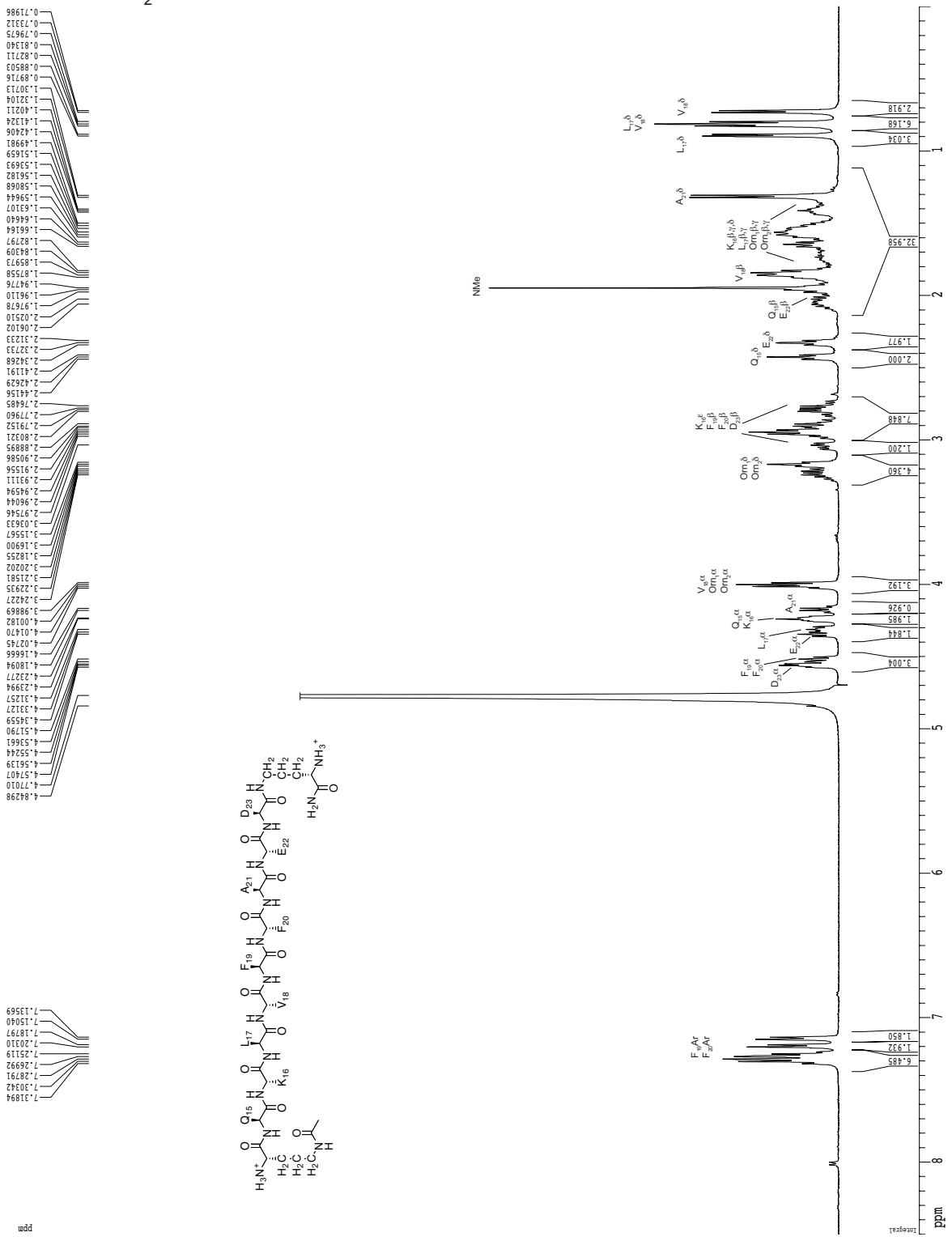

2D TOCSY NMR spectrum of linear peptide **3.5** as control
4.95 mM in D_2O, 500 MHz, 298 K
150 ms spin-locking time

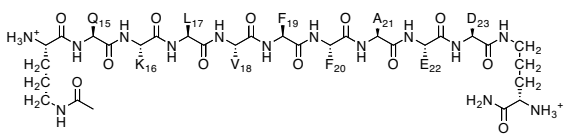

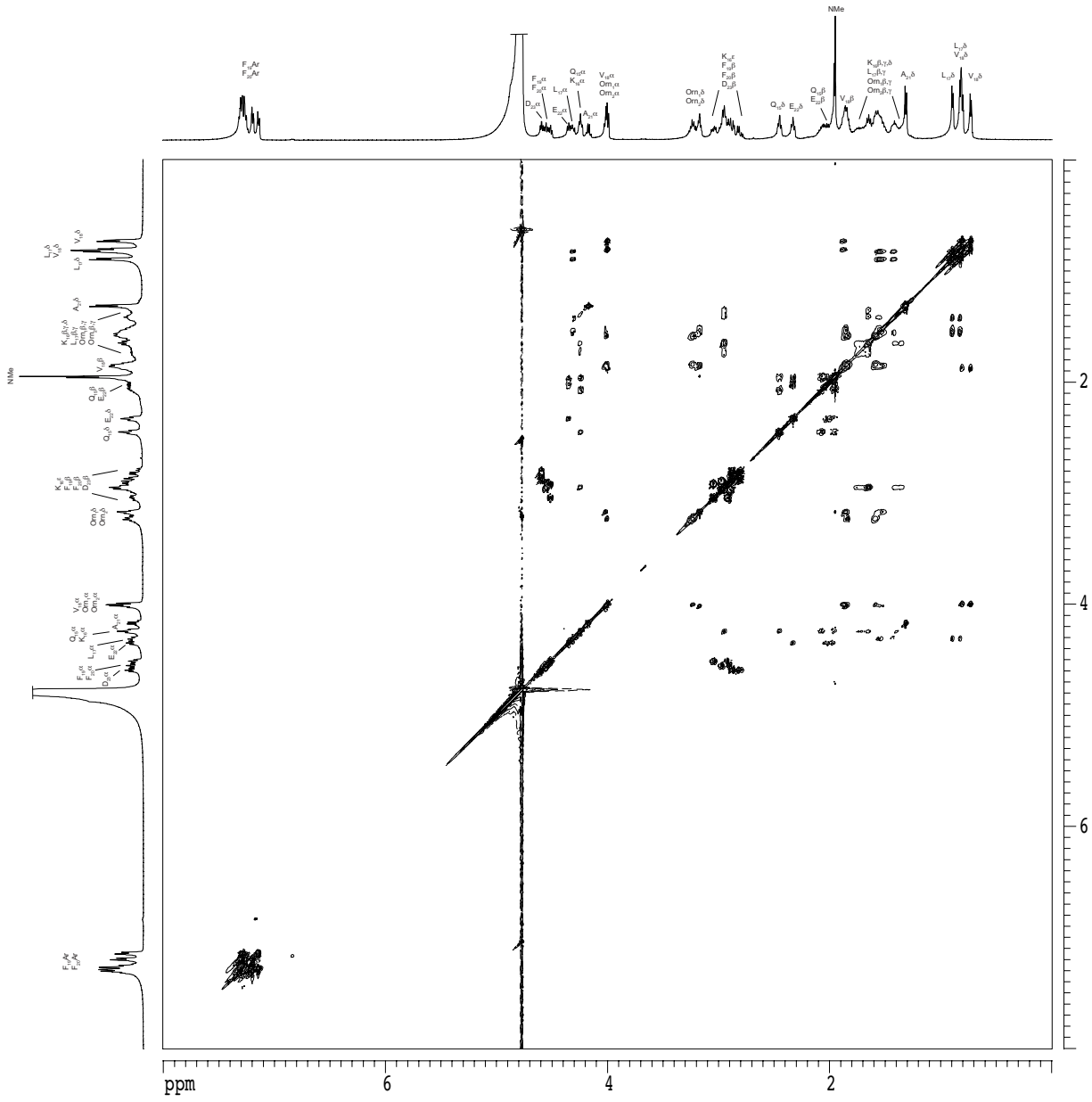

2D TOCSY NMR spectrum of linear peptide **3.5** as control
4.95 mM in D_2O, 500 MHz, 298 K
150 ms spin-locking time

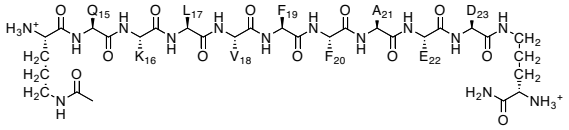

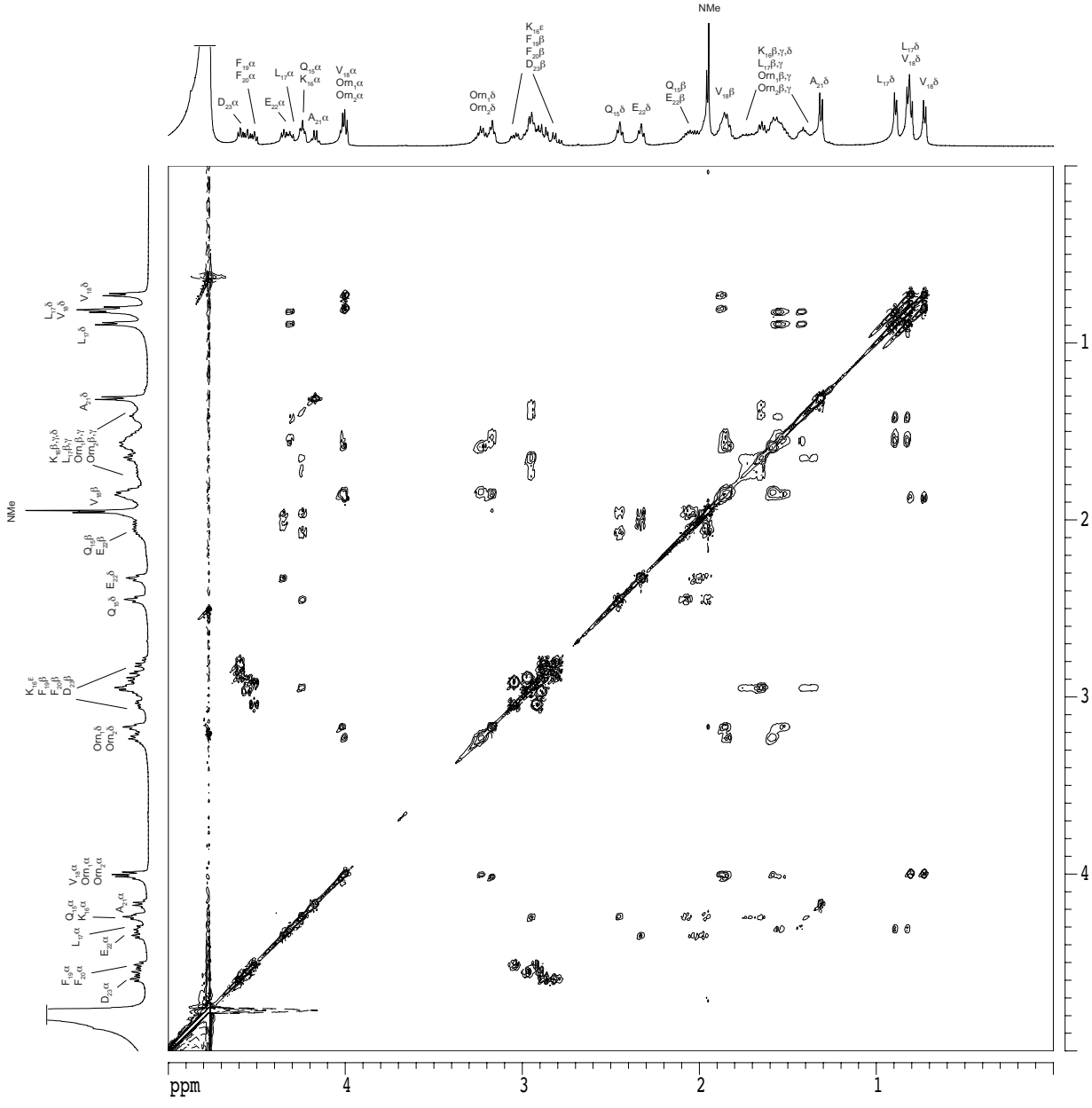

2D ROESY NMR spectrum of linear peptide **3.5** as control
4.95 mM in D_2O, 500 MHz, 298 K
200 ms spin-locking time

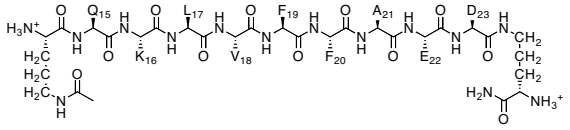

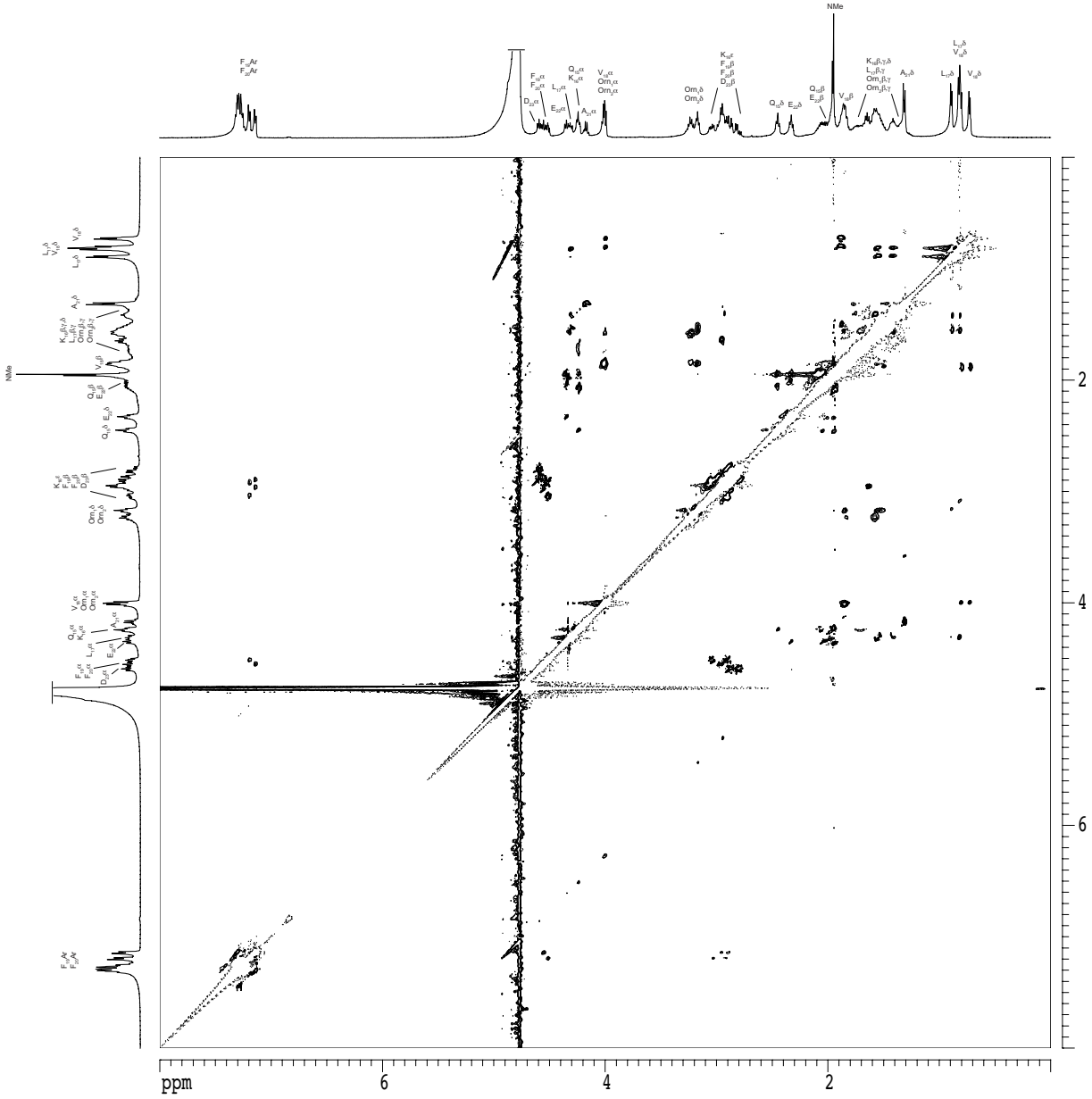

2D ROESY NMR spectrum of linear peptide **3.5** as control
4.95 mM in D_2O, 500 MHz, 298 K
200 ms spin-locking time

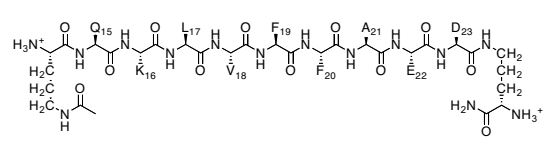

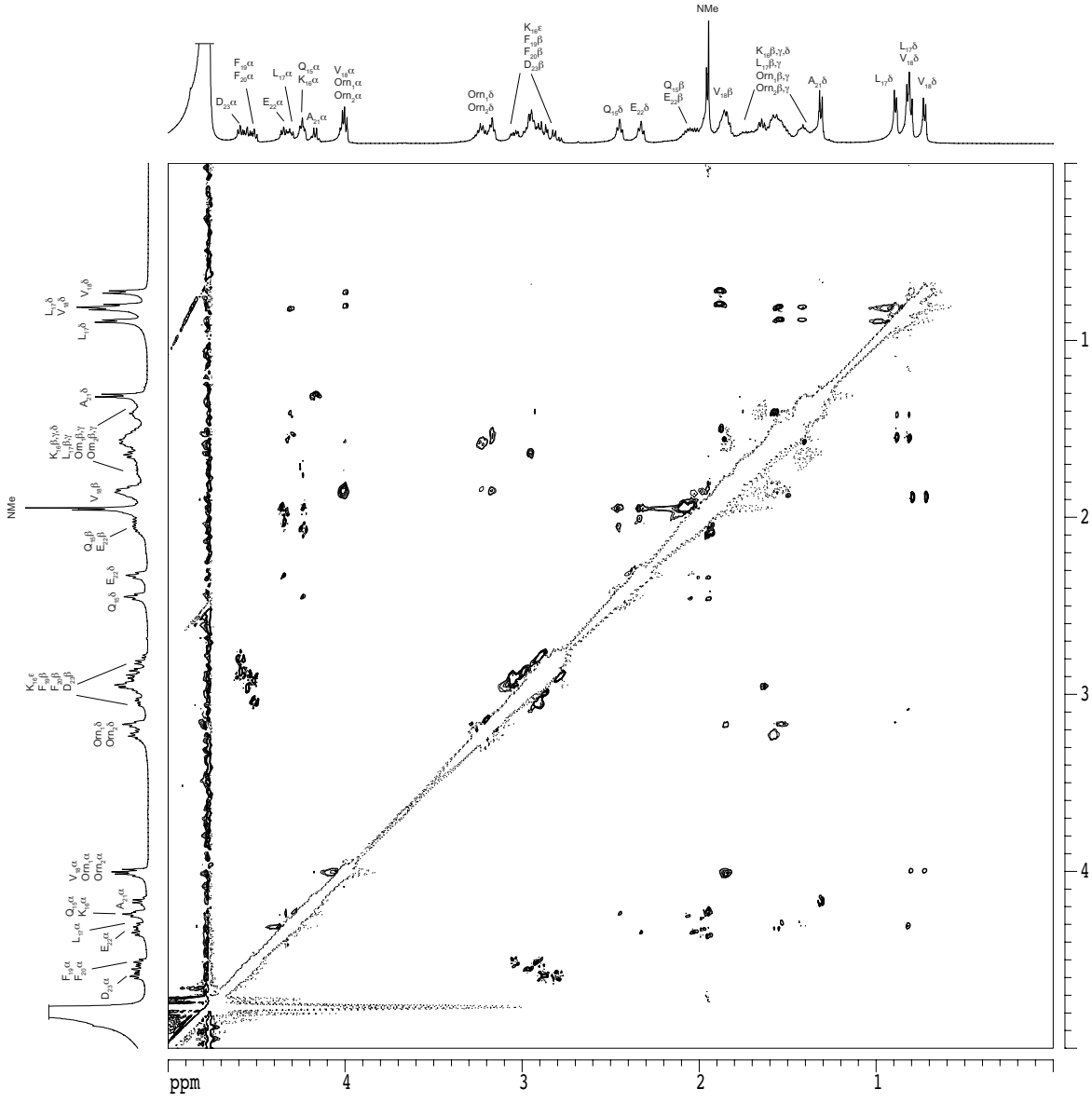

CHAPTER 4

A Fibril-Like Oligomer Assembly of a Peptide Derived from β-Amyloid

Preamble

Chapter 4 concludes the series of projects for the nonapeptide sequence QKLVFFAED ($A\beta_{15–23}$). My initial goal of this project was to incorporate two full strands of $A\beta_{15–23}$ into a macrocycle without a template strand to observe structures that may form. The peptide was difficult to synthesize, so I constructed macrocyclic β-sheet peptide **4.3** instead. Macrocyclic β-sheet peptide **4.3** incorporates a single Hao amino acid to substitute for the hydrophobic residues $F_{19}F_{20}A_{21}$ to allow for convenient synthesis, and to investigate the possible structures that form in aqueous solution by ^{1}H NMR spectroscopy and in the solid state by X-ray crystallography.

Macrocyclic β-sheet peptide **4.3** forms fibril-like assemblies of oligomers in the solid state. The X-ray crystallographic structure of macrocyclic β-sheet **4.3** was determined at 1.75 Å resolution. The macrocycle forms hydrogen-bonded dimers, which further assemble along the fibril axis in a fashion resembling a herringbone pattern. The extended β-sheet comprising the dimers is laminated against a second layer of dimers through hydrophobic interactions to form a fibril-like assembly that runs the length of the crystal lattice. This chapter reports fibril-like assemblies of oligomers formed by macrocyclic β-sheet **4.3**, and provide insights into the structures of oligomers and oligomer assemblies formed by full-length Aβ and may suggest a mechanism by which these oligomers may replicate.

This chapter is adapted from the paper that I submitted for publication to the *Journal of the American Chemical Society*.[1]

Reproduced in part with permission from *J. Am. Chem. Soc.*, submitted for publication.

Unpublished work copyright 2014 American Chemical Society.

Introduction

The supramolecular assembly of the β-amyloid peptide Aβ to form fibrils and soluble oligomers has been the subject of intense interest and study over the past two decades. The plaques formed by the 40–42 amino acid Aβ polypeptide in the brain are one of the most distinctive physiological features of Alzheimer's disease, while the more cryptic soluble Aβ oligomers that also form are now thought to be the primary culprits in the devastating neurodegeneration that occurs.[2] In β-amyloid fibrils, the central region of Aβ forms an extended network of β-sheets.[3] The oligomers also appear to involve β-sheet formation, but their structures are still largely unknown at atomic resolution.[4,5] Enhanced understanding the structures and interactions of the oligomers and fibrils offers the promise of preventing and treating Alzheimer's and other amyloid diseases.

The highly amyloidgenic central region of Aβ, which includes the hydrophobic pentapeptide sequence LVFFA ($A\beta_{17–21}$) has provided an archetype not only for the assembly of Aβ but also for amyloidogenic peptides and proteins in general.[6] Peptides derived from $A\beta_{17–21}$ have been found to inhibit the aggregation of full length Aβ.[7] The hydrophobic residues 17–21 are flanked by cationic and anionic residues K_{16} and E_{22}, making the heptapeptide sequence KLVFFAE ($A\beta_{16–22}$) especially prone to supramolecular assembly to form fibrils and nanotubes. [8]

We recently began using macrocyclic β-sheet peptides containing nonapeptide sequence QKLVFFAED ($A\beta_{15–23}$) as a model system with which to explore the structures and interactions of amyloid oligomers. We incorporated the $A\beta_{15–23}$ nonapeptide into a 66-membered ring macrocycle containing template and turn units that help enforce a β-sheet structure and block uncontrolled aggregation, and we studied the supramolecular

assembly of the resulting macrocyclic β-sheet peptides **4.1** (previously described as **2.1** in Chapter 2 and **3.1** in Chapter 3) in the solid state by X-ray crystallography and in aqueous solution by NMR spectroscopy.[9,10] Macrocyclic β-sheet peptides **4.1** contain an $A\beta_{15–23}$ peptide strand connected through two δ-linked ornithine turn units ($^{\delta}$Orn) to a template strand that contains two Hao amino acid tripeptide mimics.[11,12] In the solid state, macrocyclic β-sheet peptide **4.1a** forms tetramers, dodecamers, and porelike assemblies of oligomers. In solution, macrocyclic β-sheets **4.1** form tetramers that differ in structure from those in the solid state. The differences between the solid-state and solution state tetramers are important, because they reveal polymorphism among amyloid oligomers at atomic resolution and illustrate the importance of environment upon oligomer structure.

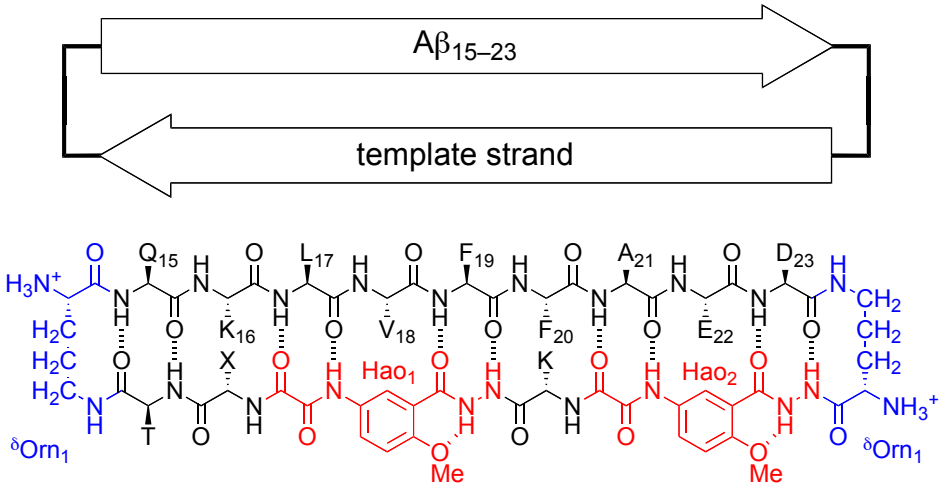

macrocyclic β-sheet peptide **4.1**
4.1a X = *p*-bromoPhe, **4.1b** X = Tyr

In the current study, we envisioned replacing the template strand with $A\beta_{15–23}$ and determine the structures of the oligomers that form. Attempts to synthesize and study

macrocyclic β-sheet peptide **4.2**, which embodies this concept, proved fruitless, yielding only an insoluble peptide hydrogel. By incorporating two full strands of $A\beta_{15–23}$ into a macrocycle without a template designed to block aggregation appeared to give a peptide that was highly amyloidogenic. To reduce the amyloidogenicity of the macrocycle, we prepared macrocyclic β-sheet **4.3**, which incorporates a single *Hao* amino acid in place of the $F_{19'}F_{20'}A_{21'}$ tripeptide segment of $A\beta_{15–23}$ in an *$A\beta_{15–23}$ hybrid strand*. To facilitate phase determination through single anomalous dispersion (SAD) phasing, we incorporated *p*-iodophenylalanine (F^I) in place of F_{20} in $A\beta_{15–23}$ the peptide strand.

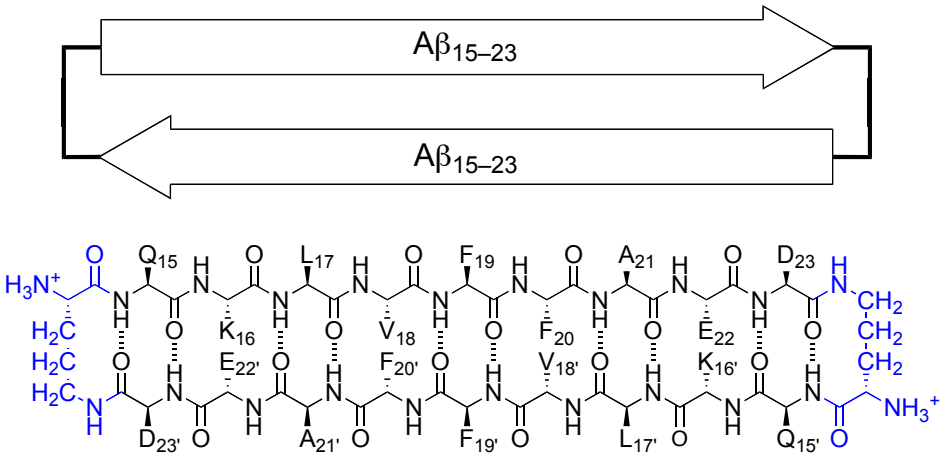

macrocyclic β-sheet peptide **4.2**

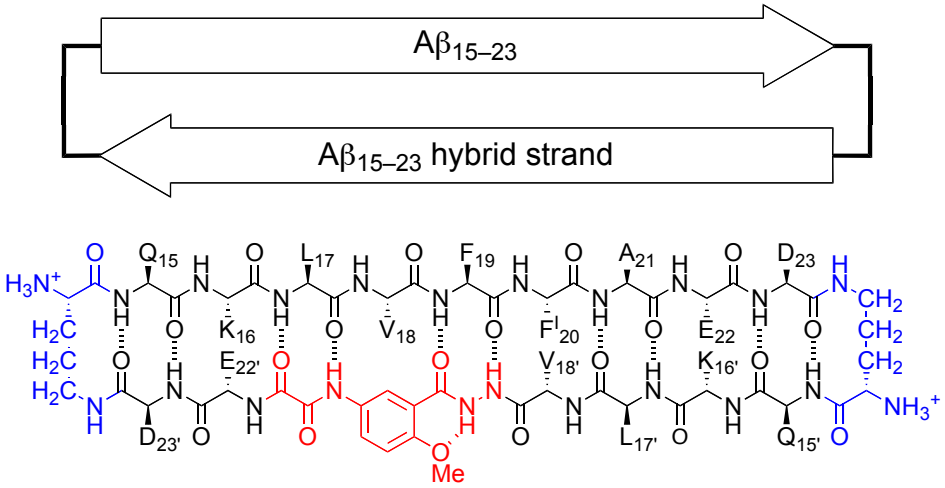

macrocyclic β-sheet peptide **4.3**

Here, we report the X-ray crystallographic structure of macrocyclic β-sheet **4.3**. We compare the solid-state supramolecular assembly to those of the oligomer observed in solution. We describe a new mode of assembly of $A\beta_{15–23}$ in the solid state — a fibril-like assembly of oligomers — that resembles both fibrils and oligomers.

Results

*X-ray Crystallographic Structure of Macrocyclic β-Sheet **4.3***. In the solid state, macrocyclic β-sheet **4.3** forms hydrogen-bonded dimers arranged in a herringbone fashion in offset layers that pack through hydrophobic interactions. The resulting supramolecular assembly differs substantially both from that which we have observed previously for macrocyclic β-sheet **4.1**[9,10] and that which others have previously observed for Aβ.

Macrocyclic β-sheet **4.3** readily formed crystals under sparse-matrix screening conditions with kits from Hampton Research. Crystals suitable for X-ray crystallography were grown from a 3.5 mg/mL solution with 0.1 M sodium citrate at pH 7.3, 0.1 M ammonium acetate, and 30% 2-methyl-2,4-pentanediol. Crystal diffraction data were collected on beamline 7-1 at the Stanford Synchotron Radiation Lightsource (SSRL) at 1.00 Å wavelength to 1.75 Å resolution. Data were integrated and scaled with XDS,[13] and merged with Aimless.[14] Iodine locations were determined with HySS in the PHENIX software suite.[15] Initial density maps and phasing were generated with Autosol. Alternating rounds of manual rebuilding with the program Coot,[16] and refinement with phenix.refine were performed. The structure was solved in the *C*2 space group with 49% pseudomerohedral twinning,[17] to give a model with R_{free} = 22.0% and R_{work} = 17.9% (Table 1). The asymmetric unit contains two molecules of macrocyclic β-sheet **4.3** and two molecules of 2-methyl-2,4-pentanediol.

Table 4.1. X-ray Crystallographic Data Collection and Refinement Statistics for Macrocyclic β-Sheet Peptide 4.3.

Crystal parameters	
Space group	*C*2
a, *b*, *c* (Å)	32.174, 62.582, 20.094
α, β, γ (°)	90.00, 89.98, 90.00
Molecules per asymmetric unit	2
Data collection	
Synchrotron beam line	SSRL beam line 7-1
Wavelength (Å)	1.00
Resolution (Å)	17.56–1.75 (1.81–1.75)
Total reflections[a]	14845 (1450)
Unique reflections[a]	4060 (398)
Completeness (%)[a]	99.2 (97.1)
Multiplicity[a]	3.7 (3.6)
R_{merge} (%)[a,b]	3.6 (6.3)
$CC_{1/2}$ (%)[a]	99.8 (99.6)
CC* (%)[a]	100 (99.9)
$I/\sigma(I)$[a]	25.4 (13.4)
Refinement	
Resolution (Å)	1.75
R_{work} (%)[c]	17.9
R_{free} (%)[d]	22.0
RMS bond lengths (Å)	0.010
RMS bond angles (°)	1.52
Ligands	2-methyl-2,4-pentanediol (2)
Water	43
Ramachandran favored (%)	100
Ramachandran outliers (%)	0
Wilson *B*-factor (Å^2)	18.5
Average *B*-factor (Å^2)	22.6
Twinning	*-h*, *-k*, *l* (α = 0.49)

[a]Statistics for the highest resolution shell are shown in parentheses
[b]$R_{merge} = \sum|I - \langle I \rangle|/\sum I$
[c]$R_{work} = \sum|F_{obs} - F_{calc}|/\sum F_{obs}$
[d]R_{free} was computed as R_{work} using a cross-validation set of 10% non-redundant data.

Macrocyclic β-sheet peptide **4.3** crystallizes as a folded monomer in which the $A\beta_{15–23}$ peptide strand and the $A\beta_{15–23}$ hybrid strand form a hydrogen-bonded β-sheet. Two conformers of the macrocycle occur in the asymmetric unit, differing in rotamer of

F_{19} and tilt of the Hao amino acid. The conformers alternate in the crystal lattice, geared together through crystal packing. Figure 1 illustrates the structure the two conformers of the macrocycle.

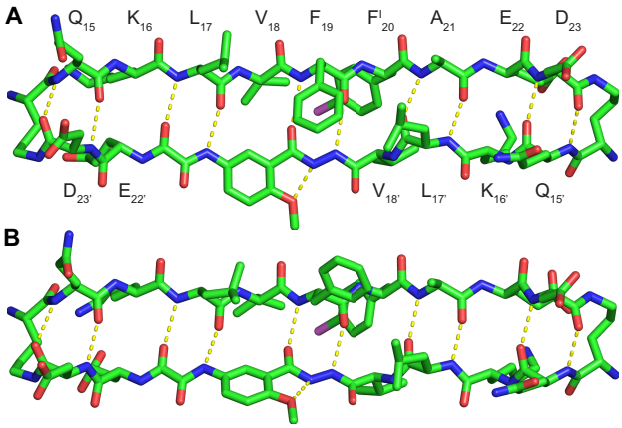

Figure 4.1. X-ray crystallographic structure of macrocyclic β-sheet peptide **4.3**. Two conformers (A and B) make up the asymmetric unit.

Macrocyclic β-sheet peptide **4.3** forms a hydrogen-bonded dimer in which two monomers hydrogen bond to form a four-stranded antiparallel β-sheet. The $A\beta_{15–23}$ peptide strands of the macrocycles make up the dimerization interface and are fully aligned, with residues 17−23 of one of the macrocycles paired with residues 23−17 of the other through eight hydrogen bonds. The side chains of residues Q_{15}, L_{17}, F_{19}, A_{21}, and D_{23} of the $A\beta_{15–23}$ peptide strands and $Q_{15'}$, $L_{17'}$, and $D_{23'}$ of the $A\beta_{15–23}$ hybrid strands decorate one of the surfaces of the four-stranded antiparallel β-sheet; the side chains of residues K_{16}, V_{18}, F^{I}_{20}, and E_{22} of the $A\beta_{15–23}$ peptide strands and $K_{16'}$, $V_{18'}$, and $E_{22'}$ of the $A\beta_{15–23}$ hybrid strands decorate the other surface. Figure 4.2 illustrates the structure of the hydrogen-bonded dimer and the two surfaces. We term the two surfaces the *LFA face* and the *VF face* for the discussion of the higher-order supramolecular assembly of the dimers

that follows.

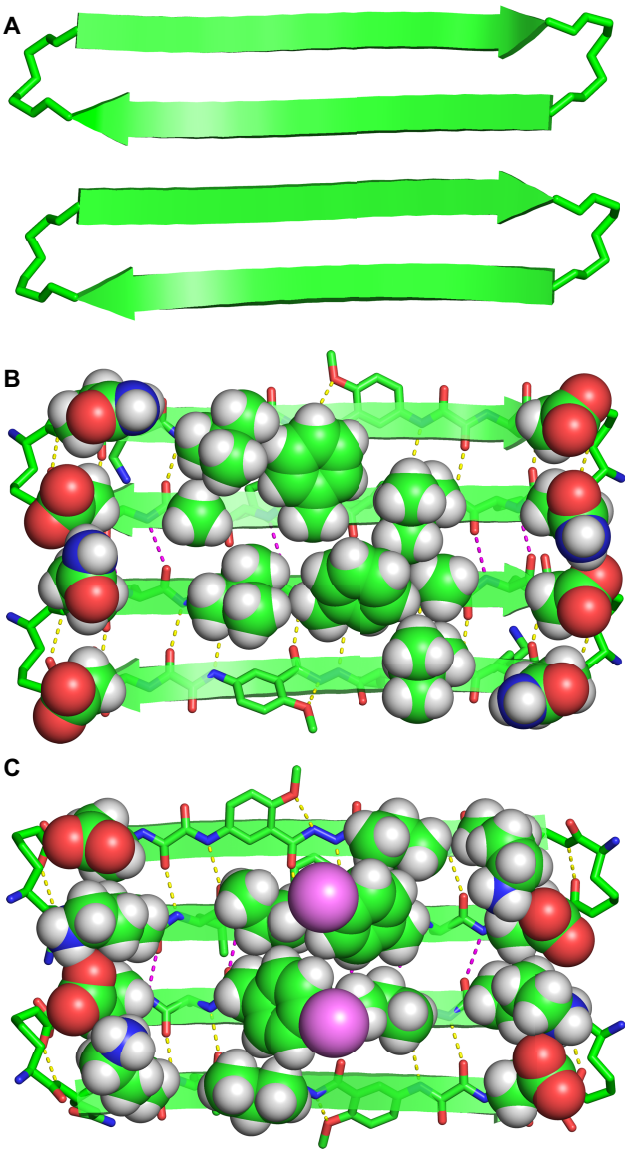

Figure 4.2. X-ray crystallographic structure of hydrogen-bonded dimer of macrocyclic β-sheet peptide **4.3**. (A) Cartoon illustration of the hydrogen-bonded dimer. (B) The *LFA face* of the hydrogen-bonded dimer, bearing the side chains of residues Q_{15}, L_{17}, F_{19}, A_{21}, and D_{23} of the $A\beta_{15-23}$ peptide strands and $Q_{15'}$, $L_{17'}$, and $D_{23'}$ of the $A\beta_{15-23}$ hybrid strands. (C) The *VF face* of the hydrogen-bonded dimer, bearing the side chains of residues K_{16}, V_{18}, F^{I}_{20}, and E_{22} of the $A\beta_{15-23}$ peptide strands and $K_{16'}$, $V_{18'}$, and $E_{22'}$ of the $A\beta_{15-23}$ hybrid strands.

The hydrogen-bonded dimers assemble to form an extended β-sheet that runs the

length of the crystal lattice. The $A\beta_{15-23}$ hybrid strands form the interface between the dimers. At these interfaces, the $A\beta_{15-23}$ hybrid strands are not fully aligned, but rather are shifted out of alignment by two residues toward the C-termini. As a result of the shift in alignment, the β-strands comprising the β-sheets are not orthogonal to the axis formed by the extended β-sheet, but rather are rotated about 20° from orthogonality. The resulting assembly of the dimers resembles a herringbone pattern. Figure 4.3A illustrates the assembly of the hydrogen-bonded dimers.

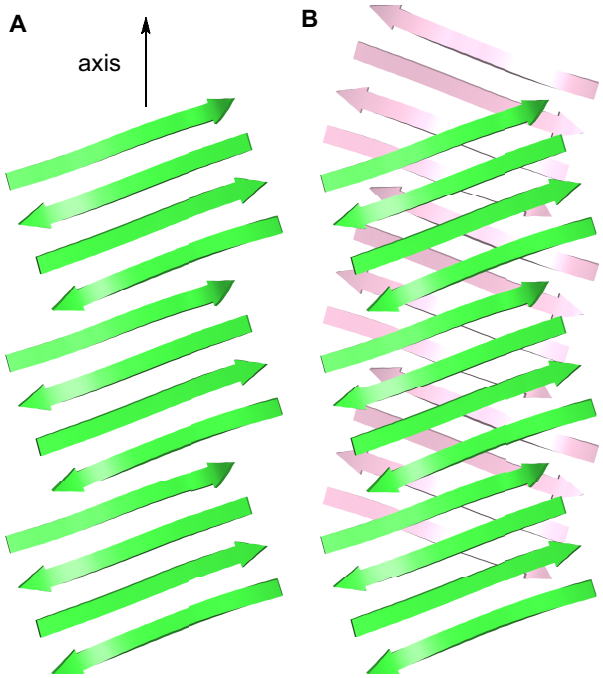

Figure 4.3. Assembly of hydrogen-bonded dimers in the X-ray crystallographic structure of macrocyclic β-sheet peptide **4.3**. (A) Extended β-sheet that runs the length of the crystal lattice. (B) Packing of the extended β-sheets to form a two-layered structure.

The extended β-sheets formed by the hydrogen-bonded dimers pack through the VF faces to form a two-layered structure. The dimers comprising each layer do not overlap directly. Instead, each dimer in one layer sits over the interface between to dimers

in the opposite layer. Figure 4.3B illustrates the packing of the two layers.

The Hao amino acids come together at the interface between the hydrogen-bonded dimers, tilting alternately upward and downward and stacking to accommodate hydrogen-bonding interactions between the $A\beta_{15–23}$ hybrid strands. Figure 4.4A illustrates the interaction between the Hao amino acids at the interface. The side chains of the V_{18}, F^{I}_{20}, and $V_{18'}$ residues create a hydrophobic core that runs along the axis formed by the extended β-sheet. Figure 4.4B illustrates the structure of the hydrophobic core. The stacked Hao amino acids and the iodine of F^{I}_{20} help fill the void created by the absence of $F_{20'}$ in the $A\beta_{15–23}$ hybrid strand. The 2-methyl-2,4-pentanediol solvent that crystallizes with macrocyclic β-sheet **4.3** packs alongside the hydrophobic core and further stabilizes the two-layered structure through additional hydrophobic interactions.

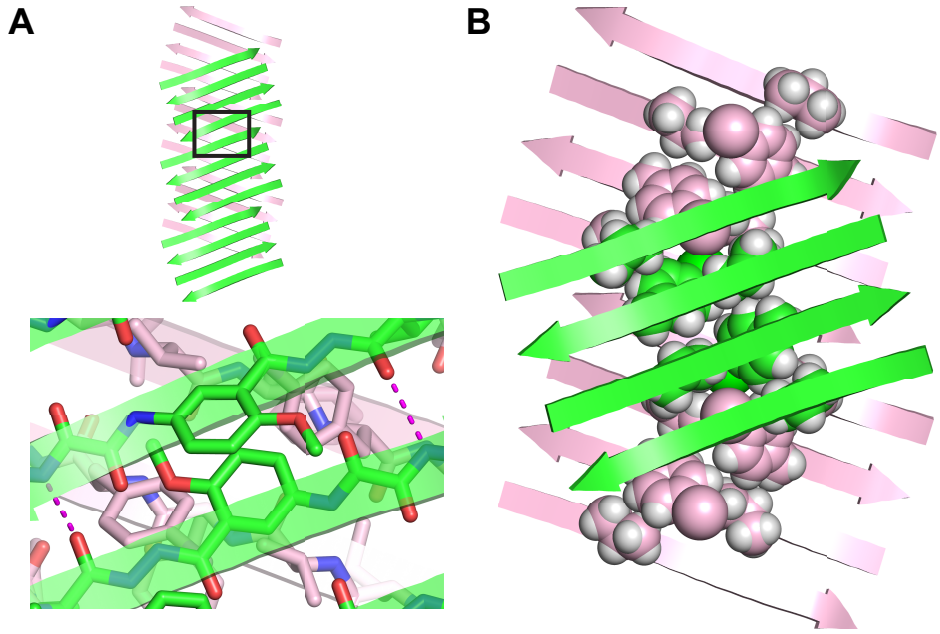

Figure 4.4. (A) Interaction between the Hao amino acids at the interface between dimers in the X-ray crystallographic structure of macrocyclic β-sheet peptide **4.3**. (B) Hydrophobic core formed by the side chains of the V_{18}, F^{I}_{20}, and $V_{18'}$ residues, between the layers of the extended β-sheets in the X-ray crystallographic structure of macrocyclic β-sheet peptide **4.3**.

*Solution-State Studies of Macrocyclic β-Sheets **4.3–4.6.*** In aqueous solution, macrocyclic β-sheet **4.3** forms discrete tetramers comprising a sandwich formed by two hydrogen-bonded dimers. The solution-state tetramers are similar in structure to that which we have previously observed for macrocyclic β-sheets **4.1**.[10] The dimer subunits form through hydrogen bonding between the $A\beta_{15–23}$ peptide strands, in which these β-strands are shifted out of alignment by two residues toward the C-termini. The dimer subunits assemble to form the tetramer through hydrophobic interactions between the LFA faces.

We studied the folding and supramolecular assembly of macrocyclic β-sheet **4.3** and homologues **4.4**, **4.5**, and **4.6** by ^{1}H NMR NOESY and DOSY experiments on the

trifluoroacetate (TFA) salts in D_2O solution. Macrocyclic β-sheet **4.4** is a homologue of macrocyclic β-sheet **4.3** with phenylalanine in place of *p*-iodophenylalanine in the $A\beta_{15\text{-}23}$ peptide strand (F_{20} in place of F^{I}_{20}). Macrocyclic β-sheet **4.5** is a double mutant in which the hydrophobic residues V_{18} and F_{20} in the $A\beta_{15–23}$ peptide strand are rendered more hydrophilic by hydroxylation: V_{18} is replaced by threonine and F_{20} is replaced by tyrosine ($V_{18}T,F_{20}Y$). Macrocyclic β-sheet **4.6** is a double mutant in which the hydrophobic residues F_{19} and A_{21} in the $A\beta_{15–23}$ peptide strand are rendered more hydrophilic by hydroxylation: F_{19} is replaced by tyrosine and A_{21} is replaced by serine ($F_{19}Y,A_{21}S$).

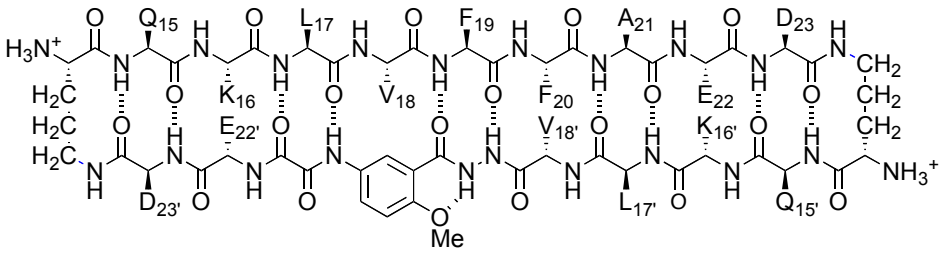

macrocyclic β-sheet peptide **4.4**

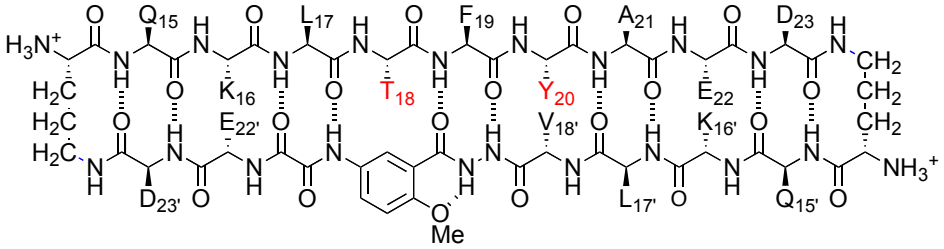

macrocyclic β-sheet peptide **4.5**

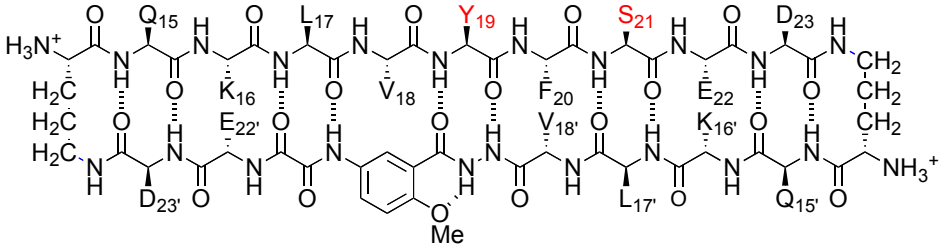

macrocyclic β-sheet peptide **4.6**

^{1}H NMR studies establish that macrocyclic β-sheets **4.3**, **4.4**, and **4.5** form tetramers comprising hydrogen-bonded dimer subunits at low millimolar concentrations.[18] The three macrocycles exhibit ^{1}H NMR spectra with similar features (Figure 4.5). All three macrocycles show downfield shifting of the α-protons characteristic of β-sheet structure, magnetic anisotropy of the δ-linked ornithine *pro-R* and *pro-S* δ-protons characteristic of well-defined turn structures,[11] and upfield shifting of the F_{19} aromatic resonances characteristic of tertiary and quaternary structure (Figures 4.5-4.6, Table 4.2).[19] In contrast, macrocyclic β-sheet **4.6** is monomeric at low millimolar concentrations and is less well folded than macrocyclic β-sheets **4.3**–**4.5**, exhibiting less downfield shifting of the α-protons and less magnetic anisotropy of the δ-linked ornithine *pro-R* and *pro-S* δ-protons (Figure 4.5).[20]

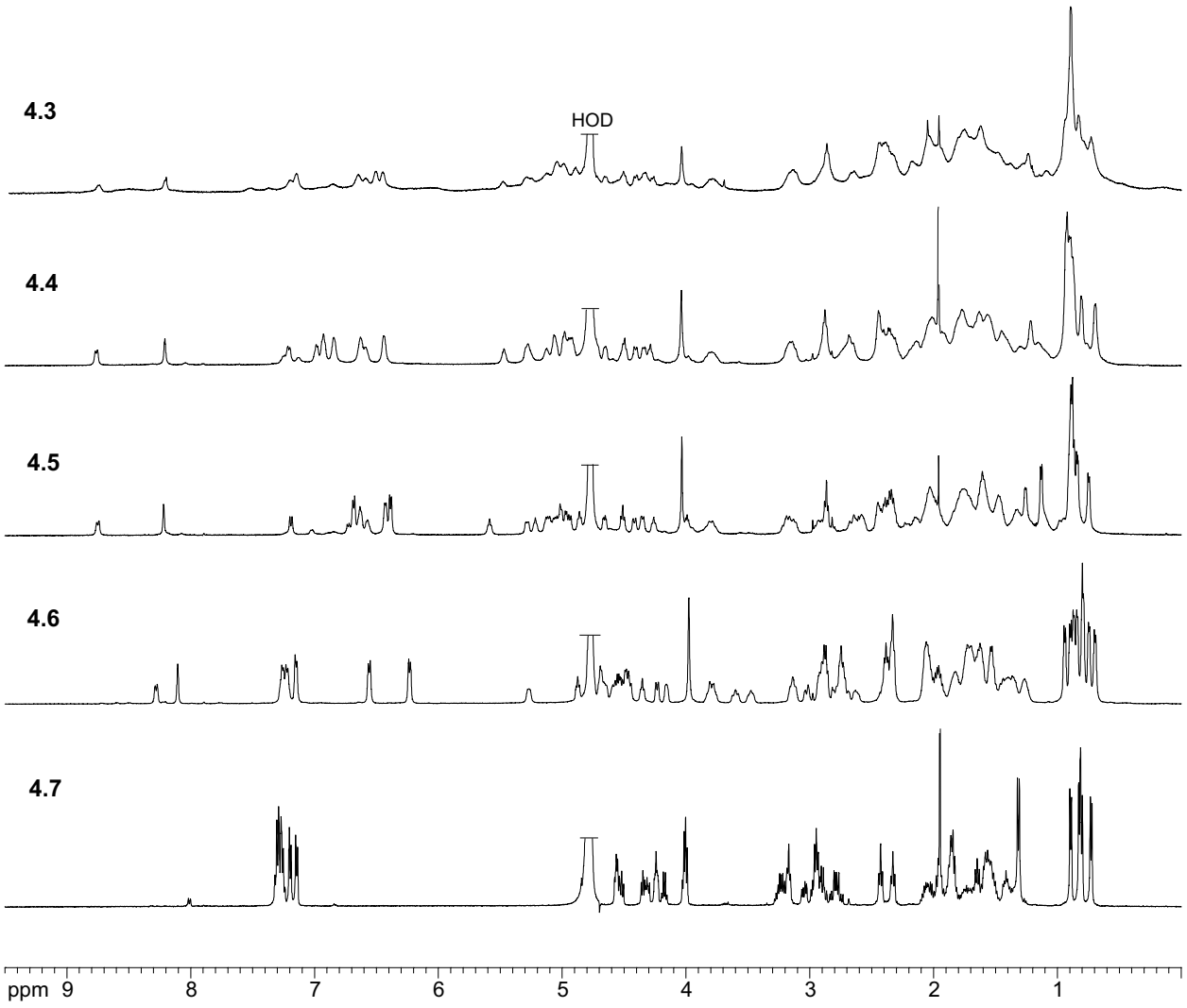

Figure 4.5. ^{1}H NMR spectra of macrocyclic β-sheet peptides at 2.0 mM at 298 K in D_2O at 500 MHz: **4.3** (tetramer predominates), **4.4** (tetramer predominates), **4.5** (tetramer predominates), and **4.5** (monomer predominates). The ^{1}H NMR spectrum of linear peptide **4.7** (1.2 mM at 298 K in D_2O at 500 MHz) is provided for comparison, to show the spectrum of an unstructured QKLVFFAED peptide.[9]

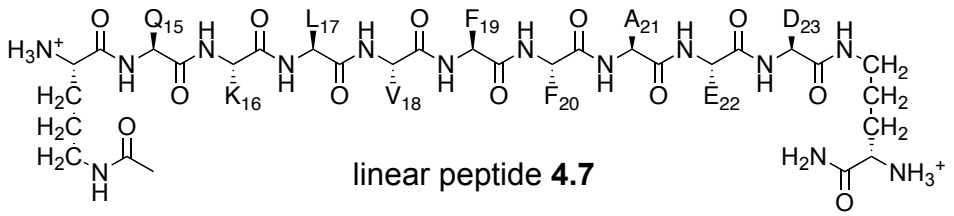

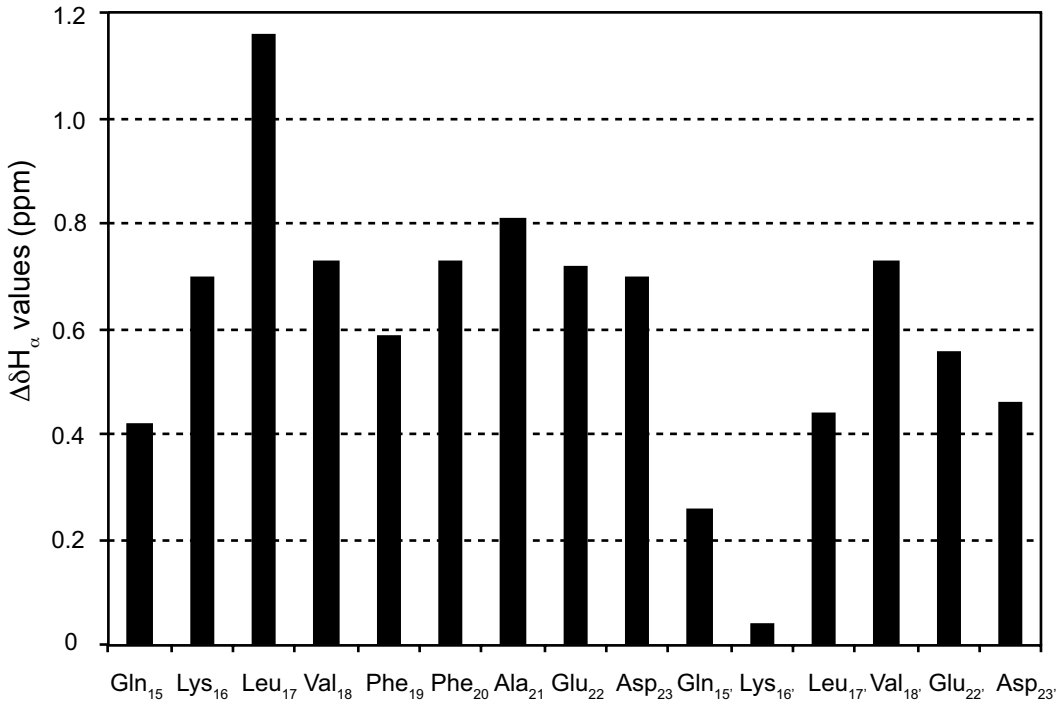

Figure 4.6. Downfield shifting of the ^{1}H NMR α-proton resonances of the **4.4** tetramer relative to linear peptide **4.7**[9]. The ^{1}H NMR spectrum of **4.4** was recorded at 2.0 mM in D_2O at 500 MHz and 298 K. Assignments of Lys_{16} vs. $Lys_{16'}$, Glu_{23} vs. $Glu_{23'}$, and Gln_{15} vs. $Gln_{15'}$ are arbitrary.

Table 4.2. Magnetic Anisotropies of the δ-Protons of the δ-Linked Ornithine Turn Units of Peptides 4.3–4.6 at 2.0 mM in D_2O at 298 K and 500 MHz

peptide	$^{\delta}Orn_1$[c] Δδ (ppm)	$^{\delta}Orn_2$[c] Δδ (ppm)	folding
4.3[a]	0.63	0.69	folded tetramer
4.4[a]	0.60	0.69	folded tetramer
4.5[a]	0.62	0.70	folded tetramer
4.6[b]	0.46	0.34	partially folded monomer

[a]Oligomer at 2.0 mM. [b] Monomer at 2.0 mM. [c]Assignment of $^{\delta}Orn_1$ vs. $^{\delta}Orn_2$ is arbitrary

In the NOESY spectra, macrocyclic β-sheets **4.3**, **4.4**, and **4.5** exhibit a rich array of NOE crosspeaks associated with folding and dimerization. The macrocycles exhibit key NOEs between α-protons associated with folding: K_{16} and $E_{22'}$; V_{18} or T_{18} and the

proton at the 6-position of the Hao residue; F_{20}^{I}, F_{20}, or Y_{20} and $V_{18'}$; and E_{22} and $K_{16'}$. The macrocycles also exhibit key NOEs between α-protons associated with dimerization: L_{17} and D_{23}; and F_{19} and A_{21}. Table 4.3 summarizes the key NOEs observed for each macrocycle; Figures 4.7 and 4.8-4.10 illustrates the structures of the dimers.

Table 4.3. Key NOEs Observed for Macrocyclic β-Sheets 4.3, 4.4, and 4.5[a]

macrocycle	K_{16}–$E_{22'}$[b]	X_{18}–Hao_6	X_{20}–$V_{18'}$	E_{22}–$K_{16'}$[b]	L_{17}–D_{23}[b]	F_{19}–A_{21}[b]
4.3	obs[c]	obs	obs	–[c,d]	obs	–[c]
4.4	obs	obs	obs	obs	obs	obs
4.5	obs	obs	obs	obs	obs	obs

[a]500 MHz NOESY spectra at 2.0 mM in D_2O at 298 K. [b]Assignments of K_{16} vs. $K_{16'}$, L_{17} vs. $L_{17'}$, E_{22} vs. $E_{22'}$, and D_{23} vs. $D_{23'}$ are inferred from the observed pattern of NOEs. [c]Assignment of K_{16}–$E_{22'}$ vs. E_{22}–$K_{16'}$ is arbitrary. [d]NOEs not observed due to overlap of the resonances. (**4.3**: X_{18} = V, X_{20} = F^{I}; **4.4**: X_{18} = V, X_{20} = F; **4.5**: X_{18} = T, X_{20} = Y)

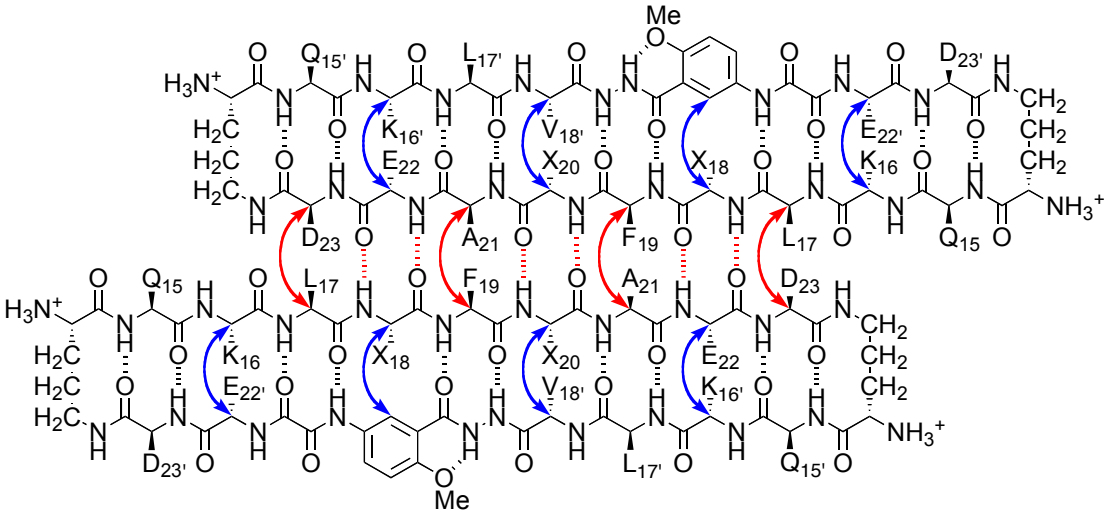

Figure 4.7. Hydrogen-bonded dimers formed by macrocyclic β-sheet peptides **4.3–4.5** in aqueous solution. Key NOEs associated with dimerization and folding are shown with red and blue arrows. (**4.3**: X_{18} = V, X_{20} = F^{I}; **4.4**: X_{18} = V, X_{20} = F; **4.5**: X_{18} = T, X_{20} = Y)

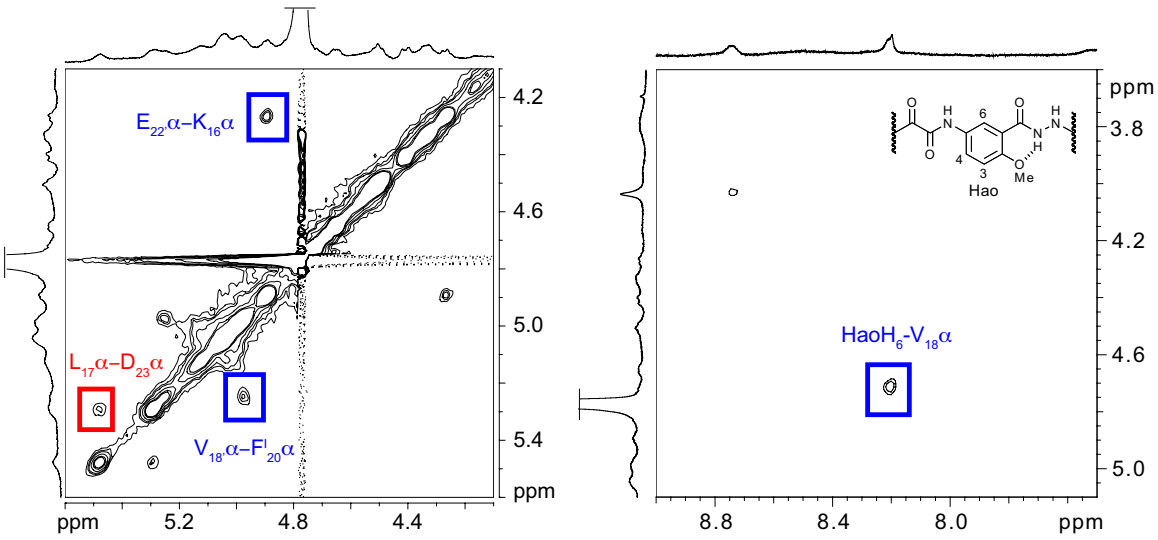

Figure 4.8. Selected expansions of the NOESY spectrum of macrocyclic β-sheet peptide **4.3** at 2.0 mM in D_2O at 500 MHz and 298 K. Key intermolecular interstrand NOEs associated with dimerization are highlighted in red; key intramolecular interstrand NOEs associated with folding are highlighted in blue.

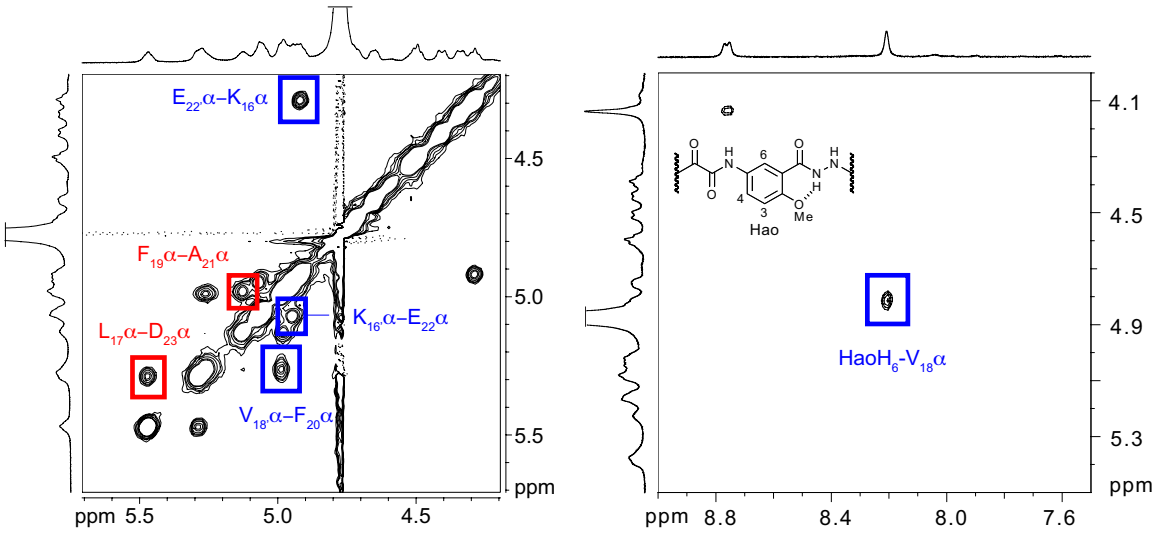

Figure 4.9. Selected expansions of the NOESY spectrum of macrocyclic β-sheet peptide **4.4** at 2.0 mM in D_2O at 500 MHz and 298 K. Key intermolecular interstrand NOEs associated with dimerization are highlighted in red; key intramolecular interstrand NOEs associated with folding are highlighted in blue.

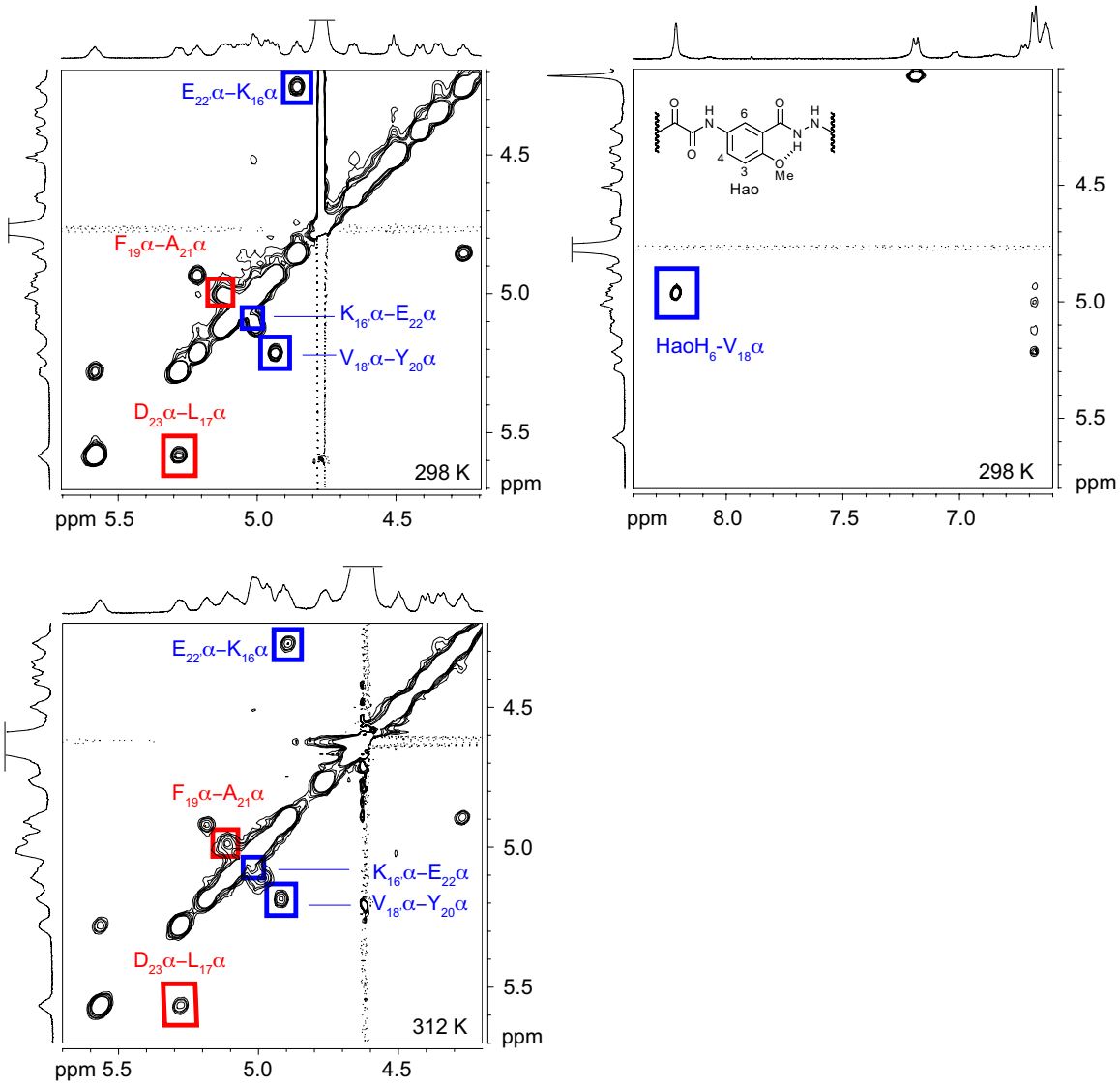

Figure 4.10. Selected expansions of the NOESY spectrum of macrocyclic β-sheet peptide **4.5** at 2.0 mM in D_2O at 500 MHz and at 298 K and 312 K. Key intermolecular interstrand NOEs associated with dimerization are highlighted in red; key intramolecular interstrand NOEs associated with folding are highlighted in blue.

DOSY studies show that the hydrogen-bonded dimers are subunits of tetramers, which are the stable species in aqueous solution.[18,19,21,22] In the DOSY spectra macrocyclic β-sheets **4.3**, **4.4**, and **4.5** exhibit diffusion coefficients of 10.1 – 10.7 x 10^{-7} cm^2/s. These values are comparable to those that we have observed previously for similar

tetramers and are 0.58 – 0.61 times smaller than that of macrocyclic β-sheet **4.6**, which is monomeric.[10,23,24]

Table 4.4. Diffusion Coefficients (D) of Peptides 4.3–4.6 at 2.0 mM in D_2O at 298 K

peptide	$MW_{monomer}$[a] (Da)	$MW_{tetramer}$[a] (Da)	D (10^{-7} cm^2/s)	oligomer state
4.3	2380	9522	10.1[b]	tetramer
4.4	2254	9018	10.3[b]	tetramer
4.5	2272	9090	10.7[b]	tetramer
4.6	2286	NA	17.4[b]	monomer

[a]Molecular weight calculated for the neutral (uncharged) macrocycle. [b]Diffusion coefficient measured at 2.0 mM.

The tetramer forms as sandwich hydrogen-bonded dimers and is sandwiched through the hydrophobic face that displays L_{17}, F_{19}, and A_{21}, and these residues help create the hydrophobic core of the tetramer (Figure 4.11). When F_{19} and A_{21} are rendered hydrophilic by hydroxylation in macrocyclic β-sheet **4.6**, the hydrophobic core cannot form and the tetramer is disrupted.[10] In contrast, when V_{18} and F_{20} are rendered hydrophilic by hydroxylation in macrocyclic β-sheet **4.5**, the hydrophobic core is unaffected and the tetramer is not disrupted.

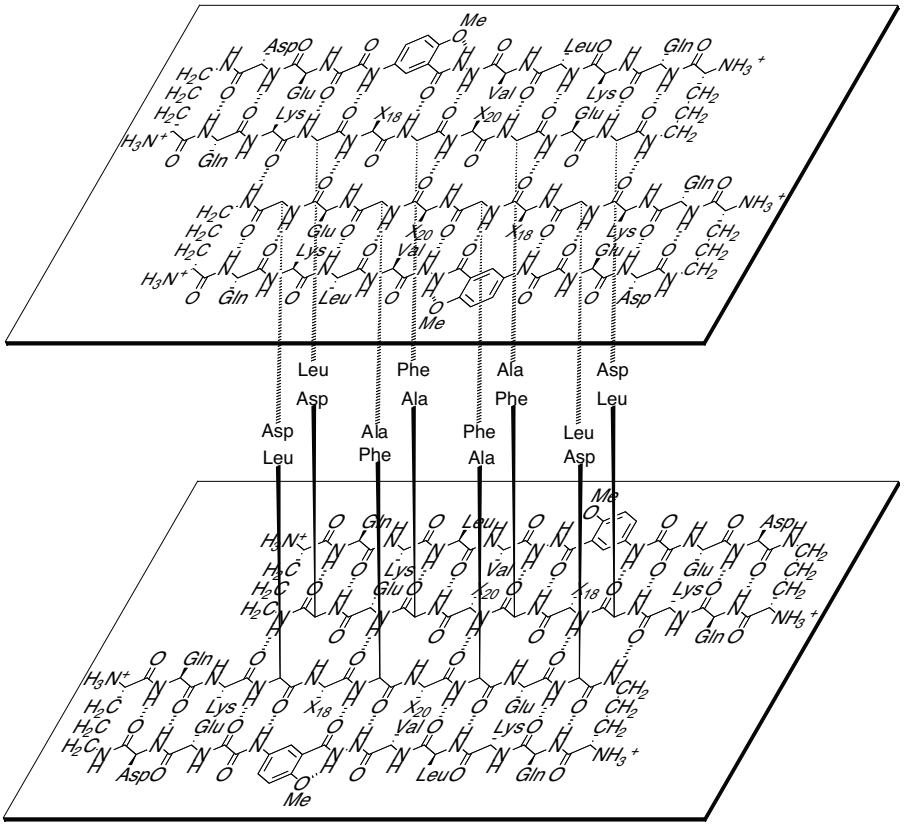

Figure 4.11. Illustration of the tetramer formed by macrocyclic β-sheets **4.3**–**4.5** in aqueous solution. The tetramer forms as a sandwich-like assembly of two hydrogen-bonded dimers, sandwiched through the LFA faces. (**4.3**: X_{18} = V, X_{20} = F^{I}; **4.4**: X_{18} = V, X_{20} = F; **4.5**: X_{18} = T, X_{20} = Y)

Discussion

The extended layered β-sheet formed by the hydrogen-bonded dimers of **4.3** (Figure 4.3B) resembles the structures of amyloid fibrils.[25,26] Amyloid fibrils consist of extended β-sheets composed of networks of hydrogen-bonded β-strands running the length of the fibril axis and laminated in pairs through hydrophobic interactions to form two-layered assemblies.[3] In the fibrils formed by $A\beta_{1-40}$, the hydrophobic central and C-terminal regions of the peptide assemble to form extended β-sheets that run the length of

the fibril axis. The β-strands comprising the β-sheets are roughly orthogonal (90°) to the fibril axis. The molecules of Aβ forms a U-shaped turns, and the hydrophobic central and C-terminal β-strands pack in a face-to-face fashion through hydrophobic interactions. The resulting two-layered β-sheets make up the basic subunit of the fibril, further assembling to form four-layered or triangular fibrils consisting of two or three of these subunits. Although most of the structures reported for $A\beta_{1-40}$ fibrils involve parallel β-sheets, antiparallel β-sheets have been reported for Iowa mutant β-amyloid fibrils.[27] Figures 4.12A and 4.12B illustrate the structures of the parallel and antiparallel two-layered β-sheets reported for $A\beta_{1-40}$. Figure 4.13A illustrates the structure of the component U-shaped turns in the resulting two-layered assemblies.

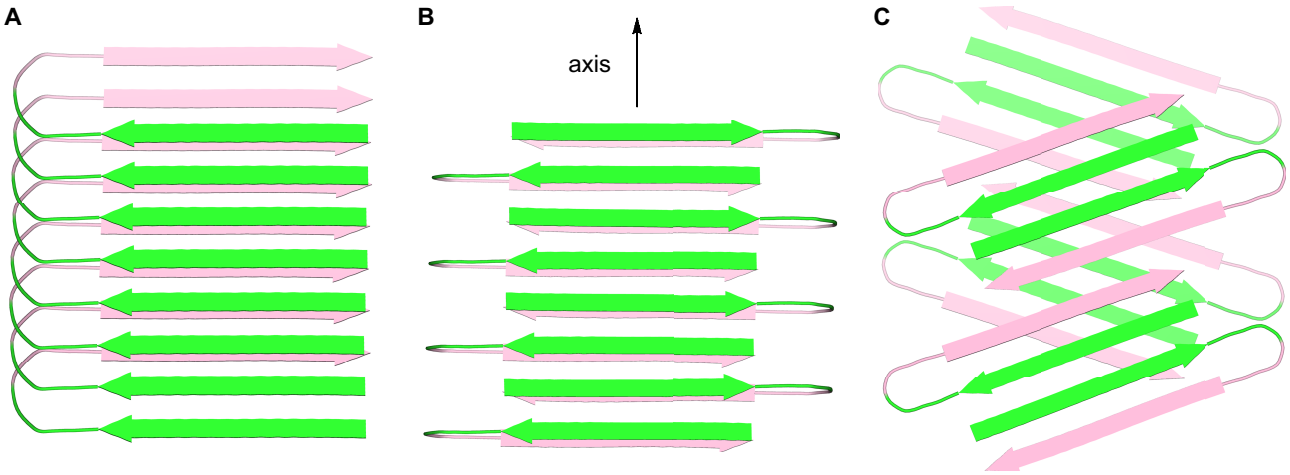

Figure 4.12. Cartoon representations of fibrils formed by Aβ. (A) Parallel β-sheet fibril composed of U-shaped turns in a staggered arrangement, observed for $A\beta_{1-40}$.[2c] (B) Antiparallel β-sheet fibril composed of U-shaped turns, observed for the Iowa mutant $A\beta_{1-40}$.[27] (C) Fibril-like assembly of oligomers composed of β-hairpins, envisioned from the X-ray crystallographic structure of macrocyclic β-sheet **4.3**. The green and pink colors represent the central and C-terminal regions of Aβ.

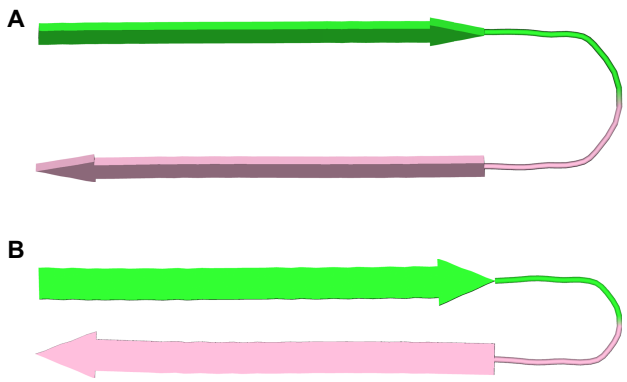

Figure 4.13. Cartoon representations of U-shaped turns (A) and β-hairpins (B) formed by Aβ. In the β-hairpins, the edges of the β-strands hydrogen bond together. In the U-shaped turns, the faces of the β-strands pack together. The green and pink colors represent the central and C-terminal regions of Aβ.

The assembly formed by the hydrogen-bonded dimers of **4.3** (Figure 4.3B) differs notably from amyloid fibrils in that it is composed of discrete oligomeric subunits. While the two-layered β-sheets of the $A\beta_{1\text{-}40}$ fibrils contain no subunit larger than the monomer, the fibril-like assemblies formed by macrocyclic β-sheet **4.3** are composed of oligomers consisting of two β-hairpin-like macrocycles, hydrogen bonded to form a four-stranded antiparallel β-sheet.

The X-ray crystallographic structure of the fibril-like assembly of oligomers formed by macrocyclic β-sheet **4.3** suggests that alternative fibril assemblies of $A\beta_{1\text{–}40}$ or $A\beta_{1\text{–}42}$ may also be possible.[24,25] In fibril-like assembly of oligomers formed by full-length Aβ, the hydrophobic central and C-terminal regions of the peptide hydrogen bond to form a β-hairpin.[28] The β-hairpins further assemble to form layered β-sheets through edge-to-edge hydrogen bonding and face-to-face hydrophobic interactions. The β-strands comprising the β-sheets are not orthogonal to the fibril axis, but rather are rotated about 20° from orthogonality. To compensate for this rotation, the β-sheets must shift

registration by two residues for every two β-hairpins. Figure 4.12C illustrates a structure of this fibril-like assembly of oligomers; Figure 4.13B illustrates the structure of the component β-hairpins.

The solid-state and solution-state structures of macrocyclic β-sheets **4.3–4.6**, show that $A\beta_{15–23}$ can form both aligned and shifted antiparallel β-sheets. In the X-ray crystallographic structure of macrocyclic β-sheet **4.3**, the $A\beta_{15–23}$ peptide strand forms an aligned β-sheet, while the $A\beta_{15–23}$ hybrid strand forms a shifted β-sheet. In the solution-state structure of macrocyclic β-sheets **4.3–4.6**, the $A\beta_{15–23}$ peptide strand forms a shifted β-sheet. Figure 4.14 illustrates the observed modes of supramolecular assembly of these peptides.

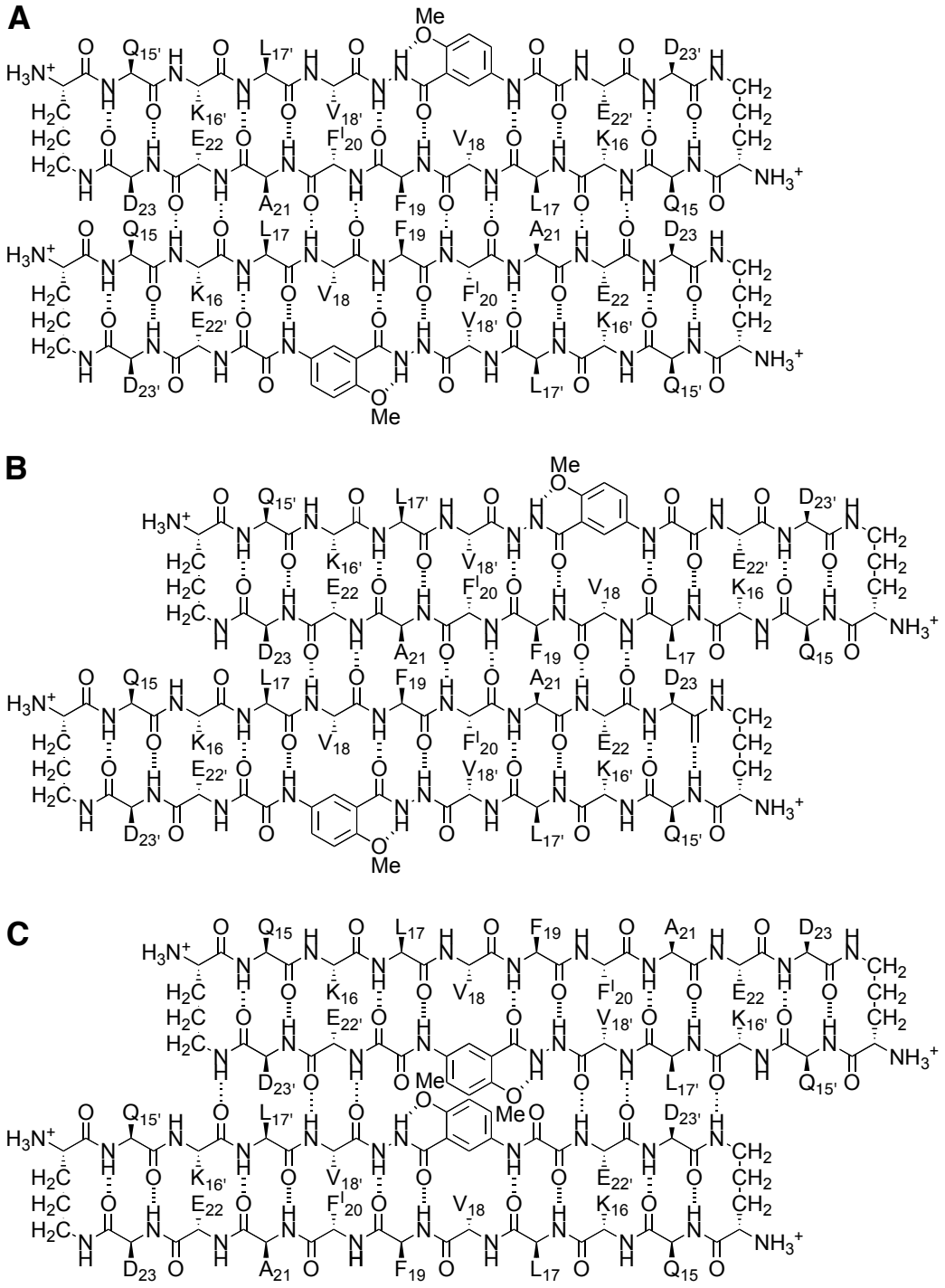

Figure 4.14. Interfaces between $A\beta_{15–23}$ observed in the solid state and in solution. (A) Interface between monomer subunits within the dimer of macrocyclic β-sheet **4.3** in the solid state. (B) Interface between monomer subunits within the dimer of macrocyclic β-sheet **4.3** in aqueous solution. (C) Interface between the dimers of macrocyclic β-sheet **4.3** in the solid state. In (A) and (B) the interface occurs between the $A\beta_{15–23}$ peptide strands; in (C) the interface occurs between the $A\beta_{15–23}$ hybrid strands.

We have previously observed both aligned and shifted antiparallel β-sheets involving $A\beta_{15–23}$ in the solid-state and solution-state structures of macrocyclic β-sheets **4.1**. In the solid state, macrocyclic β-sheet **4.1a** forms tetramers consisting of two hydrogen-bonded dimers sandwiched through the VF faces (Figure 4.15A).[9] In these hydrogen-bonded dimers, the $A\beta_{15–23}$ peptide strands are fully aligned. In aqueous solution, macrocyclic β-sheets **4.1a** and **4.1b** form tetramers consisting of two hydrogen-bonded dimers sandwiched through the LFA faces (Figure 4.15B).[10] In these hydrogen-bonded dimers, the $A\beta_{15–23}$ peptide strands are shifted out of alignment by two residues toward the C-termini. The fibril-like assembly of oligomers formed by macrocyclic β-sheet **4.3** differs from the solid-state and solution-state structures of macrocyclic β-sheets **4.1**, in that it does not contain discrete tetramers. Instead, each dimer subunit overlaps with *two* dimers in the opposing layer.

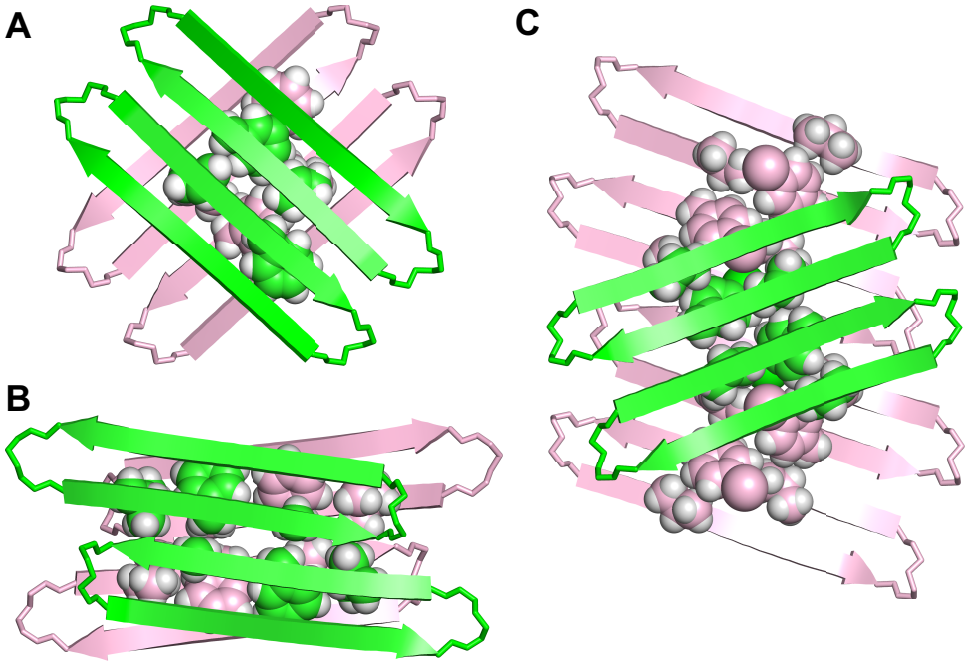

Figure 4.15. Supramolecular assemblies of macrocyclic β-sheet peptides derived from Aβ $_{15–23}$. (A) Tetramer of **4.1a** observed in the solid state (PDB: 4IVH).[9] (B) Tetramer of **4.1b** (and **4.1a**) observed in aqueous solution.[10] (C) Fibril-like assembly of dimers of **4.3** observed in the solid state.

It is easy to imagine a mechanism by which the fibril-like assemblies of oligomers catalyze oligomer formation. During crystal growth, the fibril-like oligomers of macrocyclic β-sheet **4.3** shown in Figure 4.3B must elongate by adding monomer subunits either one at a time or in small groups from tetramers or oligomers present in solution. A similar mechanism of growth can be envisioned for the fibril-like assemblies of oligomers postulated for full-length Aβ in Figure 4.12C, in which the exposed hydrogen-bonding edges and hydrophobic surfaces serve as a template that promotes the addition and folding of monomeric Aβ. The fibril-like assembly of oligomers can then serve as a reservoir of oligomers, dissociating organized dimers, tetramers, or other small homogenous assemblies of soluble toxic amyloid oligomers. Such mechanisms for oligomer replication have been seen and discussed previously but have not been observed

at atomic resolution.[29] The X-ray crystallographic structure of macrocyclic β-sheet **4.3** may thus provide a window at atomic resolution into a prion-like mechanism of amyloid oligomer propagation.

Conclusion

The X-ray crystallographic structure of macrocyclic β-sheet **4.3** provides new insights into the supramolecular assembly of peptides from β-amyloid, revealing a fibril-like assembly of hydrogen-bonded dimers. The dimers repeat along the fibril axis, to form an extended β-sheet, like in conventional amyloid fibrils. Unlike conventional amyloid fibrils, the β-strands comprising the β-sheets are rotated about 20° from orthogonality, and a two-residue shift in alignment of the β-strands occurs at the juncture between the dimers. The β-sheets are layered and laminated through hydrophobic interactions. The dimers are not layered directly over each other, but rather are offset by two strands. As a result, the fibril-like assembly of dimers is not composed of discrete tetramers.

The fibril-like assembly of oligomers formed by macrocyclic β-sheet **4.3** offers the intriguing possibility that full-length Aβ may also be able to form similar assemblies, perhaps consisting of β-hairpins formed by the amyloidogenic central and C-terminal regions of Aβ. This model further suggests the provocative hypothesis that fibril-like assemblies of Aβ oligomers might catalyze Aβ oligomer formation and replication.

References and Notes

1 Pham, J. D.; Spencer, R. K.; Chen, K. H.; Nowick, J. S. "A Fibril-Like Assembly of Oligomers of a Peptide Derived from β-Amyloid," manuscript submitted to *J. Am. Chem. Soc.*

2 (a) Hamley, I. W. *Chem. Rev.* **2012,** *112*, 5147–5192. (b) Benilova, I.; Karran, E.; De Stooper, B. *Nat. Neurosci.* **2012**, *15*, 349–357. (c) Querfurth, H. W.; LaFerla, F. H. N *N. Engl. J. Med.* **2010**, *362*, 329–344. (d) Larson, M. E.; Lesné, S. E. *J. Neurochem.* **2012**, *192* (Suppl. 1), 125–139. (e) Fändrich, M. *J. Mol. Biol.* **2012**, *421*, 427–440.

3 (a) Benzinger, T. L.; Gregory, D. M.; Burkoth, T. S.; Miller-Auer, H.; Lynn, D. G.; Botto, R. E.; Meredith, S. C. *Proc. Natl. Acad. Sci. U.S.A.* **1998**, *95*, 13407–13412. (b) Lührs, T; Ritter, C.; Adrian, M.; Riek-Loher, D.; Bohrmann, B.; Döbeli, H.; Schubert, D.; Riek, R. *Proc. Natl. Acad. Sci. U.S.A.* **2005**, *102*, 17342–17347. (c) Petkova, A. T.; Yau, W.-M.; Tycko, R. *Biochemistry* **2006**, *45*, 498–512. (d) Paravastu, A. K.; Leapman, R. D.; Yau, W.-M.; Tycko, R. *Proc. Natl. Acad. Sci. U.S.A.* **2008**, *105*, 18349–18354. (e) McDonald, M; Box, H.; Bian, W.; Kendall, A.; Tycko, R.; Stubbs, G. *J. Mol. Biol.* **2012**, *423*, 454–461.

4 (a) Yu, L.; Edalji, R.; Harlan, J. E.; Holzman, T. F.; Lopez, A. P.; Labkovsky, B.; Hillen, H.; Barghorn, S.; Ebert, U.; Richardson, P. L.; Miesbauer, L.; Solomon, L.; Bartley, D.; Walter, K.; Johnson, R. W.; Hajduk, P. J.; Olejniczak, E. T. *Biochemistry* **2009**, *48*, 1870–1877. (b) Cerf, E.; Sarroukh, R.; Tamamizu-Kato, S.; Breydo, L.; Derclaye, S.; Dufrênes, Y. V.; Narayanaswami, V.; Goormaghtigh, E.; Ruysschaert, J.-M.; Raussens, V. *Biochem. J.* **2009**, *421*, 415–423. (c) Chimon, S.; Shaibat, M. A.;

Jones, C. R.; Calero, D. C.; Aizezi, B.; Ishii, Y. *Nat. Struc. Mol. Bio.* **2010**, *14*, 1157–1164. (d) Streltsov, V. A.; Varghese, J. N.; Masters, C. L.; Nuttall, S. D. *J. Neurosci.* **2011**, *31*, 1419–1426.

5 (a) Ma, B.; Nussinov, *Proc. Natl. Acad. Sci. U.S.A.* **2002**, *99*, 14126–14131. (b) Tarus, B.; Straub, J. E.; Thirumalai, D. *J. Mol. Biol.* **2005**, *345*, 1141–1156. (c) Miller, Y.; Ma, B.; Nussinov, R. *Biophys. J.* **2009**, *97*, 1168–1177. (d) Ahmed, M.; Davis, J.; Aucoin, D.; Sato, T.; Ahuja, S.; Aimoto, S.; Elliott, J. I.; van Nostrand, W. E.; Smith, S. O. *Nat. Struct. Mol. Biol.* **2010**, 17, 561– 567

6 (a) Hilbich, C.; Kisters-Woike, B.; Reed, J. Masters, C. L; Beyreuther, K. *J. Mol. Biol.* **1992**, *228*, 460–473. (b) Wood, S. J.; Wetzel, R.; Martin, J. D.; Hurle, M. R. *Biochemistry* **1995**, *34*, 724–730. (c) Tjernberg, L. O.; Callaway, D. J. E.; Tjernberg, A.; Hahne, S.; Lilliehöök, C.; Terenius, L.; Thyberg, J.; Nordstedt, C. *J. Biol. Chem.* **1999**, *274*, 12619–12625.

7 (a) Tjernberg, L. O.; Näslund, J.; Lindqvist, F.; Johansson, J.; Karlström, A. R.; Thyberg, J.; Terenius, L.; Nordstedt, C. *J. Biol. Chem.* **1996**, *271*, 8545–8548. (b) Tjernberg, L. O.; Lilliehöök, C.; Callaway, D. J. E.; Näslund, J.; Hahne, S.; Thyberg, J.; Terenius, L.; Nordstedt, C. *J. Biol. Chem.* **1997**, *272*, 12601–12605. (c) Soto, C.; Kindy, M. S.; Baumann, M.; Frangione, B. *Biochem. Biophys. Res. Commun*. **1996**, *226*, 672−680. (d) Findeis, M. A.; Musso, G. M.; Arico-Muendel, C. C.; Benjamin, H. W.; Hundal, A. M.; Lee, J. J.; Chin, J.; Kelley, M.; Wakefield, J.; Hayward, N. J.; Molineaux, S. M. *Biochemistry* **1999**, *38*, 6791−6800.

8 (a) Balbach, J. J.; Ishii, Y.; Antzutkin, O. N.; Leapman, R. D.; Rizzo, N. W.; Dyda, F.; Reed, J.; Tycko, R. *Biochemistry* **2000**, *39*, 13748−13759. (b) Ishii, Y.; Tycko, R.

J. Am. Chem. Soc. **2003**, *125*, 6606−6607. (c) Klimov, D.; Thirumalai, D. *Structure* **2003**, *11*, 295–307. (d) Petkova, A. T.; Buntkowsky, G.; Dyda, F.; Leapman, R. D.; Yau, W. M.; Tycko, R. *J. Mol. Biol.* **2004**, *335*, 247–260. (e) Lu, K.; Jacob, J.; Thiyagarajan, P.; Conticello, V. P.; Lynn, D. G. *J. Am. Chem. Soc.* **2003**, *125*, 6391–6393. (f) Mehta, A. K.; Lu, K.; Childers, W. S.; Liang, Y.; Dublin, S. N.; Dong, J.; Snyder, J. P.; Pingali, S. V.; Thiyagarajan, P.; Lynn, D. G. *J. Am. Chem. Soc.* **2008**, *130*, 9829–9835. (g) Liang, Y.; Pingali, S. V.; Jogalekar, A. S.; Snyder, J. P.; Thiyagarajan, P.; Lynn, D. G. *Biochemistry* **2008**, *47*, 10018–10026. (h) Senguen, F. T.; Lee, N. R.; Gu, X.; Ryan, D. M.; Doran, T. M.; Anderson, E. A.; Nilsson, B. L. *Mol. BioSyst.* **2011**, *7*, 486–496. (i) Senguen, F. T.; Doran, T. M.; Anderson, E. A.; Nilsson, B. L. *Mol. BioSyst.* **2011**, *7*, 497–510. (j) Colletier, J.-P.; Laganowsky, A.; Landau, M.; Zhao, M.; Soriaga, A. B.; Goldschmidt, L.; Flot, D.; Cascio, D.; Sawaya, M. R.; Eisenberg, D. *Proc. Natl. Acad. Sci. U.S.A.* **2011**, *108*, 16938–16943. (k) Cheng, P.-N.; Liu, C.; Zhao, M.; Eisenberg, D.; Nowick, J. S. *Nature Chemistry* **2012**, *4*, 927–933.

9 Pham, J. D.; Chim, N.; Goulding, C. W.; Nowick, J. S. *J. Am. Chem. Soc.* **2013**, *135*, 12460–12467.

10 Pham, J. D.; Demeler, B.; Nowick, J. S. *J. Am. Chem. Soc.* **2014**, *136*, 5432–5442.

11 Nowick, J. S.; Brower, J. O. *J. Am. Chem. Soc.* **2003**, *125*, 876–877.

12 Nowick, J. S.; Chung, D. M.; Maitra, K.; Maitra, S.; Stigers, K. D.; Sun, Y. J. *J. Am. Chem. Soc.* **2000**, *122*, 7654–7661.

13 Kabsch, W. *Acta Crystallogr. Sect. D: Biol. Crystallogr.* **2010**, *66*, 125–132.

14 (a) Evans, P. *Acta Crystallogr. Sect. D: Biol. Crystallogr.* **2006**, *62*, 72–82. (b) Evans, P. R.; Murshudov, G. N. *Acta Crystallogr. Sect. D: Biol. Crystallogr.* **2013**, *69*, 1204–1214.

15 (a) Grosse-Kunstleve, R. W.; Adams, P. D. *Acta Crystallogr. Sect. D: Biol. Crystallogr.* **2003**, *59*, 1966–1973. (b) Adams, P. D.; Afonine, P. V.; Bunkoczi, G.; Chen, V. B.; Davis, I. W.; Echols, N.; Headd, J. J.; Hung, L. W.; Kapral, G. J.; Grosse-Kunstleve, R. W.; McCoy, A. J.; Moriarty, N. W.; Oeffner, R.; Read, R. J.; Richardson, D. C.; Richardson, J. S.; Terwilliger, T. C.; Zwart, P. H. *Acta Crystallogr. Sect. D: Biol. Crystallogr.* **2010**, *66*, 213–221.

16 Emsley, P.; Lohkamp, B.; Scott, W. G.; Cowtan, K. *Acta Crystallogr. Sect. D: Biol. Crystallogr.* **2010**, *66*, 486–501.

17 Larsen, N. A.; Heine, A.; de Prada, P.; Redwan, E.-R.; Yeates, T. O.; Landry, D. W.; Wilson, I. A. *Acta Crystallogr. Sect. D: Biol. Crystallogr.* **2002**, *58*, 2055–2059.

18 Macrocyclic β-sheet **4.5** shows predominantly or wholly the tetramer in the ^{1}H NMR spectrum at concentrations as low as 0.1 mM in D_2O at 298 K.

19 The ^{1}H NMR spectra of macrocyclic β-sheets **4.3** and **4.4** are broader than that of **4.5**, suggesting that while the tetramers predominate for all of these peptides, the tetramers formed by the more hydrophobic peptides **4.3** and **4.4** may participate in minor equilibria with additional tetramers that differ in structure or oligomers that differ in molecularity.

20 Macrocyclic β-sheet **4.6** shows only monomer in the ^{1}H NMR spectrum at 2.0 mM in D_2O at 298 K, but shows resonances for both monomer and oligomer at 8.0 mM.

21 (a) Berger, S.; Braun, S. *200 and More NMR Experiments: A Practical Course*;

Wiley-VCH: Weinheim, 2004; pp 515–517. (b) Findeisen, M; Berger, S. *50 and More Essential NMR Experiments*; Wiley-VCH: Weinheim, 2012; pp 163–166.

22 (a) Altieri, A. S.; Hinton, D. P.; Byrd, R. A. *J. Am. Chem. Soc.* **1995**, *117*, 7566–7567. (b) Johnson, C. S. *Progr. NMR Spectrosc.* **1999**, *34*, 203–256. (c) Yao, S.; Howlett, G. J.; Norton, R. S. *J. Biomol. NMR* **2000**, *16*, 109–119. (d) Cohen, Y.; Avram, L.; Frish, L. *Angew. Chem. Int. Ed.* **2005**, *44*, 520–554. (e) Cohen, Y.; Avram, L.; Evan-Salem, T.; Slovak, S.; Shemesh, N.; Frish, L. In *Analytical Methods in Supramolecular Chemistry*, 2nd ed.; Schalley, C. A., Ed; Wiley-VCH: Weinheim, 2012; 197–285.

23 Khakshoor, O.; Demeler, B.; Nowick, J. S. *J. Am. Chem. Soc.* **2007**, *129*, 5558–5569.

24 (a) Polson, A. *J. Phys. Colloid Chem.* **1950**, *54*, 649–652. (b) Teller, D. C.; Swanson, E.; DeHaen, C. *Methods Enzymol.* **1979**, *61*, 103–124.

25 Fibril-like assemblies of oligomers have also been envisioned and observed previously for macrocyclic β-sheet peptides containing amyloidogenic peptide sequences: (a) Liu, C.; Sawaya, M. R.; Cheng, P.-N.; Zheng, J.; Nowick, J. S.; Eisenberg, D. *J. Am. Chem. Soc.* **2011**, *133*, 6736–6744. (b) Liu, C.; Zhao, M.; Jiang, L.; Cheng, P.-N.; Park, J.; Sawaya,. M. R.; Pensalfini, A.; Gou, D.; Berk, A. J.; Glabe, C. G.; Nowick, J. S.; Eisenberg, D. *Proc. Natl. Acad. Sci. U. S. A.* **2012**, *109*, 20913–20918.

26 Stroud, J. C.; Liu, C.; Teng, P. K.; Eisenberg, D. *Proc. Natl. Acad. Sci. U. S. A.* **2012**, *109*, 7717–7722.

27 (a) Qiang, W.; Yau, W-M.; Tycko, R.; *J. Am. Chem. Soc.* **2011**, *133*, 4018–4029. (b) Qiang, W.; Yau, W-M.; Luo, Y.; Mattson, M. P.; Tycko, R. *Proc. Natl. Acad. Sci. U.S.A.* **2012**, *109*, 4443–4448.

28 (a) Hoyer, W.; Grönwall, C.; Jonsson, A.; Ståhl, S.; Härd, T. *Proc. Natl. Acad. Sci. U.S.A.* **2008**, *105*, 5099–5104. (b) Sandberg, A.; Luheshi, L. M.; Söllvander, S.; de Barros, T. P.; Macao, B.; Knowles, T. P. J.; Biverstål, H.; Lendel, C.; Ekholm-Petterson, F.; Dubnovitsky, A.; Lannfelt, L.; Dobson, C. M.; Härd, T. *Proc. Natl. Acad. Sci. U.S.A.* **2010**, *107*, 15595–15600.

29 (a) Lansbury Jr., P. T.; Caughey, B. *Chem. Biol.* **1995**, *2*, 1–5. (b) Petkova, A. T.; Leapman, R. D.; Guo, Z.; Yau, W.-M.; Mattson, M. P.; Tycko, R. *Science* **2005**, *307*, 262–265. (c) Cremades, N.; Cohen, S. I.; Deas, E.; Abramov, A. Y.; Chen, A. Y.; Orte, A.; Sandal, M.; Clarke, R. W.; Dunne, P.; Aprile, F. A.; Bertoncini, C. W.; Wood, N. W.; Knowles, T. P.; Dobson, C. M.; Klenerman, D. *Cell* 2012, *149*, 1048–1059. (d) Soto, C. *Cell* **2012**, *149*, 968–977. (e) Shahnawaz, M.; Soto, C.; *J. Biol. Chem.* **2012**, *287*, 11665–11676. (f) Nussbaum, J. M.; Schilling, S.; Cynis, H.; Silva, A.; Swanson, E.; Wangsanut, T.; Tayler, K.; Wiltgen, B.; Hatami, A.; Rönicke, R.; Reymann, K.; Hutter-Paier, B.; Alexandru, A.; Jagla, W.; Graubner, S.; Glabe, C. G.; Demuth, H.-U.; Bloom, G. S. *Nature* **2012**, *485*, 651–655. (g) Morales, R.; Duran-Aniotz, C.; Castilla, J.; Estrada, L. D.; Soto, C. *Mol. Psychiatry* **2012**, *17*, 1347–1353.

Experimental Section For Chapter 4

Materials and Methods:

Peptides **4.3–4.6** were prepared and studied as the trifluoroacetate (TFA) salts. ^{1}H NMR 1D, TOCSY, NOESY, ROESY, and DOSY experiments for peptides **4.3–4.6** were carried out as previously described. [1]

*Synthesis of macrocyclic β-sheet peptides **4.3–4.6**.*

Macrocyclic peptide **4.3–4.6** were synthesized using procedures previously reported for the synthesis of **4.1** and of other macrocyclic β-sheet peptides.[2,3,4] Boc-Orn(Fmoc)-OH was used to introduce the δ-linked ornithine turn units. Fmoc-Hao-OH was used to introduce the unnatural amino acid Hao.[3,5] Standard Fmoc-protected amino acids were used to introduce the other residues: Fmoc-Ala-OH, Fmoc-Asp(OtBu)-OH, Fmoc-Gln(Trt)-OH, Fmoc-Glu(OtBu)-OH, Fmoc-Leu-OH, Fmoc-Lys(Boc)-OH, Fmoc-Phe-OH, Fmoc-Phe(*p*-iodo)-OH, Fmoc-Ser(OtBu)-OH, Fmoc-Thr(OtBu)-OH, Fmoc-Tyr(OtBu)-OH, and Fmoc-Val-OH.

---

1 Pham, J. D.; Demeler, B.; Nowick, J. S. *J. Am. Chem. Soc.* **2014**, *136*, 5432–5442.

2 Pham, J. D.; Chim, N.; Goulding, C. W.; Nowick, J. S. *J. Am. Chem. Soc.* **2013**, *135*, 12460–12467.

3 Cheng, P.-N.; Nowick, J. S. *J. Org. Chem.* **2011**, *76*, 3166–3173.

4 Cheng, P.-N.; Liu, C.; Zhao, M.; Eisenberg, D.; Nowick, J. S. *Nat. Chem.* **2012**, *4*, 927–933.

5 Nowick, J. S.; Chung, D. M.; Maitra, K.; Maitra, S.; Stigers, K. D.; Sun, Y. J. *J. Am. Chem. Soc.* **2000**, *122*, 7654–7661.

X-ray diffraction data collection, processing, and structure refinement.

Crystals of macrocyclic β-sheet peptide **4.3** were flash-frozen in liquid nitrogen prior to data collection. Diffraction data for macrocyclic β-sheet peptide **4.3** were collected on beamline 7-1 at the Stanford Synchrotron Radiation Lightsource (Stanford, CA) at 1.00 Å wavelength to a resolution 1.75 Å at 100 K. [Data were collected at 1.00 Å wavelength to take advantage of the maximum flux of the beamline and obtain a reasonable anomalous signal from the iodine groups (f'' = 3.3).] Data were collected over 180 degrees with a 0.5 degree oscillation. The data were integrated and scaled with XDS,[6] and merged with Aimless.[7] The space group was initially determined to be $C222_1$; after an analysis of the data with Xtriage in the PHENIX software suite,[8] it became apparent (multivariate Z score L-test > 3.5) that the data better fit a lower space group with pseudomerohedral twinning.[9] Data were reprocessed in the $C2$ space group and refined with the appropriate twin law (-h, -k, l).

---

6 Kabsch, W. *Acta Crystallogr. Sect. D: Biol. Crystallogr.* **2010**, *66*, 125–132.

7 (a) Evans, P. *Acta Crystallogr. Sect. D: Biol. Crystallogr.* **2006**, *62*, 72–82. (b) Evans, P. R.; Murshudov, G. N. *Acta Crystallogr. Sect. D: Biol. Crystallogr.* **2013**, *69*, 1204–1214.

8 Adams, P. D.; Afonine, P. V.; Bunkoczi, G.; Chen, V. B.; Davis, I. W.; Echols, N.; Headd, J. J.; Hung, L. W.; Kapral, G. J.; Grosse-Kunstleve, R. W.; McCoy, A. J.; Moriarty, N. W.; Oeffner, R.; Read, R. J.; Richardson, D. C.; Richardson, J. S.; Terwilliger, T. C.; Zwart, P. H. *Acta Crystallogr. Sect. D: Biol. Crystallogr.* **2010**, *66*, 213–221.

9 Larsen, N. A.; Heine, A.; de Prada, P.; Redwan, E.-R.; Yeates, T. O.; Landry, D. W.; Wilson, I. A. *Acta Crystallogr. Sect. D: Biol. Crystallogr.* **2002**, *58*, 2055–2059.

Initial positions for the iodine groups were determined using hybrid substructure search (HySS) in the PHENIX software suite.[8,10] Coordinates for the iodine groups determined by HySS were used with Autosol to generate the initial electron density map. Two macrocyclic β-sheet peptides **3** and two 2-methyl-2,4-pentanediol molecules were found in the asymmetric unit. Iterative rounds of refinement and model building were done with phenix.refine and Coot,[11] respectively. Each structure during the iterative model building was refined with riding hydrogens, TLS parameters, anisotropic *B*-factors for 4-iodophenylalanine residues, and with the twin law (-*h*, -*k*, *l*). Statistics for the final refinement of macrocyclic β-sheet peptides **4.3** were R_{work} = 17.94% and R_{free} = 21.97%. The crystal structure was deposited to the Protein Data Bank (PDB) with PDB code 4Q8D.

PyMOL was used to generate images from the crystallographic data. A β-strand of three glycine residues (G3) was used to replace Hao in generating a cartoon of the $A\beta_{15–23}$ hybrid strand, QKLV-Hao-ED. Specifically, the pdb coordinates for the unnatural amino acid Hao were used to generate triglycine segments.

---

[10] Grosse-Kunstleve, R. W.; Adams, P. D. *Acta Crystallogr. Sect. D: Biol. Crystallogr.* **2003**, *59*, 1966–1973.

[11] Emsley, P.; Lohkamp, B.; Scott, W. G.; Cowtan, K. *Acta Crystallogr. Sect. D: Biol. Crystallogr.* **2010**, *66*, 486–501.

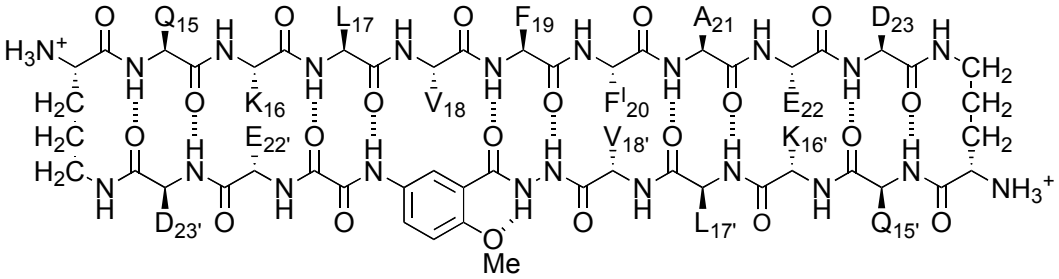

macrocyclic β-sheet peptide **4.3** (as the TFA salt)

molecular weight calculated for $C_{103}H_{155}IN_{26}O_{31} \cdot 4CF_3CO_2H$ (TFA salt of **4.3**): 2836.49
molecular weight calculated for $C_{103}H_{155}IN_{26}O_{31}$ (free base of **4.3**): 2380.39
exact mass calculated for $C_{103}H_{155}IN_{26}O_{31}$ (free base of **4.3**): 2379.04

Analytical RP-HPLC of macrocyclic β-peptide **4.3**

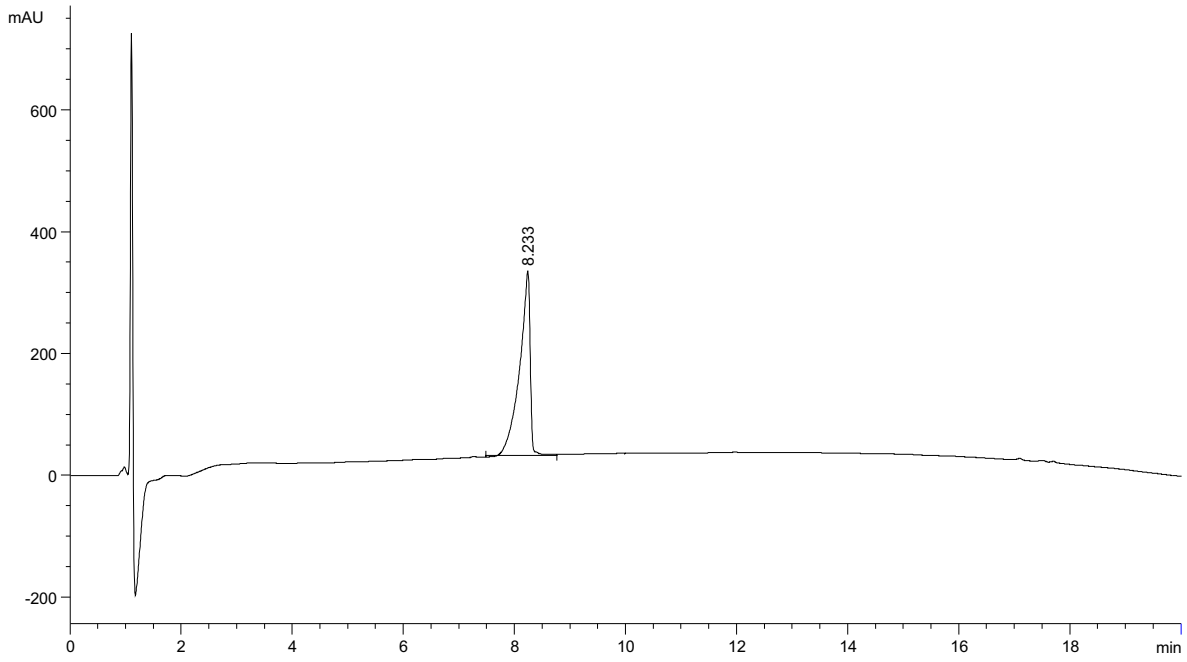


```
Signal 1: VWD1 A, Wavelength=214 nm

Peak RetTime Type  Width     Area      Height     Area
  #   [min]        [min]  mAU   *s    [mAU   ]      %
----|-------|----|-------|----------|----------|--------|
   1   8.233 MM    0.2195 3995.70361  303.33344 100.0000

Totals :                  3995.70361  303.33344
```

Macrocyclic β-sheet peptide **4.3**

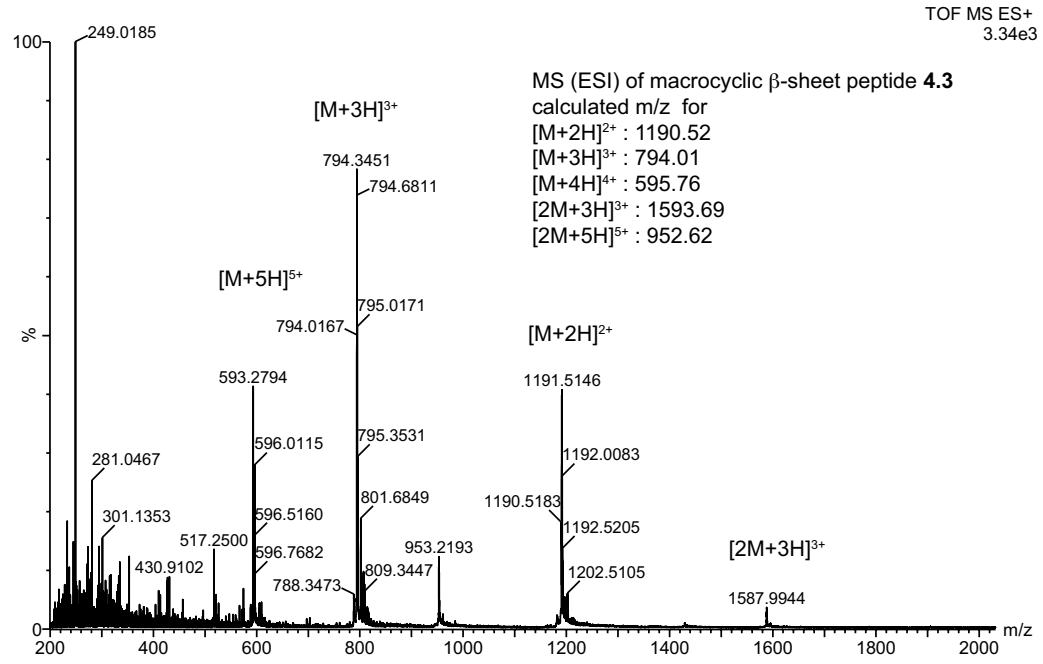

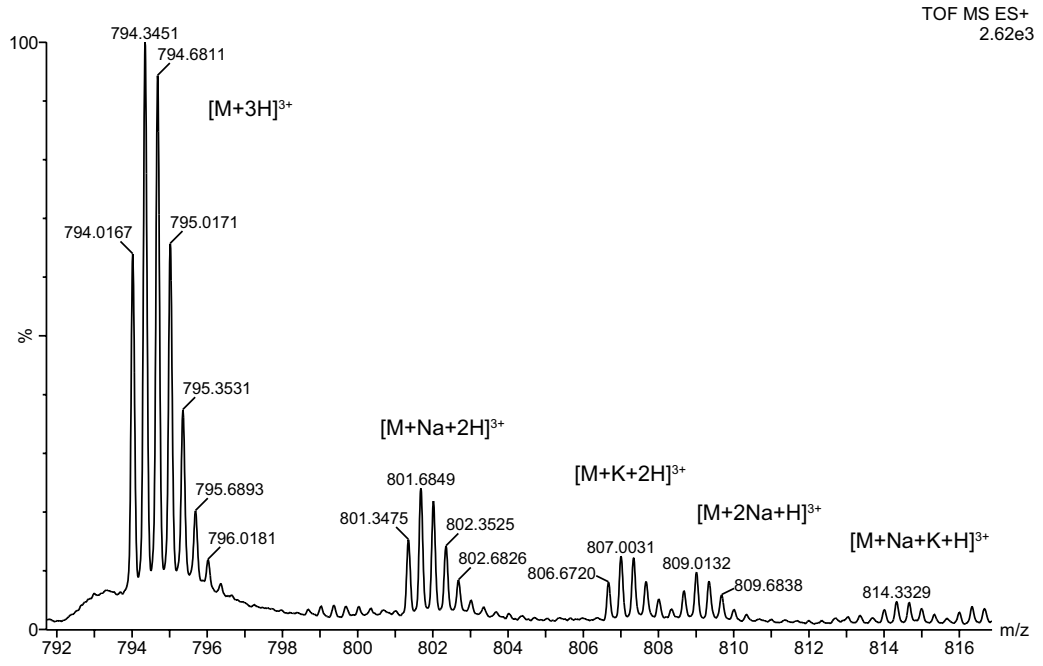

Macrocyclic β-sheet peptide **4.3**

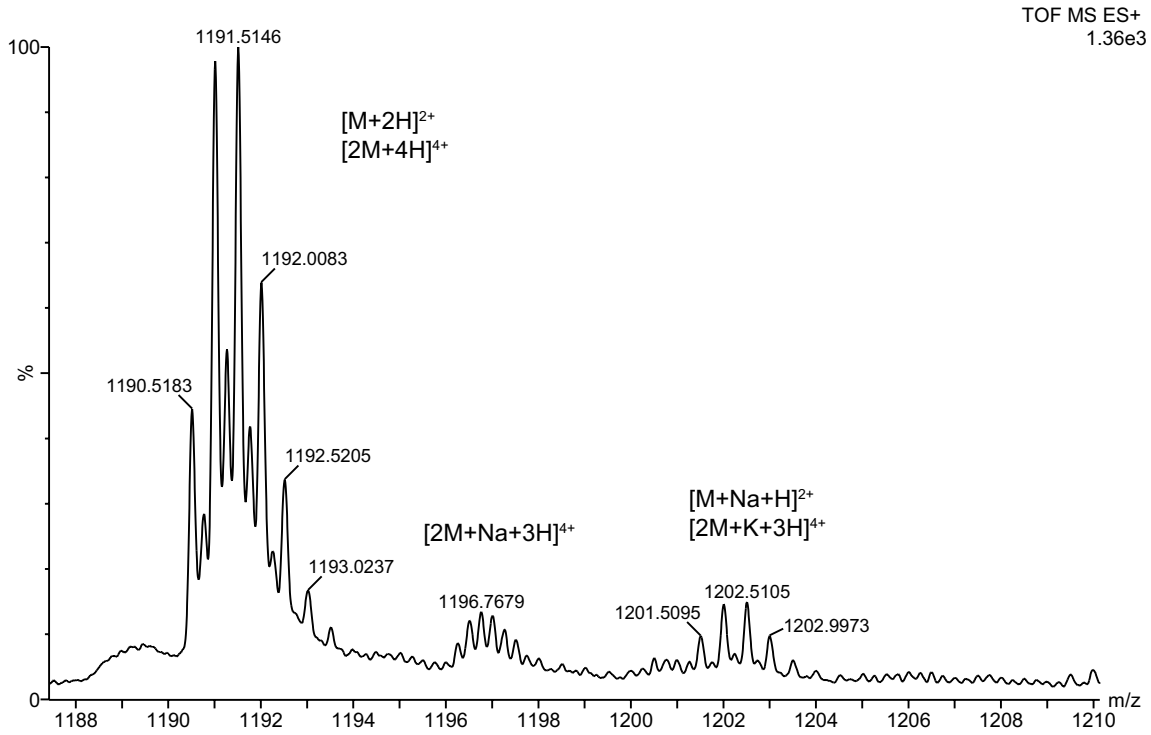

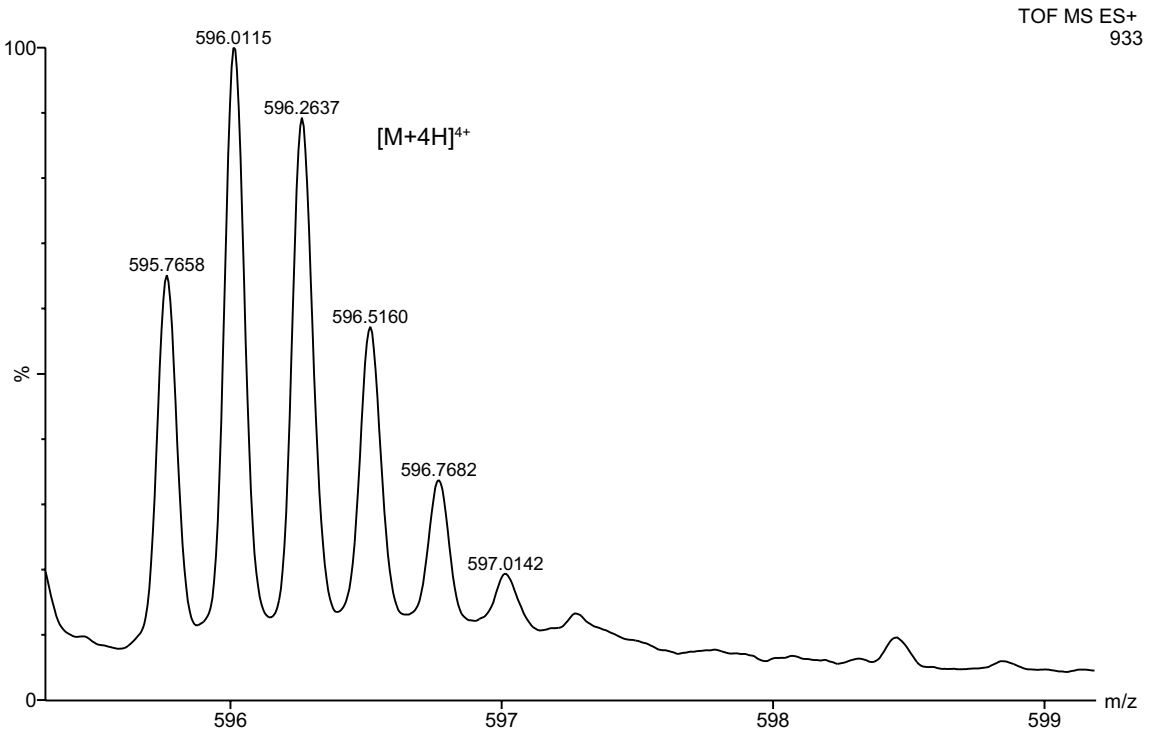

Macrocyclic β-sheet peptide **4.3**

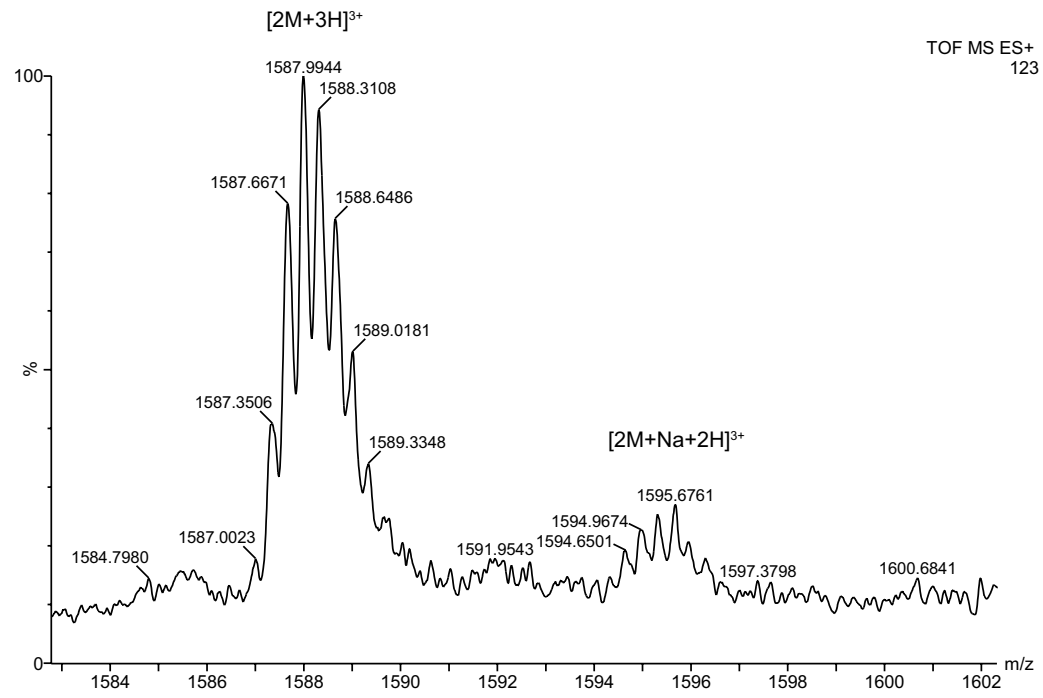

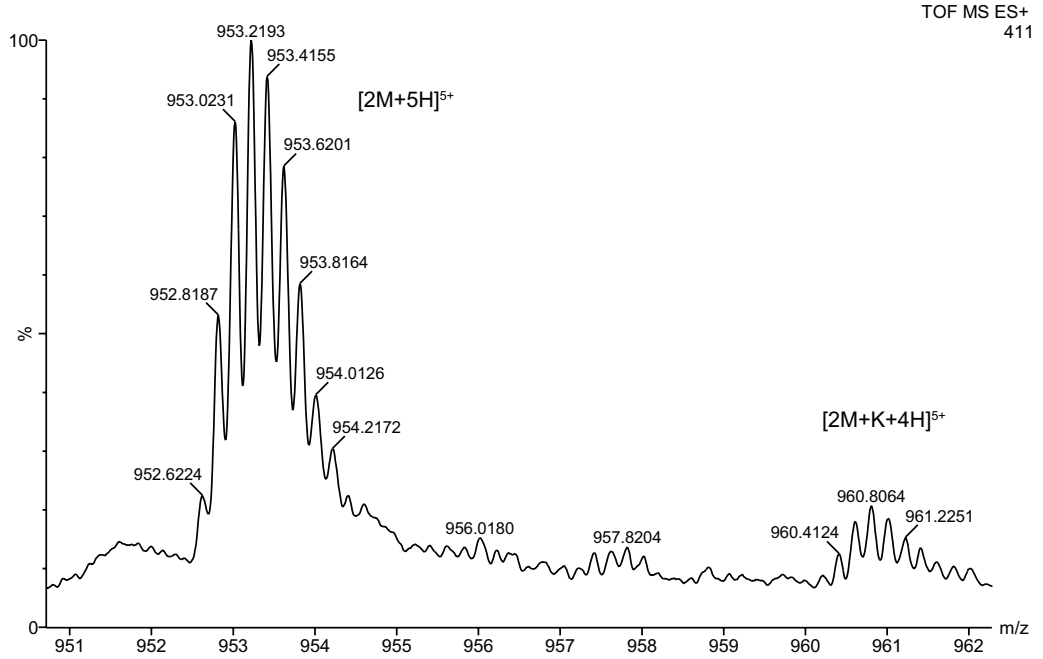

1D ^{1}H NMR spectrum of macrocyclic β-sheet **4.3**
2 mM in D_2O, 500 MHz, 298 K
tetramer predominates

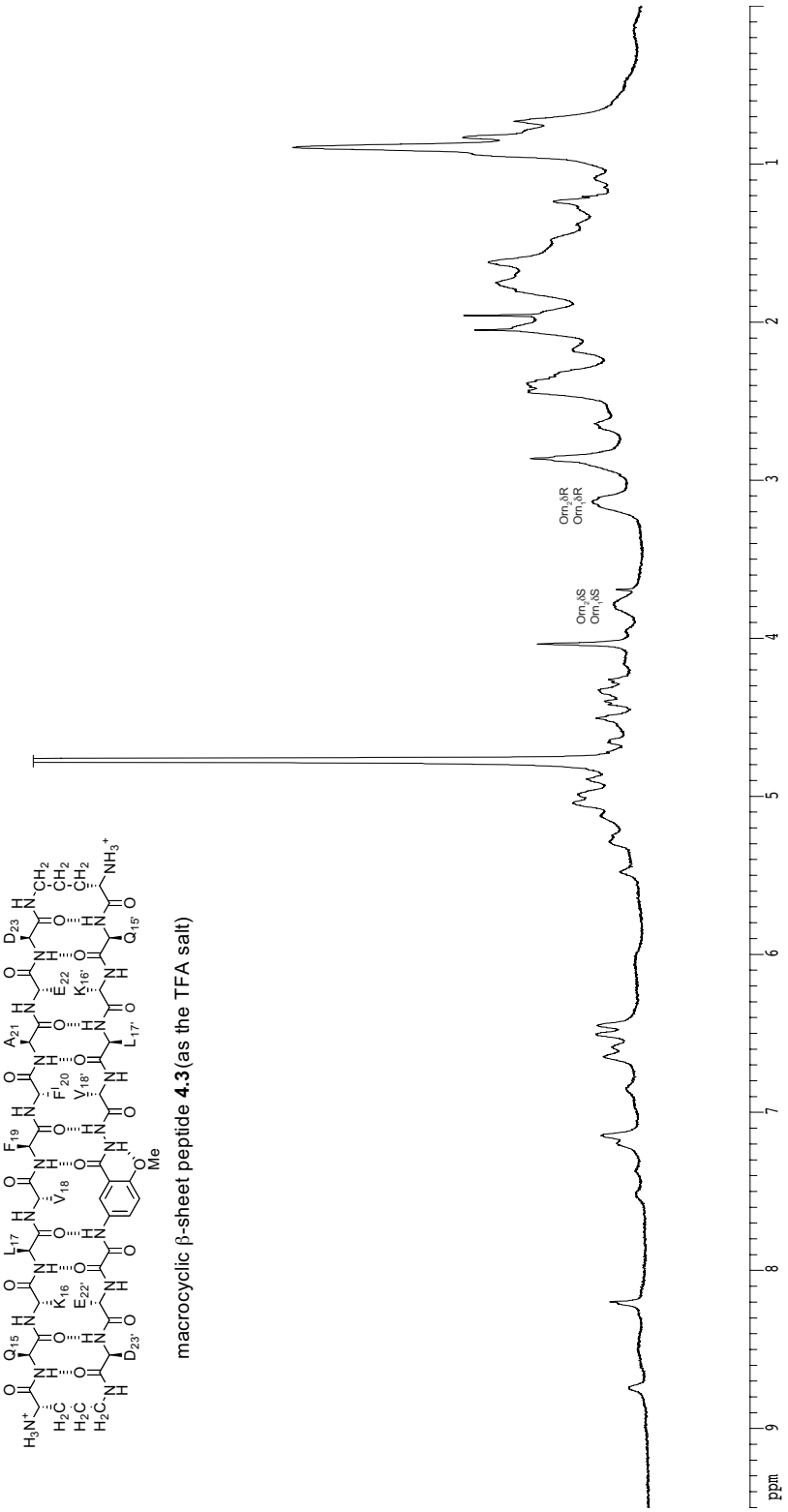

macrocyclic β-sheet peptide **4.3**(as the TFA salt)

2D TOCSY spectrum of macrocyclic β-sheet **4.3**
2 mM in D_2O, 500 MHz, 298 K
150-ms spin-locking mixing time
tetramer predominates

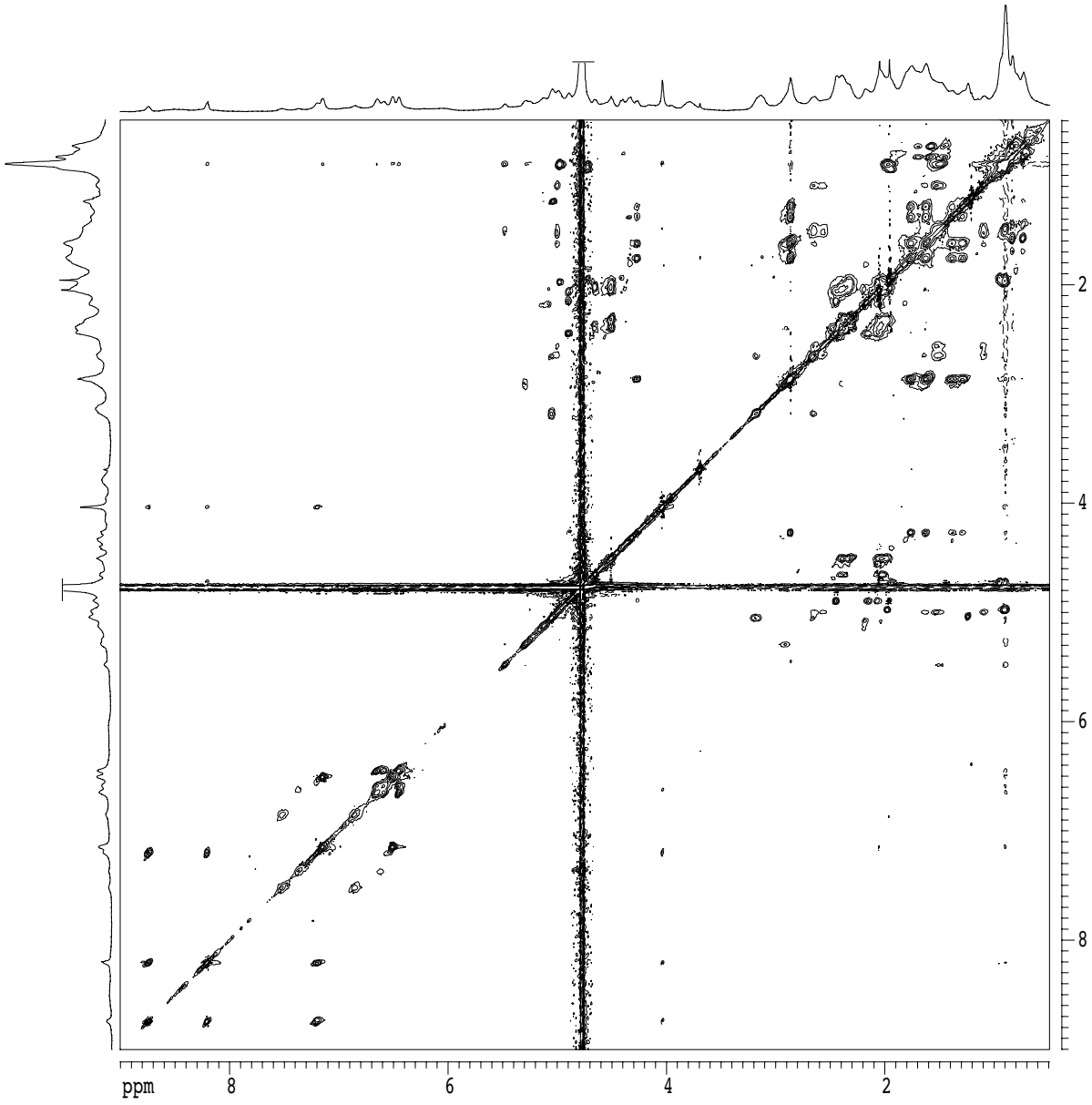

2D NOESY spectrum of macrocyclic β-sheet **4.3**
2 mM in D_2O, 500 MHz, 298 K
200-ms spin-locking mixing time
tetramer predominates

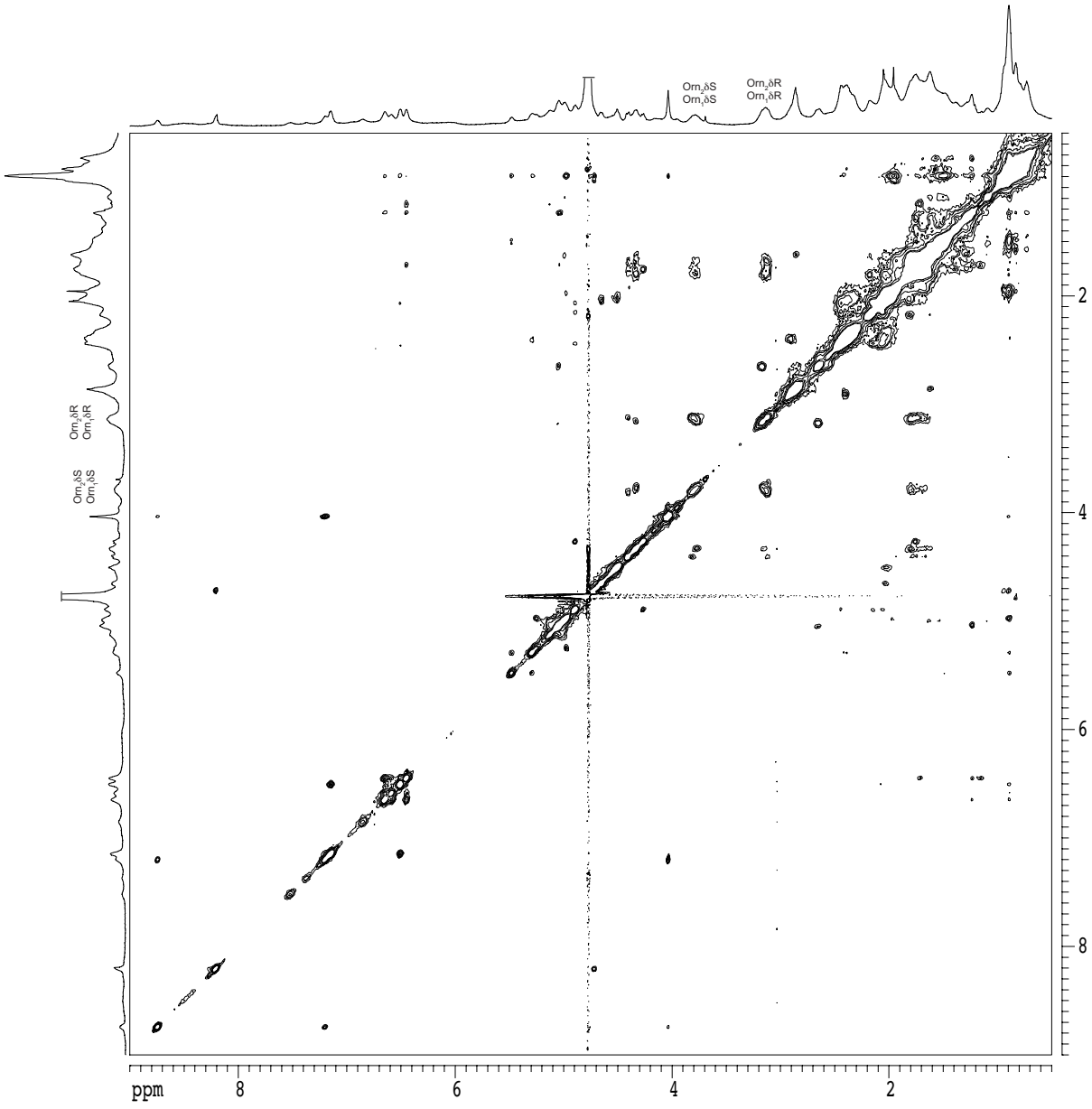

2D DOSY spectrum of macrocyclic β-sheet **4.3**
2 mM in D_2O, 600 MHz, 298 K
tetramer predominates

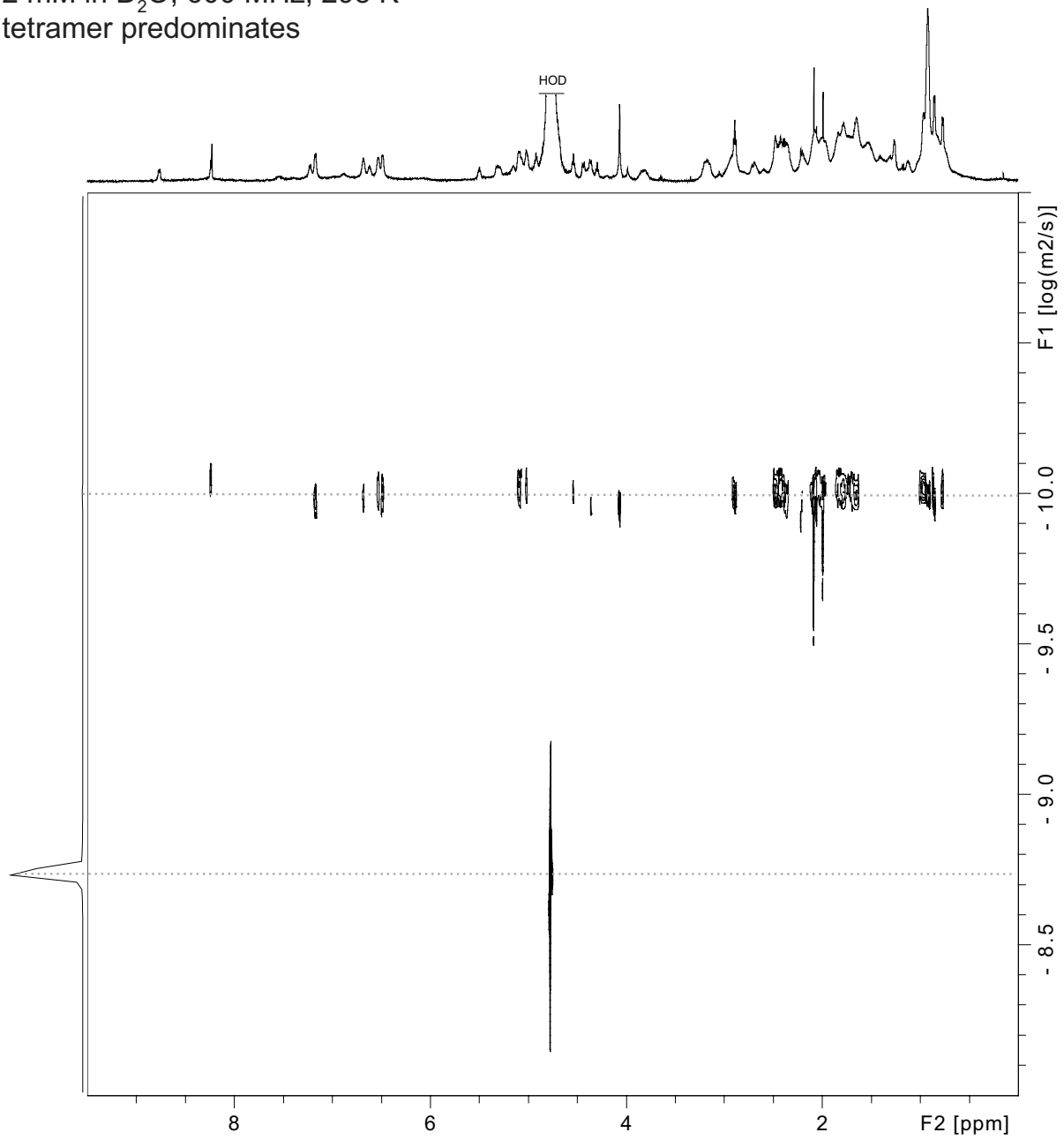

Calculation for peptide **4.3** at 2.0 mM

DC_{HOD} = 19.0 x 10^{-10} m^2/s [a]
log DC_{HOD} = -8.721

For peptide **4.3** tetramer, log DC (m^2/s) = -9.99(4), DC = $10^{-9.994}$ m^2/s = 10.1 x 10^{-11} m^2/s = 10.1 x 10^{-7} cm^2/s

[a] Longsworth, L. G. J. Phys. Chem. 1960, 64, 1914–1917.

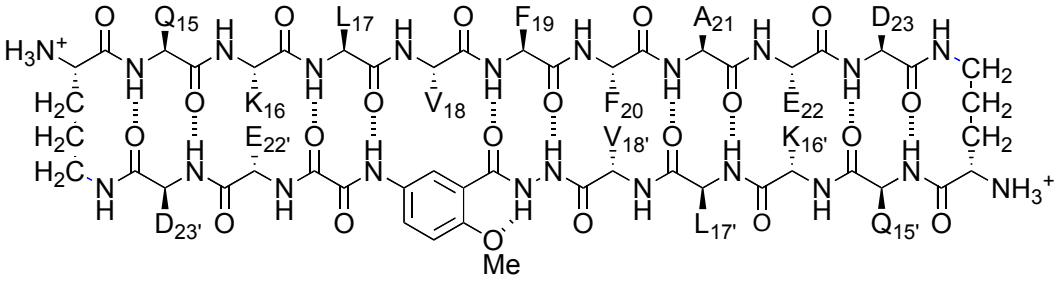

macrocyclic β-sheet peptide **4.4** (as the TFA salt)

molecular weight calculated for $C_{103}H_{156}N_{26}O_{31} \bullet 4CF_3CO_2H$ (TFA salt of **4.4**): 2710.59
molecular weight calculated for $C_{103}H_{156}N_{26}O_{31}$ (free base of **4.4**): 2254.50
exact mass calculated for $C_{103}H_{156}N_{26}O_{31}$ (free base of **4.4**): 2253.14

Analytical RP-HPLC of macrocyclic β-peptide **4.4**

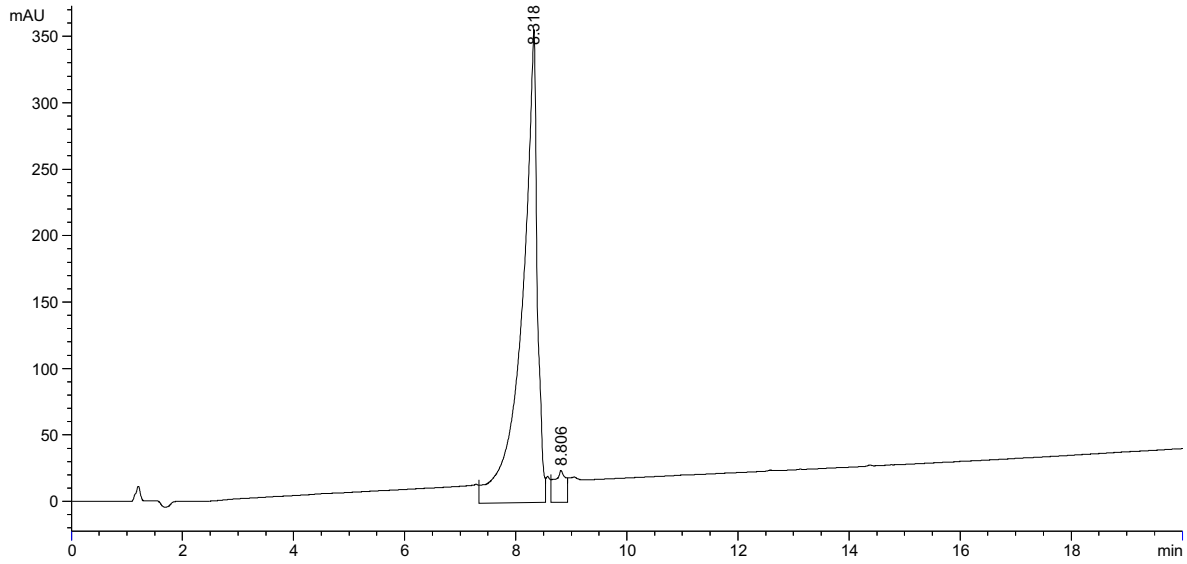

Signal 1: VWD1 A, Wavelength=254 nm

Peak #	RetTime [min]	Type	Width [min]	Area mAU *s	Height [mAU]	Area %
1	8.318	VV	0.2395	6692.11328	356.28714	95.1129
2	8.806	VV	0.1819	343.85294	23.96618	4.8871

Macrocyclic β-sheet peptide **4.4**

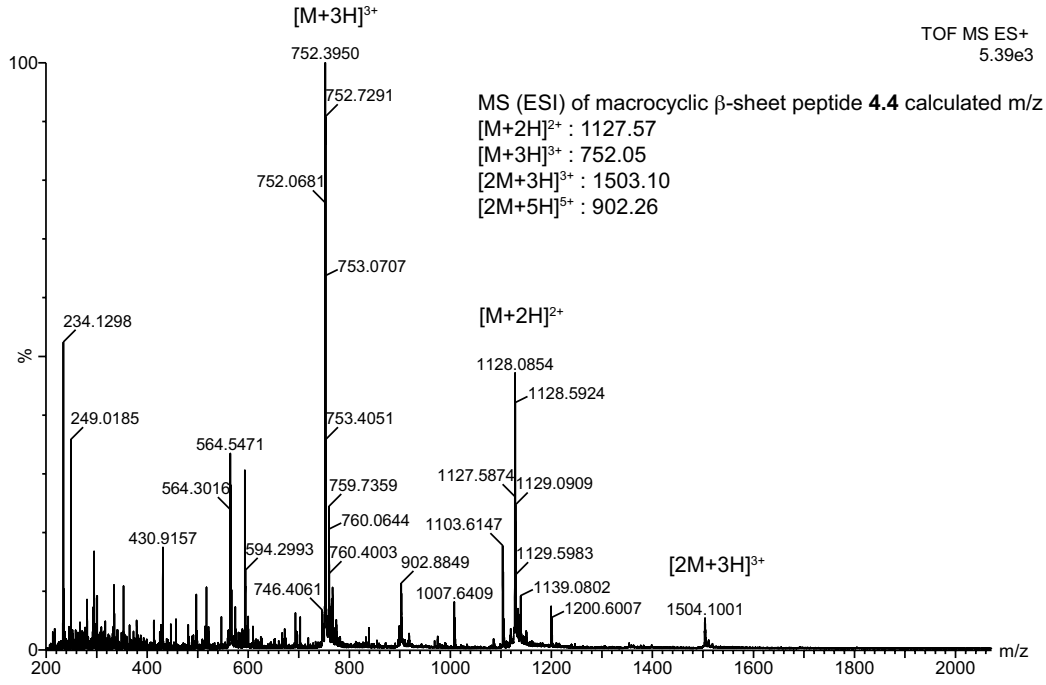

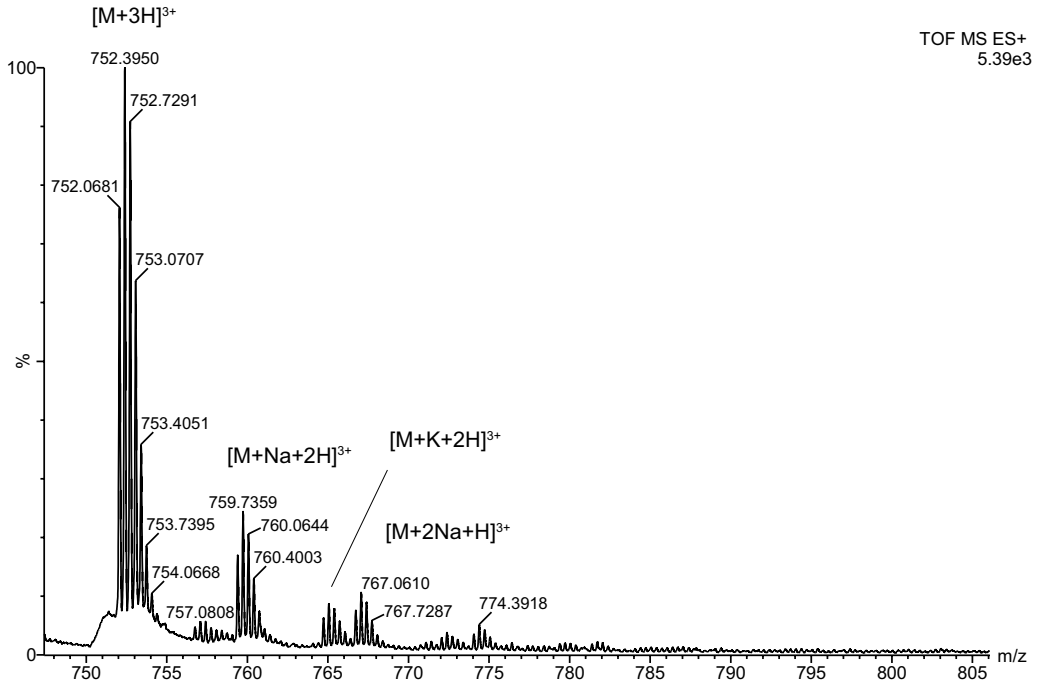

Macrocyclic β-sheet peptide **4.4**

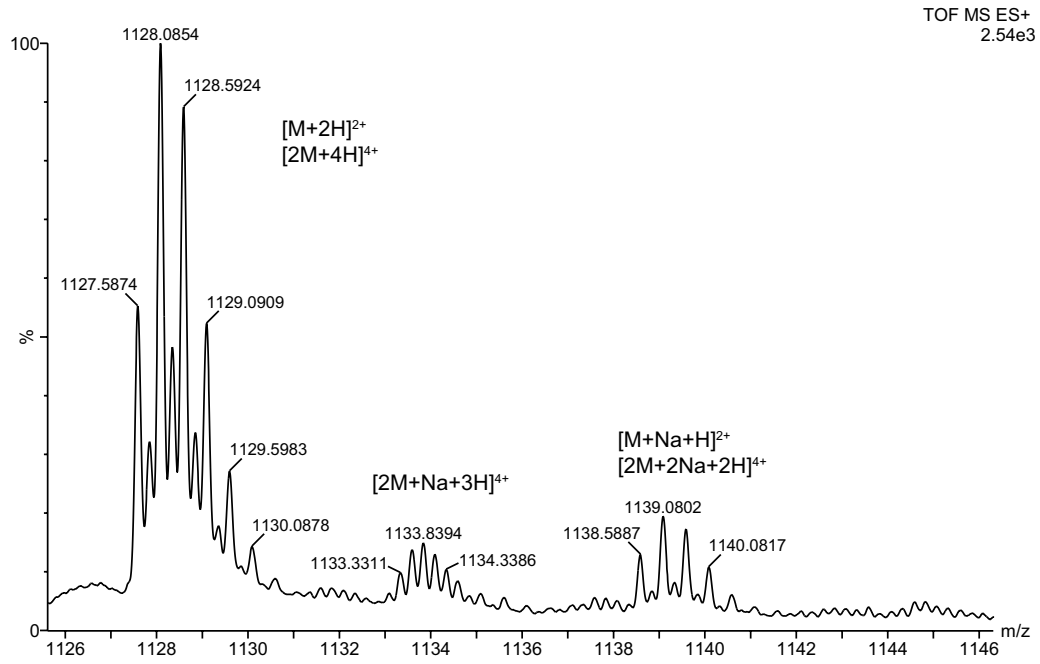

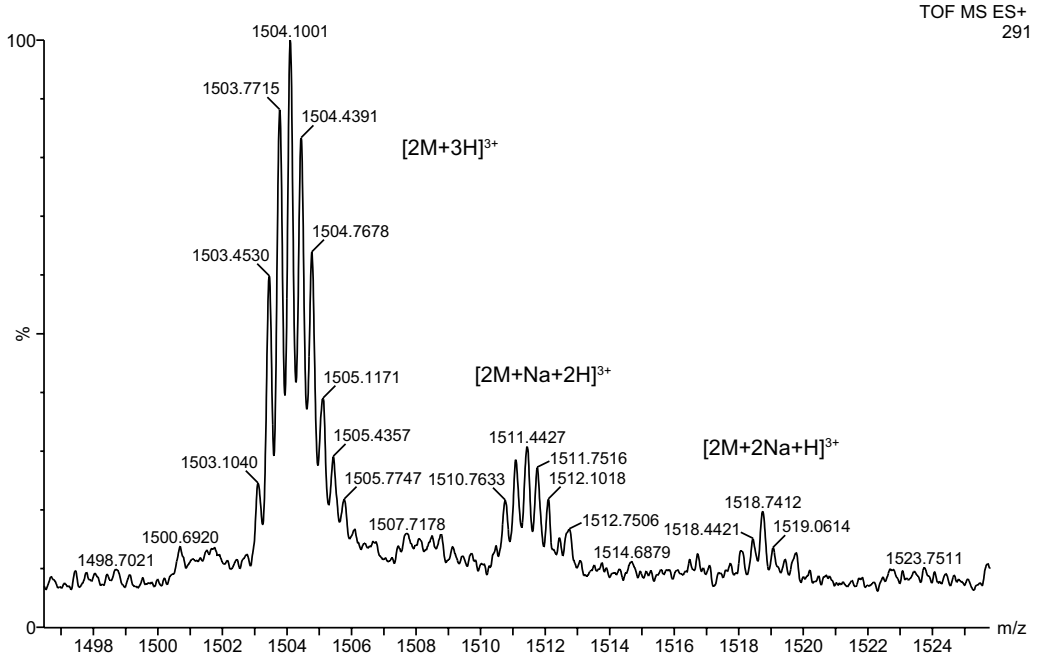

Macrocyclic β-sheet peptide **4.4**

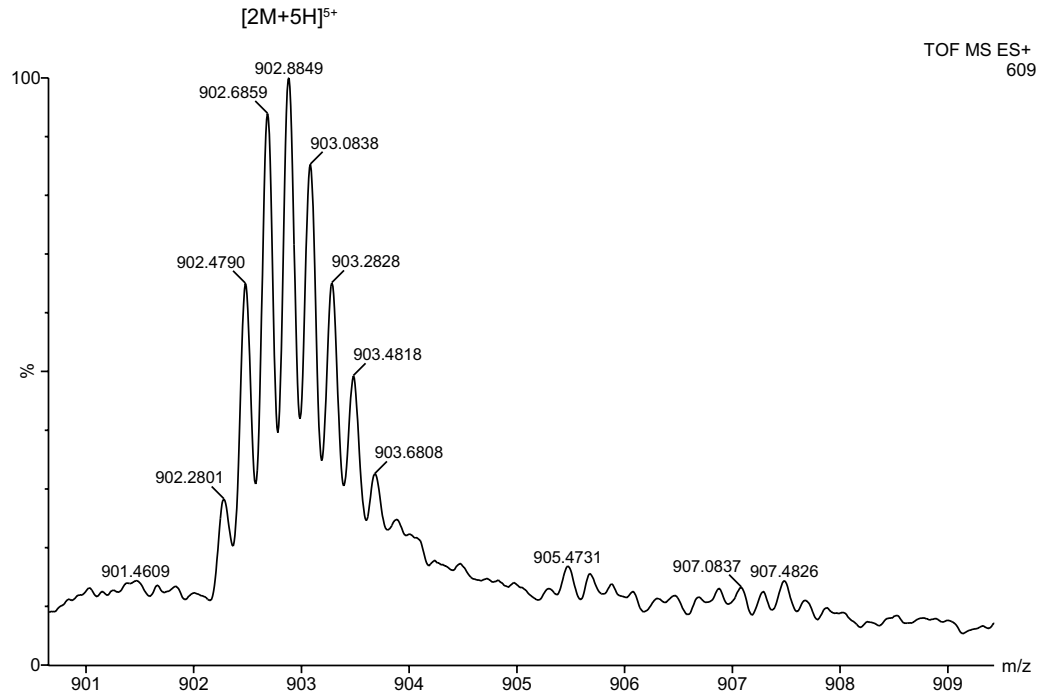

1D ^{1}H NMR spectrum of macrocyclic β-sheet **4.4**
2 mM in D_2O, 500 MHz, 298 K
tetramer predominates

Assignments of Lys_{16} vs. $Lys_{16'}$, Glu_{23} vs. $Glu_{23'}$, Gln_{15} vs. $Gln_{15'}$, and Orn_1 vs Orn_2 are arbitrary

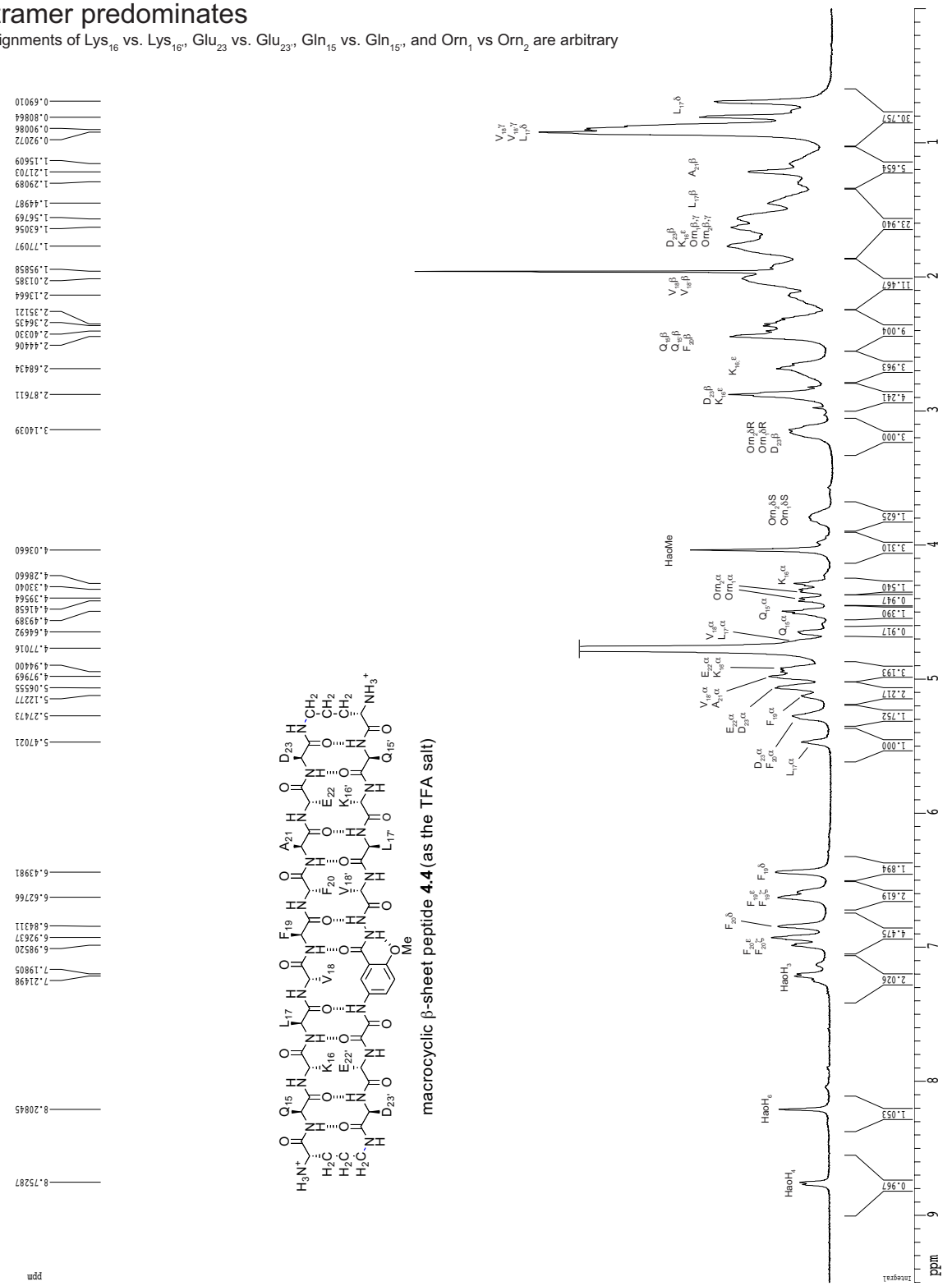

macrocyclic β-sheet peptide **4.4** (as the TFA salt)

2D TOCSY spectrum of macrocyclic β-sheet **4.4**
2 mM in D_2O, 500 MHz, 298 K
150-ms spin-locking mixing time
tetramer predominates

Assignments of Lys_{16} vs. $Lys_{16'}$, Glu_{23} vs. $Glu_{23'}$, Gln_{15} vs. $Gln_{15'}$, and Orn_1 vs Orn_2 are arbitrary

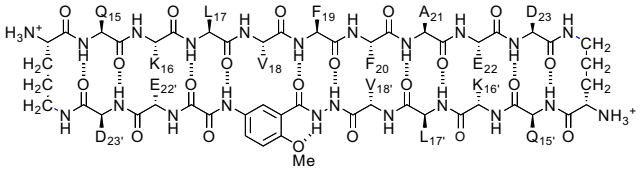

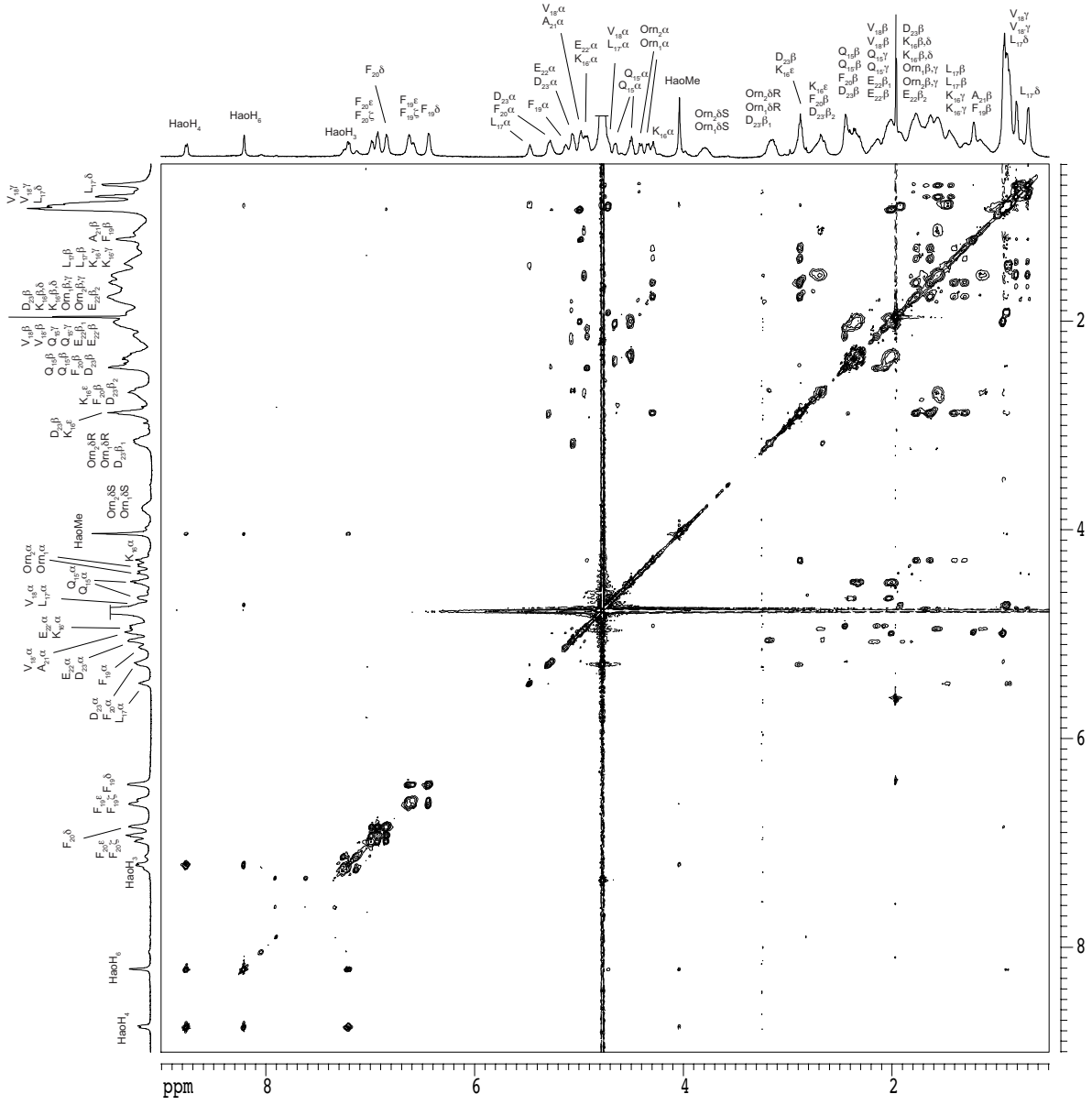

2D TOCSY spectrum of macrocyclic β-sheet **4.4**
2 mM in D_2O, 500 MHz, 298 K, 150-ms spin-locking mixing time
tetramer predominates

Assignments of Lys_{16} vs. $Lys_{16'}$, Glu_{23} vs. $Glu_{23'}$, Gln_{15} vs. $Gln_{15'}$, and Orn_1 vs Orn_2 are arbitrary

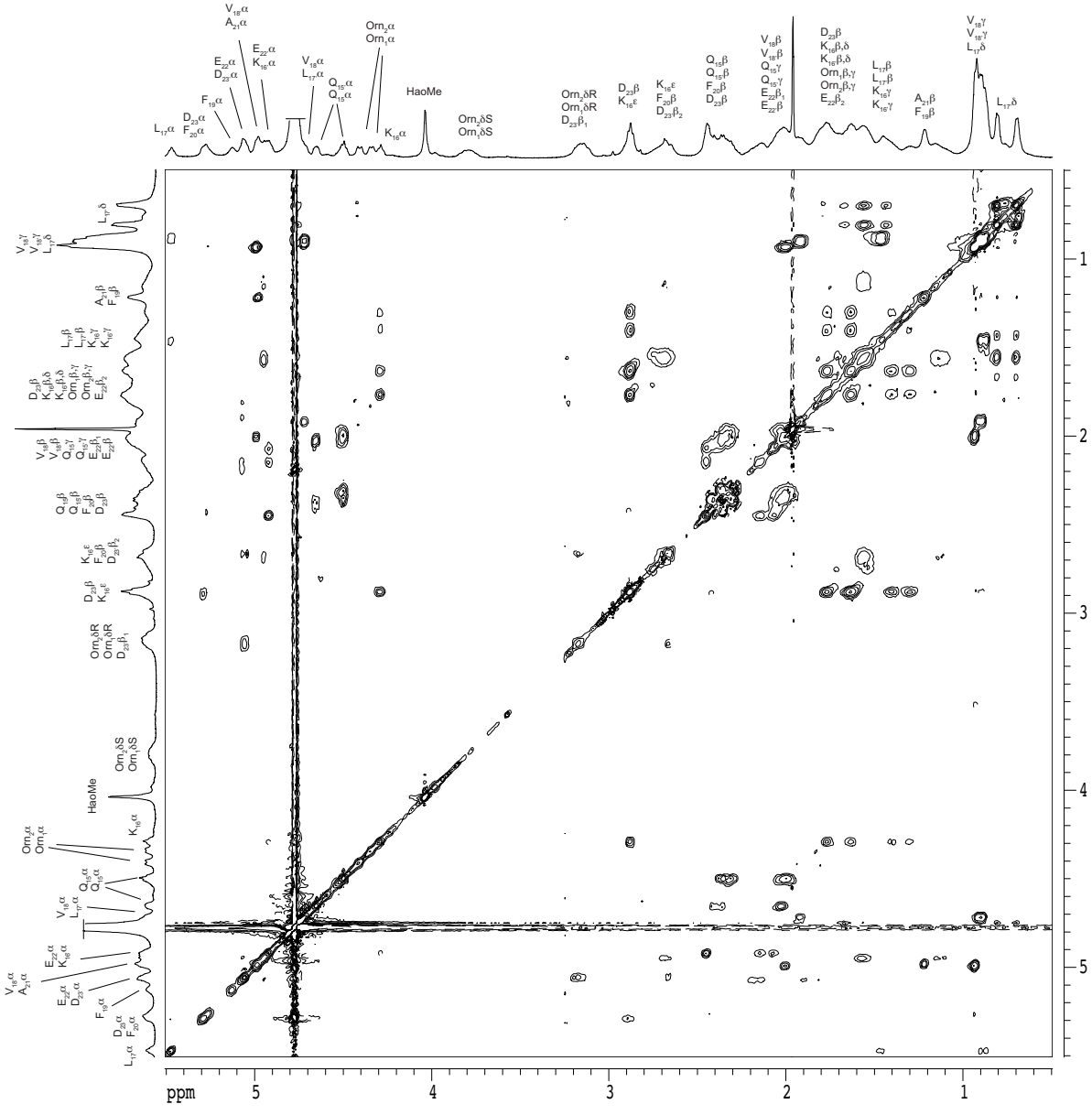

2D TOCSY spectrum of macrocyclic β-sheet **4.4**
2 mM in D_2O, 500 MHz, 298 K, 150-ms spin-locking mixing time
tetramer predominates

Assignments of Lys_{16} vs. $Lys_{16'}$, Glu_{23} vs. $Glu_{23'}$, Gln_{15} vs. $Gln_{15'}$, and Orn_1 vs Orn_2 are arbitrary

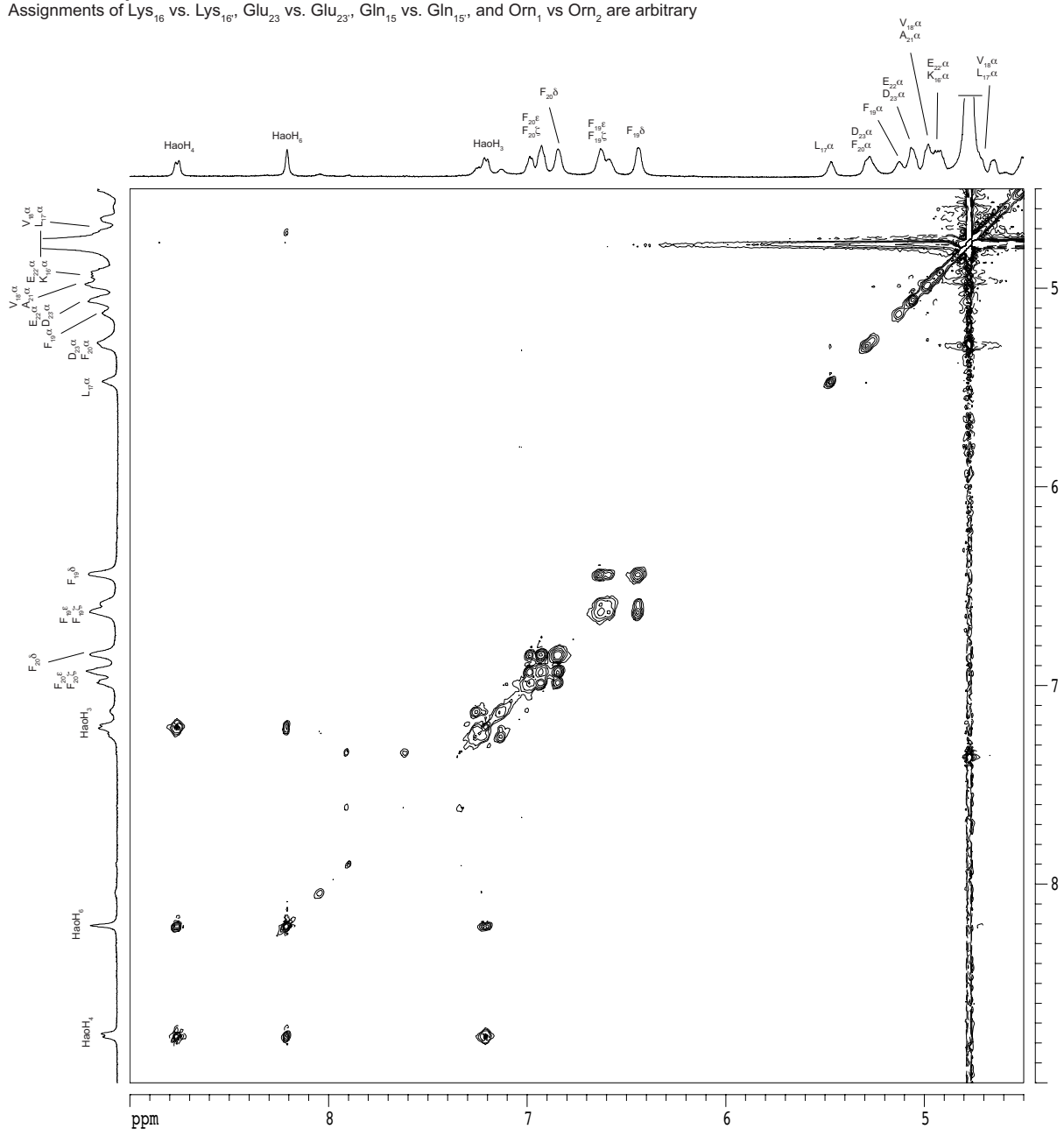

2D NOESY spectrum of macrocyclic β-sheet **4.4**
2 mM in D_2O, 500 MHz, 298 K
200-ms spin-locking mixing time
tetramer predominates

Assignments of Lys_{16} vs. $Lys_{16'}$, Glu_{23} vs. $Glu_{23'}$, Gln_{15} vs. $Gln_{15'}$, and Orn_1 vs Orn_2 are arbitrary

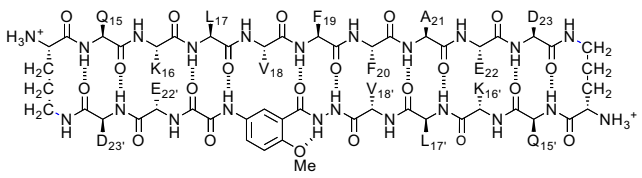

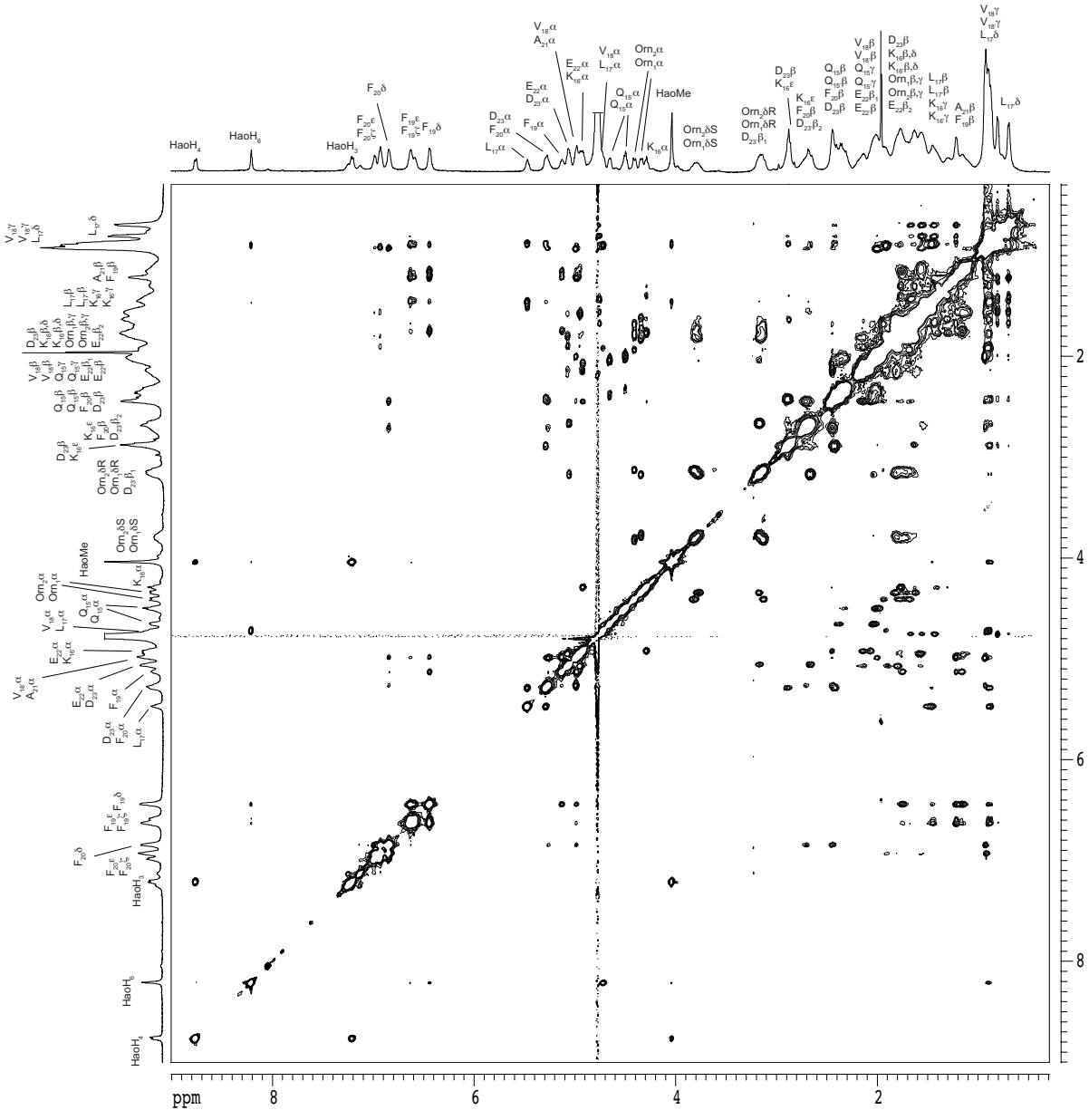

2D NOESY spectrum of macrocyclic β-sheet **4.4**
2 mM in D_2O, 500 MHz, 298 K, 200-ms spin-locking mixing time
tetramer predominates

Assignments of Lys_{16} vs. $Lys_{16'}$, Glu_{23} vs. $Glu_{23'}$, Gln_{15} vs. $Gln_{15'}$, and Orn_1 vs Orn_2 are arbitrary

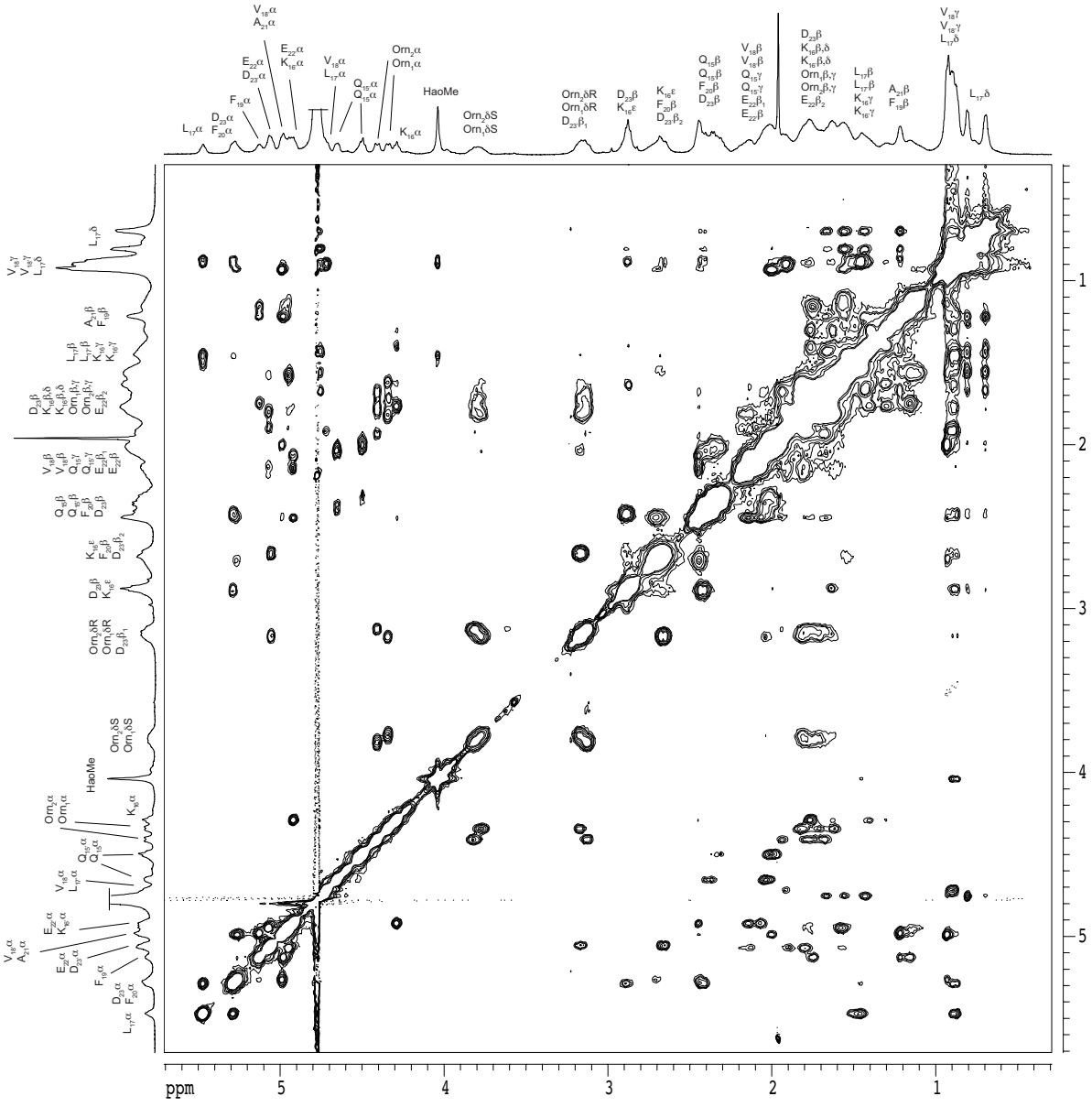

2D NOESY spectrum of macrocyclic β-sheet **4.4**
2 mM in D_2O, 500 MHz, 298 K, 200-ms spin-locking mixing time
tetramer predominates

Assignments of Lys_{16} vs. $Lys_{16'}$, Glu_{23} vs. $Glu_{23'}$, Gln_{15} vs. $Gln_{15'}$, and Orn_1 vs Orn_2 are arbitrary

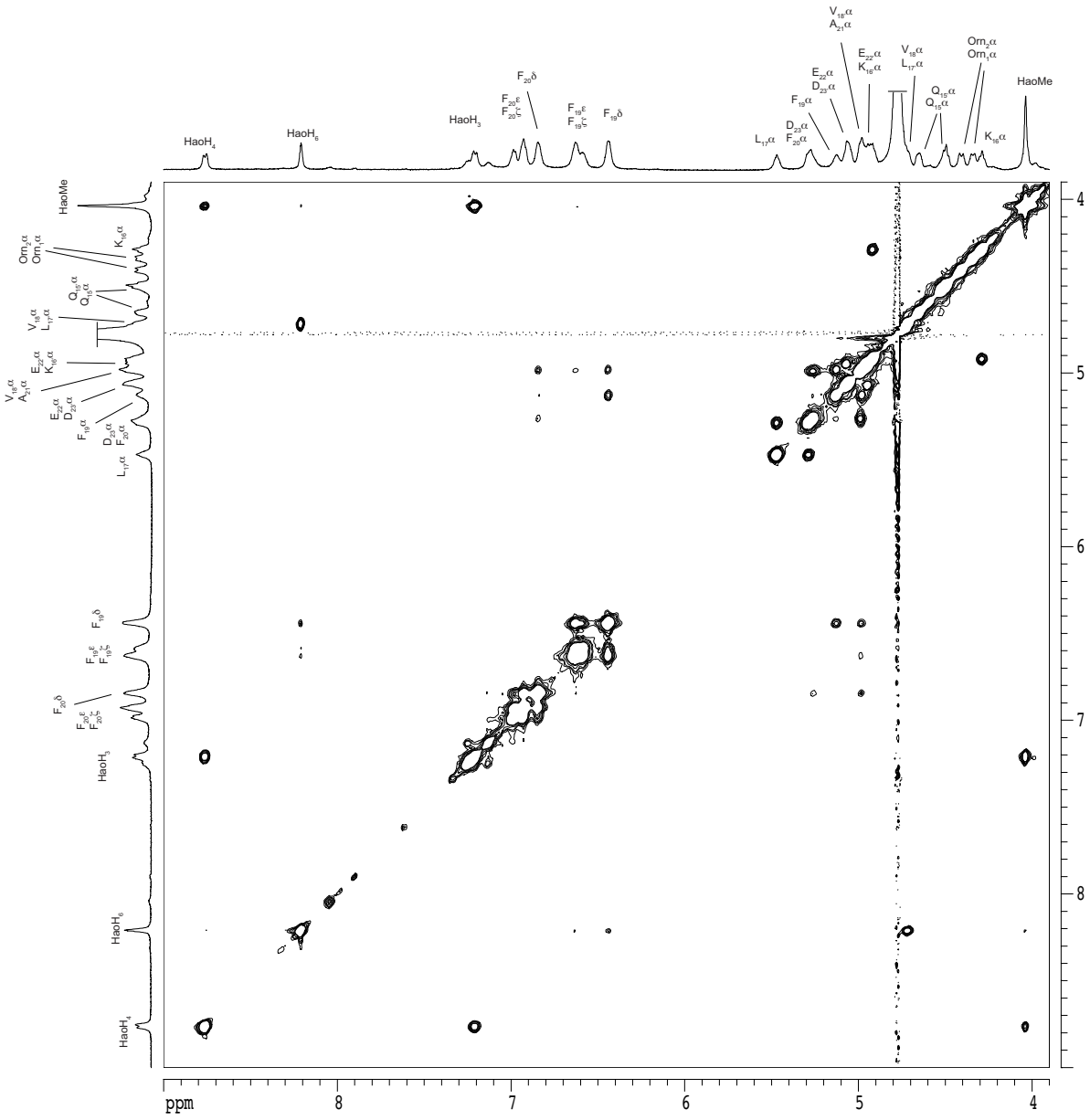

2D NOESY spectrum of macrocyclic β-sheet **4.4**
2 mM in D_2O, 500 MHz, 298 K, 200-ms spin-locking mixing time
tetramer predominates

Assignments of Lys_{16} vs. $Lys_{16'}$, Glu_{23} vs. $Glu_{23'}$, Gln_{15} vs. $Gln_{15'}$, and Orn_1 vs Orn_2 are arbitrary

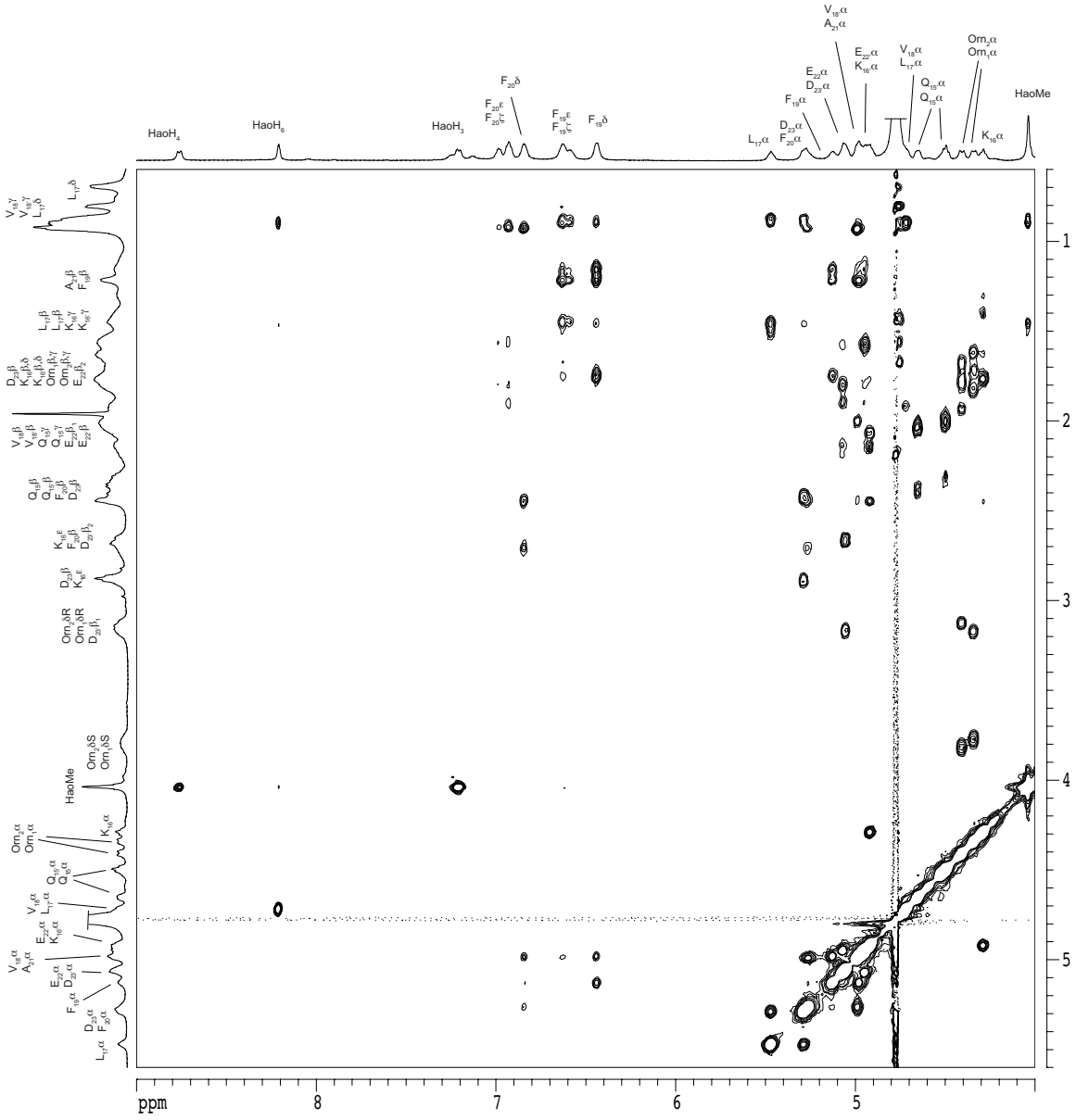

2D DOSY spectrum of macrocyclic β-sheet **4.4**
2 mM in D_2O, 600 MHz, 298 K
tetramer predominates

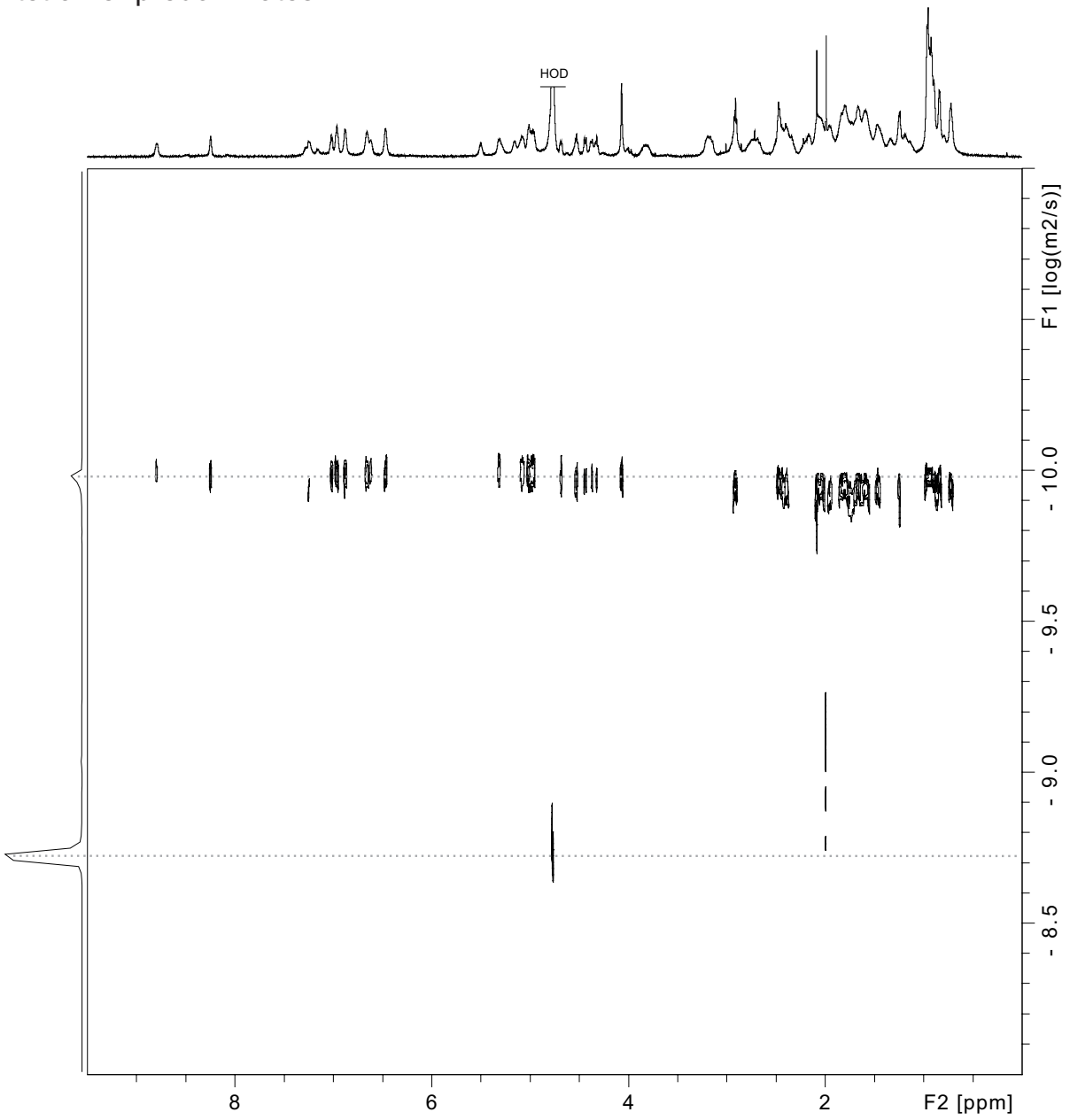

Calculation for peptide **4.4** at 2.0 mM

DC_{HOD} = 19.0 x 10^{-10} m^2/s [a]
log DC_{HOD} = -8.721

For peptide **4.4** tetramer, log DC (m^2/s) = -9.98(8), DC = $10^{-9.988}$ m^2/s = 10.3 x 10^{-11} m^2/s = 10.3 x 10^{-7} cm^2/s

[a] Longsworth, L. G. J. Phys. Chem. 1960, 64, 1914–1917.

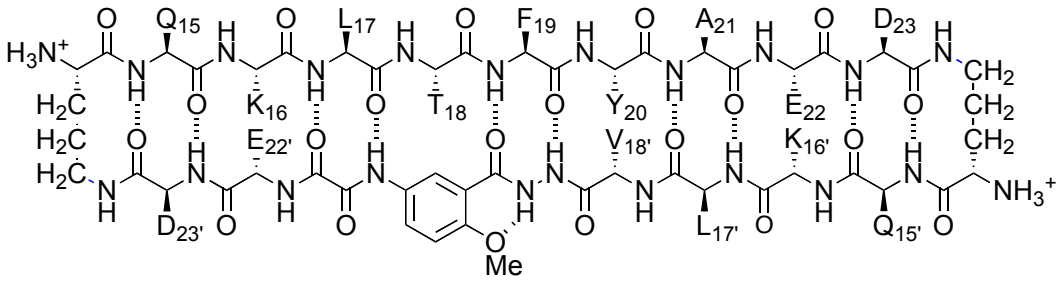

macrocyclic β-sheet peptide **4.5** (as the TFA salt)

molecular weight calculated for $C_{102}H_{154}N_{26}O_{33} \cdot 4CF_3CO_2H$ (TFA salt of **4.5**): 2728.56
molecular weight calculated for $C_{102}H_{154}N_{26}O_{33}$ (free base of **4.5**): 2272.47
exact mass calculated for $C_{102}H_{154}N_{26}O_{33}$ (free base of **4.5**): 2271.12

Analytical RP-HPLC of macrocyclic β-peptide **4.5**

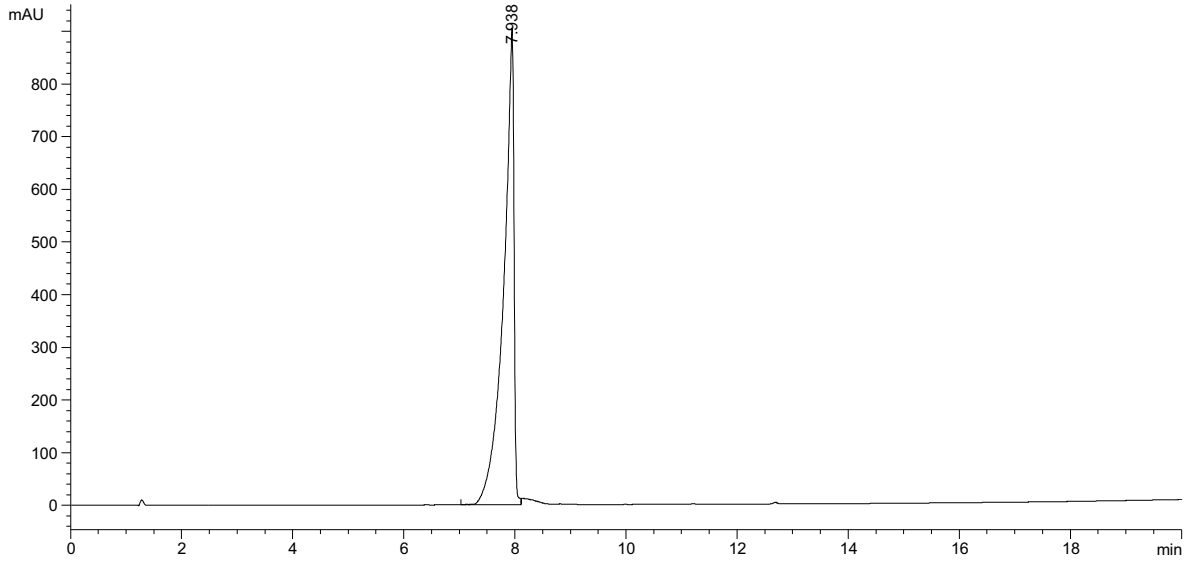


```
Signal 1: VWD1 A, Wavelength=254 nm

Peak RetTime Type  Width     Area      Height     Area
  #   [min]        [min]  mAU   *s   [mAU   ]       %
----|-------|----|-------|----------|----------|--------|
   1   7.938 VV    0.1715 1.17436e4   906.91034 100.0000

Totals :                  1.17436e4   906.91034
```

Macrocyclic β-sheet peptide **4.5**

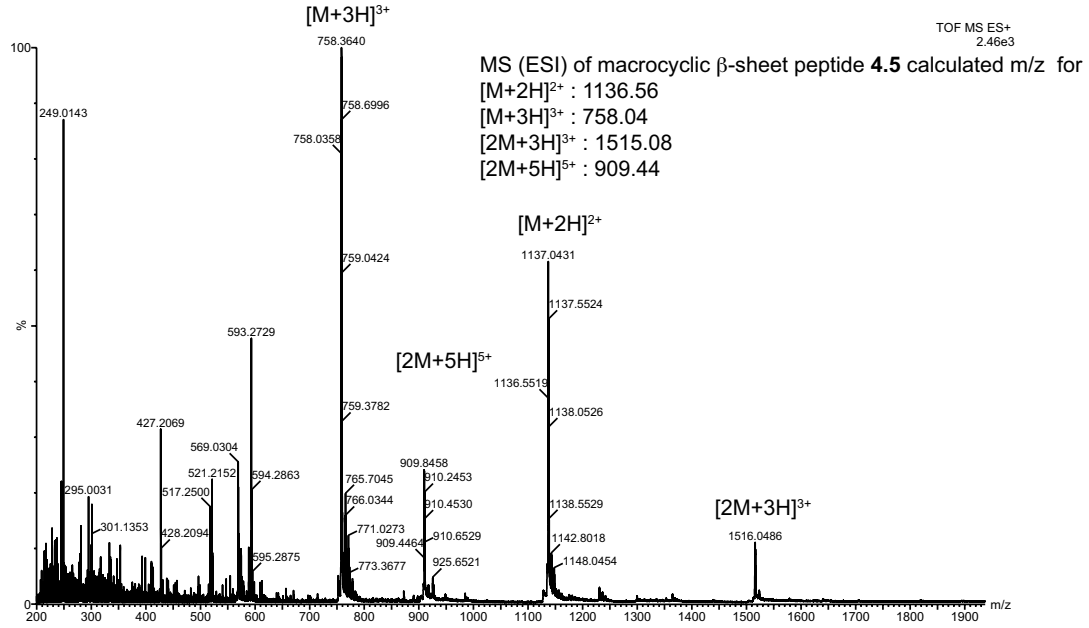

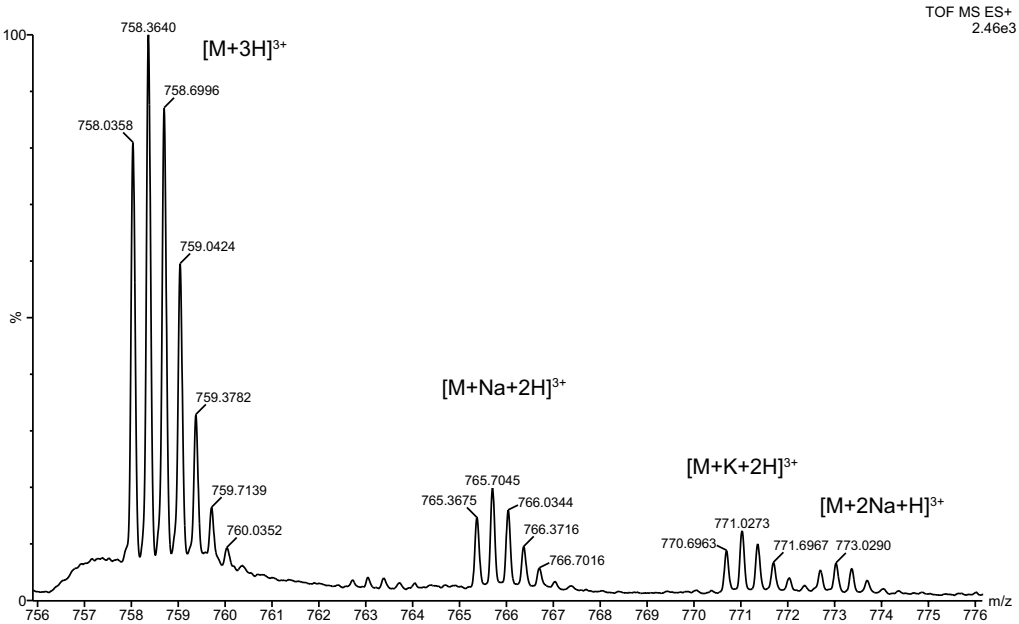

Macrocyclic β-sheet peptide **4.5**

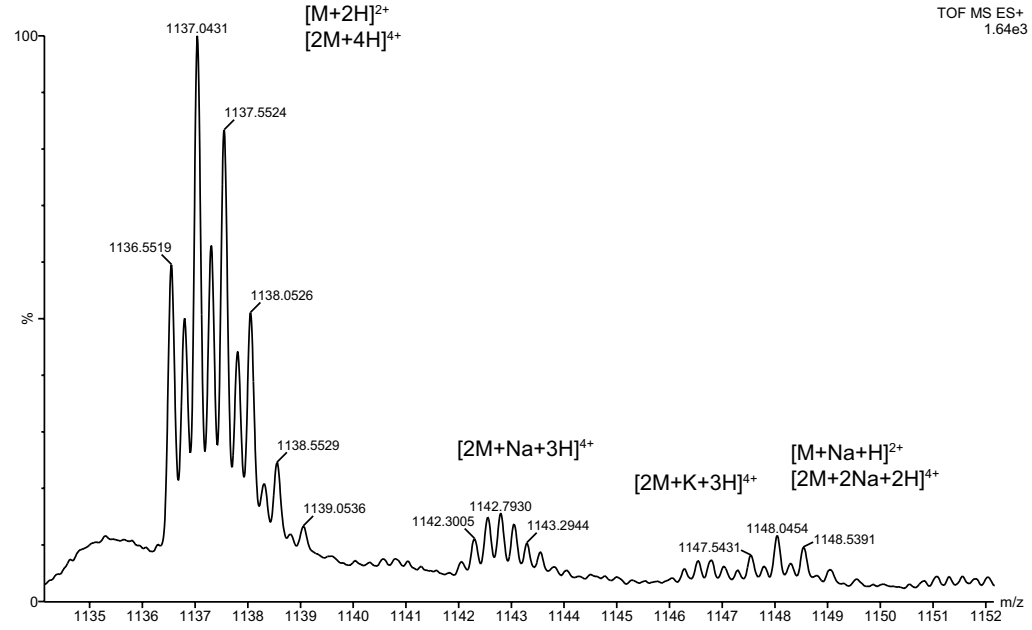

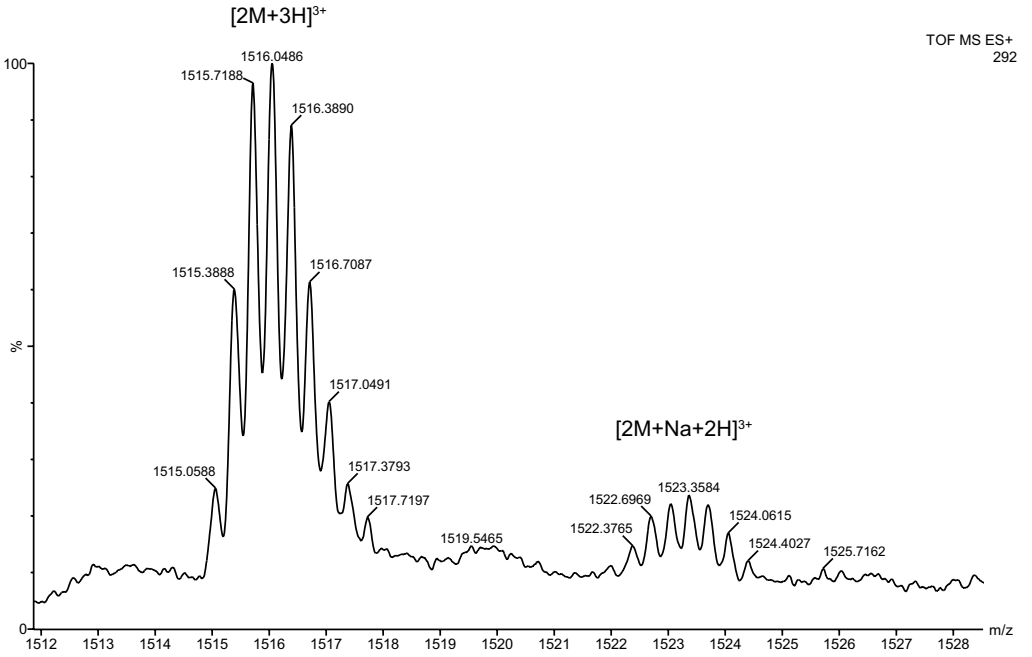

Macrocyclic β-sheet peptide **4.5**

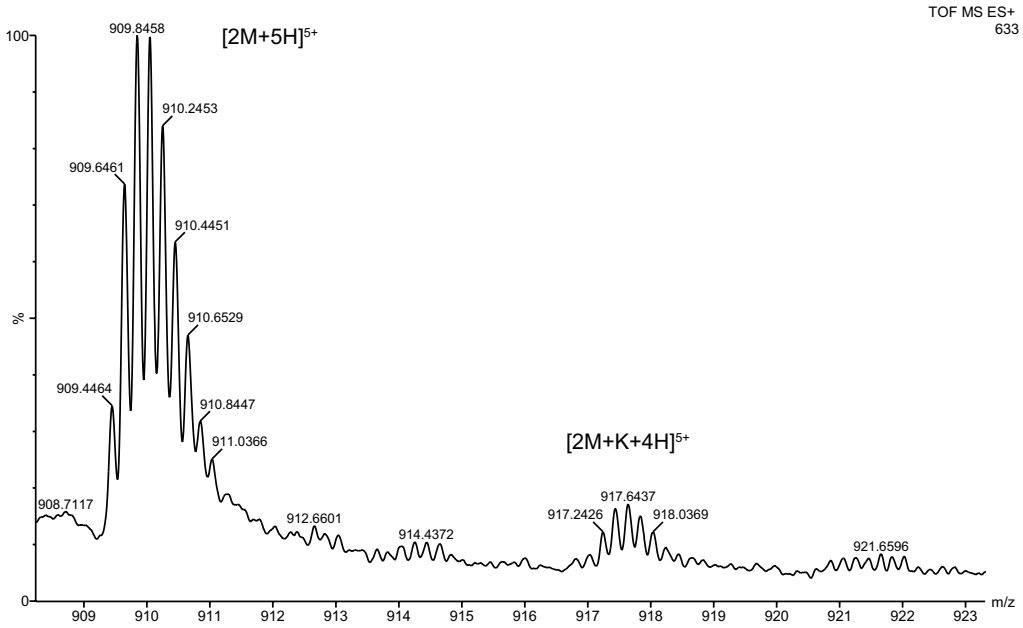

1D ^{1}H NMR spectrum of macrocyclic β-sheet **4.5**
2 mM in D_2O, 500 MHz, 298 K
tetramer predominates

Assignments of Lys_{16} vs. $Lys_{16'}$, Glu_{23} vs. $Glu_{23'}$, Gln_{15} vs. $Gln_{15'}$, and Orn_1 vs Orn_2 are arbitrary

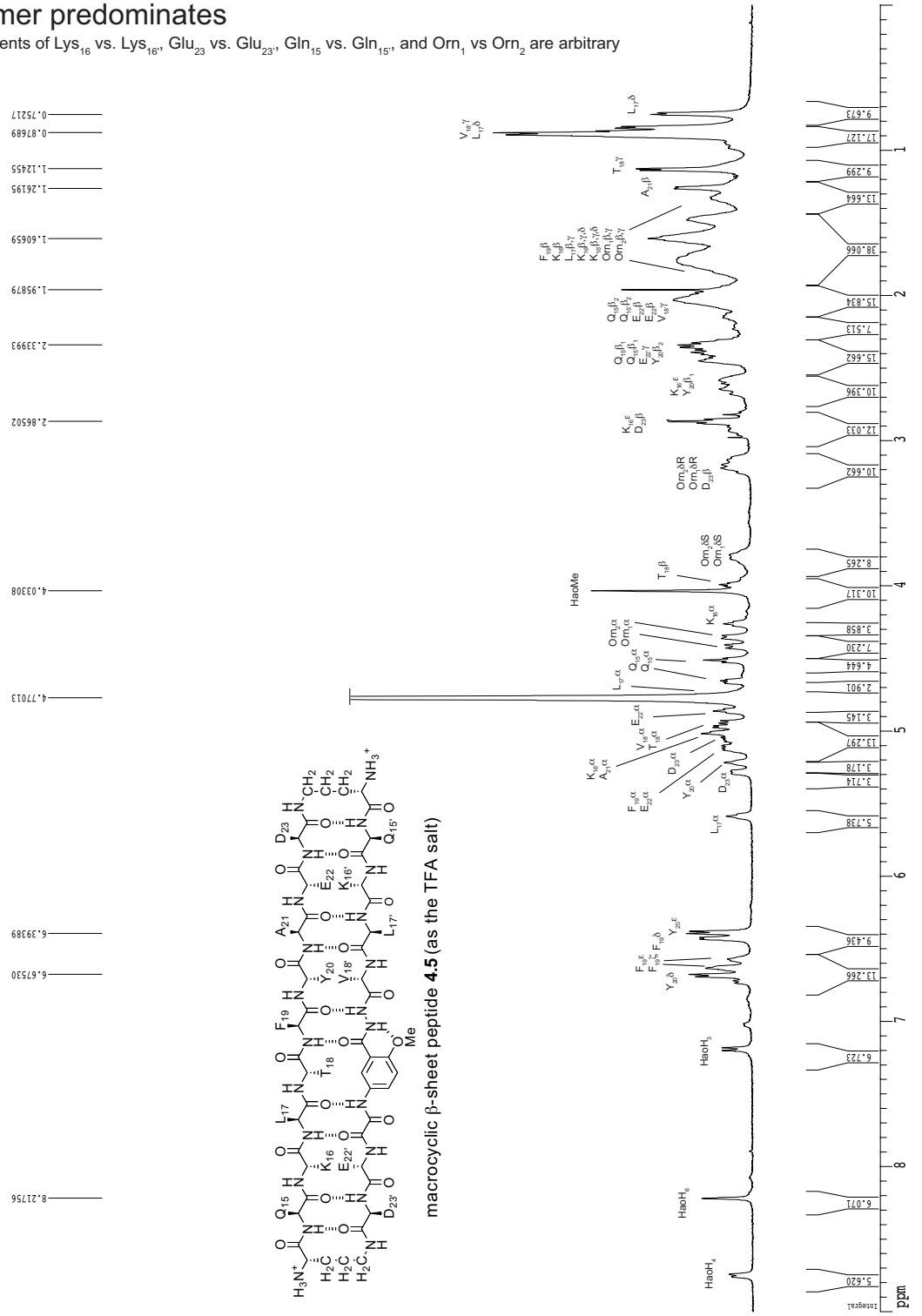

2D TOCSY spectrum of macrocyclic β-sheet **4.5**
2 mM in D_2O, 500 MHz, 298 K
150-ms spin-locking mixing time
tetramer predominates

Assignments of Lys_{16} vs. $Lys_{16'}$, Glu_{23} vs. $Glu_{23'}$, Gln_{15} vs. $Gln_{15'}$, and Orn_1 vs Orn_2 are arbitrary

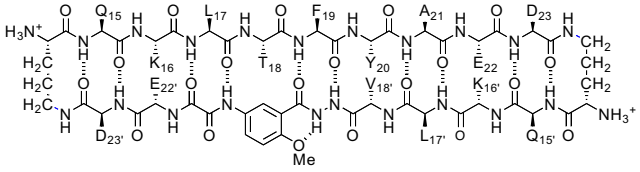

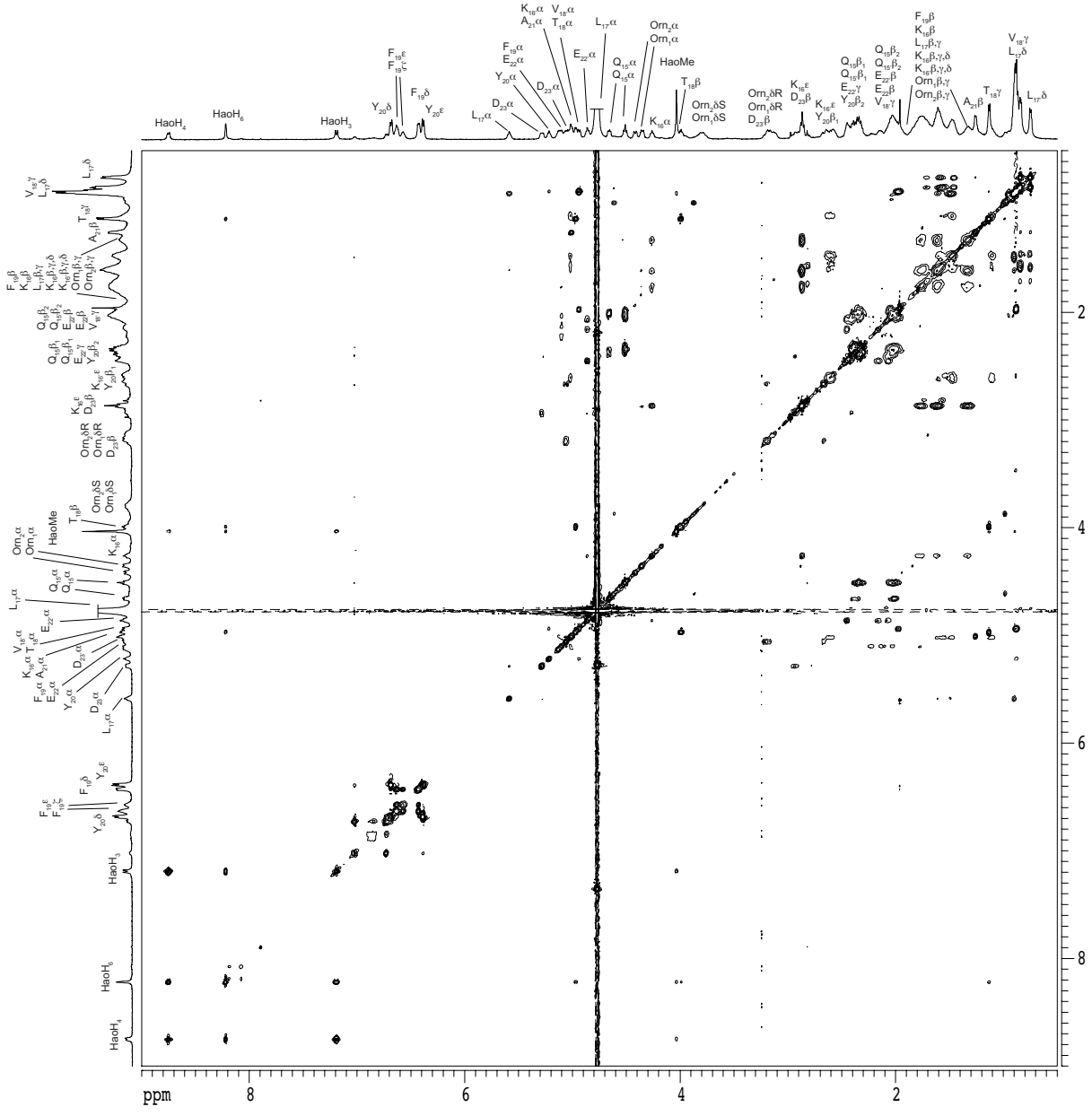

2D TOCSY spectrum of macrocyclic β-sheet **4.5**
2 mM in D_2O, 500 MHz, 298 K
150-ms spin-locking mixing time
tetramer predominates

Assignments of Lys_{16} vs. $Lys_{16'}$, Glu_{23} vs. $Glu_{23'}$, Gln_{15} vs. $Gln_{15'}$, and Orn_1 vs Orn_2 are arbitrary

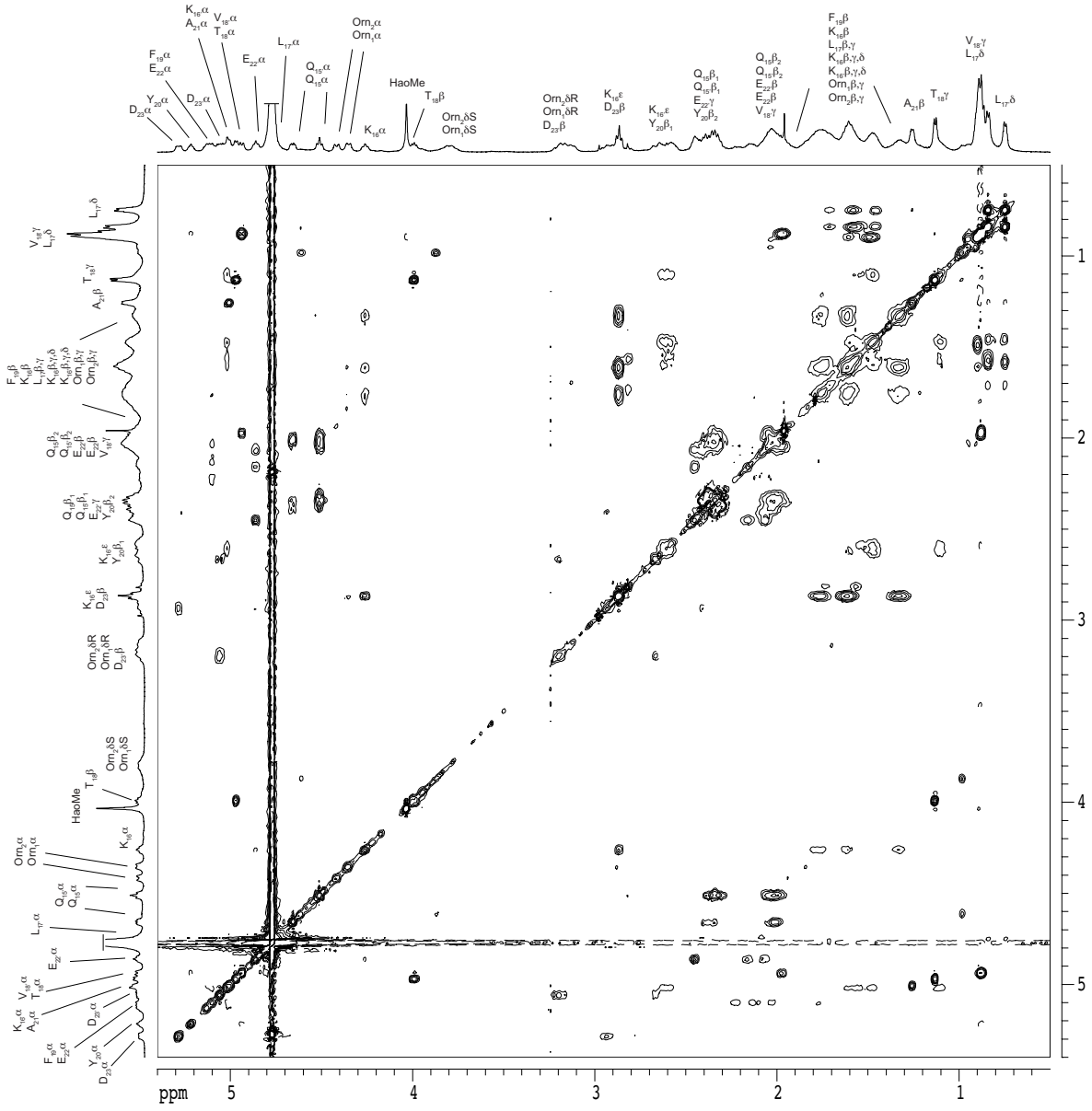

2D TOCSY spectrum of macrocyclic β-sheet **4.5**
2 mM in D_2O, 500 MHz, 298 K
150-ms spin-locking mixing time
tetramer predominates

Assignments of Lys_{16} vs. $Lys_{16'}$, Glu_{23} vs. $Glu_{23'}$, Gln_{15} vs. $Gln_{15'}$, and Orn_1 vs Orn_2 are arbitrary

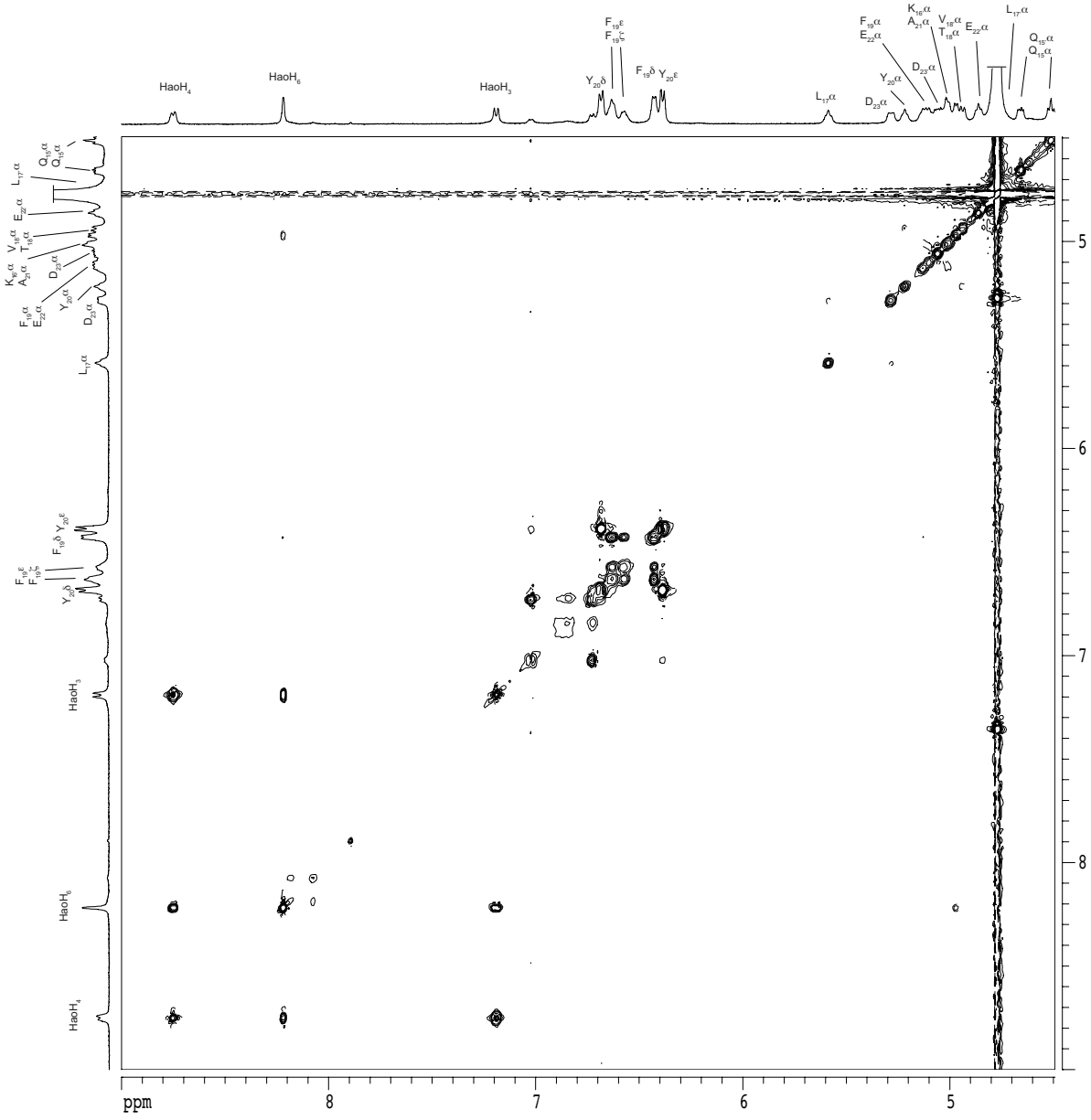

2D NOESY spectrum of macrocyclic β-sheet **4.5**
2 mM in D_2O, 500 MHz, 298 K
200-ms spin-locking mixing time
tetramer predominates

Assignments of Lys_{16} vs. $Lys_{16'}$, Glu_{23} vs. $Glu_{23'}$, Gln_{15} vs. $Gln_{15'}$, and Orn_1 vs Orn_2 are arbitrary

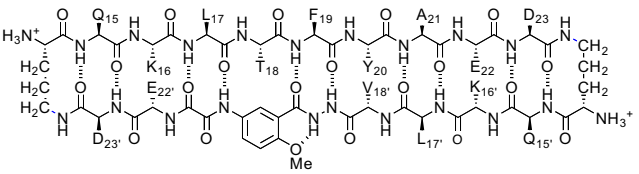

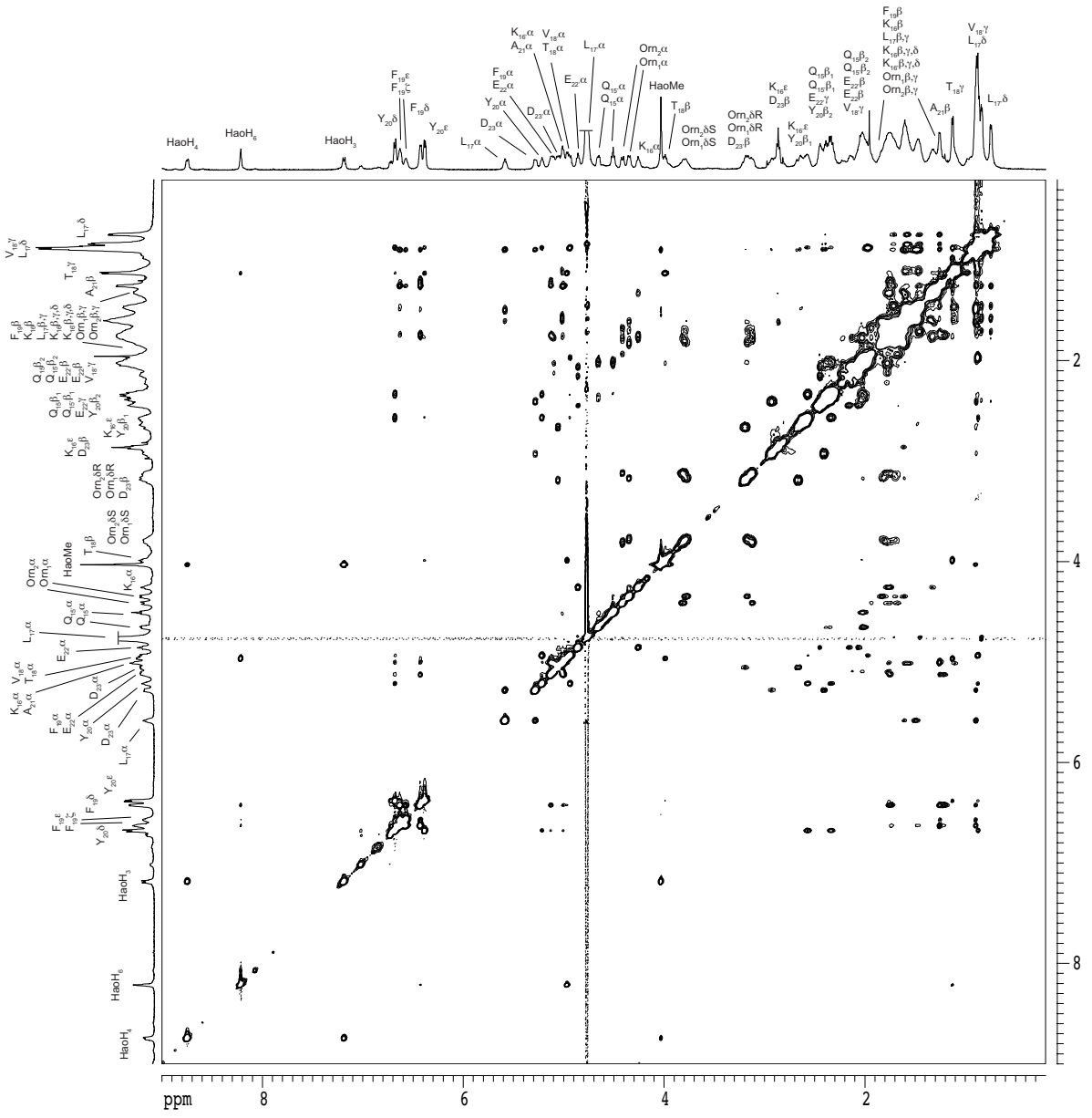

2D NOESY spectrum of macrocyclic β-sheet **4.5**
2 mM in D_2O, 500 MHz, 298 K
200-ms spin-locking mixing time
tetramer predominates

Assignments of Lys_{16} vs. $Lys_{16'}$, Glu_{23} vs. $Glu_{23'}$, Gln_{15} vs. $Gln_{15'}$, and Orn_1 vs Orn_2 are arbitrary

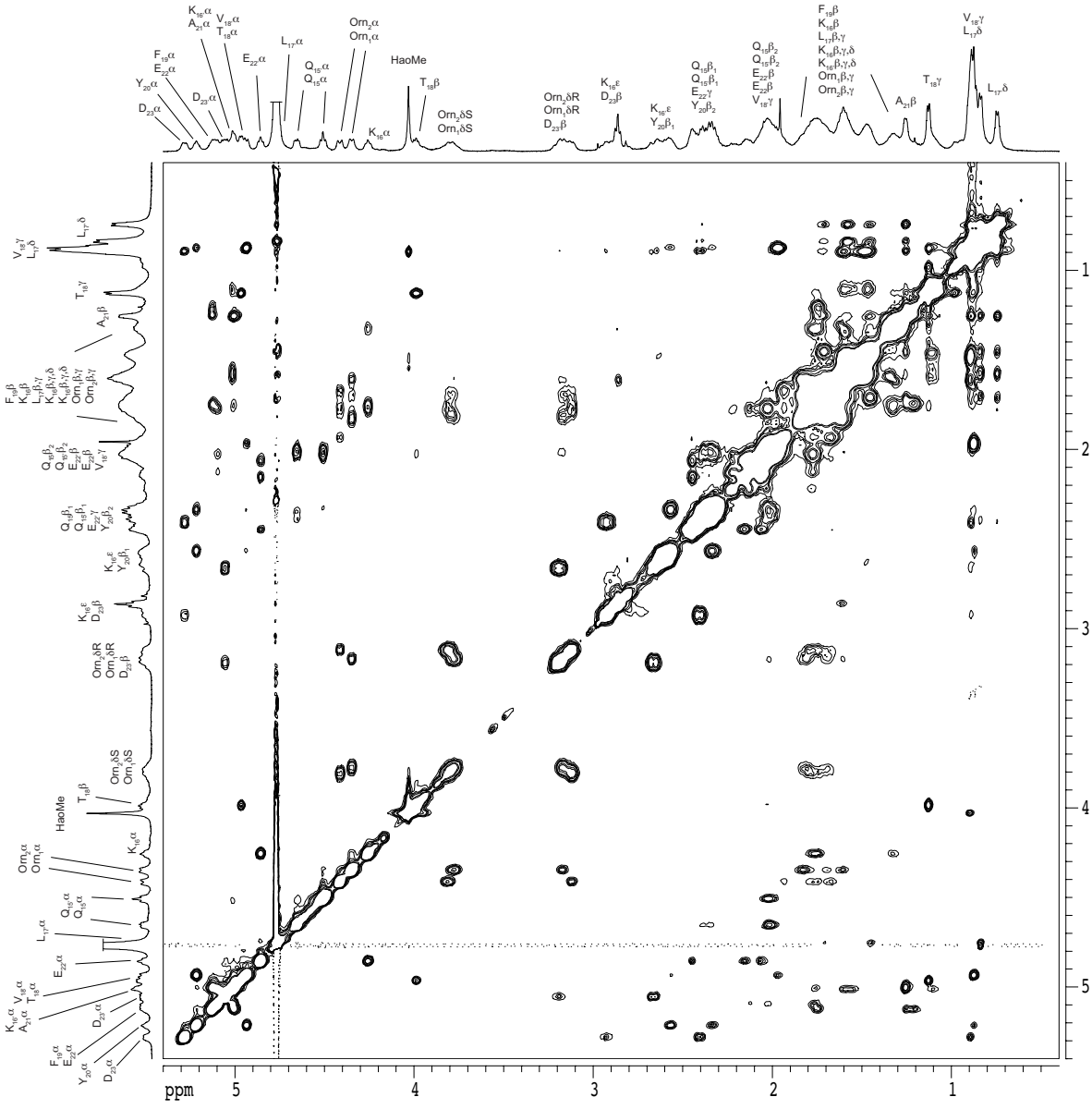

2D NOESY spectrum of macrocyclic β-sheet **4.5**
2 mM in D_2O, 500 MHz, 298 K
200-ms spin-locking mixing time
tetramer predominates

Assignments of Lys_{16} vs. $Lys_{16'}$, Glu_{23} vs. $Glu_{23'}$, Gln_{15} vs. $Gln_{15'}$, and Orn_1 vs Orn_2 are arbitrary

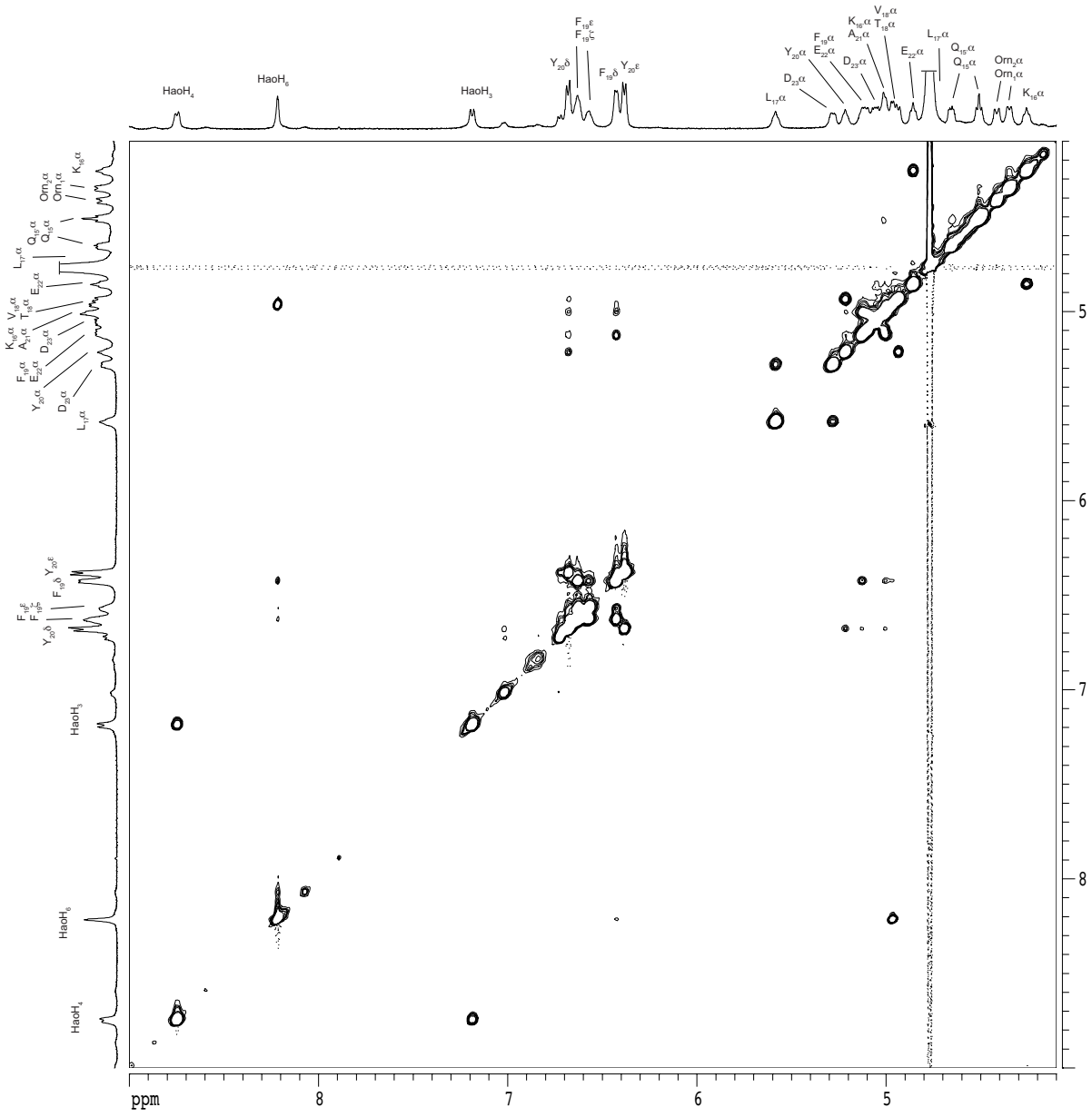

2D NOESY spectrum of macrocyclic β-sheet **4.5**
2 mM in D_2O, 500 MHz, 298 K
200-ms spin-locking mixing time
tetramer predominates

Assignments of Lys_{16} vs. $Lys_{16'}$, Glu_{23} vs. $Glu_{23'}$, Gln_{15} vs. $Gln_{15'}$, and Orn_1 vs Orn_2 are arbitrary

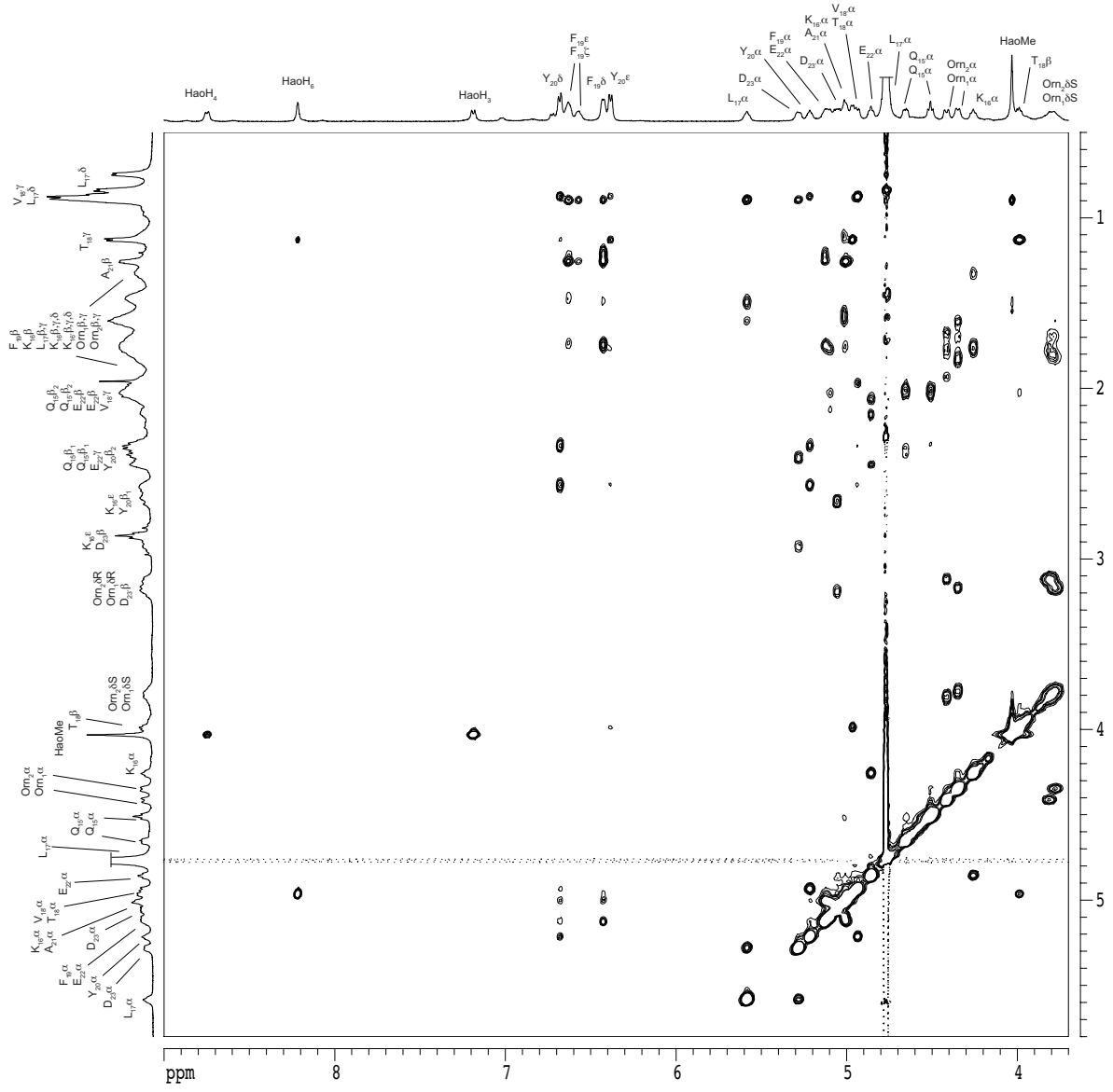

2D DOSY spectrum of macrocyclic β-sheet **4.5**
2 mM in D_2O, 600 MHz, 298 K
tetramer predominates

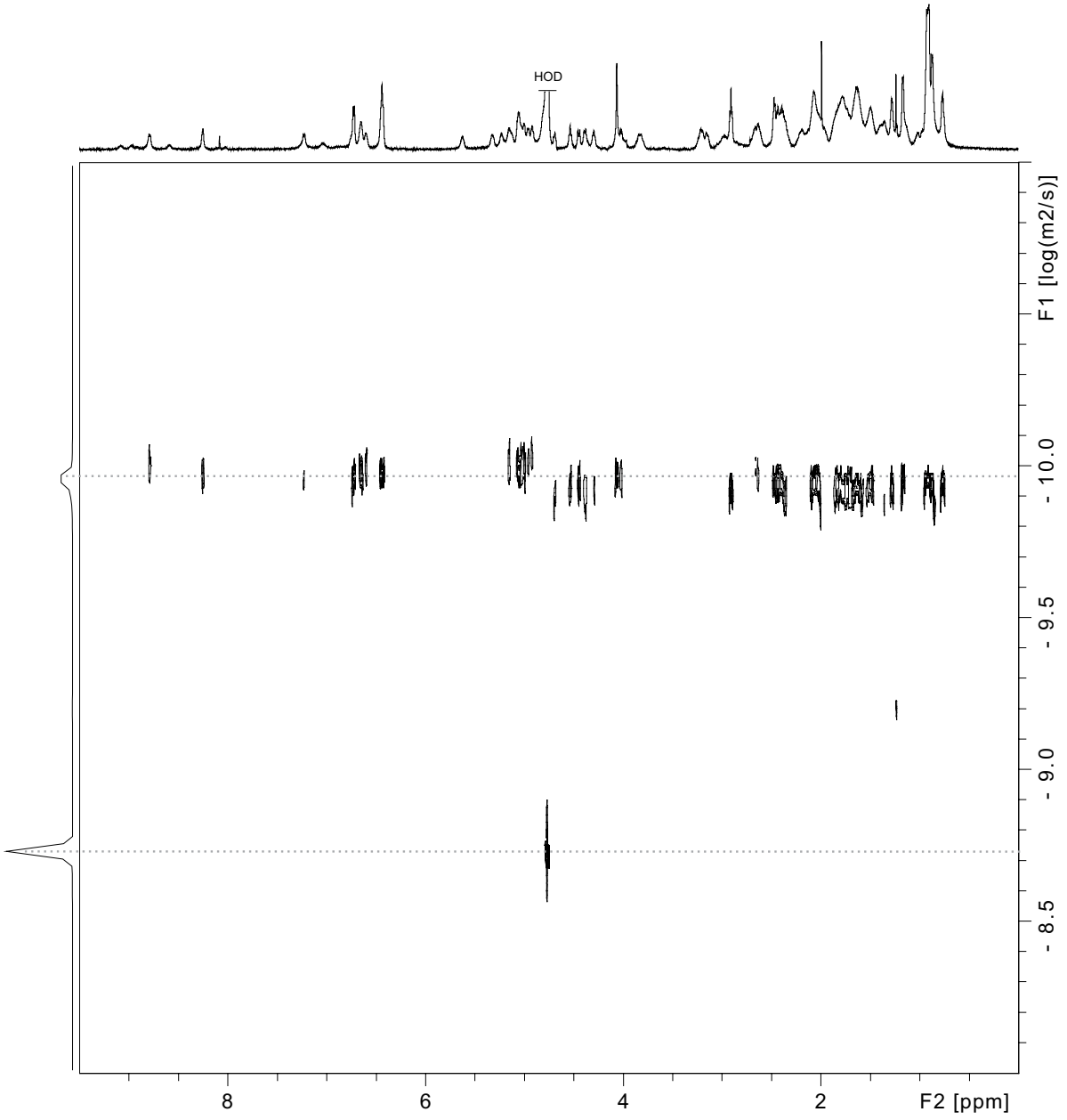

Calculation for peptide **4.5** at 2.0 mM

DC_{HOD} = 19.0 x 10^{-10} m^2/s [a]
log DC_{HOD} = -8.721

For peptide **4.5** tetramer, log DC (m^2/s) = -9.97(0), DC = $10^{-9.970}$ m^2/s = 10.7 x 10^{-11} m^2/s = 10.7 x 10^{-7} cm^2/s

[a] Longsworth, L. G. J. Phys. Chem. 1960, 64, 1914–1917.

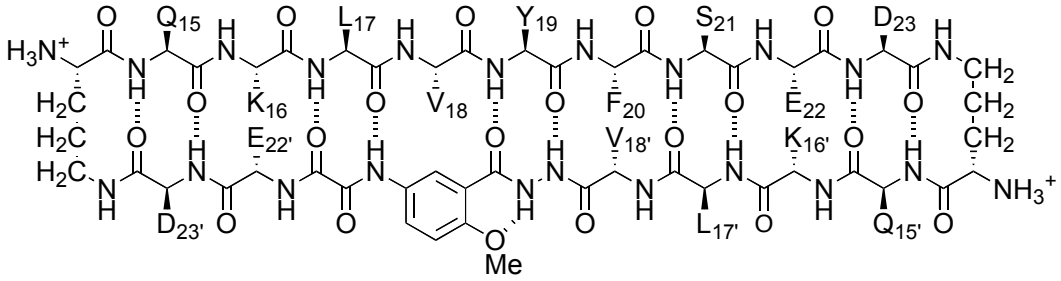

macrocyclic β-sheet peptide **4.6** (as the TFA salt)

molecular weight calculated for $C_{103}H_{156}N_{26}O_{33} \cdot 4CF_3CO_2H$ (TFA salt of **4.6**): 2742.59
molecular weight calculated for $C_{103}H_{156}N_{26}O_{33}$ (free base of **4.6**): 2286.50
exact mass calculated for $C_{103}H_{156}N_{26}O_{33}$ (free base of **4.6**): 2285.13

Analytical RP-HPLC of macrocyclic β-sheet **4.6**

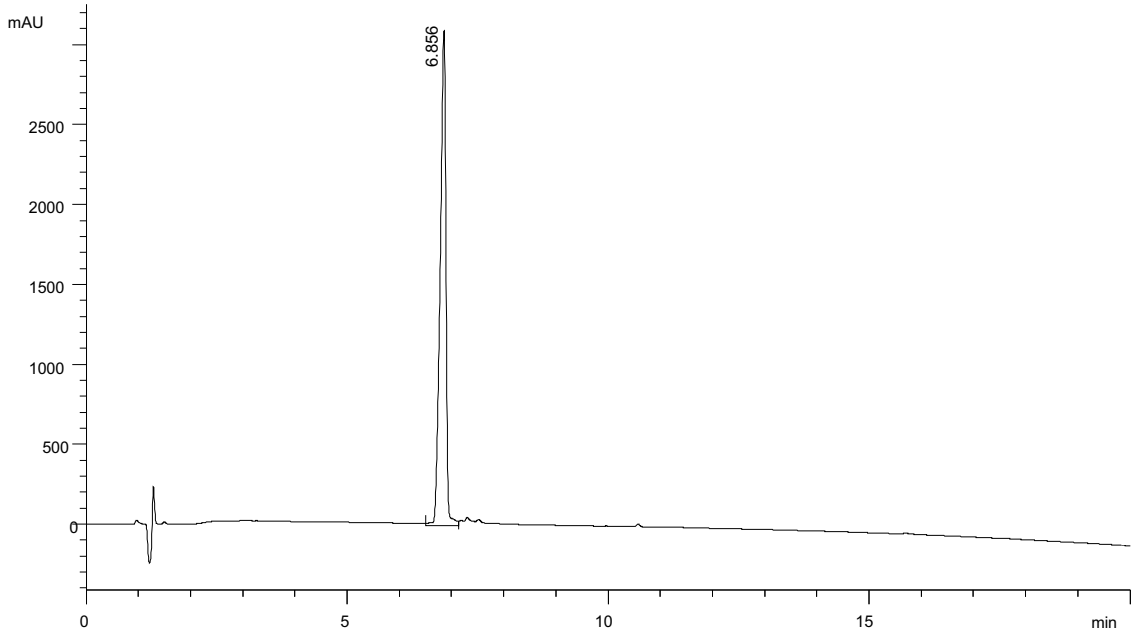

Signal 1:VWD1 A, Wavelength=214 nm

Peak #	RT [min]	Type	Width [min]	Area mAU*s	Height [mAU]	Area %
1	6.856	VV	0.108	23348.021	100.000	100.000

Macrocyclic β-sheet peptide **4.6**

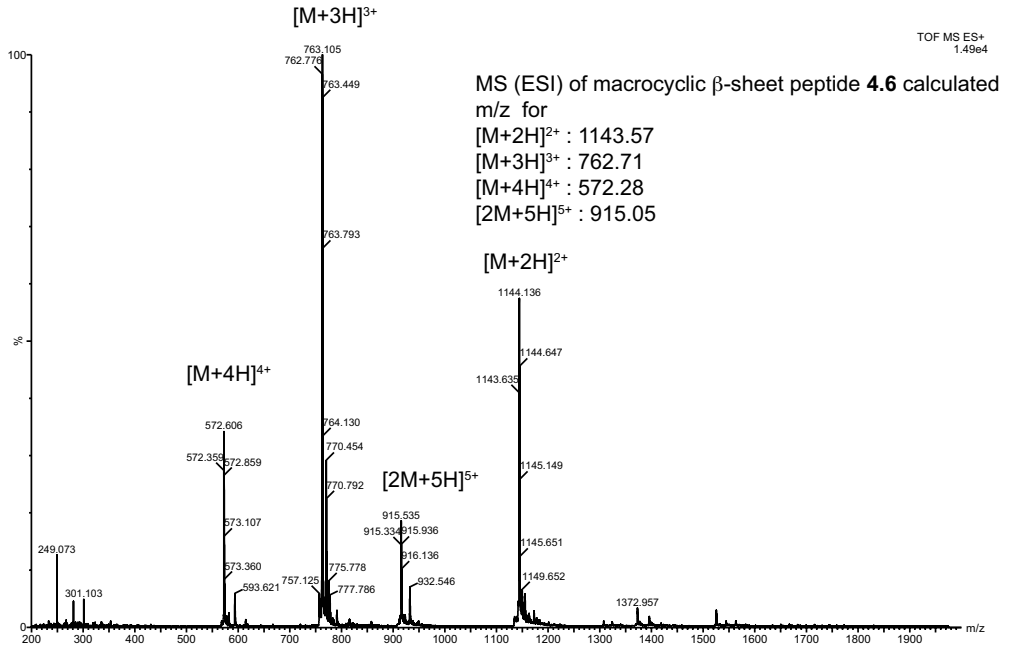

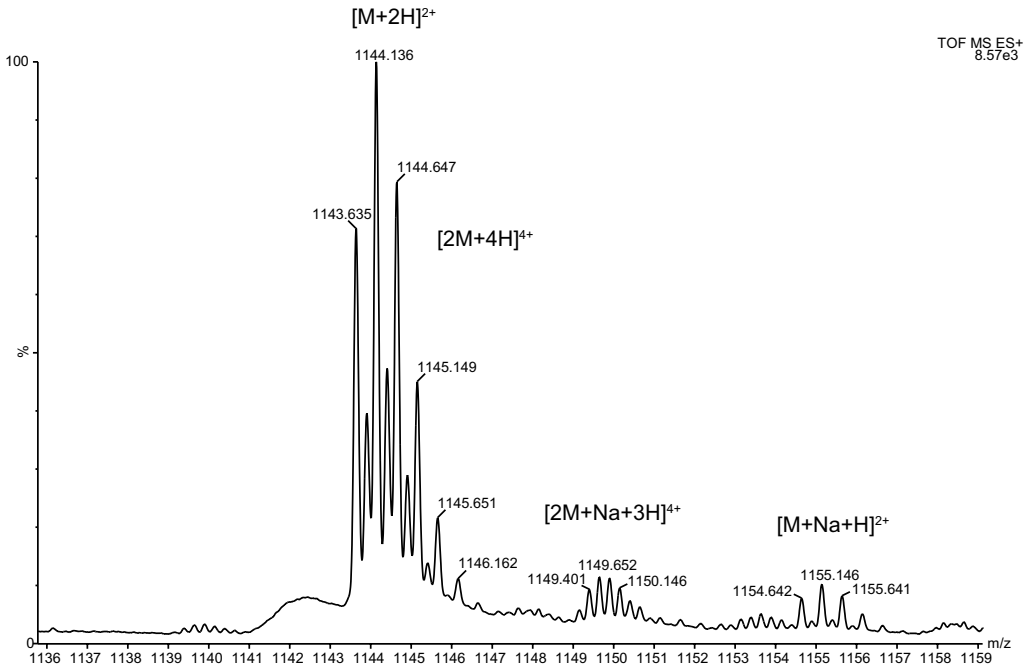

Macrocyclic β-sheet peptide **4.6**

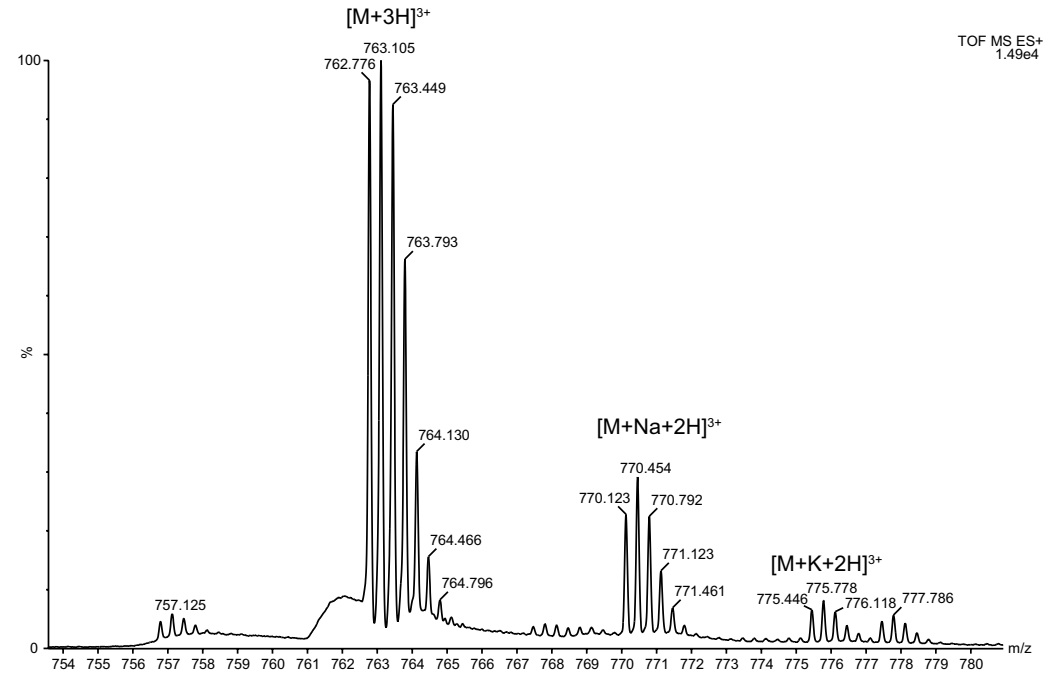

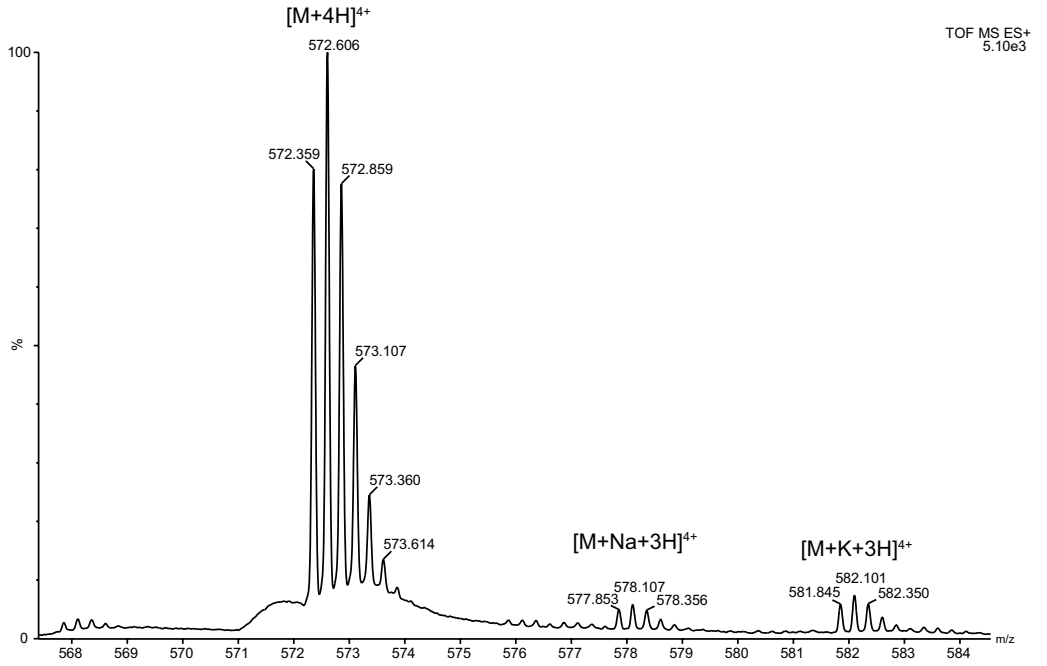

Macrocyclic β-sheet peptide **4.6**

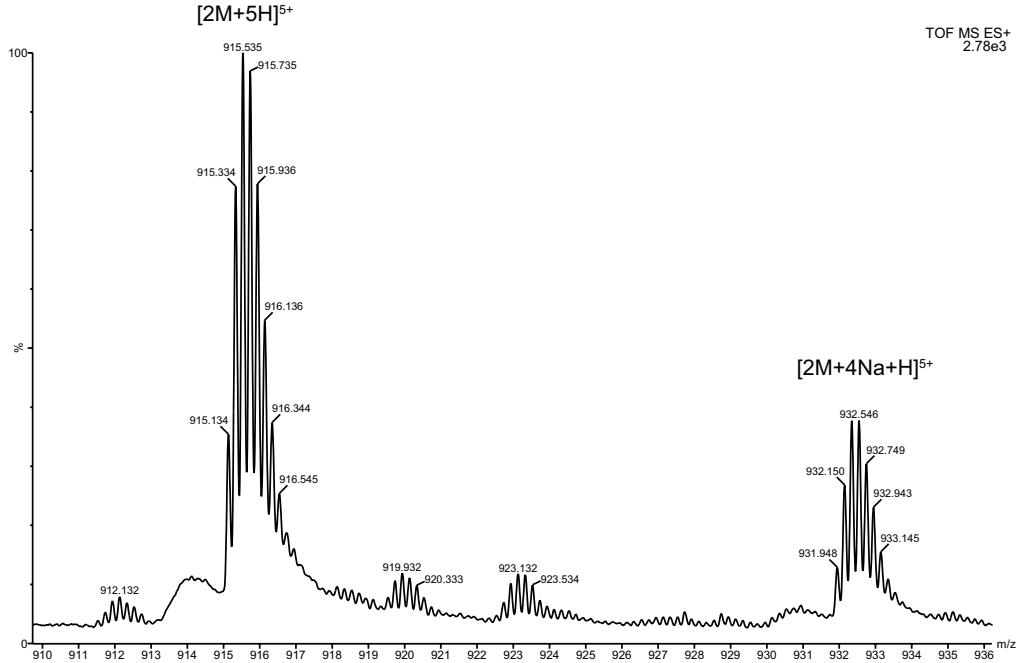

1D ^{1}H NMR spectrum of macrocyclic β-sheet **4.6**
2 mM in D_2O, 500 MHz, 298 K
monomer predominates

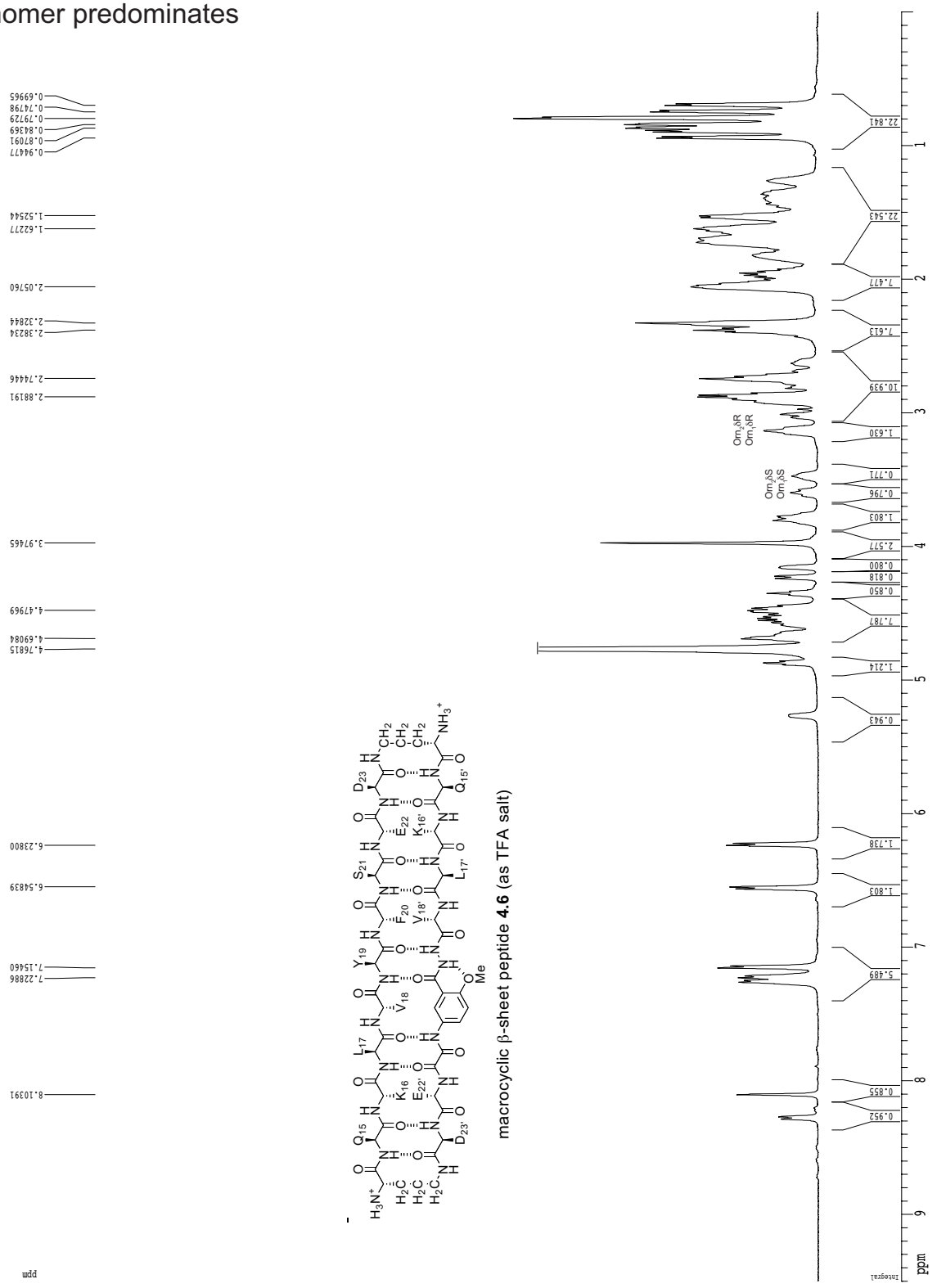

2D ROESY spectrum of macrocyclic β-sheet **4.6**
2 mM in D_2O, 500 MHz, 298 K
150-ms spin-lock mixing time
monomer predominates

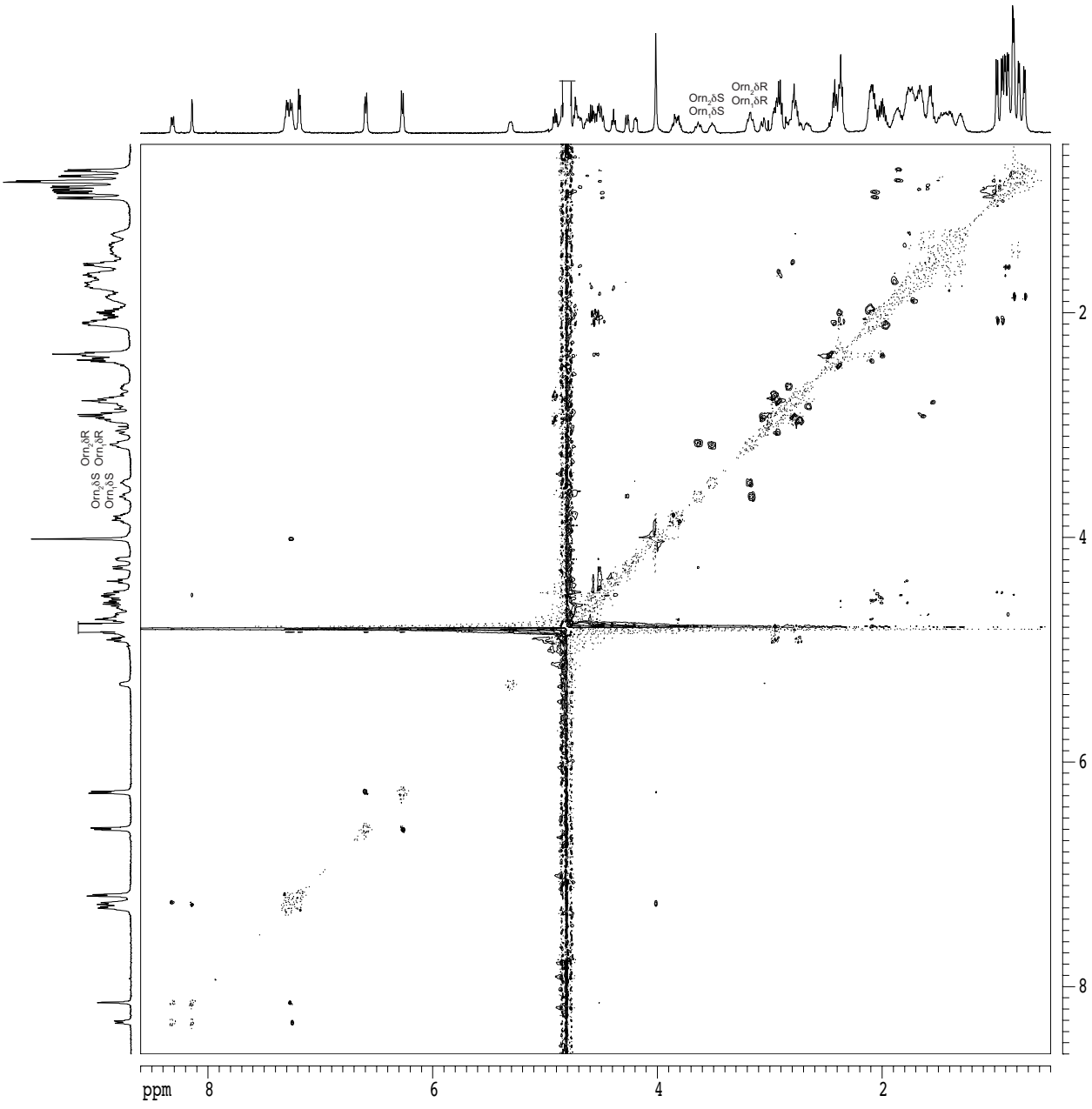

2D DOSY spectrum of macrocyclic β-sheet **4.6**
2 mM in D_2O, 600 MHz, 298 K
monomer predominates

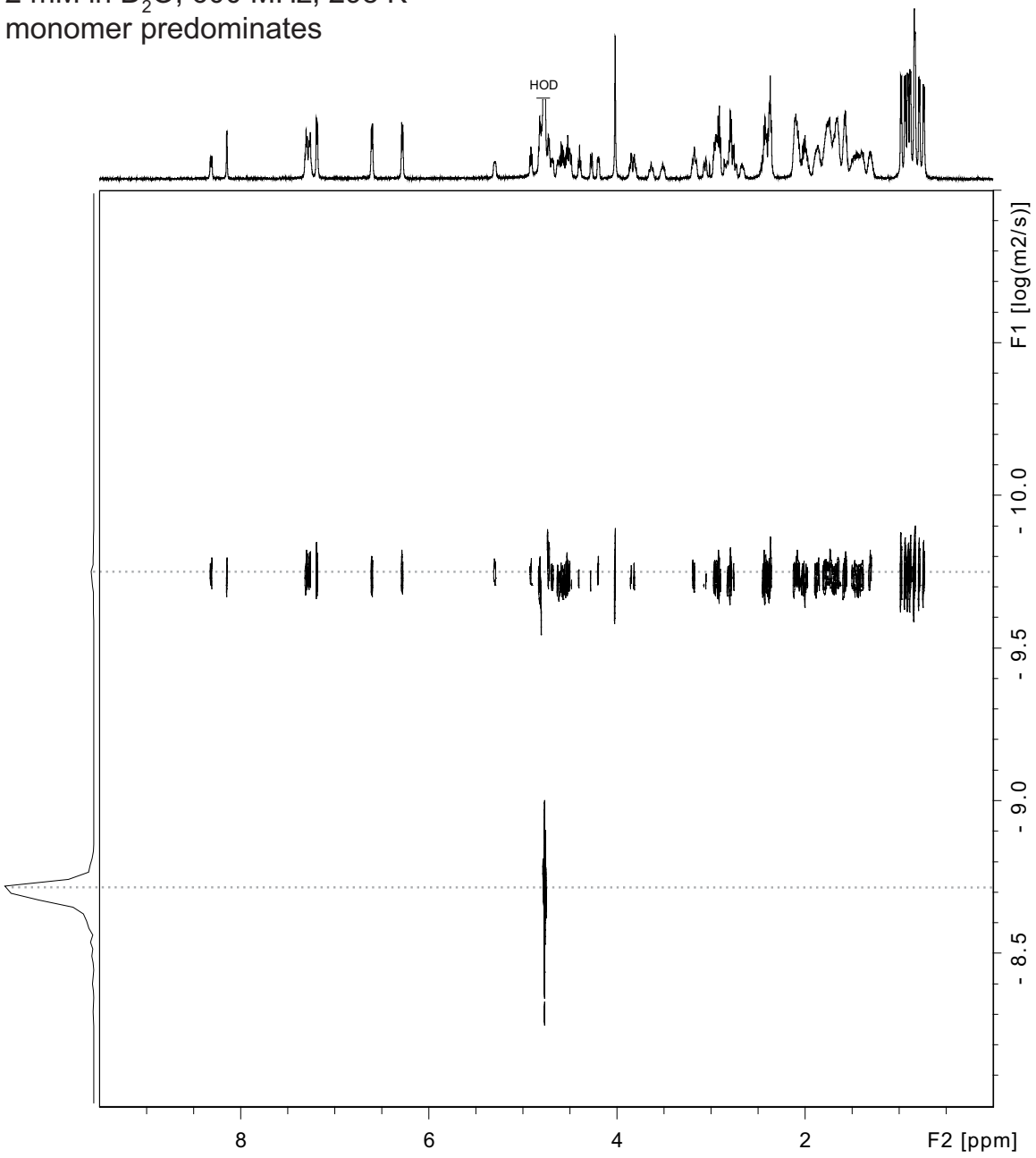

Calculation for peptide **4.6** at 2.0 mM

$DC_{HOD} = 19.0 \times 10^{-10}$ m^2/s [a]
$\log DC_{HOD} = -8.721$

For peptide **4.6** tetramer, log DC (m^2/s) = -9.76(0), DC = $10^{-9.760} m^2/s$ = 17.4×10^{-11} m^2/s = 17.4×10^{-7} cm^2/s

[a] Longsworth, L. G. J. Phys. Chem. 1960, 64, 1914–1917.